INSIGHTS IN HOMOCHIRAL METAL-ORGANIC FRAMEWORKS: FROM THEIR SYNTHESIS TO ENANTIOSELECTIVE APPLICATIONS

Juanjo Cabezas Giménez

UNIVERSITAT ROVIRA i VIRGILI

Insights in Homochiral Metal–Organic Frameworks: From Their Synthesis to Enantioselective Applications

Juanjo Cabezas Giménez

DOCTORAL THESIS

2022

UNIVERSITAT ROVIRA I VIRGILI
INSIGHTS IN HOMOCHIRAL METAL-ORGANIC FRAMEWORKS: FROM THEIR SYNTHESIS TO ENANTIOSELECTIVE
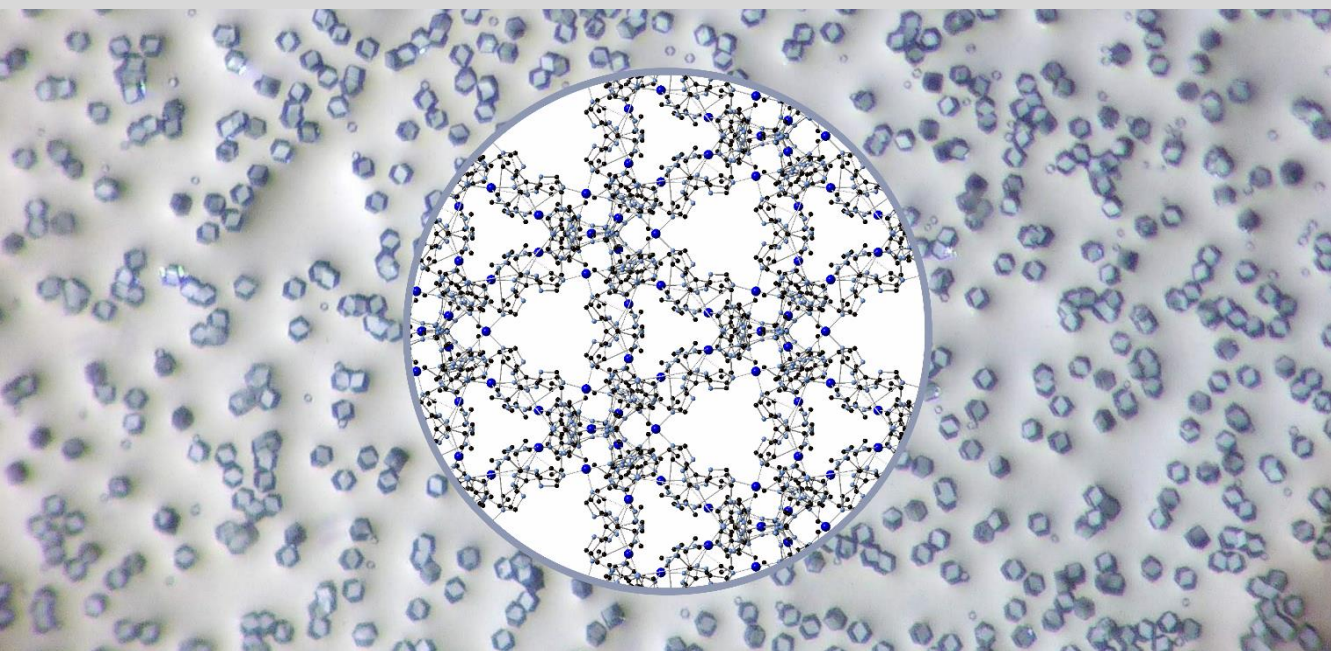APPLICATIONS
Juanjo Cabezas Giménez

UNIVERSITAT ROVIRA I VIRGILI
INSIGHTS IN HOMOCHIRAL METAL-ORGANIC FRAMEWORKS: FROM THEIR SYNTHESIS TO ENANTIOSELECTIVE
APPLICATIONS
Juanjo Cabezas Giménez

UNIVERSITAT ROVIRA I VIRGILI
INSIGHTS IN HOMOCHIRAL METAL-ORGANIC FRAMEWORKS: FROM THEIR SYNTHESIS TO ENANTIOSELECTIVE
APPLICATIONS
Juanjo Cabezas Giménez

Juanjo Cabezas Giménez

Insights in Homochiral Metal–Organic Frameworks: From Their Synthesis to Enantioselective Applications

DOCTORAL THESIS

Supervised by Prof. Dr. José Ramón Galán Mascarós and Prof. Dr. Anton Vidal i Ferran

Institut Català d'Investigació Química (ICIQ)

UNIVERSITAT
ROVIRA i VIRGILI

ICIQ R
Institut
Català
d'Investigació
Química

Tarragona 2022

UNIVERSITAT ROVIRA I VIRGILI
INSIGHTS IN HOMOCHIRAL METAL-ORGANIC FRAMEWORKS: FROM THEIR SYNTHESIS TO ENANTIOSELECTIVE
APPLICATIONS
Juanjo Cabezas Giménez

We state that the present study, entitled "*Insights in homochiral metal-organic frameworks: from their synthesis to enantioselective applications*", presented by **Juanjo Cabezas Giménez** to receive the degree of Doctor, has been carried out under our supervision at the Institut Català d'Investigació Química (ICIQ).

Tarragona, 01st of February 2022.

Doctoral thesis supervisors,

Prof. Dr. José Ramón Galán Mascarós   Prof. Dr. Anton Vidal Ferran

II

ACKNOWLEDGEMENTS

I would like to start the acknowledgements by thanking Profs. José Ramón Galán-Mascarós and Anton Vidal for the opportunity to carry out my PhD studies in their research groups at the *Institut Català d'Investigació Química* (ICIQ). I would like to thank all the members of their research groups (Andrea, David, Jiahao, Felipe, Irene, Stefano, Santiago, Jesús, Neus, Katherine, Scott, Ilario and Khalid) for all the good moments during these four years.

En particular, me gustaría mencionar a **Andrés Romero** por tener un corazón que no le cabe en el pecho. Eres una gran persona y un gran amigo (Simpson), y agradezco mucho que nuestros caminos se hayan cruzado en este no tan fácil proceso. Las peores situaciones sacan lo mejor de algunas personas. Del grupo Galán-Mascarós quería agradecer a **Vanesa Lillo**, coordinadora del grupo Galán-Mascarós, por haber sido mi confidente y mi compañera de risas y lágrimas. Me llevo muy buenos recuerdos contigo, ¡y espero que nos queden muchos más por crear! Finalmente, **Mabel de Fez**, eres un ser maravilloso y te mereces que la vida te depare lo mejor por todo lo que has trabajado, en todos los sentidos. Cada vez que olía a vainilla en el laboratorio sabía que iba a ser un buen día.

I am grateful to Prof. David Fairén-Jiménez for the opportunity to spend three months in his research group in the Chemical Engineering and Biotechnology department in University of Cambridge. I would like to thank Yue Yang his support and kindness, I have learnt a lot thanks to you! Also, a big, huge thank you to all the group members for making me feel a part of their big family: Marta, Elena, Jon, Francesca, Sergio and the rest of the group. Por último, gracias a la *spanish mafia* por haber hecho que estos tres meses me sienta como en casa (¡también va por vosotros, Manu y Nacho!).

Thank you to the ICIQ Research Support Area for all the help during these years. Específicamente, me gustaría agradecer al equipo de ChromTAE (Marta, Simona, Meritxell and Maria José) por todo lo que me han ayudado, ha sido "perturbadoramente" divertido trabajar con vosotras, y al equipo de X-Ray Diffraction (Eduardo, Marta y Jordi) por toda la ayuda ofrecida.

Fora de l'àmbit acadèmic, volia agrair als membres del "BBQ de verdat" per ser la família que s'escull. Iraida (¡PARAD, PARAD!), Steve, Nagore, Ariadna, Alícia, Fran, Eric, Adela, Anna, Ollé, Clàudia, Lídia, Mireia i Marcel, us estimo (menys quan sou *saboteurs*).

No podía olvidarme de ti, **Isaac**. Las vueltas que ha dado la vida desde que nos conocimos, y aun así te sigo teniendo muy presente en todas las etapas por las que he pasado. Si he llegado hasta donde he llegado también ha sido gracias a ti, doctor. Gracias por esa noche en la colina de Zarautz hablando de la vida, éramos felices y aún no lo sabíamos.

Mafe, gracias por haber hecho del confinamiento en la torre y de vivir en Vendrell una aventura. Bicicleta, playa, barbacoas, caminatas, esquivar al COVID-19 como ninjas durante *casi* dos años, charlas hasta las tantas de la madrugada, piscineo, birras, muchas risas y muchos dramas. Eres el gran descubrimiento de mi periodo de tesis (junto con Marta, Marga y Laura), y que lo que nos ha dado Vendrell que no nos lo quite Girona.

Quiero agradecer a mi familia, a la directa y a la política, todo el soporte y el cariño que he recibido siempre, en especial en esta difícil etapa. **Manolo** y **Antonia**, gracias por hacerme sentir uno más de la familia y el cariño que me dais, os quiero mucho. Eva, Xavi, Isel, Eva, Álex, Cristian, Mari y Dolores, gracias a todos, de corazón. **Iván**, estos últimos años he encontrado en ti a algo más que un hermano: a un amigo. Eres un adulto espectacular, siéntete orgulloso de quién eres, es un placer poder contar contigo en mi vida y compartir el humor tontísimo que tanto nos caracteriza. **Manolo**, por muchos años más juntos. **Mama**, mi gordi. Si es que qué voy a decir de ti, si cualquier cosa que escriba me va a parecer poco. Qué afortunado soy de tenerte, qué suerte la mía de poder llamarte "mama", no me faltes nunca. **Papa**, después de nueve años te tengo más presente que nunca, tengo tantas cosas que contarte que no sabría por dónde empezar. Hace poco leí en una carta tuya de hace 16 años: "[…] *quién sabe, a lo mejor le estoy escribiendo a un futuro científico*", y ahora que lo he conseguido no estás aquí para verlo, pero quiero creer que de alguna manera puedes verme. Esta tesis te la dedico especialmente a ti.

Por último, **Manu**. Gracias por haberme acompañado en este viaje y haberlo hecho un poco más bonito y un poco más ameno, a pesar de las cuatro mudanzas que llevamos. Te agradezco más todavía que sigamos viajando juntos, estoy impaciente por ver qué nos depara el futuro, aunque estoy seguro de que será espectacular (en una casa llena de perretes). Qué bonita es la vida a tu lado, pitu. Te quiero.

VI

Á miña familia e Manu.

VIII

"Die Chemie muss zur Astronomie der Molekularwelt werden"

Alfred Werner

X

LIST OF PUBLICATIONS

At the moment of the submission of this doctoral thesis, the results contained herein have so far resulted in the following publications:

- "Homochiral Metal–Organic Frameworks for Enantioselective Separations in Liquid Chromatography" Corella-Ochoa, M. N.; Tapia, J. B.; Rubin, H. N., Lillo, V.; González-Cobos, J.; Núñez-Rico, J. L.; Balestra, S. R. G.; Almora-Barrios, N.; Lledós, M.; Güell-Bara, A.; Cabezas-Giménez, J.; Escudero-Adán, E. C.; Vidal-Ferran, A.; Calero, S.; Reynolds, M.; Martí-Gastaldo, C.; Galán-Mascarós, J. R., *J. Am. Chem. Soc.* **2019**, *141*, 14306-14316.

- "Differentiation of Epoxide Enantiomers in the Confined Spaces of an Homochiral Cu^{2+} Metal–Organic Framework by Kinetic Resolution" Cabezas-Giménez, J.; Lillo, V.; Núñez-Rico, J. L.; Corella-Ochoa, M. N.; Jover, J.; Galán-Mascarós, J. R.; Vidal-Ferran, A., *Chem. Eur. J.* **2021**, *27*, 16956-16965 (Hot paper).

TABLE OF CONTENTS

XVIII

LIST OF ACRONYMS AND ABBREVIATIONS

The acronyms and abbreviations used in this doctoral thesis have been used following the recommendations given by the American Chemical Society. Additional abbreviations and acronyms used in this thesis are listed below:

5-Hmtz	5-methyltetrazole
AA	amino acid
AcOH	acetic acid
ADC	adamantane-1,3-carboxylic acid
BDC	benzene-1,4-dicarboxylic acid
BTC	benzene-1,3,5-tricarboxylic acid
BET	Brunauer-Emmett-Teller
BINAP	2,2′-bis(diphenylphosphino)-1,1′-binaphthyl
BINOL	1,1'-bi-2-naphthol
BPDC	4,4'-biphenyldicarboxylic acid
BTEX	benzene, toluene, ethylbenzene and xylenes
CMOF	chiral metal-organic framework
COF	covalent-organic framework
CSP	chiral stationary phase
CV	column volume
DCM	dichloromethane
DLS	dynamic light scattering
DMFA	dimethylformamide azine
DoF	degree of freedom
DPEN	diphenylethylenediamine
DUT	Dresden University of Technology
EDX	energy dispersive X-ray
ESEM	environmental scanning electron microscope

FESEM	field emission scanning electron microscope
H_2bdh	benzene-1,4-dihydroxamic acid
HETP	height equivalent to the theoretical plate
HKUST	Hong Kong University of Science and Technology
HPLC	high performance liquid chromatography
HRMS	high resolution mass spectrometry
IUPAC	International Union of Pure and Applied Chemistry
MIL	*Matériaux Institut Lavoisier*
MOF	metal-organic framework
NP	nanoparticle
PSM	post-synthetic modification
PVP	polyvinylpyrrolidone
PXRD	powder X-ray diffraction
PYI	pyrrolidine-2-yl-imidazole
QSDFT	quenched solid density functional theory
rac-	racemic
salen	2,2'-((1*E*,1'*E*)-(ethane-1,2-diylbis(azaneylylidene))bis-(methaneylylidene))diphenol)
SBU	secondary building unit
SCXRD	single-crystal X-ray diffraction
SPS	solvent purification system
STP	standard temperature and pressure
TEM	transmission electron microscopy
TGA	thermogravimetric analysis
TPDC	4,4''-terphenyldicarboxylic acid
Tr	trityl
Trz	triazole
TSO	*trans*-stilbene oxide
XRD	X-ray diffraction

XX

SUMMARY/RESUM/RESUMEN

Summary in English

The present doctoral thesis has been focused on the study of an amino acid-based CMOF, TAMOF-1, and its enantioselective applications. Then, we directed our interest to the design and synthesis of new ligands structurally similar to the one used to synthesise TAMOF-1 and the subsequent screening of coordination conditions for the obtention of analogues of TAMOF.

The thesis has been divided into six sections: a general introduction about CMOFs using enantiopure ligands and triazole-based MOFs, and five chapters about the research activities performed. Each chapter has been divided into the following sections: (1) abstract, (2) introduction, (3) results and discussion, (4) conclusions and (5) experimental section. References can be found as footnotes and are numbered jointly throughout the thesis. The crystallographic data and a molecule index can be found in the Annex. Molecules have been numbered independently in each chapter.

The general introduction briefly explains the history of coordination chemistry, the discovery of MOFs and their applications. Next, more thoroughly, the development of CMOFs using different kinds of enantiopure ligands and their applications are described. Then, a brief description of MOFs constructed with triazole ligands is developed. Later, it focuses on the description of the CMOF developed in our research group, in which the present doctoral thesis is based. After the introduction, the general objectives of the thesis are described.

Chapter I presents the synthetic optimisation of TAMOF-1 regarding particle size, surface area and nanoparticle (NP) incorporation into the structure, and the pH effect in TAMOF-1 synthesis has been studied. A preliminary study on the catalytic behaviour of NP@TAMOF-1 has been carried out. Self-shaping techniques have been explored for the formation of TAMOF-1 monoliths.

Chapter II discloses the role of TAMOF-1 as a heterogeneous catalyst in the kinetic resolution of styrene oxide with aniline. The meticulous exploration of the catalytic process allowed us to observe that two kinetic resolutions were taking place consecutively. The manuscript summarising the results has been published in *Chem. Eur. J.* **2021**, *27*, 16956-16965.

Chapter III describes the behaviour of TAMOF-1 as a platform for the separation of racemic mixtures in gravity columns. The research was continued with handmade HPLC columns with different lengths and inner diameters to expand the scope of chiral separations with this CMOF. For the first time, this chapter unfolds the use of a CMOF in semi-preparative separations in HPLC. The results enclosed in this chapter have been published in *J. Am. Chem. Soc.* **2019**, *141*, 14306-14316.

Chapter IV details the performance of TAMOF-1 as stationary phase for the separation of regioisomers of organic compounds. The mixtures analysed in this chapter are complex mixtures to separate with conventional separation techniques, such as distillation.

Chapter V is a compendium of different synthetic routes to transform enantiopure primary amines into their 4*H*-1,2,4-triazole analogues through a transamination process. These ligands were further used to explore the synthesis of novel porous CMOFs.

Resum en català

La present tesi doctoral ha estat enfocada a l'estudi d'un CMOF basat en un lligand aminoàcid, TAMOF-1, i les seves aplicacions enantioselectives. Llavors, vàrem dirigir el nostre interès al disseny i la síntesi de lligands nous estructuralment semblants a l'utilitzat en la síntesi del TAMOF-1, i el subseqüent cribratge de les condicions de coordinació per a la obtenció d'anàlegs de TAMOF.

La tesi ha estat dividida en sis seccions: una introducció general sobre CMOFs utilitzant lligands enantiopurs i MOFs fets amb lligands triazol, i cinc capítols sobre les activitats de recerca dutes a terme. Cada capítol s'ha dividit en cinc seccions: (1) resum, (2) introducció, (3) discussió de resultats, (4) conclusions i (5) secció experimental. Les referències es poden trobar com a peus de pàgina i es troben numerades de manera contínua durant tota la tesi. Les dades cristal·logràfiques i l'índex de molècules es poden trobar a l'Annex. Les molècules s'han numerat de manera independent en cada capítol.

La introducció general explica breument la història de la química de coordinació, el descobriment dels MOFs i les seves aplicacions. A continuació, més exhaustivament, es descriu el desenvolupament dels CMOFs utilitzant diferents tipus de lligands enantiopurs i les seves aplicacions. Just després es fa una breu descripció dels MOF construïts amb lligands triazole i les seves aplicacions. Posteriorment, es centra en la

descripció del CMOF sintetitzat al nostre grup de recerca, en el qual es basa la present tesi doctoral. Després de la introducció, es descriuen els objectius generals de la tesi.

El capítol I presenta la optimització de la síntesi del TAMOF-1 pel que fa a la mida de partícula, l'àrea superficial i la incorporació de nanopartícules (NPs) a l'estructura, i s'ha estudiat l'efecte del pH a la síntesi del TAMOF-1. S'ha dut a terme un estudi preliminar del comportament catalític de NP@TAMOF-1. Finalment, s'han explorat diverses tècniques d'autoformació per a la obtenció de monòlits de TAMOF-1.

El capítol II revela el paper del TAMOF-1 com a catalitzador heterogeni en la resolució cinètica d'òxid d'estirè amb anilina. L'exploració meticulosa del procés catalític ens ha permès observar que dues resolucions cinètiques tenen lloc consecutivament. El manuscrit resumint els resultats ha estat publicat en *Chem. Eur. J.* **2021**, *27*, 16956-16965.

El capítol III descriu el comportament del TAMOF-1 com a plataforma per a la separació de mescles racèmiques en columnes de gravetat. Vam continuar la recerca amb columnes d'HPLC emplenades a mà amb diferents llargades i diàmetres interns per ampliar l'abast de les separacions quirals amb aquest CMOF. Per primera vegada, aquest capítol explica l'ús d'un CMOF en separacions semipreparatives en HPLC. Els resultats inclosos en aquest capítol han estat publicats en *J. Am. Chem. Soc.* **2019**, *141*, 14306-14316.

El capítol IV detalla l'aplicació del TAMOF-1 com a fase estacionària per a la separació de regioisòmers de molècules orgàniques en cromatografia líquida emprant les mateixes columnes descrites en el capítol III. Les mescles analitzades en aquest capítol són complicades de separar amb tècniques de separació convencionals, com la destil·lació.

El capítol V és un compendi de diferents rutes sintètiques per a la transformació d'amines primàries enantiopures en els seus anàlegs 4*H*-1,2,4-triazol a través d'un procés de transaminació. Aquests lligands s'ha utilitzat en la exploració de la síntesi de nous CMOFs porosos.

Resumen en castellano

La presente tesis doctoral se ha enfocado al estudio de un CMOF basado en un ligando aminoácido, TAMOF-1, y sus aplicaciones enantioselectivas. Entonces, dirigimos nuestro interés al diseño y síntesis de nuevos ligandos estructuralmente similares al usado en la síntesis de TAMOF-1, y el

subsecuente cribado de las condiciones de coordinación para la obtención de nuevos análogos de TAMOF.

La tesis ha sido dividida en seis secciones: una introducción general sobre los CMOF usando ligandos enantiopuros y MOFs hechos con ligandos triazol, y cinco capítulos sobre las actividades de investigación realizadas. Cada capítulo ha sido dividido en las siguientes secciones: (1) resumen, (2) introducción, (3) discusión de resultados, (4) conclusiones y (5) sección experimental. Las referencias se pueden encontrar en los pies de página y se encuentran numeradas de manera continua durante toda la tesis. Los datos cristalográficos y el índice de moléculas se pueden encontrar en el Anexo. Las moléculas se han numerado de manera independiente en cada capítulo.

La introducción general explica brevemente la historia de la química de coordinación, el descubrimiento de los MOF y sus aplicaciones. A continuación, de una manera más exhaustiva, se describe el desarrollo de los CMOF utilizando diferentes tipos de ligandos enantiopuros y sus aplicaciones. Después se desarrolla una breve descripción de MOFs construidos con ligandos triazol y sus aplicaciones. Posteriormente, se centra en la descripción del CMOF desarrollado en nuestro grupo de investigación, en el cual se basa la presente tesis doctoral. Después de la introducción, se presentan los objetivos generales de la tesis.

El capítulo I presenta la optimización de la síntesis del TAMOF-1 por lo que se refiere al tamaño de partícula, el área superficial y la incorporación de nanopartículas (NPs) a la estructura, y se ha estudiado el efecto del pH en la síntesis de TAMOF-1. Se ha llevado a cabo un estudio preliminar del comportamiento catalítico de NP@TAMOF-1. Finalmente, se han explorado diversas técnicas sintéticas para la obtención de monolitos de TAMOF-1.

El capítulo II revela el papel de TAMOF-1 como catalizador heterogéneo en la resolución cinética de óxido de estireno con anilina. La exploración meticulosa del proceso catalítico nos permitió observar que dos resoluciones cinéticas tenían lugar consecutivamente. El manuscrito resumiendo los resultados se ha publicado en *Chem. Eur. J.* **2021**, *27*, 16956-16965.

El capítulo III describe el comportamiento de TAMOF-1 como plataforma para la separación de mezclas racémicas en columnas de gravedad. Continuamos la investigación con columnas de HPLC llenadas a mano con diferentes longitudes y diámetros internos para ampliar el alcance de las separaciones quirales con este CMOF. Por primera vez, este capítulo explica el uso de un CMOF en separaciones semipreparativas en HPLC. Los resultados incluidos en este capítulo se han publicado en *J. Am. Chem. Soc.* **2019**, *141*, 14306-14316.

El capítulo IV detalla la aplicación de TAMOF-1 como fase estacionaria para la separación de regioisómeros de moléculas orgánicas en cromatografía líquida usando las mismas columnas descritas en el capítulo III. Las mezclas analizadas son mezclas complejas de separar con técnicas de purificación convencionales, como la destilación.

El capítulo V es un compendio de diferentes rutas sintéticas para la transformación de aminas primarias enantiopuras en sus correspondientes análogos 4*H*-1,2,4-triazol a través de un proceso de transaminación. Estos ligandos se han usado en la exploración de la síntesis de nuevos CMOF.

UNIVERSITAT ROVIRA I VIRGILI
INSIGHTS IN HOMOCHIRAL METAL-ORGANIC FRAMEWORKS: FROM THEIR SYNTHESIS TO ENANTIOSELECTIVE
APPLICATIONS
Juanjo Cabezas Giménez

INTRODUCTION
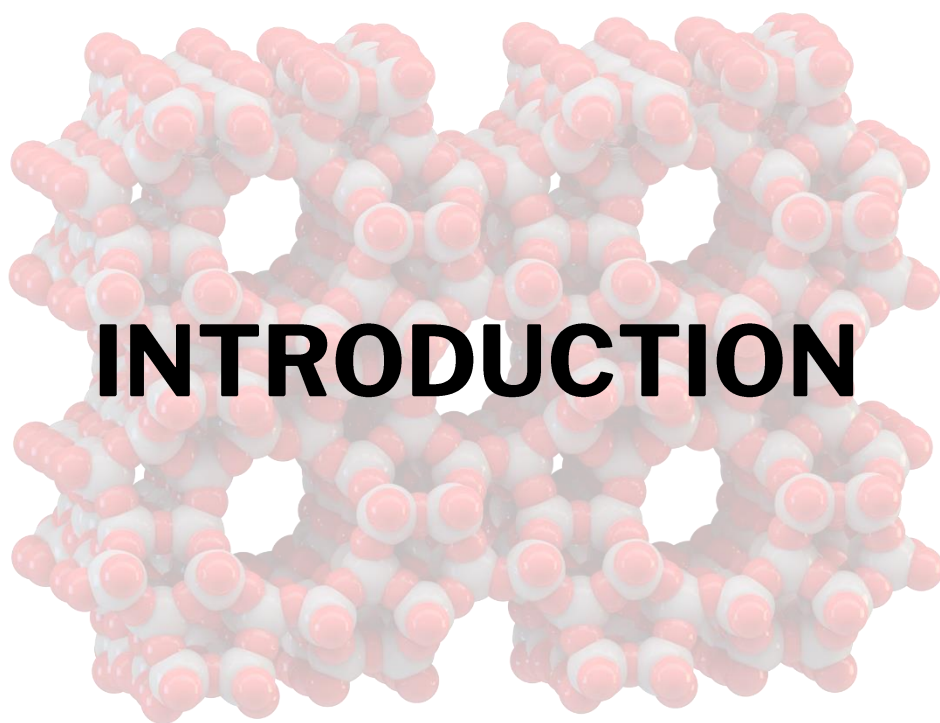
COORDINATION CHEMISTRY

Coordination compounds[1] have been among us for millennia. They have been with us, humans, since our very beginning – for instance, haemoglobin contains iron-porphyrin complexes (heme) to carry oxygen to cells. A well-known family of products arising from coordination chemistry are pigments, insoluble inorganic compounds that have been historically used in cave paintings. Of course, these pigments were found in nature, such as ochre, charcoal and calcite.

Little was known about coordination compounds until the eighteenth century. There is evidence that synthetic pigments like Egyptian blue (the oldest synthetic pigment) have been manufactured since the third millennium BCE.[2] Either if they were found by serendipity or not, and regardless of the reproducibility of the processes conducting to those, no knowledge existed about their composition and structure.

The serendipitous discovery of a well-known pigment – actually, the first modern synthetic pigment – changed the historical course of coordination chemistry: Prussian Blue.[3] It was discovered in 1704 in Berlin, Germany, by Johann Jacob Diesbach, a Swiss chemist, dye and pigment producer, although the recipe was described in the literature by John Woodward. Diesbach worked in the production of cochineal lake,[4] an organic red pigment extracted from cochineal (*Dactylopius coccus*), and the process was based on the precipitation of an extract of cochineal with potassium carbonate (or potash, K_2CO_3), the addition of alum [$KAl(SO_4)_2 \cdot 12H_2O$] and iron sulphate ($FeSO_4$).

At this time, Diesbach worked in Johann Konrad Dippel's laboratory, where he prepared a distillation product of animal blood, called "animal oil", where he added potash to remove impurities. Diesbach borrowed some potash of Dippel's animal oil production – what he did not know is that the decomposition of organic molecules in the distillation process ultimately produced cyanide ions that subsequently reacted with iron(III) centres from the blood to yield hexacyanoferrate ions [$Fe^{3+}(CN)_6$]$^{3-}$. These ions were substantially present in the potash he borrowed, and by addition to his mixture, he observed an unexpected, deep blue precipitate. This precipitate, $Fe_4^{3+}[Fe^{2+}(CN)_6]_3 \cdot H_2O$, was first named *Preußisch blau* and *Berlinisch blau*, to be

---

[1] Coordination entity: an assembly consisting of a central atom (usually metallic) to which is attached a surrounding array of other groups or atoms (ligands). *IUPAC. Compendium of Chemical Terminology, 2nd ed. (the "Gold Book"). Blackwell Scientific Publications, Oxford (1997).*

[2] Rossotti, H. *Colour: Why the World Isn't Grey*. Princeton University Press: Princeton, N. J., 1984.

[3] (a) Woodward, J. *Philos. Trans. R. Soc. Lond.* **1724**, *33*, 15-17. (b) Dunbar, K. R.; Heintz, R. A. In *Prog. Inorg. Chem.*; 1996; pp 283-391.

[4] Meloan, S. N.; Valentine, L. S.; Puchtler, H. *Histochemie* **1971**, *27*, 87-95.

ultimately named Prussian blue. Despite its discovery, the serendipitous character of this synthetic procedure endowed pigments with the mystery of its structure and composition.

Numerous theories were proposed to explain the behaviour of coordination compounds, resulting in unsuccessful trials. It was not until the late 19th century that the concept of coordination chemistry was established when a French chemist, Alfred Werner, was working on the rationalisation of the atom disposition in coordination complexes.[5] Werner's findings distinguished the oxidation state (*Hauptvalenz*) and coordination number (*Nebenvalenz*) and provided him with the title of "Founder of Coordination Chemistry" and the Nobel Prize in Chemistry for his findings in coordination chemistry (1913).[6]

From this point, coordination chemistry extended from the molecular (0D) scale to complex layers (2D) or three-dimensional networks (3D). Subsequent changes, like the rationalisation of the molecular geometry and the use of building units radically evolved the chemistry of coordination networks. A new field of chemistry was born when these conceptual changes were tested experimentally – **reticular chemistry**.[7]

Reticular chemistry is the study of linking molecular building blocks into extended crystalline structures. COFs[8] and MOFs[9] are part of these crystalline structures. The difference between these two crystalline materials is that COFs are made exclusively by organic ligands, while MOFs are constructed from organic ligands and metallic nodes.

METAL-ORGANIC FRAMEWORKS

As stated by the IUPAC, "*A metal-organic framework, abbreviated to MOF, is a coordination network with organic ligands containing potential voids*".[10] Interest in MOFs has grown exponentially since the first example was published in 1999 when Omar Yaghi reported the design and synthesis of MOF-5 (**Figure 1**).[11] Curiously, this was not the first time the term "metal-organic framework" was

---

[5] Bailar, J. C. *J. Chem. Educ.* **1986**, *63*, A116.
[6] (a) Kauffman, G. B. *Alfred Werner: Founder of Coordination Chemistry*. Springer-Verlag: Berlin, Heidelberg, 1966. (b) Constable, E. C.; Housecroft, C. E. *Chem. Soc. Rev.* **2013**, *42*, 1429-1439.
[7] (a) Yaghi, O. M. *J. Am. Chem. Soc.* **2016**, *138*, 15507-15509. (b) Jiang, H.; Alezi, D.; Eddaoudi, M. *Nat. Rev. Mater.* **2021**, *6*, 466-487.
[8] Huang, N.; Wang, P.; Jiang, D. *Nat. Rev. Mater.* **2016**, *1*, 16068.
[9] (a) James, S. L. *Chem. Soc. Rev.* **2003**, *32*, 276-288. (b) Furukawa, H.; Cordova Kyle, E.; O'Keeffe, M.; Yaghi Omar, M. *Science* **2013**, *341*, 1230444.
[10] Batten, S. R.; Champness, N. R.; Chen, X.-M.; Garcia-Martinez, J.; Kitagawa, S.; Öhrström, L.; O'Keeffe, M.; Paik Suh, M.; Reedijk, J. *Pure Appl. Chem.* **2013**, *85*, 1715-1724.
[11] Li, H.; Eddaoudi, M.; O'Keeffe, M.; Yaghi, O. M. *Nature* **1999**, *402*, 276-279.

used – it was first reported by Ibers and co-workers. However, it did not refer to an actual MOF.[12] Furthermore, the inherent properties of MOFs that have attracted the attention of the researchers are their permanent porosities, large surface areas, their thermal and chemical stability and the tunability of their pores, among many others.

Introduction
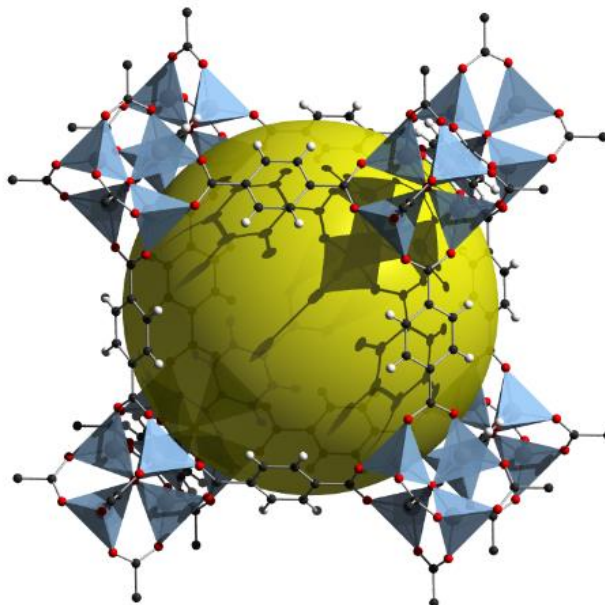
Figure 1. The unit cell of MOF-5. The pore volume is represented as a yellow sphere.

So far, more than 90000 MOF structures have been reported according to the literature.[13] Among these, there are several MOFs that are widely known, and their structures have served as a template to develop similar materials with modified properties. These include but are not limited to:

- MIL-53 (**Figure 2**) and MIL-101[14] (**Figure 3**). These Cr^{3+} MOFs were developed in 2002 and 2005 in the Institut Lavoisier de Versailles by Gérard Ferey and co-workers. These microporous MOFs possess BET (*i.e.* Brunauer, Emmett and Teller, a theory to evaluate the gas adsorption data) surface areas of ~1500 and ~4100 m^2 g^{-1}, respectively.

---

[12] Palmer, S. M.; Stanton, J. M.; Hoffman, B. M.; Ibers, J. A. *Inorg. Chem.* **1986**, *25*, 2296-2300.
[13] (a) Moghadam, P. Z.; Li, A.; Wiggin, S. B.; Tao, A.; Maloney, A. G. P.; Wood, P. A.; Ward, S. C.; Fairen-Jimenez, D. *Chem. Mater.* **2017**, *29*, 2618-2625. (b) Moosavi, S. M.; Nandy, A.; Jablonka, K. M.; Ongari, D.; Janet, J. P.; Boyd, P. G.; Lee, Y.; Smit, B.; Kulik, H. J. *Nat. Commun.* **2020**, *11*, 4068.
[14] For MIL-53 see (a) Millange, F.; Serre, C.; Férey, G. *Chem. Commun.* **2002**, 822-823. (b) Serre, C.; Millange, F.; Thouvenot, C.; Noguès, M.; Marsolier, G.; Louër, D.; Férey, G. *J. Am. Chem. Soc.* **2002**, *124*, 13519-13526. For MIL-101 see Férey, G.; Mellot-Draznieks, C.; Serre, C.; Millange, F.; Dutour, J.; Surblé, S.; Margiolaki, I. *Science* **2005**, *309*, 2040-2042.
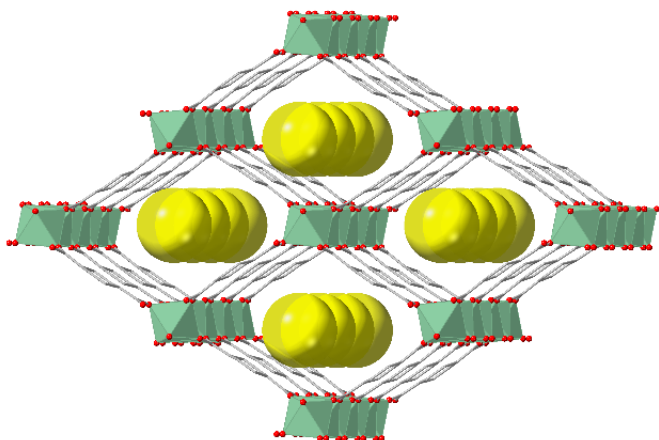
Figure 2. Structure of MIL-53.
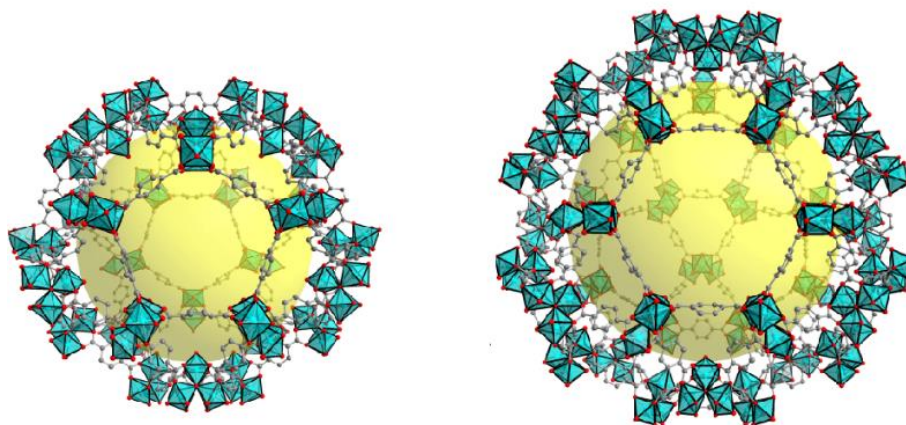
Figure 3. Structure of the mesoporous cages made of pentagonal (left) and hexagonal (right) rings in MIL-101. Adapted from *Membranes* **2013**, *3*, 331-353.

- UiO-66[15] (**Figure 4**). Synthesised in 2008 in University of Oslo, in Karl Peter Lillerud's research group. Constructed with Zr^{4+} and BDC, this MOF is exceptionally stable, although its BET surface area is not among the highest, being 1187 m^2 g^{-1}. Changing the ligand to BPDC or TPDC yielded the analogues UiO-67 and UiO-68, with a BET surface area of 3000 and 4170 m^2 g^{-1}, respectively. Like the aforementioned MOFs, these three materials are also microporous.

---

[15] Cavka, J. H.; Jakobsen, S.; Olsbye, U.; Guillou, N.; Lamberti, C.; Bordiga, S.; Lillerud, K. P. *J. Am. Chem. Soc.* **2008**, *130*, 13850-13851.

4
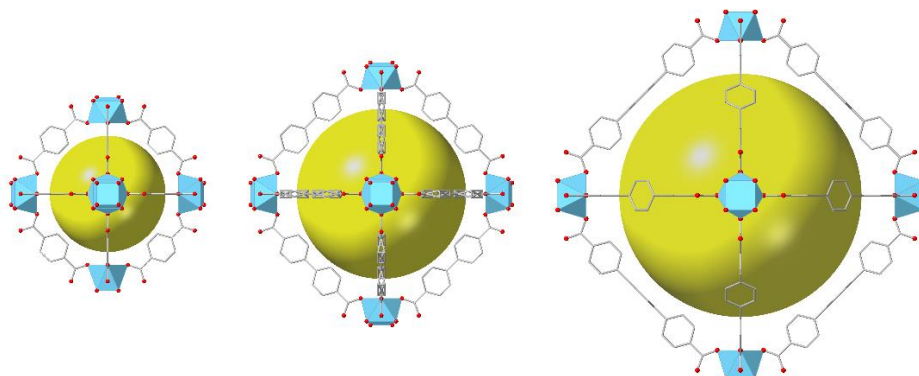
Figure 4. Structures of UiO-66, UiO-67 and UiO-68 (from left to right).

- ZIF-8[16] (**Figure 5**). Omar Yaghi and co-workers developed the zeolitic imidazolate framework-8, a subclass of MOF with Zn^{2+} as the metal centre and imidazole ligands. It is highly stable, it has a BET surface area of ~1800 m^2 g^{-1}, and its pores and surface are hydrophobic.
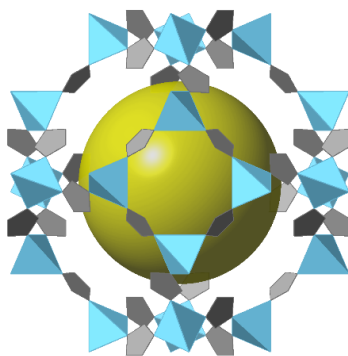
Figure 5. Structure of ZIF-8.

The surface area and porosity of MOFs are exceptional and have not ceased growing.[17] In fact, in 2018 was reported the highest BET surface area in a MOF up to date, DUT-60,[18] with 7839 m^2 g^{-1}. Theoretical calculations[19] have limited the surface area of MOFs up to 14600 m^2 g^{-1}, and after 20 years of research in MOFs, we are halfway of the maximum predicted surface area.

[16] Park, K. S.; Ni, Z.; Côté, A. P.; Choi, J. Y.; Huang, R.; Uribe-Romo, F. J.; Chae, H. K.; O'Keeffe, M.; Yaghi, O. M. *PNAS* **2006**, *103*, 10186.

[17] Furukawa, H.; Cordova, K. E.; O'Keeffe, M.; Yaghi, O. M. *Science* **2013**, *341*, 1230444.

[18] Hönicke, I. M.; Senkovska, I.; Bon, V.; Baburin, I. A.; Bönisch, N.; Raschke, S.; Evans, J. D.; Kaskel, S. *Angew. Chem. Int. Ed.* **2018**, *57*, 13780-13783.

[19] Farha, O. K.; Eryazici, I.; Jeong, N. C.; Hauser, B. G.; Wilmer, C. E.; Sarjeant, A. A.; Snurr, R. Q.; Nguyen, S. T.; Yazaydın, A. Ö.; Hupp, J. T. *J. Am. Chem. Soc.* **2012**, *134*, 15016-15021.

MOFs have opened the door to a world of possibilities and can be classified by their applications in several scientific disciplines. The most representative examples are gas storage and separation,[20] sensors,[21] LEDs,[22] drug delivery[23] and a long list of other applications. MOFs can also be divided into subclasses, like the aforementioned ZIFs and chiral MOFs.

CHIRAL METAL-ORGANIC FRAMEWORKS

Chiral MOFs are a subclass of MOFs possessing intrinsic chirality due to enantiopure precursors, asymmetric environment or special arrangements. CMOFs can be classified into homochiral or heterochiral (**Figure 6**).

On the one hand, homochiral MOFs are enantiomorphous materials constructed with a single enantiomer, therefore enantiopure. On the other hand, heterochiral MOFs are built with racemic mixtures but in an ordered manner through a process of self-discrimination. Up to date, only a few examples of heterochiral MOFs have been reported compared with homochiral.[24] Heterochiral MOFs will not be further described in the present introduction. The intrinsic chirality inside CMOF pores expands the scope of the inherent applications of these materials.
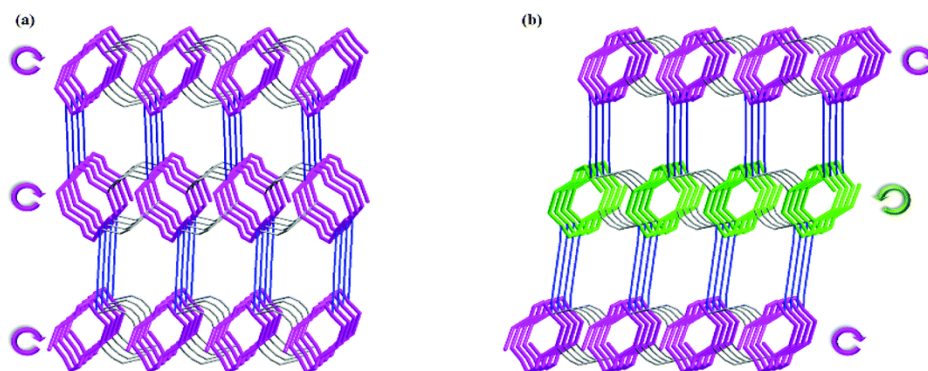
Figure 6. 3D representation of (a) homochiral and (b) heterochiral MOFs. Adapted with permission from *Dalton Trans.* **2016**, *45*, 1335-1338. Copyright 2016 Royal Society of Chemistry.

[20] Fan, W.; Zhang, X.; Kang, Z.; Liu, X.; Sun, D. *Coord. Chem. Rev.* **2021**, *443*, 213968.
[21] Zhang, L.-T.; Zhou, Y.; Han, S.-T. *Angew. Chem. Int. Ed.* **2021**, *60*, 15192-15212.
[22] Tang, Y.; Wu, H.; Cao, W.; Cui, Y.; Qian, G. *Adv. Opt. Mater.* **2020**, *9*, 2001817.
[23] Lawson, H. D.; Walton, S. P.; Chan, C. *ACS Appl. Mater. Interfaces* **2021**, *13*, 7004-7020.
[24] (a) Wu, Y.; Li, D.; Fu, F.; Tang, L.; Wang, J.; Yang, X. G. *J. Coord. Chem.* **2009**, *62*, 2665-2674. (b) Wen, G.-L.; Liu, D.-F.; Chen, Y.-H.; Wei, Y.-J.; Zhu, Q.-Y.; Wang, X.-L.; Xu, M.; Yao, Y.; Ma, L.-F. *Inorg. Chem. Commun.* **2016**, *74*, 86-89. (c) Yue, Q.; Wang, N.-N.; Guo, S.-Y.; Liang, L.-L.; Gao, E.-Q. *Dalton Trans.* **2016**, *45*, 1335-1338.

6

Introduction

Applications of CMOFs

As known since the thalidomide disaster,[25] pharmaceutically active products are enantiopure in most cases. However, some drugs like ibuprofen are clinically administrated as a racemic mixture.[26] The challenge to obtain these products enantiomerically pure can be tackled in two ways: enantioselective synthesis or chiral separation. It has been shown that CMOFs are promising heterogeneous platforms for these two asymmetric processes.

Enantioselective catalysis

On account of their inherent chiral cavities, permanent porosities, the density of catalytic sites and potential recyclability, CMOFs are propitious catalytic platforms for enantioselective transformations. The asymmetric processes in which CMOFs have been successfully used include, but are not limited to cyanosilylations,[27] oxidations,[28] 1,2-[29] and 1,4-additions,[30] carbonyl-ene reactions,[31] aldol reactions,[32] asymmetric hydrogenations[33] and ring-opening of epoxides.[34]

Chiral separations

The stability and tunability of the pores inside CMOFs have also made them excellent CSPs for chiral separations. Up to date, several CMOFs have been tested in the enantiomeric separation of racemates containing a wide range of functional groups, such as sulfoxides,[35] amines[36] and other interesting molecules.[37] Up to date, these separations are limited to analytical scale.

---

[25] Kim, J. H.; Scialli, A. R. *Toxicol. Sci.* **2011**, *122*, 1-6.

[26] Evans, A. M. *Clin. Rheumatol.* **2001**, *20*, 9-14.

[27] Li, J.; Ren, Y.; Qi, C.; Jiang, H. *Chem. Commun.* **2017**, *53*, 8223-8226.

[28] Chen, X.; Peng, Y.; Han, X.; Liu, Y.; Lin, X.; Cui, Y. *Nat. Commun.* **2017**, *8*, 2171.

[29] Ma, L.; Wu, C.-D.; Wanderley, M. M.; Lin, W. *Angew. Chem. Int. Ed.* **2010**, *49*, 8244-8248.

[30] Sawano, T.; Ji, P.; McIsaac, A. R.; Lin, Z.; Abney, C. W.; Lin, W. *Chem. Sci.* **2015**, *6*, 7163-7168.

[31] Han, J.; Lee, M. S.; Thallapally, P. K.; Kim, M.; Jeong, N. *ACS Catal.* **2019**, *9*, 3969-3977.

[32] Kutzscher, C.; Nickerl, G.; Senkovska, I.; Bon, V.; Kaskel, S. *Chem. Mater.* **2016**, *28*, 2573-2580.

[33] Li, X.; Jiang, J. *Catal. Sci. Technol.* **2019**, *9*, 4888-4897.

[34] Jiao, J.; Tan, C.; Li, Z.; Liu, Y.; Han, X.; Cui, Y. *J. Am. Chem. Soc.* **2018**, *140*, 2251-2259.

[35] Tanaka, K.; Muraoka, T.; Hirayama, D.; Ohnish, A. *Chem. Commun.* **2012**, *48*, 8577-8579.

[36] Peng, Y.; Gong, T.; Zhang, K.; Lin, X.; Liu, Y.; Jiang, J.; Cui, Y. *Nat. Commun.* **2014**, *5*, 4406.

[37] (a) Hailili, R.; Wang, L.; Qv, J.; Yao, R.; Zhang, X.-M.; Liu, H. *Inorg. Chem.* **2015**, *54*, 3713-3715. (b) Ding, W.; Yu, T.; Du, Y.; Sun, X.; Feng, Z.; Zhao, S.; Ma, X.; Ma, M.; Chen, C. *Microchim. Acta* **2019**, *187*, 51. (c) Yu, Y.; Xu, N.; Zhang, J.; Wang, B.; Xie, S.; Yuan, L. *ACS Appl. Mater. Interfaces* **2020**, *12*, 16903-16911.

Synthesis of CMOFs

There are several strategies to yield CMOFs, and these can be divided into three methods: 1) spontaneous resolution, 2) indirect synthesis, and 3) direct synthesis (**Figure 7**).
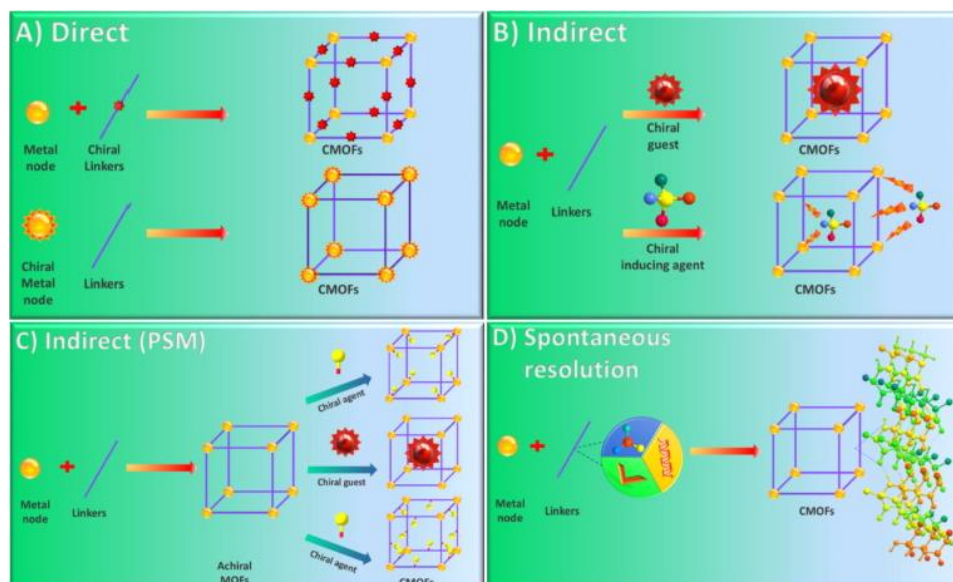
Figure 7. Synthetic strategies for the obtention of CMOFs. Reprinted with permission from *Coord. Chem. Rev.* **2021**, *445*, 214083. Copyright Elsevier 2021.

Spontaneous resolution

In this method, crystallisation happens towards one of the two possible enantiomers while the starting materials are achiral, and no chiral auxiliaries are used in the synthetic process. This can happen due to several factors, such as the arrangement of the achiral ligand in the structure.[38] Helicoidal arrangements dominated by non-covalent interactions (such as hydrogen bonding or π-π interactions) can endow the desired structure with chirality. It is worth mentioning that the number of structures obtained by this method is scarce as the factors mentioned above are difficult to predict and reproduce.

---

[38] (a) Sun, D.; Collins, D. J.; Ke, Y.; Zuo, J. L.; Zhou, H. C. *Chem. Eur. J.* **2006**, *12*, 3768-3776. (b) Verma, A.; Tomar, K.; Bharadwaj, P. K. *Inorg. Chem.* **2017**, *56*, 13629-13633. (c) Rizzuto, F. J.; Pröhm, P.; Plajer, A. J.; Greenfield, J. L.; Nitschke, J. R. *J. Am. Chem. Soc.* **2019**, *141*, 1707-1715.

The first example of CMOF described in the literature belongs to this category. Reported in 2000 by Rosseinsky and co-workers, the use of non-chiral diols yielded homochiral helical structures caused by hydrogen bonding between the diols and BTC ligands (**Figure 8**).[39]
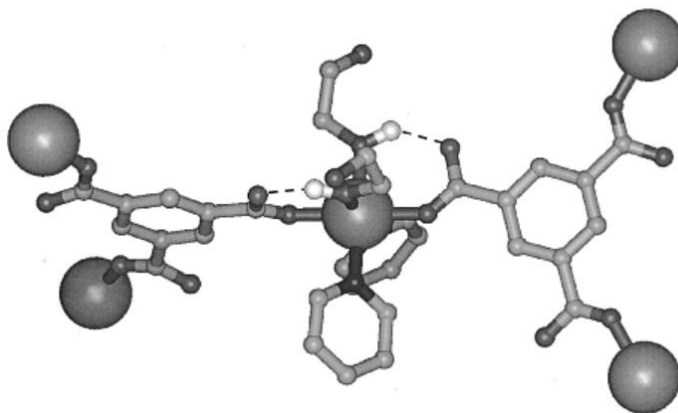
Figure 8. Control of the orientation of BTC ligands (left and right) by hydrogen bonding (dashed line) to the two monodentate ethylene glycol (top and pointing out of the page) molecules to form a chiral structure. Adapted with permission of *J. Am. Chem. Soc.* **2000**, *122*, 5158-5168. Copyright 2000 American Chemical Society.

Indirect synthesis (chiral induction)

Modifying the experimental procedure for the obtention of an achiral MOF by adding an enantiopure molecule that interacts **reversibly** with the metal centre induces chirality. The use of achiral precursors can yield CMOFs if chiral auxiliaries are used. For instance, the use of D- or L-camphoric acid in the synthesis of an achiral MOF [Mn(ADC)] yielded (+)- and (-)-[Mn$_3$(HCOO)$_4$(ADC)], respectively (**Figure 9**).[40] The use of D- and L-glutamic acid yielded the opposite enantiomers, (-) and (+), respectively.

---

[39] Kepert, C. J.; Prior, T. J.; Rosseinsky, M. J. *J. Am. Chem. Soc.* **2000**, *122*, 5158-5168.
[40] Zhang, J.; Chen, S.; Nieto, R. A.; Wu, T.; Feng, P.; Bu, X. *Angew. Chem. Int. Ed.* **2010**, *49*, 1267-1270.
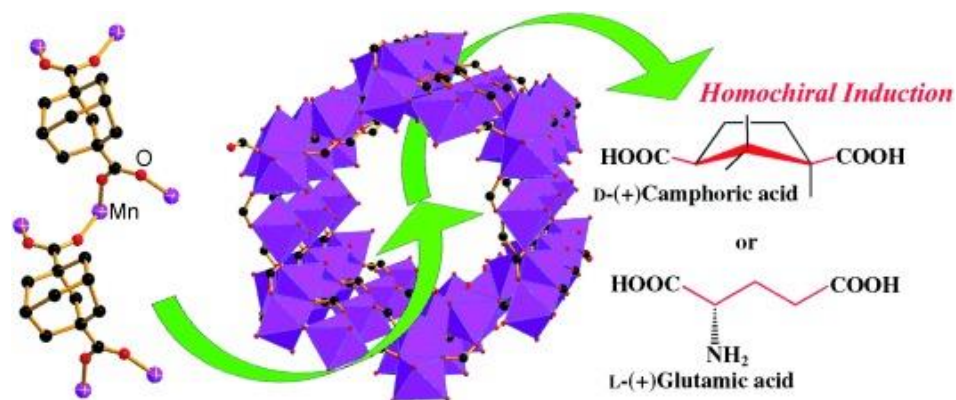
Figure 9. Chiral induction in an achiral MOF. Reprinted with permission of *Angew. Chem. Int. Ed.* **2010**, *49*, 1267-1270. Copyright 2010 Wiley.

Indirect synthesis (post-synthetic modification)

Using prochiral ligands or metal centres/clusters includes the possibility of, after obtaining the MOF, modifying it with enantiopure moieties. One example of PSM in the ligand is UiO-66-NH$_2$, which contains free amino groups that can be decorated with optically active moieties.[41] Conversely, this method involves the risk of pore size reduction. Furthermore, it has been found that ligands can be replaced, as tested in UiO-68-Me with an enantiopure M(salen) ligand (**Figure 10**).[42]
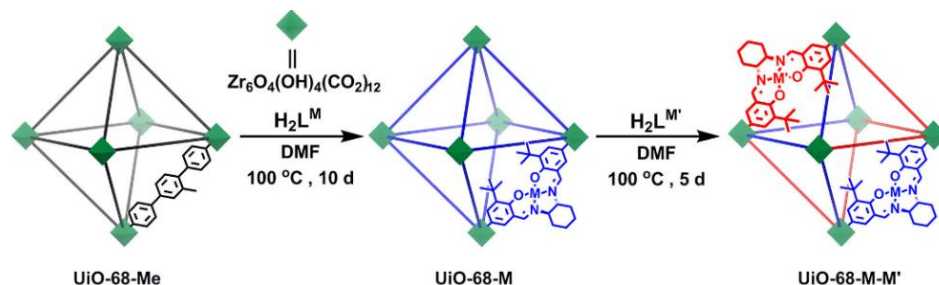
Figure 10. Ligand exchange in UiO-68-Me by PSM. Adapted with permission of *J. Am. Chem. Soc.* **2018**, *140*, 16229-16236. Copyright 2018 American Chemical Society.

Enantiopure molecules that bind to the metal nodes may furnish the MOF with chirality. One example of this would be the use of L- or D-PYI in the

---

[41] Kou, W.-T.; Yang, C.-X.; Yan, X.-P. *J. Mater. Chem. A* **2018**, *6*, 17861-17866.
[42] Tan, C.; Han, X.; Li, Z.; Liu, Y.; Cui, Y. *J. Am. Chem. Soc.* **2018**, *140*, 16229-16236.

10

synthesis of MOF-150,[43] that yielded the CMOFs Zn-PYI1 and Zn-PYI2 (**Figure 11**).[44]
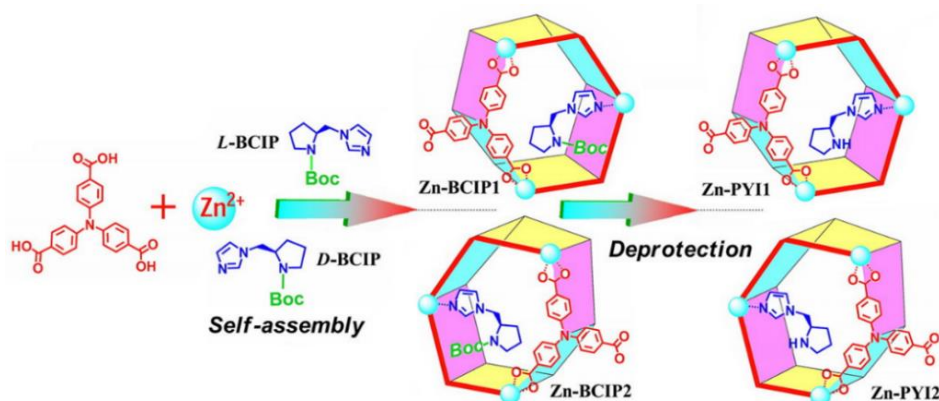
Figure 11. Synthetic scheme of the synthesis of Zn-PYI1 and Zn-PYI2 by self-assembly and subsequent deprotection. Adapted with permission of *J. Am. Chem. Soc.* **2012**, *134*, 14991-14999. Copyright 2012 American Chemical Society.

Direct synthesis

This can be achieved by either using an enantiopure ligand, a mixture of enantiopure and racemic ligands or using a chiral cluster. Although all three strategies have been used and adequately described, the first one – the use of an enantiopure ligand – is the easiest method used to yield CMOFs. The following section is based on such method to give a comprehensive overview of the use of enantiopure ligands to construct CMOFs.

Enantiopure ligands

Although any multidentate enantiopure molecule can be used as a ligand for the synthesis of CMOFs if it contains the appropriate coordinating moieties (*e.g.* carboxylates, imidazoles or triazoles, among others),[45] these can be

---

[43] Chae, H.K.; Kim, J.; Friedrichs, O.D.; O'Keeffe, M.; Yaghi, O. M. *Angew. Chem. Int. Ed.* **2003**, *42*, 3907-3909.

[44] Wu, P.; He, C.; Wang, J.; Peng, X.; Li, X.; An, Y.; Duan, C. *J. Am. Chem. Soc.* **2012**, *134*, 14991-14999.

[45] (a) Seo, J. S.; Whang, D.; Lee, H.; Jun, S. I.; Oh, J.; Jeon, Y. J.; Kim, K. *Nature* **2000**, *404*, 982-986. (b) Zhang, J.; Yao, Y.-G.; Bu, X. *Chem. Mater.* **2007**, *19*, 5083-5089. (c) Zhang, S.-Y.; Wojtas, L.; Zaworotko, M. J. *J. Am. Chem. Soc.* **2015**, *137*, 12045-12049. (d) Cai, K.; Zhao, N.; Zhang, N.; Sun, F.-X.; Zhao, Q.; Zhu, G.-S. *Nanomaterials* **2017**, *7*, 88.

divided into two major groups: (a) privileged enantiopure ligands and (b) biomolecules.

Privileged enantiopure ligands

Privileged enantiopure ligands are used for the formation of synthetic catalysts. These are "enantioselective over a wide range of different reactions, creating effective asymmetric environments for mechanistically unrelated reactions",[46] as described in 2003 by Yoon and Jacobsen in the work where this concept was forged.

The most representative ligands included in this group are BINOL and BINAP, salen and salan (salen reduced form), bisoxazoline, phosphoramidite and many others (**Figure 12**). Due to their ease of coordination to a significant number of metals (alkali, alkaline earth and transition metals) and structural adaptability, BINOL/BINAP and salen/salan ligands are among the most used in the synthesis of CMOFs.

BINOL [X = OH] **phosphoramidite** **salen** **salan** **bisoxazoline**
BINAP [X = PPh$_3$]

Figure 12. Chemical structure of some privileged ligands.

BINOL and BINAP

The binaphthyl-based ligands BINOL[47] and BINAP[48] possess axial chirality – molecules lacking a stereogenic centre but with a stereogenic axis where its substituents are not superimposed.[49] This is common in atropisomeric molecules, such as the ligands mentioned above.

Wenbin Lin and co-workers reported the first example of a CMOF using this type of ligands in 2001, where they used a BINOL derivative **L₁** (2,2'-

[46] Yoon T. P.; Jacobsen, E. N. *Science* **2003**, *299*, 1691-1693.
[47] Brussee, J.; Jansen, A. C. A. *Tetrahedron Lett.* **1983**, *24*, 3261-3262.
[48] Miyashita, A.; Yasuda, A.; Takaya, H.; Toriumi, K.; Ito, T.; Souchi, T.; Noyori, R. *J. Am. Chem. Soc.* **1980**, *102*, 7932-7934.
[49] Moss, G. P. *Pure Appl. Chem.* **1996**, *68*, 2193-2222.

diethoxy-1,1'-binaphthalene-6,6'-bisphosphonic acid) coordinated to several lanthanides (**Figure 13**).[50]
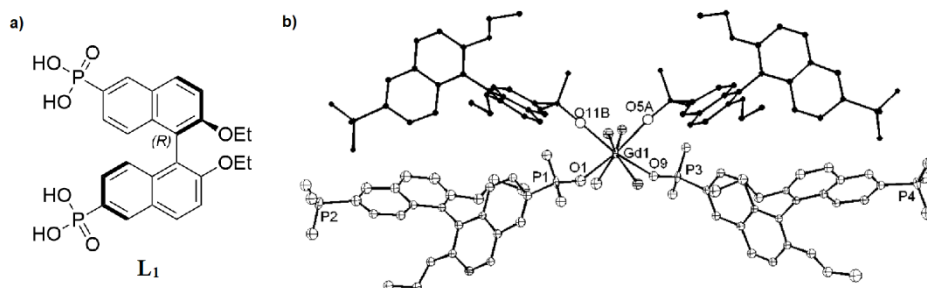
Figure 13. (a) Structure of **L₁** and (b) coordination environment of **CMOF-1** using Gd as a metal centre. Adapted with permission of *J. Am. Chem. Soc.* **2001**, *123*, 10395-10396. Copyright 2001 American Chemical Society.

In 2003, they reported the first use of a BINAP derivative **L₂** ((*R*)-2,2′-bis(diphenylphosphino)-1,1′-binaphthyl-4,4′-bis(phosphonic acid)) that was reacted with Zr(O^{t}Bu)₄ to obtain **CMOF-2** Zr[Ru(**L₂**)(DPEN)Cl₂]·4H₂O.

By using **L₃** ((*R*)-2,2′-bis(diphenylphosphino)-1,1′-binaphthyl-6,6′-bis(phosphonic acid)), a ligand similar to the previously mentioned, they obtained **CMOF-3** Zr[Ru(**L₃**)(DPEN)Cl₂]·4H₂O. The difference between **L₃** and **L₂** relies on the phosphoric acid groups position, being the 6 and 6' positions instead of the 4,4', respectively (**Figure 14**). In these porous solids, each P(O)(OH)₂ is coordinated to two Zr^{4+}. These CMOFs were used in the asymmetric hydrogenation of aromatic ketones.[51]
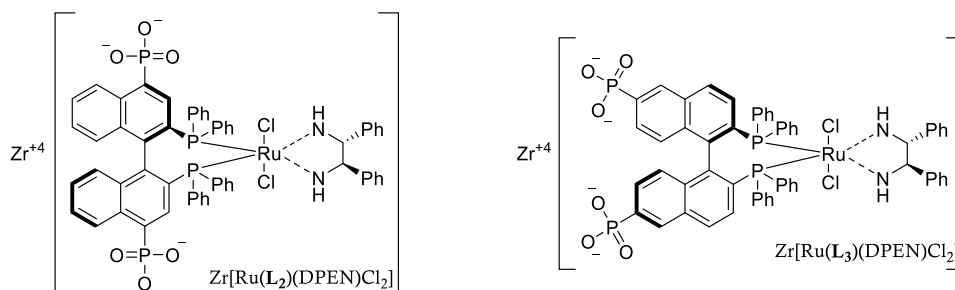
Figure 14. Schematic structures of **CMOF-2** (left) and **CMOF-3** (right).

[50] Evans, O. R.; Ngo, H. L.; Lin, W. *J. Am. Chem. Soc.* **2001**, *123*, 10395-10396.
[51] Hu, A.; Ngo, H. L.; Lin, W. *J. Am. Chem. Soc.* **2003**, *125*, 11490-11491.

Further development of BINOL-based ligands was described in 2005, where the ligand **L₄** ((*R*)-6,6'-dichloro-4,4'-di(pyridin-4-yl)-[1,1'-binaphthalene]-2,2'-diol) contained two pyridyl groups in the 4,4' positions as coordinating moieties. The 2,2'-dihydroxy functional group served as a platform to host the catalytically active Ti^{4+} centres to be further used in enantioselective organozinc additions to carbonyl compounds (**Figure 13**).[52] The same ligand was later used for the synthesis of two new CMOFs.[53]
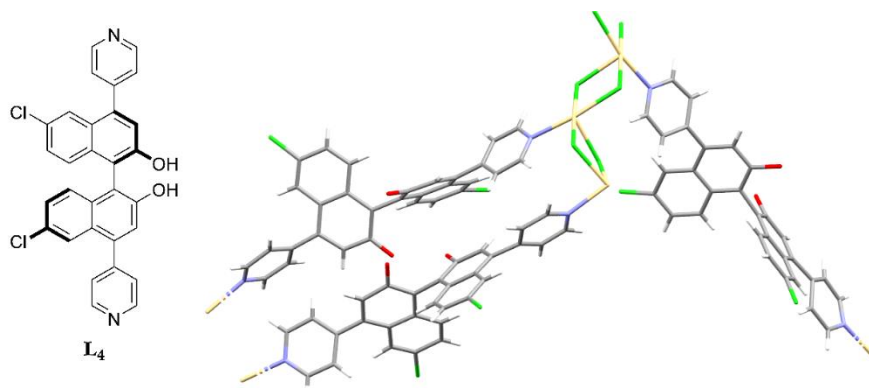
Figure 15. Structure of L₄ (left) and crystalline structure of **CMOF-4** $[Cd_3Cl_6(L_4)_3]\cdot$ $4DMF\cdot6MeOH\cdot3H_2O$ (right). The solvent molecules have been omitted for clarity.

With the same catalytic purpose, they reported in 2010 the synthesis of eight novel BINOL-based ligands containing –COOH coordinating groups (**Figure 16**) for the development of eight isoreticular CMOFs (**Figure 17**).[54]
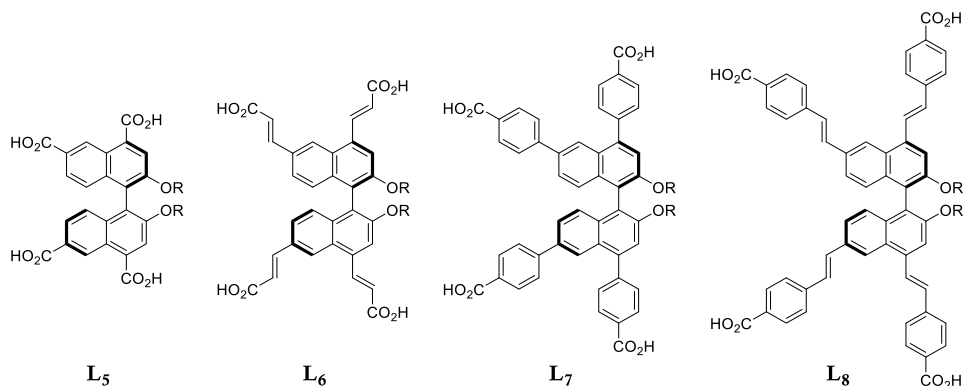
Figure 16. Structure of the ligands L₅-L₈. R = Et (a), H (b).

[52] Wu, C.-D.; Hu, A.; Zhang, L.; Lin, W. *J. Am. Chem. Soc.* **2005**, *127*, 8940-8941.
[53] Wu, C.-D.; Lin, W. *Angew. Chem. Int. Ed.* **2007**, *46*, 1075-1078.
[54] Ma, L.; Falkowski, J. M.; Abney, C.; Lin, W. *Nat. Chem.* **2010**, *2*, 838-846.

14
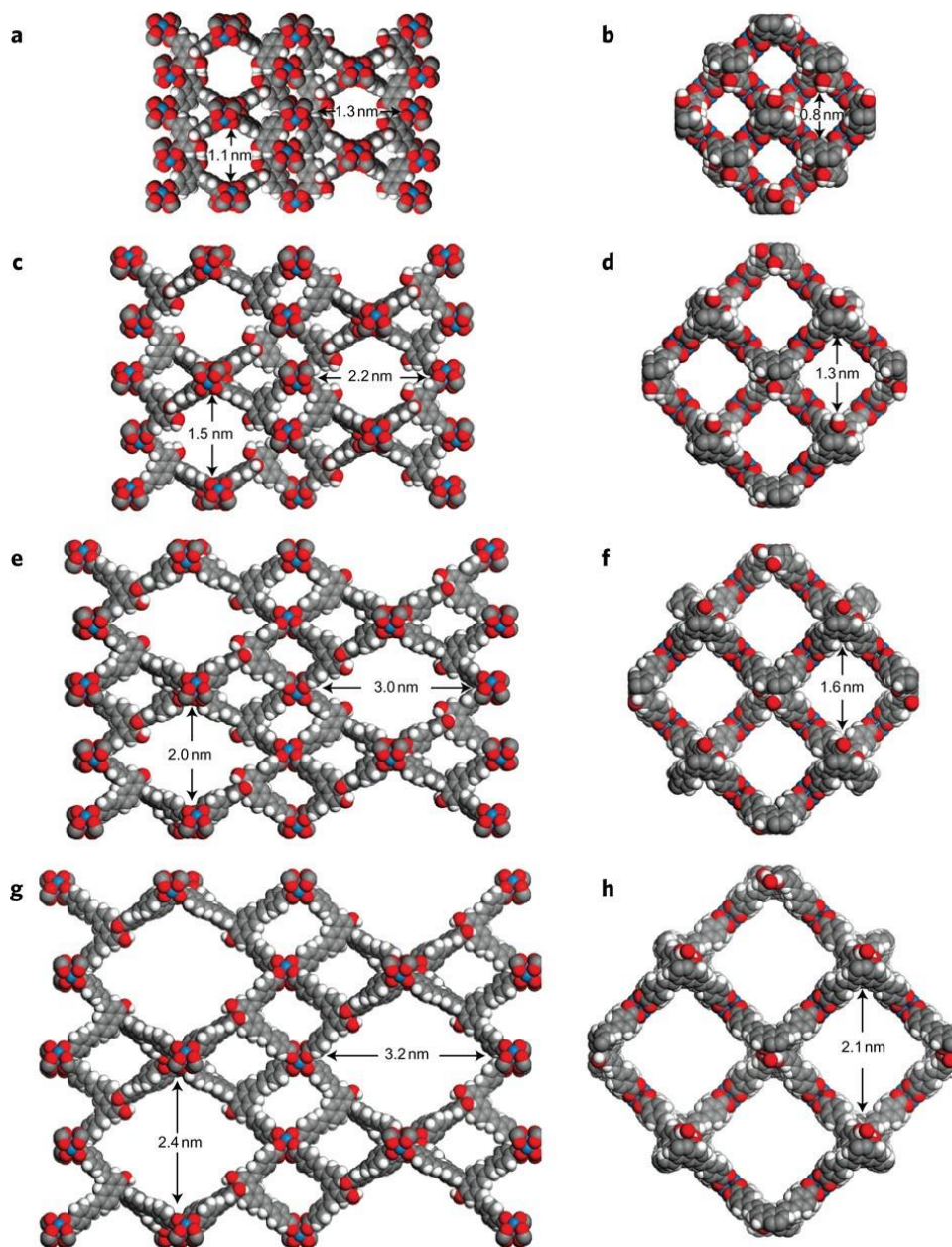
Figure 17. Structure of **CMOF**-**5b** (top) to -**8b** (bottom). Reproduced with permission of *Nat. Chem.* **2010**, *2*, 838-846. Copyright 2010 Springer Nature.

Koichi Tanaka and co-workers have also pioneered the use of BINOL-based ligands to synthesise CMOFs. In fact, since 2008, they have reported the synthesis of eight ligands for the construction of eight CMOFs with enantioselective properties (**Figure 18**). These CMOFs do not require

PSM to add a catalytically active metal for their applications. These applications are the asymmetric ring-opening of epoxides,[55] kinetic resolutions,[56] enantioselective Diels-Alder cycloadditions,[57] Friedel-Crafts alkylations,[58] and enantiomeric separation of racemic mixtures.[59] As a representative example, the **CMOF-10a** is shown in **Figure 19**.
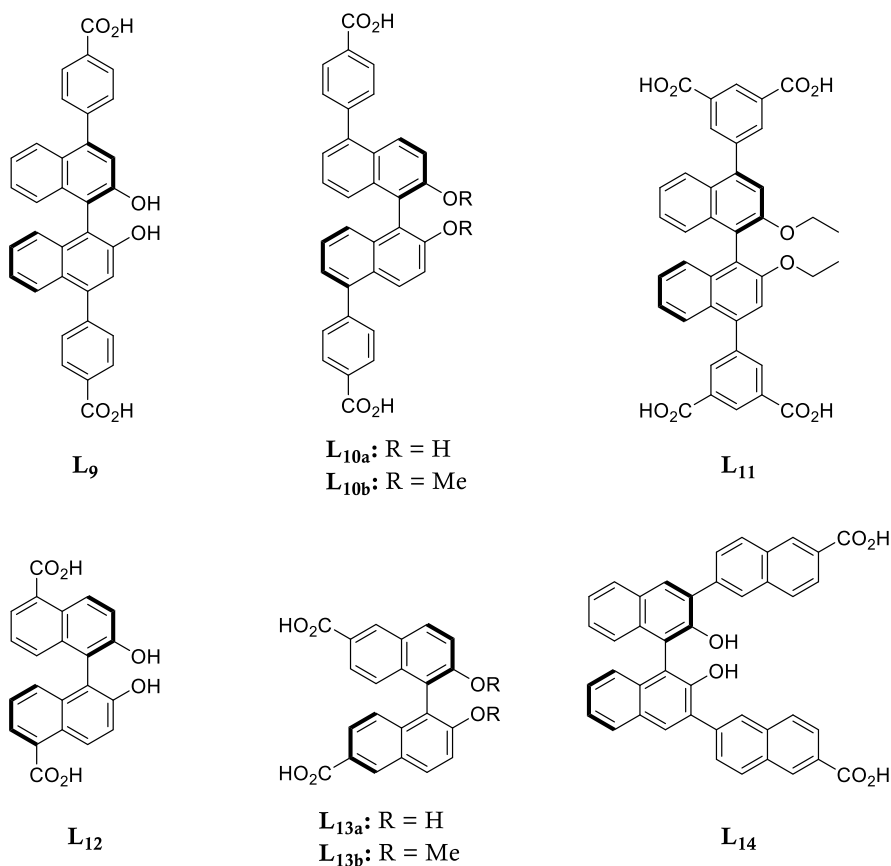
Figure 18. Structure of the eight ligands **L9**-**L14** synthesised by Tanaka and co-workers.

---

[55] (a) Tanaka, K.; Oda, S.; Shiro, M. *Chem. Commun.* **2008**, 820-822. (b) Tanaka, K.; Kinoshita, M.; Kayahara, J.; Uebayashi, Y.; Nakaji, K.; Morawiak, M.; Urbanczyk-Lipkowska, Z. *RSC Adv.* **2018**, *8*, 28139-28146.

[56] Tanaka, K.; Otani, K.. *New J. Chem.* **2010**, *34*, 2389-2391.

[57] (a) Tanaka, K.; Yanamoto, D.; Yoshimura, K.; Anami, T.; Urbanczyk-Lipkowska, Z. *CrystEngComm* **2015**, *17*, 1291-1295. (b) Tanaka, K.; Nagase, S.; Anami, T.; Wierzbicki, M.; Urbanczyk-Lipkowska, Z. *RSC Adv.* **2016**, *6*, 111436-111439.

[58] Tanaka, K.; Sakuragi, K.; Ozaki, H.; Takada, Y. *Chem. Commun.* **2018**, *54*, 6328-6331.

[59] (a) Tanaka, K.; Muraoka, T.; Otubo, Y.; Takahashi, H.; Ohnishi, A. *RSC Adv.* **2016**, *6*, 21293-21301. (b) Tanaka, K.; Kawakita, T.; Morawiak, M.; Urbanczyk-Lipkowska, Z. *CrystEngComm* **2019**, *21*, 487-493.

16
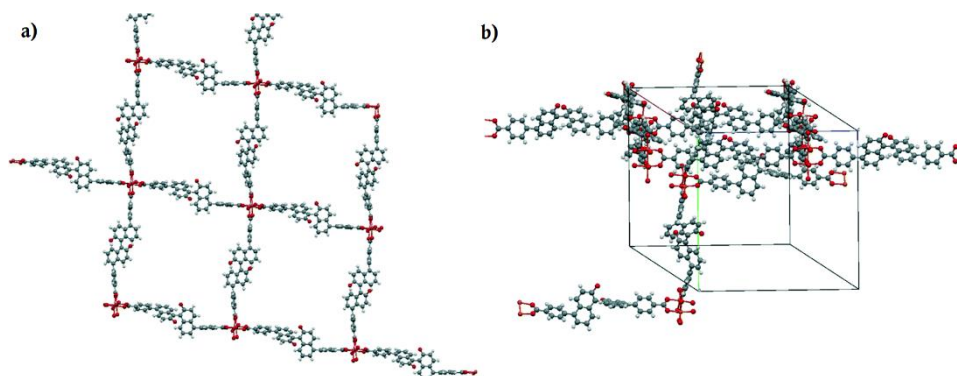
Figure 19. (a) 2D coordination polyhedron of **CMOF-10a** viewed down the *b*-axis and (b) interpenetration mode in **CMOF-10a**. Reprinted with permission of *CrystEngComm* **2015**, *17*, 1291-1295. Copyright 2015 Royal Society of Chemistry.

The use of BINAP/BINOL-containing CMOFs is not limited to asymmetric transformations. In 2014, Evamarie Hey-Hawkins and co-workers designed and synthesised a heterobimetallic CMOF (**CMOF-15**) containing Na^+ and Pb^{2+} with luminescence properties (**Figure 20**). The ligand L_{15} ((*S*)-5,5′-bis(4-carboxyphenyl)-2,2′-bis(diphenylphosphinoyl)-1,1′-binaphthyl) used for the construction of this CMOF is BINAP-based.[60]
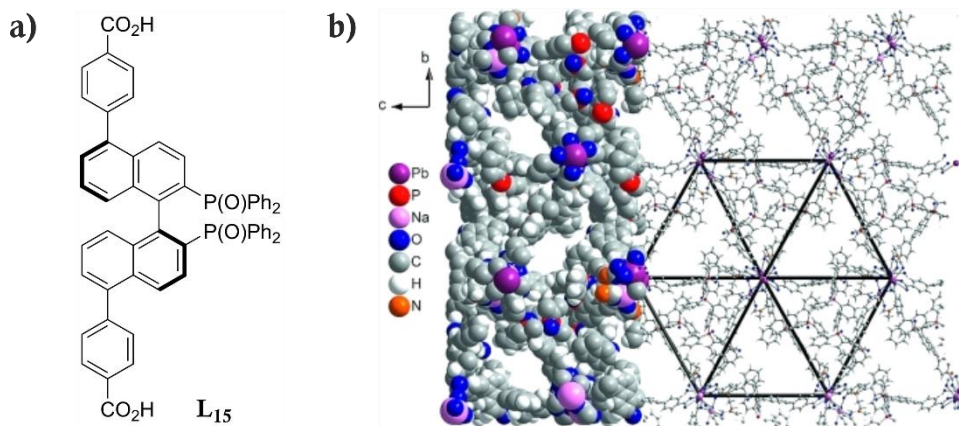
Figure 20. (a) Structure of L_{15} and (b) 3D framework of **CMOF-15**{[$Na_2Pb_2(L_{15})_3(H_2O)(DMF)_4$]·9DMF}$_n$ shown as ball-and-stick and space-filling models, viewed along the [100] direction. Reprinted with permission of *Eur. J. Inorg. Chem.* **2014**, 1775-1782. Copyright 2015 Wiley.

[60] Lestari, W. W.; Lönnecke, P.; Streit, H. C.; Handke, M.; Wickleder, C.; Hey-Hawkins, E. *Eur. J. Inorg. Chem.* **2014**, 1775-1782.

Salen and salan[61]

Salen-type ligands (sal from salicylaldehyde and en from ethylenediamine) can host metallic species due to their excellent chelation capacity. These ligands can be endowed with chirality by tuning the diamino backbone. Enantiopure salen ligands have been commonly used in asymmetric transformations, *e.g.* Jacobsen epoxidations (**Scheme 1**).[62]
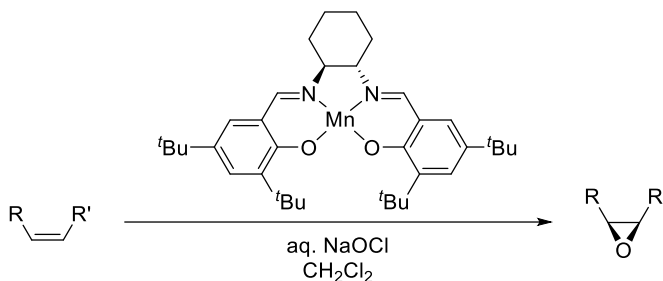
Scheme 1. Jacobsen epoxidation. The transformation employs a Salen-type catalyst.

Using this ligand as a precursor for the synthesis of CMOFs has two main benefits: (a) leads to enantiopure materials, and (b) the CMOF becomes a bimetallic system, where one of the metals can be hosted by the ligand. These features leave the door open to the use of non-catalytic yet robust metallic species for the CMOF scaffold, whereas the ligand contains the catalytically active species. Moreover, their facile obtention and excellent complexation capability make these ligands outstanding precursors for synthesising CMOFs.

The first structure reported using a salen ligand was described in 2006 by Joseph Hupp and co-workers.[63] In this work, they used a Mn(salen) ligand L_{16} (6,6' ((1E,1'E) (((1R,2R) cyclohexane 1,2 diyl)bis(azaneylylidene))bis(methan eylylidene))bis(2-(*tert*-butyl)-4 (pyridine-4-yl)phenol)) with pyridyl coordinating groups to axially connect Zn^{2+}-BPDC pillared paddlewheel layers, yielding the interpenetrated **CMOF-16a**. The paddlewheel structure stabilised the CMOF because the metal-pyridine bonds can collapse when removing the solvent.

[61] (a) Pfeiffer, P.; Breith, E.; Lübbe, E.; Tsumaki, T. *Justus Liebigs Ann. Chem.* **1933**, *503*, 84-130. (b) Tsumaki, T. *Bull. Chem. Soc. Jpn.* **1938**, *13*, 252-260.
[62] Zhang, W.; Loebach, J. L.; Wilson, S. R.; Jacobsen, E. N. *J. Am. Chem. Soc.* **1990**, *112*, 2801-2803.
[63] Cho, S.-H.; Ma, B.; Nguyen, S. T.; Hupp, J. T.; Albrecht-Schmitt, T. E. *Chem. Commun.* **2006**, 2563-2565.

18

Later, in 2011, they replaced the BPDC connector with a tetracarboxylate ligand (1,2,4,5-tetrakis(4-carboxyphenyl)benzene) to obtain **CMOF-16b**, a noncatenated CMOF (**Figure 21**).[64]
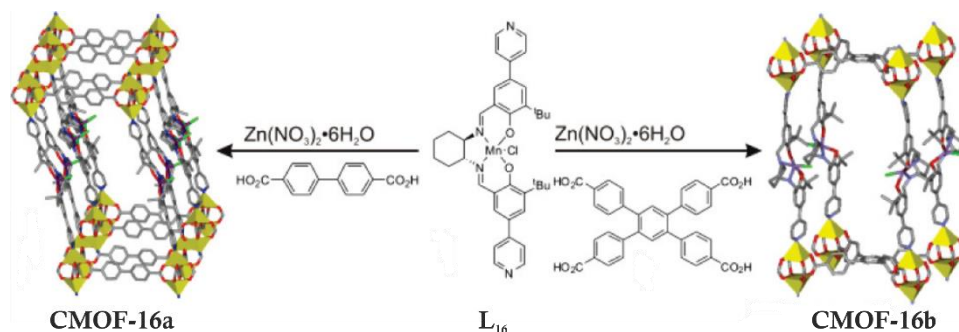
Figure 21. The Mn(salen)-type ligand **L₁₆** used in the synthesis of **CMOF-16a** (left) and **CMOF-16b** (right). Adapted with permission of *Inorg. Chem.* **2011**, *50*, 3174-3176. Copyright 2011 American Chemical Society.

Yong Cui and co-workers have also fine-tuned the use of M(salen) ligands in the construction of CMOFs. Among their numerous works, it is worth highlighting some of them. In 2014, they reported the use of the salen-type ligand **L₁₇** (5,5'-((1*E*,1'*E*)-(((*S*)-2,2'-dihydroxy-5,5',6,6'-tetramethyl-[1,1'-biphenyl]-3,3'-diyl)bis(azaneylylidene))bis(methaneylylidene))bis(3-(*tert*-butyl)-4-hydroxybenzoic acid)) for the obtention of two CMOFs: **CMOF-17a** (Cd^{2+}) and **CMOF-17b** (Zn^{2+}), the latter being a mesoporous structure.

This is an atypical example of using a salen-based ligand: the tetradentate coordinating centre serves as a platform for forming a helicate – four salen-based ligands bonded through a Zn₇ cluster (**Figure 22**). **CMOF-17b** was employed as a catalyst for aldolic reactions after being functionalised with (*S*)-2-(dimethylaminomethyl)pyrrolidine by PSM.

---

[64] Shultz, A. M.; Farha, O. K.; Adhikari, D.; Sarjeant, A. A.; Hupp, J. T.; Nguyen, S. T. *Inorg. Chem.* **2011**, *50*, 3174-3176.

a)

b) **c)** **d)**
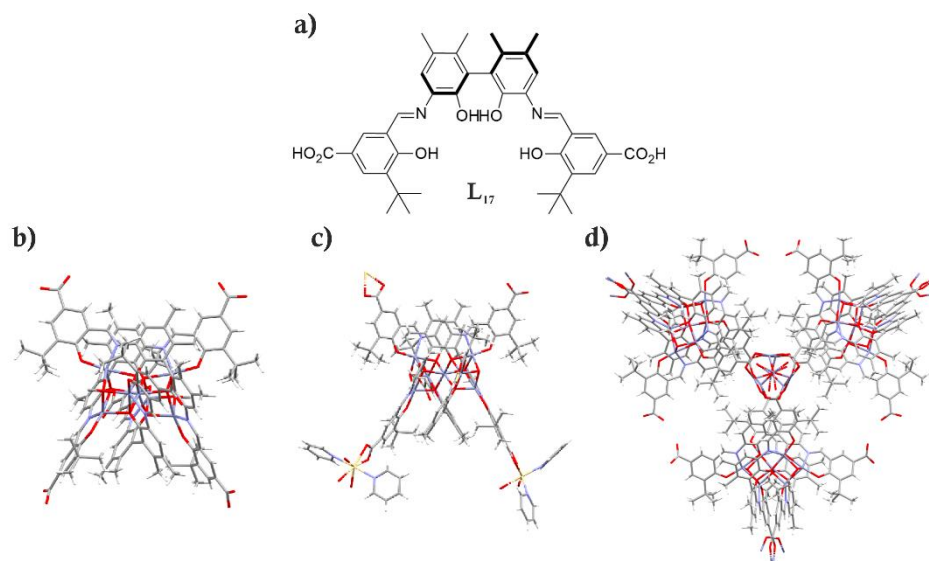
Figure 22. Structures of (a) L_{17}, (b) L_{17}-Zn_7 helicate, (c) **CMOF-17a** and (d) **CMOF-17b**.

In 2017, they described multivariate two-fold penetrated Cu^{2+} CMOFs containing up to three metal centres hosted by the salen ligand L_{18} (5,5'-((1*E*,1'*E*)-(((1*R*,2*R*)-cyclohexane-ethaneylylidene))bis(3-(*tert*-butyl)-4-hydroxy benzoic acid)). These CMOFs were exploited for asymmetric transformations, such as enantioselective epoxidation by **CMOF-18CuMn** and **CMOF-18CuFe** (the latter also oxidises sulfides to sulfoxides), cyanosilylation of aldehydes with **CMOF-18CuV** after oxidation of V^{4+} to V^{5+}, aminolysis of TSO with **CMOF-18CuCr**, Diels-Alder cycloaddition with **CMOF-18CuCo** and **CMOF-18CuMnCr** for the sequential epoxidation and ring-opening of alkenes (**Figure 23**).[65]

---

[65] Xia, Q.; Li, Z.; Tan, C.; Liu, Y.; Gong, W.; Cui, Y. *J. Am. Chem. Soc.* **2017**, *139*, 8259-8266.

20

Introduction
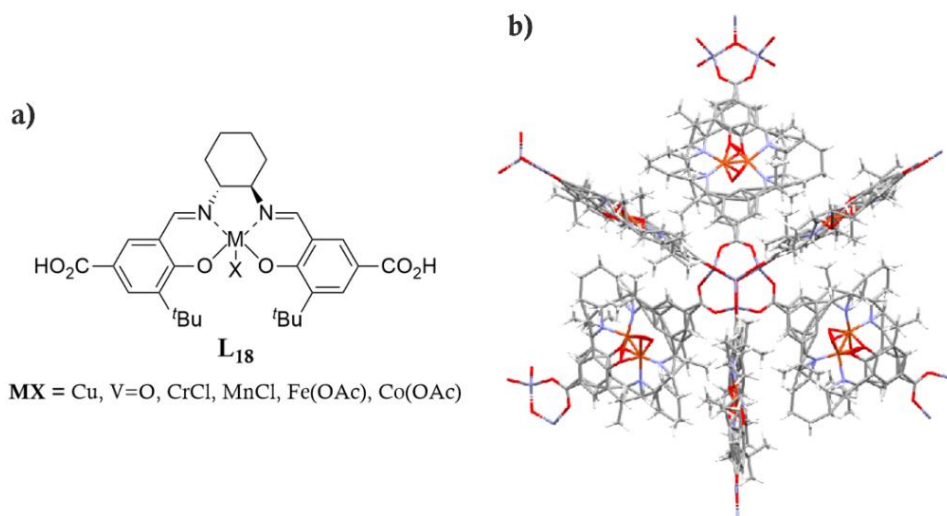
Figure 23. Structures of (a) L_{18} and (b) the 2-fold interpenetrated network of **CMOF-18Cu**.

Despite their structural similarity, the use of salan (**Figure 12**) ligands for synthesising CMOFs has been underexplored. Nonetheless, promising features such as inherent flexibility and strong nitrogen donors make these ligands promising candidates. Following the previously mentioned line of research, Yong Cui and co-workers have also instigated the use of salan building blocks for CMOF design and synthesis.

In 2012, they depicted the use of the salan-based ligand L_{19} (6,6'-(((((1R,2R)-cyclohexane-1,2-diyl)bis(azanediyl))bis(methylene))bis(4-(*tert*-butyl)-2-((*E*)-2-(pyridin-4-yl)vinyl)phenol)) to afford **CMOF-19** containing Zn_8 helicate cages – this is the first example in the literature of enantiopure helical cages with inner spaces (**Figure 24**).[66]

[66] Xuan, W.; Zhang, M.; Liu, Y.; Chen, Z.; Cui, Y. *J. Am. Chem. Soc.* **2012**, *134*, 6904-6907.

a)

b)
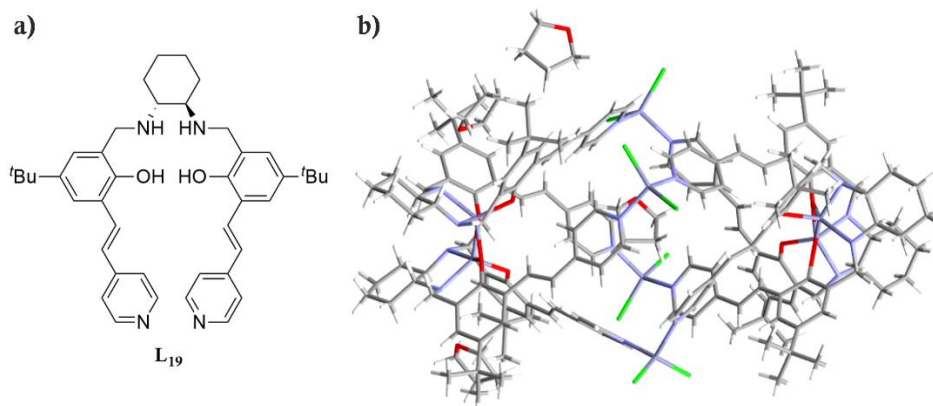
Figure 24. Structure of (a) L_{19} and (b) helicate octanuclear cage in **CMOF-19**.

The use of a very similar Ti(salan) ligand L_{20} (6,6'-((((1R,2R)-cyclohexane-1,2-diyl)bis(azanediyl))bis(methylene))bis(2-(*tert*-butyl)-4-(pyridin-4-yl)phenol)) in 2013 afforded the zeolite-like **CMOF-20** with tetranuclear Ti^{+4} clusters connected by Cd^{2+}-BPDC chains (**Figure 25**).[67]

b)

a)
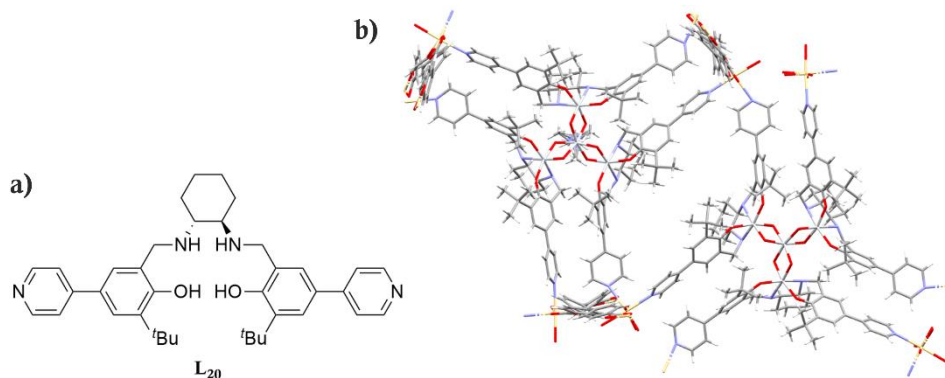
Figure 25. Structure of (a) L_{20} and (b) zeolite-like **CMOF-20**.

Although these enantiopure ligands are a success for the synthesis of CMOFs due to their rigid backbones and fixed geometries of their coordinating moieties, the synthetic procedures for their synthesis are challenging. Their synthesis requires enantioselective catalysts or tedious purification protocols, and their obtention is unlikely scalable to gram scale. To that end, the use of readily available enantiopure organic molecules is desirable for the scale-up of their enantioselective properties.

---

[67] Xuan, W.; Ye, C.; Zhang, M.; Chen, Z.; Cui, Y. *Chem. Sci.* **2013**, *4*, 3154-3159.

22

Biomolecules

Biomolecules are promising candidates for the synthesis of CMOFs as they are (a) enantiopure, (b) easy to obtain on kilogram scale and (c) contain coordinating moieties. The biomolecules family includes but is not limited to nucleobases, amino acids, peptides and porphyrins, among others. Among these molecular groups, amino acids are the most promising ones.

Amino acids

AAs (**Figure 26**) are organic molecules with a carboxylic acid (–COOH) and an amino group (–NH$_2$). α-AAs, which are mostly present in nature, bear the amino group in the α position. AAs are the monomeric units that build peptides and proteins through amide bonds, making them essential for life. Some AAs bear a third coordinating group in the lateral chain, such as L-His (imidazole).
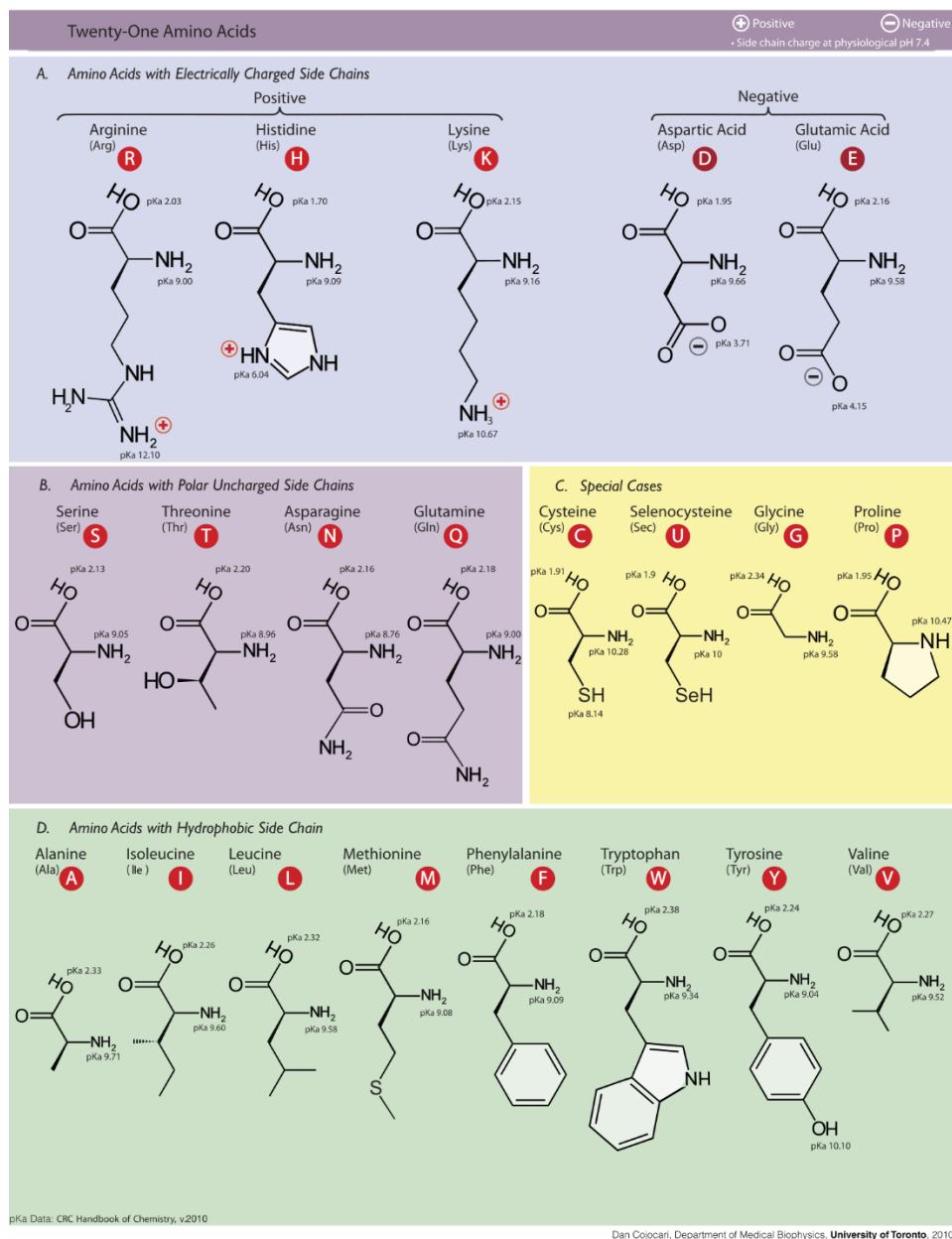
Figure 26. Structure of the 21 proteinogenic amino acids classified by the chemical properties of their side chain.[68]

24

Only a few examples of CMOFs constructed solely from amino acids are reported. Some examples encompass the use of L-Asp with Ni^{2+} to obtain 1D[69] and 3D[70] structures, with Zr^{2+} and with Zn^{2+} to yield 3D frameworks MIP-202(Zr)[71] and [Zn(asp)],[72] respectively. L-Glu, which contains an extra $-CH_2-$ unit compared to L-Asp, was also used to construct a Co^{2+} CMOF, $[Co(L\text{-}Glu)(H_2O)]\cdot H_2O$.[73]

On the other hand, the number of structures built from a mixture of AAs and organic ligands is higher as the latter confers robustness to the network. Rosseinsky and co-workers have reported several works using this strategy, specifically by incorporating five organic ligands (L_{21}-L_{25}) with bipyridyl moieties (**Figure 27**) in the formation of $[Ni(L\text{-}Asp)_2(L_X)]$ structures.[74] The same strategy was followed by Zhang and co-workers to synthesise D- and L-Ala, L-Ser and L-Val CMOFs using 5-Hmtz as bridging ligand.[75]
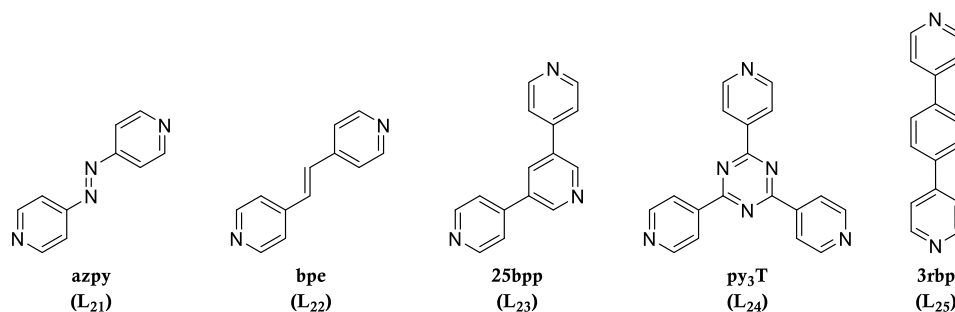
Figure 27. Ligands used in the construction of $[Ni(L\text{-}Asp)_2(L_X)]$ structures.

Peptides

Peptides have also been exploited in the synthesis of CMOFs for their flexibility and coordinating versatility. Following their work with AAs, Rosseinsky and co-workers also explored the use of peptides in the assembly

[69] Anokhina, E. V.; Jacobson, A. J. *J. Am. Chem. Soc.* **2004**, *126*, 3044-3045.
[70] Anokhina, E. V.; Go, Y. B.; Lee, Y.; Vogt, T.; Jacobson, A. J. *J. Am. Chem. Soc.* **2006**, *128*, 9957-9962.
[71] Wang, S.; Wahiduzzaman, M.; Davis, L.; Tissot, A.; Shepard, W.; Marrot, J.; Martineau-Corcos, C.; Hamdane, D.; Maurin, G.; Devautour-Vinot, S.; Serre, C. *Nat. Commun.* **2018**, *9*, 4937.
[72] Gould, J. A.; Jones, J. T. A.; Bacsa, J.; Khimyak, Y. Z.; Rosseinsky, M. J. *Chem. Commun.* **2010**, *46*, 2793-2795.
[73] Zhang, Y.; Saha, M. K.; Bernal, I. *CrystEngComm* **2003**, *5*, 34-37.
[74] Perez Barrio, J.; Rebilly, J.-N.; Carter, B.; Bradshaw, D.; Bacsa, J.; Ganin, A. Y.; Park, H.; Trewin, A.; Vaidhyanathan, R.; Cooper, A. I.; Warren, J. E.; Rosseinsky, M. J. *Chem. Eur. J.* **2008**, *14*, 4521-4532.
[75] Li, M.-Y.; Wang, F.; Gu, Z.-G.; Zhang, J. *RSC Adv.* **2017**, *7*, 4872-4875.

of CMOFs. They reported the Zn-based **CMOFs-26**,[76] **-27**,[77] **-28**[78] and **CMOF-29**.[79] Tripeptides, such as **L₃₀** and **L₃₁**, were also explored by coordination with Cu^{2+}, yielding isoreticular **CMOF-30** and **CMOF-31** with sponge-like behaviour due to the tripeptide flexibility (**Figure 28**).[80]
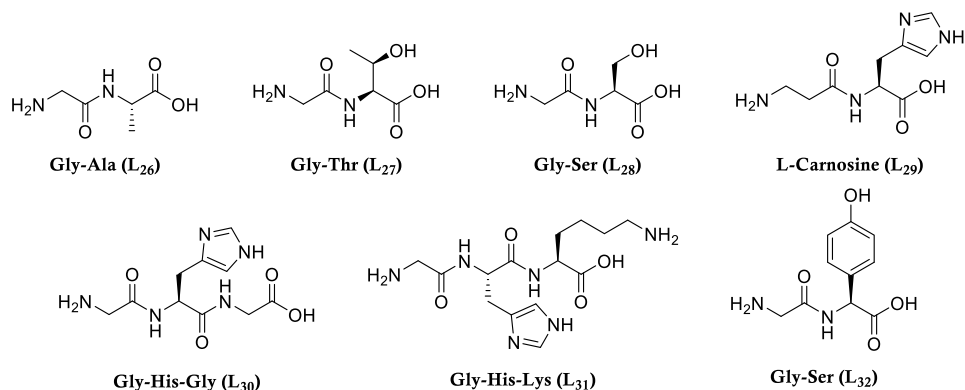
Figure 28. Structure of the peptides **L₂₆-L₃₁** used for the synthesis of CMOFs.

Martí-Gastaldo and co-workers pioneered the design and applications of metal-peptide frameworks, specifically **CMOF-32**[81] and the exploration of enantioselective applications of some of the aforementioned CMOFs (*e.g.* **CMOF-30**).[82]

Proteins

Proteins are biomolecules made of several polypeptide chains. They are structurally complex and with numerous coordinating groups located in the

[76] Rabone, J.; Yue, Y. F.; Chong, S. Y.; Stylianou, K. C.; Bacsa, J.; Bradshaw, D.; Darling, G. R.; Berry, N. G.; Khimyak, Y. Z.; Ganin, A. Y.; Wiper, P.; Claridge, J. B.; Rosseinsky, M. J. *Science* **2010**, *329*, 1053-1057.

[77] Martí-Gastaldo, C.; Warren, J. E.; Stylianou, K. C.; Flack, N. L. O.; Rosseinsky, M. J. *Angew. Chem. Int. Ed.* **2012**, *51*, 11044-11048.

[78] Martí-Gastaldo, C.; Antypov, D.; Warren, J. E.; Briggs, M. E.; Chater, P. A.; Wiper, P. V.; Miller, G. J.; Khimyak, Y. Z.; Darling, G. R.; Berry, N. G.; Rosseinsky, M. J. *Nat. Chem.* **2014**, *6*, 343-351.

[79] Katsoulidis, A. P.; Park, K. S.; Antypov, D.; Martí-Gastaldo, C.; Miller, G. J.; Warren, J. E.; Robertson, C. M.; Blanc, F.; Darling, G. R.; Berry, N. G.; Purton, J. A.; Adams, D. J.; Rosseinsky, M. J. *Angew. Chem. Int. Ed.* **2014**, *53*, 193-198.

[80] Martí-Gastaldo, C.; Warren, J. E.; Briggs, M. E.; Armstrong, J. A.; Thomas, K. M.; Rosseinsky, M. J. *Chem. Eur. J.* **2015**, *21*, 16027-16034.

[81] Navarro-Sánchez, J.; Mullor-Ruíz, I.; Popescu, C.; Santamaría-Pérez, D.; Segura, A.; Errandonea, D.; González-Platas, J.; Martí-Gastaldo, C. *Dalton Trans.* **2018**, *47*, 10654-10659.

[82] Navarro-Sánchez, J.; Argente-García, A. I.; Moliner-Martínez, Y.; Roca-Sanjuán, D.; Antypov, D.; Campíns-Falcó, P.; Rosseinsky, M. J.; Martí-Gastaldo, C. *J. Am. Chem. Soc.* **2017**, *139*, 4294-4297.

Introduction

residues of the monomeric units. There is no consensus of the minimum units of AAs to form a protein, but it can be considered somewhere above 50 units.

Tezcan and co-workers managed to synthesise a MOF containing ferritin nodes: they modified the AA position 122 replacing Thr with His (^{T122H}ferritin) to create a trinuclear node for the coordination of Zn^{2+}, then they used L_{33} (H_2bdh) to link Zn-^{T122H}ferritin units to build **MOF-33** (**Scheme 2**).[83]

Zn-^{T122H}ferritin   bdh-Zn-^{T122H}ferritin
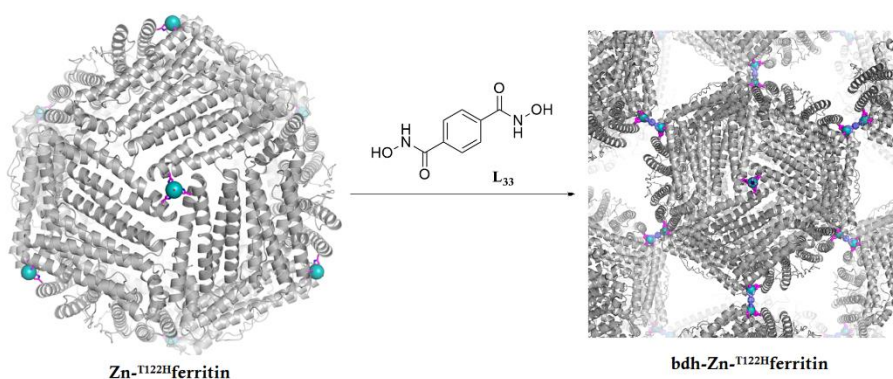
Scheme 2. Schematic representation of the synthesis of bdh-Zn-^{T122H}ferritin. Adapted with permission from *J. Am. Chem. Soc.* **2015**, *137*, 11598-11601. Copyright 2015 American Chemical Society.

Following this work, they created a library of 15 ferritin-MOFs with cubic or tetragonal lattice arrangements using different metal nodes (Zn^{2+}, Ni^{2+} and Co^{2+}) and five different ligands (L_{33}-L_{37}) (**Figure 29**).[84]
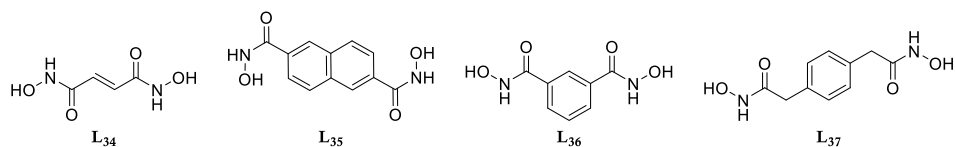
Figure 29. Structure of the ligands used in the synthesis of the ferritin-MOF library.

Although amino acids, peptides and proteins can be used as building blocks for the synthesis of promising biomimetic networks, the lability of primary amines in N–M bonds can lead to chemically unstable materials. The synthetic versatility of primary amines opens the possibility to transform them into more chemically stable moieties. Amidst the promising transformations that can take place in the α-amino functional group, triazoles are propitious candidates.

[83] Sontz, P. A.; Bailey, J. B.; Ahn, S.; Tezcan, F. A. *J. Am. Chem. Soc.* **2015**, *137*, 11598-11601.
[84] Bailey, J. B.; Zhang, L.; Chiong, J. A.; Ahn, S.; Tezcan, F. A. *J. Am. Chem. Soc.* **2017**, *139*, 8160-8166.

TRIAZOLE-BASED METAL-ORGANIC FRAMEWORKS

Triazoles (or pyrrodiazoles)[85] are five-membered heterocyclic compounds containing three *N* atoms. They occur in two isomeric forms: the 1,2,3-triazole and 1,2,4-triazole skeletons (**Scheme 3**), prone to tautomeric equilibria.

Scheme 3. Isomeric forms of triazoles: 1,2,3-triazole (left) and 1,2,4-triazole (right), and their NH tautomeric forms.

Up to date, several synthetic methods have been reported for the synthesis of 1,2,4-triazoles. 4-substituted 4*H*-1,2,4-triazoles can be readily synthesised from a primary amine by transamination of *N,N*-dimethylformamide azine (abbreviated to DMFA), a method reported by R. K. Bartlett and I. R. Humphrey in 1967 (**Scheme 4**).[86]
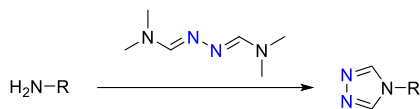
Scheme 4. Schematic synthesis of 4-substituted 4*H*-1,2,4-triazoles using DMFA.

Other methods, such as the use of formyl hydrazide and triethyl orthoformate for the *in-situ* formation of 1,2-diformylhydrazine (**Scheme 5**), known as the Bayer synthesis,[87] are also of interest.
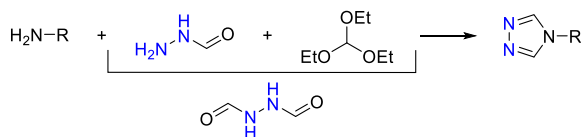
Scheme 5. Schematic synthesis of 4-substituted 4*H*-1,2,4-triazoles using formyl hydrazine and triethyl orthoformate through a 1,2-diformylhydrazine intermediate.

[85] Ji Ram, V.; Sethi, A.; Nath, M.; Pratap, R. In *The Chemistry of Heterocycles*; Elsevier: 2019; pp 364-369.
[86] Bartlett, R. K.; Humphrey, I. R. *J. Chem. Soc. C* **1967**, 1664-1666.
[87] (a) Gural'skiy, I. y. A.; Reshetnikov, V. A.; Omelchenko, I. V.; Szebesczyk, A.; Gumienna-Kontecka, E.; Fritsky, I. O. *J. Mol. Struct.* **2017**, *1127*, 164-168. (b) Gural'skiy, I. y. A.; Reshetnikov, V. A.; Omelchenko, I. V.; Szebesczyk, A.; Gumienna-Kontecka, E.; Fritsky, I. O. *J. Mol. Struct.* **2017**, *1127*, 164-168.

Introduction

Triazoles are of high interest in coordination chemistry.[88] For instance, 1,2,4-triazoles can bind with two metal centres through N^1,N^2 through several bonding modes (these are terminal, bridging or chelating, **Figure 30**),[89] resulting in the formation of polynuclear compounds such as materials with magnetic properties[90] or metal-organic frameworks.
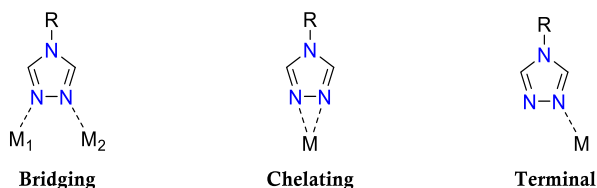
Figure 30. Bridging, chelating and terminal coordination modes of 4-substituted 4*H*-1,2,4-triazoles.

Applications of triazole-based MOFs

Several examples of MOFs constructed with 1,2,4-triazole-containing ligands have been reported in the literature, with properties such as gas capture and separation, catalysis, luminescence, guest adsorption and others. A few examples will be described hereunder based on their properties.

Gas adsorption and separation

Yue-Biao Zhang and co-workers reported in 2020 the synthesis of four isoreticular MOFs using 1,2,4-triazolate molecules with appending amino and methyl groups (**L₃₈-L₄₁**). The presence of rod (–Zn–F–Zn–F–)$_n$ SBUs formed channels with honeycomb shape for selective CO_2 capture from highly humid flue gas (**Figure 31**).[91]

[88] Aromí, G.; Barrios, L. A.; Roubeau, O.; Gamez, P. *Coord. Chem. Rev.* **2011**, *255*, 485-546.

[89] (a) Tahli, A.; Maclaren, J. K.; Boldog, I.; Janiak, C. *Inorg. Chim. Acta* **2011**, *374*, 506-513. (b) Bahemmat, S.; Ghassemzadeh, M.; Neumüller, B. *Inorg. Chim. Acta* **2015**, *435*, 159-166. (c) Bahemmat, S.; Ghassemzadeh, M.; Neumüller, B. *Inorg. Chim. Acta* **2015**, *435*, 159-166. (d) Zhang, J.; Jia, W.; Wu, J.; Tang, G.; Zhang, C. *New J. Chem.* **2019**, *43*, 16078-16088.

[90] (a) Nieto-Castro, D.; Garcés-Pineda, F. A.; Moneo-Corcuera, A.; Pato-Doldan, B.; Gispert-Guirado, F.; Benet-Buchholz, J.; Galán-Mascarós, J. R. *Inorg. Chem.* **2020**, *59*, 7953-7959. (b) Nieto-Castro, D.; Garcés-Pineda, F. A.; Moneo-Corcuera, A.; Sánchez-Molina, I.; Galán-Mascarós, J. R. *Adv. Funct. Mater.* **2021**, *31*, 2102469. (c) Sánchez-Molina, I.; Moneo-Corcuera, A.; Nieto-Castro, D.; Benet-Buchholz, J.; Galán-Mascarós, J. R. *Eur. J. Inorg. Chem.* **2021**, *2021*, 112-116.

[91] Shi, Z.; Tao, Y.; Wu, J.; Zhang, C.; He, H.; Long, L.; Lee, Y.; Li, T.; Zhang, Y.-B. *J. Am. Chem. Soc.* **2020**, *142*, 2750-2754.
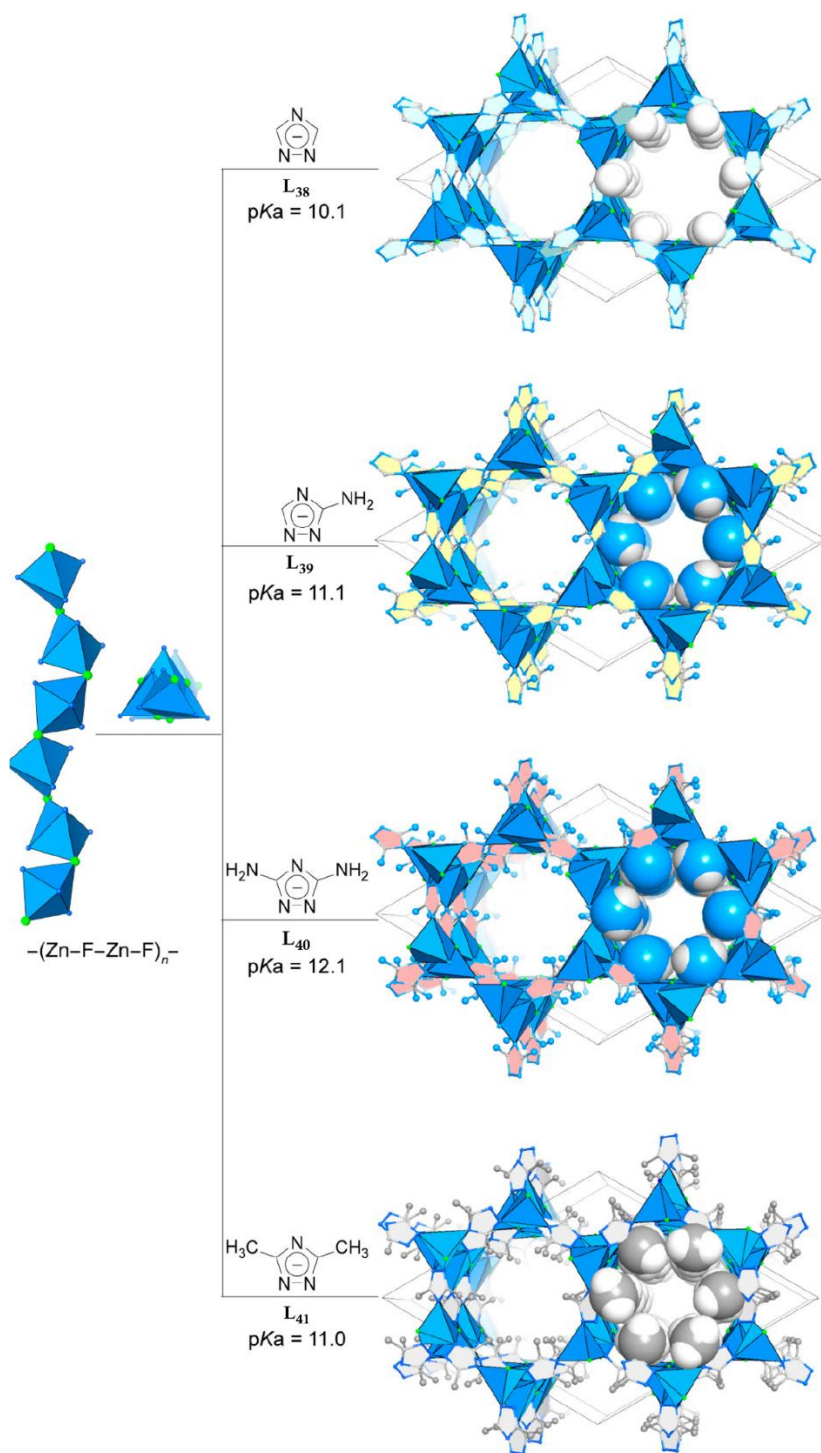
Figure 31. Synthetic scheme for the construction of the four isoreticular triazole-based MOFs and their corresponding crystal structures. Adapted with permission of *J. Am. Chem. Soc.* **2020**, *142*, 2750-2754. Copyright 2020 American Chemical Society.

30

Regarding gas separation, Zhizhi Yao *et al.* described the hydrothermal synthesis (high-temperature solutions at high vapour pressures) of two novel triazole-based MOFs using ligand **L₄₂** (5-(4*H*-1,2,4-triazol-4-yl)-isophthalic acid), **MOF-42a** and **MOF-42b**. These MOFs were used for the selective separation of acetylene from a mixture with ethylene (**Figure 32**).[92]
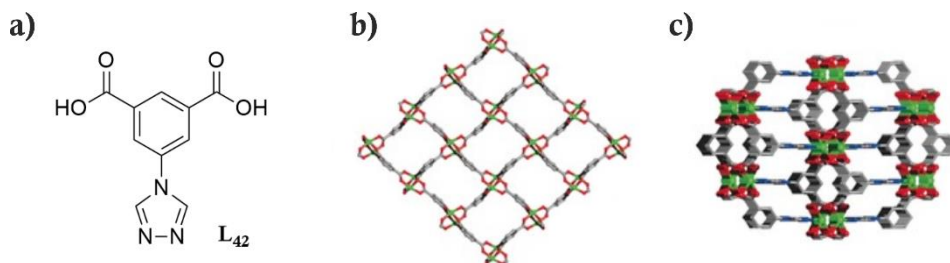
Figure 32. Structure of (a) **L₄₂**, (b) **MOF-42a** and (c) **MOF-42b** along the *a* axis. Adapted with permission of *Chem. Eur. J.* **2016**, *22*, 5676-5683. Copyright 2016 Wiley.

Although the ligand used for both MOFs was the same, changing the solvent under the same experimental conditions produced two different MOFs. Selectivity towards acetylene retention was achieved by the open oxygen donors and the acidic protons in acetylene.

Catalysis

MOFs containing 1,2,4-triazole-based ligands also have been used as heterogeneous catalysts. Specifically, in 2019, Feng Guo reported the synthesis of a Cu^{2+} MOF (**MOF-43**) using a triazole-based ligand **L₄₃** (3-methyl-5-(4*H*-1,2,4-triazol-4-yl)pyridine) and its dual role as a heterogeneous catalyst. It catalysed the cycloaddition of CO_2 to epoxides to form cyclic carbonates and the Knoevenagel condensation reaction between aldehydes and malononitrile (**Figure 33**).[93]

---

[92] Yao, Z.; Zhang, Z.; Liu, L.; Li, Z.; Zhou, W.; Zhao, Y.; Han, Y.; Chen, B.; Krishna, R.; Xiang, S. *Chem. Eur. J.* **2016**, *22*, 5676-5683.
[93] Guo, F. *Inorg. Chem. Commun.* **2019**, *101*, 87-92.
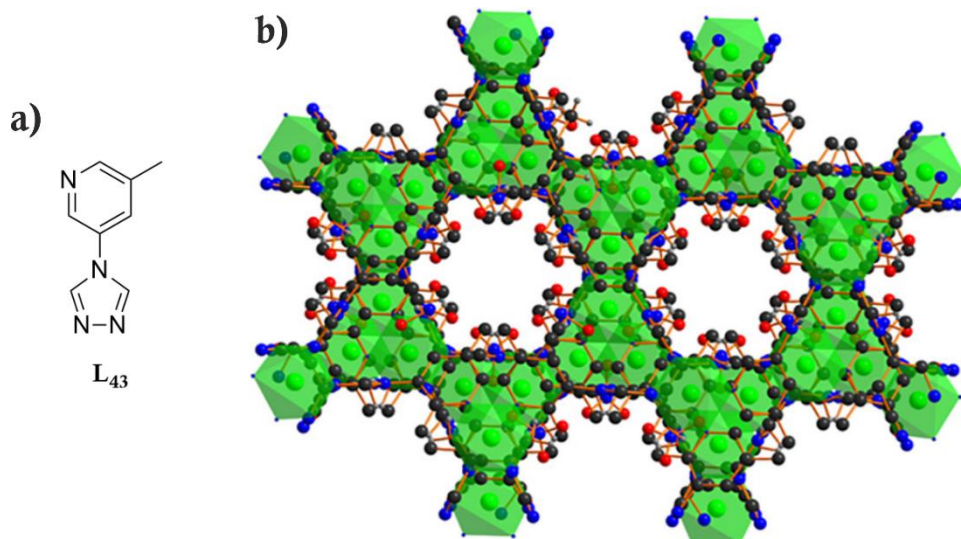
Figure 33. (a) Structure of L_{43} and (b) view of a single 2D network of **MOF-43**. Reproduced with permission of *Inorg. Chem. Commun.* **2019**, *101*, 87-92. Copyright 2019 Elsevier.

Another 1,2,4-triazole-based MOF was also used in the cycloaddition of CO_2 to epoxides. **MOF-44**, which was constructed with $L_{44.1}$ (3,5-di(pyridine-4-yl)-4H-1,2,4-triazol-4-amine) and $L_{44.2}$ (4,4',4''-nitrilotribenzoic acid), was reported by Jian Wang and co-workers in 2021 (**Figure 34**).[94]
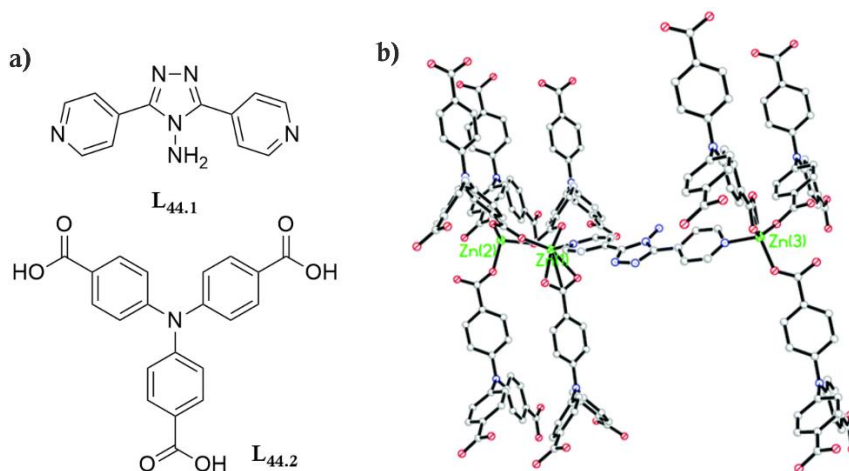
Figure 34. Structure of (a) $L_{44.1}$, $L_{44.2}$ and (b) **MOF-44**. Adapted with permission of *Chem. Commun.* **2021**, *57*, 10803-10806. Copyright 2019 Royal Society of Chemistry.

[94] Li, Y.; Tian, X.; Jiang, W.; Wu, P.; Li, H.-S.; Wang, M.; Lin, C.; Wang, J. *Chem. Commun.* **2021**, *57*, 10803-10806.

32

Luminescence

By using ligand L_{45} (4,4'-(4H-1,2,4-triazole-3,5-diyl)dibenzoic acid), Qi-Long Zhu and co-workers constructed four different MOFs. MOFs containing Co^{2+} (**MOF-45a**) and Ni^{2+} (**MOF-45b**) possess magnetic properties, while MOFs constructed with Cd^{2+} (**MOF-45c,d**) display intense blue emission under UV excitation. Moreover, **MOF-45d** was used for the sensing of acetone in water based on luminescence quenching effect (**Figure 35**).[95]
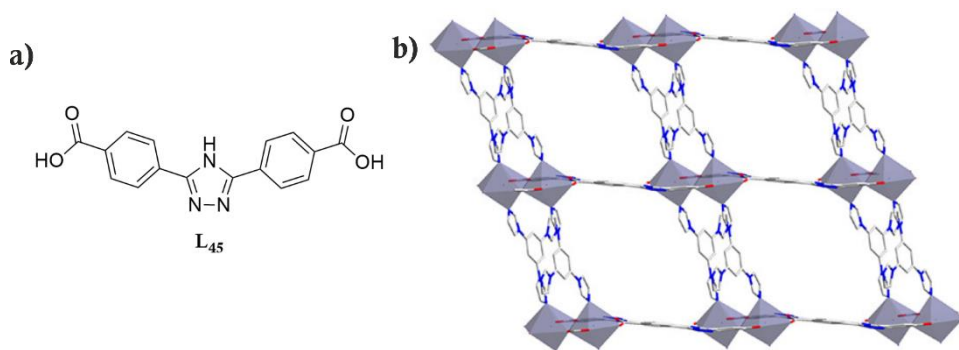
Figure 35. Structure of (a) L_{45} and (b) **MOF-45d** 2D layer along the [111] orientation. Adapted with permission of *Cryst. Growth Des.* **2019**, *19*, 1057-1063. Copyright 2019 American Chemical Society.

Devices

MOFs are also promising materials for electronic devices. In this example, Banglin Chen and co-workers synthesised **CMOF-42c** in 2019 using an achiral ligand (the same for **MOF-42a/b**, L_{42}, page **31**). Chirality was obtained by spontaneous resolution, and the CMOF was used in the development of an RRAM device based on hydrogen bonding (**Figure 36**).[96]

---

[95] Zhang, Y.-X.; Lin, H.; Wen, Y.; Zhu, Q.-L. *Cryst. Growth Des.* **2019**, *19*, 1057-1063.

[96] Yao, Z.; Pan, L.; Liu, L.; Zhang, J.; Lin, Q.; Ye, Y.; Zhang, Z.; Xiang, S.; Chen, B. *Sci. Adv.* **2019**, *5*, eaaw4515.
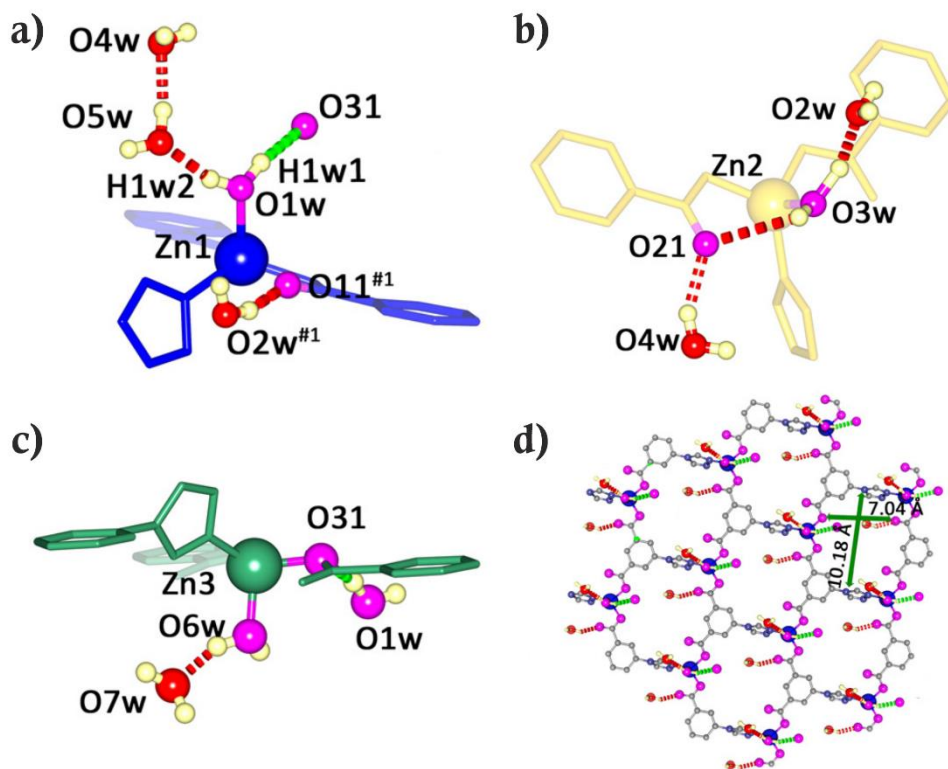
Figure 36. (**a** to **c**)Hydrogen bonding interaction between the lattice water and the MOF in **CMOF-42c** and (**d**) honeycomb sheet of Zn_1 atoms. Adapted from *Sci. Adv.* **2019**, *5*, eaaw4515. Licensed under CC BY 4.0.

Amino acid-derived 1,2,4-triazoles

The availability of structurally diverse AAs and the possibility to transform them into the corresponding 4*H*-1,2,4-triazole derivatives encouraged us to explore the transformation of several amino acids into their triazole analogues. These ligands could be further used in the synthesis of coordination compounds. Hitherto, only the derivatisation of five amino acids to their 4*H*-1,2,4-triazole analogues (Gly, Ala, His, Met and Phe) has been described in the literature (**Figure 37**).[97]

---

[97] **Trz-Glycine**: Naik, A. D.; Marchand-Brynaert, J.; Garcia, Y. *Synthesis* **2008**, *1*, 149-154. **Trz-Alanine and Trz-Phenylalanine**: Vasylevs'kyy, S. I.; Lysenko, A. B.; Krautscheid, H.; Karbowiak, M.; Rusanov, E. B.; Domasevitch, K. V. *Inorg. Chem. Commun.* **2015**, *62*, 51-54. **Trz-Histidine**: Lysenko, A. B.; Senchyk, G. A.; Domasevitch, K. V.; Kobalz, M.; Krautscheid, H.; Cichos, J.; Karbowiak, M.; Neves, P.; Valente, A. A.; Gonçalves, I. S. *Inorg. Chem.* **2017**, *56*, 4380-4394. **Trz-Methionine**: Naik, A. D.; Beck, J.; Dîrtu, M. M.; Bebrone, C.; Tinant, B.; Robeyns, K.; Marchand-Brynaert, J.; Garcia, Y. *Inorg. Chim. Acta* **2011**, *368*, 21-28.

34

Introduction

Trz-Gly-OR	Trz-Ala-OH	Trz-His-OH	Trz-Met-OH	Trz-Phe-OH
L_{46a}: R = H	L_{47}	L_{48}	L_{49}	L_{50}
L_{46b}: R = Me				
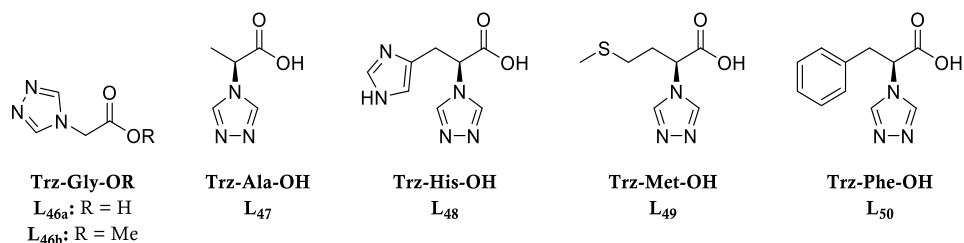
Figure 37. Structure of the AA-based 4*H*-1,2,4-triazol-4-yl derivatives.

Despite the successful synthesis of these ligands, only a few MOFs using these have been reported, and none of them were exploited in enantioselective processes.

Yann-Garcia and co-workers reported in 2010 the use of L_{46a} (2-(4*H*-1,2,4-triazol-4-yl)acetic acid, Trz-Gly-OH) and L_{46b} (methyl 2-(4*H*-1,2,4-triazol-4-yl)acetate, Trz-Gly-OEt) for the synthesis of **MOF-46i (Figure 38)**.[98] In 2015, they used L_{46a} for the synthesis of a single-walled Cu^{2+} metal-organic nanotube (SWMONT) **MOF-46ii**, capable of storing metallic mercury inside (**Figure 39**).[99]
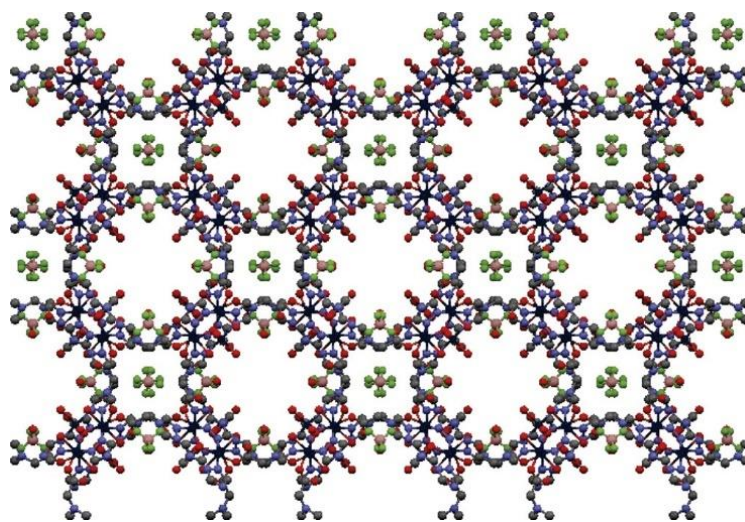
Figure 38. Hydrophilic (large) and hydrophobic (small, includes BF_4^- anions) channels in **MOF-46i** ([$Cu_3(\mu_3\text{-}O)(L_{46a})_3\cdot(H_2O)_3$]$BF_4\cdot H_2O$). Reproduced with permission of *Cryst. Growth Des.* **2010**, *10*, 1798-1807. Copyright 2010 American Chemical Society.

[98] Naik, A. D.; Dîrtu, M. M.; Léonard, A.; Tinant, B.; Marchand-Brynaert, J.; Su, B.-L.; Garcia, Y. *Cryst. Growth Des.* **2010**, *10*, 1798-1807.
[99] Adarsh, N. N.; Dîrtu, M. M.; Naik, A. D.; Léonard, A. F.; Campagnol, N.; Robeyns, K.; Snauwaert, J.; Fransaer, J.; Su, B. L.; Garcia, Y. *Chem. Eur. J.* **2015**, *21*, 4300-4307.
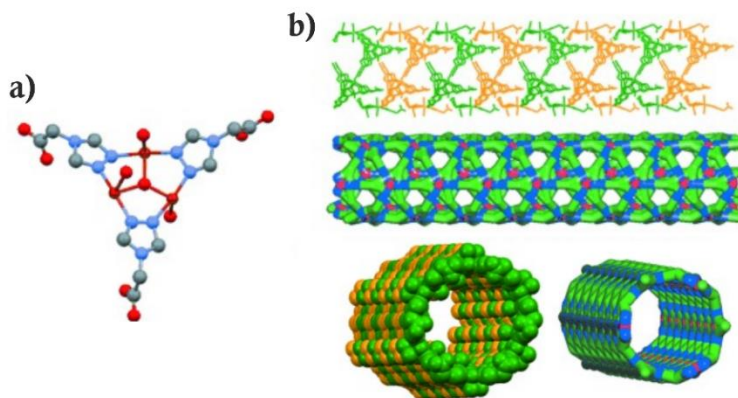
Figure 39. (**a**) L_{46a} SBU and (**b**) view of **MOF-46ii** along various crystallographic axis. Adapted with permission of *Chem. Eur. J.* **2015**, *21*, 4300-4307. Copyright 2015 Wiley.

In 2014, Andrew Ozarowski and co-workers synthesised L_{46a} and (*R*)-L_{47} ((*R*)-2-(4*H*-1,2,4-triazol-4-yl)propanoic acid, (D)-Trz-Ala-OH) for the formation of three Cu^{2+} MOFs (**MOF-46iii**, **MOF-46iv** and **MOF-47**) with magnetic properties (**Figure 40**).[100] **MOF-47** was optically active due to the enantiopurity of the organic ligand (Flack parameter = -0.02(3)).[101]
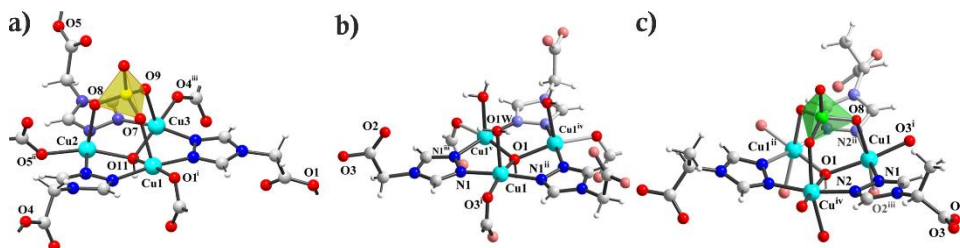
Figure 40. Structure of (a) **MOF-46iii**, (b) **MOF-46iv** and (c) **MOF-47** clusters. Adapted with permission of *Inorg. Chem.* **2014**, *53*, 3642-3654. Copyright 2014 American Chemical Society.

Our group explored in the past the use of several triazoles derived from AAs for the synthesis of a porous compound and succeeded in achieving this goal by using L_{48} ((*S*)-3-(1*H*-imidazol-4-yl)-2-(4*H*-1,2,4-triazol-4-yl)propanoic acid, abbreviated to **S-HTA**), which was synthesised from L-histidine. The deprotonated form of *S*-HTA is abbreviated to **S-TA**.

[100] Vasylevs'kyy, S. I.; Senchyk, G. A.; Lysenko, A. B.; Rusanov, E. B.; Chernega, A. N.; Jezierska, J.; Krautscheid, H.; Domasevitch, K. V.; Ozarowski, A. *Inorg. Chem.* **2014**, *53*, 3642-3654.
[101] The **Flack parameter** is used in crystallography to estimate the absolute configuration of a structural model determined by SCXRD. **Flack ≈ 0** means that the absolute configuration is correct. **Flack ≈ 1** means that the opposite configuration is correct. **Flack ≈ 0.5** means that the crystal could be racemic or twinned.

Introduction

TAMOF-1

TAMOF-1[102] (Triazole Acid Metal-Organic Framework), a highly porous, homochiral and chemically stable MOF, was obtained. This CMOF can be easily synthesised by the reaction of *S*-HTA and Cu^{2+} in water. The phase purity of TAMOF-1 was confirmed by LeBail refinement of PXRD data (**Figure 41**).
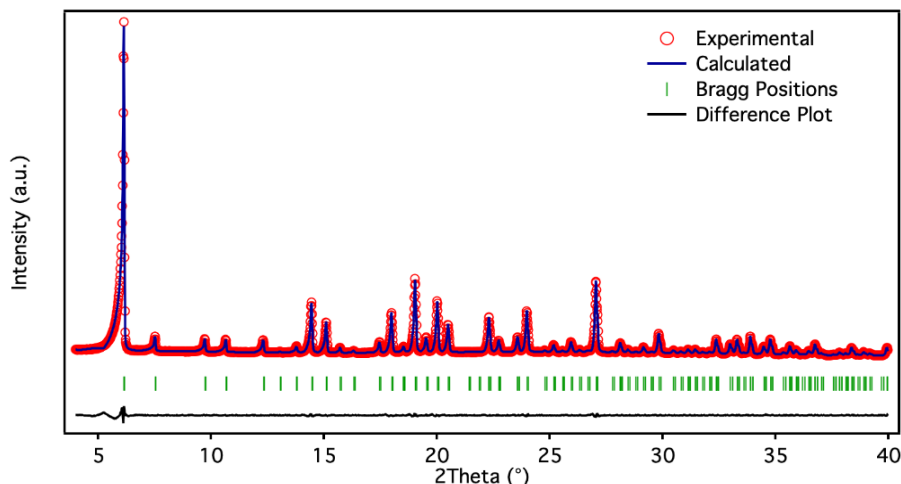
Figure 41. Experimental (red dots), calculated (blue line), difference plot [($I_{obs}-I_{calc}$)] (black line, bottom panel), and Bragg positions (green ticks, bottom panel) for the Le Bail refinement of experimental diffraction data of TAMOF-1 collected at room temperature, confirming the isostructurality for TAMOF-1.[103]

SCXRD showed that TAMOF-1 is a 3D structure built from linked Cu(*S*-TA)$_2$ units (**Figure 42**). The octahedral Cu^{2+} centres are connected to four deprotonated ligands (two imidazole and two triazole moieties) in the equatorial positions and two H_2O molecules in the axial ones. Each metal centre is coordinated to four neighbouring sites by four ligands, and the carboxylates remain uncoordinated to yield a neutral framework with a cubic space group (*P*4$_3$32).

---

[102] Corella-Ochoa, M. N.; Lillo, V.; Galán-Mascaros, J. R. WO 2018/073400 A1, 2018.
[103] Reprinted with permission from *J. Am. Chem. Soc.* **2019**, *141*, 14306–14316. Copyright 2019 American Chemical Society.
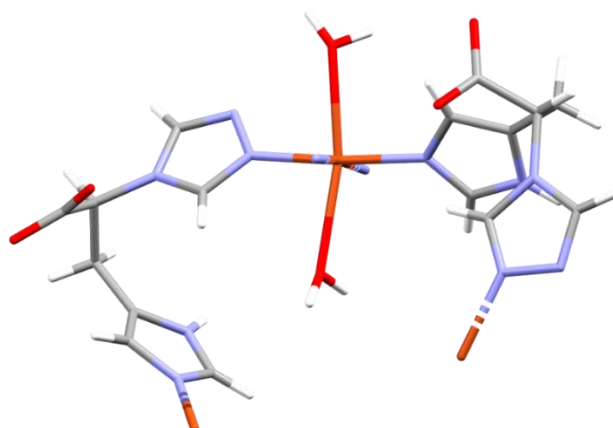
Figure 42. Cu(S-TA)$_2$ unit of TAMOF-1.

TGA analysis showed that TAMOF-1 is stable up to 200 °C. PXRD analysis at different temperatures confirmed the stability of the crystal structure up to the aforementioned temperature (**Figure 43**). Moreover, PXRD analysis of samples subjected to acid or base confirmed the chemical stability of this CMOF (**Figure 44**).
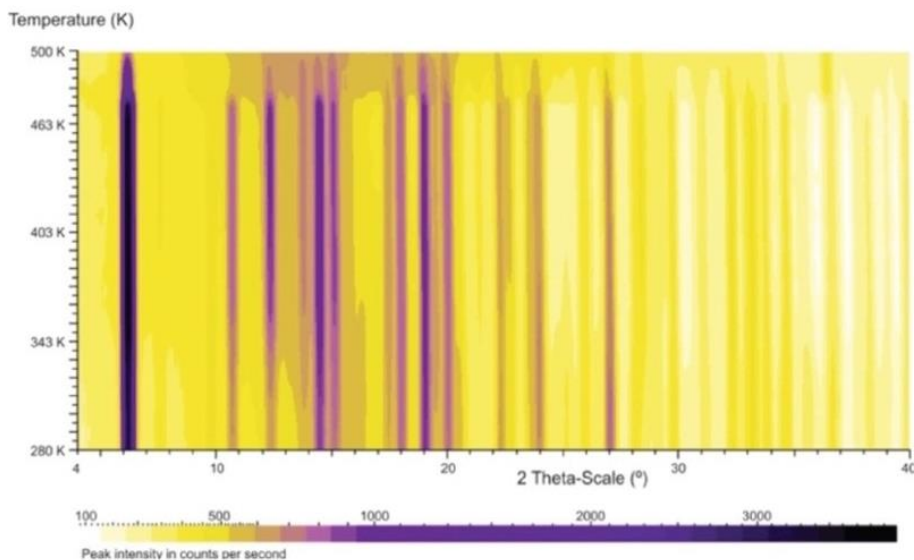
Figure 43. Temperature dependence of the powder pattern of TAMOF-1 under N$_2$ stream atmosphere, showing persistence of the crystal structure up to 470 K.[103]
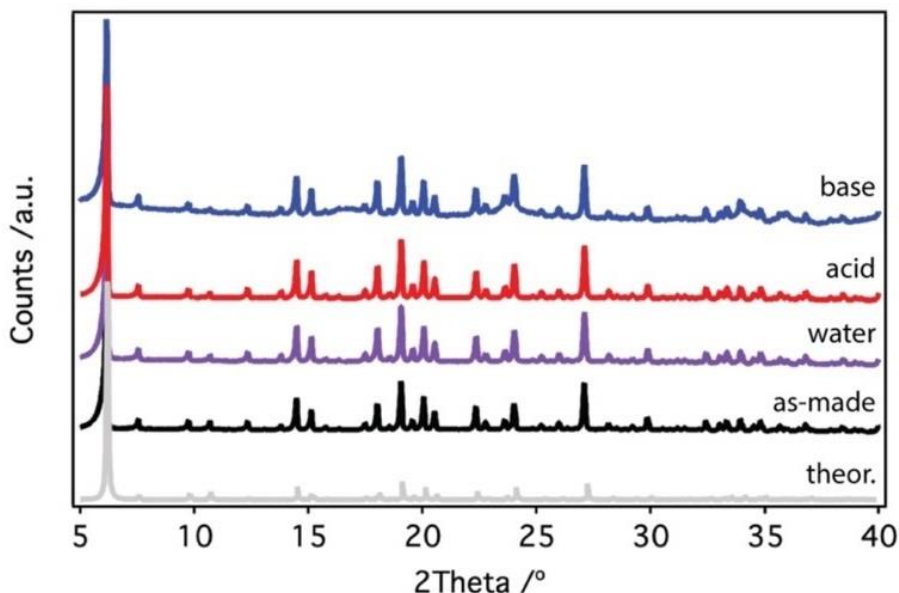
Figure 44. PXRDs of TAMOF-1 confirming structural integrity after incubation in water during 96 hours at neutral (purple), acid (red) and basic (blue) conditions.[103]

N_2 adsorption/desorption isotherms at 77 K were performed to assess the permanent porosity of TAMOF-1 (**Figure 45**). It displayed a type-I isotherm, characteristic of microporous materials, with a multipoint BET over 980 ± 50 m^2 g^{-1} and a micropore volume of 0.38 ± 0.02 cm^3 g^{-1} (**Table 1**).
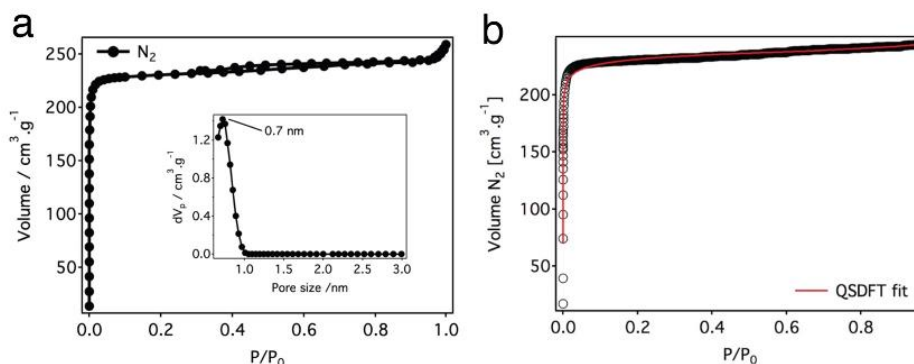
Figure 45. N_2 adsorption/desorption isotherms for TAMOF-1 at 77 K. Surface area, pore size and volume values were calculated from nitrogen adsorption/desorption isotherms at 77 K recorded on an AUTOSORB-6 apparatus. Before analysis, samples were degassed for 24 hours at 150 ºC and 10^{-6} Torr. **(a)** N_2 isotherm of TAMOF-1 and pore size distribution centred at 0.7 nm. **(b)** QSDFT fit to experimental data. Fitting error was below 2%.[103]

Table 1. Parameters obtained from N_2 adsorption isotherms of TAMOF-1 at 77 K.[103]

Sample	SA_{BET}^a [$m^2 \cdot g^{-1}$]		V_t^b [$cm^3 g^{-1}$]		PSD_{NLDFT}^c [nm]
	Exp.	Theor.[d]	Exp.	Theor.[e]	
TAMOF-1	962.5	873.25	0.379	0.260	0.723

[a] Specific surface area (SA) was calculated by multipoint Brunauer-Emmett-Teller (BET) method.[104] [b] Total pore volume at $P/P_0=0.96$. [c] Pore size distribution was analysed by using QSDFT. [d] Calculated with Zeo++[105] by using a probe radius of 1.8 Å (equal to the kinetic diameter of 3.6 Å for N_2). [e] based on solvent accessible volume of single-crystal structure, calculated with a probe diameter of 3.6 Å.

Morphological analysis by ESEM revealed a homogeneous cubic solid with particle size between 3.5 and 7 μm (**Figure 46**).
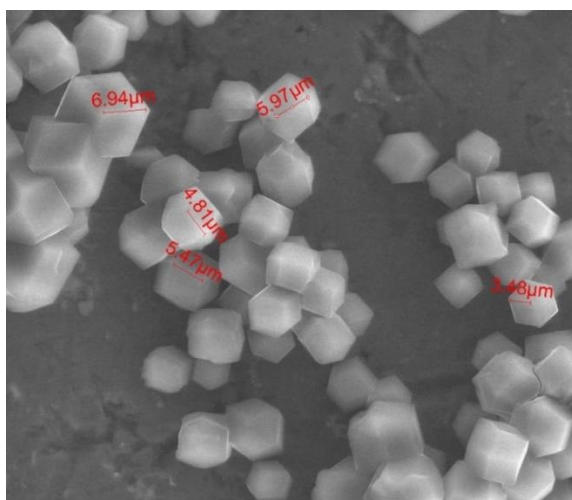
Figure 46. ESEM image of TAMOF-1 powder (Scale: 40 μm). The analysis was performed with a FEI ESEM Quanta 600 equipped with EDX.[103]

Compared to other CMOFs, the derivatisation of the α-amino group to a triazole yields a stable framework that maintains its porosity after activation. Moreover, it has been shown that TAMOF-1 is chemically stable, whereas other AA or peptide-based solids have weak metal binding sites.

In addition to the privileged stability and robustness, TAMOF-1 helical channels dispose of numerous sites and polar functional groups. These polar groups (*i.e.* free carboxylates, imidazole and triazole units) can serve as a platform for guest-host interactions with chiral molecules, endowing TAMOF-1 with potential enantioselective properties.

[104] Brunauer, S.; Emmett, P. H.; Teller, E. *J. Am. Chem. Soc.* **1938**, *60*, 309-319.
[105] Willems, T. F.; Rycroft, C. H.; Kazi, M.; Meza, J. C.; Haranczyk, M. *Microporous Mesoporous Mater.* **2012**, *149*, 134-141.

OBJECTIVES

Overall, reported CMOFs in the literature are excellent heterogeneous platforms for enantioselective applications, and these materials have been demonstrated to have an outstanding performance compared to their homogeneous counterparts. Sadly, they are limited either by physical or chemical stability. Even though there are reports about highly stable CMOFs, several drawbacks (*e.g.* problematic access to large-scale ligand synthesis, complex synthetic procedures to yield CMOFs) prevent them from being used on industrial scale.

As described in the previous section, TAMOF-1 is a promising platform for enantioselective applications for its permanent porosity (*ca.* 1000 m^2 g^{-1}), excellent thermal stability (up to 200 °C) and chemical resistance (polar and non-polar solvents, acid and base). The ligand, *S*-HTA, can be synthesised on kilogram scale, so can TAMOF-1. Additionally, polar groups in the chiral pores are promising modulators for guest-host interactions, translating into enantiodiscrimination.

Taking into account these properties and the limitations of CMOFs previously described in the literature, the objectives of the present thesis are:

1. To study the structure, synthesis, tunability of the pores and the shaping of TAMOF-1.

2. To analyse the enantioselectivity of TAMOF-1 in its use in heterogeneous enantioselective catalytic processes.

3. To elucidate the capability of TAMOF-1 as CSP for the separation of racemic mixtures.

4. To use TAMOF-1 in other chromatographic separations, such as the separation of aromatic regioisomers.

5. To design and synthesise new triazole-based ligands with more extended spaces between coordinating moieties to build novel CMOFs with enlarged pore sizes.
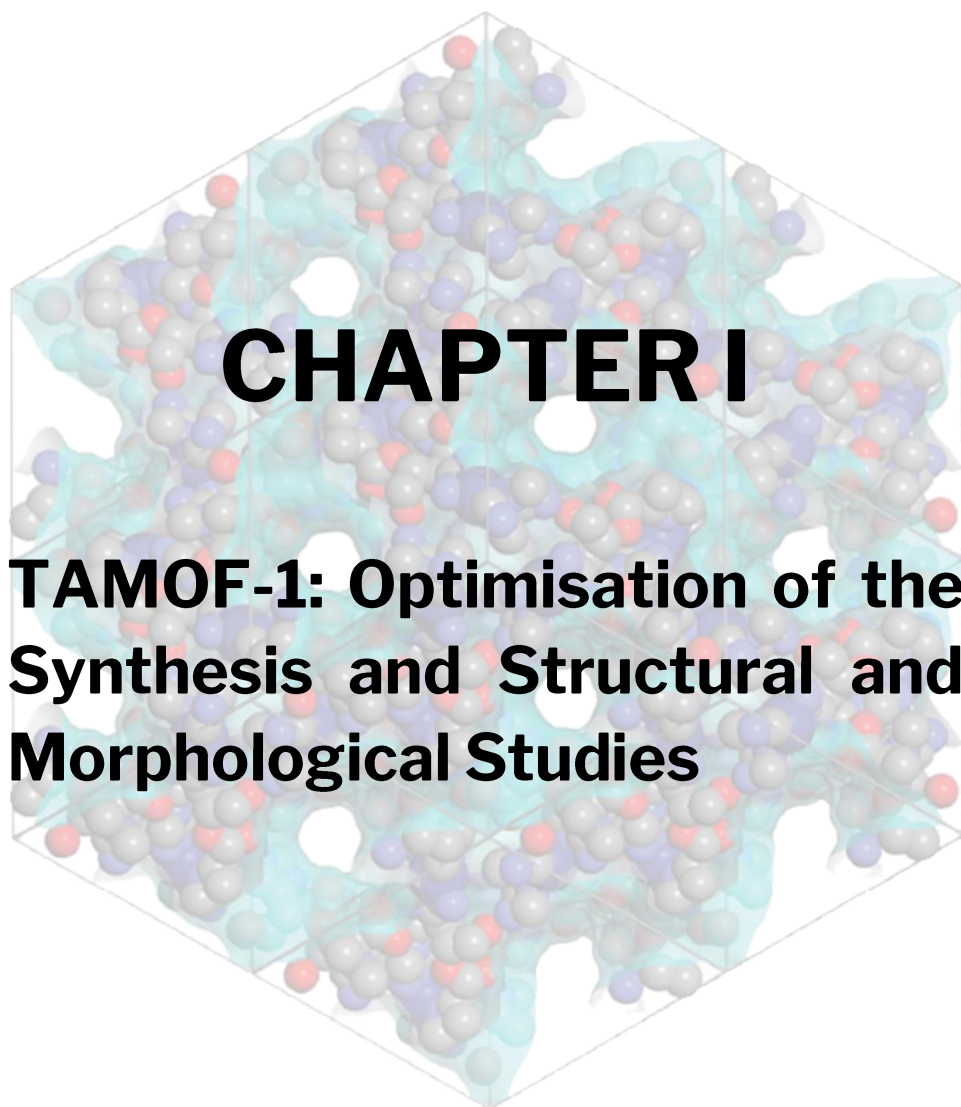
Objectives

41

CHAPTER I

TAMOF-1: Optimisation of the Synthesis and Structural and Morphological Studies

1.1. ABSTRACT

In this chapter, we describe the synthesis, synthetic variations to control particle size and BET surface area of TAMOF-1 and the study of the pH in the synthetic process. Then, we investigate the crystallisation conditions to obtain large single crystals (up to mm scale) to study of guest molecules inside TAMOF-1 pores by neutron diffraction. We further exploited the crystallisation conditions for introducing metallic NPs inside the pores of TAMOF-1 to expand its catalytic scope and study their effect in its catalytic activity. Finally, self-shaping has been used for the formation of monolithic TAMOF-1 ($_{mono}$TAMOF-1) and its use in gas separation and capture has been studied.

Chapter I

1.2. INTRODUCTION

Metal-organic frameworks (MOFs) are a family of porous materials, assembled by metal ions or clusters and organic ligands, creating three-dimensional networks exhibiting outstanding porosities (up to 8,000 m^2 g^{-1})[106] and exceptional chemical tunability. Up to date, these materials have been proposed for applications such as gas storage,[107] separation of gas mixtures,[108] sensing,[109] drug delivery,[110] enantioselective processes (catalysis and separation),[111] among others.

One of the main challenges in the development of MOFs is the engineering of these materials in terms of shape and porosity. In the standard synthetic procedures (*e.g.* solution-based methods by mixing solutions, solvothermal conditions or layering), MOFs may be obtained as polycrystalline powders (nm-μm scale) or single crystals (up to mm scale).[112]

Our research group we synthesised the already described homochiral MOF, TAMOF-1. With excellent thermal and chemical stability, this MOF has found applications in separation of gas mixtures, chiral separation and

[106] Hönicke, I. M.; Senkovska, I.; Bon, V.; Baburin, I. A.; Bönisch, N.; Raschke, S.; Evans, J. D.; Kaskel, S. *Angew. Chem. Int. Ed.* **2018**, *57*, 13780-13783.
[107] Connolly, B. M.; Madden, D. G.; Wheatley, A. E. H.; Fairen-Jimenez, D. *J. Am. Chem. Soc.* **2020**, *142*, 8541-8549.
[108] Qian, Q.; Asinger, P. A.; Lee, M. J.; Han, G.; Mizrahi Rodriguez, K.; Lin, S.; Benedetti, F. M.; Wu, A. X.; Chi, W. S.; Smith, Z. P. *Chem. Rev.* **2020**, *120*, 8161-8266.
[109] Li, H.-Y.; Zhao, S.-N.; Zang, S.-Q.; Li, J *Chem. Soc. Rev.* **2020**, *49*, 6364-6401.
[110] Osterrieth, J. W. M.; Fairen-Jimenez, D. *Biotechnol. J.* **2021**, *16*, 2000005.
[111] Bhattacharjee, S.; Khan, M. I.; Li, X.; Zhu, Q. L.; Wu, X. T. *Catalysts* **2018**, *8*, 120.
[112] Sorrenti, A.; Jones, L.; Sevim, S.; Cao, X.; deMello, A. J.; Martí-Gastaldo, C.; Puigmartí-Luis, J. *J. Am. Chem. Soc.* **2020**, *142*, 9372-9381.

TAMOF-1: Optimisation of the Synthesis and Structural and Morphological Studies

enantioselective catalysis, the latter two being the main subject of this thesis and will be described in the next chapters.[113] Although these applications were developed using the as-synthesised TAMOF-1 with particle sizes ranging from 1 to 10 μm, we envisaged that the optimisation of the synthetic conditions could control the particle size and the BET surface area.[114]

In terms of catalytic applications, the porosity of a MOF could act as a scaffold to host catalytically active complexes or metallic NPs inside their pores or channels.[115] The combination of a homochiral environment and diverse catalytic sites could create a vast range of enantioselective synthetic possibilities. Additionally, the recyclability of these materials could overcome expensive processes in industry.

Concerning shape, changes in the synthetic procedures and processing techniques of MOFs have allowed researchers to obtain these materials as monoliths (*mono*MOFs) through self-shaping conditions.[116] These monoliths possess high bulk densities (close to single-crystal densities). Usually, the processed materials see their microporosity (0-2 nm) reduced compared to its powdered analogues. However, due to the packing of the microparticles in the synthetic process, the interstitial spaces endow monoliths with mesoporosity (2-50 nm). Monoliths are useful for liquid applications, such as chiral separations, as mesoporosity offers less resistance to mass transfer.

The diminishment of the microporosity slightly worsens the BET area and the gravimetric gas uptake of the MOF (expressed as cm^3 of gas per g of MOF). Nonetheless, the high density of monoliths drastically increases the volumetric BET surface, pore volume and volumetric uptake (cm^3 of gas per cm^3 of MOF). However, the formation of these monoliths can be rather difficult. For instance, mechanical shaping could compact TAMOF-1 powder to a monolith, but the use of high pressure could compromise the structure of the microcrystallites.[117] An already-known synthetic method called sol-gel,[118] which is widely used in the synthesis of aerogels, overcomes the issues mentioned above yielding robust monoliths.

[113] (a) Corella-Ochoa, M. N.; Tapia, J. B.; Rubin, H. N.; Lillo, V.; González-Cobos, J.; Núñez-Rico, J. L.; Balestra, S. R. G.; Almora-Barrios, N.; Lledós, M.; Güell-Bara, A.; Cabezas-Giménez, J.; Escudero-Adán, E. C.; Vidal-Ferran, A.; Calero, S.; Reynolds, M.; Martí-Gastaldo, C.; Galán-Mascarós, J. R. *J. Am. Chem. Soc.* **2019**, *141*, 14306-14316. (b) Cabezas-Giménez, J.; Lillo, V.; Luis Núñez-Rico, J.; Nieves Corella-Ochoa, M.; Jover, J.; Galán-Mascarós, J. R.; Vidal-Ferran, A. *Chem. Eur. J.* **2021**, *27*, 16956-16965.
[114] Wahiduzzaman; Allmond, K.; Stone, J.; Harp, S.; Mujibur, K. *Nanoscale Res. Lett.* **2017**, *12*, 6.
[115] (a) Juan-Alcañiz, J.; Gascon, J.; Kapteijn, F. *J. Mater. Chem.* **2012**, *22*, 10102-10118. (b) Yang, Q.; Xu, Q.; Jiang, H.-L. *Chem. Soc. Rev.* **2017**, *46*, 4774-4808. (c) Li, X.; Zhang, Z.; Xiao, W.; Deng, S.; Chen, C.; Zhang, N. *J. Mater. Chem. A* **2019**, *7*, 14504-14509.
[116] Hou, J.; Sapnik, A. F.; Bennett, T. D. *Chem. Sci.* **2020**, *11*, 310-323.
[117] Lorignon, F.; Gossard, A.; Carboni, M. *Chem. Eng. J.* **2020**, *393*, 124765.
[118] **Sol-gel** is a method where a colloidal solution (*i.e.* "sol") gradually evolves to a biphasic system similar to a gel to produce solid materials from small molecules. (a) Danks, A. E.; Hall, S. R.; Schnepp, Z. *Mater. Horiz.* **2016**, *3*, 91-112. (b) Feinle, A.; Elsaesser, M. S.; Hüsing, N. *Chem. Soc. Rev.* **2016**, *45*, 3377-3399.

The first monolith reported was $_{mono}$ZIF-8,[119] and, since then, other examples of $_{mono}$MOFs can be found in the literature.[120] Among all the monolithic MOFs that have been reported, $_{mono}$HKUST-1 stands out for reaching the US Department of Energy (DOE) target for methane storage, which was set in a volumetric uptake of 263 cm^3 (STP) cm^{-3}.[121]

In this chapter the synthesis of TAMOF-1 is described. Different synthetic conditions were tried, and the particle size and the BET surface area of such trials were analysed. To better understand the interaction between the metal centre and the ligand, the pH of the reaction was thoroughly analysed. Metal NPs were incorporated to bring additional catalytic properties to the material. Finally, the self-shaping conditions for the formation of $_{mono}$TAMOF-1 were explored, and the resulting materials were comprehensively characterised.

Chapter I

[119] Tian, T.; Velazquez-Garcia, J.; Bennett, T. D.; Fairen-Jimenez, D. *J. Mater. Chem. A* **2015**, *3*, 2999-3005.
[120] (a) Mehta, J. P.; Tian, T.; Zeng, Z.; Divitini, G.; Connolly, B. M.; Midgley, P. A.; Tan, J.-C.; Fairen-Jimenez, D.; Wheatley, A. E. H. *Adv. Funct. Mater.* **2018**, *28*, 1705588. (b) Connolly, B. M.; Aragones-Anglada, M.; Gandara-Loe, J.; Danaf, N. A.; Lamb, D. C.; Mehta, J. P.; Vulpe, D.; Wuttke, S.; Silvestre-Albero, J.; Moghadam, P. Z.; Wheatley, A. E. H.; Fairen-Jimenez, D. *Nat. Commun.* **2019**, *10*, 2345.
[121] Tian, T.; Zeng, Z.; Vulpe, D.; Casco, M. E.; Divitini, G.; Midgley, P. A.; Silvestre-Albero, J.; Tan, J.-C.; Moghadam, P. Z.; Fairen-Jimenez, D. *Nat. Mater.* **2018**, *17*, 174-179.

UNIVERSITAT ROVIRA I VIRGILI
INSIGHTS IN HOMOCHIRAL METAL-ORGANIC FRAMEWORKS: FROM THEIR SYNTHESIS TO ENANTIOSELECTIVE
APPLICATIONS
Juanjo Cabezas Gimenez

TAMOF-1: Optimisation of the Synthesis and Structural and Morphological Studies

1.3. RESULTS AND DISCUSSION

1.3.1. Synthesis of TAMOF-1

The synthetic route for the obtention of TAMOF-1 began by synthesising the required reagent DMFA for the transformation of the AA into its triazole-containing analogue. This reagent was easily obtained in excellent yields following a literature procedure (**Scheme 6**).[122]
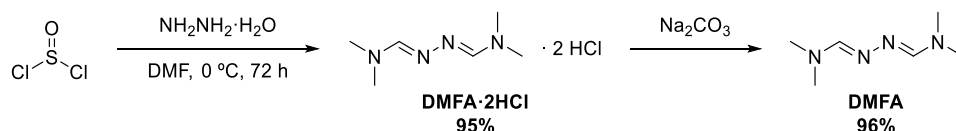
Scheme 6. Synthesis of DMFA.

The next step was the synthesis of the ligand, (*S*)-3-(1*H*-imidazol-5-yl)-2-(4*H*-1,2,4-triazol-4-yl)-propanoic acid (*S*-HTA), a L-histidine derivative. This reaction – transamination of DMFA – yielded the desired ligand in excellent yields (**Scheme 7**). The synthesis of the racemic ligand was already described in the literature;[123] nevertheless, our group developed a different procedure to yield the enantiopure ligand.[102]
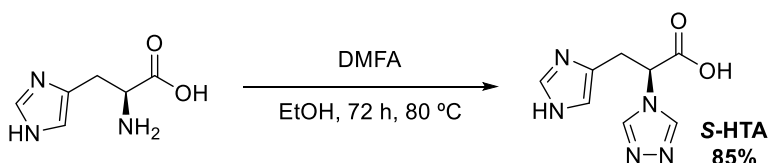
Scheme 7. Synthesis of (*S*)-3-(1*H*-imidazol-5-yl)-2-(4*H*-1,2,4-triazol-4-yl)-propanoic acid (*S*-HTA).

With the ligand in hand, the last step was the precipitation of TAMOF-1. The reaction between an aqueous solution of *S*-HTA and an aqueous solution of $Cu(OAc)_2$ gave a light blue powder in 70% yield with the formula $[Cu(H_2O)_2(S\text{-}TA)_2]\cdot6H_2O$ (**Scheme 8**).

[122] Bartlett, R. K.; Humphrey, I. R. *J. Chem. Soc. C* **1967**, 1664-1666.
[123] Lysenko, A. B.; Senchyk, G. A.; Domasevitch, K. V.; Kobalz, M.; Krautscheid, H.; Cichos, J.; Karbowiak, M.; Neves, P.; Valente, A. A.; Gonçalves, I. S. *Inorg. Chem.* **2017**, *56*, 4380-4394.
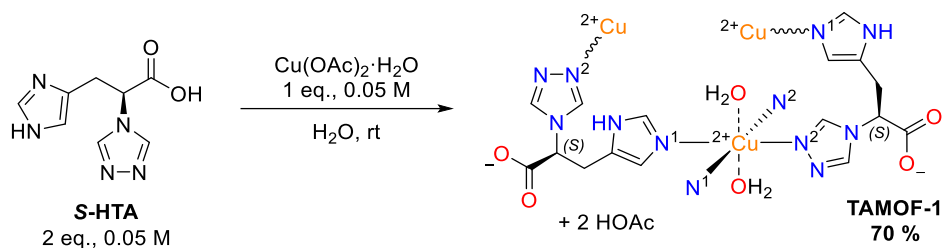
Scheme 8. Synthesis of TAMOF-1.

Single crystals of TAMOF-1 (**Figure 47**) were easily obtained by slow diffusion of an aqueous solution of Cu(OAc)$_2$·H$_2$O and an aqueous solution of *S*-HTA in an H-Cell. The preparation of this MOF was protected by filing a European Patent Application.[102]
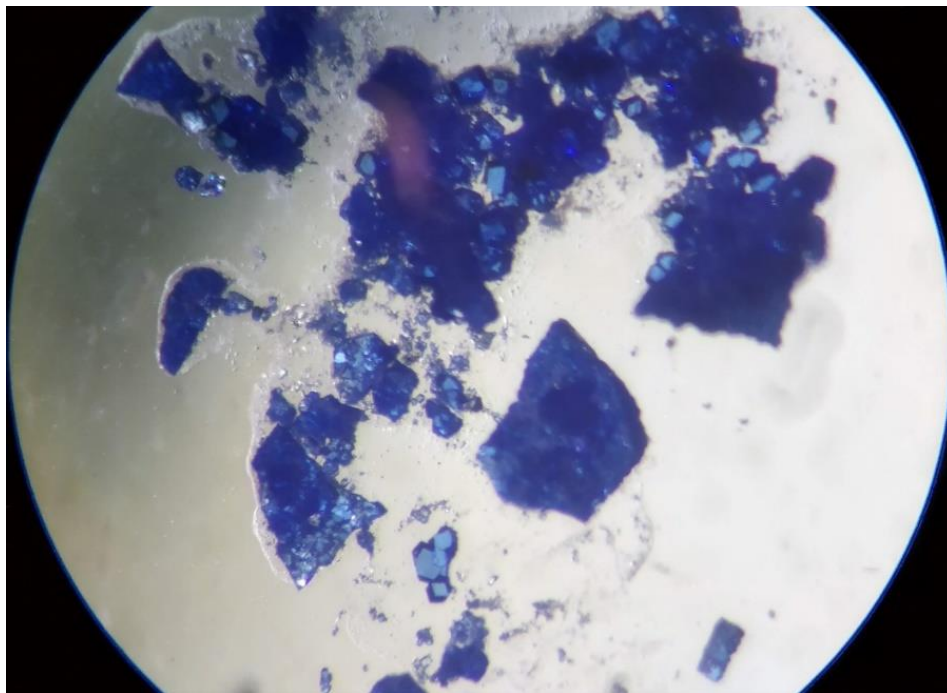
Figure 47. Single crystals of TAMOF-1 with different sizes.

TAMOF-1: Optimisation of the Synthesis and Structural and Morphological Studies

1.3.2. Optimisation of particle size of TAMOF-1

The as-synthesised MOF presented a random particle size between 0.2 and 10 μm, according to ESEM and DLS data (**Figure 48**).
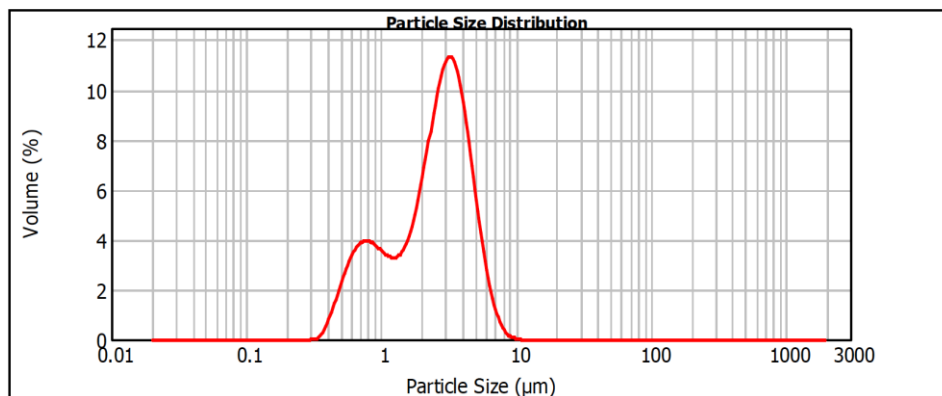
Figure 48. DLS data obtained from a suspension of TAMOF-1 in distilled water with Mastersizer 2000 (MALVERN) showing a large size distribution between 0.2 and 10 μm.

We wondered if the particle size would change by varying the reaction conditions. We considered that the relative concentration of the starting materials and the temperature could be crucial for the obtention of TAMOF-1. Thus, we changed parameters such as addition rate and stirring rate (**Table 2**). We analysed the effect of changing these parameters in the yield, the particle size and the uniformity of the material.

Table 2. Particle size and BET area of different TAMOF-1 batches.

Entry	Stirring (rpm)	Addition[a]	D[4,3] (μm)[b]	Uniformity[b]	BET Area (m² g⁻¹)[c]
1	400	Slow	2,839	0,518	429
2	800	Slow	2,821	0,483	618
3	400	Medium	3,300	0,545	767
4	800	Medium	3,174	0,504	973
5	1200	Medium	2,142	0,618	1088
6	1200	Fast	1,394	0,288	1210

[a] The addition rate was controlled with a NE-1010 Higher Pressure Syringe Pump. [b] Analysed from a suspension in distilled water with Mastersizer 2000 (MALVERN). D[4,3] is the weighted mean value by volume, and the uniformity is the absolute deviation from the median [c] Nitrogen adsorption/desorption isotherms at 77 K were measured on a Quantachrome Autosorb iQ gas adsorption analyser.

At slow stirring and addition rates (**Table 2, Entries 1-4**), similar particle size distributions as in **Figure 48** were observed. Although the quantity of particles between 0.1 and 1 μm decreased by increasing the stirring rate or the addition rate, the modification of these parameters did not yield homogeneous particle sizes (**Figure 49**).
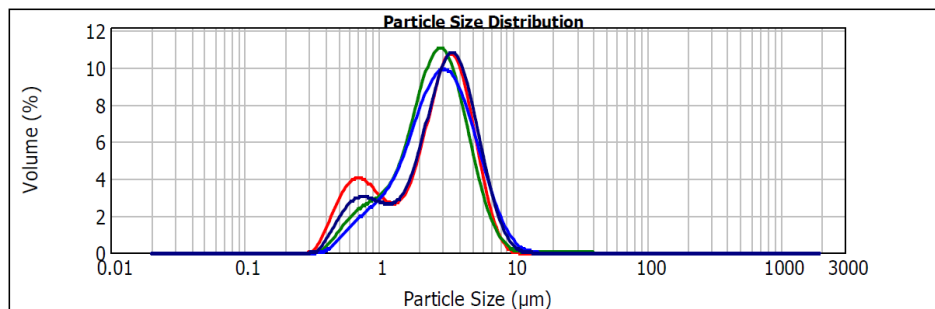
Figure 49. DLS data obtained with Mastersizer 2000 (MALVERN) of entries 1-4.

When the stirring rate was increased to 1200 rpm at medium addition rates (**Table 2, Entry 5**), the particle size homogeneity increased towards small particle sizes (0.4-6 μm). A small number of particles between 7 and 20 μm were observed, possibly due to particle aggregation (**Figure 50**).
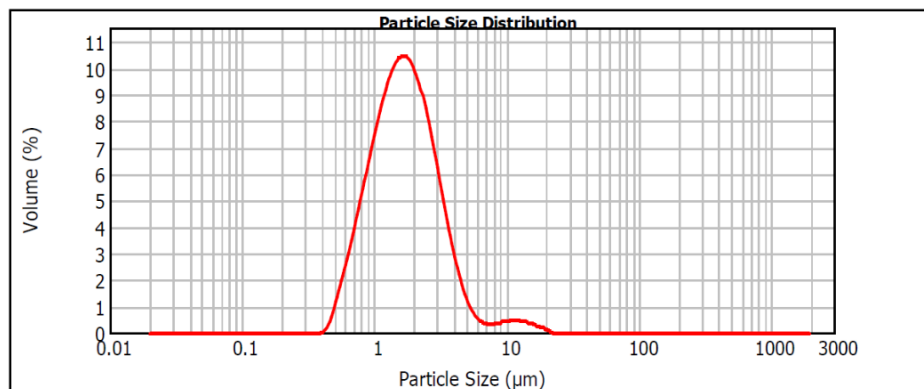
Figure 50. DLS data obtained with Mastersizer 2000 (MALVERN) of entry 5.

When the stirring (1200 rpm) and the addition rate were increased simultaneously (**Table 2, Entry 6**), we found that particle size homogeneity notably increased, having a particle size between 0.3 and 3 μm centred at 1.39 μm (**Figure 51**). On the other hand, variations in the above mentioned parameters did not affect the yields, which ranged from 61 to 70 %.

Chapter I

TAMOF-1: Optimisation of the Synthesis and Structural and Morphological Studies
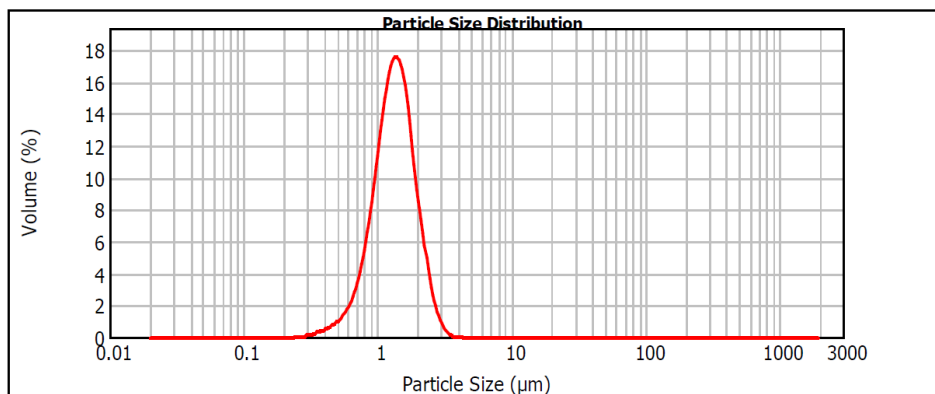
Figure 51. DLS data obtained with Mastersizer 2000 (MALVERN) of entry 6.

It is worth mentioning that a correlation between the particle size and the BET surface area has been observed. As described in **Table 2**, the smaller the particle size and the higher the homogeneity, the greater the BET surface area. If we look at the most oversized particles (**Table 2, Entry 1**), the BET surface area was 429 m^2 g^{-1}, whereas the smallest ones have a BET surface area of 1210 m^2 g^{-1}.

The particle size and its homogeneity are different by changing reaction conditions, and a correlation between the particle size and the BET surface area exists. This is extremely important for the applications of this MOF. For instance, to fill an analytic HPLC column, it is desirable to have a TAMOF-1 batch with a median particle size between 5 and 10 μm.

1.3.3. pH effect in TAMOF-1 synthesis

To the best of our knowledge, the obtention of TAMOF-1 is limited to the acetate salt of Cu^{2+}. A plausible hypothesis could be that acetate acts a buffer that maintains the pH of the system and allows the ligand to stay in the proper protonation state to form the MOF. In order to rationalise the hypothesis, we measured the pK_a of *S*-HTA (**Figure 52**), which contains three possibly protonable functional groups: the carboxylic acid group, the imidazole ring and the 4*H*-1,2,4-triazole ring.

52
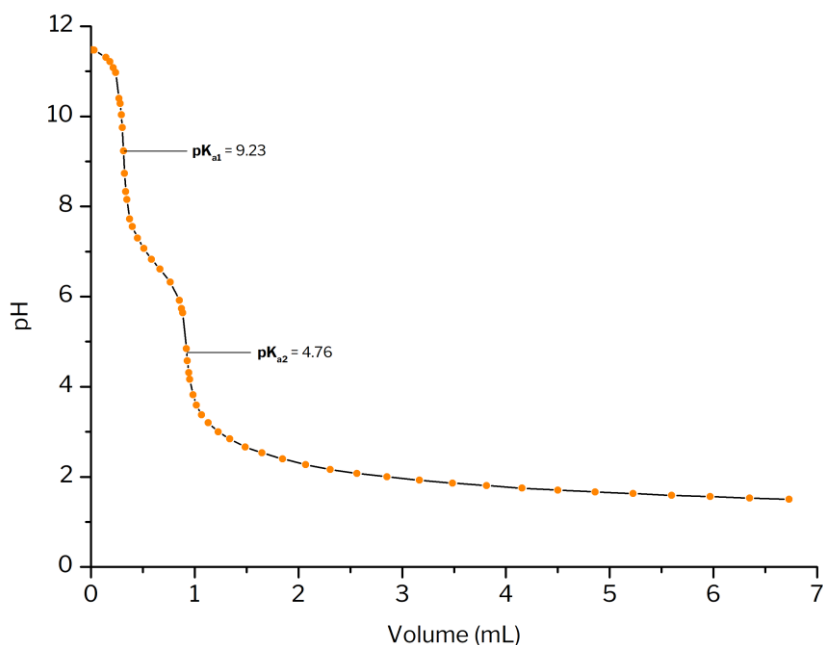
Figure 52. Determination of the pKa values of *S*-HTA by titration with 0.1M HCl. Recorded with a Potentiometer Metrohm 836 Titrando Dosino 800 instrument.

The titration of a basified solution of *S*-HTA with HCl 0.1M allowed us to conclude that the pK_a values of *S*-HTA are pK_{a1} = 9.23 and pK_{a2} = 4.76 (**Scheme 9**). The pK_a values have been tentatively assigned to the imidazole ring and the carboxylate, respectively, although the imidazole value does not agree with the expected literature value (~7.0).[124] On the other hand, the pK_a of the carboxylate is in agreement with the pK_a value of AcOH (4.75).[125]
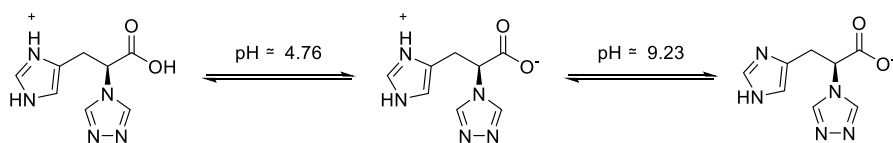
Scheme 9. Acid-base equilibria of *S*-HTA according to the experimental pK_a values.

Predicted pK_a values[126] do not fit the experimental values precisely, even though the pH value of the predominant zwitterionic form (5.10) fits the

[124] Ebel, K.; Koehler, H.; Gamer, A. O.; Jäckh, R. Imidazole and Derivatives. In *Ullmann's Encyclopedia of Industrial Chemistry*, Wiley-VCH: Weinheim, 2012; pp 637-645.
[125] Goldberg, R. N.; Kishore, N.; Lennen, R. M. *J. Phys. Chem. Ref. Data* **2002**, *31*, 231-370.
[126] pKa values of *S*-HTA were predicted using Chemicalize, developed by ChemAxon.

measured value in the curve, which is 5.20 for a 0.05 M concentration (**Figure 53**, dark blue curve).

a)

b)

c)
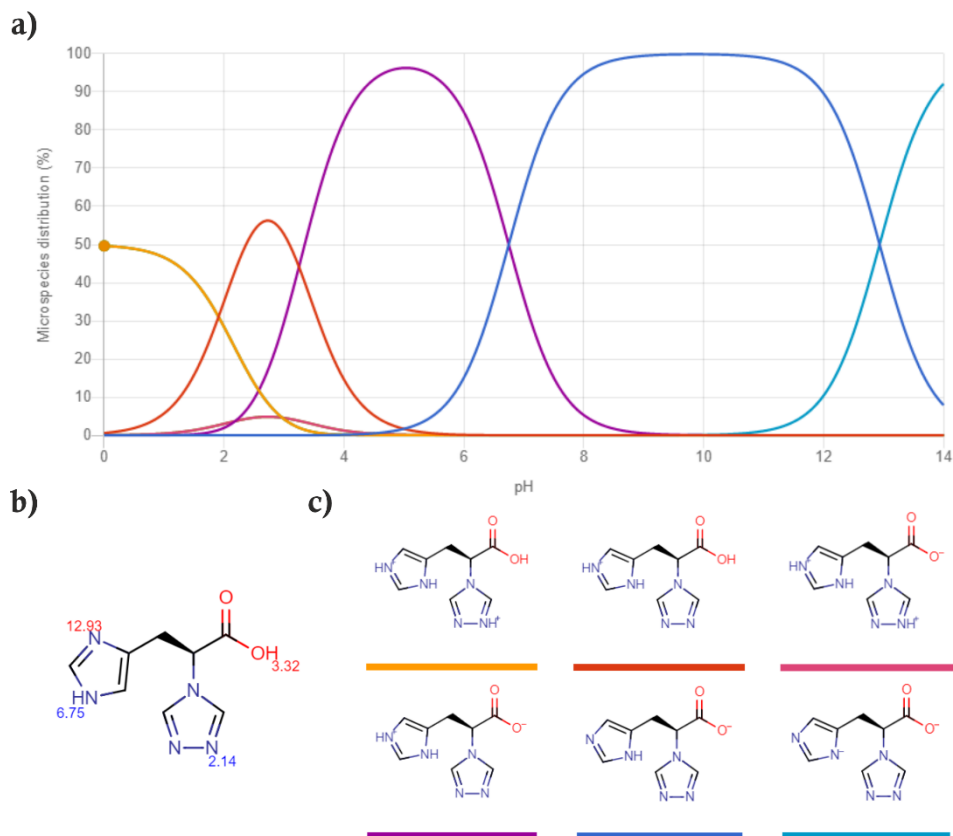
Figure 53. (a) Predicted microspecies distribution. (b) pK$_a$ of the functional groups of *S*-HTA. (c) Structure of the species depending on the pH. Chemicalize was used for structural prediction of pK$_a$ values, January 2022, Chemicalize developed by ChemAxon.

With the experimental pK$_a$ values of *S*-HTA in hand, we measured the pH of the starting materials and the continuous measurement of the pH of the reaction mixture. The starting materials provide acidic pH values (pH$_{Cu}$ = 5.61 and pH$_{S\text{-}HTA}$ = 5.20) in a concentration of 0.05 M. The Cu^{2+} solution is added on top of the *S*-HTA solution, and the pH profile throughout the reaction is shown in **Figure 54**.

54
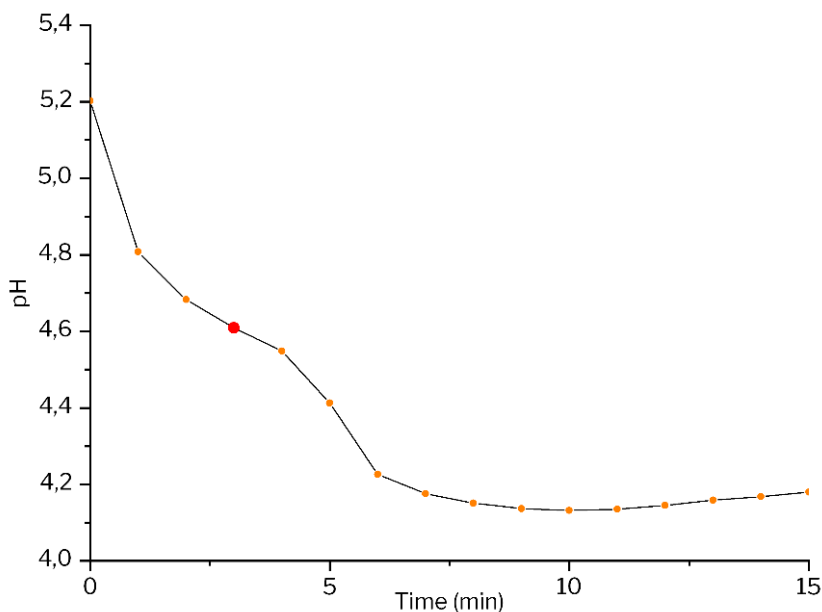
Figure 54. pH profile of the reaction mixture of TAMOF-1. The pH was measured with an 877 Titrino Plus instrument. The precipitation started at the red dot (~3 min, pH ~ 4.6).

The precipitation started at ~3 min, in a pH value of approximately 4.6. In spite of the fact that the starting pH of both solutions is above 5, the pH of the reaction decreases with time. Therefore, we wanted to assess if the precipitation of TAMOF-1 took place regardless of the starting pH. For that, we changed the pH of the *S*-HTA solution to more acidic with AcOH (**Figure 55**) and less acidic with NaOAc (**Figure 56**).

Chapter I

TAMOF-1: Optimisation of the Synthesis and Structural and Morphological Studies
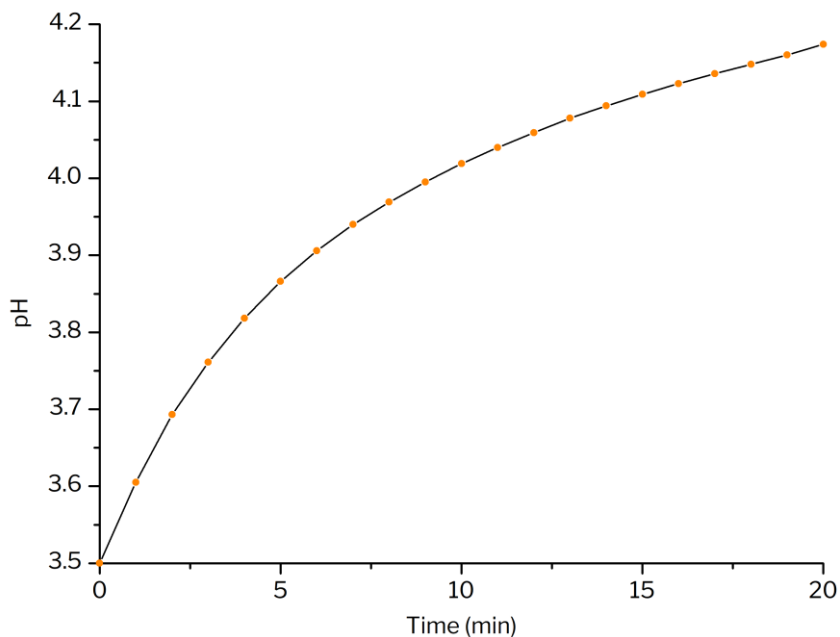
Figure 55. pH profile of the reaction mixture of TAMOF-1 with the initial pH adjusted at 3.5 with AcOH 2M. pH measured with a Metrohm 877 Titrino Plus instrument.
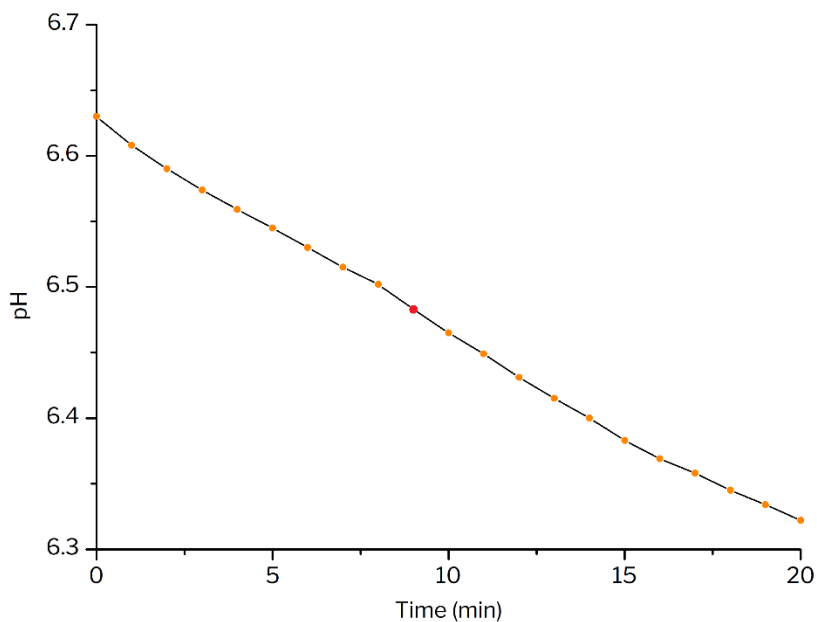
Figure 56. pH profile of the reaction mixture of TAMOF-1 with the initial pH adjusted at 6.63 with NaOAc 2M. pH measured with a Metrohm 877 Titrino Plus instrument. The precipitation started at the red dot (~9 min, pH ~ 6.5).

56

The acidification of the *S*-HTA solution did not yield any precipitate in the short term, although after five days, we observed TAMOF-1 precipitate. The carboxylate group might be deprotonated to form TAMOF-1, and the acidic media delays substantially the precipitation. On the other hand, the increase of the pH to 6.63 using NaOAc 2M allowed us to obtain TAMOF-1 (precipitation started at ~9 min of reaction).

Taking in account the aforementioned observations, we can hypothesise that the reaction must happen with the zwitterionic form of *S*-HTA. As expected from the reaction stoichiometry shown in **Scheme 8**, the acetate ion captures the proton released by the ligand, acting as a buffer. The presence of the buffer favours the formation of TAMOF-1 and maintains the pH in a value that prevents the formation of the protonated carboxylic acid as the dominant species, allowing the continuity of the reaction.

1.3.4. Crystal structure of TAMOF-1

The crystallisation process of TAMOF-1 has been described in page **48**. Analysis by single-crystal X-ray diffraction showed that TAMOF-1 is a three-dimensional network constructed of interlinked Cu(*S*-TA)$_2$ units (**Figure 57**). The crystallographic data can be found in **ANNEX I**.

The geometry of the Cu^{2+} centres is pseudo-octahedral. The equatorial positions are coordinated by imidazole and triazole moieties from four different *S*-TA molecules. Two water molecules occupy the axial positions with long coordination bonds (Cu–O > 2.45 Å @ 100 K, Cu–O > 2.49 Å @ 300 K), being a clear example of the Jahn-Teller effect.[127] In general, each Cu^{2+} is bonded to four neighbouring sites by four *S*-TA ligands, which orientate the imidazole and triazole moieties out of the plane and keep the carboxylate groups without coordinating. This yields an electroneutral homochiral MOF with a *P*4$_3$32 cubic space group.

---

[127] Jahn, H. A.; Teller, E.; Donnan, F. G. *Proc. R. Soc. Lond. A* **1937**, *161*, 220-235.
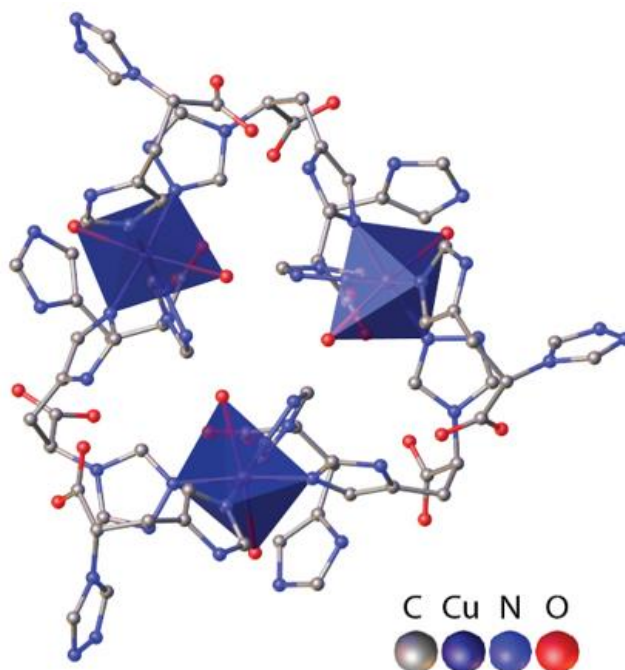
Figure 57. Projection of the crystal structure of TAMOF-1 on the [111] plane showing the interlinking of [Cu(S-TA)$_2$] secondary building units by TA ligands.[103]

TAMOF-1 is stable after removal of the water molecules, and it is a reversible process (**Figure 58**). In fact, at 403 K, the coordinating water molecules are removed as well, leaving a square planar geometry in the Cu^{2+} centres. Rehydration yields an undistinguishable structure from the initial one, confirming the robustness of the structure.
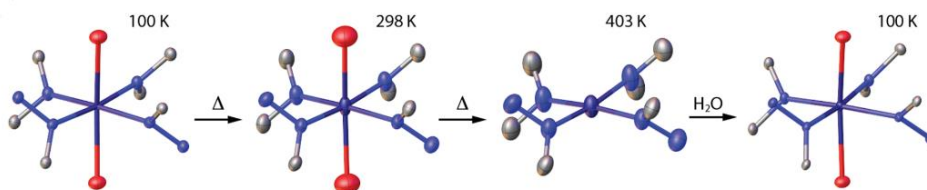
Figure 58. Thermal cycle for the coordination geometry of Cu^{2+} centres. Thermal ellipsoid plots at 3 Å from the metal crystallographic position at 100, 298, and 403 K (dehydrated state), and again at 100 K after rehydration by controlled addition of water.[103]

To exploit the benefits of the porosity of TAMOF-1, we investigated the interaction with different gaseous analytes, such as CH_4 and CO_2.

1.3.4.1. CO_2 coordination inside TAMOF-1 pores

Activation of TAMOF-1 and subsequent interaction studies by incorporating different guest molecules showed that it has an excellent affinity towards CO_2 capture. The capture of CO_2 was observed by single-crystal X-ray diffraction, but the resolution was poor. To further increase resolution and improve the quality of the structure, we required of experimental techniques such as neutron diffraction, as with this technique we could experimentally elucidate the interaction between CO_2 molecules and Cu^{2+} centres in TAMOF-1. Neutron diffraction interacts with the nucleus, while X-rays interact with electron clouds. The benefit of using neutrons for small atoms such as carbon and oxygen is that the diffracted intensity depends on each isotope due to the neutron cross section.[128]

Neutron diffraction requires crystal sizes of *ca.* 1 mm^3 that were successfully obtained with a similar procedure to the described on page **49**. The crystals were activated, cooled down to 100 K then submerged in CO_2 at room temperature (procedure described in page **81**). The interaction of CO_2 inside the pores of TAMOF-1 is shown in **Figure 59**.

Chapter I
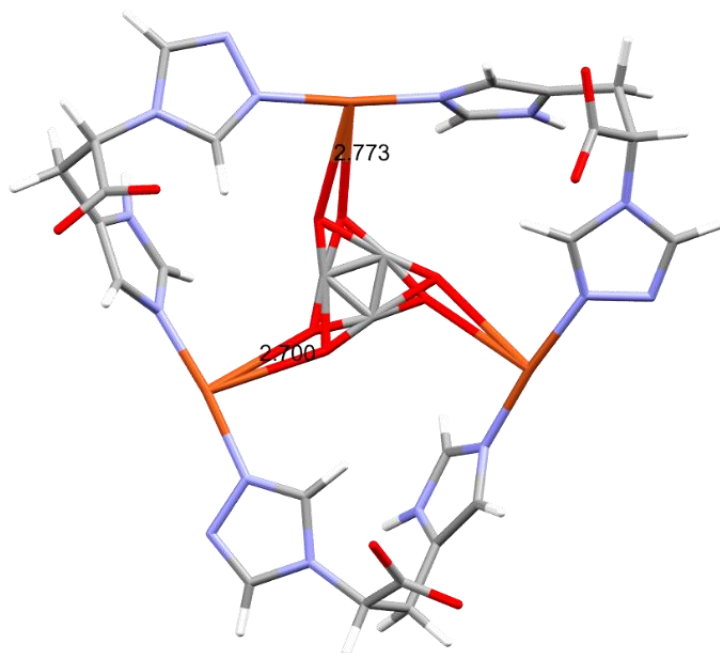
Figure 59. Interaction of a disordered CO_2 molecule (displayed as a triangle) inside a trinuclear Cu^{2+} pore of TAMOF-1. The distances are shown in black.

---

[128] Sears, V. F. *Neutron News* **1992**, *3*, 26-37.

TAMOF-1: Optimisation of the Synthesis and Structural and Morphological Studies

The occupation of the CO_2 molecule is disordered over 3 positions, which means that each CO_2 molecule is bonded to two Cu^{2+} centres, hence it appears as a triangle. This is in agreement with the trinuclear pore structure as there is no space left for another CO_2 molecule.

At room temperature, CO_2 appears delocalised due to thermal energy, which could indicate that CO_2 molecules moves through the channels instead of occupying a fixed position in the pores. We can observe that the activation at 400 K was successful since there are no H_2O molecules in the axial positions, as previously seen in X-ray diffraction. The Cu–O distances are between 2.700 and 2.773 Å, as shown in **Figure 59**. The crystallographic data can be found in **ANNEX I**.

1.3.5. Incorporation of metallic NPs inside TAMOF-1 pores

The Cu^{2+} centres in TAMOF-1 cannot participate in the catalytic process due to the fact that the oxidation state needs to be 2+ to maintain structural integrity.

The benefit of TAMOF-1 is that having a porous material with such a high micropore area (up to 1200 m^2 g^{-1}) allows us to do some modifications, like adding metallic NPs in the structure to expand or modify TAMOF-1's catalytic properties. The addition of catalytically active NPs inside TAMOF-1's chiral channels would lead to new enantioselective catalysts that could be used to synthesise enantioenriched products.

In this section, we explore the synthesis of several metal NPs, their incorporation inside TAMOF-1 structure and their activity in enantioselective catalysis.

1.3.5.1. Pt^0 nanoparticles

Our studies began by attempting to incorporate Pt NPs into TAMOF-1 channels. The synthesis of Pt^0-PVP protected NPs was performed by following a well-established method in the bibliography where hexachloroplatinic acid is used as a starting material (**Scheme 10**).[129] This method uses ethylene glycol as a reducing agent, also called the polyol method.[130]

[129] Xiao, J.-D.; Shang, Q.; Xiong, Y.; Zhang, Q.; Luo, Y.; Yu, S.-H.; Jiang, H.-L. *Angew. Chem. Int. Ed.* **2016**, *55*, 9389-9393.
[130] Fiévet, F.; Ammar-Merah, S.; Brayner, R.; Chau, F.; Giraud, M.; Mammeri, F.; Peron, J.; Piquemal, J. Y.; Sicard, L.; Viau, G. *Chem. Soc. Rev.* **2018**, *47*, 5187-5233.

$$H_2PtCl_6 \xrightarrow[\substack{\text{ethylene glycol} \\ 180\ °C,\ 10\ min}]{PVP} Pt^0$$
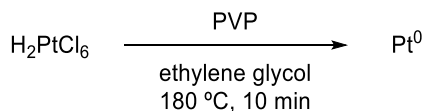
Scheme 10. Synthetic scheme of Pt^0 nanoparticles.

PVP as protecting agent has two advantages: the control of the NP size and the prevention of aggregate formation.[131] After synthesis, the NPs were precipitated and dispersed in water. Particle size distribution was measured by DLS and was found to be centred at 10 nm, ranging from 2 to 40 nm.

To incorporate the as-synthesised particles inside TAMOF-1 crystals, we followed the same crystallisation method described in page **49** but saturating the crystallisation media with NPs. Once the crystals grew to the desired size (0.1-0.5 mm), by comparing the shape and colour of the single crystals with the TAMOF-1 ones, visual analysis evidenced that NPs were introduced on or into the crystallites (**Figure 60**).

Figure 60. Visual difference of TAMOF-1 crystals (right) and Pt@TAMOF-1 (left).

To confirm the incorporation of the Pt NPs inside the TAMOF-1 crystals, we analysed the crystals by FESEM, TEM and microanalysis by EDX. Analysis by FESEM showed the morphology of the crystals (**Figure 61**), but the Pt NPs could not be adequately observed. Whilst the physical observation could not be possible, microanalysis by EDX (**Table 3**) revealed the presence of Pt on or into the channels of the aforenoted crystal.

---

[131] Koczkur, K. M.; Mourdikoudis, S.; Polavarapu, L.; Skrabalak, S. E. *Dalton Trans.* **2015**, *44*, 17883-17905.
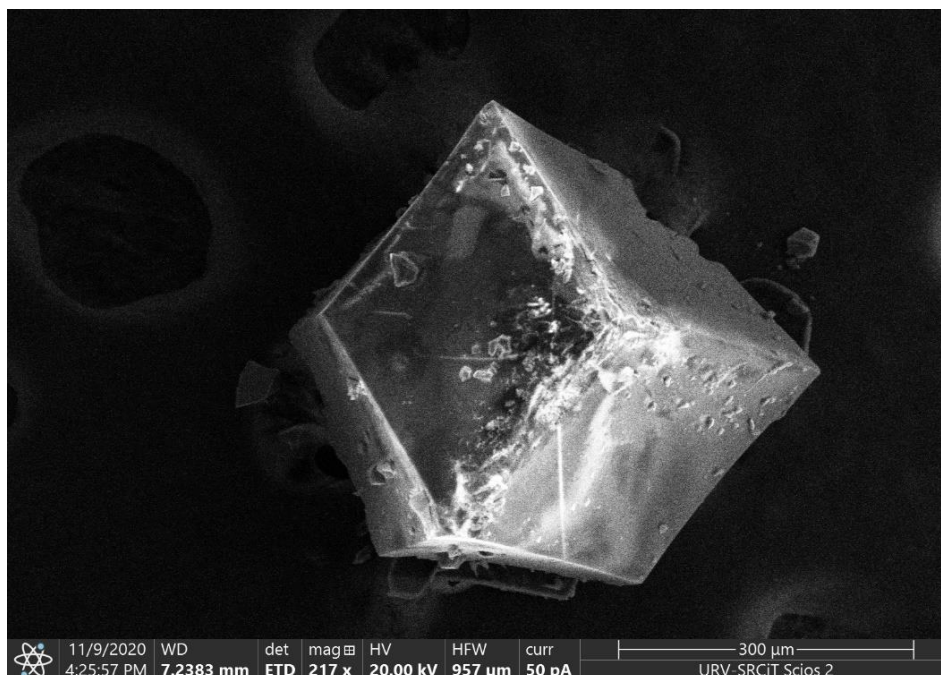
Figure 61. FESEM image of the Pt@TAMOF-1 monocrystal. *The shiny areas in the crystal are charged zones due to the poor conductivity of the sample.*

Table 3. Weight% and atomic% of Cu and Pt in Pt@TAMOF-1.

Element	Weight%[a]	Atomic%[a]
Cu	34.74	10.33
Pt	2.95	0.29

[a] Microanalysis performed with a FEI ESEM Quanta 600 equipped with EDX.

Although microanalysis by EDX showed the presence of Pt in the crystal, this technique is not accurate enough to give exact information about the weight% and atomic%. Furthermore, the concentration of Pt NPs in different areas could be different. Finally, to physically observe the Pt NPs, the sample was analysed by TEM, where we could confirm the presence of the nanoparticles inside TAMOF-1 (**Figure 62**). Moreover, this microscopy technique allowed us to measure the nanoparticle size (**Figure 63**).
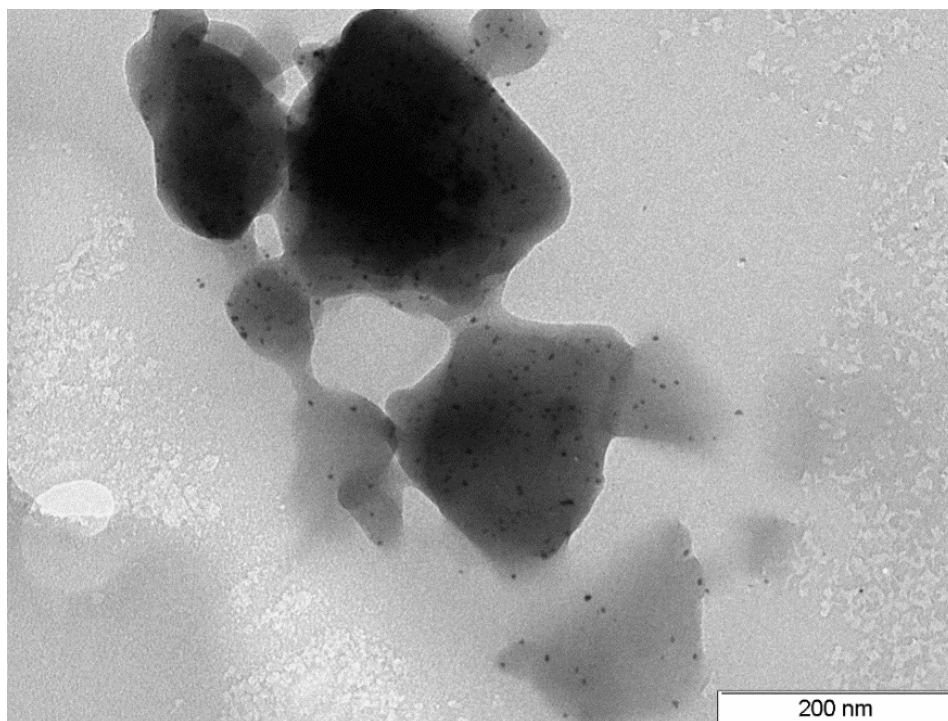
Figure 62. TEM image of Pt@TAMOF-1. The black dots are the Pt NPs. The image was taken at 150k magnification.
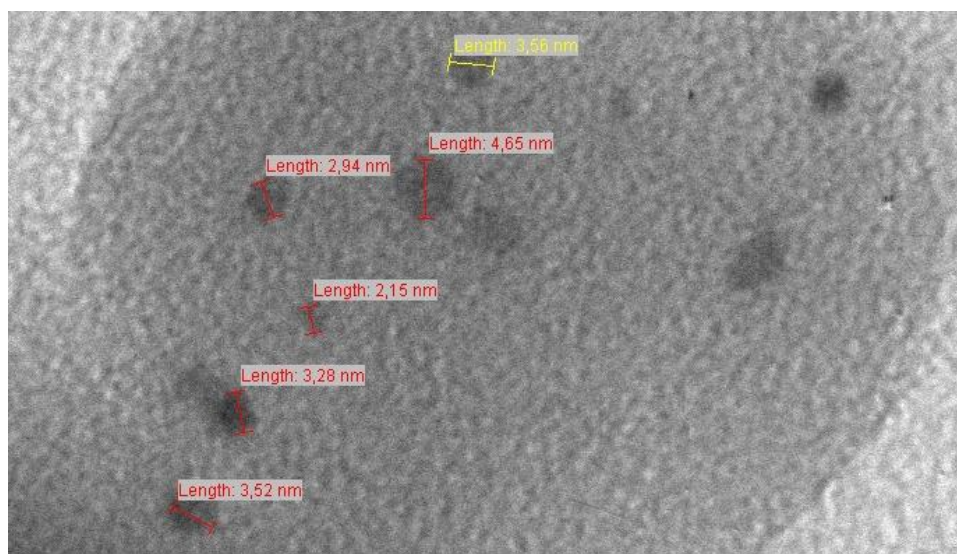
Figure 63. Measurement of the Pt NPs size. The size of the NPs was found to be between 2-5 nm approximately. The image was taken at 800k magnification.

63

TAMOF-1: Optimisation of the Synthesis and Structural and Morphological Studies

To assess the effect of the Pt NPs trapped in the pores of TAMOF-1, we measured the permanent porosity of Pt@TAMOF-1 by N_2 adsorption/desorption at 77 K (**Figure 64**). The multipoint BET in this material was 380 $m^2 \, g^{-1}$, which is ~40% of the BET in unmodified TAMOF-1, and the micropore volume of 0.14 $cm^3 \, g^{-1}$, also ~40% of the unmodified TAMOF-1 pore volume. Even though the surface area was notably compromised by the incorporation of the NPs, X-ray analysis of the Pt@TAMOF-1 crystal structure revealed no significant structural changes compared with unmodified TAMOF-1 (**Table 39**).
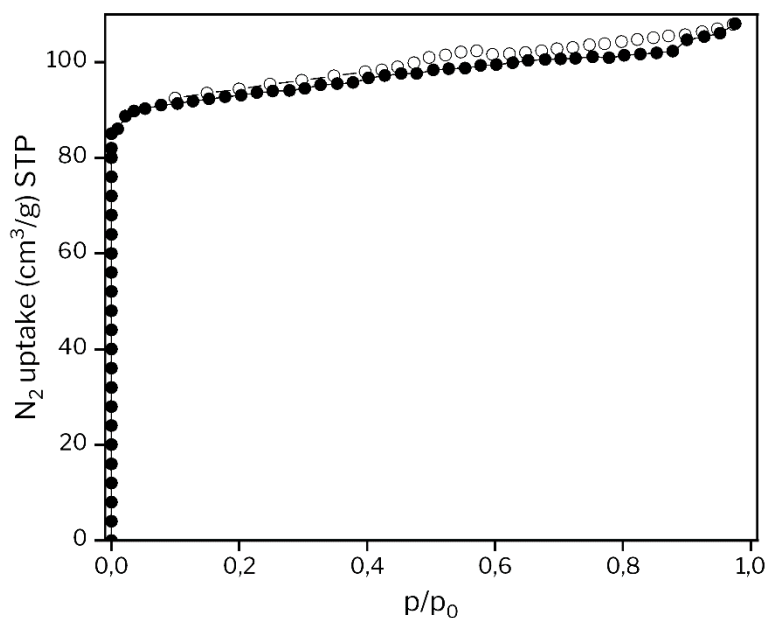
Figure 64. N_2 adsorption/desorption isotherm for Pt@TAMOF-1 at 77 K.

In conclusion, Pt NPs have been synthesised and successfully incorporated inside TAMOF-1 as visually observed and by EDX. With the aim of creating a broader collection of NP@TAMOF-1 materials with different catalytic properties, we studied the incorporation of NPs of other metals to TAMOF-1.

1.3.5.2. Rh⁰ nanoparticles

For the synthesis of Rh^0 NPs, we followed the same method and conditions than those described for Pt^0 NPs (see page **60** for details). In this case, the starting material was rhodium^{2+} acetate dimer (**Scheme 11**).

$$Rh_2(OAc)_4 \xrightarrow[\substack{\text{ethylene glycol} \\ 180\ ^\circ C,\ 10\ \text{min}}]{PVP} Rh^0$$
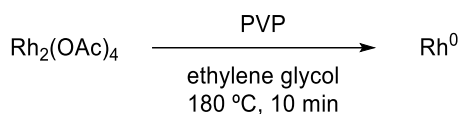
Scheme 11. Synthesis of Rh^0-PVP nanoparticles.

We repeated the same procedure to incorporate the Rh NPs inside TAMOF-1 crystals, but this time the resulting material was left to crystallise one month. The colour of the crystals was less dark than Pt@TAMOF-1, indicating that the incorporation could have been poorer.

The morphology of Rh@TAMOF-1 was observed by FESEM (**Figure 65**), and incorporation of the Rh NPs was confirmed by TEM (**Figure 66**). In this case, the presence of Rh could not be detected by microanalysis by EDX, probably due to a lower concentration of NPs inside the crystals.

Chapter I
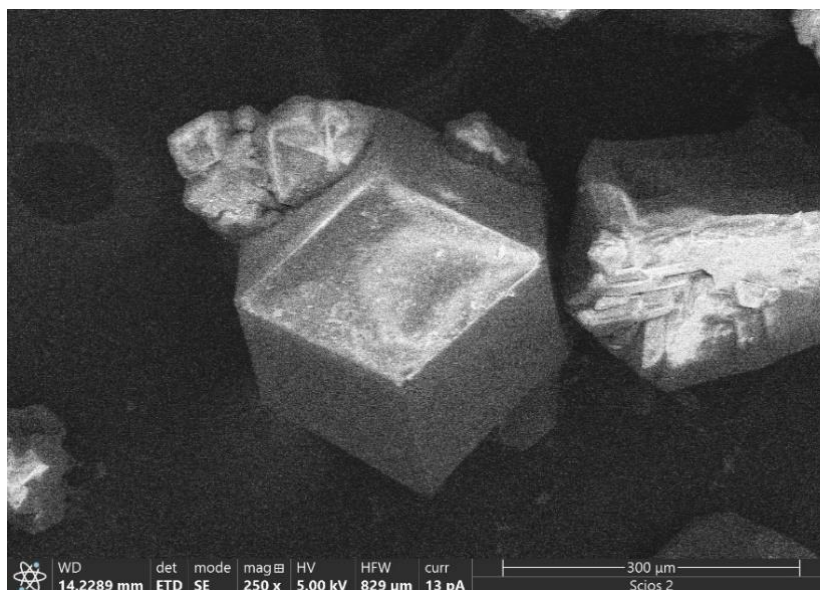
Figure 65. FESEM image of the Rh@TAMOF-1 monocrystal. *The shiny areas in the crystal are charged zones due to the poor conductivity of the sample.*

TAMOF-1: Optimisation of the Synthesis and Structural and Morphological Studies
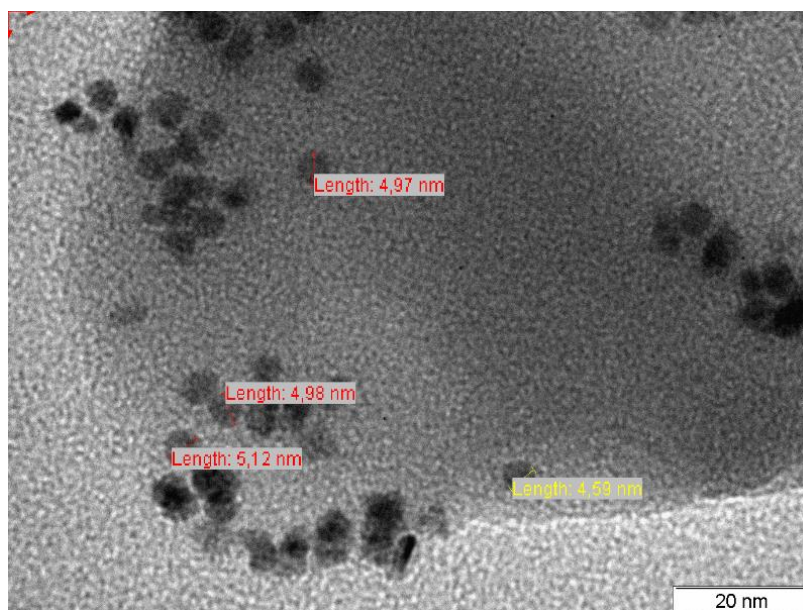
Figure 66. Measurement of the Rh NPs size. The size of the NPs was found to be 5 nm approximately. The image was taken at 1000k magnification.

1.3.5.3. Preliminary catalytic tests with NPs@TAMOF-1

As we successfully incorporated Pt and Rh NPs inside the porous structure of TAMOF-1, we wanted to test its potential as enantioselective heterogeneous catalyst for transformations like hydrogenations (Pt) or hydroformylations (Rh).

We started by trying the hydrogenation of a double bond with the naked NPs to assess their catalytic activity. The selected molecule was methyl 2-acetamidoacrylate **1** (**Figure 67**).
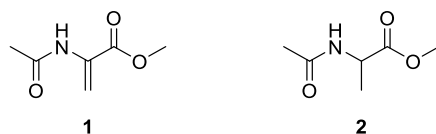
Figure 67. Structure of methyl 2-acetamidoacrylate (**1**) and methyl acetylalaninate (**2**).

The hydrogenation was conducted in a high-pressure parallel HEL reactor. The solvents selected for the trial were THF and DCM, and the reaction was performed overnight (**Table 4**).

Table 4. Hydrogenation results of **1** with Pt NPs.

Solvent	Cat. (mg)	Conv. (%)[a]
THF	0.5	63.3
DCM	0.5	>95%

Reaction conditions: Pt NP (0.5 mg), **1** (0.1 mmol), 0.5 mL solvent, 30 bar H_2, 16 h. [a] Conversion was calculated by ^{1}H-NMR without internal standard.

Since there was conversion towards **2**, **1** was subjected to hydrogenation conditions using Pt@TAMOF-1 (1, 5 and 10 wt%) as catalyst under the same conditions used for the Pt NPs. Sadly, **2** was not observed under the conditions above.

The reason why Pt@TAMOF-1 is not a good heterogeneous hydrogenation catalyst might be the pore size and BET surface area, which decreased both in Pt@TAMOF-1 crystals with respect to the as-synthesised TAMOF-1 material. As the catalytic studies with Pt@TAMOF-1 were unsuccessful, this research was discontinued.

1.3.6. Monolithic TAMOF-1 (*mono*TAMOF-1)

The sol-gel synthesis of *mono*MOFs usually requires of particle sizes lower than 100 nm, although larger particles could also form *mono*MOFs. The reason is that shape is crucial in the formation of monoliths where spherical particles are more suitable to lead to monoliths, and these shapes can be obtained in small particles at the beginning of the nucleation process. In the typical synthetic schemes for the obtention of MOFs, particles grow up to the μm scale (in TAMOF-1, the average particle size is 1-10 μm), therefore the level of crystallisation needs to be decreased to obtain smaller particle sizes.

In collaboration with Prof. Fairén-Jimenez's group in University of Cambridge, we explored the synthesis of *mono*TAMOF-1. Several methods were proposed for the reduction of the particle size:

- **Change L/M ratio:** excess of one of the two components of the reaction could make the nucleation process faster, thus promoting multiple nucleations instead of crystallisation due to the excess of one of the reactants.

Chapter I

67

UNIVERSITAT ROVIRA I VIRGILI
INSIGHTS IN HOMOCHIRAL METAL-ORGANIC FRAMEWORKS: FROM THEIR SYNTHESIS TO ENANTIOSELECTIVE
APPLICATIONS
Juanjo Cabezas Gimenez

TAMOF-1: Optimisation of the Synthesis and Structural and Morphological Studies

- **Change the metal counteranion:** substituting the acetate salt for SO_4^{2-}, Cl^-, NO_3^- or BF_4^- could drastically change the outcome of the reaction due to a change in the system's pH. Furthermore, electronic attractions between ligands and metals can be affected by this change.

- **Change in the solvent:** increasing the solvent's polarity prevents the growth of primary particles. As the synthesis solvent is water, the polarity cannot be increased substantially. Increasing the viscosity can also prevent the growth of primary particles.

- **Changes in the temperature:** decreasing the reaction temperature could make nucleation slower.

- **Use of modulators:** adding a "quenching" reagent could help the process stop in small particle sizes. There are two types of modulators:

  1. **Ligand modulators:** the use of molecules similar to the ligand could create a competing environment, where presence of these can hinder the interaction between the ligand and the metal. These modulators must be related to the ligand; therefore, we decided to use 4H-1,2,4-triazole and imidazole (the two coordination moieties of TAMOF-1) as ligand modulators.

  2. **pH modulators:** changes in the pH can change the protonation state of the ligand, limiting the kinetics of the reaction and yielding smaller particles.

Aside of the aforementioned changes in the reaction process, the critical step in the synthesis of monoliths is to stop the reaction as soon as the primary particles precipitate to achieve optimal particle sizes (nm scale). This is a challenge with TAMOF-1 because the precipitation takes place fast (~10 min). In a general way, the reactions were stopped as soon as the precipitate was clearly observed, unless otherwise indicated.

Amidst all the conditions mentioned above, we observed an apparent change in the morphology by adding different solvents to the reaction mixture, by using acid/base modulators, and by changing the reaction temperature. These reactions follow the same general experimental procedure, which is described in the Experimental Section (page **84**).

68

1.3.6.1. Changes in the solvent

Among the solvents tried in the synthetic screening, DMF and *t*-BuOH yielded morphologically different materials.

In terms of changing the polarity of the reaction, the addition of DMF to the *S*-HTA solution yielded a compact pellet with upper glassy surface, although it seemed powder-like in the bottom. This pellet was named **M1** (**Figure 68**), and albeit visually resembled TAMOF-1, we confirmed the isostructurality by comparing their PXRD patterns (**Figure 69**).

Figure 68. Morphology of **M1** pellet.

2θ (°)
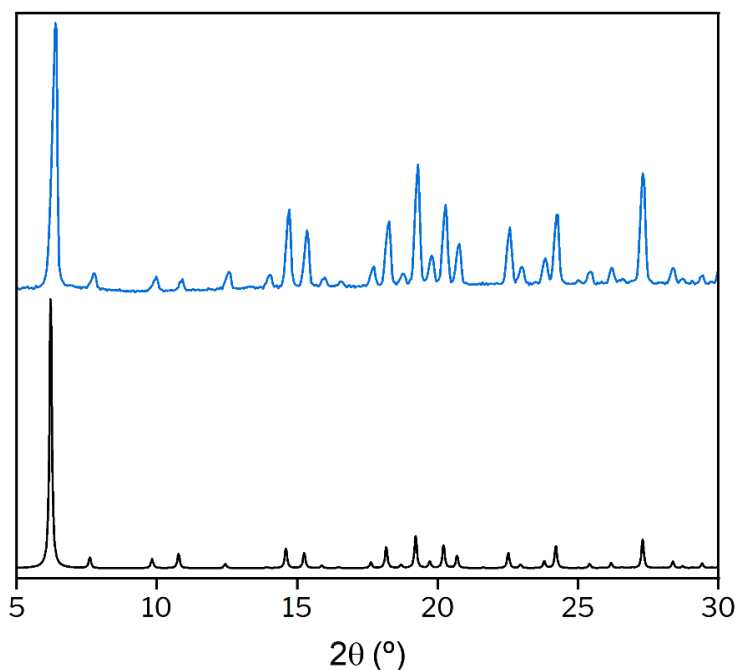
Figure 69. Comparison of the simulated (black) and **M1** (blue) PXRD patterns.

TAMOF-1: Optimisation of the Synthesis and Structural and Morphological Studies

We observed by SEM imaging that the morphology of the particles is cubical, as TAMOF-1 powder (**Figure 70**). Measurement of the particle size by SEM exhibited an average size of **0.63 ± 0.31 μm** (**Figure 71**), which is a substantial reduction of the particle size compared to the original TAMOF-1.
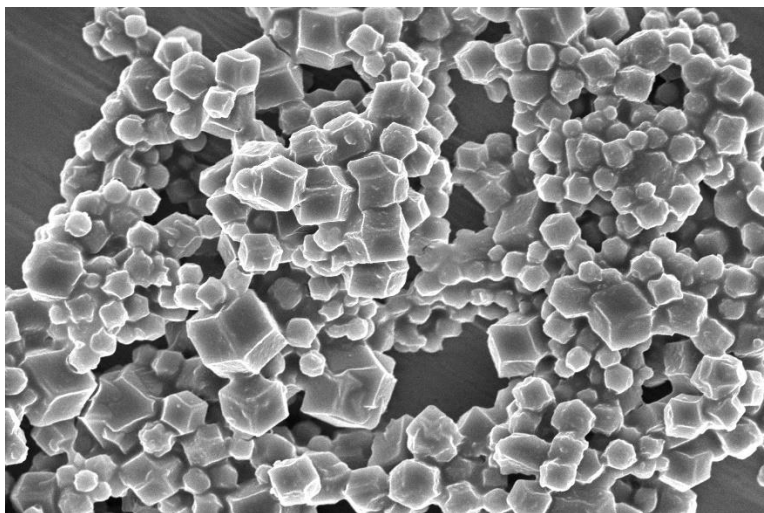
Figure 70. SEM image of **M1**. Scale: 5 μm.
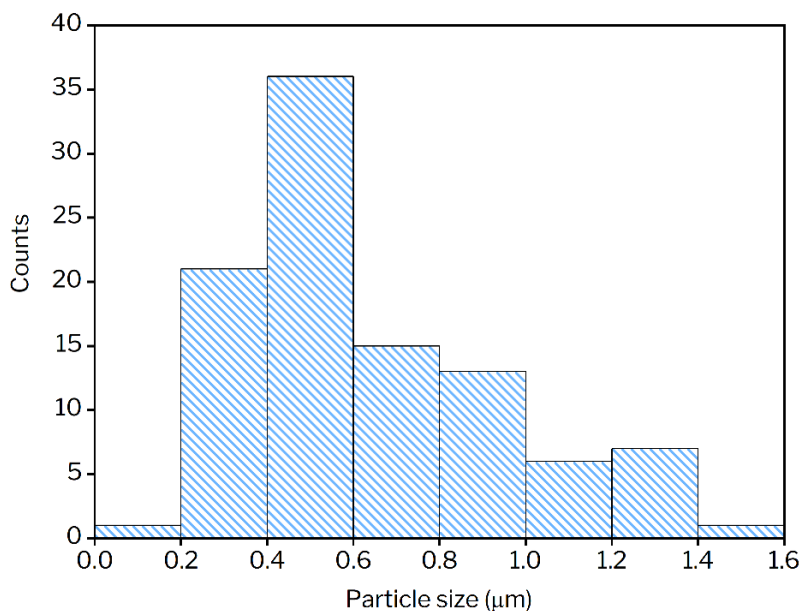
Figure 71. Particle size distribution of **M1**.

70

The N_2 adsorption isotherm showed a slight growth of the mesoporosity that is not observed in TAMOF-1 powder (**Figure 72**). This means that the packing is relatively improved. The BET surface area of **M1** is 835 m^2 g^{-1}.
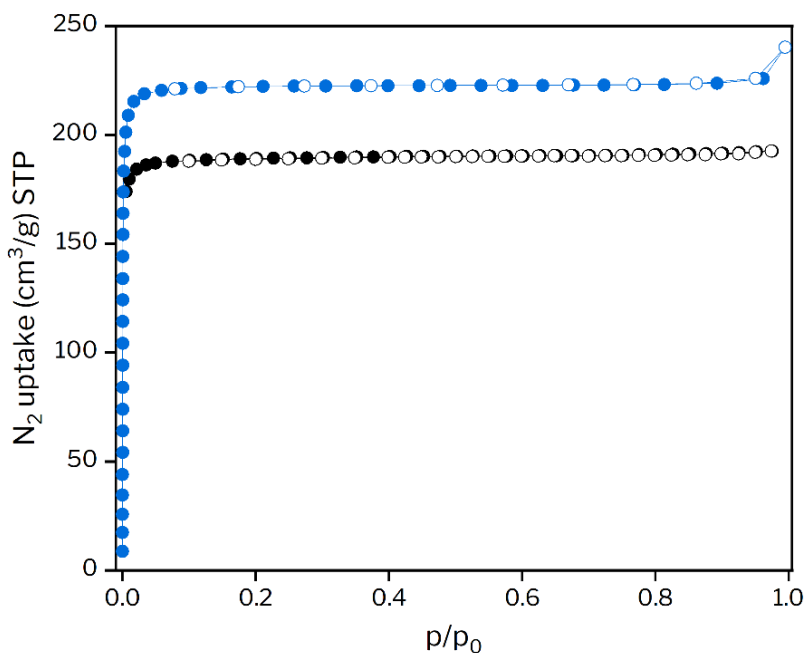
Figure 72. Comparison of the N_2 adsorption profiles of the original TAMOF-1 (black) and **M1** (blue). Hollow circles represent the desorption isotherms.

Changes in the viscosity of the reaction yielded a completely different material. The addition of *t*-BuOH to the *S*-HTA solution yielded a glassy deep-blue pellet named **M2** (**Figure 73**).
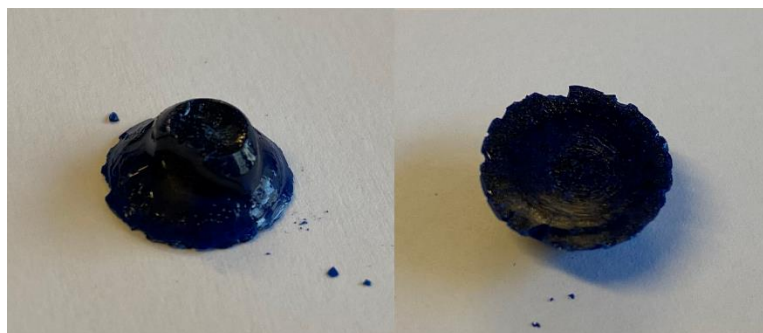
Figure 73. Morphology of **M2** pellet.

Chapter I

71

UNIVERSITAT ROVIRA I VIRGILI
INSIGHTS IN HOMOCHIRAL METAL-ORGANIC FRAMEWORKS: FROM THEIR SYNTHESIS TO ENANTIOSELECTIVE
APPLICATIONS
Juanjo Cabezas Gimenez

TAMOF-1: Optimisation of the Synthesis and Structural and Morphological Studies

PXRD analysis concluded that it was isostructural to TAMOF-1, although the intensity of the peaks in **M2** is different (**Figure 74**). SEM images showed that this material was morphologically different from the previously obtained (**Figure 75**), which hindered the proper particle size measurement. N_2 adsorption isotherm showed no porosity.
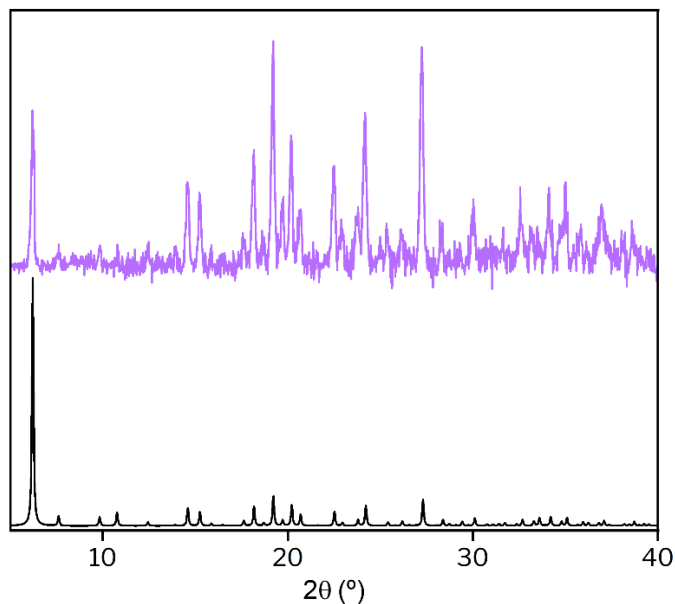
Figure 74. Comparison of the simulated (black) and **M2** (purple) PXRD patterns.
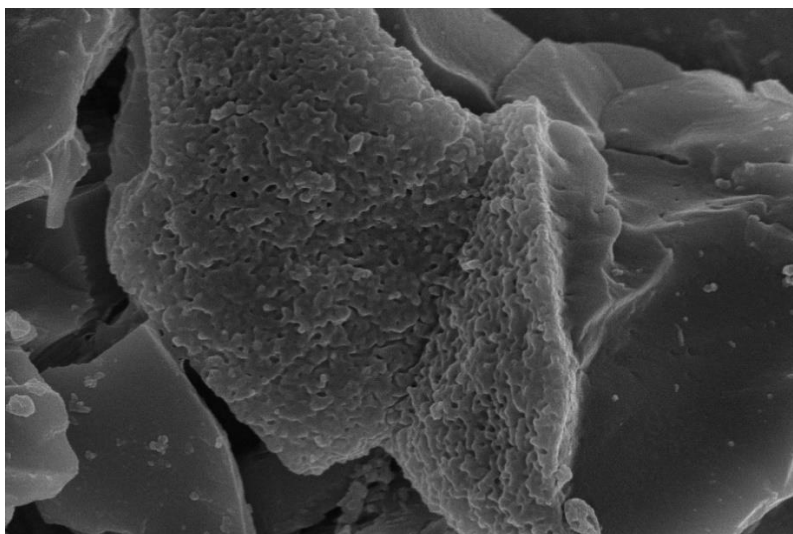
Figure 75. SEM image of **M2**. Scale: 1 μm.

72

1.3.6.2. Acid/base modulators

As previously commented in page **52**, the obtention of TAMOF-1 is limited to the acetate salt of Cu^{2+}. Therefore, we used AcOH and NaOAc as acidic and basic modulators, respectively. The experimental procedure is analogous to the previous one, where the modulator is added to the ligand solution.

Adding AcOH, with concentrations ranging from 0.05 to 1 M, yielded TAMOF-1 pellets morphologically similar to **M1**. We selected for characterisation the pellet obtained using 0.5 M AcOH, named **M3**. Isostructurality was confirmed by PXRD (**Figure 76**).
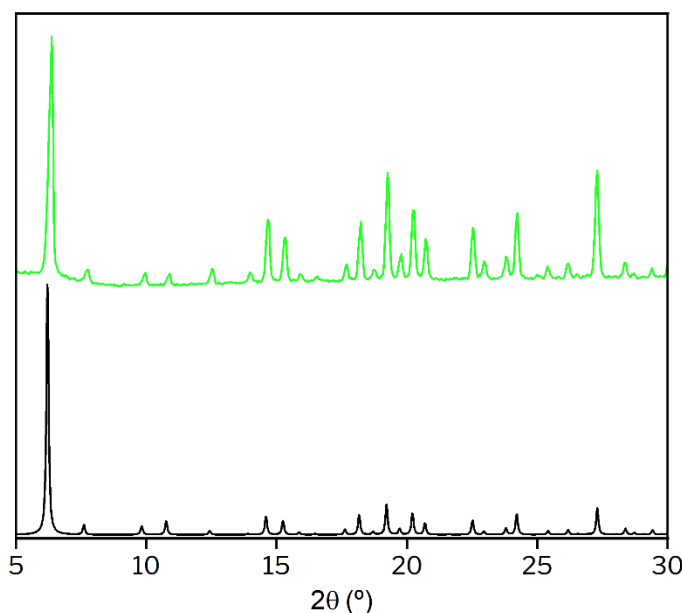
Figure 76. Comparison of the simulated (black) and **M3** (green) PXRD patterns.

SEM images showed that the presence of AcOH affected the morphology of TAMOF-1. Although it is isostructural by PXRD, no cubic particles could be observed (**Figure 77**). Due to there is not homogeneity in the particle shape, we did not measure the particle size.

TAMOF-1: Optimisation of the Synthesis and Structural and Morphological Studies
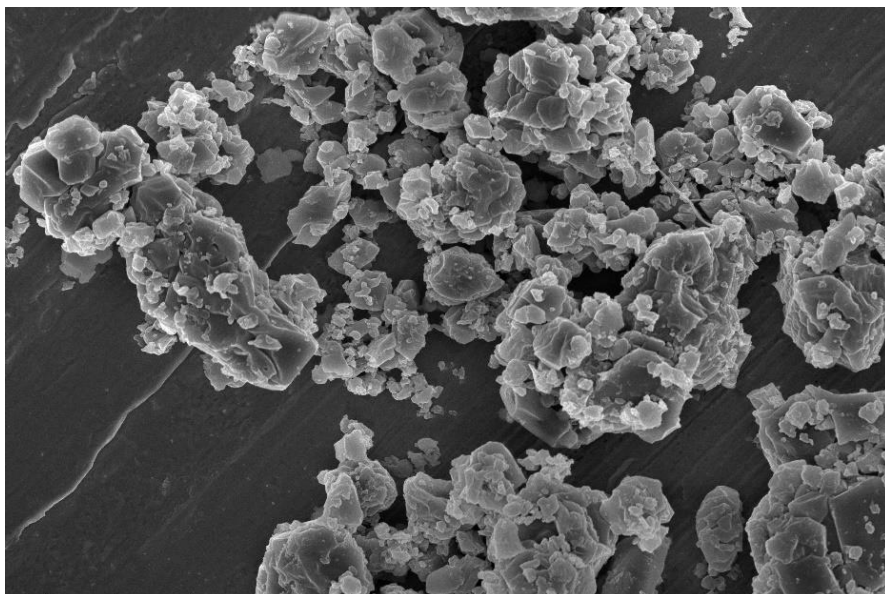
Figure 77. SEM image of **M3**. Scale: 5 μm.

The use of this acidic modulator did not improve the packing, as it was seen by the N_2 adsorption isotherm, where no mesoporosity was observed and the BET surface area was decreased to 700 m^2 g^{-1} (**Figure 78**).
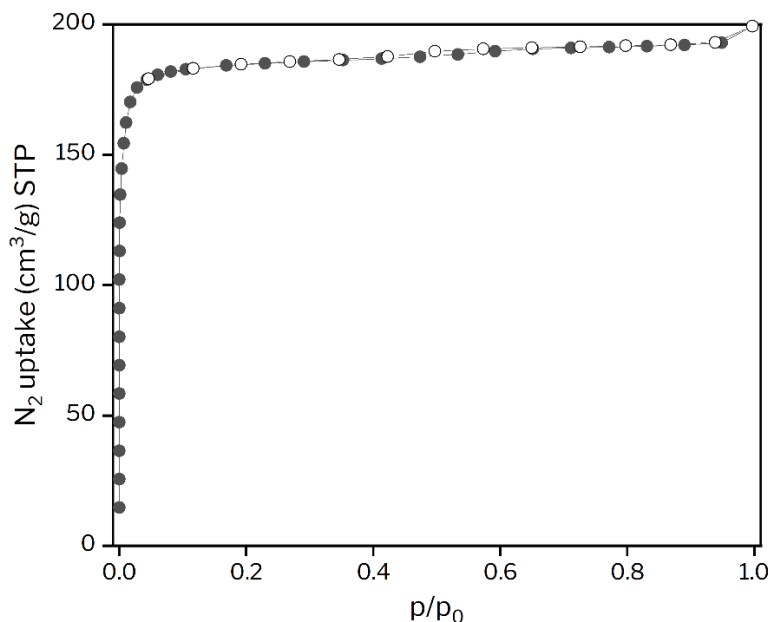
Figure 78. N_2 adsorption/desorption isotherm of **M3**.

74

Moving to the use of the basic modulator NaOAc, the same concentration conditions were used as in AcOH. In this case, the product precipitated instantly using 0.5 M, with a morphology similar to **M2** (**Figure 79**). This compound was named **M4**.

Figure 79. Morphology of **M4** pellet.

M4 was visually related to **M2**. Likewise, we found that the structure was indeed the one of TAMOF-1 (**Figure 80**). Analogously, we observed that the structure is non-porous by its N_2 adsorption isotherm.
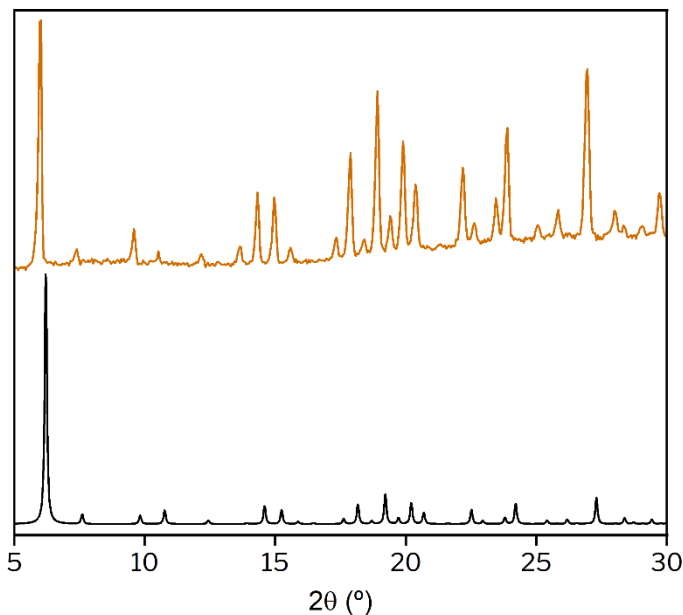
Figure 80. Comparison of the simulated (black) and **M4** (orange) PXRD patterns.

75

1.3.6.3. Modification of the temperature

Finally, we analysed the role of the reaction temperature in the nucleation process. Following the general synthetic procedure at 0 °C, we obtained a pellet with a glassy surface named **M5** (**Figure 81**).
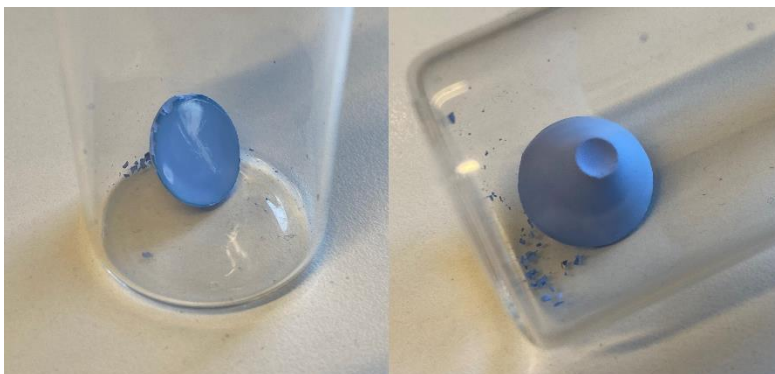
Figure 81. Morphology of **M5** pellet.

As in the previous examples, structure confirmation was performed by PXRD comparison (**Figure 82**).
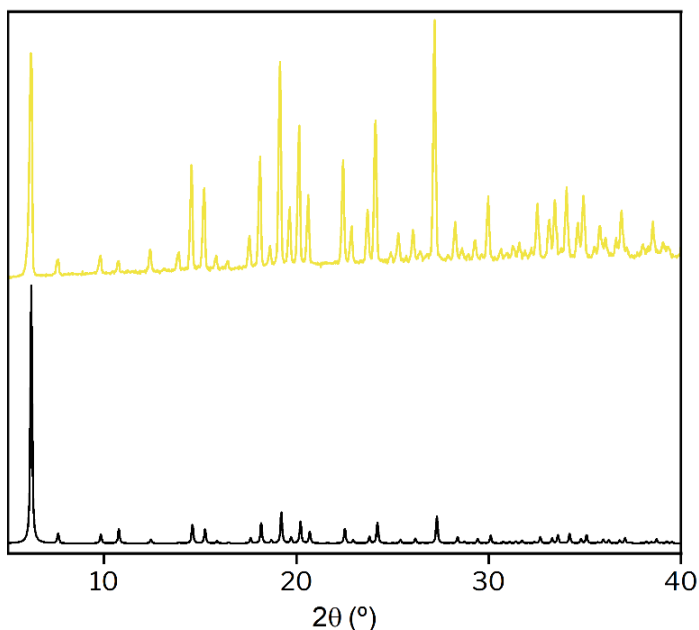
Figure 82. Comparison of the simulated (black) and **M5** (yellow) PXRD patterns.

The increased glassiness of **M5** indicates that better packing has occurred. As observed in the N_2 adsorption/desorption isotherm, mesoporosity was notably increased compared to **M1** (**Figure 83**).
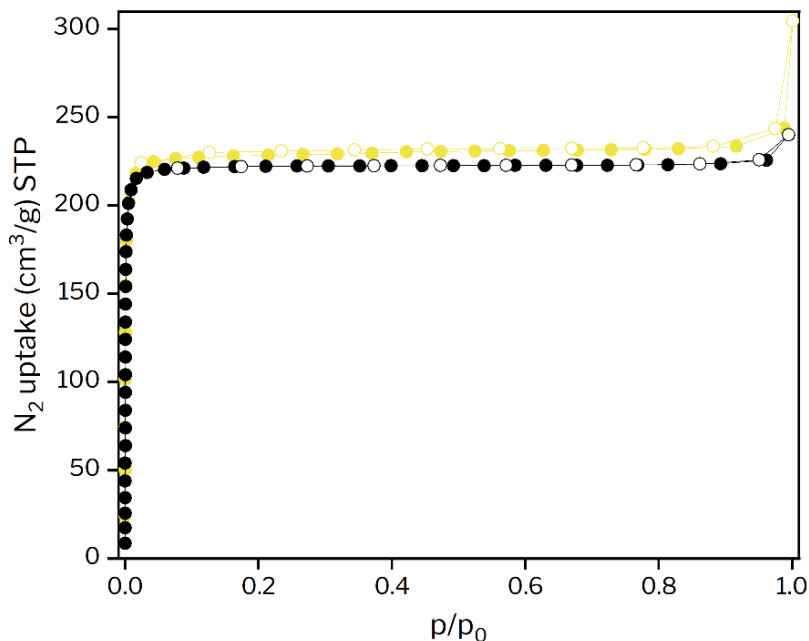
Figure 83. Comparison of the N_2 adsorption/desorption isotherm of **M5** (yellow) and **M1** (black).

Having seen that the mesoporosity is increased, this could mean that smaller particle size has been obtained in this synthetic procedure. SEM images showed us that the particle size was drastically decreased to nanometre scale, where the average particle size is **375 ± 120 nm** (**Figure 84**). The morphology of the particles is cubical, such as **M1**.

Chapter I

UNIVERSITAT ROVIRA I VIRGILI
INSIGHTS IN HOMOCHIRAL METAL-ORGANIC FRAMEWORKS: FROM THEIR SYNTHESIS TO ENANTIOSELECTIVE
APPLICATIONS
Juanjo Cabezas Gimenez

TAMOF-1: Optimisation of the Synthesis and Structural and Morphological Studies
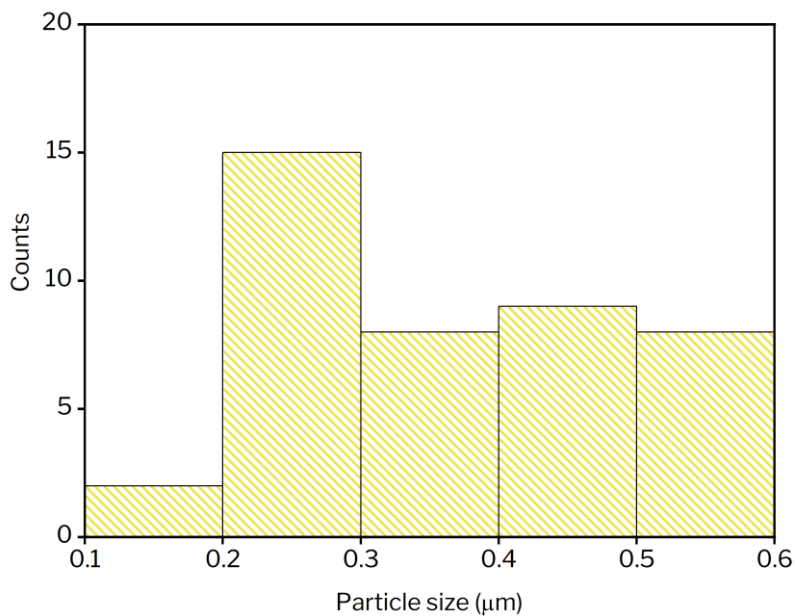
Figure 84. Particle size distribution of **M5**.

1.4. CONCLUSIONS

In conclusion, the synthesis and crystallisation of TAMOF-1 have been reproduced. The optimisation of the synthesis has been explored to control the particle size, and it was found that there is a correlation between the particle size and the BET surface area – the smaller the particles, the greater the area.

The study of the pH in the synthesis of TAMOF-1 allowed us to conclude that the ligand must be in zwitterionic form for precipitation to occur. The synthesis of TAMOF-1 may be limited to the use of $Cu(OAc)_2 \cdot H_2O$ due to the role of the acetate ion as a buffer, which captures the released proton from *S*-HTA and maintains the pH of the system to allow the reaction to happen.

The obtention of crystals up to mm scale allowed us to carry out neutron diffraction studies to identify the interaction of CO_2 with the trinuclear Cu^{2+} pore. Each trinuclear pore can host a CO_2 molecule though Cu–O interactions.

TAMOF-1 has been modified by incorporating metallic NPs in its structure (Pt and Rh), confirmed by TEM and FESEM-EDX. Preliminary catalytic trials showed that Pt@TAMOF-1 was inactive in the hydrogenation of a functionalised alkene.

Finally, among several reaction conditions tried to obtain a monolithic structure, decreasing the reaction temperature down to 0 ºC allowed us to obtain a TAMOF-1 pellet with increased mesoporosity and smaller particle size, which settles a precedent for the formation of TAMOF-1 monoliths, although this process requires further investigation.

Chapter I

79

TAMOF-1: Optimisation of the Synthesis and Structural and Morphological Studies

1.5. EXPERIMENTAL SECTION

1.5.1. Materials and general

All syntheses were carried out on chemicals purchased from commercial sources unless otherwise indicated. Air and moisture sensitive manipulations or reactions were run under inert atmosphere using anhydrous solvents and Schlenk techniques. All solvents were purchased commercially anhydrous or dried using a Solvent Purification System (SPS). NMR spectra were recorded in D_2O and $CDCl_3$ as solvent on a Bruker Advance 300, 400 or 500 MHz Ultrashield spectrometers. ^1H and ^{13}C-NMR chemical shifts are quoted in ppm relative to residual solvent peaks. Data for ^1H-NMR are given as follows: chemical shift, multiplicity (s = singlet, d = doublet, t = triplet, m = multiplet, dd = doublet of doublets, tt = triplet of triplets), coupling constants and intensities. High-resolution mass spectra (HRMS) were recorded by using ESI as ionization method in positive mode. IR spectra were recorded using Attenuated Total Reflection (ATR) spectroscopy. Specific optical rotation ($[\alpha]_\lambda^T$) was recorded using a Jasco P1030 Polarimeter with a wavelength of 589 nm (sodium, D line) at 25 ºC in the corresponding solvent, in a 10 cm cell, unless otherwise indicated. Crude mixtures of the hydrogenation were analysed by ^1H-NMR and HPLC chromatography with an Agilent 1200 Series system equipped with a diode array detector. TGA was performed in a thermogravimetric balance Mettler Toledo TGA/SDTA851. FESEM images were acquired using a Scios 2 from FEI Company equipped with an X-ray detector for EDX analysis. TEM images were acquired using a Transmission Electron Microscope JEOL 1100. Powder X-ray diffraction analysis was performed using a Bruker Apex II Duo Single Crystal Diffractometer. Particle size distributions were measured using ImageJ software.[132]

1.5.2. Crystallography

1.5.2.1. X-ray diffraction

X-ray single-crystal diffraction data of TAMOF-1 were collected at 100(2) K (as prepared), 298 K, 403 K, and again at 100(2) K (rehydrated) on a Bruker APEX duo diffractometer with an APEX II CCD detector using Mo Kα (λ = 0.71073 Å) and equipped with an Oxford Cryostream 700 plus. Crystal

---

[132] Schneider, C.A.; Rasband, W.S.; Eliceiri, K.W. *Nat. Methods* **2012**, *9*, 671-675.

structure solution was obtained using SIR2011,[133] and refinement was performed using SHELXL21 v. 2018/3 under the ShelXle (Rev. 912) interface.[134] All non-hydrogen atoms were refined anisotropically. Crystallographic data have been deposited at the Cambridge Crystallographic Database Centre, with deposition numbers 1898811 (as-prepared, 100 K), 1898970 (298 K), 1898969 (404 K), and 1898971 (100 K, rehydrated).

1.5.2.2. Neutron diffraction

The experiments were carried out at the Institut Max Von Laue - Paul Langevin (ILL), located in Grenoble (France). The instrument used was a thermal neutron diffractometer for single-crystal and fibre diffraction (D19). The instrument was operated with a wavelength of 1.4556(1) Å, provided by a flat Cu(220) monochromator (at $2\theta M = 69.91°$ take-off angle). The measurement strategy consisted of a series of five ω-scans with steps of 0.07° at different χ and φ positions. The acquisition time was *ca.* 45s step^{-1}, which corresponds to 500000 counts on the instrument monitor. The data collection was performed using the instrument control program NOMAD from ILL. Indexing and unit-cell determination were done using the programs PFIND and DIRAX.[135] The integration of the raw data and refinement of the UB-matrix, including the off-sets, were done using the programs RETREAT[136] and RAFD19, respectively; the Lorentz correction was applied to the intensities. XABS2[137] was used for the absorption correction. The structure was refined with SHELX 2018.3.[138]

The experiment setup was the following: the TAMOF-1 crystal was activated under a N_2 stream (400 K) for an hour. A drastic change of colour was observed on the single-crystal from sea-blue to dark blue. Then, the sample was cooled down to 100 K. Data collection was performed, and the resulting crystal structure confirmed that the TAMOF was activated. The N_2 stream was cut off, and a CO_2 stream (298 K) was passed through the activated crystal for 1 min, then immediately retaken to 100 K with a N_2 stream. A second data collection was carried out using the same acquisition sequence.

[133] Burla, M. C.; Caliandro, R.; Camalli, M.; Carrozzini, B.; Cascarano, G.L.; Giacovazzo, C.; Mallamo, M.; Mazzone, A.; Polidori, G.; Spagna, R. *J. Appl. Cryst.* **2012**, *45*, 351-356.
[134] Hubschle, C. B.; Sheldrick, G. M.; *J. Appl. Cryst.* **2011**, *44*, 1281-1284.
[135] Duisenberg, A. *J. Appl. Crystallogr.* **1992**, *25*, 92-96.
[136] Wilkinson, C.; Khamis, H.; Stansfield, R.; McIntyre, G. *J. Appl. Crystallogr.* **1988**, *21*, 471-478.
[137] Parkin, S.; Moezzi, B.; Hope, H. *J. Appl. Crystallogr.* **1995**, *28*, 53-56.
[138] Sheldrick, G. *Acta Crystallogr. C* **2015**, *71*, 3-8.

Chapter I

1.5.3. Synthetic procedures

1.5.3.1. Synthesis of *N,N*-dimethylformamide azine (DMFA)

Part 1: 150 mL of ice-cooled DMF were placed in a 250 mL three-neck round-bottom flask (RBF). Then, 28.6 mL of $SOCl_2$ (0.39 mol) were slowly added, and the reaction mixture was stirred for 24 h. After cooling to rt, a solution of 5 mL of $NH_2NH_2 \cdot H_2O$ (0.1 mol) in 15 mL of DMF was slowly added, and the reaction mixture was stirred at rt for 48 h. The precipitate was then filtered and washed with DMF (20 × 3 mL), Et_2O (10 × 3 mL) and dried in the air to yield 20.5 g (0.095 mol, 95% yield) of **DMFA·2HCl**. The solid was used in the next step without further purification.

Part 2: 20.5 g of **DMFA·2HCl** (0.095 mol) were dissolved in 100 mL of H_2O. Then, a solution of 10.6 g of Na_2CO_3 (0.1 mol) in 100 mL of H_2O was slowly added, and the desired product was purified by continuous extraction with 750 mL of Et_2O for 2 days. The organic layer was concentrated *in vacuo*, and 12.95 g of **DMFA** (0.09 mol, 96% yield) were obtained as an orange solid, which was used without further purification.[102]

1.5.3.2. Synthesis of (*S*)-3-(1H-imidazol-5-yl)-2-(4*H*-1,2,4-triazol-4-yl)propanoic acid (*S*-HTA)

DMFA (6.3 g, 0.044 mol) and L-histidine (3.1 g, 0.02 mol) were mixed together in 150 mL of EtOH and heated at reflux for 48 h. Unreacted L-histidine was filtered off from the reaction mixture, and the solvent was removed *in vacuo* to afford an orange gel that was washed with EtOH to yield a white precipitate of *S*-**HTA**, that was filtered, washed with EtOH (15 × 3 mL), Et_2O (15 × 3 mL) and dried in the air. Yield: 3.5 g (0.017 mol, 85%). Anal. Calcd for $C_8H_9N_5O_2$ (%): C, 46.38; H, 4.38; N, 33.80. Found: C, 46.36; H, 4.52; N, 33.78. MS-ESI (m/z): $[M + H]^+$ calcd for $C_8H_{10}N_5O_2$, 208.1; found, 208.1. **IR** (ATR, cm^{-1}): 1637, 1601, 1535, 1463, 1440, 1397, 1359, 1294, 1261, 1209, 1080, 1031, 1009, 971, 921, 872, 838, 796, 731, 710, 681, 647, 630, 483, 424. **¹H-NMR** (400 MHz, D_2O): δ (ppm) 8.54 (d, $J = 1.4$ Hz, 1H), 8.49 (s, 2H), 7.11 (s, 1H), 5.23 (dd, $J = 9.4, 5.4$ Hz, 1H), 3.63 (dd, $J = 15.7, 5.4$ Hz, 1H), 3.52 (dd, $J = 15.7, 9.4$ Hz, 1H). **¹³C-NMR** (101 MHz, D_2O): δ (ppm) 173.00 (C), 143.64 (CH), 133.79 (CH), 128.63 (C), 117.16 (CH), 60.14 (CH), 28.55 (CH$_2$). $[\alpha]^{25}_D = +4.64°$ (c = 0.74, H_2O).[102]

1.5.3.3. Synthesis of [Cu(H$_2$O)$_2$(S-TA)$_2$]·6H$_2$O (TAMOF-1)

Cu(OAc)$_2$·H$_2$O (0.48 g, 2.4 mmol) was dissolved in 50 mL of H$_2$O, and the resulting solution was slowly added to a 100 mL aqueous solution of *S*-HTA (1.0 g, 4.8 mmol). After 30 min, a blue polycrystalline powder appeared (TAMOF-1), and it was filtered with a Nylon membrane filter (pore size: 0.45 μm, Filter-Lab), washed with H$_2$O (50 × 3 mL), and dried in the air. Yield: 1.1 g (70%). Anal. Calcd for C$_{16}$H$_{32}$CuN$_{10}$O$_{12}$(%): C, 30.99; H, 5.2; N, 22.59. Found: C, 30.79; H, 4.83; N, 22.30. **IR** (ATR, cm^{-1}): 3289, 1615, 1532, 1495, 1395, 1355, 1263, 1242, 1211, 1180, 1116, 1087, 1015, 979, 891, 845, 752, 701, 660, 647, 549, 511, 472. Single crystals of TAMOF-1 were obtained by slow diffusion of Cu(CH$_3$COO)$_2$·H$_2$O and *S*-HTA solutions in an H-tube.[102]

1.5.3.4. Synthesis of TAMOF-1 crystals

To an H-cell equipped with a porous frit, *S*-HTA (400 mg, 1.92 mmol) was added in one side and Cu(OAc)$_2$·H$_2$O (193 mg, 0.96 mmol) in the other side. Then, H$_2$O (20 mL) was added to each side at the same time, and it was left to crystallise by slow diffusion for a week to obtain TAMOF-1 crystals. To obtain crystals of *ca.* 1 mm^3, the Cu(OAc)$_2$ side was heated at 40 ºC.

1.5.3.5. Synthesis of Pt and Rh NPs

H$_2$PtCl$_6$·6H$_2$O (50.75 mg, 0.098 mmol) or Rh$_2$(OAc)$_4$ (44.6 mg, 0.1 mmol) was dissolved in 20 mL of ethylene glycol (0.005 M) with 222 mg of poly(vinylpyrrolidone) (PVP, MW = 40000) in a two-necked RBF, and the reaction mixture was stirred at 180 ºC for 10 min. The as-synthesised PVP-protected NPs were precipitated by adding acetone and then collected by centrifugation (6000 rpm, 15 min). The solvent was decanted, the remaining NPs were cleaned with acetone and n-Hex and centrifuged again (6000 rpm, 10 min). The organic solvent was decanted, and the NPs were redispersed in water to give a colloidal dispersion of NPs (~1 mg mL^{-1}).[129]

1.5.3.6. Synthesis of Pt@TAMOF-1

In an H-cell, Cu(CH$_3$COO)$_2$·H$_2$O (300 mg, 1.5 mmol) was added in one compartment and *S*-HTA (623 mg, 3.01 mmol) in the other compartment. Then, a solution of Pt NPs was added to each compartment, and the resulting solutions were left to crystallise by slow diffusion for 14 days.

Chapter I

83

1.5.3.7. Synthesis of Rh@TAMOF-1

In an H-cell, $Cu(CH_3COO)_2 \cdot H_2O$ (300 mg, 1.5 mmol) was added in one compartment and *S*-HTA (623 mg, 3.01 mmol) in the other compartment. Then, a solution of Rh NPs was added to each compartment, and the resulting solutions were left to crystallise by slow diffusion for 30 days.

1.5.3.8. General procedure for the hydrogenation of double bonds

1 (0.1 mmol) was added to 2 mL glass tubes. Then, it was dissolved in 0.5 mL of DCM or THF (0.2 M). The catalyst (1, 5 or 10 mol% of Pt@TAMOF-1 or 0.5 mg of Pt NPs) was added to the solutions, then the tubes were placed inside a high-pressure HEL multireactor, pressurised to 30 bar of H_2 and the reaction mixtures were left to stir at 700 rpm overnight at room temperature. The reactor was slowly depressurised, the solutions were then filtered, concentrated *in vacuo* and the crudes analysed by ^{1}H-NMR and HPLC if required.

1.5.3.9. Synthesis of $_{mono}$TAMOF-1

To a stirred solution of *S*-HTA (208 mg, 1 mmol) in H_2O (10 mL, 0.1 M) at a specific temperature was added a solution of $Cu(OAc)_2 \cdot H_2O$ (100 mg, 0.5 mmol) in H_2O (5 mL, 0.1 M) at a specific temperature, and the reaction mixture was stirred at a specific temperature until the solution became cloudy. As soon as the precipitate was observed, the suspension was transferred to a Falcon tube and centrifuged for 10 min. The supernatant liquid was decanted, fresh water was added, the suspension was sonicated and centrifuged for 20 min. The supernatant liquid was decanted, and the pellet was left to dry at rt.

1.5.4. NMR spectra
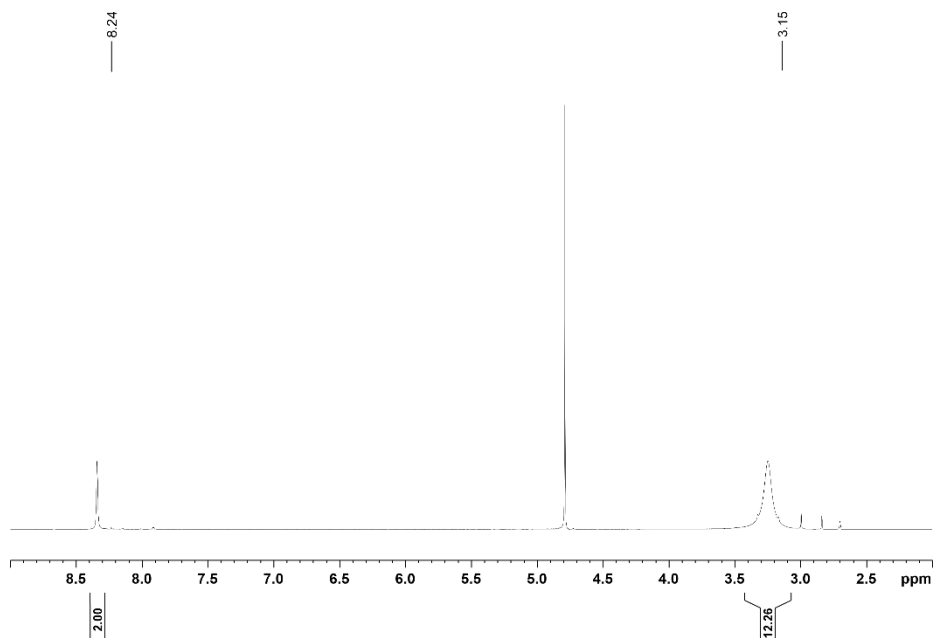
Figure 85. ^{1}H-NMR (400 MHz, D$_2$O) spectra of **DMFA·2HCl**.
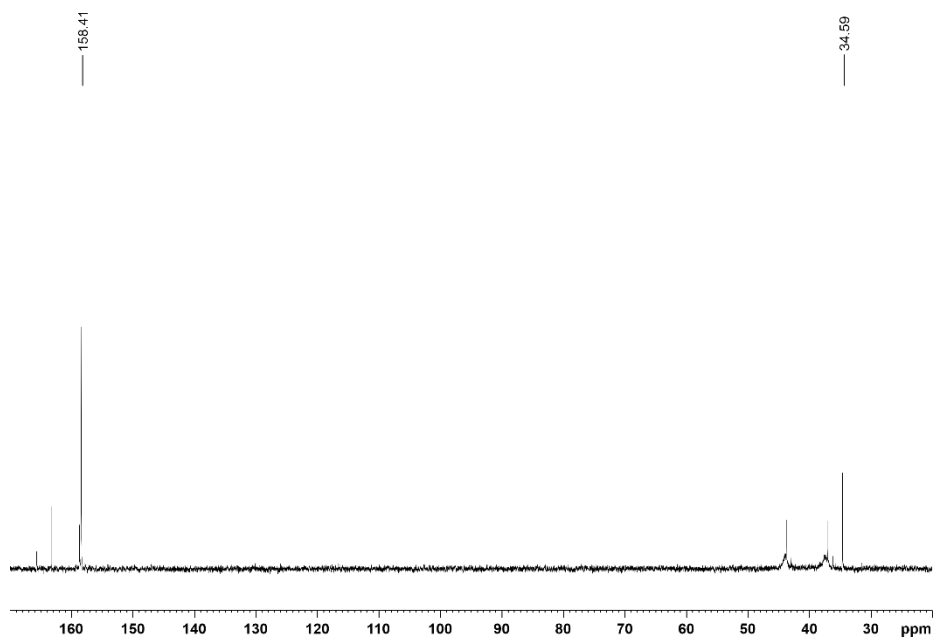
Figure 86. ^{13}C-NMR (101 MHz, D$_2$O) spectra of **DMFA·2HCl**.

85

TAMOF-1: Optimisation of the Synthesis and Structural and Morphological Studies
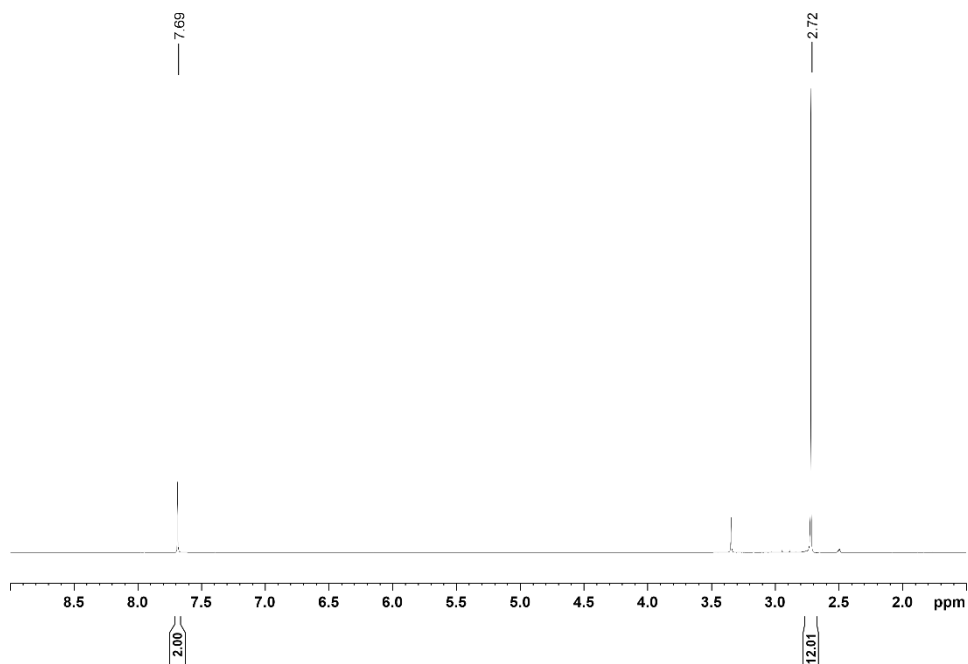
Figure 87. ^{1}H-NMR (400 MHz, D$_2$O) spectra of **DMFA**.
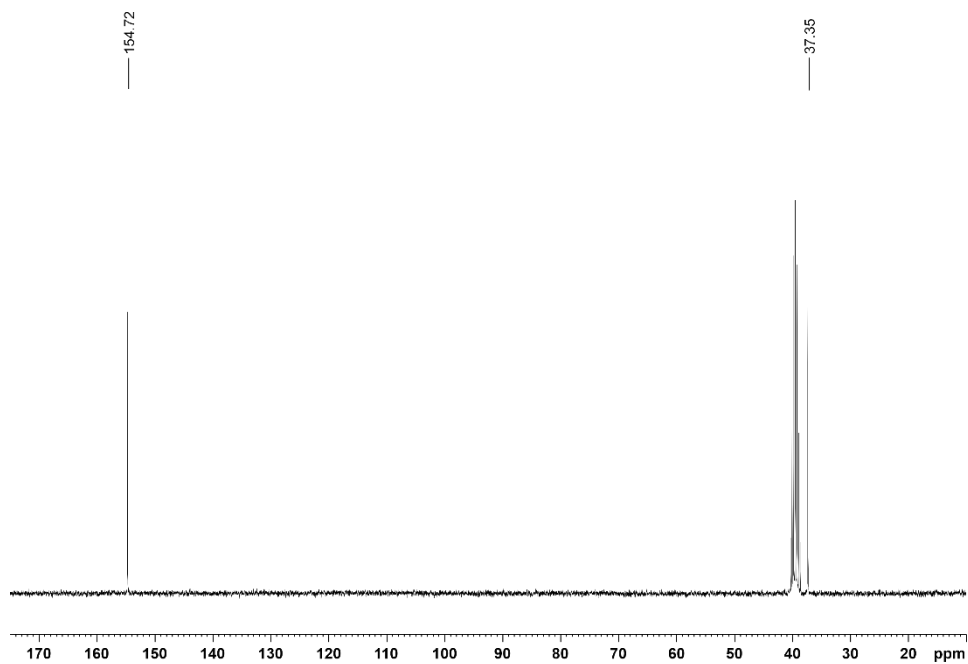
Figure 88. ^{13}C-NMR (101 MHz, D$_2$O) spectra of **DMFA**.

86
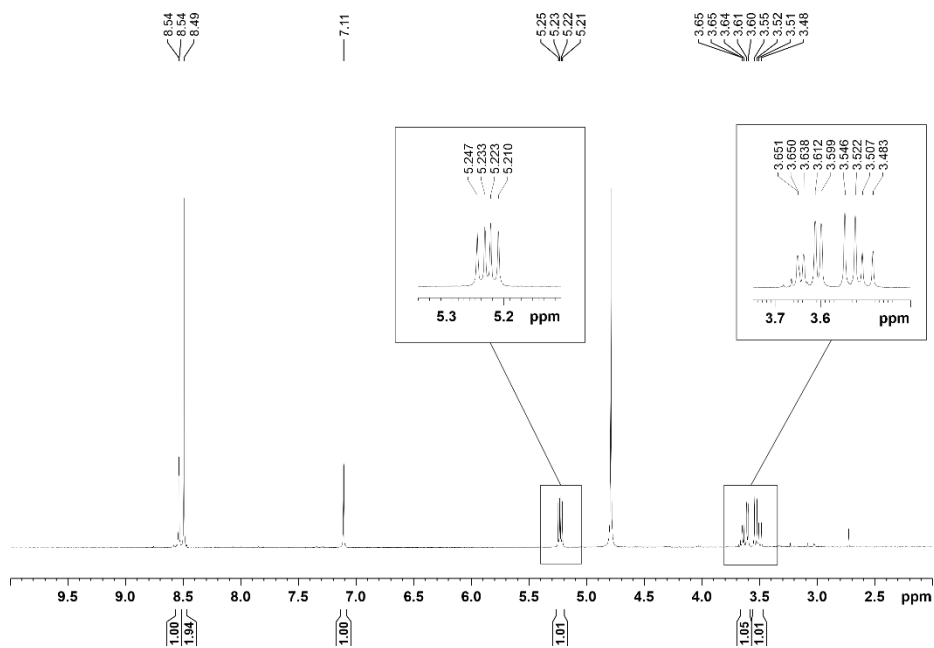
Figure 89. ^{1}H-NMR (400 MHz, D$_2$O) spectra of **S-HTA**.
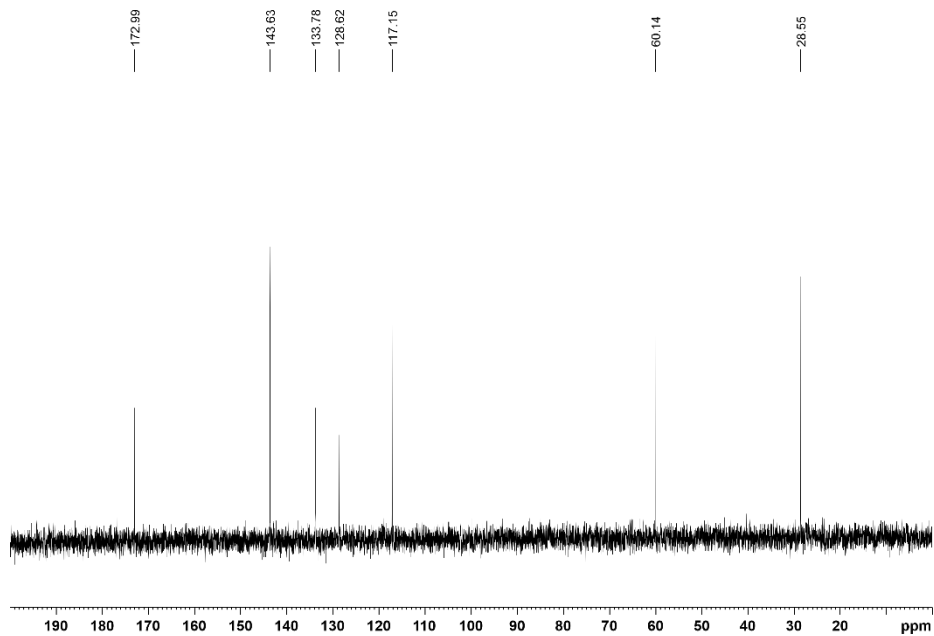
Figure 90. ^{13}C-NMR (101 MHz, D$_2$O) spectra of **S-HTA**.

87

TAMOF-1: Optimisation of the Synthesis and Structural and Morphological Studies
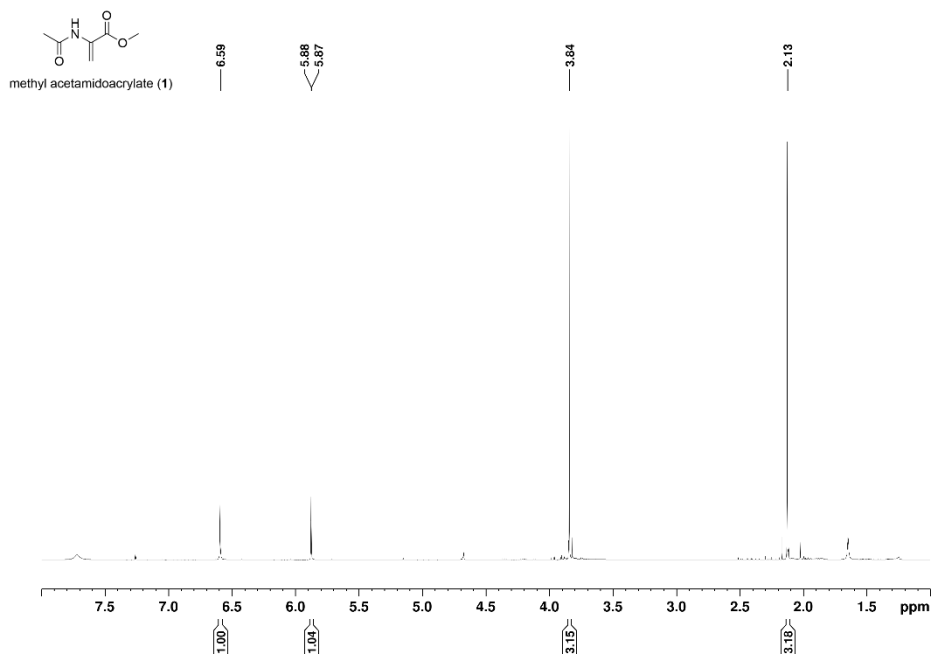
Figure 91. ^{1}H-NMR (400 MHz, CDCl$_3$) spectra of **1**.
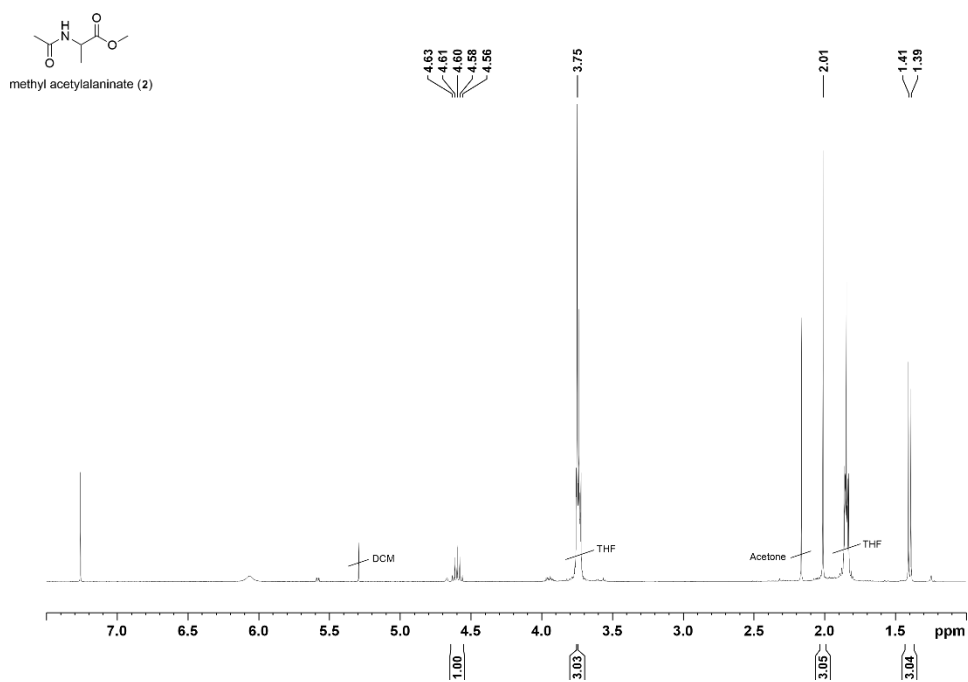
Figure 92. ^{1}H-NMR (400 MHz, CDCl$_3$) spectra of **2**.

CHAPTER II

Differentiation of Epoxide Enantiomers in the Confined Spaces of an Homochiral Cu²⁺ MOF by Kinetic Resolution

UNIVERSITAT ROVIRA I VIRGILI
INSIGHTS IN HOMOCHIRAL METAL-ORGANIC FRAMEWORKS: FROM THEIR SYNTHESIS TO ENANTIOSELECTIVE
APPLICATIONS
Juanjo Cabezas Giménez

Differentiation of Epoxide Enantiomers in the Confined Spaces of an Homochiral Cu²⁺ MOF by Kinetic Resolution

Juanjo Cabezas-Giménez,[a,b] Vanesa Lillo,[a] José Luis Núñez-Rico,[a,c] M. Nieves Corella-Ochoa,[a] Jesús Jover,[c,*] José Ramón Galán-Mascarós[a,d,*] and Anton Vidal-Ferran[a,c,d,e,*]

a Institut Català d'Investigació Química (ICIQ) and the Barcelona Institute of Science and Technology (BIST), Av. Països Catalans 16, 43007 Tarragona (Spain).

b Departament de Química Física i Inorgànica, Universitat Rovira i Virgili (URV), C/Marcel·lí Domingo S/N, 43007 Tarragona (Spain).

c Departament de Química Inorgànica i Orgànica, Universitat de Barcelona (UB), C/Martí Franqués 1-11, 08028 Barcelona (Spain).

d Institució Catalana de Recerca i Estudis Avançats (ICREA), Pg. Lluís Companys 23, 08010 Barcelona (Spain).

e Institut de Nanociència i Nanotecnologia (IN2UB), Av. Diagonal 645, 08028 Barcelona (Spain)

Chapter II

UNIVERSITAT ROVIRA I VIRGILI
INSIGHTS IN HOMOCHIRAL METAL-ORGANIC FRAMEWORKS: FROM THEIR SYNTHESIS TO ENANTIOSELECTIVE
APPLICATIONS
Juanjo Cabezas Giménez

Differentiation of Epoxide Enantiomers by Kinetic Resolution
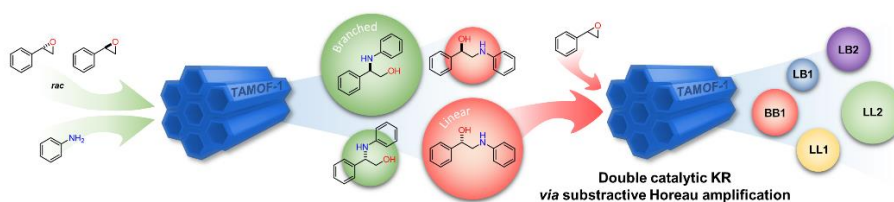
2.1. ABSTRACT

TAMOF-1 was investigated as a heterogeneous catalyst in kinetic resolutions involving the ring-opening of styrene oxide with a set of anilines. The branched products generated from the ring opening of styrene oxide with anilines and the unreacted epoxide were obtained with moderately high enantiomeric excesses. The linear product arising from the attack on the non-benzylic position of styrene oxide underwent a second kinetic resolution by reacting with the epoxide, amplifying its final enantiomeric excess and a concomitant formation of an array of isomeric aminodiols. Computational studies confirmed the experimental results, providing a deep understanding of the process involving the two successive kinetic resolutions. Furthermore, TAMOF-1 activity was conserved after several catalytic cycles. The ring-opening of a meso-epoxide with aniline catalysed by TAMOF-1 was also studied, and moderate enantioselectivities were obtained.

2.2. INTRODUCTION

Metal-organic frameworks (MOFs) are porous coordination polymers composed of organic ligands and metal centres or clusters. With high porosities and thermal stabilities, these materials have captured the attention of many researchers due to their remarkable chemical and physical versatility.[139] They have been used in gas storage[140] and separation,[141] sensors[142] and LEDs,[143] among other applications.

[139] a) Eddaoudi, M.; Kim, J.; Rosi, N.; Vodak, D.; Wachter, J.; O'Keeffe, M.; Yaghi, O. M. *Science* **2002**, *295*, 469-472. b) Eddaoudi, M.; Moler, D. B.; Li, H.; Chen, B.; Reineke, T. M.; O'Keeffe, M.; Yaghi, O. M. *Acc. Chem. Res.* **2001**, *34*, 319-330. c) Férey, G. *Chem. Soc. Rev.* **2008**, *37*, 191-214.
[140] a) Feng, D.; Lei, T.; Lukatskaya, M. R.; Park, J.; Huang, Z.; Lee, M.; Shaw, L.; Chen, S.; Yakovenko, A. A.; Kulkarni, A.; Xiao, J.; Fredrickson, K.; Tok, J. B.; Zou, X.; Cui, Y.; Bao, Z. *Nat. Energy* **2018**, *3*, 30-36. b) Furukawa, H.; Ko, N.; Go, Y. B.; Aratani, N.; Choi, S. B.; Choi, E.; Yazaydin, A. Ö.; Snurr, R. Q.; O'Keeffe, M.; Kim, J.; Yaghi, O. M. *Science* **2010**, *329*, 424-428. c) Millward, A. R.; Yaghi, O. M. *J. Am. Chem. Soc.* **2005**, *127*, 17998-17999.
[141] a) Li, L.; Guo, L.; Pu, S.; Wang, J.; Yang, Q.; Zhang, Z.; Yang, Y.; Ren, Q.; Alnemrat, S.; Bao, Z. *Chem. Eng. J.* **2019**, *358*, 446-455. b) Xiang, S.-C.; Zhang, Z.; Zhao, C.-G.; Hong, K.; Zhao, X.; Ding, D.-R.; Xie, M.-H.; Wu, C.-D.; Das, M. C.; Gill, R.; Thomas, K. M.; Chen, B. *Nat. Commun.* **2011**, *2*, 204. c) Yang, S.; Ramirez-Cuesta, A. J.; Newby, R.; Garcia-Sakai, V.; Manuel, P.; Callear, S. K.; Campbell, S. I.; Tang, C. C.; Schröder, M. *Nat. Chem.* **2014**, *7*, 121.
[142] a) Hu, Z.; Deibert, B. J.; Li, J. *Chem. Soc. Rev.* **2014**, *43*, 5815-5840. b) Li, J.; Li, J. *Inorg. Chem. Commun.* **2018**, *89*, 51-54. c) Wanderley, M. M.; Wang, C.; Wu, C.-D.; Lin, W. *J. Am. Chem. Soc.* **2012**, *134*, 9050-9053. d) Yao, Q.; Bermejo Gómez, A.; Su, J.; Pascanu, V.; Yun, Y.; Zheng, H.; Chen, H.; Liu, L.; Abdelhamid, H. N.; Martín-Matute, B.; Zou, X. *Chem. Mater.* **2015**, *27*, 5332-5339.
[143] a) Angioni, E.; Marshall, R. J.; Findlay, N. J.; Bruckbauer, J.; Breig, B.; Wallis, D. J.; Martin, R. W.; Forgan, R. S.; Skabara, P. J. *J. Mater. Chem. C* **2019**, *7*, 2394-2400. b) Tang, Y.; Xia, T.; Song, T.; Cui, Y.; Yang, Y.; Qian, G. *Adv. Opt. Mater.* **2018**, *6*, 1800968. c) Wang, Z.; Wang, Z.; Lin, B.; Hu, X.; Wei, Y.; Zhang, C.; An, B.; Wang, C.; Lin, W. *ACS Appl. Mater. Interfaces* **2017**, *9*, 35253-35259. d) Zhao, S.-S.; Zhang, H.; Wang, L.; Chen, L.; Xie, Z. *J. Mater. Chem. C* **2018**, *6*, 11701-11706.

Differentiation of Epoxide Enantiomers by Kinetic Resolution

Homochiral MOFs may be obtained from enantiopure precursors. Well-known enantiopure ligands have been used in the construction of homochiral MOFs, such as BINOL- or salen-based porous materials.[144] These MOFs, possessing rigid structures and tunable pores, have been exploited in asymmetric catalysis and chiral separations, two areas of high interest in the pharmaceutical industry.

Homochiral MOFs have already been used as enantioselective catalysts for directing the preferential formation of a stereoisomer from a pro-chiral substrate. For instance, in the cyanosilylation of aldehydes,[145] epoxidation of alkenes,[146] additions to carbonyl groups,[147] carbonyl-ene[148] and Diels-Alder reactions,[149] cyclopropanations[150] and aldol reactions.[151]

Kinetic resolution is also an interesting tool in enantioselective catalysis for the generation of enantiopure (or highly enantioenriched) products.[152] The success of a catalytic kinetic resolution relies on distinct reaction rates occurring in the presence of a catalyst for the reaction between the two enantiomers of the starting material and an additional reactant/reagent. There are very few examples in the literature of kinetic resolutions of epoxides with homochiral MOFs as catalysts. Moreover, these examples mainly comprise the reaction of oxygen-containing nucleophiles and epoxides outside the confined spaces of the MOFs.[153,154]

Our research group has recently reported a new homochiral MOF, TAMOF-1, constructed from copper(II) and a ligand prepared from natural L-histidine. The strong metal-nitrogen coordination bonds of TAMOF-1

---

[144] a) Ma, L.; Abney, C.; Lin, W. *Chem. Soc. Rev.* **2009**, *38*, 1248. b) Tanaka, K.; Kawakita, T.; Morawiak, M.; Urbanczyk-Lipkowska, Z. *CrystEngComm* **2019**, *21*, 487-493. c) Zhu, C.; Xia, Q.; Chen, X.; Liu, Y.; Du, X.; Cui, Y. *ACS Catal.* **2016**, *6*, 7590-7596.

[145] a) Bhunia, A.; Dey, S.; Moreno, J. M.; Diaz, U.; Concepcion, P.; Van Hecke, K.; Janiak, C.; Van Der Voort, P. *Chem. Commun.* **2016**, *52*, 1401-1404. b) Li, Z.; Liu, Y.; Kang, X.; Cui, Y. *Inorg. Chem.* **2018**, *57*, 9786-9789. c) Mo, K.; Yang, Y.; Cui, Y. *J. Am. Chem. Soc.* **2014**, *136*, 1746-1749.

[146] a) Noh, H.; Cui, Y.; Peters, A. W.; Pahls, D. R.; Ortuño, M. A.; Vermeulen, N. A.; Cramer, C. J.; Gagliardi, L.; Hupp, J. T.; Farha, O. K. *J. Am. Chem. Soc.* **2016**, *138*, 14720-14726. b) Song, F.; Wang, C.; Falkowski, J. M.; Ma, L.; Lin, W. *J. Am. Chem. Soc.* **2010**, *132*, 15390-15398. c) Song, F.; Zhang, T.; Wang, C.; Lin, W. *Proc. R. Soc. Lond. A* **2012**, *468*, 2035-2052.

[147] a) Hu, A.; Ngo, H. L.; Lin, W. *J. Am. Chem. Soc.* **2003**, *125*, 11490-11491. b) Wu, C.-D.; Hu, A.; Zhang, L.; Lin, W. *J. Am. Chem. Soc.* **2005**, *127*, 8940-8941.

[148] Han, J.; Lee, M. S.; Thallapally, P. K.; Kim, M.; Jeong, N. *ACS Catal.* **2019**, *9*, 3969-3977.

[149] a) Jeong, K. S.; Go, Y. B.; Shin, S. M.; Lee, S. J.; Kim, J.; Yaghi, O. M.; Jeong, N. *Chem. Sci.* **2011**, *2*, 877-882. b) Tanaka, K.; Nagase, S.; Anami, T.; Wierzbicki, M.; Urbanczyk-Lipkowska, Z. *RSC Adv.* **2016**, *6*, 111436-111439.

[150] Falkowski, J. M.; Wang, C.; Liu, S.; Lin, W. *Angew. Chem. Int. Ed.* **2011**, *50*, 8674-8678.

[151] a) Banerjee, M.; Das, S.; Yoon, M.; Choi, H. J.; Hyun, M. H.; Park, S. M.; Seo, G.; Kim, K. *J. Am. Chem. Soc.* **2009**, *131*, 7524-7525. b) Lun, D. J.; Waterhouse, G. I. N.; Telfer, S. G. *J. Am. Chem. Soc.* **2011**, *133*, 5806-5809. c) Sartor, M.; Stein, T.; Hoffmann, F.; Fröba, M. *Chem. Mater.* **2016**, *28*, 519-528.

[152] Studer, M.; Burkhardt, S.; Blaser, H.-U. *Adv. Synth. Catal.* **2001**, *343*, 802-808.

[153] Tanaka, K.; Otani, K.-I. *New J. Chem.* **2010**, *34*, 2389.

[154] Zhu, C.; Yuan, G.; Chen, X.; Yang, Z.; Cui, Y. *J. Am. Chem. Soc.* **2012**, *134*, 8058-8061.

produce a structurally robust porous material, with a very high permanent porosity (*ca.* 1200 $m^2 g^{-1}$) and excellent thermal and chemical stabilities.

TAMOF-1 has been used as a chiral stationary phase in chromatographic separations for the quantitative separation of racemic mixtures of drugs (for instance, *rac*-ibuprofen and *rac*-thalidomide), as well as in HPLC columns for highly efficient analytical separations of racemic mixtures. The 3D intersected channels with a diameter ≤ 10 Å and the internal binding sites for chiral molecular recognition led to the fabrication of in-house HPLC columns that outperformed several commercial HPLC columns.

The interesting properties of TAMOF-1[102] (*i.e.*, capability of chiral recognition inside wide channels combined with broad tolerance to solvents) prompted us to study its catalytic activity in kinetic resolutions within confined spaces.

Herein, we describe our interesting findings for the kinetic resolution of styrene oxide with a set of anilines in the presence of TAMOF-1. The unreacted epoxide and products generated from the ring-opening at the benzylic position were kinetically resolved in an efficient way. Computational studies carried out by Dr. Jesús Jover from *Universitat de Barcelona* provided a deep understanding of the whole process, based on the different reactivity of the substrates when confined in the helical channels of TAMOF-1.

Chapter II

95

2.3. RESULTS AND DISCUSSION

2.3.1. Reaction conditions for TAMOF-1 catalysed ring openings of epoxides with anilines

The beginning of the screening of the reaction conditions for the ring-opening of epoxides was the exploration of the resolution of *rac*-styrene oxide (*rac*-**1**) with aniline (**2**) catalysed by TAMOF-1 (**Scheme 12**).
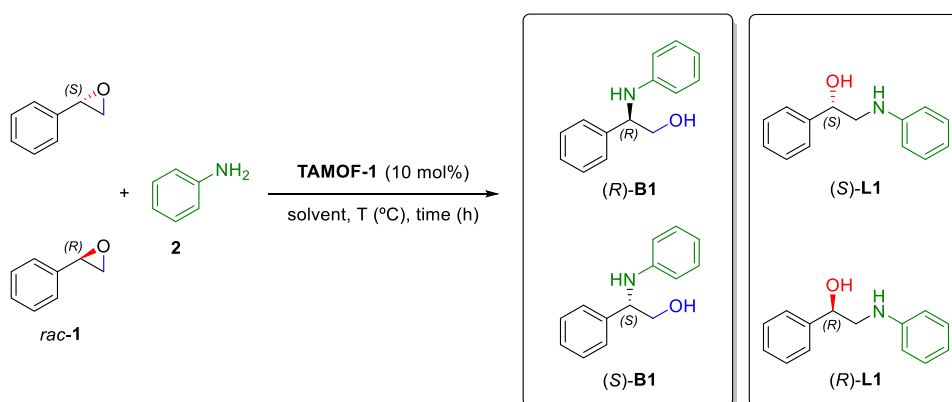
Scheme 12. Reaction between *rac*-**1** and **2** catalysed by TAMOF-1.

The ring-opening of *rac*-**1** with **2** provides four possible products: two enantiomers arising from the nucleophilic attack on the benzylic methine carbon of each enantiomer of the epoxide, called branched products, (*R*)-**B1** and (*S*)-**B1**; and the nucleophilic attack on the non-benzylic methylene carbon, called linear products, (*R*)-**L1** and (*S*)-**L1**.

The standard screening conditions used were 10 mol% of TAMOF-1 as a catalyst, equimolar amounts of *rac*-**1** and **2** (0.5 eq.) and 2 mL (0.25 M) of solvent. Different solvents, such as DCM, EtOAc, Toluene, THF and ACN, were used. Also, different reaction temperatures were tried, going from 0 °C to 100 °C. The screening conditions are described in **Table 5**.

96

Table 5. Screening conditions for the kinetic resolution of *rac*-**1**.

Entry	Solvent	T (ºC)	Conv. (%)[b]	(R)-B1 (%)[c]	(S)-B1 (%)[c]	(S)-L1 (%)[c]	(R)-L1 (%)[c]
1	-	rt	44.4	34.0	42.2	10.7	13.1
2	-	80	87.9	35.3	31.9	16.0	16.8
3	CH_2Cl_2	80	76.4	38.4	38.7	11.5	11.4
4	EtOAc	80	32.2	30.1	39.0	12.6	18.3
5	Toluene	rt	≤1.0	n.d.	n.d.	n.d.	n.d.
6	Toluene	80	10.8	24.2	44.9	11.4	19.5
7	Toluene	100	21.8	27.0	39.6	13.4	20.0
8	THF	rt	≤1.0	n.d.	n.d.	n.d.	n.d.
9	THF	60	≤1.0	n.d.	n.d.	n.d.	n.d.
10	THF	80	30.6	39.1	41.6	7.8	11.5
11[d]	ACN	0	33.0	44.4	39.3	8.4	8.0
12	ACN	rt	26.1	64.3	29.8	3.4	2.5
13	ACN	40	53.1	57.3	28.6	7.5	6.5
14	ACN	60	64.0	57.8	34.0	4.1	4.1
15	ACN	80	84.0	52.2	34.8	7.0	6.0
16	ACN	100	49.0	49.4	30.6	11.6	8.4
17[e]	ACN	40	54.0	54.1	33.8	6.4	5.7
18[f]	ACN	40	26.6	65.0	29.5	3.1	2.4
19[g]	ACN	40	24.1	54.6	24.6	12.2	8.6
20[h]	ACN	40	31.0	58.5	26.3	8.7	6.5
21[i]	ACN	60	66.7	52.2	37.8	5.2	4.8

[a] Reaction conditions: *rac*-**1** (0.5 mmol), **2** (0.5 mmol), TAMOF-1 (10 mol%), 2 mL solvent, 16 h. No conversion was observed in absence of the catalyst. [b] Calculated by ^{1}H-NMR, using durene as internal standard. [c] Calculated by SFC (Acquity UPC2, CHIRALPAK® IA column, CO_2/IPA gradient, from 0 to 40%, 1500 psi). [d] Reaction time: 3 days. [e] 1.5 eq. of **2** were used. [f] 1.5 eq. of *rac*-**1** were used. [g] 3 mol% of catalyst were used. [h] 7 mol% of catalyst were used. [i] 20 mol% of catalyst were used.

Control experiments in the absence of the catalyst revealed that ring-opening did not occur place to a measurable extent. In the presence of the catalyst, the ring-opening reaction proceeded smoothly, yielding variable amounts of the four possible diastereomers depending on the solvent and the temperature of the reaction. As expected, the major products were the branched enantiomers **B1**, the products obtained from the attack on the benzylic position, the most electrophilic position.

UNIVERSITAT ROVIRA I VIRGILI
INSIGHTS IN HOMOCHIRAL METAL-ORGANIC FRAMEWORKS: FROM THEIR SYNTHESIS TO ENANTIOSELECTIVE
APPLICATIONS
Juanjo Cabezas Giménez

Differentiation of Epoxide Enantiomers by Kinetic Resolution

Conversions of the ring-opening with solvents such as toluene, THF and ethyl acetate were poor, regardless of the reaction temperature. Consequently, no further investigation was carried out with these solvents. ACN was an appropriate solvent, with conversions ranging from 26% to 84% at different reaction times and temperatures.
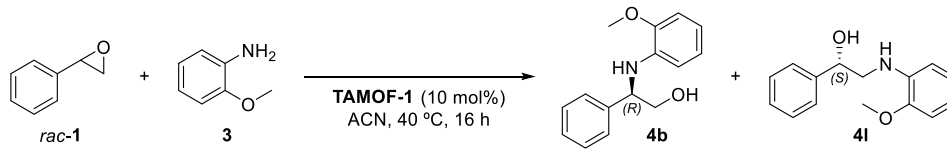
As expected, the enantiomeric excesses of both branched and linear products increased by lowering the reaction temperature, allowing the system to react thermodynamically. The best e.e.'s with ACN were found at room temperature – 36.6% for (*R*)-**B1** and 15.2% for (*S*)-**L1**. However, at 40 ºC, the e.e.'s were quite similar – 33.4% for (*R*)-**B1** and 7.1% for (*S*)-**L1** – but the conversion was significantly higher than at rt (53% *vs.* 26%). We decided to move forward with the kinetic resolution studies at the aforenoted conditions (ACN, 40 ºC), which balanced conversion and stereoselectivity.

At this point of the study, we also explored the effects of the ratio epoxide/amine (**Table 5**, entries 17-18), demonstrating that there were no significant effects on the regio- and enantioselectivity of the final products. Thus, the standard concentrations previously indicated were used in subsequent catalytic studies.
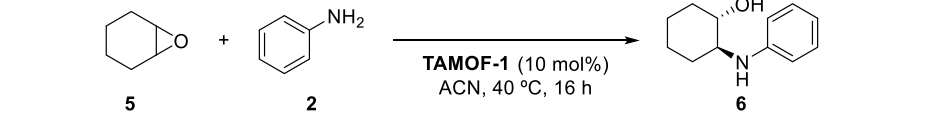
Other control experiments were performed to determine whether racemisation of the starting materials or products was taking place. These processes were studied by reacting enantiopure (*R*)-**1** or (*S*)-**1** separately with aniline (**2**) in the presence of TAMOF-1 under the same reaction conditions as those in the catalytic assays. The products obtained were diastereomerically and enantiomerically pure, as expected for an epoxide-opening process This process is a stereospecific S_N2 reaction without any epimerisation.

In order to expand the scope of this reaction, 10 mol% of TAMOF-1 were used in the reaction of *rac*-**1** and *o*-anisidine **3** (**Table 6**). Similar results were observed to those reported for aniline (51% conv.; 60% e.e. for (*R*)-**4b** and 35% e.e. for (*S*)-**4l**).

In the reaction between meso-epoxide **5** and aniline with the same catalyst loading, lower conversion and e.e. were obtained compared to its analogue *rac*-**1** (15% conversion and 35% e.e. in favour of product (1*S*,2*S*)-**6**, **Table 7**).

Table 6. Conversion, selectivity, and enantiomeric excess of **4b** and **4l**.

Conv. (%)[a]	Sel. 4b (%)[a]	e.e. 4b (%)[b]	Sel. 4l (%)[a]	e.e. 4l (%)[b]
50.5	74.1	56.6 (R)	25.9	34.8 (S)

[a] Calculated by ^{1}H-NMR.
[b] Calculated by SFC (Acquity UPC2, CHIRALPAK® IA column, CO_2/MeOH 95:5, 1500 psi, 240 nm t_R(S-**4b**) = 3.56 min, t_R(R-**4b**) = 3.80 min, t_R(S-**4l**) = 6.94 min, t_R(R-**4l**) = 9.27 min.

Table 7. Conversion and enantiomeric excess of **6**.

Conv. (%)[a]	e.e. 6 (%)[b]
15.0	35.4 (1S,2S)

[a] Calculated by ^{1}H-NMR.
[b] Calculated by HPLC: CHIRALCEL® OD-H, *n*-Hex/IPA 85:15, 1 mL min^{-1}, 247 nm, t_R(1S, 2S-**6**) = 8.2 min (lit. 10.3 min), t_R(1R, 2R-**6**) = 9.2 min (lit. 11.9 min).[155]

2.3.2. Monitoring of the kinetic resolution

Using the optimised conditions, we studied the kinetic resolution of *rac*-**1** by measuring conversions and e.e. at different reaction times (4, 12, 17 and 48 h, **Figure 93**). The concentrations of **1** and **2** decreased rapidly, yielding **B1** as the major product and small amounts of **L1**. Regarding the stereoselectivity of the kinetic resolution, the e.e. of the unreacted starting material increased with the conversion, whilst the e.e. of the products dropped as the conversion increased. These trends are in agreement with the expected behaviour of a kinetic resolution.[156]

[155] Mai, E.; Schneider, C. *Chem. Eur. J.* **2007**, *13*, 2729-2741.
[156] Keith, J. M.; Larrow, J. F.; Jacobsen, E. N. *Adv. Synth. Catal.* **2001**, *343*, 5-26.

Differentiation of Epoxide Enantiomers by Kinetic Resolution
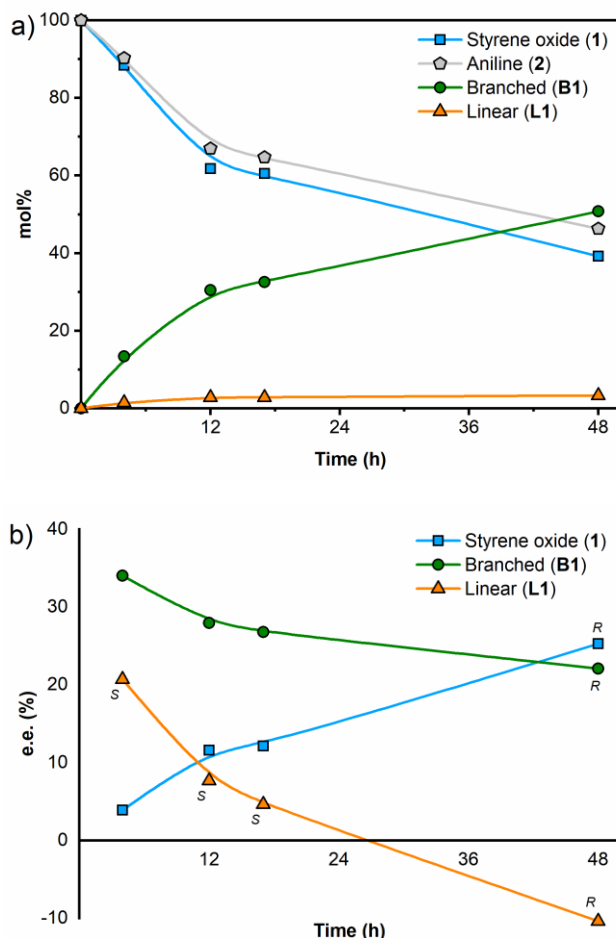
Figure 93. (a) Kinetic resolution profile in mol% at 4, 12, 17 and 48 h, using 10 mol% of TAMOF-1. (b) Enantiomeric excess of **1**, **B1** and **L1** against time.

Ring-opening of the (*R*)-enantiomer of **1** with aniline proceeded at a lower rate when using TAMOF-1 as the catalyst, with the concentration of (*R*)-**1** increasing with time. As shown in **Figure 93**, an e.e. of 25.3% in favour of (*R*)-**1** was recorded after 48 h. As (*S*)-**1** reacts faster with aniline, the major product formed was the branched product derived from (*S*)-**1** by the benzylic attack of aniline with an inversion of the configuration at the attacked carbon. Consequently, the branched product (*R*)-**B1** mainly was formed, and its absolute configuration was confirmed by comparison with previous data.[157] The e.e. for this compound after four hours was 34.3%.

---

[157] Tak, R.; Kumar, M.; Menapara, T.; Gupta, N.; Kureshy, R. I.; Khan, N.-u. H.; Suresh, E. *Adv. Synth. Catal.* **2017**, *359*, 3990-4001.

The product arising from the non-benzylic attack (**L1**) was also observed in the reaction mixture. However, it was formed in lower amounts compared to **B1**. Comparing **B1** and **L1** yields through time (**Figure 93a**) showed that **L1**'s was much lower than **B1**'s throughout the reaction.

The stereoselectivity of **L1** after four hours was slightly lower than that for **B1** (e.e. of 20.0% for (*S*)-**L1** and 34.3% for (*R*)-**B1**). This indicates a slightly lower degree of stereodifferentiation of the two enantiomers of *rac*-**1** by TAMOF-1 for the non-benzylic position. Surprisingly, an inversion of the configuration of the product **L1** was observed at long reaction times (formation of (*R*)-**L1** with an extended e.e. of 9.1%). This finding was not consistent with a simple kinetic resolution.

To further understand the stereochemical outcome, we performed analogous experiments with increased TAMOF-1 amounts (from 10 mol% to 50 mol%) and extended reaction times. The results of this study are summarised in **Figure 94.** With the new reaction conditions, the conversion of the ring-opening increased up to 97% after 96 h.

The e.e. of the unreacted starting material and the stereoselectivity pattern of **B1** agree with a standard kinetic resolution. However, the final configuration of **L1** using 50 mol% of TAMOF-1 was again opposite to the one expected, as observed with 10 mol% of TAMOF-1.

Chapter II

101

UNIVERSITAT ROVIRA I VIRGILI
INSIGHTS IN HOMOCHIRAL METAL-ORGANIC FRAMEWORKS: FROM THEIR SYNTHESIS TO ENANTIOSELECTIVE
APPLICATIONS
Juanjo Cabezas Giménez

Differentiation of Epoxide Enantiomers by Kinetic Resolution
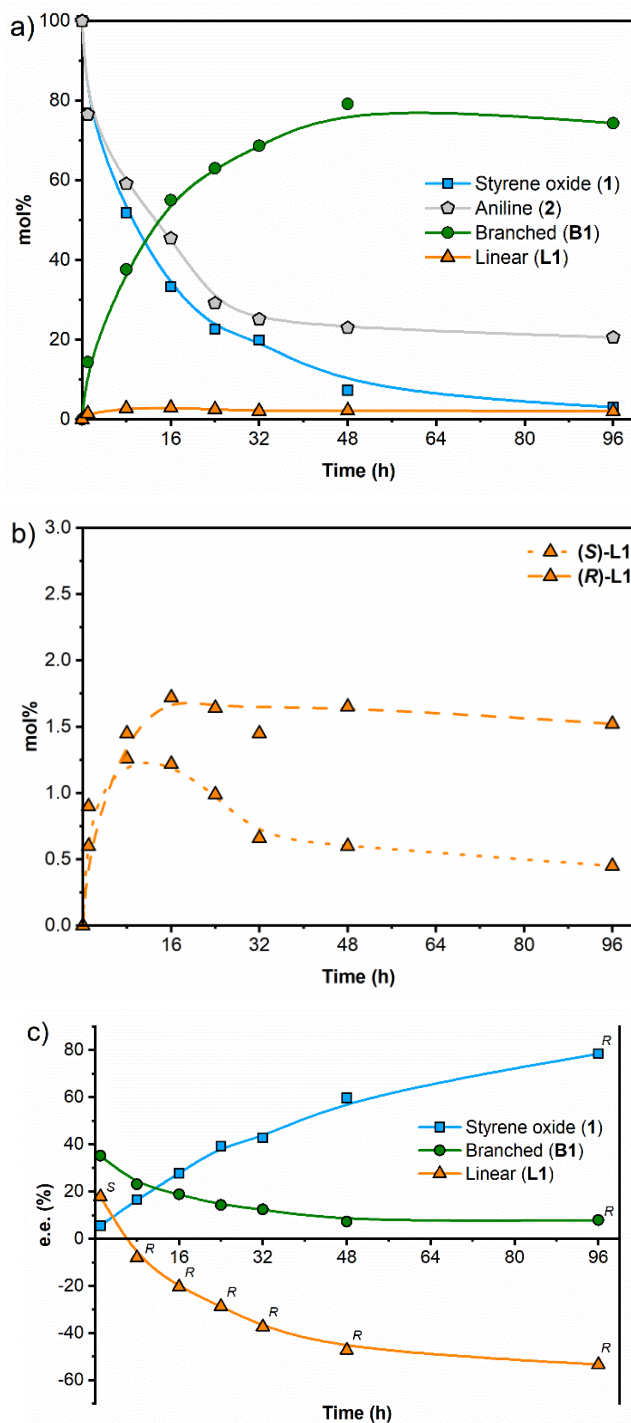
Figure 94. (a) Kinetic resolution profile in mol% at 1, 8, 16, 24, 32, 48 and 96 h, using 50 mol% TAMOF-1. (b) Kinetic resolution profile of (*R*)-**L1** and (*S*)-**L1** in mol%. (c) Enantiomeric excesses of **1**, **B1** and **L1** against time.

102

Analyses of crude reaction mixtures in an HPLC equipped with an APCI+ identified unexpected reaction products consistent with adducts formed from one molecule of aniline and two molecules of styrene oxide. These findings suggested that a second ring-opening reaction was occurring since the products arising from the first ring-opening (*i.e.*, **B1** and **L1**) could still attack a second molecule of styrene oxide to form dialkyl aryl tertiary aminodiols.

It should be noted that the ring-opening of a second unit of a racemic epoxide, at the benzylic and non-benzylic positions, by amino alcohols (*R*)-**B1**, (*S*)-**B1**, (*R*)-**L1** or (*S*)-**L1** may generate up to 10 diastereoisomeric aminodiols, whose structures are shown in **Figure 95.** Interestingly, five peaks with [M+H]$^+$ ions consistent with the suggested aminodiol structures were observed. In particular, **LB1**, **LL1**, **LB2** and **LL2** were identified in the reaction mixtures by comparative HPLC analyses of the crude reaction mixtures and pure samples of these compounds.[158] In addition, the aminodiol **BB1** arising from the ring-opening of the fastest reacting enantiomer (*S*)-**1** by the most abundant amino alcohol (*R*)-**B1** was unequivocally identified in the reaction mixture by comparative HPLC analysis.[158]
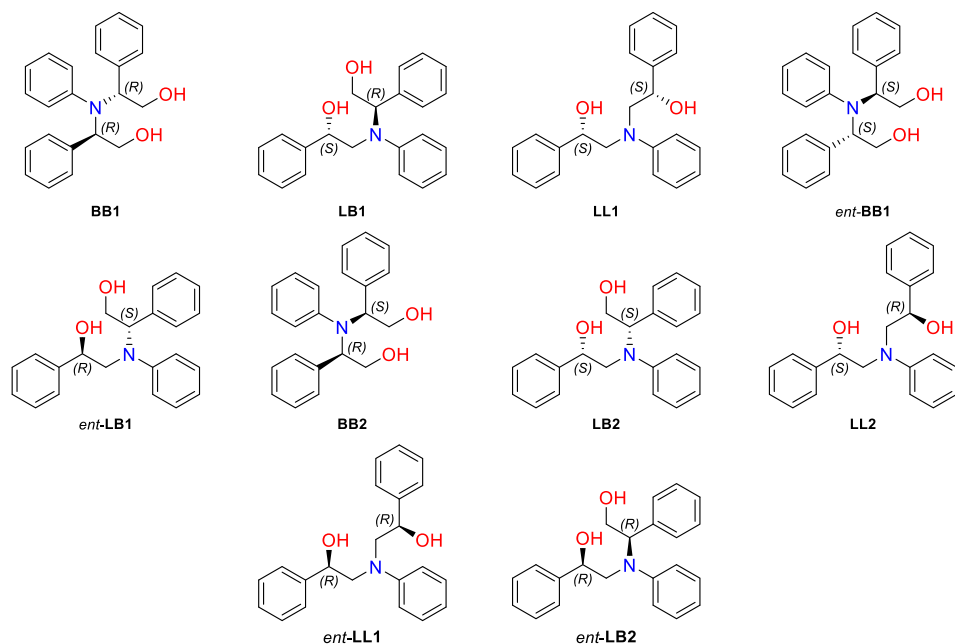
Figure 95. Isomeric aminodiols derived from the reaction between two units of *rac*-**1** and one unit of **2**.

[158] To confirm that the HPLC peaks assigned to **LB1**, **LL1**, **LB2** and **LL2** corresponded to the ring opening of (*S*)-**L1** with *rac*-**1**, these reagents were used in the reactions in the presence of **TAMOF-1**, yielding 5%, 4%, 12% and 9% of **LB1**, **LL1**, **LB2** and **LL2**, respectively.

UNIVERSITAT ROVIRA I VIRGILI
INSIGHTS IN HOMOCHIRAL METAL-ORGANIC FRAMEWORKS: FROM THEIR SYNTHESIS TO ENANTIOSELECTIVE
APPLICATIONS
Juanjo Cabezas Giménez

Differentiation of Epoxide Enantiomers by Kinetic Resolution

2.3.3. Matched double catalytic kinetic resolutions via subtractive Horeau amplification

Intrigued by the origin of the inversion of the configuration of **L1** at high conversions, we looked closely at the concentration profile of both enantiomers of **L1** *vs.* time (see **Figure 94b**).

There was an excess of (*S*)-**L1** compared to (*R*)-**L1** at short reaction times. As previously indicated, the formation of (*S*)-**L1** in the presence of TAMOF-1 was slightly preferred in the reaction between *rac*-**1** and **2**. However, (*S*)-**L1** reacted faster than (*R*)-**L1** with styrene oxide to form the corresponding aminodiol. This can be seen in **Figure 94b**, where the concentration of (*S*)-**L1** decreased with time (dotted curve in **Figure 94b**), whilst that of (*R*)-**L1** reached a plateau and remained relatively constant (dashed line in **Figure 94b**).

As (*S*)-**L1** was abstracted from the reaction media forming **LL1**, the whole process led to the formation of **L1** with an increased e.e. of 57.9% in favour of (*R*)-**L1** (orange curve in **Figure 94c**). These observations were confirmed by performing the kinetic resolution of *rac*-**L1** with *rac*-**1** in the presence of TAMOF-1 (**Figure 96**).
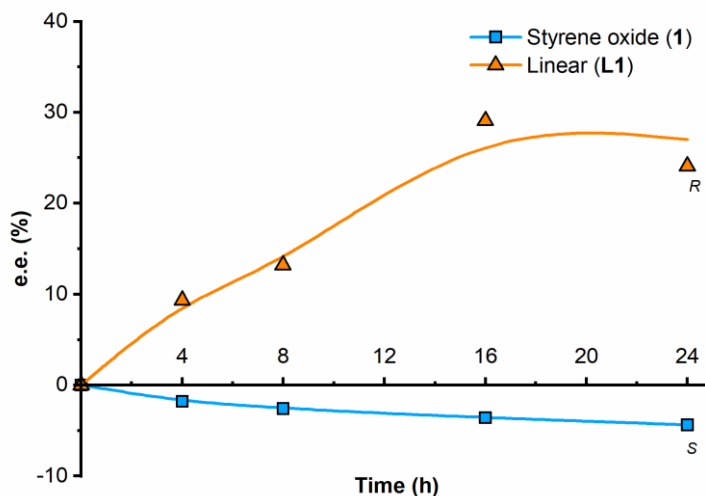
Figure 96. Enantiomeric excess profile of the second kinetic resolution. The kinetic resolution takes place with the **L** isomer, where (*R*)-**L1** reacts faster than (*S*)-**L1**. (The absolute configuration of the product is the same throughout the reaction).

As shown in **Figure 96**, the kinetic resolution of *rac*-**L1** led to (*R*)-**L1**, leaving (*S*)-**1** as the unreacted enantiomer of the starting epoxide. It should be noted that (*R*)-**1** is the fastest reacting enantiomer of the epoxide with the amino alcohol (*S*)-**L1**, whilst the other enantiomer of styrene oxide is the fastest reacting enantiomer with aniline.

It is also interesting to note the chiral amplification effect observed in (*R*)-**L1**: from an e.e. of 20.0% with one kinetic resolution to 57.9% after two kinetic resolutions. The most abundant enantiomer of the linear product formed after one kinetic resolution ((*S*)-**L1**) reacted faster through a second kinetic resolution process than (*R*)-**L1**, leading to an accumulation of the latter (by abstraction of the former).

Overall, through two matched kinetic resolutions, the stereoselectivity of the formation of (*R*)-**L1** is enhanced. These results constitute a fascinating example of subtractive Horeau amplification within the pores of TAMOF-1 (see **Scheme 13** for a summary of the processes involved).[159] To demonstrate that kinetic resolutions were occurring inside the pores of TAMOF-1, reactants with more demanding steric profiles were used (*i.e.*, racemic *trans*-2,3-diphenyloxirane instead of its mono-substituted analogue *rac*-**1** and *tert*-butylamine instead of **2**).

Interestingly, the kinetic resolution of *trans*-2,3-diphenyloxirane and **2** under the same reaction conditions did not occur to any measurable extent. Analogously, the kinetic resolution of styrene oxide with *tert*-butylamine did not proceed either. These results are strong evidence suggesting that kinetic resolution processes occur inside the pores of TAMOF-1.

Chapter II

---

[159] For the seminal work of A. Horeau see Vigneron, J. P.; Dhaenens, M.; Horeau, A. *Tetrahedron* **1973**, *29*, 1055-1059. For an overview on its application in synthesis see Harned, A. M. *Tetrahedron* **2018**, *74*, 3797-3841.

Differentiation of Epoxide Enantiomers by Kinetic Resolution
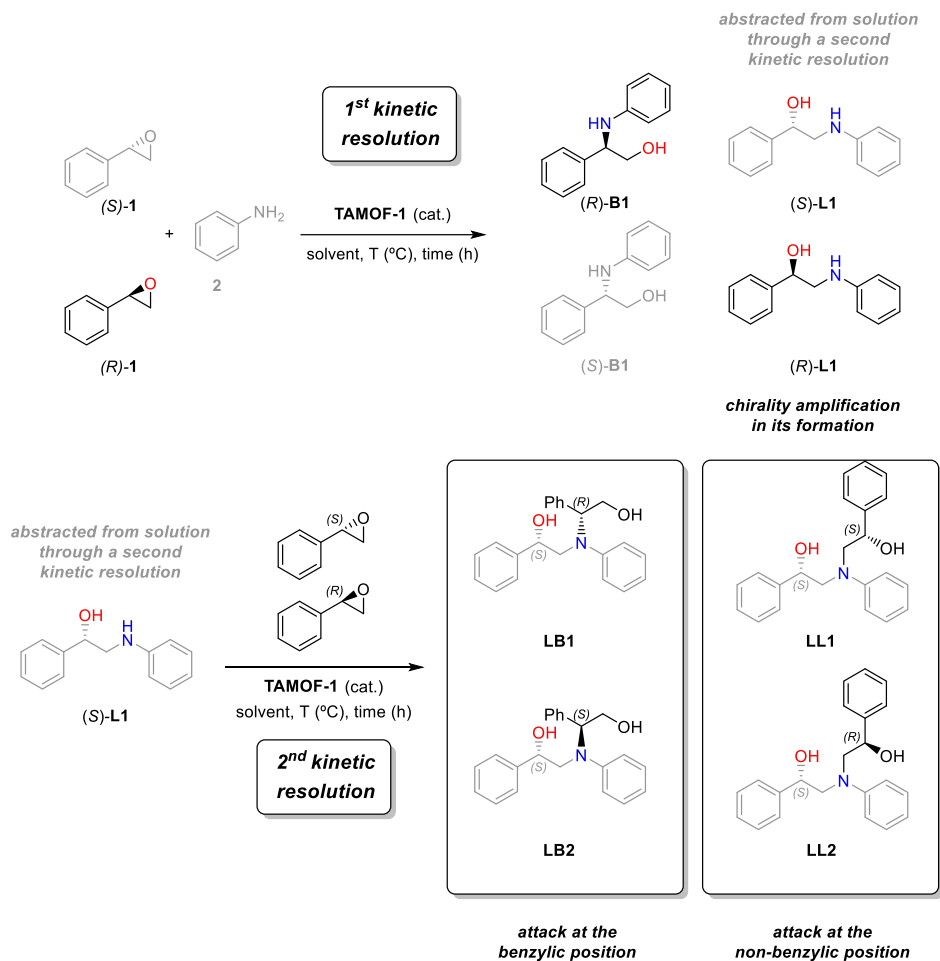
Scheme 13. General scheme of the kinetic resolution process.

2.3.4. Reaction mechanism

Carried out by Jesús Jover from *Universitat de Barcelona*, DFT calculations have been employed to investigate the reaction pathways leading to the experimentally observed amino alcohol and aminodiol products in both kinetic resolutions. The computed transition state energies, directly related to the new C–N bonds formed, constituted the key point for each pathway and were able to describe the preferential reactivity of the catalytic system. The reaction mechanism for the TAMOF-1-catalysed ring-opening of both (*S*)-**1** and (*R*)-**1** styrene oxides by aniline (**2**) (**Figure 97**) to produce (*R*)/(*S*)-**L1** or (*R*)/(*S*)-**B1** has been explored.

The reaction starts by the coordination of the epoxide **1** to the free axial position of one of the copper atoms in the TAMOF-1 structure; this process is exothermic for both styrene oxides by more than 50 kJ mol^{-1}. In intermediates **I-R** and **I-S**, the distance between the oxygen and the copper is around 2.4 Å. In addition, other weak contacts contribute to the stabilisation of these structures (e.g., the hydrogen atoms of the epoxide functionality point to the vacant axial position of the other two copper centres at distances ranging between 2.6 and 2.9 Å).

Chapter II
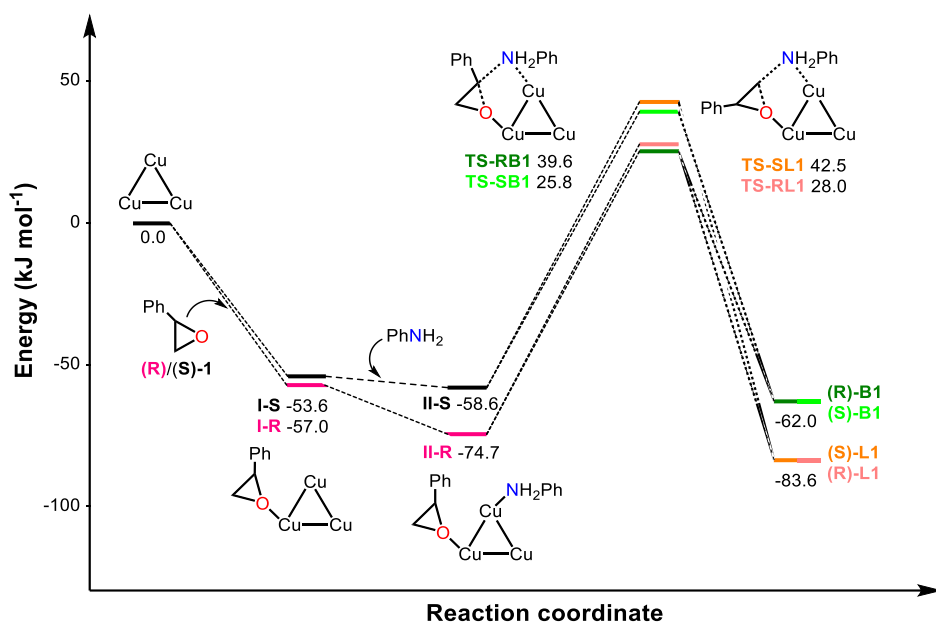
Figure 97. Computed energy profiles (in kJ mol^{-1}) for the TAMOF-1 catalysed enantioselective ring-opening of (*S*)-**1** and (*R*)-**1** with aniline.

UNIVERSITAT ROVIRA I VIRGILI
INSIGHTS IN HOMOCHIRAL METAL-ORGANIC FRAMEWORKS: FROM THEIR SYNTHESIS TO ENANTIOSELECTIVE
APPLICATIONS
Juanjo Cabezas Giménez

Differentiation of Epoxide Enantiomers by Kinetic Resolution

The epoxide molecules are not strongly activated upon coordination to the copper, as their C–O distances remain practically the same in the free and copper-bound styrene oxides. Subsequent aniline **2** attachment to one of the remaining two copper atoms leads to the formation of intermediates **II-R/II-S**. The Cu–N distance in these complexes is around 2.35 Å and, although one of the Cu–H$_{epox}$ contacts is lost, the other one is maintained, helping to stabilise these intermediates. This coordination process is also exothermic, and the associated energy gain varies depending on which enantiomer of styrene oxide is already present within TAMOF-1.

The results indicate that the binding of aniline is *ca.* 12 kJ mol^{-1} stronger in the presence of (*R*)-**1**, indicating that the MOF differentiation for both styrene oxide enantiomers take place in the presence of aniline. After the addition of aniline, the whole cavity is practically full and both substrates lie quite close to each other; additional contacts, shorter than 2.6 Å, are established between the styrene oxide and aniline in both **II-R** and **II-S**.

Nucleophilic attack of **2** onto the epoxide takes place producing either the linear or the branched product. The energy barriers leading to the latter are lower for both styrene oxides by 2.2 and 2.8 kJ mol^{-1} for the (*R*)-**B1**/(*S*)-**L1** and (*S*)-**B1**/(*R*)-**L1** pairs, respectively. Although these energy differences are not very large, they are enough to favour the formation of one regioisomer over the other in agreement with the experimental observations, which state that the branched products (**B1**) are favoured.

The energy barrier heights range between 98.2 and 102.7 kJ mol^{-1}, indicating that the reaction should not be very fast, as observed experimentally. It should be noted that the S$_N$2 barriers for the reaction of (*S*)-**1** with aniline are lower than for its (*R*)-**1** counterpart: 98.2 and 100.5 kJ mol^{-1} for the branched products, and 101.1 and 102.7 kJ mol^{-1} for the linear products. These differences in barrier heights are responsible for the observed enantioselectivity, with products (*R*)-**B1** and (*S*)-**L1** being preferably formed.

The intramolecular proton transfer steps to transform the zwitterionic amino alcohols into **B1** and **L1** have not been studied, since they are expected to be fast processes not determining the reaction outcome. The release of the final product is exothermic in all cases, except for (*S*)-**B1**. In this case, this product should be easily displaced by an incoming styrene oxide or aniline molecules, which would enable the catalytic process to proceed smoothly. As observed, TAMOF-1 favours the formation of the branched products **B1** over their –more stable– linear counterparts **L1**, as expected for a transformation that takes place under kinetic control.

The transition states for the nucleophilic attack of aniline onto *R*-**1** and *S*-**1** have also been computed without TAMOF-1. In these cases, the energy barriers leading to the branched and linear products are as high as 155.3 and 148.9 kJ mol^{-1}, respectively, around 50 kJ mol^{-1} higher than those computed within TAMOF-1. Interestingly, the uncatalysed reaction favours the formation of the linear products, which are in all cases the preferred thermodynamic products (see **Figure 98** and **Figure 99**).

These results indicate that the copper atoms in TAMOF-1 cooperatively mediate the formation of the products in the first kinetic resolution, probably by bringing styrene oxide and aniline close together inside the TAMOF-1 cavities. This effect has been already observed in reactions with supramolecular catalysts such as cucurbiturils, where the encapsulation of the reactants largely reduces the entropic cost of bringing reagents together and enhances reaction rates.[160] In addition, the coordination of one aniline and one styrene oxide molecules within TAMOF-1 has a positive accumulation effect on the reaction rate; the formation of species **II-S** and **II-R** is energetically favoured over other possible non-productive bimolecular arrangements containing either one aniline and one acetonitrile, one styrene oxide and one acetonitrile, and two aniline molecules.[161] Therefore, TAMOF-1 has two different functions in this process: first, it lowers the reaction barrier leading to the formation of all products, and second, allows for the preferential formation of the kinetic products over their thermodynamic counterparts, in contrast to the uncatalysed process.

The observed final configuration of **L1** enantiomers at long reaction times, producing a second kinetic resolution of aminodiols, has also been computed. In particular, we have studied the TAMOF-1-catalysed reaction between (*R*)/(*S*)-**L1** intermediates and (*R*)/(*S*)-**1** to deliver the linear products **LL1**, **LL2**, and their enantiomers, which constitute the most abundant products at this stage (**Figure 98**). The second kinetic resolution reaction starts by coordination of styrene oxide to one of the copper atoms in TAMOF-1 with this process being exactly the same than that found in the first kinetic resolution. The reaction should subsequently proceed by coordination of **L1** products to TAMOF-1. The computed transition states indicate that the fastest reaction is between (*S*)-**L1** and (*R*)-**1** to produce **LL1**, as experimentally observed (see **Figure 98** and **Figure 99**). This reaction has a barrier of 100.5

[160] a) Mock, W. L.; Irra, T. A.; Wepsiec, J. P.; Adhya, M. *J. Org. Chem.* **1989**, *54*, 5302-5308. b) Carlqvist, P.; Maseras, F. *Chem. Commun.* **2007**, 748-750. c) Goehry, C.; Besora, M.; Maseras, F. *ACS Catal.* **2015**, *5*, 2445-2451. d) Gil-Ramírez, G.; Hoekman, S.; Kitching, M. O.; Leigh, D. A.; Vitorica-Yrezabal, I. J.; Zhang, G. *J. Am. Chem. Soc.* **2016**, *138*, 13159-13162. e) Shybeka, I.; Aster, A.; Cheng, Y.; Sakai, N.; Frontera, A.; Vauthey, E.; Matile, S. *Chem. Eur. J.* **2020**, *26*, 14059-14063.
[161] We also attempted to compute the corresponding intermediates with two styrene oxide molecules within the cavity of **TAMOF-1** but it was not possible to find any configuration where both substrates remained attached to the copper atoms.

Chapter II

kJ mol^{-1}; in contrast, the reaction between (*S*)-**L1** and (*S*)-**1** to produce **LL2** has a larger barrier of 112.9 kJ mol^{-1}, confirming the preference of (*S*)-**L1** to engage with (*R*)-**1**.
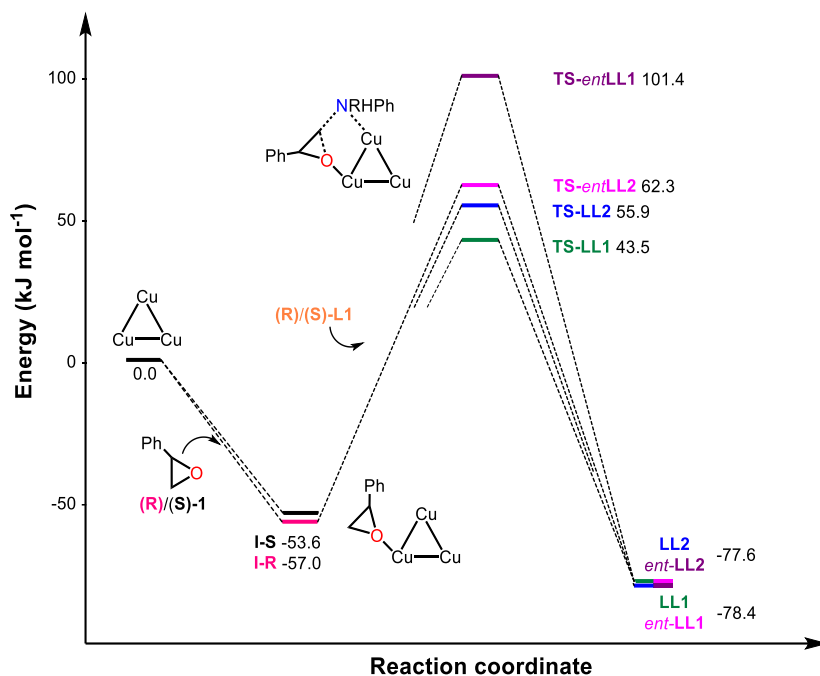
Figure 98. Computed energy profiles (in kJ mol^{-1}) for the TAMOF-1 catalysed enantioselective ring-opening of (*S*)-**1** and (*R*)-**1** with (*S*)-**L1** and (*R*)-**L1**.

These results indicate that, under experimental conditions, (*S*)-**L1** would engage faster in a second C–N bond formation process, hence producing the accumulation of (*R*)-**L1** and the reversal of the expected enantioselectivity for these amino alcohol intermediates at long reaction times.

The energy barriers for the formation of **LL1** and **LL2** from (*S*)-**L1** and (*R*)/(*S*)-**1** have also been computed in the absence of TAMOF-1. The reaction of (*S*)-**L1** with (*R*)-**1** and (*S*)-**1** produces high barriers of 150.4 and 161.4 kJ mol^{-1}, respectively. In this case, the reactivity order with and without TAMOF-1 is not altered but it can be observed that the presence of the MOF catalyst drastically reduces the energy barriers for most of the reaction pathways.
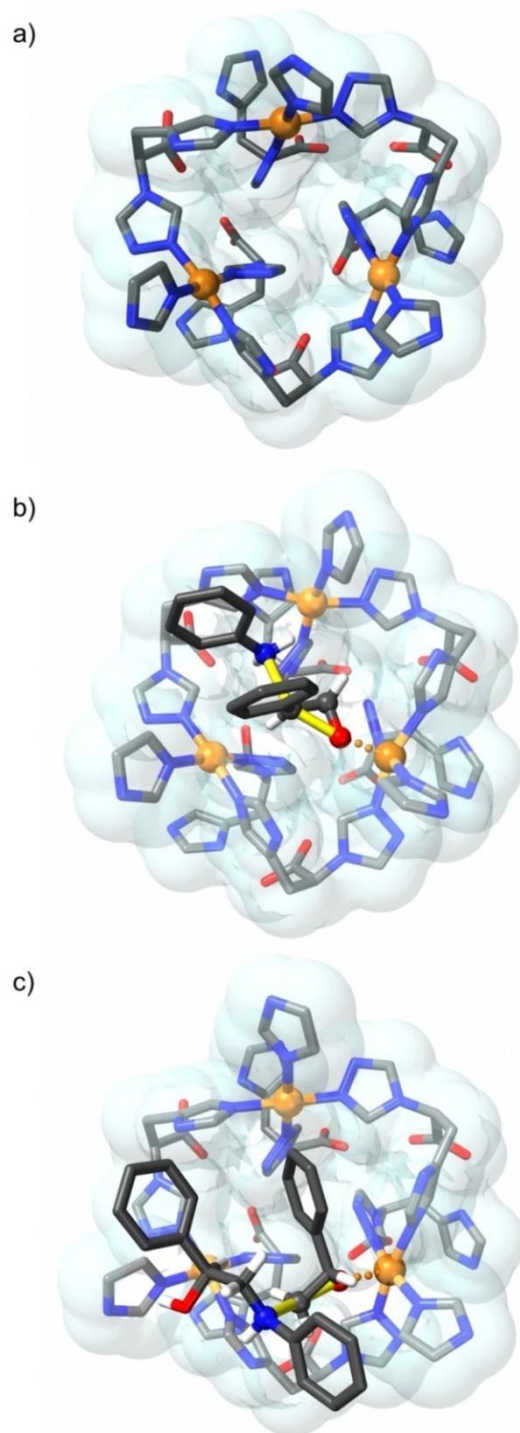
Figure 99. (a) Catalytic site of TAMOF-1. (b) Catalytic site for the preferred TS of the first ring-opening. (c) Catalytic centre for the preferred TS of the second ring-opening. *Bonds being broken/formed are indicated in yellow.*

111

UNIVERSITAT ROVIRA I VIRGILI
INSIGHTS IN HOMOCHIRAL METAL-ORGANIC FRAMEWORKS: FROM THEIR SYNTHESIS TO ENANTIOSELECTIVE
APPLICATIONS
Juanjo Cabezas Giménez

Differentiation of Epoxide Enantiomers by Kinetic Resolution

2.3.5. Recyclability of TAMOF-1

Recyclability is another relevant feature for heterogeneous catalysts. A series of reaction cycles were performed to assess the performance of TAMOF-1 as a recoverable and reusable catalyst. After each run (ACN, 40 °C, 16 h), the catalyst was collected through filtration, dried in the oven at 40 °C and reused in the next run of reactions under the same conditions. There was no loss of reactivity and enantioselectivity in the first two reaction cycles, whilst catalytic activity in terms of conversion was affected after the third run (**Figure 100**), attributed to a loss of catalyst due to handling between cycles. Regioselectivity and stereoselectivity remained constant throughout the five consecutive reaction cycles. Moreover, the crystallinity of the used catalyst after one reaction cycle remained unaltered compared to the as-prepared catalyst (**Figure 101**).
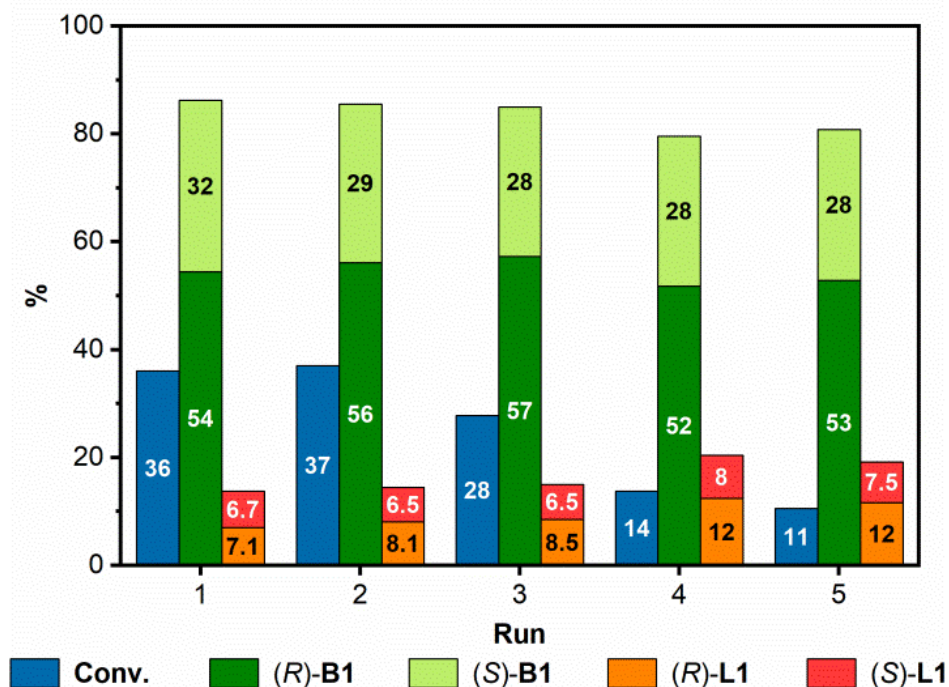
Figure 100. Conversion and enantiomeric ratio (indicated in the bar graphs) of **B1**, **B2**, **L1** and **L2** after recycling TAMOF-1 five times. Reaction conditions: 0.5 mmol of *rac*-**1**, 0.5 mmol of **2**, TAMOF-1 (10 mol%) and 2 mL of ACN at 40 °C for 16 h.
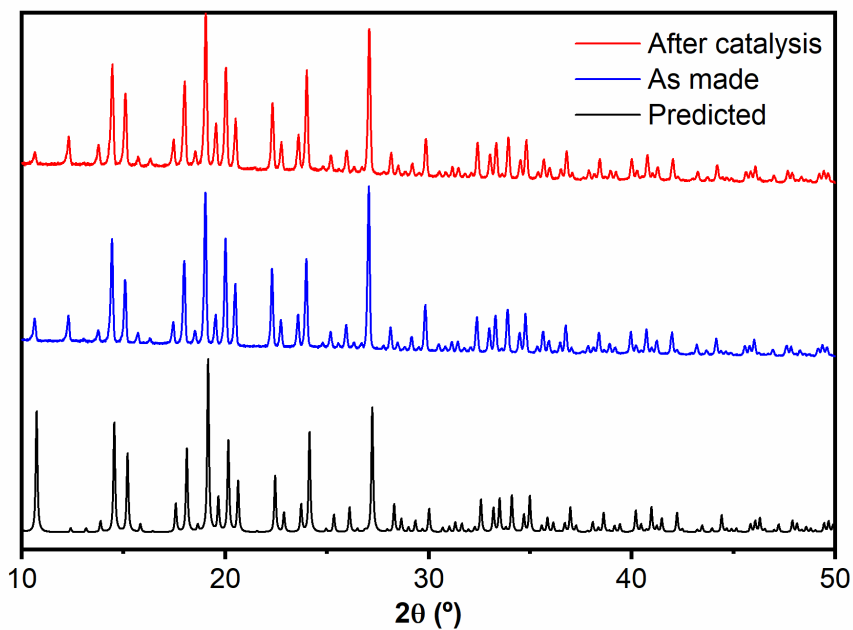
Figure 101. PXRD comparison of TAMOF-1 after one catalytic cycle (red pattern), as made (blue pattern) and simulated from its crystal structure (black pattern).

Chapter II

UNIVERSITAT ROVIRA I VIRGILI
INSIGHTS IN HOMOCHIRAL METAL-ORGANIC FRAMEWORKS: FROM THEIR SYNTHESIS TO ENANTIOSELECTIVE
APPLICATIONS
Juanjo Cabezas Giménez

Differentiation of Epoxide Enantiomers by Kinetic Resolution

2.4. CONCLUSIONS

In conclusion, TAMOF-1 is a recyclable catalyst for the efficient kinetic resolution of *rac*-**1** with aniline (**2**), yielding secondary amino alcohols (**Scheme 14**).

The linear products arising from the attack on the non-benzylic position underwent a second kinetic resolution, amplifying its final enantiomeric excess and forming isomeric aminodiols (subtractive Horeau amplification effect).

The ring-opening of a *meso*-epoxide with aniline catalysed by TAMOF-1 was also studied, and moderate enantioselectivities were obtained.

We found strong evidence that suggest that the reaction takes place inside the pores of TAMOF-1 by substituting the epoxide and the amine for bulkier analogues (*i.e. trans*-2,3-diphenyloxirane and *tert*-butylamine), and no conversion was observed in the reaction with **2** and *rac*-**1**, respectively.

Computational studies revealed that TAMOF-1 lowered the reaction barriers of all ring-opening processes inside channels. The calculated energy barriers agreed with the experimental observations: preferential formation of (*R*)-**B1** in the first kinetic resolution and preferential consumption of (*S*)-**L1** in the second kinetic resolution.

The regioselectivity and enantioselectivity of TAMOF-1 remained constant throughout five consecutive reaction cycles, and the structure remained unaltered after catalysis.
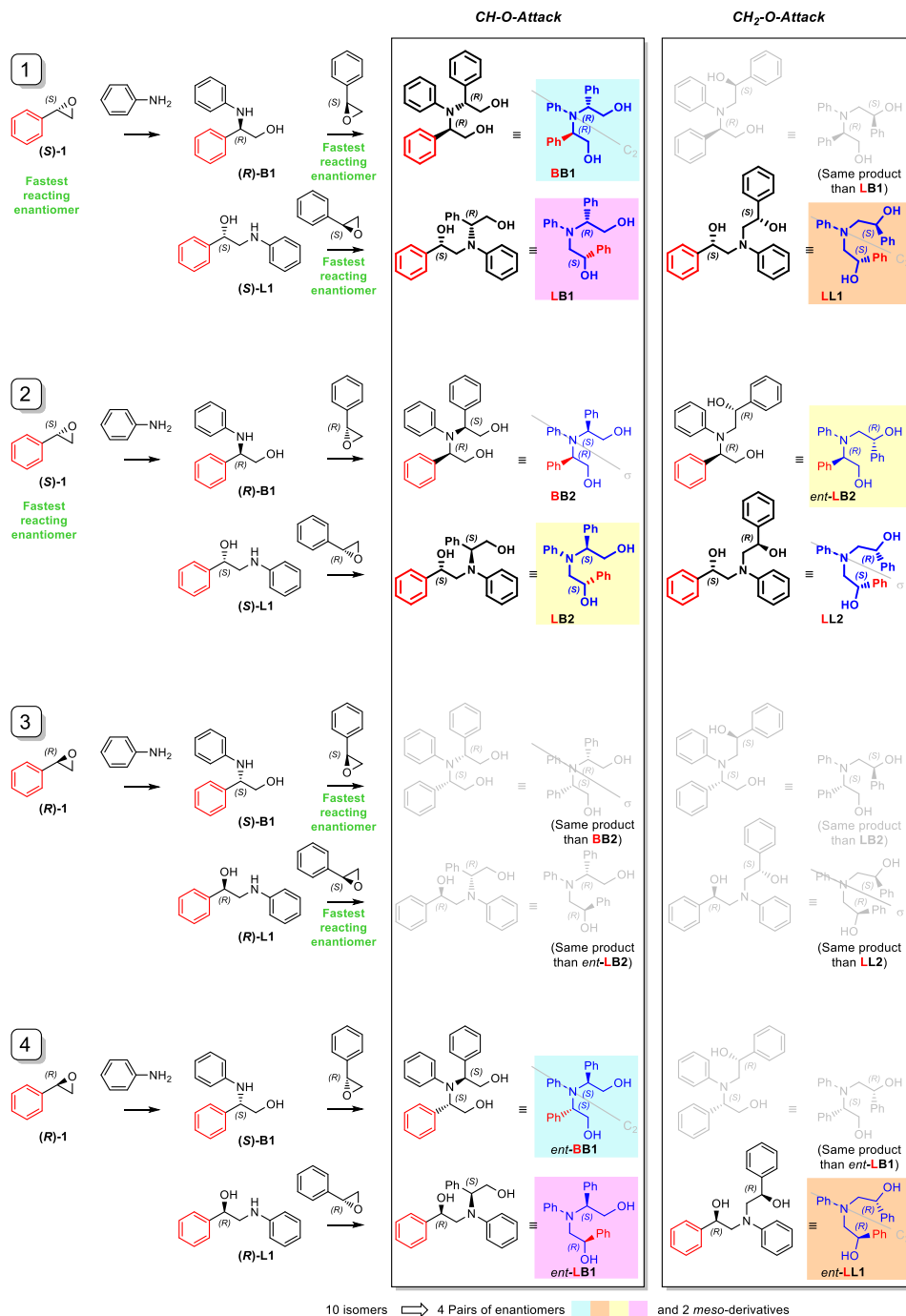
Scheme 14. Full scheme of the kinetic resolution process.

2.5. EXPERIMENTAL SECTION

2.5.1. Materials and general

All syntheses were carried out on chemicals purchased from commercial sources unless otherwise indicated. Air and moisture sensitive manipulations or reactions were run under inert atmosphere using anhydrous solvents and Schlenk techniques. All solvents were purchased commercially anhydrous or dried using a Solvent Purification System (SPS). Silica gel 60 (230–400 mesh) was used for column chromatography. NMR spectra were recorded in CDCl$_3$ as solvent on a Bruker Advance 300, 400 or 500 MHz Ultrashield spectrometers. ^{1}H and ^{13}C-NMR chemical shifts are quoted in ppm relative to residual solvent peaks. Data for ^{1}H-NMR are given as follows: chemical shift, multiplicity (s = singlet, d = doublet, t = triplet, m = multiplet, dd = doublet of doublets, tt = triplet of triplets), coupling constants and intensities. High-resolution mass spectra (HRMS) were recorded by using ESI as ionisation method in positive mode. IR spectra were recorded using Attenuated Total Reflection (ATR) spectroscopy. Specific optical rotation ([α]$_\lambda^T$) was recorded using a Jasco P1030 Polarimeter with a wavelength of 589 nm (sodium, D line) at 25 °C in the corresponding solvent, in a 10 cm cell, unless otherwise indicated. Crude mixtures of the kinetic resolution or *rac*-**1** were analysed by HPLC chromatography with an Agilent 1200 Series system equipped with a Chiralpak® IC column (4.6 x 250 mm) and a diode array detector, at a flow rate of 1 mL min^{-1} and a gradient solvent system of Hex/IPA 99:1 to 95:5 [(min, %IPA): (0, 1); (7, 1); (14, 5); (40, 5)], unless otherwise indicated. Powder X-ray diffraction analysis was performed using a Bruker Apex II Duo Single Crystal Diffractometer. DMFA and *S*-HTA were synthesised following the procedures described in Chapter 1, page **48**.

2.5.2. Computational details

The periodic structure of TAMOF-1 was truncated when carrying out the computational studies. The trinuclear copper cavity present in the MOF was preserved as such; the metal centres remain connected through 6 *S*-HTA ligands, and the coordination environment for each copper atom is completed by a truncated *S*-HTA, which has been modelled as a 3-(1*H*-imidazol) ligand. This truncated structure is charge neutral and accounts for 168 atoms.

All the calculations have been carried out using the Gaussian09[162] software with the unrestricted formalism of the dispersion-corrected B3LYP(D3)[163] functional and the Ahlrichs def2svp basis set[164] for all atoms. The geometries have been optimised in acetonitrile using the PCM method[165] and employing the SMD solvation model.[166] In all cases, the spin multiplicity was kept as a quartet, corresponding to a situation where the three copper(II) atoms do not interact with each other.

The nature of the stationary points along the reaction coordinate has been confirmed by vibrational analysis; the number of imaginary frequencies for minima and transition states is zero or none, respectively. Unless otherwise stated, all the reported energy values correspond to relative electronic energy differences corrected to include the translational entropy of the small molecules (aniline, styrene oxide, aminoalcohols and aminodiols) in THF at 40 °C.

In the case of the uncatalysed transition states (*i.e.* those where TAMOF-1 is not involved), computed Gibbs energies at 40 °C are provided. All the transition states were sought using the linear transit scan method, consisting of a series of optimisations keeping the reaction coordinate of interest fixed at different values. In this case, this process corresponds to scanning along the C–N bond that leads to the formation of the four possible enantiomers. When using this method, the structure with the highest energy is considered the transition state. All the relevant structures are published in the ioChem-BD database and can be retrieved at the following link: https://doi.org/10.19061/iochem-bd-1-177.

[162] Frisch, M. J. T., G. W.; Schlegel, H. B.; Scuseria, G. E.; Robb, M. A.; Cheeseman, J. R.; Scalmani, G.; Barone, V.; Mennucci, B.; Petersson, G. A.; Nakatsuji, H.; Caricato, M.; Li, X.; Hratchian, H. P.; Izmaylov, A. F.; Bloino, J.; Zheng, G.; Sonnenberg, J. L.; Hada, M.; Ehara, M.; Toyota, K.; Fukuda, R.; Hasegawa, J.; Ishida, M.; Nakajima, T.; Honda, Y.; Kitao, O.; Nakai, H.; Vreven, T.; Montgomery, J., J. A.; Peralta, J. E.; Ogliaro, F.; Bearpark, M.; Heyd, J. J.; Brothers, E.; Kudin, K. N.; Staroverov, V. N.; Kobayashi, R.; Normand, J.; Raghavachari, K.; Rendell, A.; Burant, J. C.; Iyengar, S. S.; Tomasi, J.; Cossi, M.; Rega, N.; Millam, N. J.; Klene, M.; Knox, J. E.; Cross, J. B.; Bakken, V.; Adamo, C.; Jaramillo, J.; Gomperts, R.; Stratmann, R. E.; Yazyev, O.; Austin, A. J.; Cammi, R.; Pomelli, C.; Ochterski, J. W.; Martin, R. L.; Morokuma, K.; Zakrzewski, V. G.; Voth, G. A.; Salvador, P.; Dannenberg, J. J.; Dapprich, S.; Daniels, A. D.; Farkas, Ö.; Foresman, J. B.; Ortiz, J. V.; Cioslowski, J.; Fox, D. J. Gaussian09, Revision D.01, Gaussian, Inc.: Wallingford CT, 2009.
[163] a) Lee, C.; Yang, W.; Parr, R. G. *Phys. Rev. B* **1988**, *37*, 785-789. b) Miehlich, B.; Savin, A.; Stoll, H.; Preuss, H. *Chem. Phys. Lett.* **1989**, *157*, 200-206. c) Becke, A. D. *J. Chem. Phys.* **1993**, *98*, 5648-5652. d) Grimme, S.; Antony, J.; Ehrlich, S.; Krieg, H. *J. Chem. Phys.* **2010**, *132*, 154104.
[164] a) Weigend, F.; Ahlrichs, R. *Phys. Chem. Chem. Phys.* **2005**, *7*, 3297-3305. b) Weigend, F.; Ahlrichs, R. *Phys. Chem. Chem. Phys.* **2005**, *7*, 3297-3305, Weigend, F. *Phys. Chem. Chem. Phys.* **2006**, *8*, 1057-1065, Weigend, F. *Phys. Chem. Chem. Phys.* **2006**, *8*, 1057-1065.
[165] a) Tannor, D. J.; Marten, B.; Murphy, R.; Friesner, R. A.; Sitkoff, D.; Nicholls, A.; Honig, B.; Ringnalda, M.; Goddard, W. A. *J. Am. Chem. Soc.* **1994**, *116*, 11875-11882. b) Marten, B.; Kim, K.; Cortis, C.; Friesner, R. A.; Murphy, R. B.; Ringnalda, M. N.; Sitkoff, D.; Honig, B. *J. Phys. Chem.* **1996**, *100*, 11775-11788.
[166] Marenich, A. V.; Cramer, C. J.; Truhlar, D. G. *J. Phys. Chem. B* **2009**, *113*, 6378-6396.

Chapter II

2.5.3. Synthetic procedures

2.5.3.1. General procedure for the kinetic resolution of *rac*-1

Prior to start the reaction, TAMOF-1 (10 or 50 mol%) was activated at 130 °C *in vacuo* for at least 3 h in a Schlenk flask. The Schlenk flask was filled with nitrogen and left to cool at rt, then, a solution of *rac*-**1** (1 eq.) and the corresponding amine (1 eq.) in ACN (0.25 M) was added to the Schlenk flask and the reaction mixture was stirred under nitrogen atmosphere at the desired temperature for the required time. The reaction mixture was left to cool at rt, then the suspension was filtered using a syringe filter with PTFE membrane (0.2 μm) and the filter was washed three times with ACN. Crude products of catalytic reactions were analysed in an Agilent 1200 series HPLC system equipped with diode array detector and quantified using external standards.

2.5.3.2. Ring-opening of *rac*-1 with *o*-anisidine (3)

The catalyst (TAMOF-1, 10 mol%) was activated at 130 °C *in vacuo* for at least 3 h in a Schlenk flask. The Schlenk flask was filled with nitrogen and left to cool at rt, then, a solution of *rac*-**1** (1 eq.) and **3** (1 eq.) in ACN (0.25 M) was added to the Schlenk flask and the reaction mixture was stirred under nitrogen atmosphere at 40 °C for 16 h. The reaction mixture was left to cool at rt, then the suspension was filtered using a syringe filter with PTFE membrane (0.2 μm) and the filter was washed three times with ACN, then the crude was analysed by ^{1}H-NMR (determination of the ratio of **4b** and **4l**) and SFC to determine the enantioselectivity.

2.5.3.3. Ring-opening of cyclohexene oxide (5) with 2

The catalyst (TAMOF-1, 10 mol%) was activated at 130 °C *in vacuo* for at least 3 h in a Schlenk flask. The Schlenk flask was filled with nitrogen and left to cool at rt, then, a solution of **5** (1 eq.) and **2** (1 eq.) in ACN (0.25 M) was added to the Schlenk flask and the reaction mixture was stirred under nitrogen atmosphere at 40 °C for 16 h. The reaction mixture was left to cool at rt, then the suspension was filtered using a syringe filter with PTFE membrane (0.2 μm) and the filter was washed three times with ACN, then the crude was analysed by HPLC to determine the enantioselectivity.[155]

2.5.3.4. Synthesis of products (*R*)-B1, (*S*)-L1, BB1, LB1, LL1[167]

(*S*)-**1** (3 g, 24.5 mmol) and **2** (2.73 g, 29.4 mmol) were dissolved in H_2O (40 mL, 0.625 M) and the reaction mixture was stirred for 18 h at 60 ºC. The reaction mixture was extracted with EtOAc (3 x 100 mL), and the combined organic layers were combined, dried over Na_2SO_4, and concentrated *in vacuo*. The residue obtained was then purified by flash column chromatography recursively using the following solvent systems:

- DCM (100%) to eliminate **2** from the crude and to isolate **BB1** (34 mg, 0.42% yield).
- DCM/MeOH 99:1 to obtain a mixture of (*R*)-**B1** and (*S*)-**L1**, and to isolate **LB1** (97 mg, 1.19%).
- Cy/MTBE 1:1 to isolate (*R*)-**B1** (3.68 g, 70.4%), (*S*)-**L1** (193 mg, 3.69%) and **LL1** (45 mg, 0.55%).
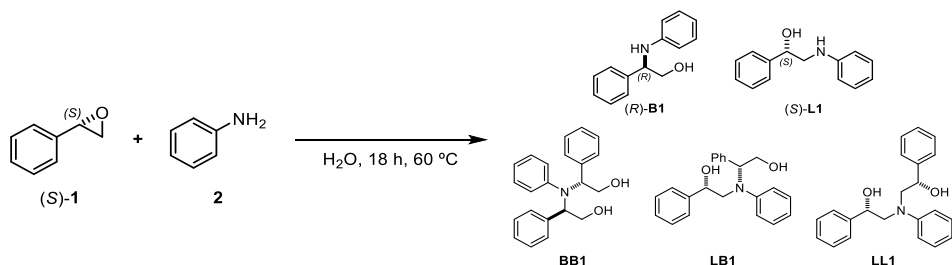
Scheme 15. Scheme of the synthesis of (*R*)-**B1**, (*S*)-**L1**, **BB1**, **LB1** and **LL1**.

2.5.3.5. Synthesis of products LB2 and LL2

The catalyst (TAMOF-1, 50 mol%) was activated at 130 ºC *in vacuo* for at least 3 h in a Schlenk flask. Then it was filled with nitrogen and left to cool at rt, then, a solution of the (*R*)-**1** (70 mg, 0.59 mmol) and (*S*)-**L1** (125 mg. 0.59 mmol) in ACN (2.3 mL, 0.25 M) was added to the Schlenk flask and the reaction mixture was stirred under nitrogen atmosphere at 40 ºC for 70 h. The reaction mixture was left to cool at rt, then the suspension was filtered using a syringe filter with PTFE membrane (0.2 μm) and the filter was washed three times with ACN. The crude solution was concentrated *in vacuo* and the residue was purified by flash column chromatography, using first Cy/EtOAc 1:1 to isolate **BL2** as a light-yellow oil (39 mg, 27.3% yield) and then Cy/MTBE 7:3 to isolate **LL2** (72.6 mg, 50.8% yield) as a light-yellow oil.

---

[167] Ziyaei-Halimehjani, A.; Gholami, H.; Saidi, M. R. *J. Iran. Chem. Soc.* **2013**, *10*, 7-11.

UNIVERSITAT ROVIRA I VIRGILI
INSIGHTS IN HOMOCHIRAL METAL-ORGANIC FRAMEWORKS: FROM THEIR SYNTHESIS TO ENANTIOSELECTIVE
APPLICATIONS
Juanjo Cabezas Giménez

Differentiation of Epoxide Enantiomers by Kinetic Resolution
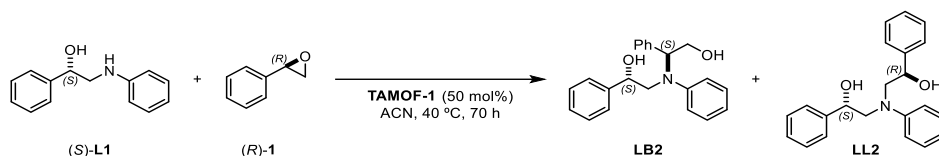
Scheme 16. Scheme of the synthesis of **LB2** and **LL2.**

2.5.3.6. Synthesis of *rac*-4b and *rac*-4l[168]

To 10 mL round-bottom flask, **3** (123 mg, 1 mmol), *rac*-**1** (124 mg, 1 mmol) and Schreiner's thiourea (*N*,*N'*-Bis[3,5(trifluoromethyl)phenyl]thiourea, 25 mg, 5 mol%) were added. The reaction mixture was stirred at 60 °C under free-solvent conditions for 2 h. The completion of the reaction was monitored by TLC (*n*-Hex/EtOAc 85:15). After completion of the reaction, the crude mixture was loaded onto a silica column, and it was purified by flash column chromatography (*n*-Hex/EtOAc 85:15). *rac*-**4b** was isolated as a yellow oil and *rac*-**4l** was isolated as a pale-yellow oil; yield of *rac*-**4b** = 68% and yield of *rac*-**4l** = 12%.
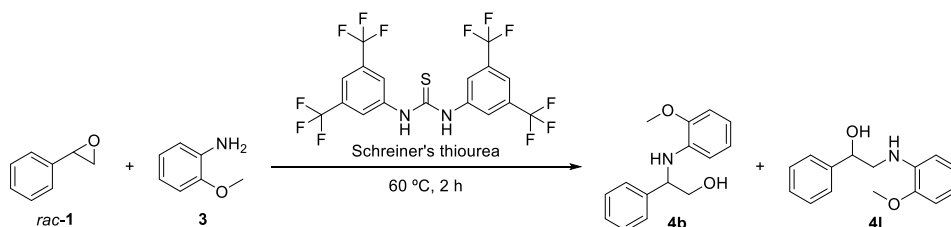
Scheme 17. Synthesis of the racemic mixtures of **4b** and **4l**.

2.5.3.7. Synthesis of (*S*)-4b and (*R*)-4l[169]

To an 8 mL vial equipped with a stirring bar, **3** (185 mg, 1.5 mmol), (*R*)-**1** (123 mg, 1 mmol) and zinc trifluoromethanesulfonate (37 mg, 10 mol%) were added. Then, the mixture was taken into the glovebox, where anhydrous toluene (2.5 mL, 0.4 M) was added. The reaction mixture was then taken outside the glovebox, heated to 100 °C and stirred for 12 h. The solvent was removed *in vacuo*, and the crude purified by flash column chromatography (*n*-Hex/EtOAc 85:15); yield of (*S*)-**4b** = 62% and (*R*)-**4l** = 7.8%.

[168] Chimni, S. S.; Bala, N.; Dixit, V. A.; Bharatam, P. V. *Tetrahedron* **2010**, *66*, 3042-3049.
[169] Xu, G.; Yang, G.; Wang, Y.; Shao, P.-L.; Yau, J. N. N.; Liu, B.; Zhao, Y.; Sun, Y.; Xie, X.; Wang, S.; Zhang, Y.; Xia, L.; Zhao, Y. *Angew. Chem. Int. Ed.* **2019**, *58*, 14082-14088.
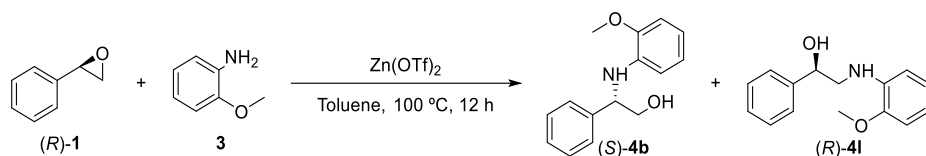
Scheme 18. Synthesis of (*S*)-**4b** and (*R*)-**4l**.

2.5.3.8. Synthesis of *rac-trans*-6[170]

rac-**5** (302 mg, 3.05 mmol), **2** (285 mg, 3.05 mmol) and acetic acid (0.18 mL, 3.05 mmol) were stirred together in a 1 mL vial under free-solvent conditions for 1 h. Then, K$_2$CO$_3$ (426 mg, 3.05 mmol) was added to the reaction mixture and the crude was purified by flash column chromatography (deactivated silica, *n*-Hex/EtOAc 3:1 + 3% Et$_3$N for deactivation, *n*-Hex/EtOAc 3:1 to elute the sample); yield = 74%.
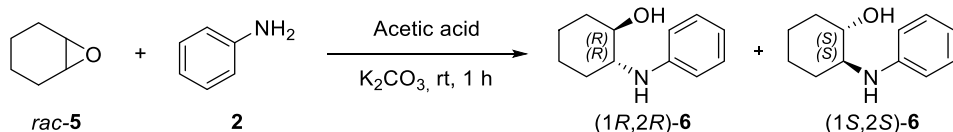
Scheme 19. Synthesis of *rac-trans*-**6**.

[170] Li, D.; Wang, J.; Yu, S.; Ye, S.; Zou, W.; Zhang, H.; Chen, J. *Chem. Commun.* **2020**, *56*, 2256-2259.

121

UNIVERSITAT ROVIRA I VIRGILI
INSIGHTS IN HOMOCHIRAL METAL-ORGANIC FRAMEWORKS: FROM THEIR SYNTHESIS TO ENANTIOSELECTIVE
APPLICATIONS
Juanjo Cabezas Giménez

Differentiation of Epoxide Enantiomers by Kinetic Resolution

2.5.4. Calibration with external standards in HPLC

The analyte (*rac*-**1**, **2**, (*R*)-**B1**, (*S*)-**L1**, **BB1**, **LB1**, **LL1**, **LL2** or **LB2**) was dissolved in an exact volume of *n*-Hex/IPA 99:1, then the solution was aliquoted in different concentrations and analysed by HPLC (CHIRALPAK® IC, *n*-Hex/IPA 99:1 to 95:5, 1 mL min^{-1}, 2 µL injection, gradient (min, %IPA): (0, 1); (7, 1); (14, 5); (40, 5). A linear regression was performed between the area (x) and the concentration (y), giving a linear formula to extrapolate the area values obtained in the catalytic studies.

- 2: $y = 0.000180x\ (R^2 = 0.999332)$
- *rac*-1: $y = 0.000317x\ (R^2 = 0.999834)$
- (*R*)-B1: $y = 0.000189x\ (R^2 = 0.999751)$
- (*S*)-L1: $y = 0.000158x\ (R^2 = 0.999653)$
- BB1: $y = 0.000543x\ (R^2 = 0.999992)$
- LB1: $y = 0.000507x\ (R^2 = 0.999932)$
- LL1: $y = 0.000257x\ (R^2 = 0.999898)$
- LL2: $y = 0.000232x\ (R^2 = 0.999886)$
- LB2: $y = 0.000308x\ (R^2 = 0.999843)$

2.5.5. Results of the kinetic resolutions

Table 8. Results of the kinetic resolution with 10 mol% of TAMOF-1. Reaction conditions: *rac*-**1** (0.5 mmol), **2** (0.5 mmol), TAMOF-1 (10 mol%), 2 mL ACN. Crude products of catalytic reactions were analysed by HPLC and quantified using external standards. (CHIRALPAK® IC, *n*-Hex/IPA 99:1 to 95:5, 1 mL min⁻¹, 5 μL injection, gradient (min, %IPA): (0, 1); (7, 1); (14, 5); (40, 5). ᵃ Results are expressed in mol%: the sum of these amounts within a row equals to 100 mol% of the starting epoxide.

Entry	Time (h)	(R)-1ᵃ	(S)-1ᵃ	2	(R)-B1ᵃ	(S)-B1ᵃ	(S)-L1ᵃ	(R)-L1ᵃ	e.e. 1 (%)	e.e. B1 (%)	e.e. L1 (%)
1	0	50	50	100	0	0	0	0	0	0	0
2	4	45.6	42.5	90.2	9.0	4.4	0.9	0.6	3.5 (R)	34.3 (R)	20.0 (S)
3	12	34.5	27.2	66.9	20.1	11.3	1.5	1.3	11.8 (R)	28.0 (R)	7.1 (S)
4	17	34.0	26.6	64.7	20.6	11.9	1.5	1.4	12.2 (R)	26.8 (R)	5.3 (S)
5	48	24.5	14.6	46.3	31.0	19.8	1.5	1.8	25.3 (R)	22.0 (R)	-9.1 (R)

Entry	Time (h)	BB1ᵃ	LB1ᵃ	LL1ᵃ	LB2ᵃ	LL2ᵃ
1 cont.	0	0	0	0	0	0
2 cont.	4	0	0	0	0	0
3 cont.	12	0.18	0.16	0.22	0.05	0.36
4 cont.	17	0.27	0.21	0.25	0.09	0.47
5 cont.	48	0.79	0.70	0.68	0.37	1.40

Chapter II

123

Differentiation of Epoxide Enantiomers by Kinetic Resolution

Table 9. Results of the kinetic resolution with 50 mol% of TAMOF-1**.** Reaction conditions: *rac*-**1** (0.5 mmol), **2** (0.5 mmol), TAMOF-1 (50 mol%), 2 mL ACN. Crude products of catalytic reactions were analysed by HPLC and quantified using external standards. (CHIRALPAK® IC, *n*-Hex/IPA 99:1 to 95:5, 1 mL min^{-1}, 5 µL injection, gradient (min, %IPA): (0, 1); (7, 1); (14, 5); (40, 5). [a] Results are expressed in mol%: the sum of these amounts within a row equals to 100 mol% of the starting epoxide.

Entry	Time (h)	(R)-1[a]	(S)-1[a]	2	(R)-B1[a]	(S)-B1[a]	(S)-L1[a]	(R)-L1[a]	e.e. 1 (%)	e.e. B1 (%)	e.e. L1 (%)
1	0	50	50	100	0	0	0	0	0	0	0
2	1	40.6	36.3	76.5	9.7	4.7	0.9	0.6	5.6 (R)	34.7 (R)	20.0 (S)
3	8	30.0	21.9	59.2	23.1	14.5	1.3	1.5	15.6 (R)	22.9 (R)	-3.7 (R)
4	16	21.2	12.2	45.5	32.4	22.7	1.2	1.7	26.9 (R)	17.6 (R)	-17.2 (R)
5	24	15.6	7.1	29.2	36.0	27.0	0.9	1.6	37.4 (R)	14.3 (R)	-28.0 (R)
6	32	14.1	5.6	25.2	38.6	30.1	0.7	1.5	41.7 (R)	12.4 (R)	-36.4 (R)
7	48	5.8	1.5	23.0	42.4	36.8	0.6	1.7	58.9 (R)	7.1 (R)	-45.5 (R)
8	96	2.7	0.4	20.5	39.8	34.5	0.5	1.5	74.2 (R)	7.1 (R)	-57.9 (R)

Entry	Time (h)	BB1[a]	LB1[a]	LL1[a]	LB2[a]	LL2[a]
1 cont.	0	0	0	0	0	0
2 cont.	1	0	0	0	0	0
3 cont.	8	0.02	0	0.41	0.08	0.47
4 cont.	16	0.20	0.08	0.59	0.14	0.99
5 cont.	24	0.64	0.08	0.86	0.26	1.57
6 cont.	32	0.79	0.16	1.00	0.29	1.84
7 cont.	48	1.10	0.22	1.04	0.73	2.38
8 cont.	96	1.73	0.46	1.09	1.08	2.62

2.5.6. Characterisation of amino alcohols and aminodiols

2.5.6.1. (*R*)-B1

(*R*)-B1
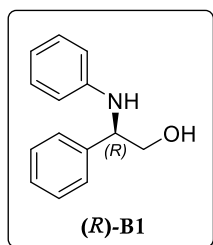
¹H NMR (400 MHz, CDCl₃) δ 7.41 – 7.31 (m, 4H), 7.31 – 7.24 (m, 1H), 7.16 – 7.05 (m, 2H), 6.75 – 6.65 (m, 1H), 6.63 – 6.55 (m, 2H), 4.51 (dd, J = 7.0, 4.2 Hz, 1H), 3.95 (dd, J = 11.1, 4.2 Hz, 1H), 3.76 (dd, J = 11.1, 7.0 Hz, 1H). **¹³C NMR** (101 MHz, CDCl₃) δ 147.37 (C), 140.25 (C), 129.30 (CH), 128.99 (CH), 127.77 (CH), 126.87 (CH), 118.05 (CH), 114.00 (CH), 67.53 (CH), 60.02 (CH₂).

HRMS-ESI (*m/z*): [M + H]⁺ calcd for $C_{14}H_{16}NO$, 214.1226; found, 214.1219. **[α]²⁵_D** = –21.9 (c = 0.5, CHCl₃), lit. (*S*)-**B1** = +27.5 (c = 0.5, CHCl₃); **IR** (neat, cm⁻¹) ῡ 3396, 3053, 3025, 2927, 2873, 1600, 1502, 1451, 1430, 1353, 1315, 1264, 1180, 1064, 1027, 749, 693. HPLC (CHIRALPAK® IC, *n*-Hex/IPA 99:1 to 95:5, 1 mL min⁻¹, 5 µL injection, gradient (min, %IPA): (0, 1); (7, 1); (14, 5); (40, 5)): t_R(*R*)-**B1**= 20.4 min, t_R(*S*)-**B1**= 28.4 min.[157]

2.5.6.2. (*S*)-L1

(*S*)-L1
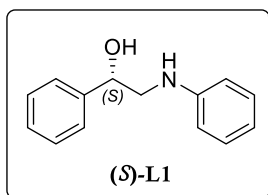
¹H NMR (400 MHz, CDCl₃) δ 7.48 – 7.39 (m, 4H), 7.39 – 7.31 (m, 1H), 7.28 – 7.18 (m, 2H), 6.78 (tt, J = 7.3, 1.1 Hz, 1H), 6.73 – 6.67 (m, 2H), 4.96 (dd, J = 8.4, 3.2 Hz, 1H), 4.07 (s, 1H), 3.47 (dd, J = 13.1, 3.9 Hz, 1H), 3.33 (dd, J = 13.1, 8.4 Hz, 1H), 2.40 (d, J = 3.3 Hz, 1H). **¹³C NMR** (101 MHz, CDCl₃) δ 148.02 (C), 142.14 (C), 129.49 (CH), 128.80 (CH), 128.17 (CH), 126.03 (CH), 118.28 (CH), 113.60 (CH), 72.65 (CH), 51.95 (CH₂). **HRMS-ESI** (*m/z*): [M + H]⁺ calcd for $C_{14}H_{16}NO$, 214.1226; found, 214.1220. **[α]²⁵_D** = –19.5 (c = 0.97, acetone), lit. (*R*)-**L1** = +17.2 (c = 0.98, acetone). **IR** (neat, cm⁻¹) ῡ 3393, 3053, 3026, 2923, 2823, 1602, 1504, 1453, 1432, 1317, 1259, 1058, 750, 693. HPLC (CHIRALPAK® IC, *n*-Hex/IPA 99:1 to 95:5, 1 mL min⁻¹, 5 µL injection, gradient (min, %IPA): (0, 1); (7, 1); (14, 5); (40, 5)): t_R(*S*)-**L1**= 22.9 min, t_R(*R*)-**L1**= 21.9 min.[171]

---

[171] Xu, Z.; Zhu, S.; Liu, Y.; He, L.; Geng, Z.; Zhang, Y. *Synthesis* **2010**, 811-817.

Chapter II

UNIVERSITAT ROVIRA I VIRGILI
INSIGHTS IN HOMOCHIRAL METAL-ORGANIC FRAMEWORKS: FROM THEIR SYNTHESIS TO ENANTIOSELECTIVE
APPLICATIONS
Juanjo Cabezas Giménez

Differentiation of Epoxide Enantiomers by Kinetic Resolution

2.5.6.3. BB1
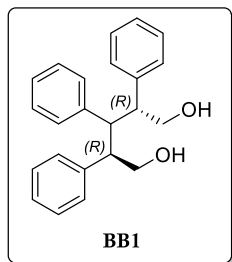
^{1}H NMR (500 MHz, CDCl$_3$) δ 7.30 – 7.25 (m, 6H), 7.22 (dd, J = 8.4, 7.2 Hz, 2H), 7.15 – 7.07 (m, 5H), 6.93 (d, J = 7.9 Hz, 2H), 4.57 (dd, J = 7.9, 5.7 Hz, 2H)23.89 (dd, J = 11.2, 7.9 Hz, 2H), 3.69 (dd, J = 11.3, 5.7 Hz, 2H), 2.31 (s, 2H). **^{13}C NMR** (126 MHz, CDCl$_3$) δ 144.61 (C), 138.21 (C), 128.89 (CH), 128.57 (CH), 128.53 (CH), 128.02 (CH), 126.64 (CH), 124.41 (CH), 64.23 (CH), 63.29 (CH$_2$). **HRMS-ESI** (*m/z*): [M + H]$^+$ calcd for C$_{22}$H$_{24}$NO$_2$, 334.1802; found, 334.1787. **[α]$^{25}_D$** = −30.53 (c = 0.16, CH$_2$Cl$_2$). **IR** (neat, cm^{-1}) $\bar{v}$ 3345, 3060, 2926, 1596, 1499, 1453, 1404, 1263, 1149, 1025, 735, 697. HPLC (CHIRALPAK® IC, *n*-Hex/IPA 99:1 to 95:5, 1 mL min^{-1}, 5 μL injection, gradient (min, %IPA): (0, 1); (7, 1); (14, 5); (40, 5)): t_R = 36.2 min.

2.5.6.4. LB1
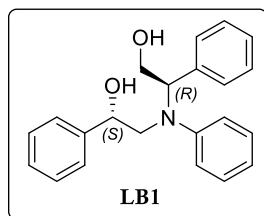
^{1}H NMR (400 MHz, CDCl$_3$) δ 7.40 – 7.27 (m, 10H), 7.10 – 7.04 (m, 2H), 6.98 (d, J = 8.1 Hz, 2H), 6.92 (t, J = 7.3 Hz, 1H), 4.94 (t, J = 6.7 Hz, 1H), 4.86 (t, J = 6.7 Hz, 1H), 4.00 – 3.89 (m, 2H), 3.53 (s, 1H), 3.39 (d, J = 6.7 Hz, 2H), 2.49 (s, 1H). **^{13}C NMR** (101 MHz, CDCl$_3$) δ 148.80 (C), 142.70 (C), 137.61 (C), 129.21 (CH), 128.68 (CH), 128.66 (CH), 128.16 (CH), 127.59 (CH), 127.16 (CH), 126.00 (CH), 119.97 (CH), 118.44 (CH), 71.73 (CH), 68.13 (CH), 61.64 (CH$_2$), 56.73 (CH$_2$). **HRMS-ESI** (*m/z*): [M + H]$^+$ calcd for C$_{22}$H$_{24}$NO$_2$, 334.1802; found, 334.1792. **[α]$^{25}_D$** = −26.29 (c = 0.25, CH$_2$Cl$_2$). **IR** (neat, cm^{-1}) $\bar{v}$ 3360, 3060, 3028, 2923, 1597, 1495, 1451, 1349, 1264, 1195, 1028, 915, 804, 750, 698. HPLC (CHIRALPAK® IC, *n*-Hex/IPA 99:1 to 95:5, 1 mL min^{-1}, 5 μL injection, gradient (min, %IPA): (0, 1); (7, 1); (14, 5); (40, 5)): t_R = 29.7 min.

2.5.6.5. LL1
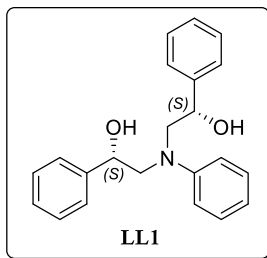
^{1}H NMR (400 MHz, CDCl$_3$) δ 7.47 – 7.36 (m, 8H), 7.35 – 7.27 (m, 4H), 6.96 (d, J = 8.1 Hz, 2H), 6.82 (t, J = 7.3 Hz, 1H), 5.06 (dd, J = 9.6, 3.4 Hz, 2H), 3.61 (dd, J = 15.0, 3.4 Hz, 2H), 3.51 (dd, J = 15.0, 9.6 Hz, 2H), 3.19 (s, 2H). **^{13C} NMR** (101 MHz, CDCl$_3$) δ 148.61 (C), 142.03 (C), 129.44 (CH), 128.77 (CH), 128.04 (CH), 126.03 (CH), 118.22 (CH), 114.64 (CH), 71.39 (CH), 60.60 (CH$_2$). **HRMS-ESI** (*m/z*): [M + H]$^+$ calcd for C$_{22}$H$_{24}$NO$_2$, 334.1802; found, 334.1793. **[α]$^{25}_D$** = −38.98 (c = 0.31, CH$_2$Cl$_2$). **IR** (neat, cm^{-1}) $\bar{v}$ 3362, 3061, 3028, 2920, 2853, 1597, 1503, 1452, 1346, 1262, 1195, 1171, 1090, 1059, 1027, 994, 745, 698. HPLC (CHIRALPAK® IC, *n*-Hex/IPA 99:1 to 95:5, 1 mL min^{-1}, 5 µL injection, gradient (min, %IPA): (0, 1); (7, 1); (14, 5); (40, 5)): t_R = 25.1 min.

2.5.6.6. LB2
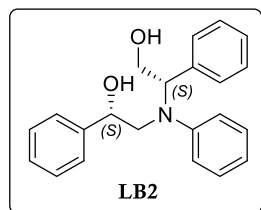
^{1}H NMR (400 MHz, CDCl$_3$) δ 7.40 – 7.27 (m, 7H), 7.25 – 7.15 (m, 3H), 7.13 – 7.04 (m, 4H), 6.86 (t, J = 7.3 Hz, 1H), 5.21 (dd, J = 10.4, 4.8 Hz, 1H), 5.03 (dd, J = 10.4, 2.1 Hz, 1H), 4.29 – 4.13 (m, 2H), 3.40 (dd, J = 15.3, 2.1 Hz, 1H), 3.14 (dd, J = 15.3, 10.4 Hz, 1H). **^{13}C NMR** (101 MHz, CDCl$_3$) δ 149.29 (C), 142.17 (C), 138.83 (C), 129.56 (CH), 128.82 (CH), 128.65 (CH), 128.20 (CH), 127.43 (CH), 127.04 (CH), 125.84 (CH), 118.88 (CH), 116.32 (CH), 70.57 (CH), 65.04 (CH), 62.00 (CH$_2$), 52.67 (CH$_2$). **HRMS-ESI** (*m/z*): [M + H]$^+$ calcd for C$_{22}$H$_{24}$NO$_2$, 334.1802; found, 334.1816. **[α]$^{25}_D$** = −51.01 (c = 0.34, CH$_2$Cl$_2$). **IR** (neat, cm^{-1}) $\bar{v}$ 3299, 3061, 3030, 2961, 2915, 1633, 1597, 1498, 1450, 1383, 1344, 1190, 1157, 1060, 1031, 751, 697. HPLC (CHIRALPAK® IC, *n*-Hex/IPA 99:1 to 95:5, 1 mL min^{-1}, 5 µL injection, gradient (min, %IPA): (0, 1); (7, 1); (14, 5); (40, 5)): t_R = 27.3 min.

Chapter II

127

UNIVERSITAT ROVIRA I VIRGILI
INSIGHTS IN HOMOCHIRAL METAL-ORGANIC FRAMEWORKS: FROM THEIR SYNTHESIS TO ENANTIOSELECTIVE
APPLICATIONS
Juanjo Cabezas Giménez

Differentiation of Epoxide Enantiomers by Kinetic Resolution

2.5.6.7. LL2

LL2
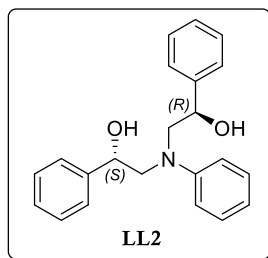
^{1}**H NMR** (400 MHz, CDCl$_3$) δ 7.49 – 7.28 (m, 12H), 6.86 (d, J = 7.4 Hz, 3H), 5.10 (dd, J = 9.8, 2.2 Hz, 2H), 4.51 (s, 2H), 3.82 (dd, J = 15.3, 2.2 Hz, 2H), 3.38 (dd, J = 15.3, 9.8 Hz, 2H). ^{13C} **NMR** (101 MHz, CDCl$_3$) δ 147.90 (C), 141.93 (C), 129.67 (CH), 128.79 (CH), 128.10 (CH), 125.98 (CH), 117.59 (CH), 112.93 (CH), 72.78 (CH), 63.23 (CH$_2$). **HRMS-ESI** (*m/z*): [M + H]$^+$ calcd for C$_{22}$H$_{24}$NO$_2$, 334.1802; found, 334.1813. **IR** (neat, cm^{-1}) $\bar{v}$ 3326, 3060, 3028, 2893, 1597, 1502, 1452, 1344, 1196, 1168, 1057, 993, 745, 678. HPLC (CHIRALPAK® IC, *n*-Hex/IPA 99:1 to 95:5, 1 mL min^{-1}, 5 μL injection, gradient (min, %IPA): (0, 1); (7, 1); (14, 5); (40, 5)): t_R = 24.4 min]

2.5.6.8. (*S*)-4b

(*S*)-4b
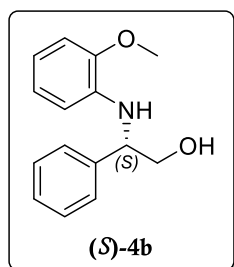
^{1}**H NMR** (400 MHz, CDCl$_3$) δ 7.39 – 7.30 (m, 4H), 7.28 – 7.23 (m, 1H), 6.78 (dd, J = 7.7, 1.6 Hz, 1H), 6.71 (td, J = 7.6, 1.6 Hz, 1H), 6.65 (td, J = 7.6, 1.7 Hz, 1H), 6.41 (dd, J = 7.7, 1.7 Hz, 1H), 5.00 (s, 1H), 4.54 (dd, J = 7.3, 4.3 Hz), 3.96 (ddd, J = 11.5, 7.3, 4.5 Hz, 1H), 3.90 (s, 3H), 3.81 (ddd, J = 11.5, 7.3, 4.5 Hz, 1H), 1.80 (dd, J = 7.3, 5.1 Hz, 1H). ^{13}**C{^{1}H. NMR** (101 MHz, CDCl$_3$) δ 147.29 (C), 140.35 (C), 137.14 (C), 128.93 (CH), 127.70 (CH), 126.85 (CH), 121.25 (CH), 117.27 (CH), 111.61 (CH), 109.58 (CH), 67.64 (CH), 59.93 (CH$_2$), 55.62 (CH$_3$). **MS-ESI** (*m/z*): [M + H]$^+$ = 244.1. [α]$^{25}_D$ = −2.5 (c = 0.60, CHCl$_3$), lit. −30.0 (c = 0.60, CHCl$_3$). SFC (Acquity UPC2, CHIRALPAK® IA column, CO$_2$/MeOH 95:5, 1500 psi, 240 nm): t_R(*S*)-**4b** = 3.6 min, t_R(*R*)-**4b** = 6.8 min.[169]

2.5.6.9. (R)-4l

(R)-4l
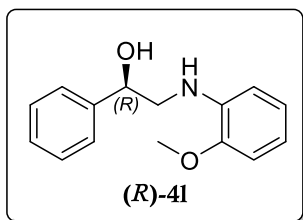
¹H NMR (400 MHz, CDCl₃) δ 7.46 – 7.36 (m, 4H), 7.35 – 7.30 (m, 1H), 6.88 (td, J = 7.6, 1.5 Hz, 1H), 6.80 (dd, J = 8.0, 1.3 Hz, 1H), 6.76 – 6.68 (m, 2H), 4.96 (dd, J = 8.9, 3.7 Hz, 1H), 4.66 (s, 1H), 3.86 (s, 3H), 3.45 (dd, J = 13.2, 3.7 Hz, 1H), 3.32 (dd, J = 13.2, 8.9 Hz, 1H), 2.50 (s, 1H). **¹³C NMR** (101 MHz, CDCl₃) δ 147.36 (C), 142.21 (C), 137.94 (C), 128.72 (CH), 128.05 (CH), 126.04 (CH), 121.41 (CH), 117.43 (CH), 110.63 (CH), 109.85 (CH), 72.68 (CH), 55.62 (CH₂), 52.01 (CH₃). **MS-ESI** (m/z): [M + H]⁺ = 244.2. **[α]²⁵_D** = −2.9 (c = 0.35, CHCl₃), lit. −2.6 (c = 0.35, CHCl₃). SFC (Acquity UPC2, CHIRALPAK® IA column, CO₂/MeOH 95:5, 1500 psi, 240 nm): t_R(R)-**4l** = 9.4 min, t_R(S)-**4l** = 6.9 min.[169]

2.5.6.10. *rac-trans*-6

rac-trans-6
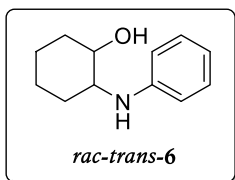
¹H NMR (300 MHz, CDCl₃) δ 7.23 – 7.14 (m, 2H), 6.79 – 6.68 (m, 2H), 3.43 – 3.22 (m, 2H), 3.22 – 3.07 (m, 1H), 2.72 (s, 1H), 2.18 – 2.07 (m, 2H), 1.83 – 1.65 (m, 2H), 1.49 – 1.20 (m, 3H), 1.16 – 0.96 (m, 1H). **¹³C NMR** (75 MHz, CDCl₃) δ 147.96 (C), 129.49 (CH), 118.54 (CH), 114.54 (CH), 74.73 (CH), 60.34 (CH), 33.28 (CH₂), 31.79 (CH₂), 25.20 (CH₂), 24.42 (CH₂). **MS-ESI** (m/z): [M + H]⁺ = 192.2. HPLC (CHIRALCEL® OD-H, *n*-Hex/IPA 85:15, 1 mL min⁻¹, 247 nm): t_R(1S, 2S-**6**) = 8.2 min (lit. 10.3 min) and t_R(1R, 2R-**6**)= 9.2 min (lit. 11.9 min).[170]

Chapter II

129

UNIVERSITAT ROVIRA I VIRGILI
INSIGHTS IN HOMOCHIRAL METAL-ORGANIC FRAMEWORKS: FROM THEIR SYNTHESIS TO ENANTIOSELECTIVE
APPLICATIONS
Juanjo Cabezas Giménez

Differentiation of Epoxide Enantiomers by Kinetic Resolution

2.5.7. NMR spectra
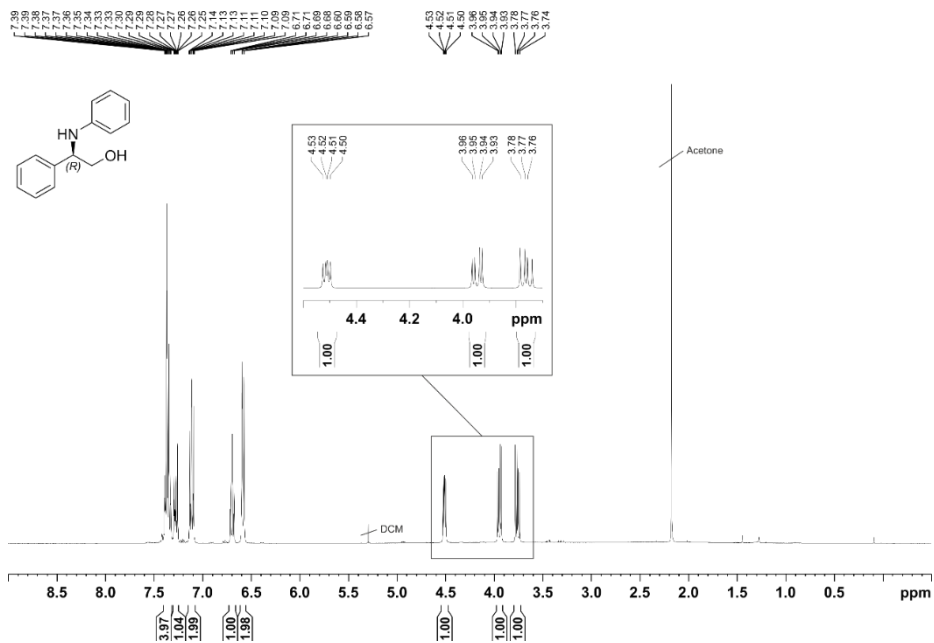
Figure 102. ^{1}H-NMR (400 MHz, CDCl$_3$) spectra of isolated compound (*R*)-**B1**.
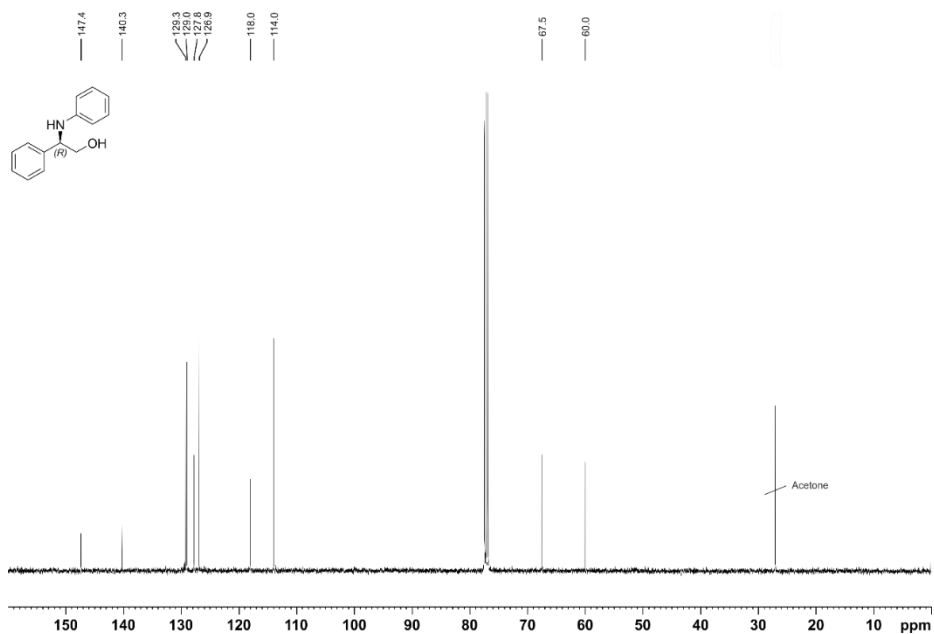
Figure 103. ^{13}C-NMR (101 MHz, CDCl$_3$) spectra of isolated compound (*R*)-**B1**.
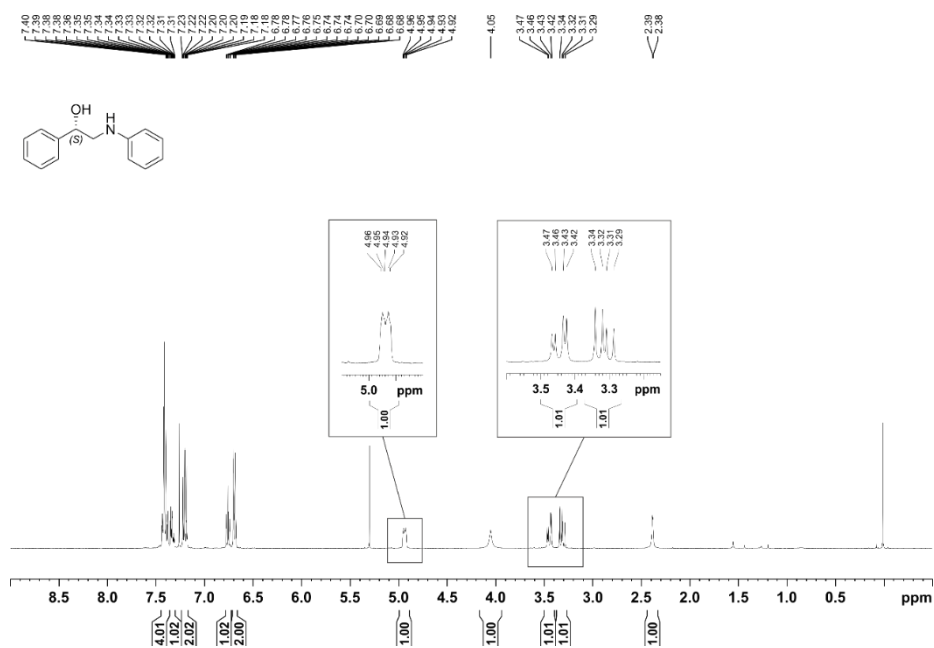
Figure 104. ^{1}H-NMR (400 MHz, CDCl$_3$) spectra of isolated compound (*S*)-**L1**.
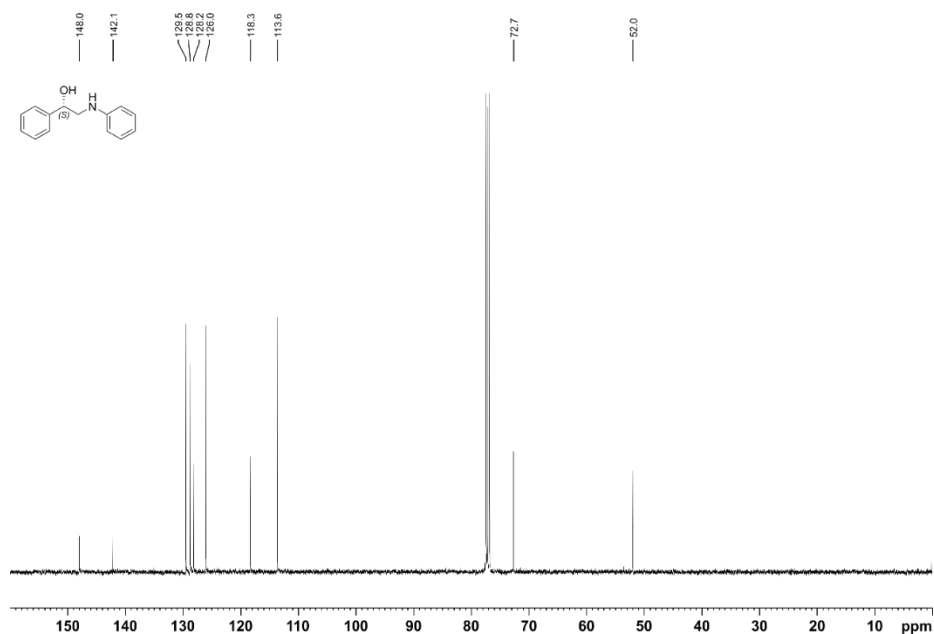
Figure 105. ^{13}C-NMR (101 MHz, CDCl$_3$) spectra of isolated compound (*S*)-**L1**.

131

UNIVERSITAT ROVIRA I VIRGILI
INSIGHTS IN HOMOCHIRAL METAL-ORGANIC FRAMEWORKS: FROM THEIR SYNTHESIS TO ENANTIOSELECTIVE
APPLICATIONS
Juanjo Cabezas Giménez

Differentiation of Epoxide Enantiomers by Kinetic Resolution
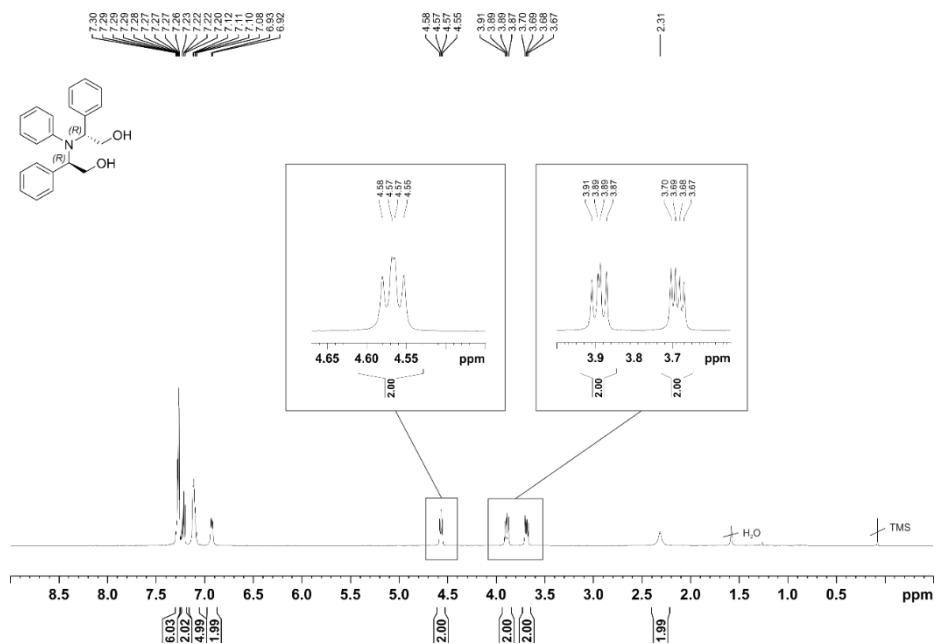
Figure 106. ^{1}H-NMR (500 MHz, CDCl$_3$) spectra of isolated compound **BB1**.
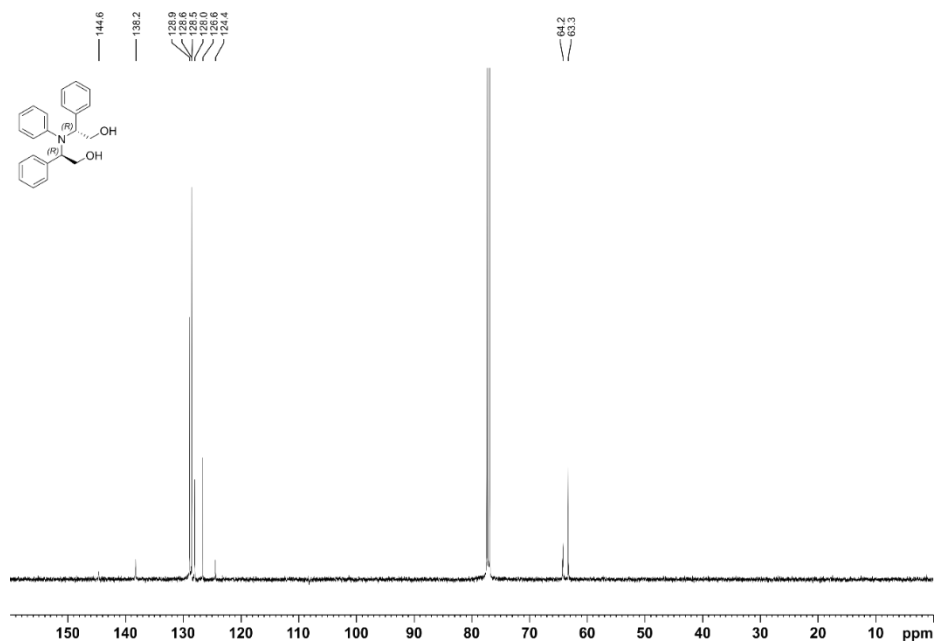
Figure 107. ^{13}C-NMR (126 MHz, CDCl$_3$) spectra of isolated compound **BB1**.
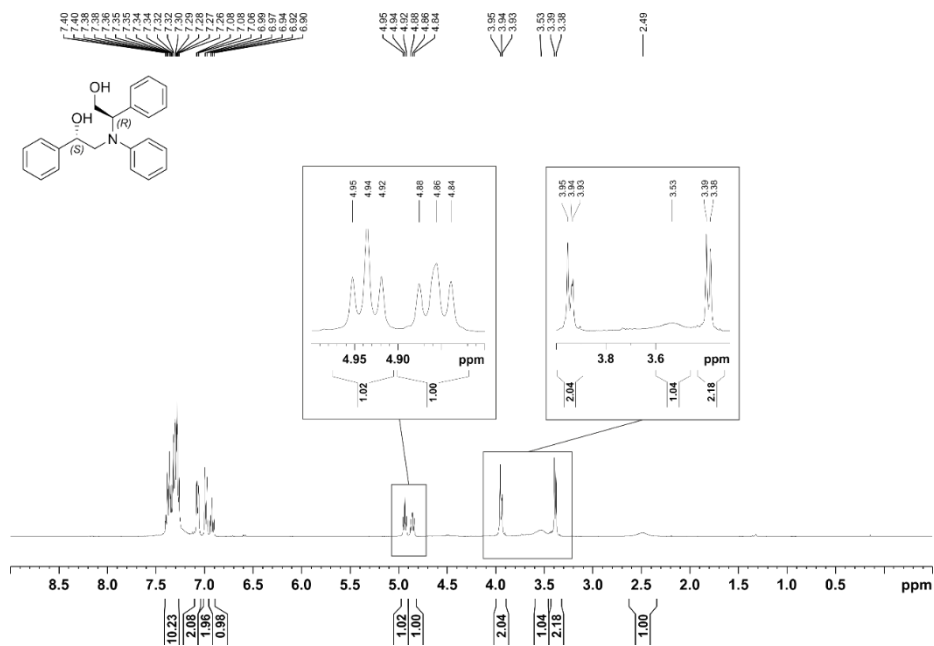
Figure 108. [^1]H-NMR (400 MHz, CDCl$_3$) spectra of isolated compound **LB1**.
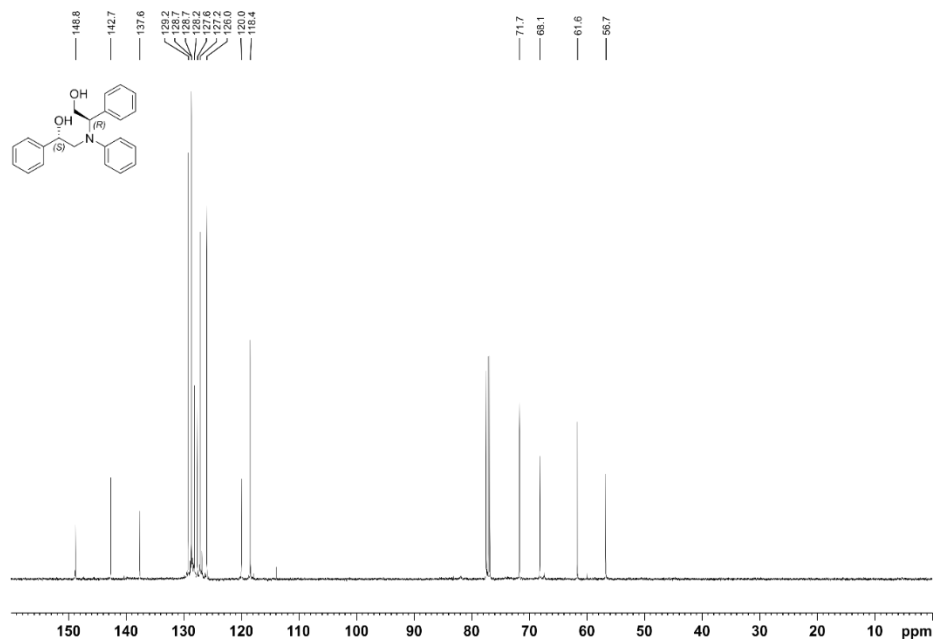
Figure 109. [^13]C-NMR (101 MHz, CDCl$_3$) spectra of isolated compound **LB1**.

133

Differentiation of Epoxide Enantiomers by Kinetic Resolution
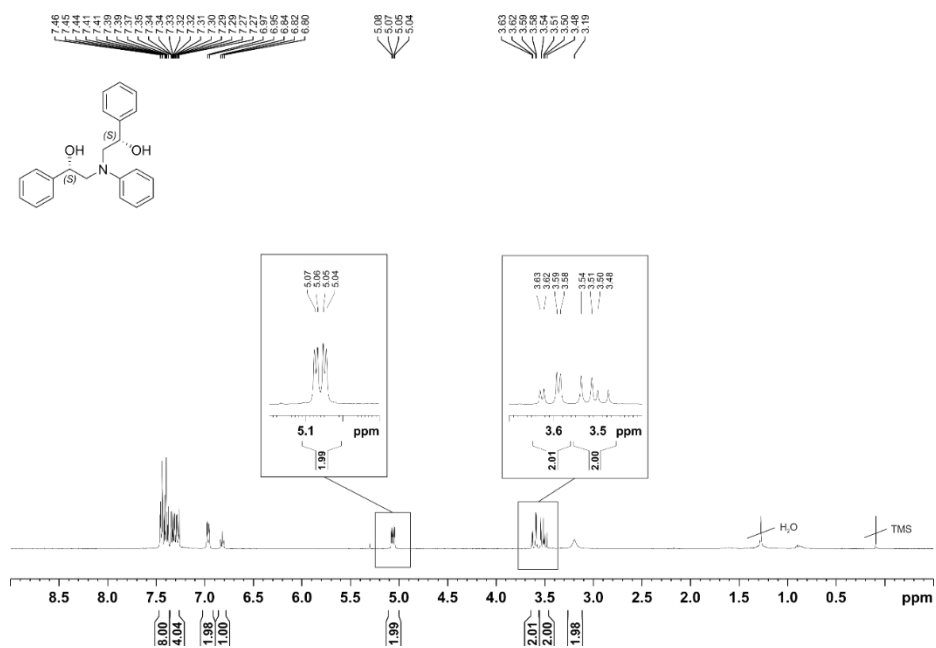
Figure 110. ^{1}H-NMR (400 MHz, CDCl$_3$) spectra of isolated compound **LL1**.
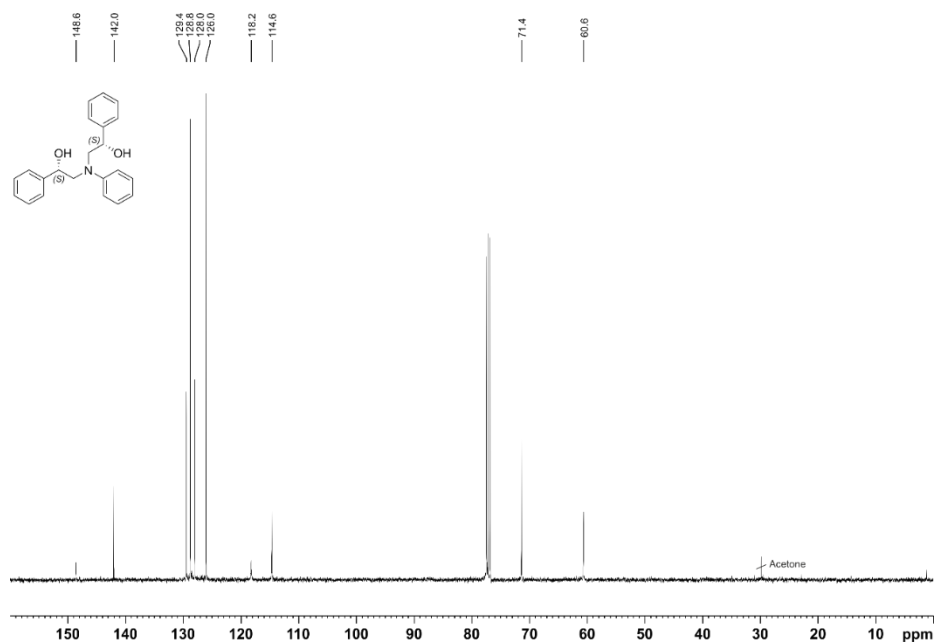
Figure 111. ^{13}C-NMR (101 MHz, CDCl$_3$) spectra of isolated compound **LL1**.
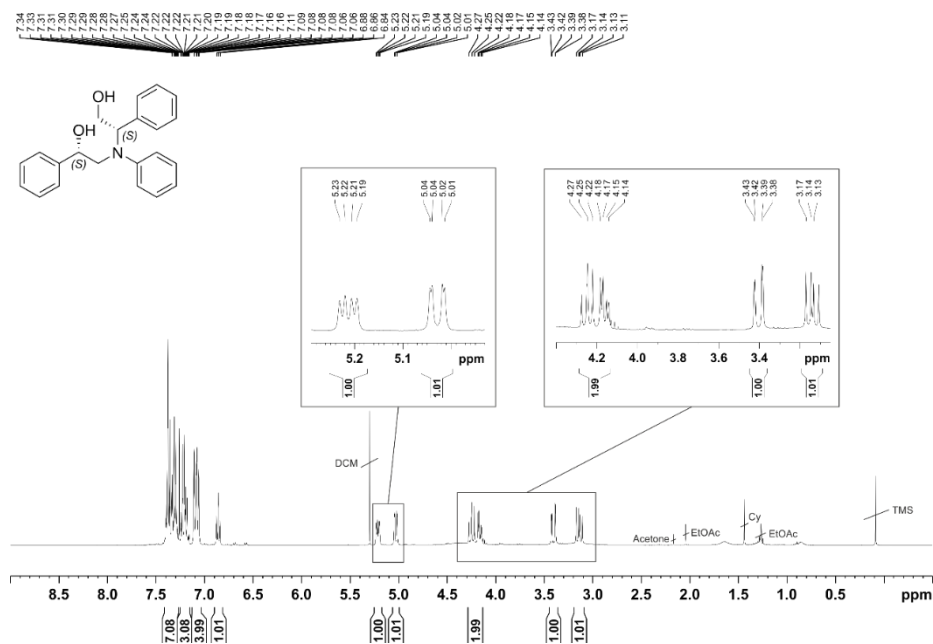
Figure 112. ^{1}H-NMR (400 MHz, CDCl$_3$) spectra of isolated compound **LB2**.
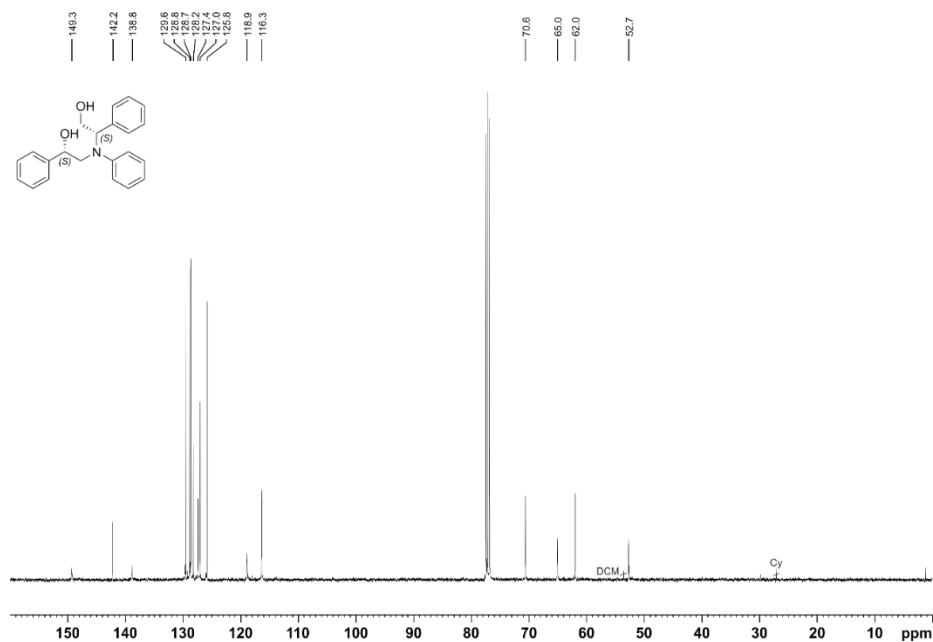
Figure 113. ^{13}C-NMR (101 MHz, CDCl$_3$) spectra of isolated compound **LB2**.

Chapter II

Differentiation of Epoxide Enantiomers by Kinetic Resolution
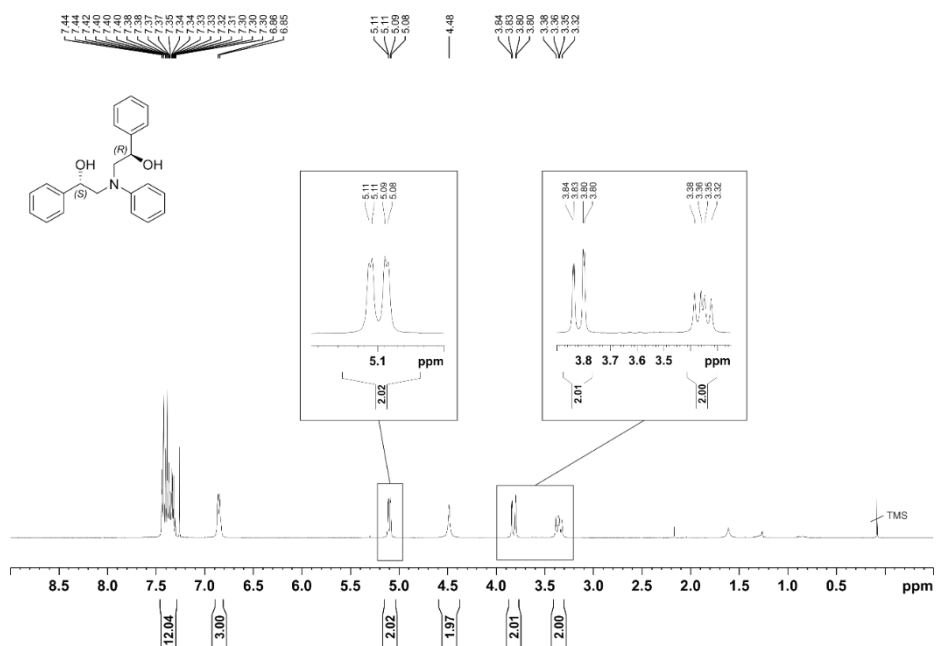
Figure 114. ^{1}H-NMR (400 MHz, CDCl$_3$) spectra of isolated compound **LL2**.
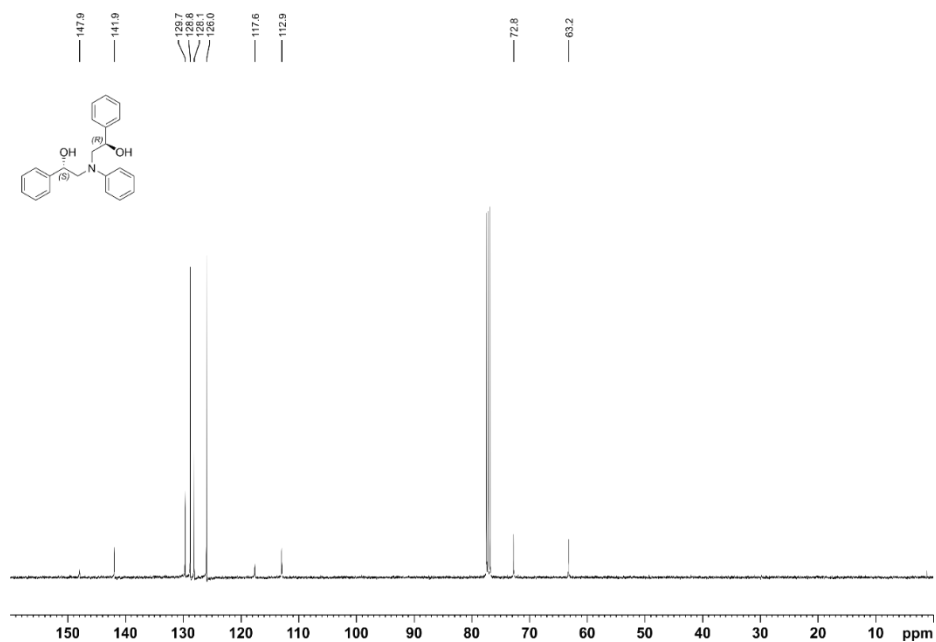
Figure 115. ^{13}C-NMR (101 MHz, CDCl$_3$) spectra of isolated compound **LL2**.
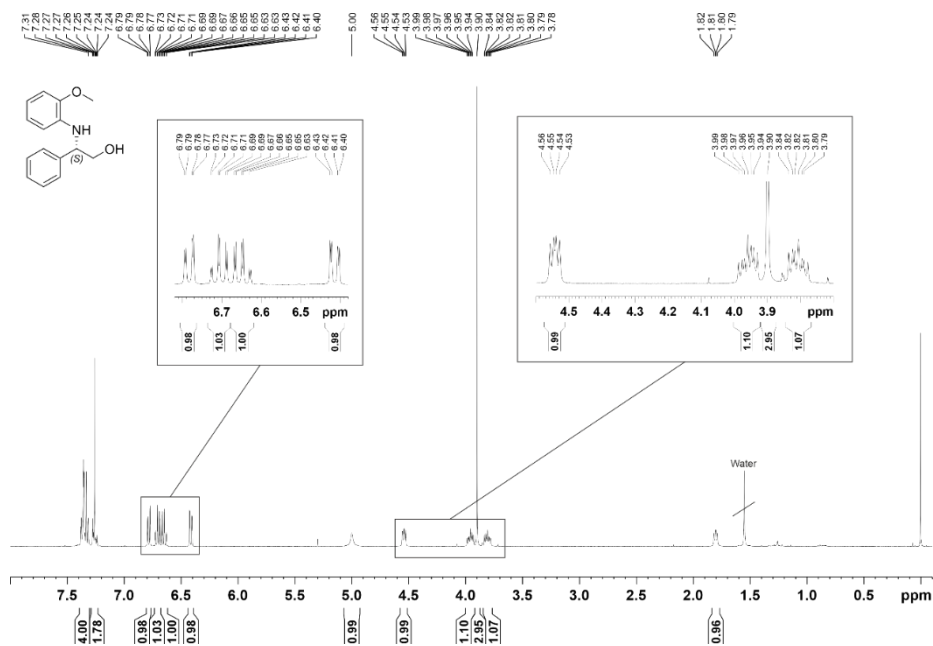
Figure 116. ^{1}H-NMR (400 MHz, CDCl$_3$) spectra of isolated compound (*S*)-**4b**.
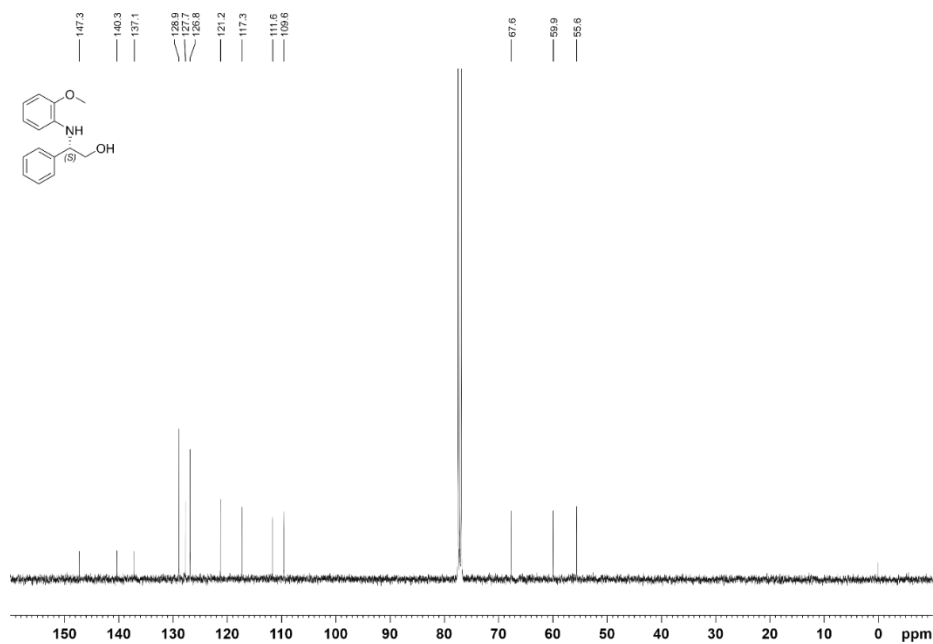
Figure 117. ^{13}C-NMR (101 MHz, CDCl$_3$) spectra of isolated compound (*S*)-**4b**.

Chapter II

137

Differentiation of Epoxide Enantiomers by Kinetic Resolution
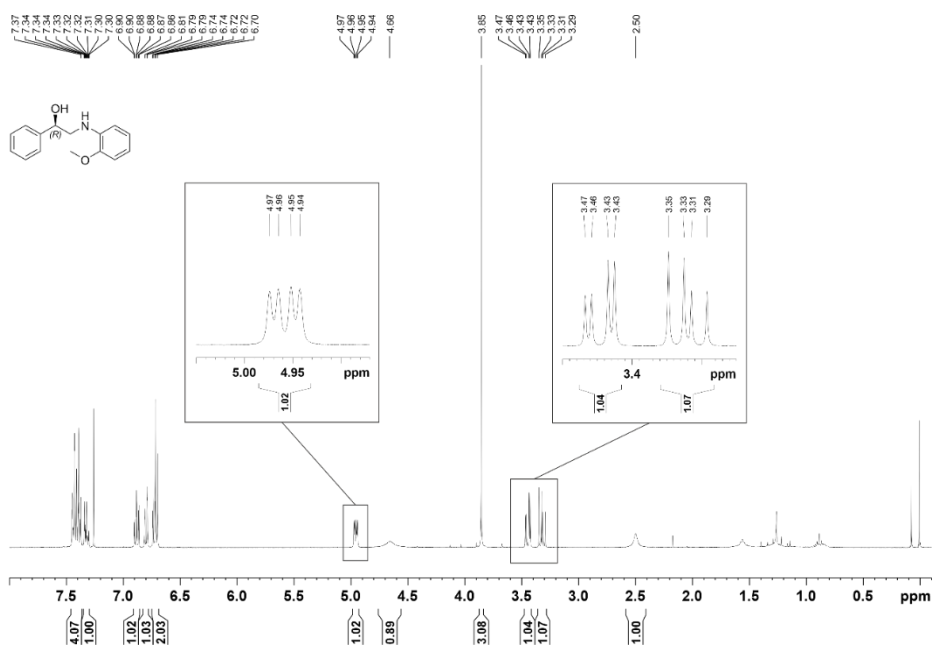
Figure 118. ¹H-NMR (400 MHz, CDCl₃) spectra of isolated compound (*R*)-**4l**.
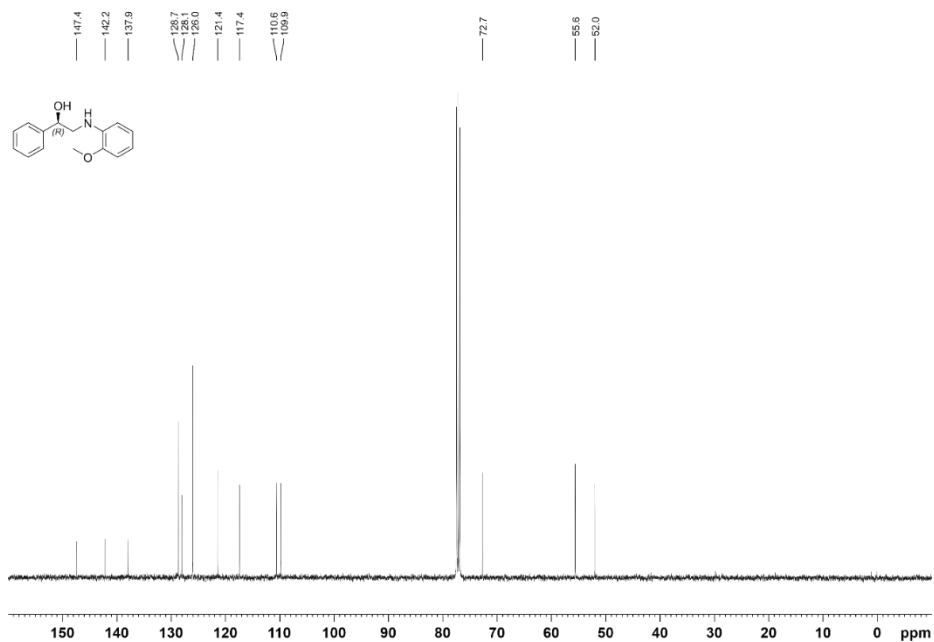
Figure 119. ¹³C-NMR (101 MHz, CDCl₃) spectra of isolated compound (*R*)-**4l**.
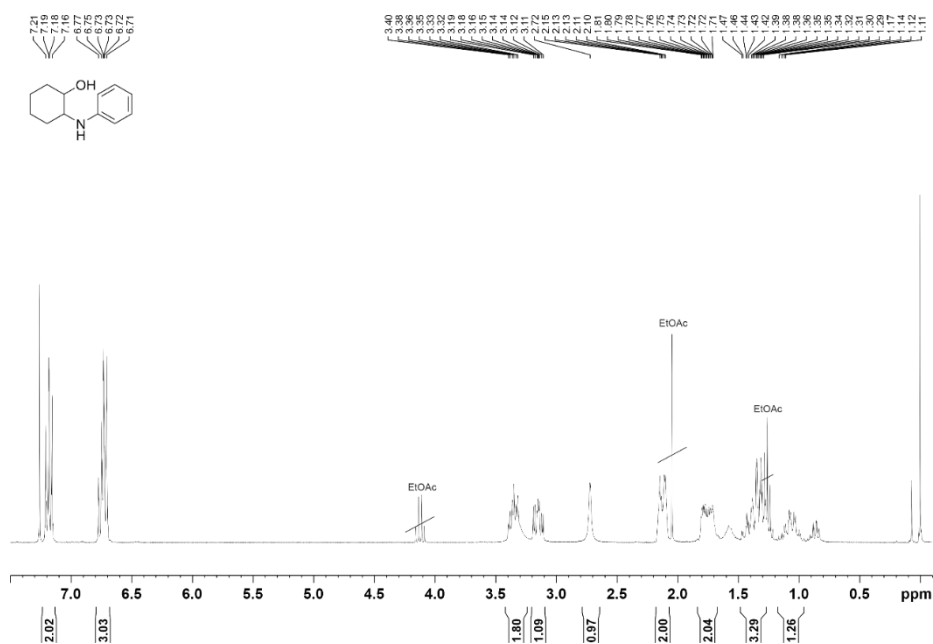
Figure 120. ^{1}H-NMR (300 MHz, CDCl$_3$) spectra of compound *rac-trans-*6.
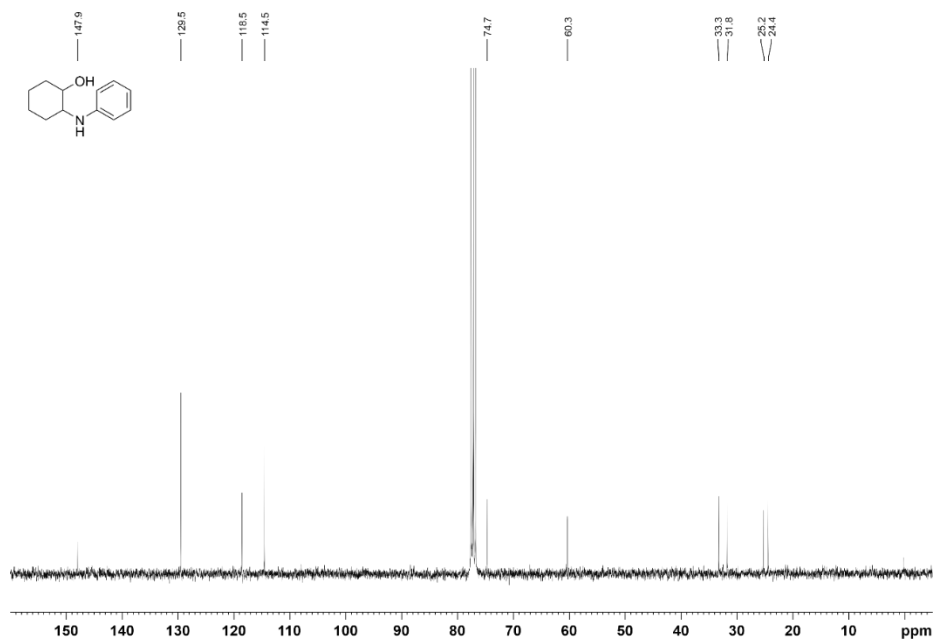
Figure 121. ^{13}C-NMR (75 MHz, CDCl$_3$) spectra of compound *rac-trans-*6.

Chapter II

Differentiation of Epoxide Enantiomers by Kinetic Resolution

2.5.8. HPLC and SFC chromatograms


```
Signal 1: DAD1 B, Sig=245,16 Ref=360,100

Peak  RetTime Type  Width     Area      Height     Area
  #    [min]        [min]    [mAU*s]     [mAU]       %
----|-------|----|-------|----------|----------|--------|
  1   15.630 VB    0.2456 1557.89001   95.84858  10.9429
  2   20.543 BV    0.1858 6210.77734  511.05444  43.6256
  3   21.959 VV    0.2344  279.94583   18.31028   1.9664
  4   22.953 VV    0.2591  186.02582   10.89963   1.3067
  5   23.905 VV    0.3252  340.22998   16.18790   2.3898
  6   25.430 VV    0.3597  189.91560    8.15403   1.3340
  7   26.637 VB    0.3967   43.84831    1.70117   0.3080
  8   28.400 BV    0.3931 5252.01465  206.22620  36.8911
  9   29.672 VB    0.5014  104.16222    3.08894   0.7317
 10   35.148 BB    0.5934   71.74158    1.87934   0.5039


Signal 2: DAD1 D, Sig=225,16 Ref=360,100

Peak  RetTime Type  Width     Area      Height     Area
  #    [min]        [min]    [mAU*s]     [mAU]       %
----|-------|----|-------|----------|----------|--------|
  1    7.217 BB    0.1357  941.10889  105.86442  61.2899
  2    8.492 BB    0.1564  594.39441   58.55555  38.7101
```

Figure 122. HPLC chromatogram of a representative reaction crude mixture of *rac*-**1** and aniline (**2**) (top: 245 nm; bottom: 225 nm). Conditions: CHIRALPAK® IC, *n*-Hex/IPA 99:1 to 95:5, 1 mL min^{-1}, gradient (min, %IPA): (0, 1); (7, 1); (14, 5); (40, 5).
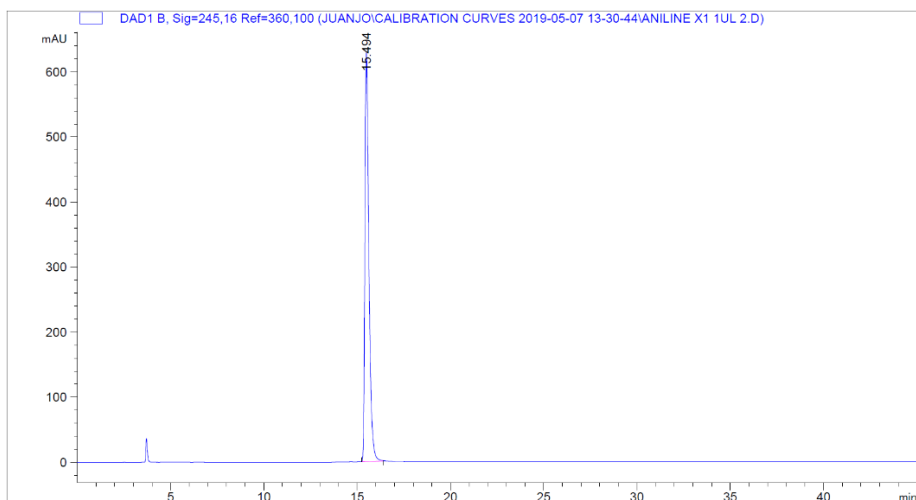
Figure 123. HPLC chromatogram of aniline (**2**). Conditions: CHIRALPAK® IC, *n*-Hex/IPA 99:1 to 95:5, 1 mL min^{-1}, gradient (min, %IPA): (0, 1); (7, 1); (14, 5); (40, 5).

Chapter II
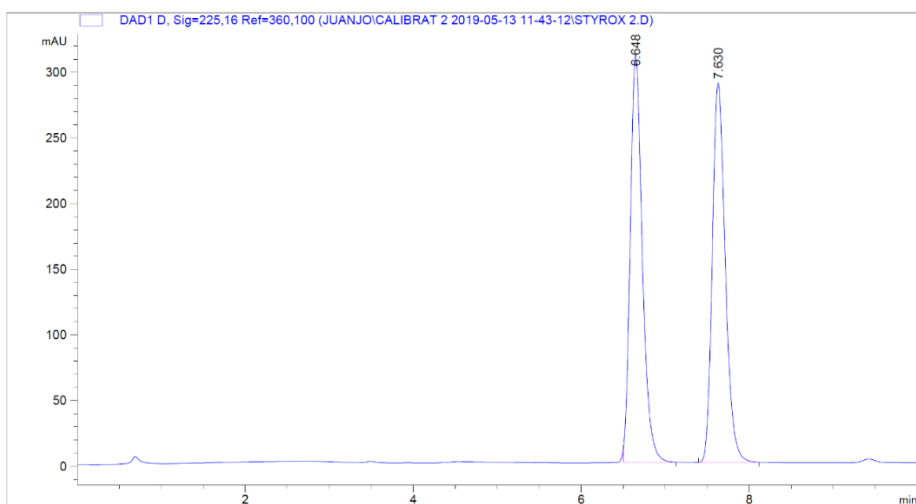
Figure 124. HPLC chromatogram of racemic styrene oxide (*rac*-**1**). Conditions: CHIRALPAK® IC, *n*-Hex/IPA 99:1 to 95:5, 1 mL min^{-1}, gradient (min, %IPA): (0, 1); (7, 1); (14, 5); (40, 5).

Differentiation of Epoxide Enantiomers by Kinetic Resolution

Figure 125. HPLC chromatogram of enantiopure (*R*)-**B1**. Conditions: CHIRALPAK® IC, *n*-Hex/IPA 99:1 to 95:5, 1 mL min^{-1}, gradient (min, %IPA): (0, 1); (7, 1); (14, 5); (40, 5).
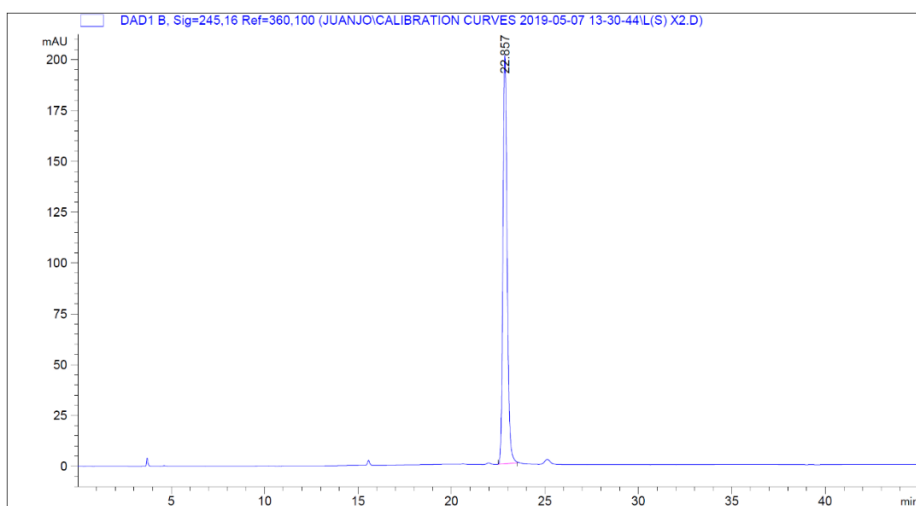
Figure 126. HPLC chromatogram of enantiopure (*S*)-**L1**. Conditions: CHIRALPAK® IC, *n*-Hex/IPA 99:1 to 95:5, 1 mL min^{-1}, gradient (min, %IPA): (0, 1); (7, 1); (14, 5); (40, 5).

142
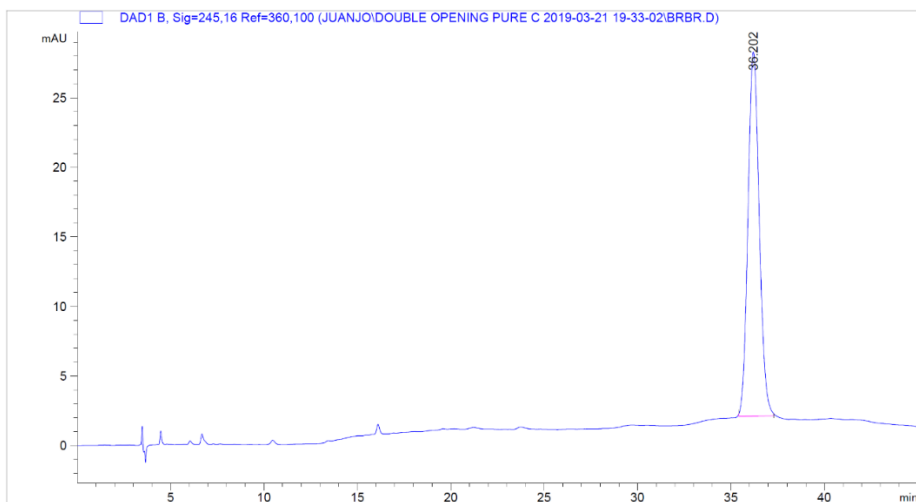
Figure 127. HPLC chromatogram of **BB1**. Conditions: CHIRALPAK® IC, n-Hex/IPA 99:1 to 95:5, 1 mL min^{-1}, gradient (min, %IPA): (0, 1); (7, 1); (14, 5); (40, 5).
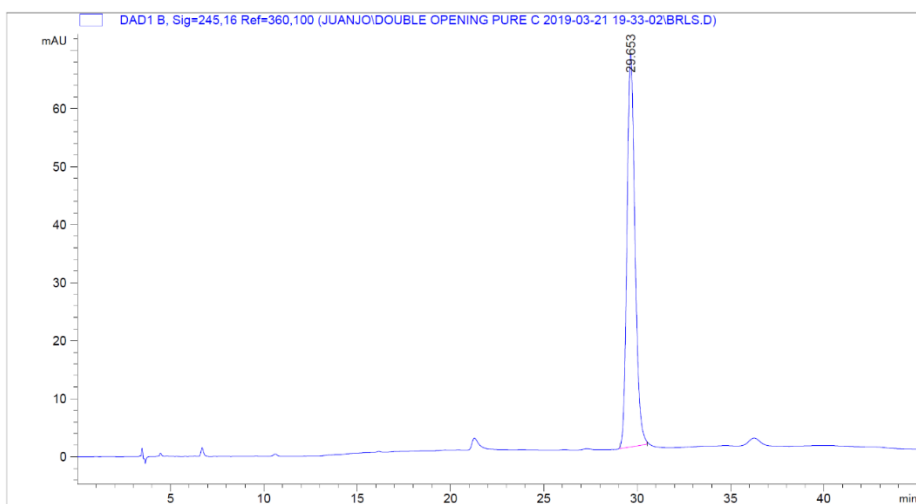
Figure 128. HPLC chromatogram of **LB1**. Conditions: CHIRALPAK® IC, n-Hex/IPA 99:1 to 95:5, 1 mL min^{-1}, gradient (min, %IPA): (0, 1); (7, 1); (14, 5); (40, 5).

143

UNIVERSITAT ROVIRA I VIRGILI
INSIGHTS IN HOMOCHIRAL METAL-ORGANIC FRAMEWORKS: FROM THEIR SYNTHESIS TO ENANTIOSELECTIVE
APPLICATIONS
Juanjo Cabezas Giménez

Differentiation of Epoxide Enantiomers by Kinetic Resolution
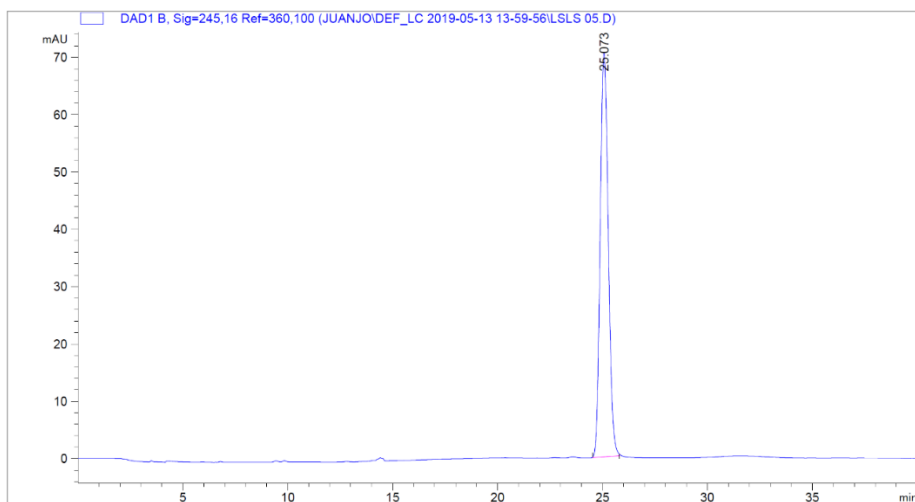
Figure 129. HPLC chromatogram of **LL1**. Conditions: CHIRALPAK® IC, *n*-Hex/IPA 99:1 to 95:5, 1 mL min^{-1}, gradient (min, %IPA): (0, 1); (7, 1); (14, 5); (40, 5).
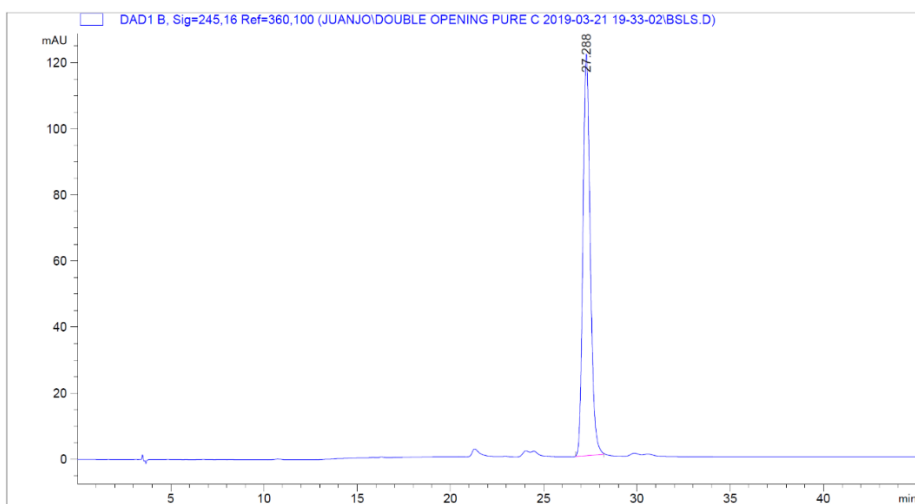
Figure 130. HPLC chromatogram of **LB2**. Conditions: CHIRALPAK® IC, *n*-Hex/IPA 99:1 to 95:5, 1 mL min^{-1}, gradient (min, %IPA): (0, 1); (7, 1); (14, 5); (40, 5).
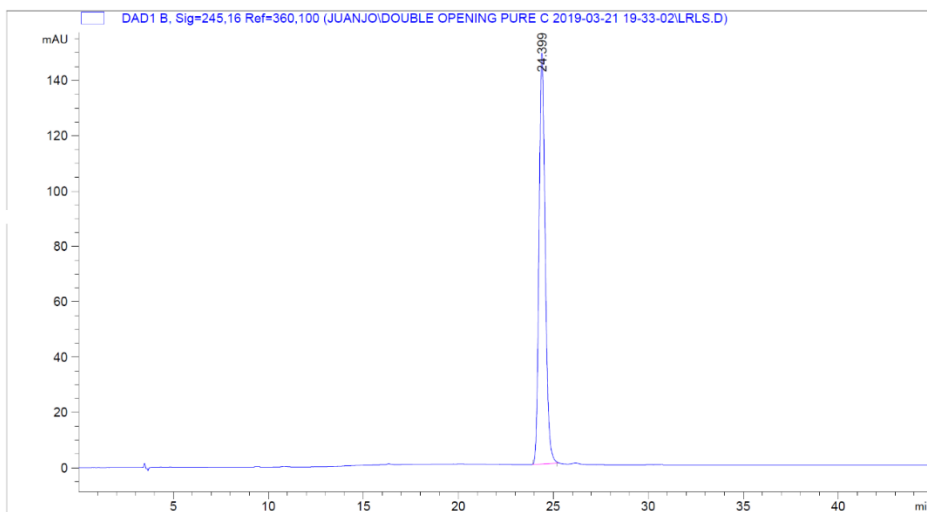
Figure 131. HPLC chromatogram of **LL2**. Conditions: CHIRALPAK® IC, n-Hex/IPA 99:1 to 95:5, 1 mL min^{-1}, gradient (min, %IPA): (0, 1); (7, 1); (14, 5); (40, 5).
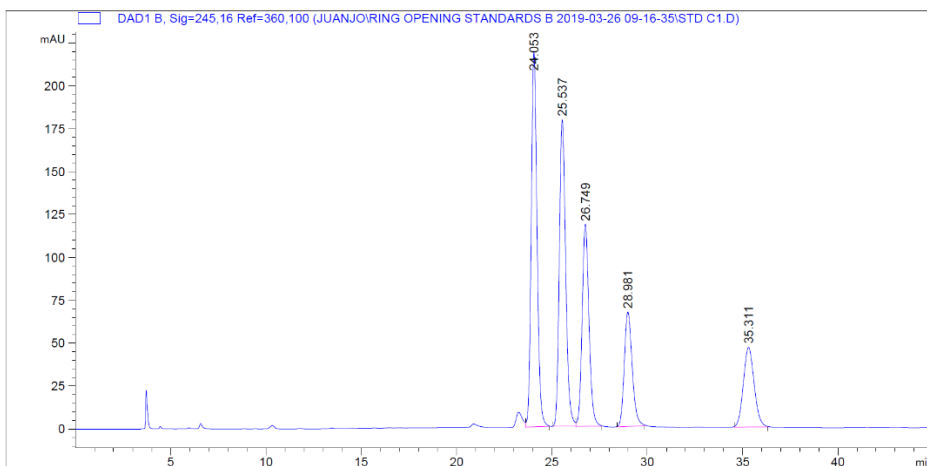
Figure 132. HPLC chromatogram of **LL2, LL1, LB2, LB1** and **BB1** (left to right). Conditions: CHIRALPAK® IC, n-Hex/IPA 99:1 to 95:5, 1 mL min^{-1}, gradient (min, %IPA): (0, 1); (7, 1); (14, 5); (40, 5).

Differentiation of Epoxide Enantiomers by Kinetic Resolution


```
Signal 1: DAD1 D, Sig=247,16 Ref=360,100

Peak RetTime Type  Width      Area       Height      Area
  #   [min]        [min]    [mAU*s]      [mAU]        %
----|-------|----|-------|-----------|-----------|--------|
  1   8.208  BB   0.2741  262.77628   14.73032   67.7085
  2   9.218  BB   0.3399  125.32330    5.71467   32.2915
```
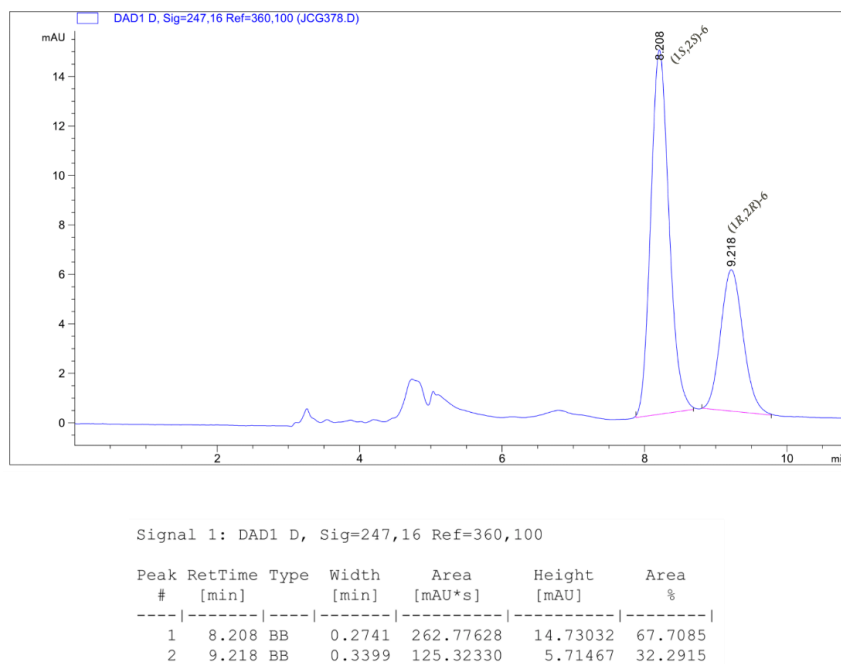
Figure 133. HPLC chromatogram of the reaction of **5** and aniline (**2**) catalysed by TAMOF-1. Conditions: CHIRALCEL® OD-H, *n*-Hex/IPA 85:15, 1 mL min^{-1}, 247 nm.
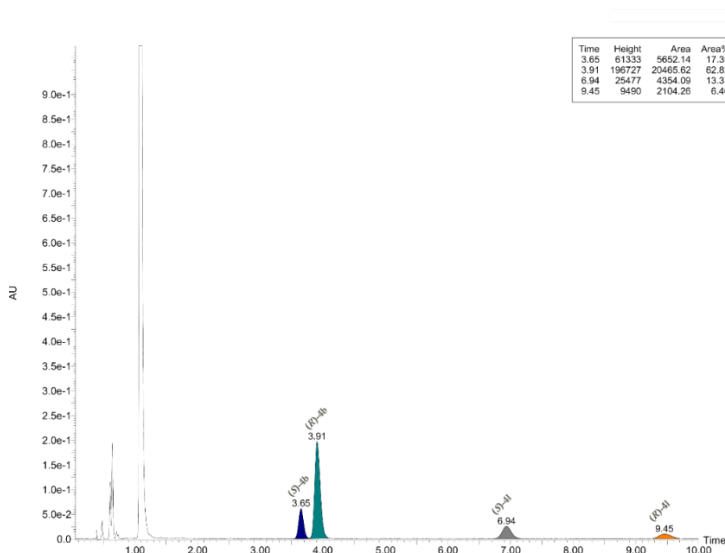
Figure 134. SFC chromatogram of the reaction of *rac*-**1** and *o*-anisidine (**3**) catalysed by TAMOF-1. Acquity UPC2, CHIRALPAK® IA column, CO_2/MeOH 95:5, 1500 psi, 240 nm.

146
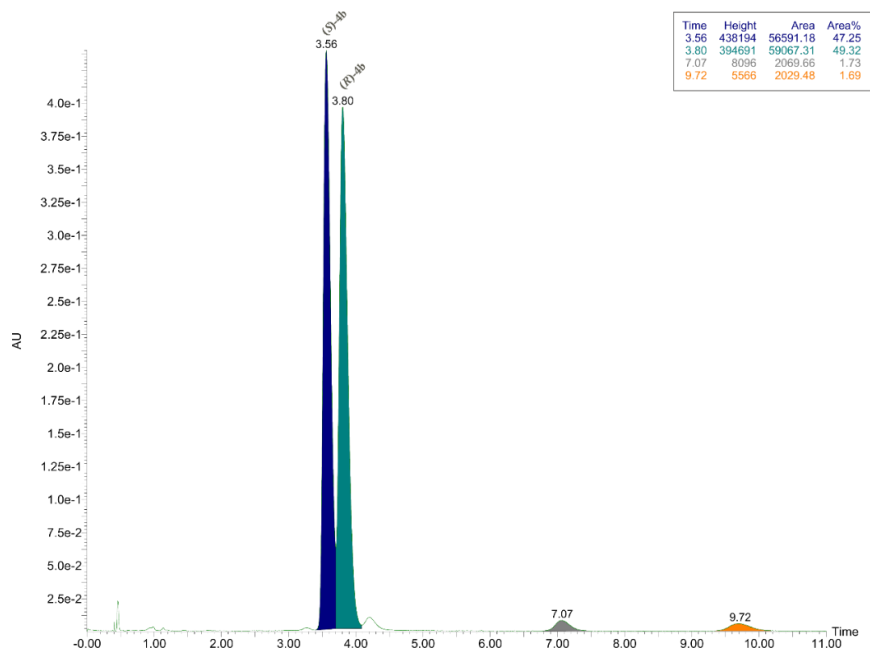
Figure 135. SFC chromatogram of *rac*-**4b**. Acquity UPC2, CHIRALPAK® IA column, CO_2/MeOH 95:5, 1500 psi, 240 nm.
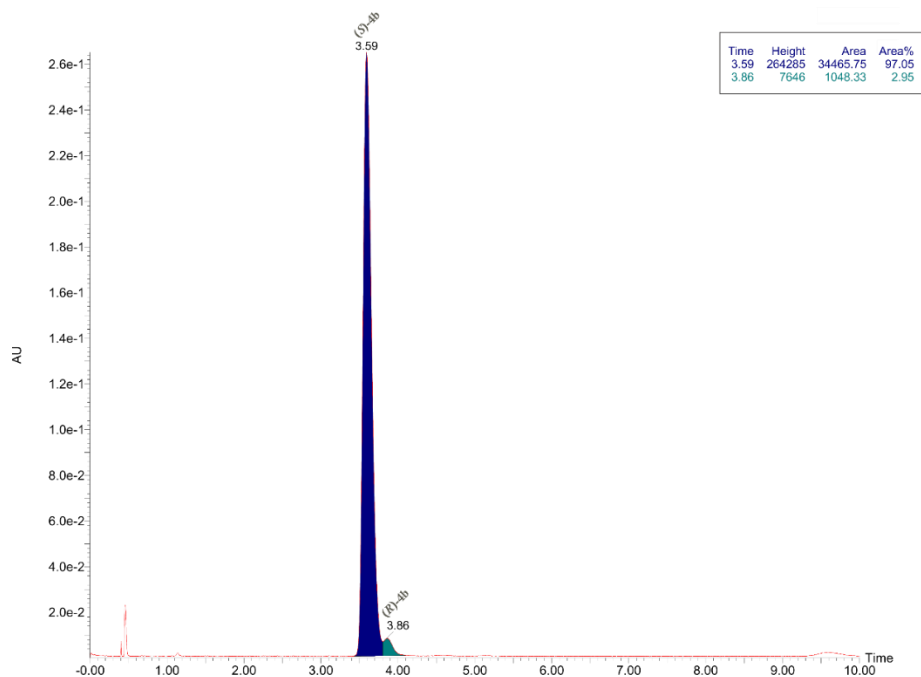
Figure 136**.** SFC chromatogram of pure (*S*)-**4b**. Acquity UPC2, CHIRALPAK® IA column, CO_2/MeOH 95:5, 1500 psi, 240 nm.

Chapter II

147
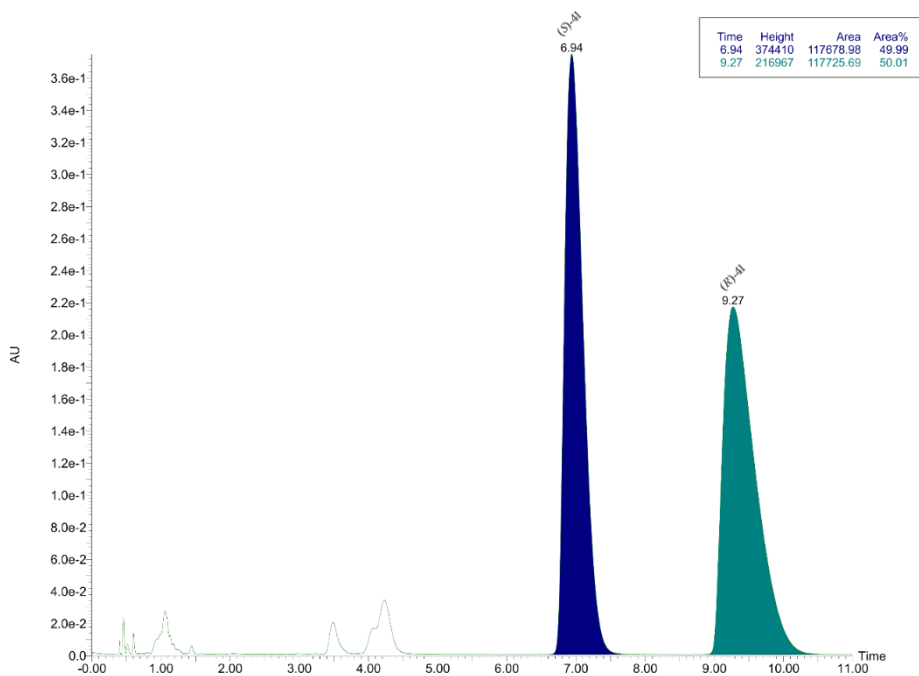
Figure 137. SFC chromatogram of *rac*-**4l**. Acquity UPC2, CHIRALPAK® IA column, CO_2/MeOH 95:5, 1500 psi, 240 nm.
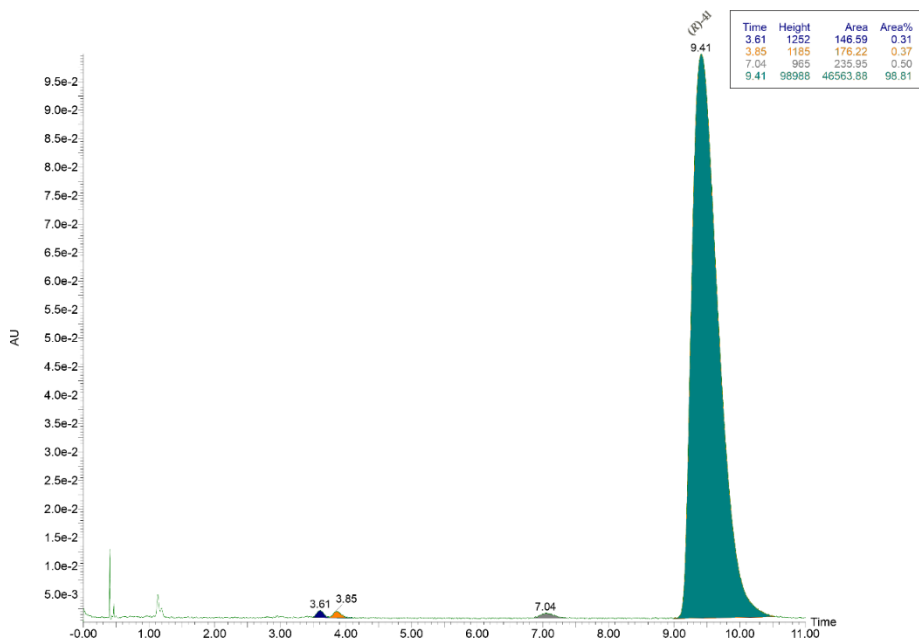
Figure 138. SFC chromatogram of pure (*R*)-**4l**. Acquity UPC2, CHIRALPAK® IA column, CO_2/MeOH 95:5, 1500 psi, 240 nm.

148

CHAPTER III

Chromatographic Separation of Enantiomers Using TAMOF-1 as Chiral Stationary Phase

UNIVERSITAT ROVIRA I VIRGILI
INSIGHTS IN HOMOCHIRAL METAL-ORGANIC FRAMEWORKS: FROM THEIR SYNTHESIS TO ENANTIOSELECTIVE
APPLICATIONS
Juanjo Cabezas Giménez

Homochiral Metal-Organic Frameworks for Enantioselective Separations in Liquid Chromatography

M. Nieves Corella-Ochoa,[a] Jesús B. Tapia,[b] Heather N. Rubin,[b] Vanesa Lillo,[a] Jesús González-Cobos,[a] José Luis Núñez-Rico,[a] Salvador R. G. Balestra,[d] Neyvis Almora-Barrios,[f] Marina Lledós,[a] Arnau Güell-Bara,[a] Juanjo Cabezas-Giménez,[a,g] Eduardo C. Escudero-Adán,[a] Anton Vidal-Ferran,[a,e] Sofia Calero,[d,g] Melissa Reynolds,[b,c] Carlos Martí-Gastaldo[e] and José Ramón Galán-Mascarós[a,f,*]

a Institut Català d'Investigació Química (ICIQ) and the Barcelona Institute of Science and Technology (BIST), Av. Països Catalans 16, Tarragona 43007, Spain.

b Department of Chemistry, and *c* School of Biomedical Engineering, Colorado State University, Fort Collins, Colorado 80523, United States.

d Departament of Physical, Chemical and Natural Systems, Universidad Pablo de Olavide, Ctra. Utrera km 1, Sevilla 41013, Spain.

e Instituto de Ciencia Molecular, Universidad de Valencia, Calle Catedratico José Beltran 2, Paterna 46980, Spain.

f Institució Catalana de Recerca i Estudis Avançats (ICREA), Pg. Lluís Companys 23, Barcelona 08010, Spain.

g Departament de Química Física i Inorganica, Universitat Rovira i Virgili, C/Marcel·lí Domingo s/n, Tarragona 43007, Spain.

Chapter III

homochiral water-stable MOF

(±)ibuprofene

151

Chromatographic Separation of Enantiomers Using TAMOF-1 as Chiral Stationary Phase
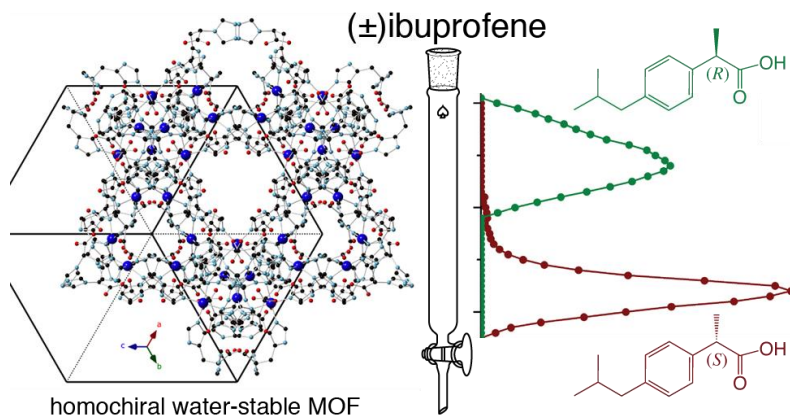
3.1. ABSTRACT

TAMOF-1 was successfully used as chiral stationary phase in the preparative chromatographic separation of *rac*-ibuprofen and *rac*-thalidomide. Packing of diverse analytical HPLC columns with TAMOF-1 allowed us to separate structurally diverse racemic mixtures such as terpenes, calcium channel blockers and *P*-stereogenic phosphorus compounds under diverse HPLC conditions. Theoretical studies suggest that chiral separation is favoured by the chiral channels inside TAMOF-1 and weak binding sites.

The TAMOF-1-packed columns are stable towards chemicals and tolerate both polar and non-polar mobile phases. Furthermore, it possesses a long-term recyclability, as no degradation of the column is observed after 2 years of use and no significant changes are observed after more than 180 consecutive injections of TSO. Semipreparative HPLC separations have been tested with two racemic analytes, allowing us to isolate up to 1 mg per run.

3.2. INTRODUCTION

Engineering chiral MOFs is a powerful strategy for developing new CSPs capable of separating racemic mixtures. Chiral drug molecules require stereoselective syntheses or challenging separations to isolate one enantiomer. Typically, only one of the enantiomers is biologically beneficial/active (*i.e.,* eutomer), while the other one (*i.e.,* distomer) is inactive or results in undesirable side effects, like thalidomide.[172] An easy separation during the early stages of drug discovery processes may reduce purification steps and save time and resources necessary to bring a new drug to the market. Despite the crucial technological relevance of chiral separations for the pharmaceutical industry, it remains an expensive and complex scientific challenge.

Current chromatographic technology depends on chiral columns composed of silica beads or polymer composites decorated with organic enantiopure molecules to confer them with chiral recognition properties.[173] Typically, these materials are mechanically fragile, expensive to manufacture, and often too specific for a single desired substrate lacking desirable versatility

[172] Stephens, T. D.; Bunde, C. J. W.; Fillmore, B. J. *Biochem. Pharmacol.* **2000**, *59*, 1489-1499.
[173] (a) Maier, N. M.; Franco, P.; Lindner, W. *J. Chromatogr. A* **2001**, *906*, 3-33. (b) Sharp, V. S.; Risley, D. S.; Oman, T. J.; Starkey, L. E. *J. Liq. Chromatogr. Relat. Technol.* **2008**, *31*, 629-666. (c) Chennuru, L. N.; Choppari, T.; Duvvuri, S.; Dubey, P. K. *J. Sep. Sci.* **2013**, *36*, 3004-3010. (d) Ahmed, M.; Gwairgi, M.; Ghanem, A. *Chirality* **2014**, *26*, 677-682. (e) Shen, J.; Okamoto, Y. *Chem. Rev.* **2016**, *116*, 1094-1138. (f) Teixeira, J.; Tiritan, M. E.; Pinto, M. M. M.; Fernandes, C. *Molecules* **2019**, *24*, 865.

Chromatographic Separation of Enantiomers Using TAMOF-1 as Chiral Stationary Phase

across structurally diverse racemic mixtures. Ongoing and future trends will involve porous materials with strategically designed target-specific interactions between the support and the molecules to be separated.[174]

MOFs as CSPs can circumvent this shortcoming, as separations on these supports are generally based on enantiodifferentiation due to the transient formation of diastereoisomeric supramolecular complexes. MOFs as CSPs have been already used in the separation of several families of racemates, such as amines,[175] sulfoxides,[176] amino acids,[177] and others.

Given this, we envisioned the use of TAMOF-1 for the separation of chiral model compounds and drugs. To assess the advantages of this new stationary phase compared to the widely used commercial columns, we explored the scope, versatility and performance of separation of a variety of racemic mixtures of organic molecules with different functional groups and different solvents as the moving phase.

These columns have proven to be excellent CSP for the purification of various products thanks to their versatility to work with solvents of different polarities. Our essays include ibuprofen, thalidomide, natural products such as terpenes and terpenoids,[178] and dihydropyridine calcium channel blockers.[179] We also achieved the separation of a chiral phosphorus compound, phenyl *N*-phenylphosphoramidochloridate. This is the first example of this purification process, particularly relevant since the synthesis of enantiopure chiral phosphorus compounds by chiral chromatographic separations avoid tedious and expensive enantioselective synthesis and the use of complex catalytic processes.[180] Some of the analytical separations were scaled up to semi-preparative scale, allowing us to isolate multi-milligram quantities, demonstrating TAMOF-1 is useful beyond analytical applications, and that can be scaled-up to preparative processes.

---

[174] Okamoto, Y.; Ikai, T. *Chem. Soc. Rev.* **2008**, *37*, 2593-2608.

[175] (a) Peng, Y.; Gong, T.; Zhang, K.; Lin, X.; Liu, Y.; Jiang, J.; Cui, Y. *Nat. Commun.* **2014**, *5*, 4406. (b) Navarro-Sánchez, J.; Argente-García, A. I.; Moliner-Martínez, Y.; Roca-Sanjuán, D.; Antypov, D.; Campíns-Falcó, P.; Rosseinsky, M. J.; Martí-Gastaldo, C. *J. Am. Chem. Soc.* **2017**, *139*, 4294-4297.

[176] (a) Tanaka, K.; Muraoka, T.; Hirayama, D.; Ohnish, A. *Chem. Commun.* **2012**, *48*, 8577-8579. (b) Wang, W.; Dong, X.; Nan, J.; Jin, W.; Hu, Z.; Chen, Y.; Jiang, J. *Chem. Commun.* **2012**, *48*, 7022-7024. (c) Tanaka, K.; Hotta, N.; Nagase, S.; Yoza, K. *New J. Chem.* **2016**, *40*, 4891-4894.

[177] (a) Xie, S.-M.; Zhang, M.; Fei, Z.-X.; Yuan, L.-M. *J. Chromatogr. A* **2014**, *1363*, 137-143. (b) Ye, N.; Ma, J.; An, J.; Li, J.; Cai, Z.; Zong, H. *RSC Adv.* **2016**, *6*, 41587-41593. (c) Wang, J.; Chen, J.; Xu, T. *Solid State Sci.* **2019**, *98*, 106032.

[178] (a) Cowan, M. M. *Clin. Microbiol. Rev.* **1999**, *12*, 564. (b) Gershenzon, J.; Dudareva, N. *Nat. Chem. Biol.* **2007**, *3*, 408-414. (c) Chen, F.; Tholl, D.; Bohlmann, J.; Pichersky, E. *Plant. J.* **2011**, *66*, 212-229. (d) Cane, D. E.; Ikeda, H. *Acc. Chem. Res.* **2012**, *45*, 463-472.

[179] (a) Trouve, R.; Nahas, G. *Proc. Soc. Exp. Biol. Med.* **1986**, *183*, 392-397. (b) Weiner, D. A. *Med. Clin. North Am.* **1988**, *72*, 83-115. (c) Mason, R. P.; Walter, M. F.; Trumbore, M. W.; Olmstead Jr, E. G.; Mason, P. E. *J. Mol. Cell. Cardiol.* **1999**, *31*, 275-281.

[180] (a) Lemouzy, S.; Giordano, L.; Hérault, D.; Buono, G. *Eur. J. Org. Chem.* **2020**, *2020*, 3351-3366. (b) Ye, X.; Peng, L.; Bao, X.; Tan, C.-H.; Wang, H. *Green Synth. Catal.* **2021**, *2*, 6-18.

3.3. RESULTS AND DISCUSSION

3.3.1. Preparative chromatographic separations

3.3.1.1. *rac*-ibuprofen

A glass preparative column was packed with a polycrystalline batch of the MOF to test the performance of TAMOF-1 as a chiral stationary phase in chromatographic preparative separation experiments (see page **178** for details), and a solution of racemic *rac*-ibuprofen was run through, using ACN as the eluent. Ibuprofen is a widely employed non-steroidal anti-inflammatory drug, typically prescribed as the racemate, even though the (*S*)-ibuprofen enantiomer exhibits a much more potent inhibitory activity than (*R*)-ibuprofen.[181]

The election of this racemic mixture involved its molecular dimensions (6.4×6.7×12.5 Å, see page **181** for details) and its relevance in previous enantiomeric separations with other MOFs,[182] and it was found that it fitted to the contour of the channels (**Figure 139**). The two enantiomers descended through the column at near-atmospheric pressure as two different fronts. Enantiopure (*S*)-ibuprofen exits the column first due to (*R*)-ibuprofen's preferred interaction with TAMOF-1. The two fronts are fully resolved in these conditions (**Figure 141a**), with almost quantitative yields for the enantiopure products; 99% of (*S*)- and 92% (*R*)-ibuprofen at e.e. > 99% were recovered starting with 6.9 mg of *rac*-ibuprofen with a flow rate of 0.09 mL min⁻¹. This process is remarkable since no high pressure, temperature, or mixture of solvents were needed for separating the two enantiomers. Furthermore, the solvent removes the enantiomers entirely, leaving the column ready for re-use without additional treatment.

Chapter III

---

[181] Boneberg, E. M.; Zou, M. H.; Ullrich, V. *J. Clin. Pharmacol.* **1996**, *36*, 16S-19S.
[182] Hailili, R.; Wang, L.; Qv, J.; Yao, R.; Zhang, X.-M.; Liu, H. *Inorg. Chem.* **2015**, *54*, 3713-3715.

Chromatographic Separation of Enantiomers Using TAMOF-1 as Chiral Stationary Phase

6.4 x 6.7 x 12.5 Å
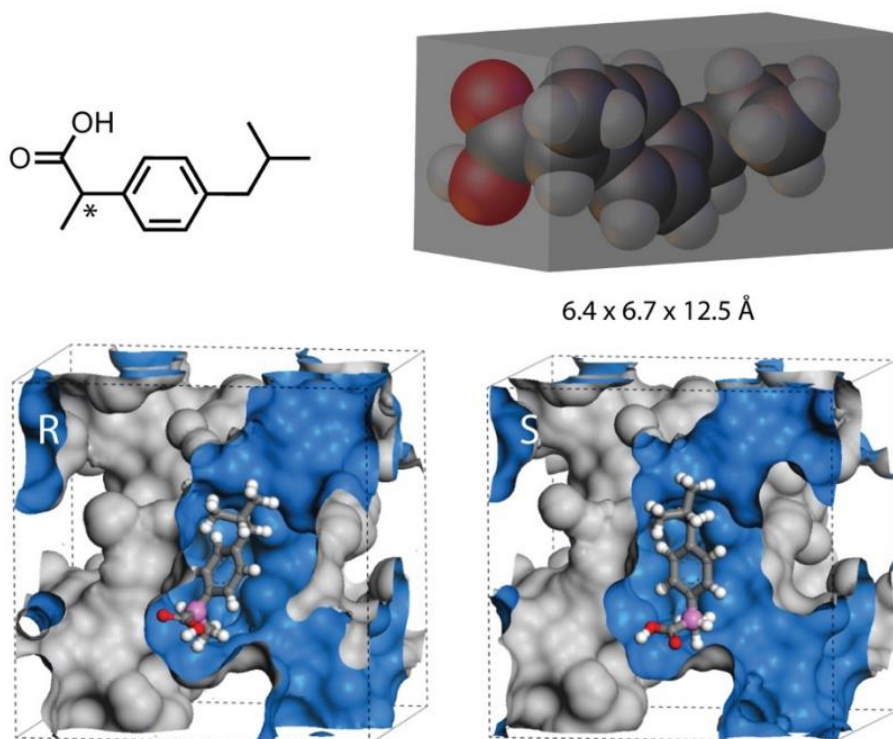
Figure 139. Molecular dimensions of racemic ibuprofen and their adsorption sites in TAMOF-1.[103]

3.3.1.2. *rac*-thalidomide

In identical conditions, we were also able to quantitatively separate *rac*-thalidomide (6.9 × 7.7 × 13.6 Å, **Figure 140**). Thalidomide was a turning point for regulatory agencies to enforce stereochemical characterisation of drugs during the 20th century due to the late discovery of the teratogenic properties of its (*S*)-enantiomer.[183] Despite ibuprofen and thalidomide being quite different in chemical functionalities, both could be separated using the same solvent and conditions, confirming TAMOF-1 versatility for separating chiral drugs. *rac*-thalidomide is also resolved (**Figure 141b**) with a yield of 78% for (*S*)- and 96% for (*R*)-thalidomide at e.e. > 99%, starting with 2 mg of *rac*-thalidomide (flow rate 0.06 mL min⁻¹). In the case of thalidomide, (*R*)-thalidomide elutes first, contrary to what is observed for ibuprofen.

[183] Schafer, W.; Chandrasekaran, T.; Pirzada, Z.; Zhang, C.; Gong, X.; Biba, M.; Regalado, E. L.; Welch, C. J. *Chirality* **2013**, *25*, 799-804.
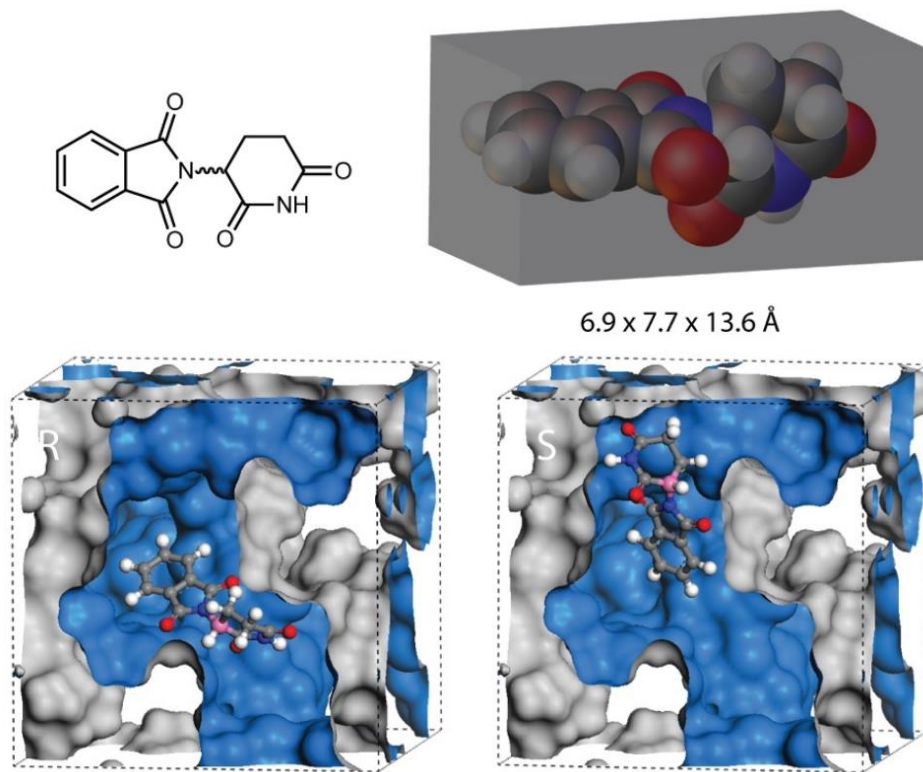
Figure 140. Molecular dimensions of racemic thalidomide and their adsorption sites in TAMOF-1.[103]

Chromatographic Separation of Enantiomers Using TAMOF-1 as Chiral Stationary Phase
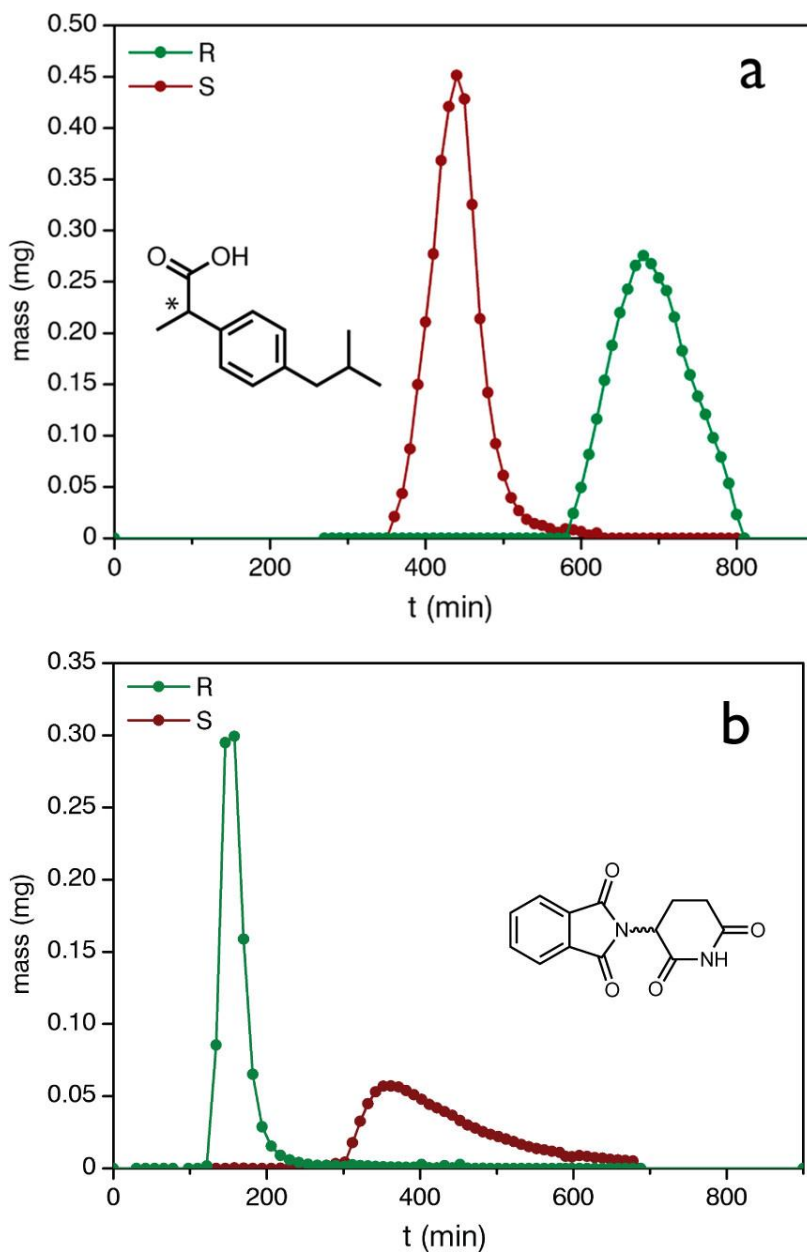
Figure 141. Preparative chromatographic separations at room temperature with a TAMOF-1 column with 100% ACN as the mobile phase: (a) of *rac*-ibuprofen; (b) *rac*-thalidomide.[103]

158

3.3.2. Calculations for the adsorption of ibuprofen and thalidomide

To better understand the mechanism of chiral separation Prof. Sofia Calero and co-workers carried out Monte-Carlo simulations for the adsorption of ibuprofen and thalidomide using well-validated methods and models (See Experimental Section, page **181** for details on the theoretical simulations).[184]

The thermodynamic contribution to the separation of both drugs was first analysed by calculating each enantiomer enthalpy of adsorption (ΔH_{st}). For ibuprofen, the calculated difference in enthalpies of adsorption (ΔH_{st}^{RS}) is -27.34 kJ mol^{-1}, which is indicative of the preference of TAMOF-1 to interact with (R)-ibuprofen. In turn, for the case of thalidomide, the difference in enthalpies of adsorption is 1.66 kJ mol^{-1} and suggests a higher preference for (S)-thalidomide.

To understand the origin of these differences, and regarding the absence of direct crystallographic evidence,[185] the binding site of the drug enantiomers in the MOF after energy minimisation was next analysed (**Figure 142**). The adsorption of ibuprofen is controlled by coordination to the vacant Cu^{2+} site and the formation of an H-bond with the triazole group. These bonds elongate from 2.35 and 1.63 Å for (R)- to 2.72 and 1.75 Å for a weaker interaction with (S)-ibuprofen due to small changes in the configuration of the adsorbed enantiomers. In turn, the smaller ΔH_{st}^{RS} calculated for thalidomide originates from the presence of an H-bond between the phthalimide ring and the free carboxylic groups in TA that elongates from 2.82 for (S)- to 2.95 Å for (R)-thalidomide combined with weak changes to the van der Waals interactions from a better fit of the first to the shape of the channels.

Chapter III

[184] (a) Caremans, T. P.; van Erp, T. S.; Dubbeldam, D.; Castillo, J. M.; Martens, J. A.; Calero, S. *Chem. Mater.* **2010**, *22*, 4591-4601. (b) van Erp, T. S.; Caremans, T. P.; Dubbeldam, D.; Martin-Calvo, A.; Calero, S.; Martens, J. A. *Angew. Chem. Int. Ed.* **2010**, *49*, 3010-3013. (c) Bueno-Perez, R.; Martin-Calvo, A.; Gómez-Álvarez, P.; Gutiérrez-Sevillano, J. J.; Merkling, P. J.; Vlugt, T. J. H.; van Erp, T. S.; Dubbeldam, D.; Calero, S. *Chem. Commun.* **2014**, *50*, 10849-10852. (d) Bueno-Perez, R.; Balestra, S. R. G.; Camblor, M. A.; Min, J. G.; Hong, S. B.; Merkling, P. J.; Calero, S. *Chem. Eur. J.* **2018**, *24*, 4121-4132.
[185] Bruno, R.; Marino, N.; Bartella, L.; Di Donna, L.; De Munno, G.; Pardo, E.; Armentano, D. *Chem. Commun.* **2018**, *54*, 6356-6359.

Chromatographic Separation of Enantiomers Using TAMOF-1 as Chiral Stationary Phase
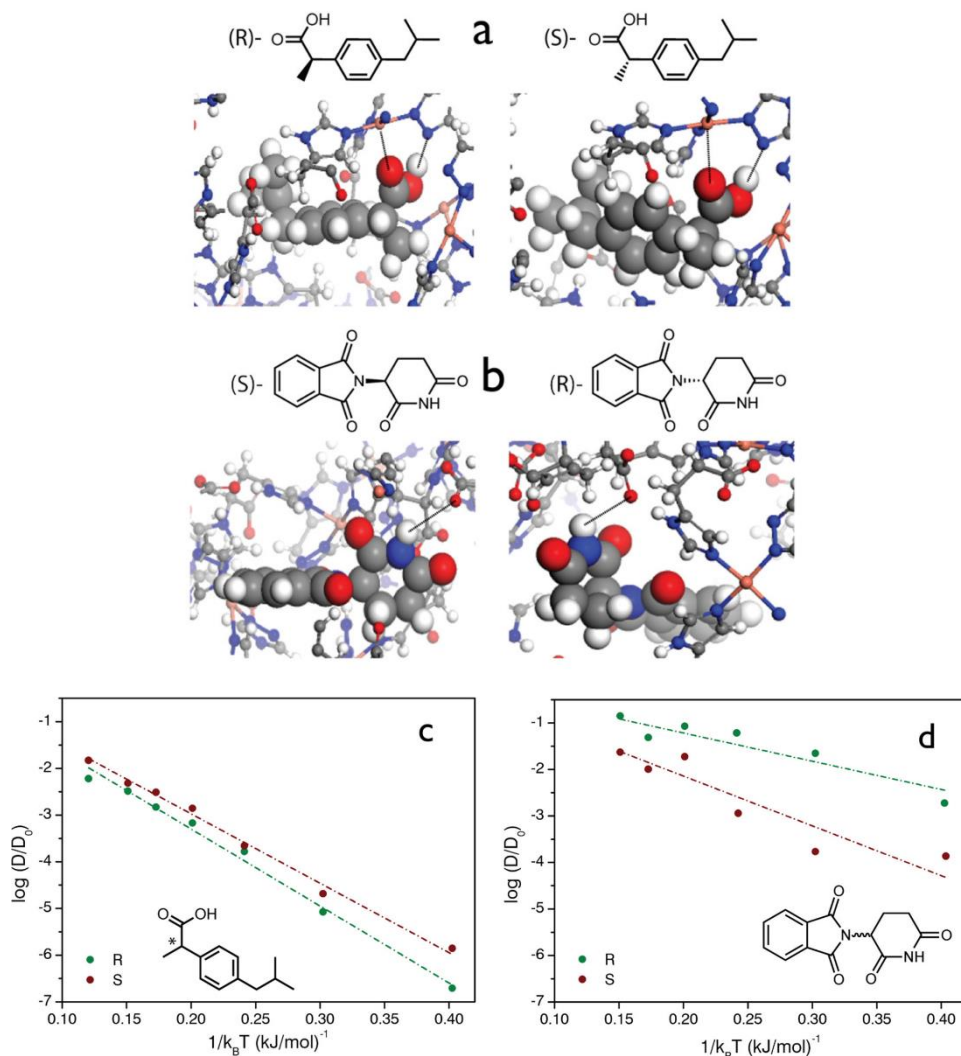
Figure 142. Binding geometries of (a) ibuprofen and (b) thalidomide enantiomers upon adsorption in TAMOF-1 calculated with Monte Carlo simulations. The most relevant interactions in directing guest binding are annotated with a dotted line. Arrhenius plot for the diffusion of ibuprofen (**c**) and thalidomide (**d**) enantiomers calculated with Molecular Dynamics.[103]

Overall, the simulations suggest that TAMOF-1 behaves as a versatile CSP due to the combination of chiral channels and weak binding sites for low-energy separation of enantiomers. The combination of weak host-guest interactions with sufficiently high ΔH_{st} differences in TAMOF-1 avoids strong pinning of one of the enantiomers to the pore walls, whereas it enables quantitative separation. It was confirmed experimentally that none of the

160

enantiomers were permanently trapped since both were quantitatively recovered by continuous elution of ACN. Considerable adsorption energies can lead to long retention times and broad chromatographic peaks. Therefore, an optimal CSP is expected to display an optimal balance between ΔH_{st}^{RS} and enantiomer diffusivity.

3.3.3. Enantioselective HPLC chromatography

3.3.3.1. Enantiomeric separation of TSO and furoin

Encouraged by the promising results in preparative chromatographic separations, we constructed an HPLC column to explore further the possibilities that TAMOF-1 has to offer as a CSP. An empty stainless-steel column (100 mm × 4.6 mm) was packed with 1.55 g of TAMOF-1 (column A, details in the Experimental section, page **178**).

As model analyte, we selected racemic TSO (*i.e.* a mixture of (2*S*,3*S*)-2,3-diphenyloxirane and (2*R*,3*R*)-2,3-diphenyloxirane), a substance typically used to calibrate HPLC columns. The versatility of TAMOF-1 allowed for baseline resolution in a variety of solvent systems encompassing different solvating abilities and polarities, such as 95:5 Hex/IPA, 100% IPA and 100% ACN (**Figure 143a**). The efficiency of the chiral resolution of TSO in terms of separation factor (α, ratio of two retention factors *k*), resolution (*R*$_S$, ability to separate two peaks), and retention times (*t*$_R$) are shown in **Table 10**, emphasizing TAMOF-1's ability to separate enantiomers under analytic HPLC conditions employing diverse elution systems.

Hence, this material can be considered as bi-functional chiral stationary phase because it operates efficiently using either non-polar (95:5 *n*-Hex/IPA) or polar (100% ACN, 100% IPA) solvent conditions. The same column was also able to resolve furoin (*i.e.* 1,2-di(furan-2-yl)-2-hydroxyethan-1-one) in a 1:1 *n*-Hex/EtOH mixture as eluent (**Table 10**, **Figure 154**), which is an additional demonstration of the versatility of TAMOF-1 as CSP regarding mobile phase and analyte.

For comparison, the chiral resolution capability of three widely-used commercial columns was also determined with racemic TSO: CHIRALPAK® AD, CHIRALCEL® OD and OJ (**Figure 143b**). The optimal separation conditions, separation times of the eluted enantiomers, and resolutions are shown in **Table 11**.

Chromatographic Separation of Enantiomers Using TAMOF-1 as Chiral Stationary Phase
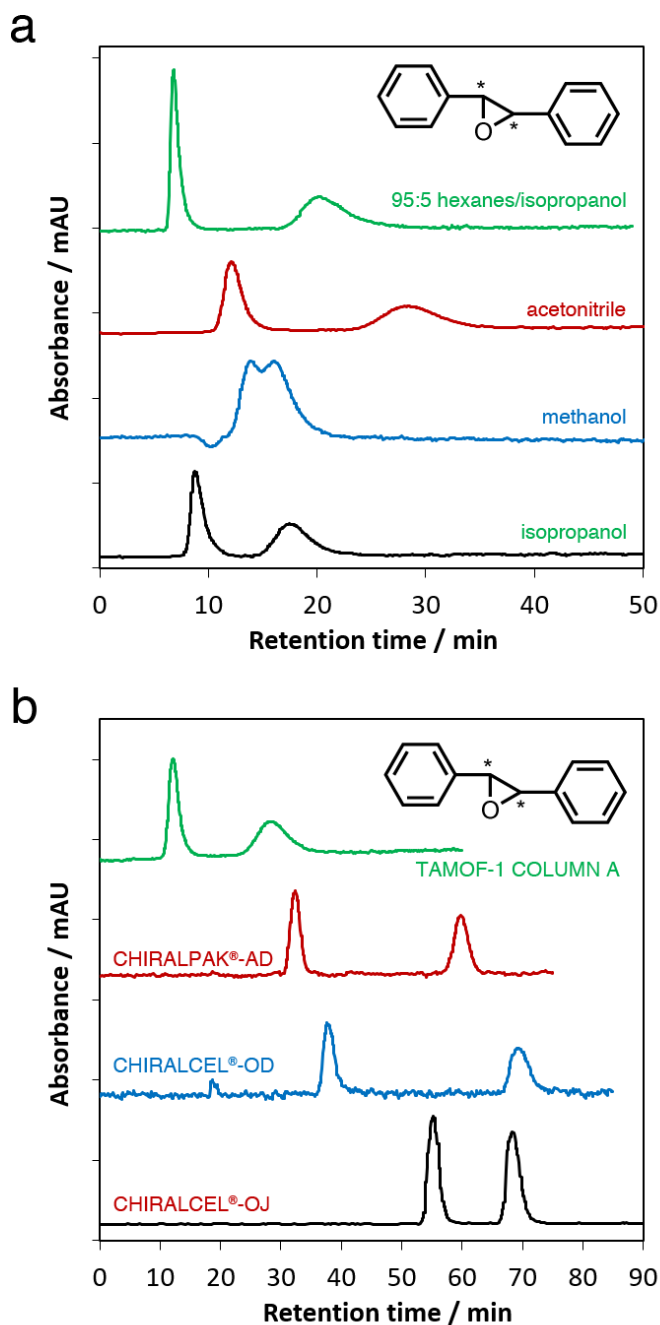
Figure 143. Representative chromatograms of the separation of TSO enantiomers with HPLC column packed with TAMOF-1: (a) Separation with different mobile phases using column A: IPA, MeOH, ACN and 95:5 *n*-Hex/IPA (v/v). (b) Comparison with commercial columns CHIRALPAK® AD, CHIRALCEL® OD and CHIRALCEL® OJ in 95:5 *n*-Hex/IPA (v/v). For detailed HPLC conditions, see **Table 10** and **Table 11**.[103] Elution order: (*R*,*R*) and (*S*,*S*).

162

Table 10. Chromatographic parameters of the separation of TSO and furoin in different solvent systems with TAMOF-1 HPLC column A.[103]

Analyte	Mobile phase[a]	R_S	α	t_{R1} (min)	t_{R2} (min)
TSO	IPA	1.73	2.92	8.71	17.38
	MeOH	–[b]	1.21	13.74	15.82
	ACN	2.55	6.38	6.70	20.12
	95:5 n-Hex/IPA	1.37	3.06	12.12	28.47
furoin	1:1 n-Hex/EtOH	1.12	1.57	67.29	103.36

[a] Flow rate = 0.15 mL min^{-1}. [b] No baseline resolution achieved.

Table 11. Comparison of the separation of TSO by the TAMOF-1 column A versus CHIRALPAK® AD, CHIRALCEL® OJ and OD commercial columns.[103]

	TAMOF-1	AD[a]	OD[b]	OJ[c]
Dimensions (mm)	100 × 4.6		250 × 4.6	
(S,S) time (min)	12.1	32.3	37.6	55.3
(R,R) time (min)	28.5	59.6	69.2	68.4
Resolution (R_S)	1.37	4.98	5.75	2.63
% area (S)	50.4	49.5	50.8	49.8
% area (R)	49.6	50.5	49.2	50.2
Total time (min)	40	75	80	80

Conditions: n-Hex/IPA 95:5 (v/v), 0.15 mL min^{-1}. [a] CHIRALPAK® AD. [b] CHIRALCEL® OJ. [c] CHIRALCEL® OD.

The data suggest that the TAMOF-1 packed HPLC column yields highly efficient chiral resolutions and may exceed commercial column performance in terms of elution system versatility. Furthermore, the TAMOF-1 packed HPLC column yields competitive separation in the same working conditions. While each column can resolve TSO, the limitation for commercial columns is the need to use highly hydrophobic solvent systems, 95:5 n-Hex/IPA in this case.

The broader peaks obtained with TAMOF-1 are likely related to its heterogeneous particle size since the columns were packed using the as-prepared material, with a random particle size between 0.2 and 10 μm, according to DLS data (Chapter 1, page **50**). A TAMOF-1 column with homogeneous particle size (as the commercial CSPs) might offer even better performance.

Chapter III

Chromatographic Separation of Enantiomers Using TAMOF-1 as Chiral Stationary Phase

3.3.3.2. Calculation of the optimal flow

In order to elucidate the optimal flow rate for TAMOF-1 packed HPLC columns, we performed three TSO injections at different flows (0.3, 0.4 and 0.5 mL min^{-1}), and by relating each flow to the corresponding HETP of the TSO peaks, we obtained the theoretical Van Deemter plot for TAMOF-1 columns (**Figure 144**), where the optimal flow is the minimum of the curve.
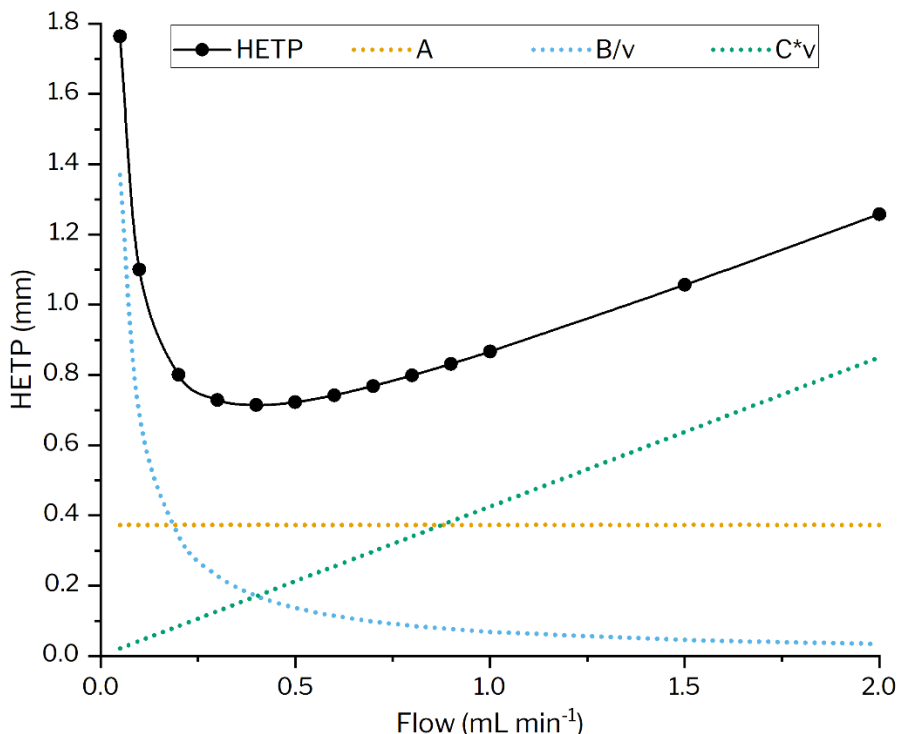
Figure 144. Theoretical Van Deemter plot. The minimum HETP (black line) is found at 0.4 mL min^{-1}.

As shown in the plot, the optimal flow rate at which the resolving power is maximised is 0.4 mL min^{-1}. Thus, we decided to move forward using this flow rate, although, some separations had to be performed in lower flow rates for practical reasons such as background pressure.

With the Van Deemter equation, we were able to calculate further other parameters such as the Eddy-diffusion parameters (A), the diffusion coefficient of eluting particles (B) and the mass transfer coefficient of the analyte between the mobile and stationary phase (C).

164

3.3.3.3. Effect of the column length in the separations

To further explore the capabilities of TAMOF-1, we packed a second HPLC column (150 mm × 4.0 mm, column B, see page **178** for details). Compared to column A, better separations were obtained for TSO using a variety of mobile phases (**Table 12** and **Figure 153**). With the same column, we successfully achieved HPLC separations of various other racemic mixtures, including 1-phenylethan-1-ol, benzoin or flavanone with different degrees of resolution (**Table 12**, **Figure 155-Figure 157**). These results ultimately demonstrate the potential versatility of TAMOF-1 to optimise chromatographic separation conditions for the direct HPLC separation of structurally diverse chiral small molecules.

Table 12. Chromatographic parameters of the separation of different racemic mixtures by a TAMOF-1 HPLC column B.

Analyte	Mobile phase[a]	R_S	α	t_{R1} (min)	t_{R2} (min)
TSO	IPA	2.32	4.50	7.60	14.2
	5:95 n-Hex/IPA	2.23	4.42	7.8	15.2
	1:9 n-Hex/IPA	2.16	4.55	8.0	16.4
	9:1 n-Hex/IPA	2.18	4.63	8.2	17.1
	95:5 n-Hex/IPA	1.52	3.55	13.2	32.3
	ACN	4.09	7.24	6.5	11.8
	95:5 ACN/TBME	1.73	7.03	6.4	10.7
	9:1 ACN/TBME	1.15	6.81	6.3	10.1
1-phenylethanol	EtOH	1.47	1.67	9.2	11.6
	1:9 n-Hex/EtOH	1.50	1.72	9.6	12.4
	9:1 n-Hex/EtOH[b]	2.00	1.57	24.6	36.5
flavanone	EtOH	1.24	1.55	17.3	23.6
	ACN	0.92	2.84	6.5	8.0
benzoin	1:9 n-Hex/EtOH	1.45	1.54	14.2	18.7

[a] 0.2 mL min^{-1} flow rate. [b] 0.3 mL min^{-1} flow rate.

Chapter III

Chromatographic Separation of Enantiomers Using TAMOF-1 as Chiral Stationary Phase

Seen the success in enantioselective HPLC chromatography using columns A and B (100 mm x 4.6 mm and 150 mm x 4.0 mm), we decided to use longer columns to improve separations. Two empty stainless-steel columns (250 mm x 4.6 mm, column C, and 250 x 2.0 mm, column D, see page **179** for details) were filled with *ca.* 3 g of TAMOF-1. Following the procedure established for columns A and B, TSO was used as a standard to calibrate columns C and D (**Table 13**), and the resolution (R_S) and selectivity (α) were compared with the results previously obtained using ACN as a model solvent. We found that column D yielded the best R_S and α (**Figure 145**). It is worth mentioning that the increase of the column length allowed us to use higher flow rates up to 1 mL min^{-1}, depending on the solvent system.

Table 13. Comparison of the separation of TSO in ACN. Wavelength: 230 nm.

Column	Dimensions (mm)	Flow rate (mL min^{-1})	t_{R1} (min)	t_{R2} (min)	*R*s	α
A	100 x 4.6	0.15	6.7 **(S,S)**	20.12 **(R,R)**	2.55	6.38
B	150 x 4.0	0.15	6.5 **(S,S)**	11.80 **(R,R)**	4.09	7.24
C	250 x 4.6	0.40	6.18 **(S,S)**	13.29 **(R,R)**	3.38	6.17
D	250 x 2.0	0.40	5.26 **(S,S)**	13.62 **(R,R)**	4.71	8.17
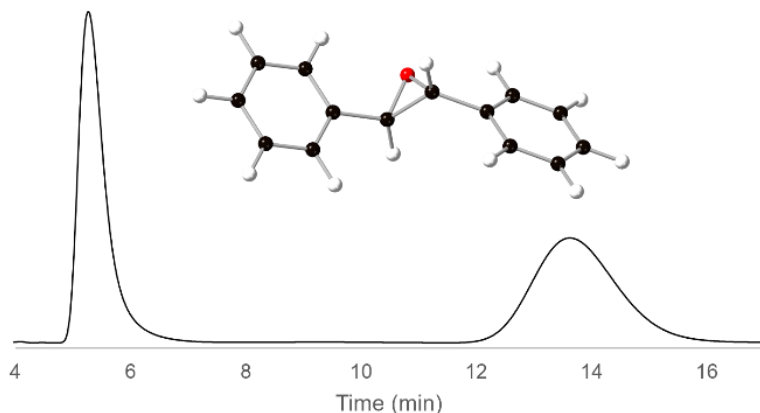
Figure 145. Representative chromatogram for the separation of TSO, column D.

In order to further test the reproducibility of columns **C** and **D**, we duplicated the analyses of 1-phenylethan-1-ol, flavanone, furoin and benzoin (**Table 14**). The chromatograms for these analytes can be found in the Experimental Section (**Figure 158** and **Figure 161**).

166

Table 14. Comparison between column B and column C in the separation of flavanone, 1-phenylethanol, furoin and benzoin.

Analyte	Column B			Column C		
	Mobile phase	Rs	α	Mobile phase	Rs	α
Flavanone	EtOH	1.24	1.55	EtOH	1.30	1.39
1-phenylethanol	n-Hex/EtOH 9:1	1.50	1.72	n-Hex/EtOH 9:1	1.36	1.25
Furoin	n-Hex/EtOH 1:1	1.12	1.57	EtOH[a]	1.13	1.29
Benzoin	n-Hex/EtOH 1:9	1.45	1.54	EtOH	1.35	1.28

Conditions: 0.2 mL min^{-1}. [a] 0.4 mL min^{-1}.

3.3.3.3.1. Structurally related racemates

We continued by separating an array of structurally related substrates with column B: anisoin (4,4'-dimethoxybenzoin), methyl mandelate and 2-phenylpropionitrile (**Table 15, Figure 146**), with phenyl rings and polar functional groups, *i.e.* alcohols, ketones, esters and nitriles. Anisoin and 2-phenylpropionitrile were successfully resolved with the same mobile phase, an *n*-Hex/EtOH mixture with good selectivity, and excellent resolution in the anisoin case. Methyl mandelate was also resolved, but with pure ACN as mobile phase.

Table 15. Retention times, resolutions and selectivities of anisoin, methyl mandelate and 2-phenylpropionitrile.

Analyte	Mobile phase	t_{R1} (min)	t_{R2} (min)	R_S	α
Anisoin	n-Hex/EtOH 1:1	44.02	84.34	1.90	2.03
Methyl mandelate	ACN	29.15 (*R*)	35.63 (*S*)	1.07	1.22
2-phenylpropionitrile	n-Hex/EtOH 1:1	14.82	16.94	0.61	1.14

Conditions: 0.4 mL min^{-1}.

Chapter III

167

Chromatographic Separation of Enantiomers Using TAMOF-1 as Chiral Stationary Phase
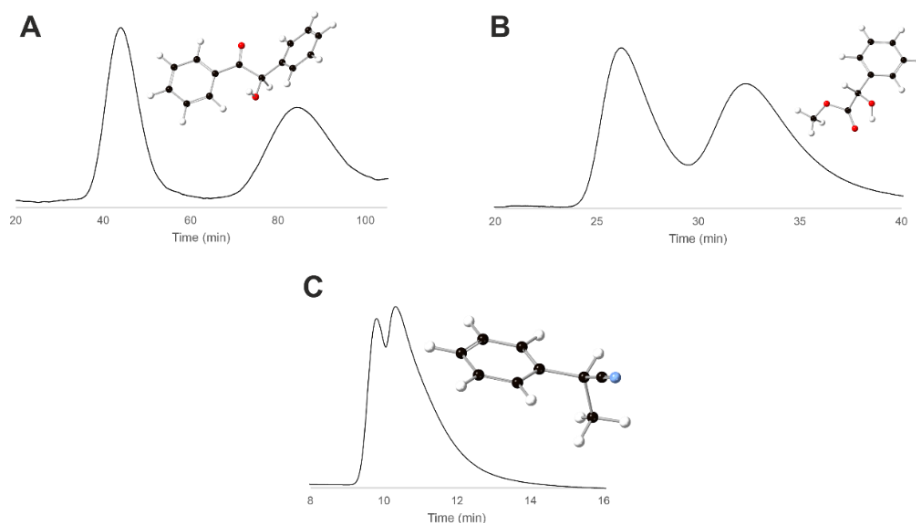
Figure 146. HPLC chromatograms of (a) anisoin, (b) methyl mandelate and (c) 2-phenylpropionitrile with the corresponding 3D representation of each molecule.

3.3.3.3.2. Terpenes and terpenoids

Terpenes are the largest family of natural products derived from isoprene with the molecular formula $(C_5H_8)_n$. Terpenoids are modified terpenes with functional groups, such as alcohols or carbonyls. These compounds are essential and, so far, minor investigations have been performed. Many methods to separate terpene enantiomers, such as limonene or carvone, have been reported in GC[186] but only a few examples in HPLC.[187] Our next target was limonene, a non-polar molecule containing only carbon and hydrogen. Thus, we screened non-polar solvents, finding excellent resolution in *n*-Hept as mobile phase (**Figure 147**). Other terpenes and terpenoids were resolved with the TAMOF-1-packed columns (**Table 16**), including carvone, camphene, β-citronellol and α-pinene, resulting in excellent separations (**Figure 148**). However, a racemic mixture of α-terpineol could not be efficiently separated (**Figure 148e**).

[186] (a) Wang, X.; Jia, C.; Wan, H. *J. Chromatogr. Sci.* **1995**, *33*, 22-25. (b) Liu, H.; Xie, S.-M.; Ai, P.; Zhang, J.-H.; Zhang, M.; Yuan, L.-M. *ChemPlusChem* **2014**, *79*, 1103-1108. (c) Pragadheesh, V. S.; Yadav, A.; Chanotiya, C. S. *J. Chromatogr. B* **2015**, *1002*, 30-41. (d) Chan, J. Y.; Zhang, H.; Nolvachai, Y.; Hu, Y.; Zhu, H.; Forsyth, M.; Gu, Q.; Hoke, D. E.; Zhang, X.; Marriot, P. J.; Wang, H. *Angew. Chem. Int. Ed.* **2018**, *57*, 17130-17134.
[187] (a) Moeder, C.; O'Brien, T.; Thompson, R.; Bicker, G. *J. Chromatogr. A* **1996**, *736*, 1-9. (b) Mookdasanit, J.; Tamura, H. *Food Sci. Technol. Res.* **2002**, *8*, 367-372. (c) Hartlieb, K. J.; Holcroft, J. M.; Moghadam, P. Z.; Vermeulen, N. A.; Algaradah, M. M.; Nassar, M. S.; Botros, Y. Y.; Snurr, R. Q.; Stoddart, J. F. *J. Am. Chem. Soc.* **2016**, *138*, 2292-2301.
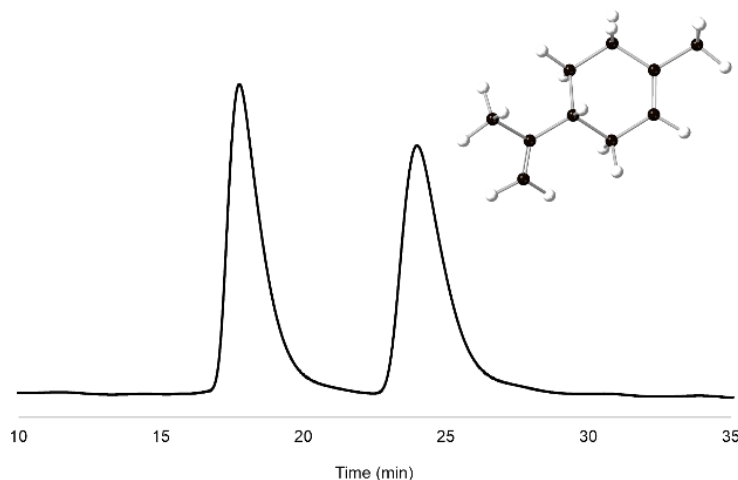
Figure 147. HPLC chromatogram of *rac*-limonene and its corresponding 3D representation.

These results are significant and support the versatility of the TAMOF-1 CSP, which can recognise the enantiomers of non-polar molecules in non-polar mobile phases. In some cases, like camphene (**Figure 148b**), a polar mobile phase, EtOH, yielded the best result, even when the substrate is non-polar. In contrast, polar molecules like β-citronellol (**Figure 148c**), were chirally recognised best in highly non-polar mobile phases (95% *n*-Hex). The results of the separation screening with terpenes and terpenoids are important for future separations, as the structurally similar molecules with similar functional groups require similar conditions for the enantiomeric separations, allowing us to make predictions prior to starting the screening – although it does not compile for every racemate.

Chapter III

Table 16. Chromatographic parameters of the separation of terpenes.

Analyte	Mobile phase	t_{R1} (min)	t_{R2} (min)	R_S	α
Limonene[c]	*n*-Hept	17.75 (*R*)	23.98 (*S*)	2.61	1.35
Carvone[b]	EtOH[a]	25.96 (*S*)	33.99 (*R*)	1.82	1.31
Camphene[b]	EtOH	19.91 (+)	26.30 (-)	1.13	1.42
β-citronellol[b]	*n*-Hex/EtOH 95:5	20.76 (*S*)	24.66 (*R*)	1.03	1.24
α-pinene[b]	*n*-Hex	30.87 (*R*)	34.18 (*S*)	1.27	1.11
α-terpineol[c]	EtOH	14.44 (*R*)	17.14 (*S*)	0.63	1.19

Conditions: 0.4 mL min^{-1}. [a] 0.2 mL min^{-1}. [b] Column C. [c] Column D.

169

Chromatographic Separation of Enantiomers Using TAMOF-1 as Chiral Stationary Phase
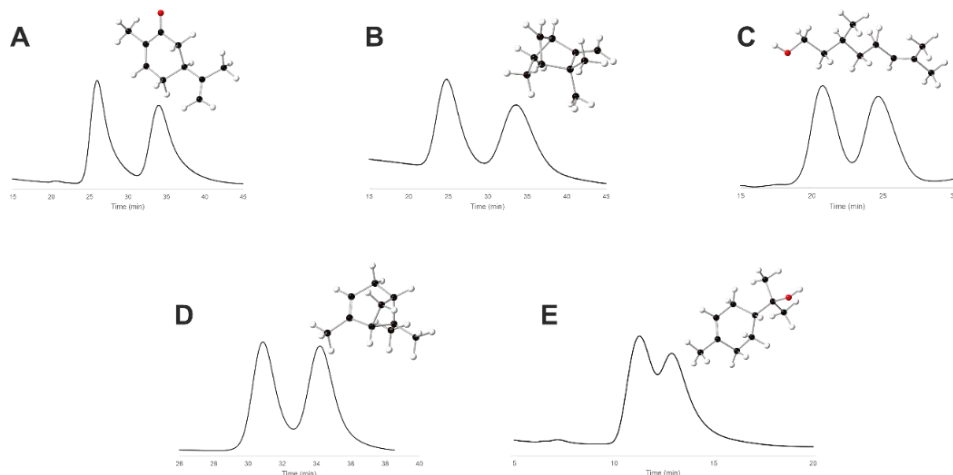
Figure 148. Chromatograms of (a) carvone, (b) camphene, (c) β-citronellol, (d) α-pinene and (e) α-terpineol with its corresponding 3D representation.

3.3.3.3.3. Calcium channel blockers

Calcium channel blockers are a group of medications used in the treatment of hypertension.[188] Most of these medications are sold as racemic mixtures, although it has been proven that some of them have a more active enantiomer, such as for (*S*)-nitrendipine and (*S*)-amlodipine.[189] These enantiopure 1,4-dihydropyridines (DHPs) can be obtained from stereoselective synthesis, resolution of 1,4-DHP salts and kinetic resolution, among other methods.[190] These methods are either expensive or experimentally challenging.

TAMOF-1-packed columns show preliminary promising results towards the separation of nitrendipine enantiomers, although further improvement is required to resolve both peaks (**Table 17**). We were able to better resolve amlodipine, which contains bulkier functional groups (**Figure 149**). In general, these molecules are significantly larger than terpenes and terpenoids, pointing again to the high versatility of TAMOF-1 for different substrates, also in terms of size.

---

[188] (a) Vardanyan, R.; Hruby, V. In *Synthesis of Best-Seller Drugs*; Vardanyan, R.; Hruby, V., Eds.; Academic Press: Boston, 2016; pp 329-356. (b) Godfraind, T. *Front. Pharmacol.* **2017**, *8*, (c) Lin, Y.; Ma, L. *Medicine* **2018**, *97*, e13152.

[189] Rucins, M.; Plotniece, A.; Bernotiene, E.; Tsai, W.-B.; Sobolev, A. *Catalysts* **2020**, *10*, 1019.

[190] (a) Goldmann, S.; Stoltefuss, J. *Angew. Chem. Int. Ed.* **1991**, *30*, 1559-1578. (b) Štěpánková, M.; Krasulová, K.; Dořičáková, A.; Kurka, O.; Anzenbacher, P.; Dvořák, Z. *Toxicol. Lett.* **2016**, *262*, 173-186.

Table 17. Chromatographic parameters of the separation of calcium channel blockers in different solvent with columns C and D.

Analyte	Mobile phase	t_{R1} (min)	t_{R2} (min)	R_S	α
Nitrendipine	EtOH[a]	10.01	11.13	0.71	1.11
Amlodipine	THF[b]	4.16	9.75	1.21	3.20[c]

[a] Conditions: 0.2 mL min⁻¹, column C. [b] 0.4 mL min⁻¹, column D. [c] The selectivity value was calculated manually following Equation 2 (Experimental Section).
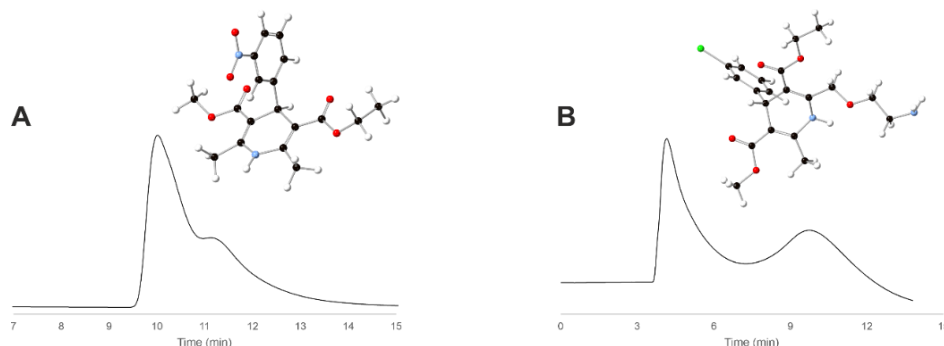
Figure 149. Chromatograms of (a) nitrendipine and (b) amlodipine with its corresponding 3D representation.

3.3.3.3.4. *P*-stereogenic compounds

Looking for stereogenic centres different to carbon, we turned our attention to the separation of *P*-stereogenic molecules. This is a highly challenging problem. To the best of our knowledge, no *P*-stereogenic molecule has been successfully purified via chiral chromatographic separation. So, these ligands are obtained by costly and complicated chiral synthetic routes.[191] As a model for these substrates, we selected phenyl *N*-phenylphosphoramidochloridate (**Table 18**), widely used for the functionalisation of nucleotides as prodrugs for the treatment of viral infections and cancer.[192] Remarkably, we observed two well-resolved peaks with our column B, with *n*-Hex/EtOH 1:1 as eluent at a flow rate of 0.4 mL min⁻¹ (**Figure 150**).

[191] Grabulosa, A. *P-Stereogenic Ligands in Enantioselective Catalysis*. RSC Publishing: Cambridge, 2011.
[192] (a) Jonckers, T. H. M.; Vandyck, K.; Vandekerckhove, L.; Hu, L.; Tahri, A.; Van Hoof, S.; Lin, T.-I.; Vijgen, L.; Berke, J. M.; Lachau-Durand, S.; Stoops, B.; Leclercq, L.; Fanning, G.; Samuelsson, B.; Nilsson, M.; Rosenquist, Å.; Simmen, K.; Raboisson, P. *J. Med. Chem.* **2014**, *57*, 1836-1844. (b) DiRocco, D. A.; Ji, Y.; Sherer, E. C.; Klapars, A.; Reibarkh, M.; Dropinski, J.; Mathew, R.; Maligres, P.; Hyde, A. M.; Limanto, J.; Brunskill, A.; Ruck, R. T.; Campeau, L.-C.; Davies, I. W. *Science* **2017**, *356*, 426. (c) Dašková, V.; Buter, J.; Schoonen, A. K.; Lutz, M.; de Vries, F.; Feringa, B. L. *Angew. Chem. Int. Ed.* **2021**, *60*, 11120-11126.

Chapter III

Chromatographic Separation of Enantiomers Using TAMOF-1 as Chiral Stationary Phase

Since none of the enantiomers of phenyl *N*-phenylphosphoramidochloridate (PNPPCl) is available in enantiopure form, we had to confirm the true nature of the two separated substances by analytical techniques. This is not trivial since it is also known that this substrate may react with alcohols to give the corresponding *O*-alkyl-*O*-phenylphosphoramides,[193] a reaction in which the labile chlorine gets replaced by an alcohol as nucleophile (**Scheme 20**).

Table 18. Chromatographic parameters of the separation of phenyl *N*-phenylphosphoramidochloridate with column C.

Analyte	Mobile phase	t_{R1}(min)	t_{R2} (min)	R_S	α
PNPPCl	*n*-Hex/EtOH 1:1[a]	16.01	32.83	1.44	2.05

[a] Conditions: 0.4 mL min^{-1}.
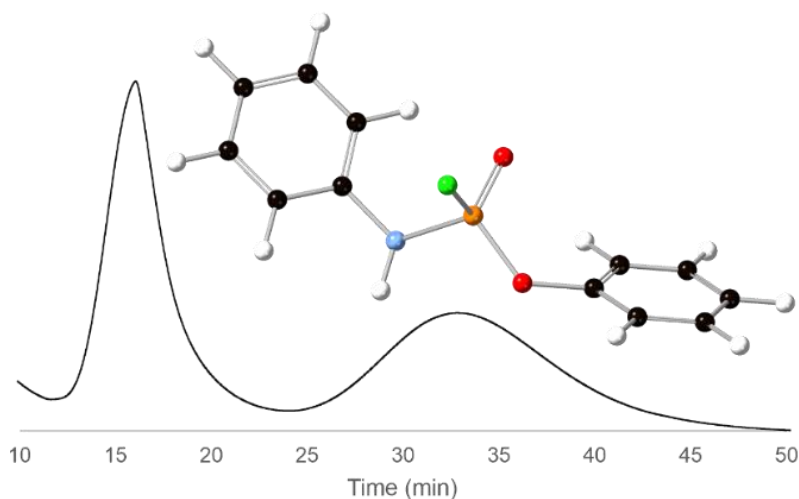
Figure 150. HPLC chromatogram of phenyl *N*-phenylphosphoramidochloridate with its corresponding 3D molecular representation.
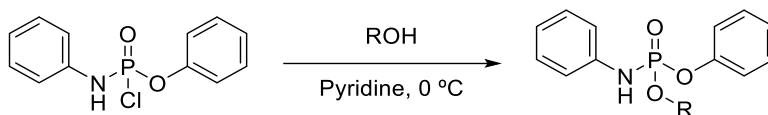
Scheme 20. Reaction scheme of the nucleophilic substitution of the chlorine atom in PNPPCl with an alcohol.

[193] Dobbs, A. P. *Phenyl N-Phenylphosphoramidochloridate* in *Encyclopedia of Reagents for Organic Synthesis*. 2001.

In order to discard the *in-situ* formation of ethyl phenyl phenylphosphoramidate by reaction with the mobile phase, we coupled our HPLC system to an ESI-MS detector to identify the nominal mass for the peaks. The mass spectra revealed that the two peaks correspond to pure samples (only one mass signal) and with identical *m/z* ratio of 267 (**Figure 186** and **Figure 187**), thus confirming the stability of phenyl *N*-phenylphosphoramidochloridate during the HPLC separation and that both enantiomers are separated adequately under these conditions.

3.3.4. Semi-preparative separations: increasing the scale

Beyond analytical applications, we finally decided to explore the practical utility that TAMOF-1-packed columns may have for the purification of products. For this aim, we fabricated columns at the semi-preparative scale to accept more significant flows while producing pure fractions of each enantiomer. For this reason, a column of size 250 x 10.0 mm was packed with TAMOF-1 (see Experimental Section for details, page **179**).

We selected limonene and carvone as model analytes for this proof-of-concept. The corresponding loading tests (**Figure 151**) showed how both substrates could be purified in 1 mg scale per injection, confirming the promising features of TAMOF-1 to be a valuable CSP for purification/preparation tools in the chemical industry in addition to analytical tools for the identification of enantiomers.

Chapter III

Chromatographic Separation of Enantiomers Using TAMOF-1 as Chiral Stationary Phase
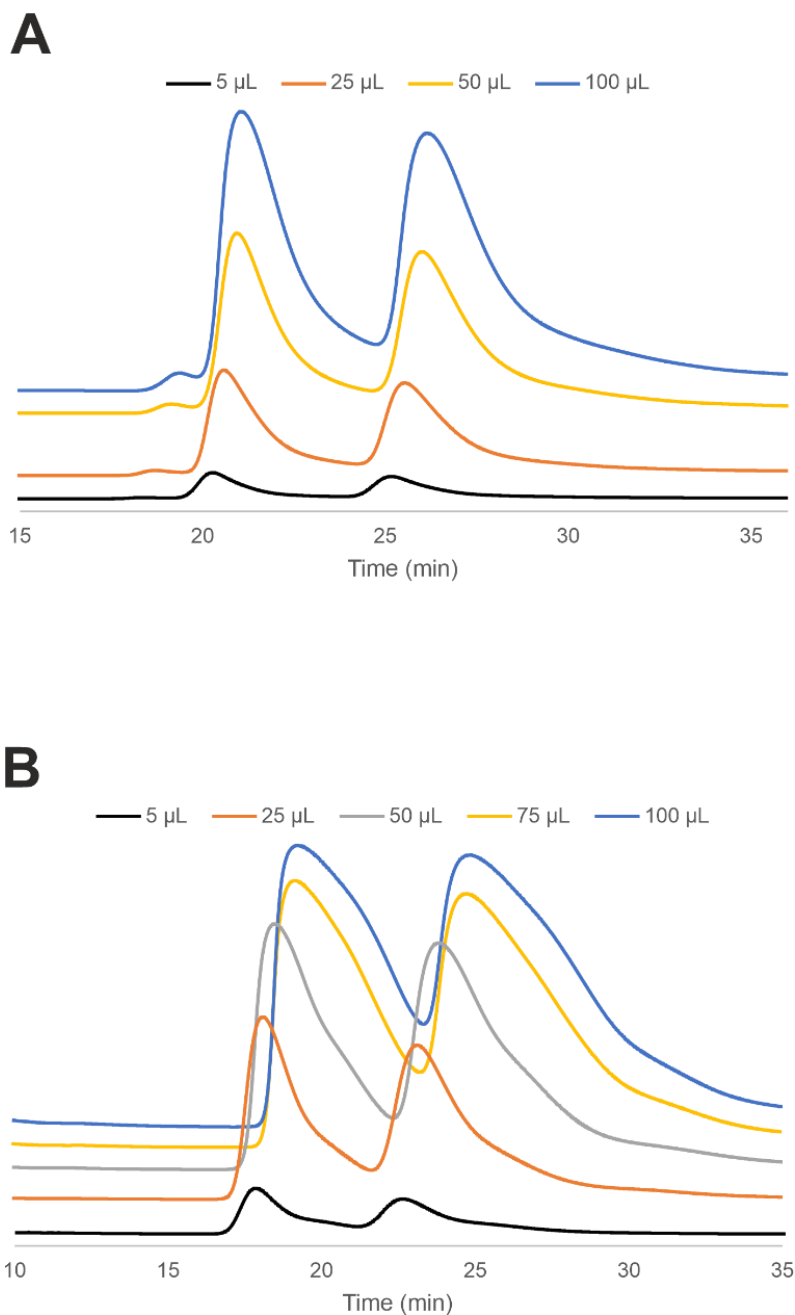
Figure 151. (A) Semi-preparative separation of limonene. Conditions: *n*-Hex, 2 mL min^{-1}, 10 mg mL^{-1}. **(B)** Semi-preparative separation of carvone. Conditions: EtOH, 1 mL min^{-1}, 10 mg mL^{-1}.

174

3.3.5. Repeatability test

To assess the proper performance of the analytical column after repeated injections, we performed >180 consecutive injections of TSO without cleaning or equilibration between injections. This test aims to observe any significant fluctuations in the resolution and the selectivity of the chiral separations. The resolution observed in these 187 injections was $R_s = 3.12 \pm 0.13$, and the selectivity was $\alpha = 7.09 \pm 0.18$. No significant changes were observed in the chromatograms, as shown in **Figure 152**.
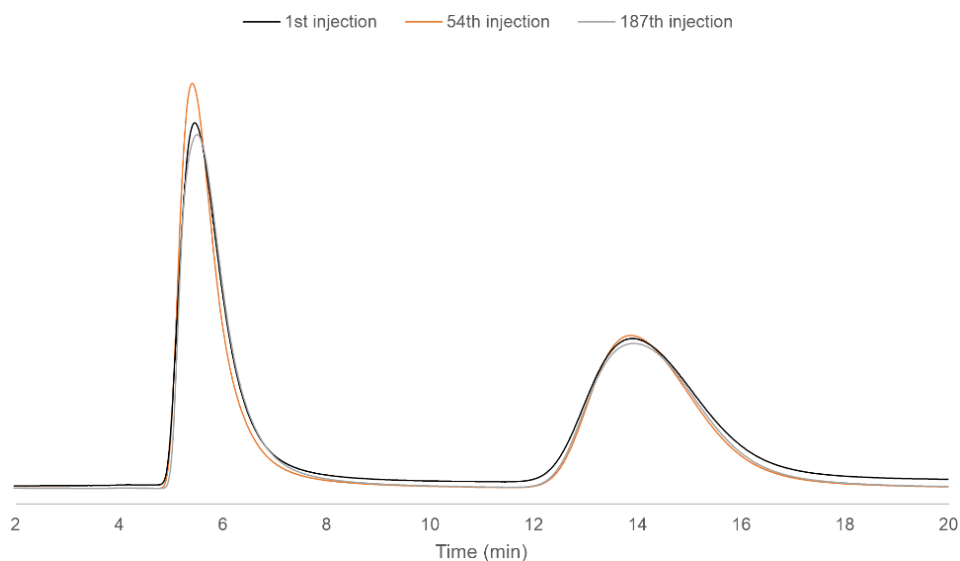
Figure 152. HPLC chromatogram of TSO (Column C) after 1, 54 and 187 injections.

Chapter III

175

3.4. CONCLUSIONS

In conclusion, TAMOF-1 works as a highly versatile and recyclable chiral stationary phase (CSP) upon a proper HPLC column packing and has been able to separate 13 racemates so far with different molecular sizes and functional groups, using both polar and non-polar solvents. The structurally diverse racemic mixtures that have been separated encompass terpenes and terpenoids, calcium channel blockers and *P*-stereogenic phosphorus compounds. In particular, the separation of configurationally stable enantiopure phosphorus compounds opens the door to their facile obtention, suitable for its use in asymmetric catalysis.

Comparative studies have shown that TAMOF-1 outperforms the chiral separation capability of some commercial chiral HPLC columns. According to theoretical studies, this performance arises from the combination of chiral channels and weak binding sites allowing for low-energy separation of enantiomers without strong binding to the recognition sites. This feature, along with its chemical and mechanical stability, allows working under diverse HPLC conditions.

The TAMOF-1-packed HPLC analytic columns possess excellent chemical stability and tolerate a wide array of mobile phases and long term cyclability. After two years of use, no column degradation is observed, being cleaned with ACN in between runs when needed. Moreover, after more than 180 consecutive injections, no significant changes were observed in the chromatograms, confirming the stability and robustness of these columns.

Finally, semi-preparative separations allowed us to obtain up to 1 mg per run. The successful trials of limonene and carvone are promising results that open the door to expand the scope of semi-preparative separations with TAMOF-1.

176

3.5. EXPERIMENTAL SECTION

3.5.1. Materials and general

All reagents were of commercial grade and used without further purification: L-histidine (≥98%, Iris Biotech GmbH), ibuprofen (≥98%, Sigma Aldrich), thalidomide (98%, Fluorochem); TSO (98%, Sigma Aldrich), furoin (≥98%, Sigma Aldrich), benzoin (98%, Sigma Aldrich), 1-phenylethan-1-ol (98%, Sigma Aldrich), flavanone (≥98%, Alfa Aesar), thionyl chloride ($SOCl_2$, reagent plus, ≥99%, Sigma Aldrich), hydrazine monohydrate ($NH_2NH_2 \cdot H_2O$, reagent grade, 98%, Sigma Aldrich), sodium carbonate anhydrous (Na_2CO_3, ACS reagent, ≥99.5%, Sigma Aldrich). All solvents were of commercial grade and used without further purification: HPLC-grade MeOH, EtOH, IPA, *n*-Hex, ACN and TBME (VWR, Chem-Lab and Sigma Aldrich), *N,N*-dimethylformamide (peptide grade, ≥99.9%, Iris Biotech GMBH) and diethyl ether (≥99%, VWR). An empty stainless-steel column (100 mm × 4.6 mm I.D.) was obtained from Restek (Bellefonte, PA, USA). An empty stainless-steel column (150 mm × 4.0 mm I.D.) was obtained from Chiral Technologies Europe SAS (Illkirch, Strasbourg, France). The synthesis of DMFA, *S*-HTA and TAMOF-1 has been described on page **48**.

Chapter III

3.5.2. Instrumentation

Ibuprofen aliquots from preparative TAMOF-1 columns were analysed by ultraperformance convergence chromatography with an ACQUITY UPC2 system equipped with a diode array detector (Waters Company), and a CHIRALPAK® IC column (4.6 ×100 mm, 3 μm) with an isocratic CO_2/ACN/TFA 88:12:0.5 mobile phase, at a 3 mL min^{-1} flow rate (1500 psi), for a volume injection of 2 μL. Ibuprofen aliquots from preparative TAMOF-1 columns were analysed by HPLC chromatography with an Agilent 1200 Series system equipped with a diode array detector, and a CHIRALPAK® IA column (4.6 × 250 mm, 5 μm) with a mobile phase MeOH/ACN 80:20 mobile phase with 0.1mM NH_4OAc, at 1 mL min^{-1} flow rate, for a volume injection of 5 μL. Comparative HPLC separations with column A were performed on a Varian 9002 HPLC pump and a Varian 9050 UV/Vis detector (Palo Alto, CA, USA). HPLC separations with column B were performed with an Agilent 1200 Series system equipped with a diode array detector.

3.5.3. Preparation of preparative TAMOF-1 columns

Glass columns (60 cm total length, 1 cm outer diameter, 0.6±1 cm inner diameter) were used to prepare TAMOF-1 separation columns. TAMOF-1 was activated in a round flask at 2×10–1 mbar and 403 K for 14 hours. The resulting TAMOF-1 powder was packed into the glass column over a 5 mm-thick compact cotton stopper by adding successive loads of ≈ 400 mg and pressurised under N_2 (99.999% purity) at ≤ 4 bar for 10 min. Then, the column was filled with 100% ACN and pressurised under N_2 until the eluent level reached the top of the TAMOF-1 bed. The bed was then covered with another 5 mm-thick cotton layer. On average, 3 g loading of TAMOF-1 corresponds to ≈ 25±1 cm bed length. Before the *rac*-ibuprofen and *rac*-thalidomide separation tests, the columns were conditioned overnight under an ACN flow (in the 0.05 - 0.10 mL min⁻¹ range, leading to column head pressure in the 10-75 kPa range). The eluent was pumped during columns conditioning and drug separation tests using a Metrohm 877 Titrino plus apparatus.

3.5.4. Preparation of packed columns

To pack **column A** (100 mm × 4.6 mm I.D.) with TAMOF-1, 737 mg (activated following previous procedure) were initially added via dry packing, and the column was pressurised using 100% ACN at a high flow rate (approx. 10 mL min⁻¹). After 10 h pressurisation with ACN, the column was opened, and an additional amount of TAMOF-1 had to be added due to packing of the material, and the eluent changed to 100% IPA (higher viscosity). This process of adding TAMOF-1 and packing was repeated until a total of 1550 mg were added to the column. After the column was fully packed, it was pressurised with 100% IPA at a high flow rate (2 mL min⁻¹, ~5000 psi) for 12 h to ensure further TAMOF-1 was properly packed. Before any separation experiment, the column was conditioned with the appropriate solvent system at a flow rate of 0.15 mL min⁻¹ with approximately 15 CV.

Another column was prepared (**column B**). To pack this second column with TAMOF-1, the 150 mm x 4.0 mm I.D. column was coupled to a 150 mm x 10 mm I.D. reservoir. This system was loaded with a slurry of TAMOF-1 in IPA/*n*-Hept 8:2 and pressurised with IPA/*n*-Hept 9:1 up to ≈ 150 bar for 20 min. The reservoir device was removed, and the column containing *ca.* 1.8 g of TAMOF-1 was closed. Before any HPLC analyses, the column was conditioned passing the mobile phase to be used (approximately the eluent volume equivalent to 15 CVs).

The column TAMOF-250 (**column C**) was prepared using the method mentioned above: *ca.* 3 g of TAMOF-1 previously activated (vacuum, 80 °C, 3 h) was added to the column (250 x 4.6 mm) via dry packing inside a glovebox, and the column was pressurised using 100% ACN at a high flow rate (10 mL min⁻¹). After 10 h of pressurisation, the column was opened, and more TAMOF-1 was added due to the packing, then the column was pressurised again using 100% IPA (2 mL min⁻¹). This process was repeated until the column was fully packed.

Column D (250 x 2.0 mm) and the semi-preparative column (250 x 10.0 mm) were purchased from Hichrom LTD. The packing of these columns followed a similar procedure to columns **A** and **B**: the columns were loaded with a slurry of TAMOF-1 in *n*-Hept/IPA 9:1, then pressurised, containing *ca.* 0.6 g of TAMOF-1 in column **D** and *ca.* 14 g of TAMOF-1 in the semi-preparative column.

3.5.5. Calculation of the chromatographic parameters

The selected parameters to assess separation efficiency were the retention factor (k), separation factor (α), and resolution (R_S). These parameters were calculated using the following equations:

$$k = \frac{t_{R1} - t_M}{t_M} \qquad \text{(Equation 1)}$$

$$\alpha = \frac{t_{R2} - t_M}{t_{R1} - t_M} \qquad \text{(Equation 2)}$$

$$R_S = \frac{2(t_{R2} - t_{R1})}{w_1 + w_2} \qquad \text{(Equation 3)}$$

where t_M is the column void time, t_{R1} and t_{R2} are the retention times and w_1 and w_2 are the peak widths of each peak. The void volumes for each column were the following: **A** = 0.76 mL; **B** = 0.89 mL; **C** = 1.92 mL and **D** = 1.64 mL.

The HETP values for the representation of the Van Deemter plot were calculated using the following formula:

$$HETP = \frac{N_t}{L} \qquad \text{(Equation 4)}$$

where N_t is the number of theoretical plates, which is automatically given by the instrument, and L is the length of the column in mm.

Chapter III

The Van Deemter plot was calculated with the Van Deemter equation by using a system of three equations with three unknown values (A, B and C). The known values were *HETP* and v:

$$HETP = A + \frac{B}{v} + C * v \qquad \text{(Equation 5)}$$

where *HETP* is the height equivalent to the theoretical plate, A is the multiple paths term, B/v is the longitudinal diffusion term, $C*v$ the mass transfer term, v the flow rate in mL min^{-1}, L is the length of the column, and N_t is the theoretical plate of the peak. The terms A, B and C were obtained with the following multiplication of matrices:

$$x^{-1} * y = z, \text{ where } x = \begin{pmatrix} 1 & 1/v_1 & v_1 \\ 1 & 1/v_2 & v_2 \\ 1 & 1/v_3 & v_3 \end{pmatrix}, y = \begin{pmatrix} HETP_1 \\ HETP_2 \\ HETP_3 \end{pmatrix} \text{ and } z = \begin{pmatrix} A \\ B \\ C \end{pmatrix}$$

3.5.6. Van Deemter equation values

The matrix multiplication stated above with the values listed below gave the values A, B and C as matrix z. Matrix x values are listed to the right of the table. Matrix y values are the HETP values listed below.

v (mL min^{-1})	N_t	L (mm)	HETP (mm)	A	1/v	v
0.3	343	250	0.728863	1	3.3333	0.3
0.4	350	250	0.714286	1	2.5	0.4
0.5	346	250	0.722543	1	2	0.5

The inverse matrix x^{-1} was calculated following the next equation, where $|x|$ is the determinant of matrix x and $(x^*)^t$ is the transpose of the adjugate matrix of x:

$$x^{-1} = \frac{1}{|x|} * (x^*)^t \qquad \text{(Equation 6)}$$

$$x^{-1} = \begin{pmatrix} -13.6 & 32.3 & -17.6 \\ 3.03 & -6.06 & 3.03 \\ 15.2 & -40.3 & 25.2 \end{pmatrix} y = \begin{pmatrix} 0.729 \\ 0.714 \\ 0.723 \end{pmatrix} z = \begin{pmatrix} 0.369 \\ 0.0692 \\ 0.429 \end{pmatrix}$$

Therefore, the resulting Van Deemter equation is the following:

$$HETP = 0.369 + \frac{0.0692}{v} + 0.429 * v \qquad \text{(Equation 7)}$$

180

3.5.7. Computational details

The preferential adsorption sites of ibuprofen and thalidomide enantiomers were determined by using the Adsorption Locator module in Materials Studio. Molecular dimensions of *rac*-ibuprofen and *rac*-thalidomide were calculated with Olex2 by using the following element radii: C, 1.7; H, 1.09; N, 1.55 and O, 1.52 Å. Default radii source: http://www.ccdc.cam.ac.uk/products/csd/radii. Classical simulations were carried out using RASPA molecular simulation software.[194] An all-atom flexible model was used to model each enantiomer, except the heterocycle part (*e.g.,* aromatic ring in the ibuprofen molecule), which is considered rigid. The intramolecular potential for the guest species comprises two-body (bond), three-body (angle), four-body (dihedral) interactions and the electrostatic Coulomb term. Parameters are given in the original reference OPLS-AA. TAMOF-1 was considered a rigid structure, and Lennard-Jones parameters are taken from DREIDING[195] force field, except for metallic atoms taken from UFF force field.[196] The charges of the host atoms are obtained via QEq calculations using the RASPA code. Finally, Lennard-Jones (LJ) potentials are used to describe the intermolecular host-guest and guest-guest interactions using Lorentz-Berthelot mixing rules. This methodology has been validated with many previous works.[197] Adsorption enthalpy was calculated with the Widom Test Particle insertion method at infinite dilution.[184] The Configurational Bias Monte Carlo (CBMC) method was used for the insertion MC move. Diffusion behaviour was studied using Molecular Dynamics (MD) simulations at several temperatures (300, 400, 500, 600, and 800 K) and fitting the self-diffusion values at infinite dilution conditions using the following Arrhenius function: $\log(D/D_0) = \varepsilon/k_B T$, where ε is the activation energy (in eV), D_0 is a pre-exponential factor (the self-diffusion coefficient at infinite temperature), k_B is the Boltzmann constant and T is temperature. ε and D_0 are fitted using a linear regression. Ten simulations for each temperature (using different random seeds) were used to estimate the average value of the self-diffusion coefficient at this temperature.

Chapter III

[194] Dubbeldam, D.; Torres-Knoop, A.; Walton, K. S. *Mol. Simul.* **2013**, *39*, 1253-1292.

[195] Mayo, S. L.; Olafson, B. D.; Goddard, W. A. *J. Phys. Chem.* **1990**, *94*, 8897-8909.

[196] Rappe, A. K.; Casewit, C. J.; Colwell, K. S.; Goddard, W. A.; Skiff, W. M. *J. Am. Chem. Soc.* **1992**, *114*, 10024-10035.

[197] (a) Karra, J. R.; Walton, K. S. *Langmuir* **2008**, *24*, 8620-8626. (b) Yazaydın, A. Ö.; Benin, A. I.; Faheem, S. A.; Jakubczak, P.; Low, J. J.; Willis, R. R.; Snurr, R. Q. *Chem. Mater.* **2009**, *21*, 1425-1430. (c) Bae, Y.; Lee, C. Y.; Kim, K. C.; Farha, O. K.; Nickias, P.; Hupp, J. T.; Nguyen, S. T.; Snurr, R. Q. *Angew. Chem. Int. Ed.* **2012**, *51*, 1857-1860. (d) Greathouse, J. A.; Allendorf, M. D. *J. Am. Chem. Soc.* **2006**, *128*, 10678-10679. (e) Vicent-Luna, J. M.; Gutiérrez-Sevillano, J. J.; Hamad, S.; Anta, J.; Calero, S. *ACS Appl. Mater. Interfaces* **2018**, *10*, 29694-29704. (f) Calero, S.; Gómez-Álvarez, P. *J. Phys. Chem. C* **2015**, *119*, 23774-23780.

Chromatographic Separation of Enantiomers Using TAMOF-1 as Chiral Stationary Phase

3.5.8. Chromatograms (Columns A and B)
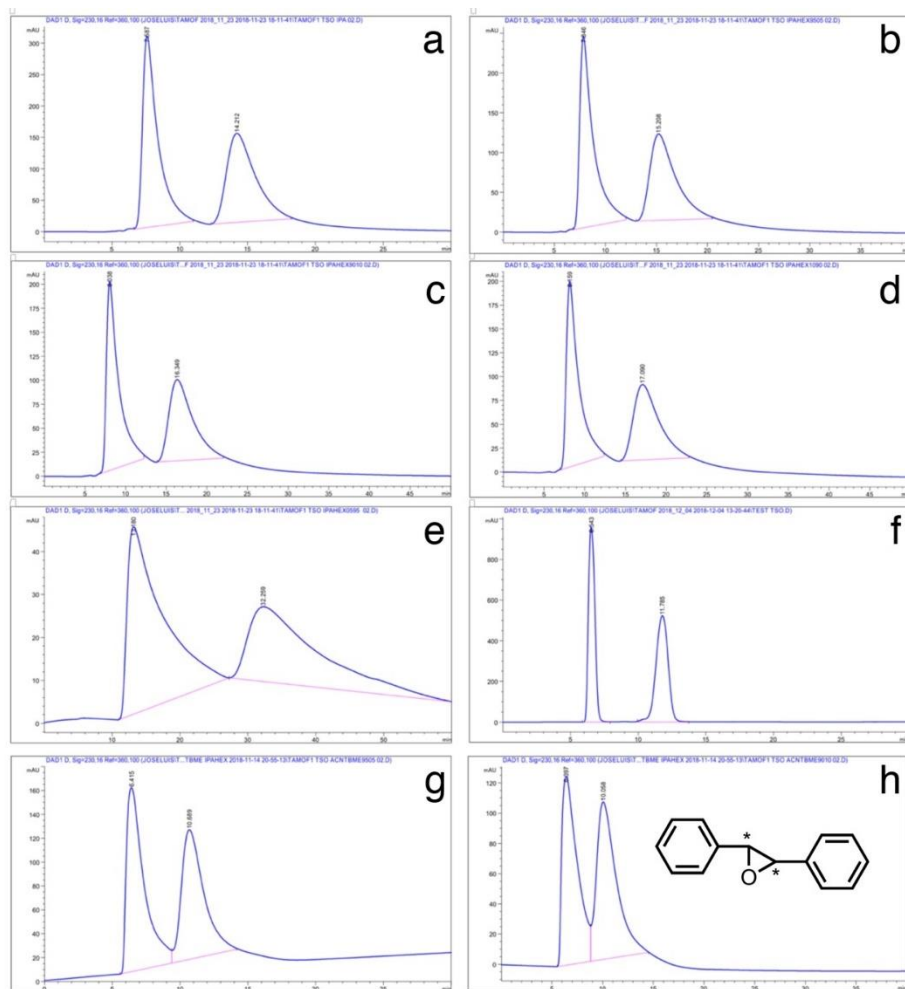
Figure 153. Chromatographic separations of *trans*-2,3-diphenyloxirane using column **B**. A number of mixtures of *n*-Hex/IPA and ACN/TBME were applied as eluting systems: (a) IPA, 0.2 mL min^{-1} flow rate; (b) *n*-Hex/IPA 5:95, 0.2 mL min^{-1}; (c) *n*-Hex/IPA 1:9, 0.2 mL min^{-1}; (d) *n*-Hex/IPA 9:1, 0.2 mL min^{-1}; (e) *n*-Hex/IPA 95:5, 0.2 mL min^{-1}; (f) ACN, 0.2 mL min^{-1}; (g) ACN/TBME 95:5, 0.2 mL min^{-1}; (h) ACN/TBME 9:1, 0.2 mL min^{-1}. A resolution (R_S) > 1.2 was achieved in all cases.[103]
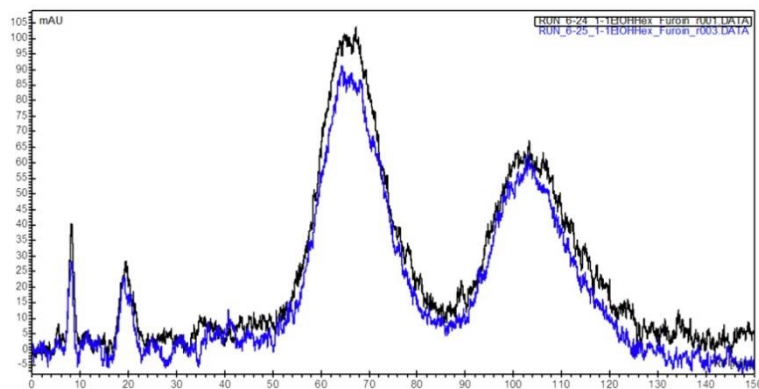
Figure 154. Chromatographic separation of furoin using column **A**. Conditions: n-Hex/EtOH 1:1, 0.15 mL min^{-1}.[103]

Chapter III
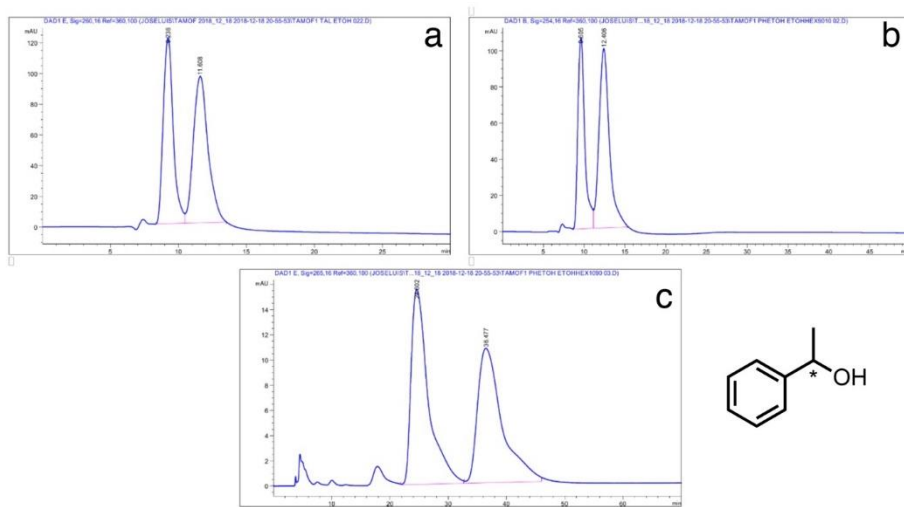
Figure 155. Chromatographic separations of 1-phenylethan-1-ol using column **B**. A number of mixtures of n-Hex/EtOH were applied as eluting systems: (a) EtOH, 0.2 mL min^{-1}; (b) n-Hex/EtOH 1:9, 0.2 mL min^{-1}; (c) n-Hex/EtOH 9:1, 0.3 mL min^{-1}. A resolution (R_S) > 1.5 was achieved in all the cases.[103]

Chromatographic Separation of Enantiomers Using TAMOF-1 as Chiral Stationary Phase
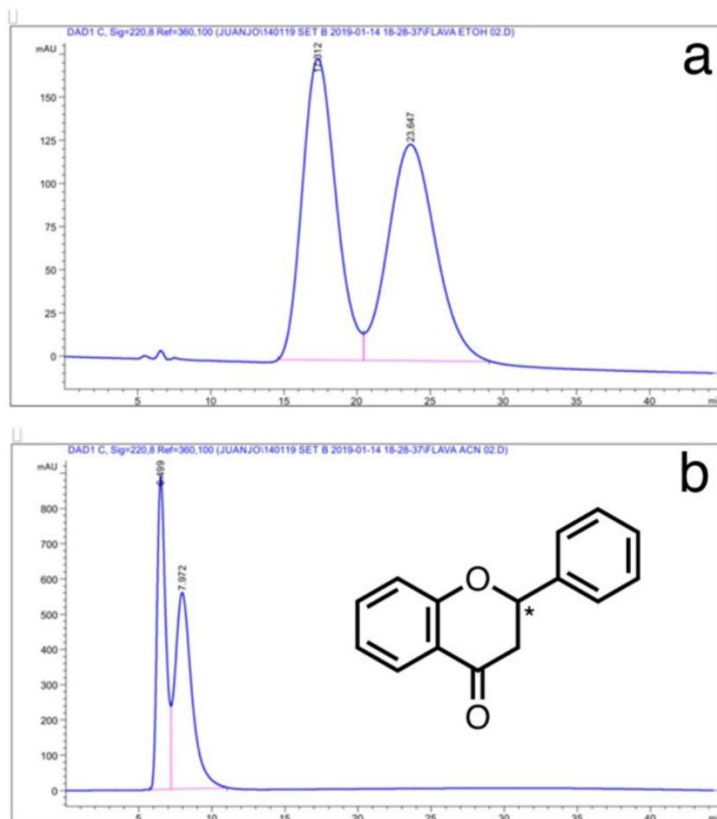
Figure 156. Chromatographic separation of flavanone using column **B**. (a) EtOH and (b) ACN were applied as eluting system, at 0.2 mL min^{-1}. A resolution (R_S) of 1.24 and 0.92 were achieved, respectively.[103]
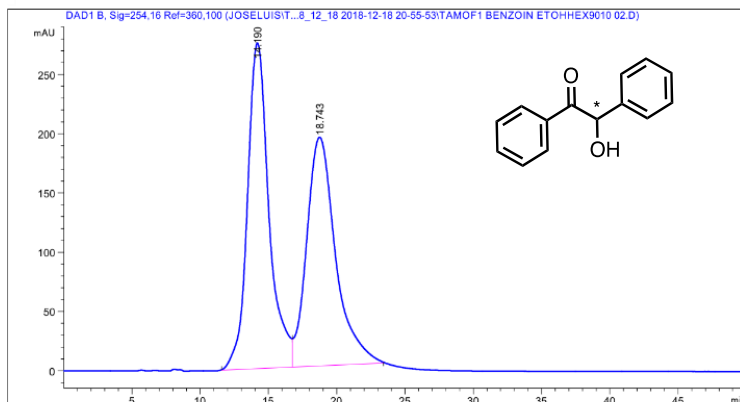
Figure 157. Chromatographic separation of benzoin using column **B**. Conditions: *n*-Hex/EtOH 1:9, 0.2 mL min^{-1}. A resolution (R_S) = 1.4 was achieved.[103]

184

3.5.9. Chromatograms (Column C)

Signal 1: DAD1 A, Sig=205,4 Ref=360,100

RetTime [min]	k'	Area [mAU*s]	Height [mAU]	Symm.	Width [min]	Plates	Resolution	Selectivity
18.210	-	1.90652e4	178.10547	0.00	1.4333	894	-	-
22.068	-	2.38357e4	138.45181	0.28	2.3800	476	1.19	1.21
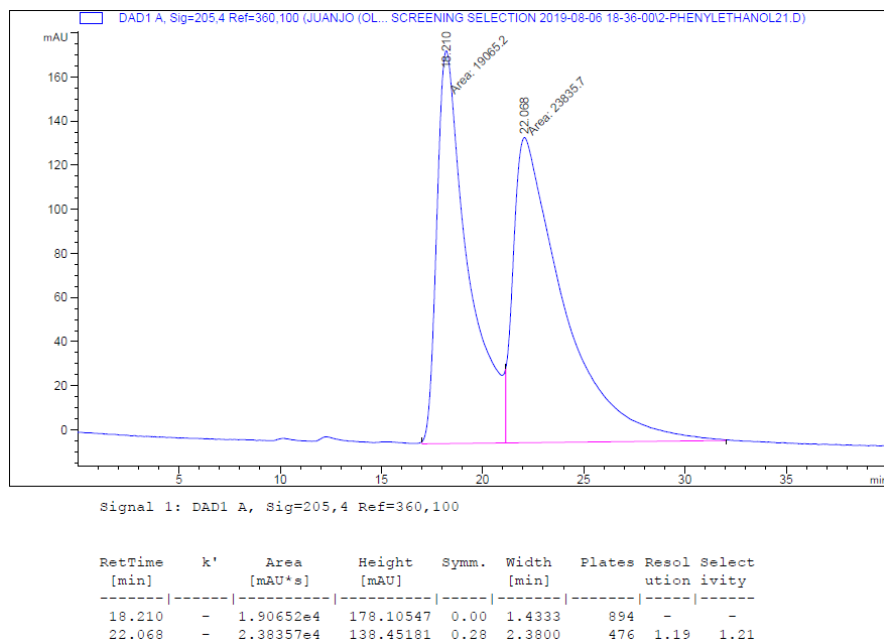
Figure 158. Chromatographic separation and values of 1-phenylethanol (205 nm).

Signal 1: DAD1 B, Sig=254,16 Ref=360,100

RetTime [min]	k'	Area [mAU*s]	Height [mAU]	Symm.	Width [min]	Plates	Resolution	Selectivity
24.936	-	7756.17480	38.51694	0.00	3.0200	378	-	-
31.944	-	8941.78906	30.31904	0.64	4.2000	320	1.14	1.28
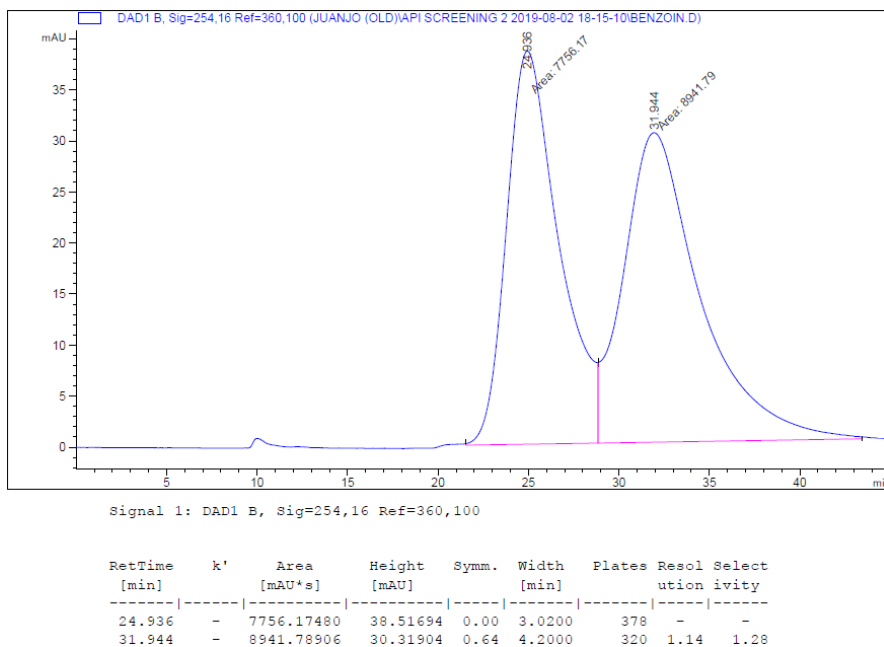
Figure 159. Chromatographic separation and values of benzoin (254 nm).

Chromatographic Separation of Enantiomers Using TAMOF-1 as Chiral Stationary Phase

Signal 1: DAD1 B, Sig=254,16 Ref=360,100

RetTime [min]	k'	Area [mAU*s]	Height [mAU]	Symm.	Width [min]	Plates	Resolution	Selectivity
33.633	-	4.06334e4	114.70412	0.69	5.4133	214	-	-
46.644	-	4.24510e4	86.43459	0.75	7.4533	217	1.19	1.39
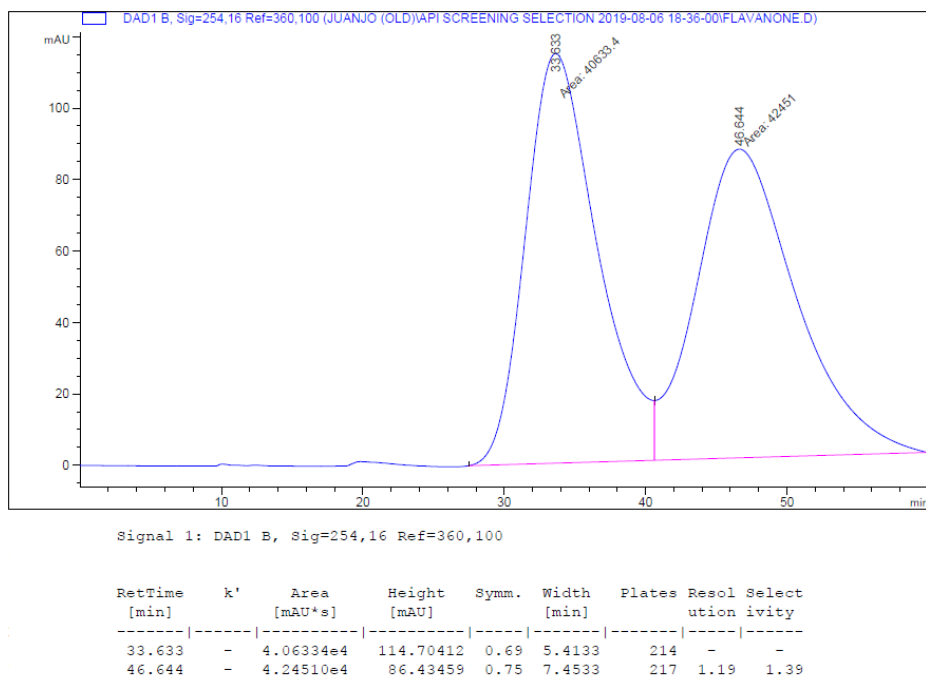
Figure 160. Chromatographic separation and values of flavanone (254 nm).

Signal 1: DAD1 C, Sig=220,8 Ref=360,100

RetTime [min]	k'	Area [mAU*s]	Height [mAU]	Symm.	Width [min]	Plates	Resolution	Selectivity
28.359	-	1.25396e4	49.60214	0.00	3.9200	290	-	-
36.660	-	1.28688e4	42.81173	0.75	4.5467	360	1.15	1.29
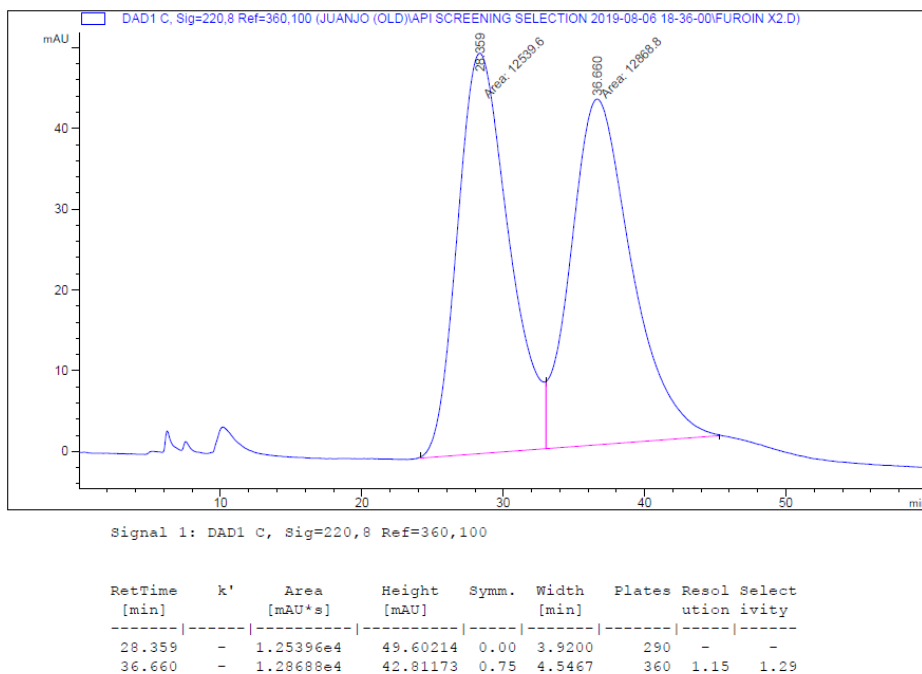
Figure 161. Chromatographic separation and values of furoin (254 nm).

186

Signal 1: DAD1 A, Sig=205,4 Ref=360,100

RetTime [min]	k'	Area [mAU*s]	Height [mAU]	Symm.	Width [min]	Plates	Resolution	Selectivity
14.439	-	2750.88794	18.37147	0.00	2.6533	164	-	-
17.139	-	2758.38379	18.16636	0.61	2.4122	280	0.63	1.19
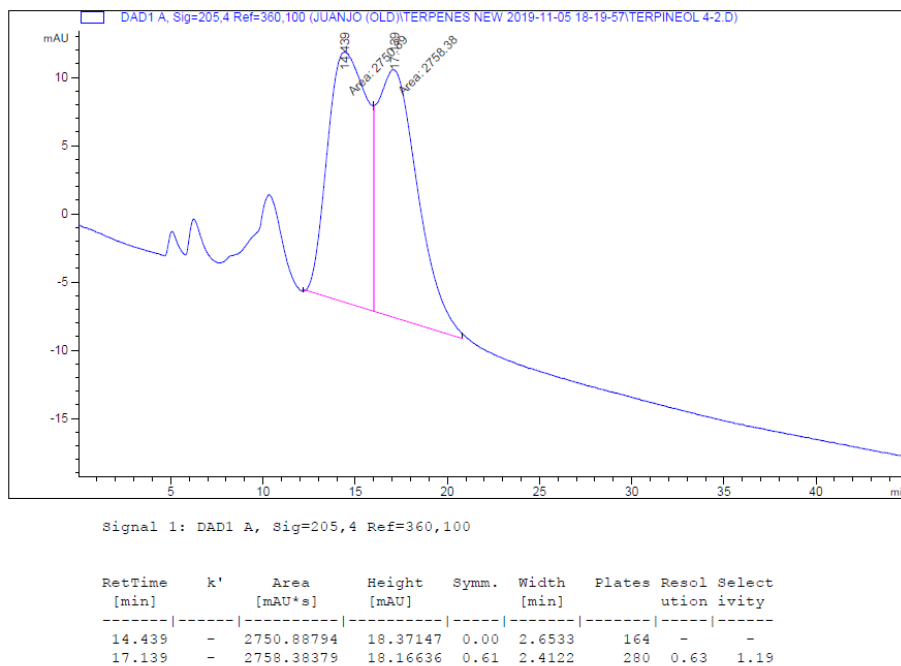
Figure 162. Chromatographic separation and values of α-terpineol (205 nm).

Signal 1: DAD1 D, Sig=230,16 Ref=360,100

RetTime [min]	k'	Area [mAU*s]	Height [mAU]	Symm.	Width [min]	Plates	Resolution	Selectivity
44.024	8.17	2979.34497	5.56479	0.79	8.2867	157	-	-
84.344	16.57	3078.78149	2.89632	0.72	16.7133	141	1.90	2.03
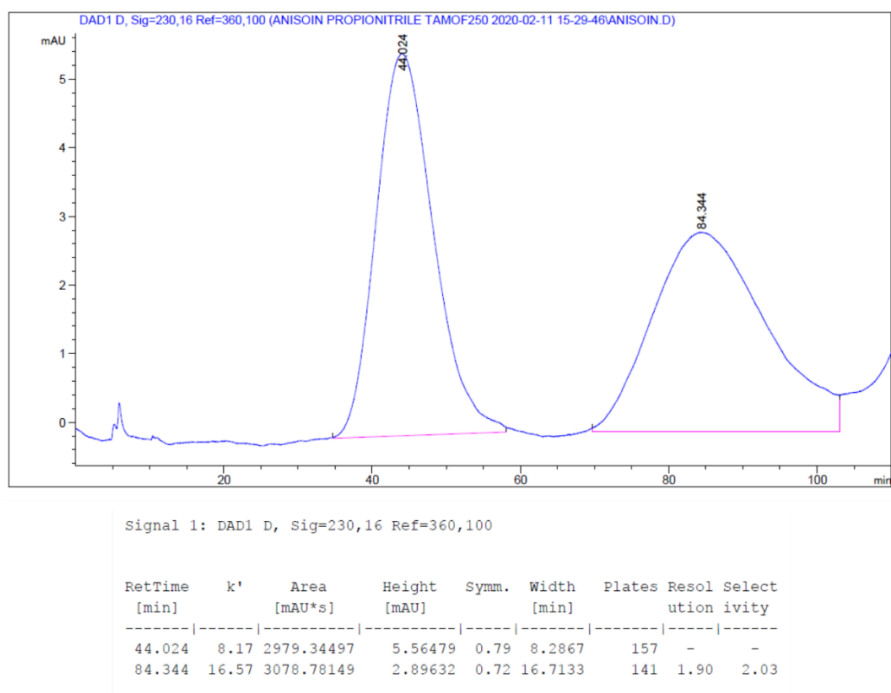
Figure 163. Chromatographic separation and values of anisoin (230 nm).

Chapter III

187

Chromatographic Separation of Enantiomers Using TAMOF-1 as Chiral Stationary Phase

Signal 1: DAD1 B, Sig=205,16 Ref=360,100

RetTime [min]	k'	Area [mAU*s]	Height [mAU]	Symm.	Width [min]	Plates	Resolution	Selectivity
19.907	3.15	2199.89722	12.12517	0.00	2.8133	278	-	-
26.301	4.48	2389.58765	9.64795	0.66	3.8133	264	1.13	1.42
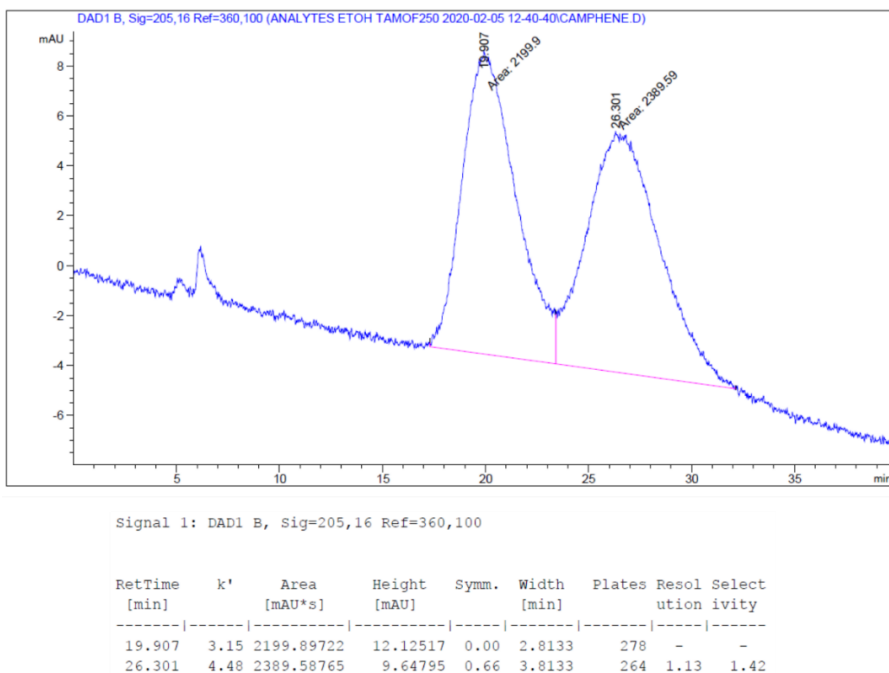
Figure 164. Chromatographic separation and values of camphene (205 nm).

Signal 1: DAD1 D, Sig=230,16 Ref=360,100

RetTime [min]	k'	Area [mAU*s]	Height [mAU]	Symm.	Width [min]	Plates	Resolution	Selectivity
25.963	-	1.05195e4	66.07133	0.60	2.3000	706	-	-
33.995	-	9749.58984	47.25256	0.56	2.8933	765	1.82	1.31
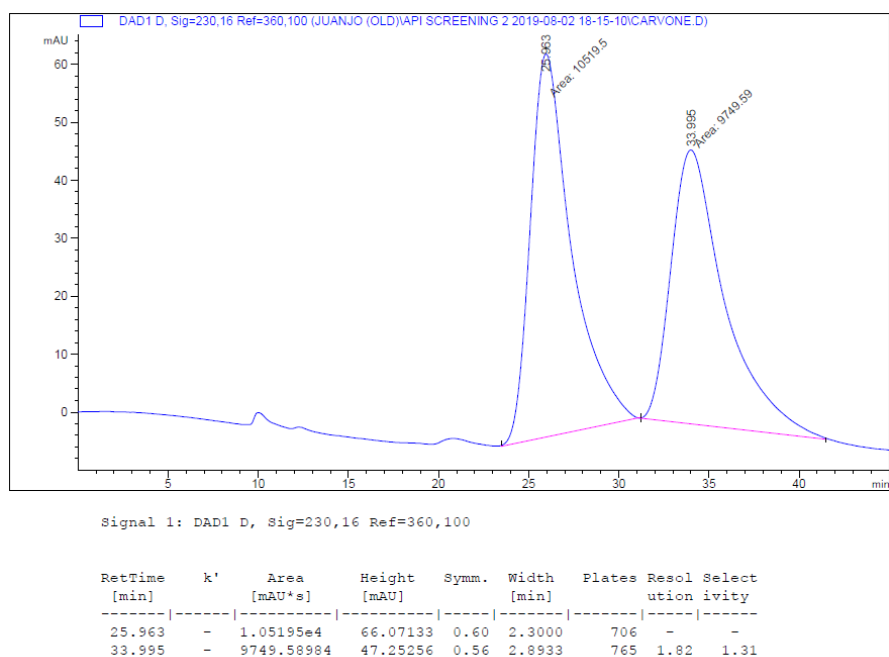
Figure 165. Chromatographic separation and values of carvone (230 nm).

188
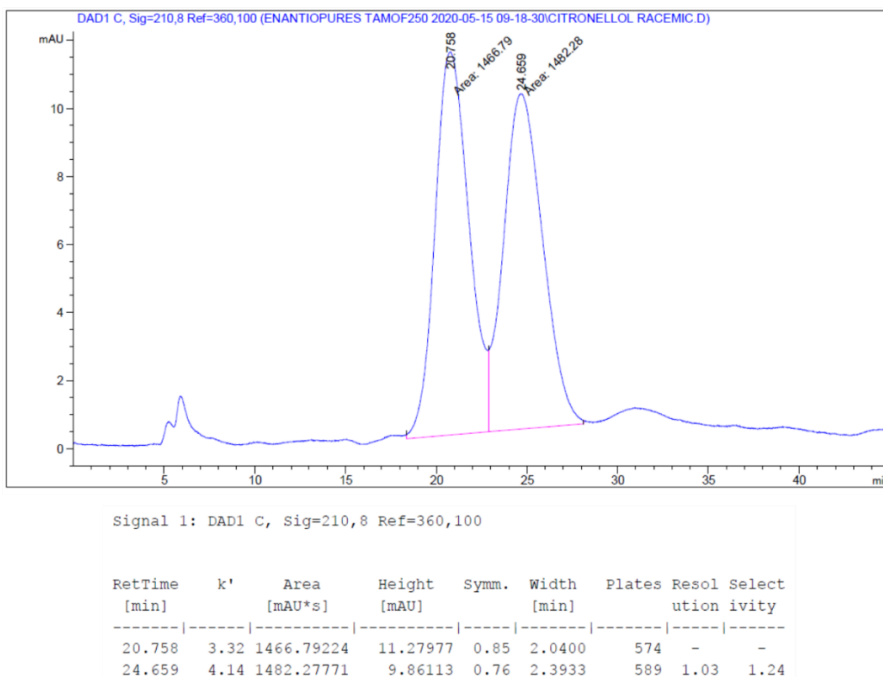
Figure 166. Chromatographic separation and values of β-citronellol (210 nm).
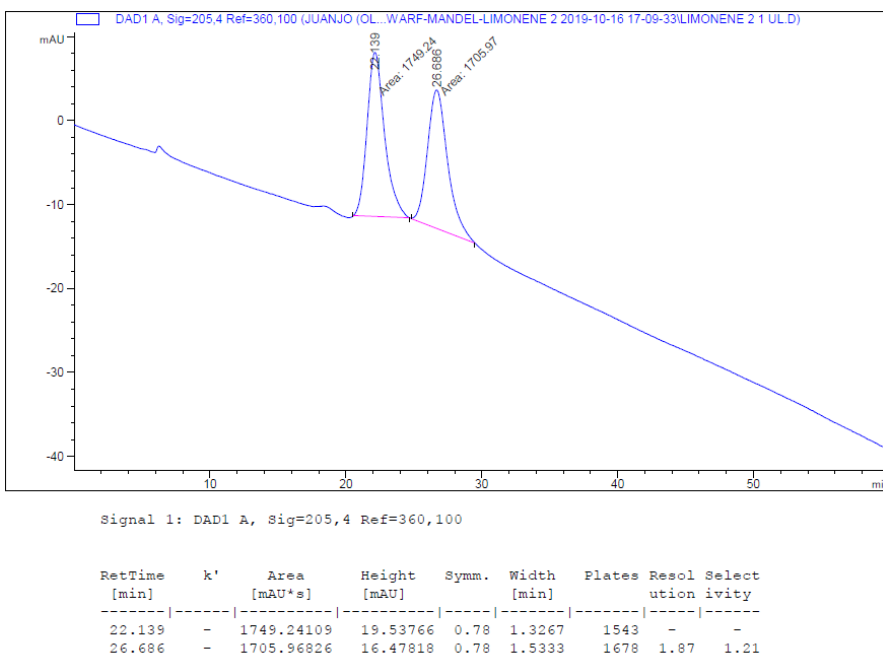
Figure 167. Chromatographic separation and values of limonene (205 nm).

189

Chromatographic Separation of Enantiomers Using TAMOF-1 as Chiral Stationary Phase

Signal 1: DAD1 C, Sig=220,8 Ref=360,100

RetTime [min]	k'	Area [mAU*s]	Height [mAU]	Symm.	Width [min]	Plates	Resolution	Selectivity
29.151	-	5638.69189	31.70293	0.70	2.8000	600	-	-
35.628	-	7998.66895	27.85743	0.77	4.2867	383	1.07	1.22
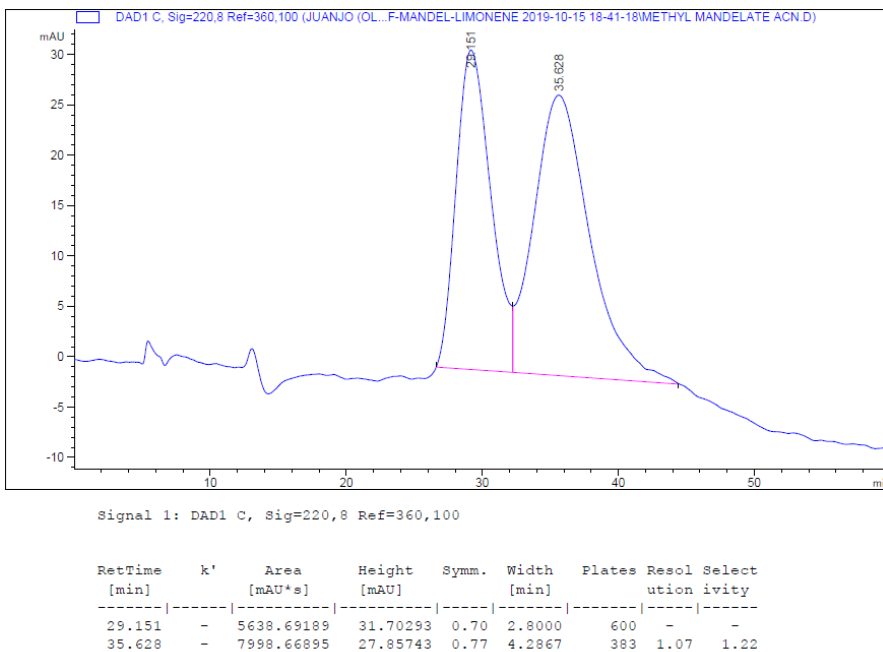
Figure 168. Chromatographic separation and values of methyl mandelate (220 nm).

Signal 1: DAD1 B, Sig=254,16 Ref=360,100

RetTime [min]	k'	Area [mAU*s]	Height [mAU]	Symm.	Width [min]	Plates	Resolution	Selectivity
10.014	-	9963.67480	191.63254	0.38	0.8733	728	-	-
11.129	-	5161.86377	75.91369	0.15	0.9732	724	0.71	1.11
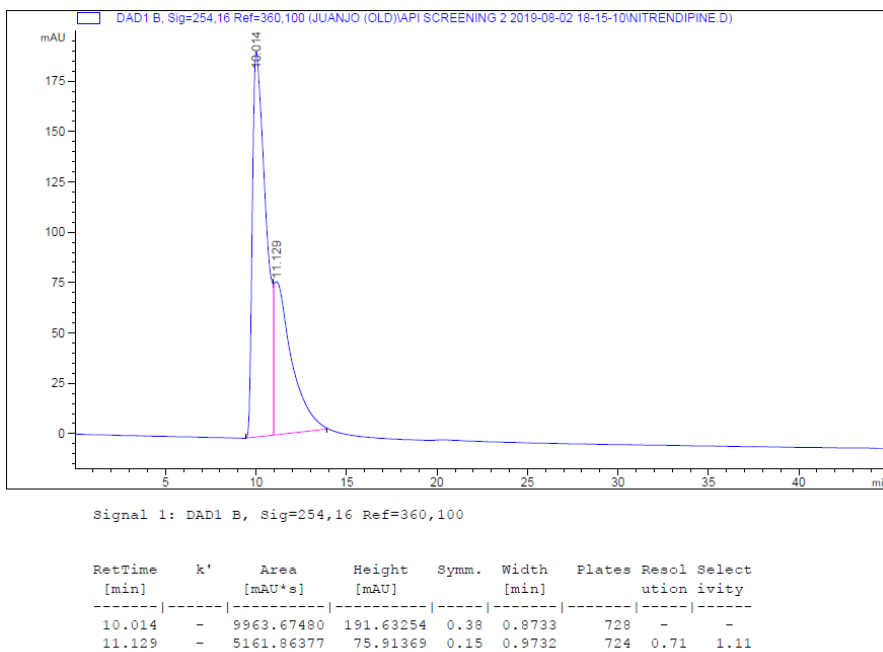
Figure 169. Chromatographic separation and values of nitrendipine (254 nm).

190

Signal 1: DAD1 B, Sig=210,8 Ref=360,100

RetTime [min]	k'	Area [mAU*s]	Height [mAU]	Symm.	Width [min]	Plates	Resolution	Selectivity
30.867	-	1635.46143	17.27071	0.76	1.4533	2499	-	-
34.182	-	1744.78284	16.36022	0.83	1.6133	2487	1.27	1.11
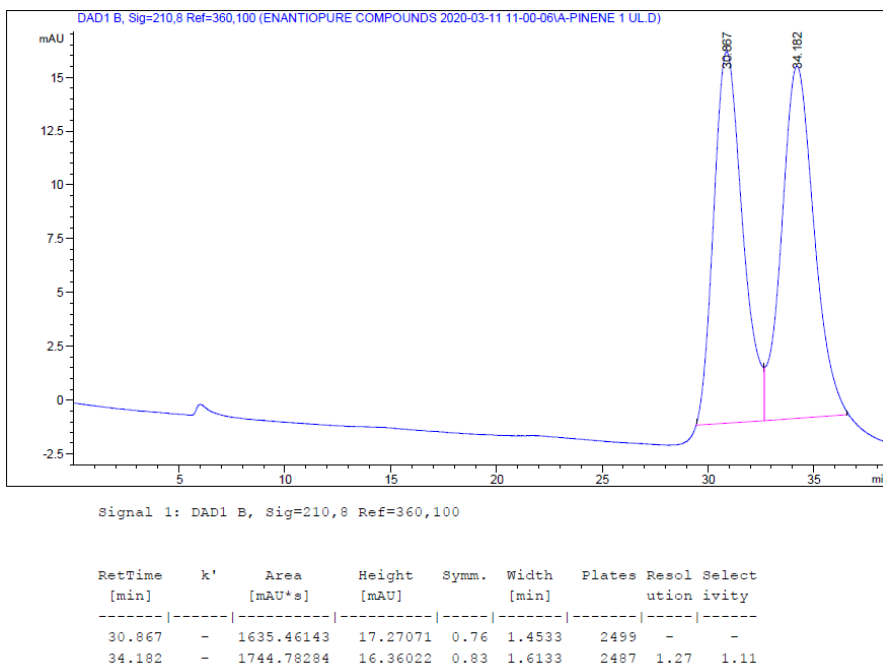
Figure 170. Chromatographic separation and values of α-pinene (210 nm).

Signal 1: DAD1 C, Sig=220,8 Ref=360,100

RetTime [min]	k'	Area [mAU*s]	Height [mAU]	Symm.	Width [min]	Plates	Resolution	Selectivity
16.018	-	1.27247e4	50.72593	0.80	3.2933	131	-	-
32.832	-	1.22327e4	17.41909	0.74	10.4000	55	1.44	2.05
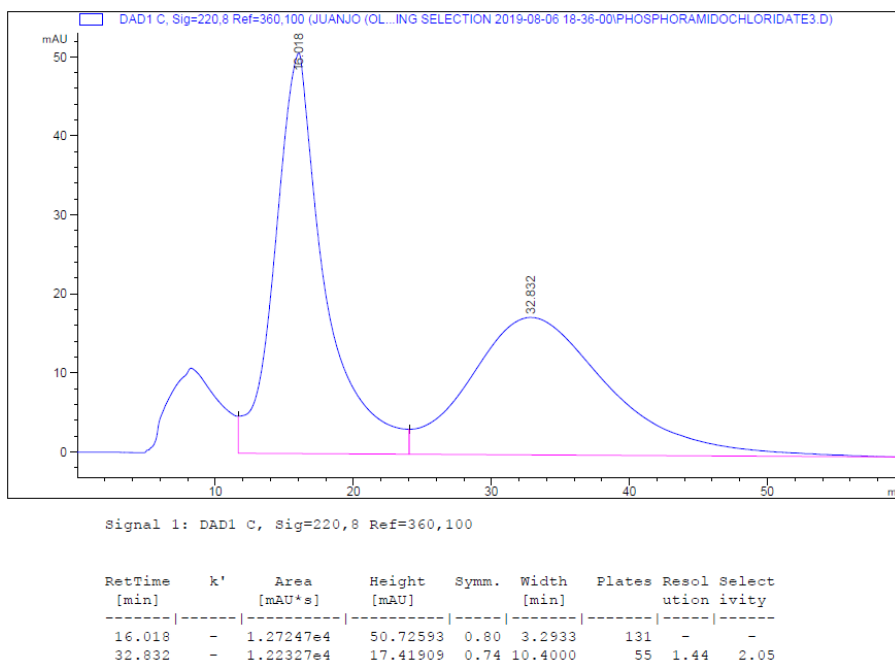
Figure 171. Chromatographic separation and values of PNPPCl (220 nm).

191

Chromatographic Separation of Enantiomers Using TAMOF-1 as Chiral Stationary Phase

Signal 1: DAD1 A, Sig=205,4 Ref=360,100

RetTime [min]	k'	Area [mAU*s]	Height [mAU]	Symm.	Width [min]	Plates	Resolution	Selectivity
14.828	-	3663.07593	37.57969	0.97	1.7352	404	-	-
16.941	-	1.01721e4	52.62583	0.35	2.3581	285	0.61	1.14
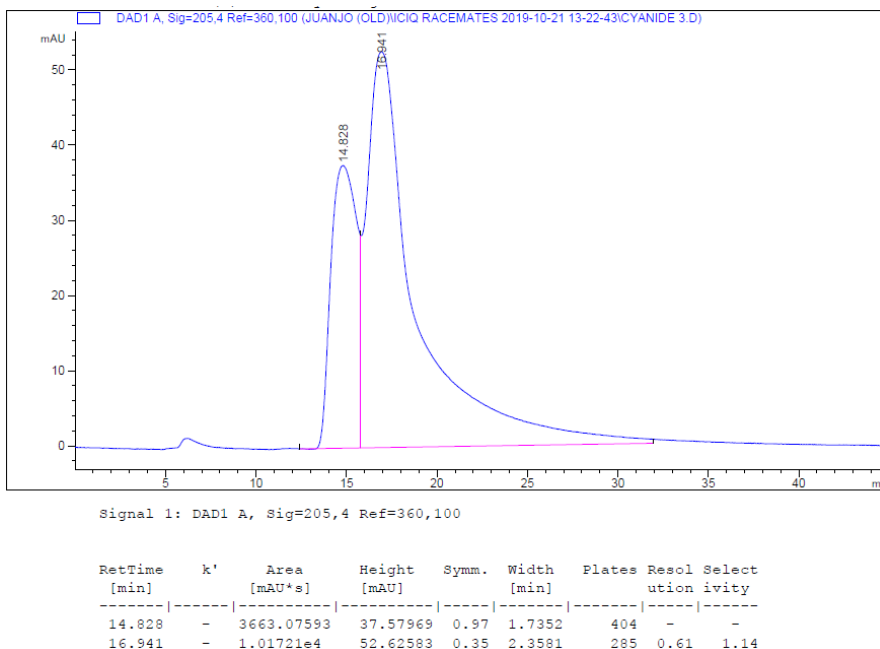
Figure 172. Chromatographic separation and values of 2-phenylpropionitrile (205 nm).

Signal 1: DAD1 D, Sig=230,16 Ref=360,100

RetTime [min]	k'	Area [mAU*s]	Height [mAU]	Symm.	Width [min]	Plates	Resolution	Selectivity
6.175	0.29	8997.31445	161.05141	0.38	0.7776	349	-	-
13.287	1.77	9125.34277	84.12326	0.71	1.6933	341	3.38	6.17
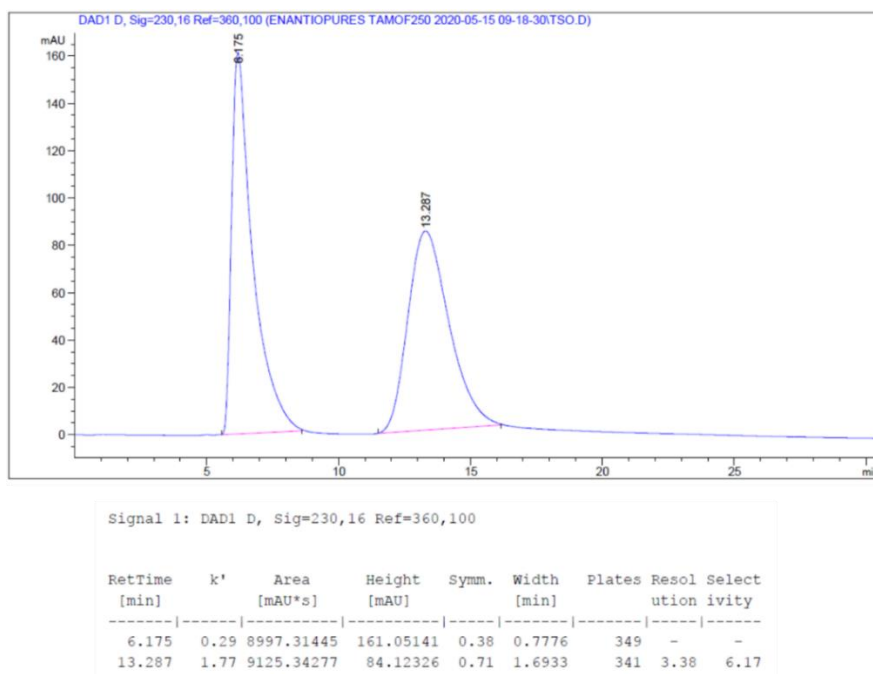
Figure 173. Chromatographic separation and values of TSO (230 nm).

192

3.5.10. Chromatograms (Column D)

Signal 1: DAD1 D, Sig=254,4 Ref=360,100

RetTime [min]	k'	Area [mAU*s]	Height [mAU]	Symm.	Width [min]	Plates	Resolution	Selectivity
4.160	1.5e-2	9351.96191	94.88011	0.25	1.1733	69	–	–
9.745	1.38	8788.58301	41.34501	0.92	3.7733	37	1.33	94.06
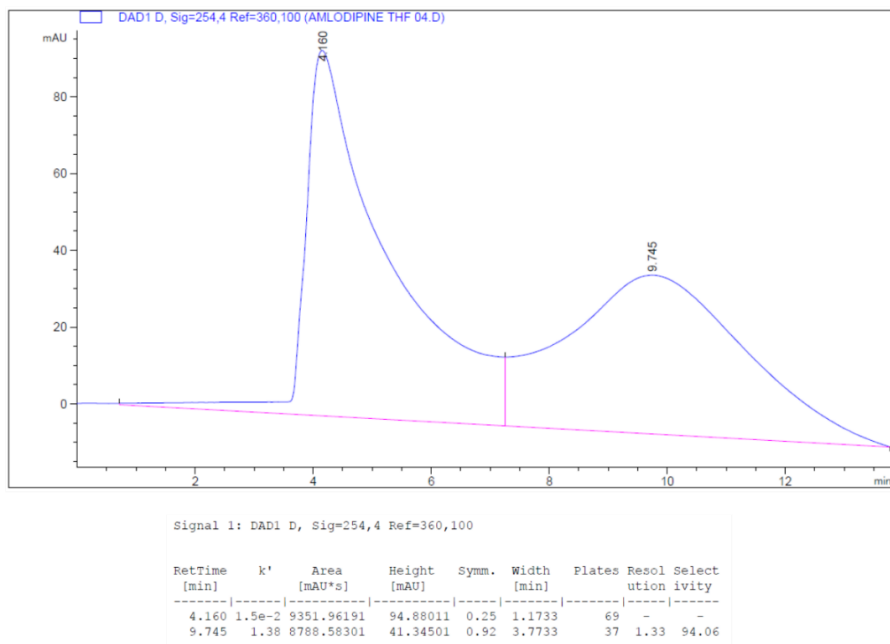
Figure 174. Chromatographic separation and values of amlodipine (254 nm).

Signal 1: DAD1 C, Sig=210,8 Ref=360,100

RetTime [min]	k'	Area [mAU*s]	Height [mAU]	Symm.	Width [min]	Plates	Resolution	Selectivity
36.537	7.91	7968.62939	15.14713	0.00	8.2933	108	–	–
53.227	11.98	7980.98828	11.02433	0.86	11.6467	116	0.98	1.51
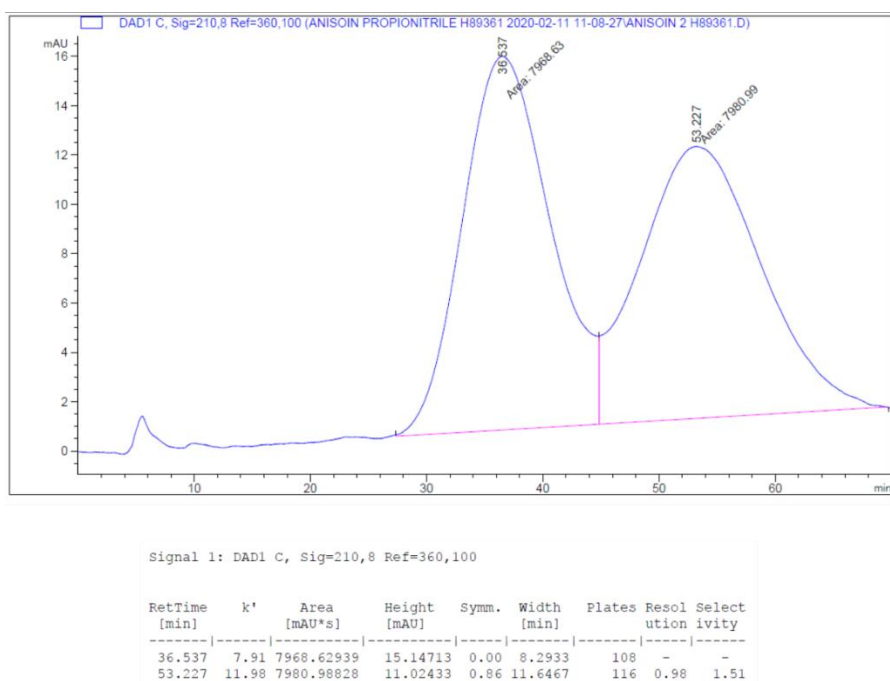
Figure 175. Chromatographic separation and values of anisoin (210 nm).

Chromatographic Separation of Enantiomers Using TAMOF-1 as Chiral Stationary Phase

Signal 1: DAD1 B, Sig=205,16 Ref=360,100

RetTime [min]	k'	Area [mAU*s]	Height [mAU]	Symm.	Width [min]	Plates	Resolution	Selectivity
30.916	2.77	5982.67676	23.11927	0.68	4.1467	308	–	–
38.978	3.75	5736.24658	18.94089	0.94	4.8933	352	1.05	1.35
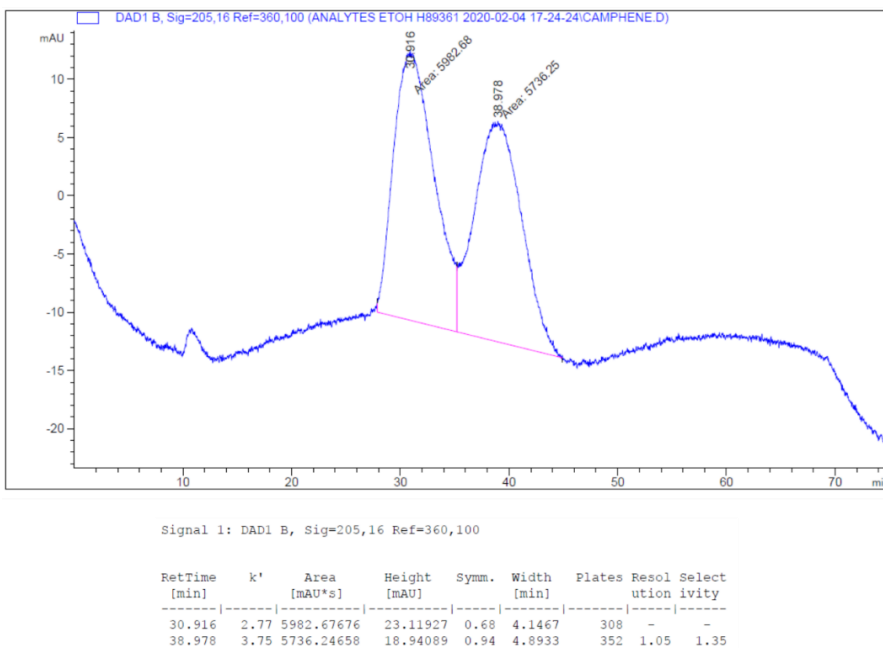
Figure 176. Chromatographic separation and values of camphene (205 nm).

Signal 1: DAD1 D, Sig=230,16 Ref=360,100

RetTime [min]	k'	Area [mAU*s]	Height [mAU]	Symm.	Width [min]	Plates	Resolution	Selectivity
17.129	1.09	8765.98340	68.72997	0.74	2.1400	355	–	–
20.814	1.54	9525.56152	57.67516	0.79	2.6600	339	0.90	1.41
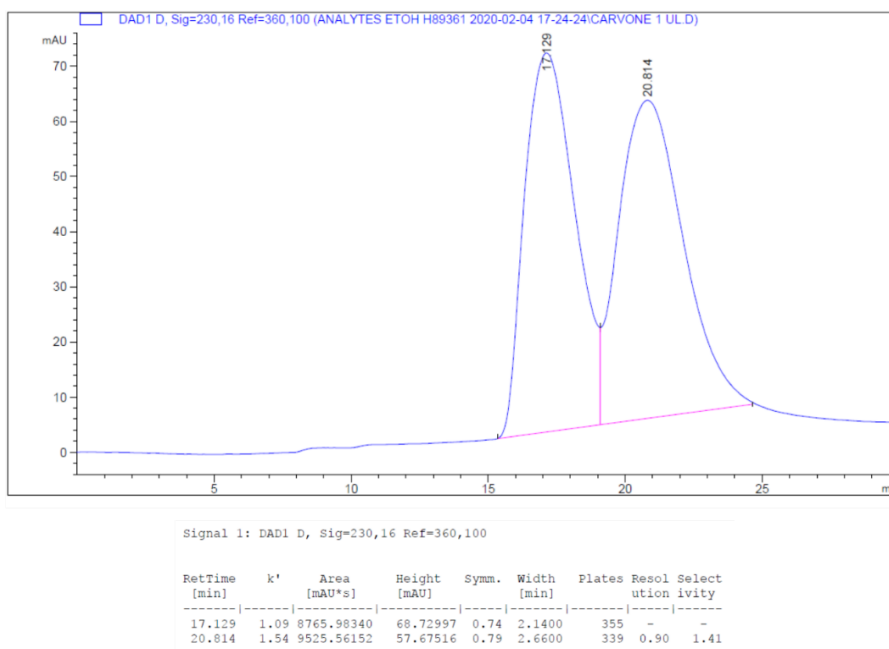
Figure 177. Chromatographic separation and values of carvone (230 nm).

194

Signal 1: DAD1 B, Sig=205,16 Ref=360,100

RetTime [min]	k'	Area [mAU*s]	Height [mAU]	Symm.	Width [min]	Plates	Resolution	Selectivity
13.964	2.41	862.30109	10.59229	0.00	1.4611	506	-	-
15.523	2.79	1260.69897	11.57244	0.41	1.8922	373	0.55	1.16
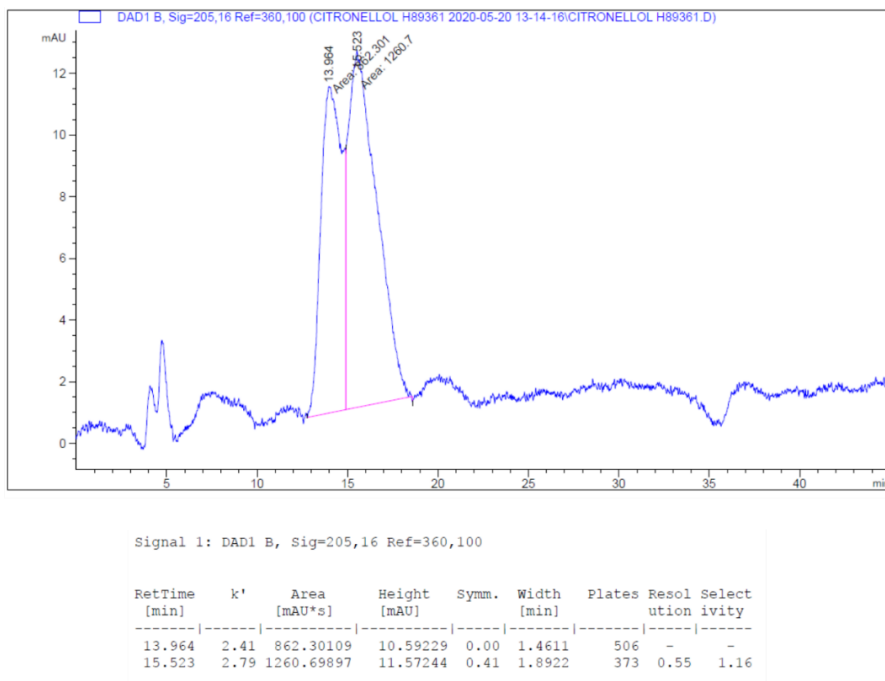
Figure 178. Chromatographic separation and values of β-citronellol (205 nm).

Signal 1: VWD1 A, Wavelength=205 nm

RetTime [min]	k'	Area mAU *s	Height [mAU]	Symm.	Width [min]	Plates	Resolution	Selectivity
17.749	-	1.63203e4	197.83546	0.48	1.2376	1139	-	-
23.983	-	1.60050e4	158.09467	0.56	1.5676	1297	2.61	1.35
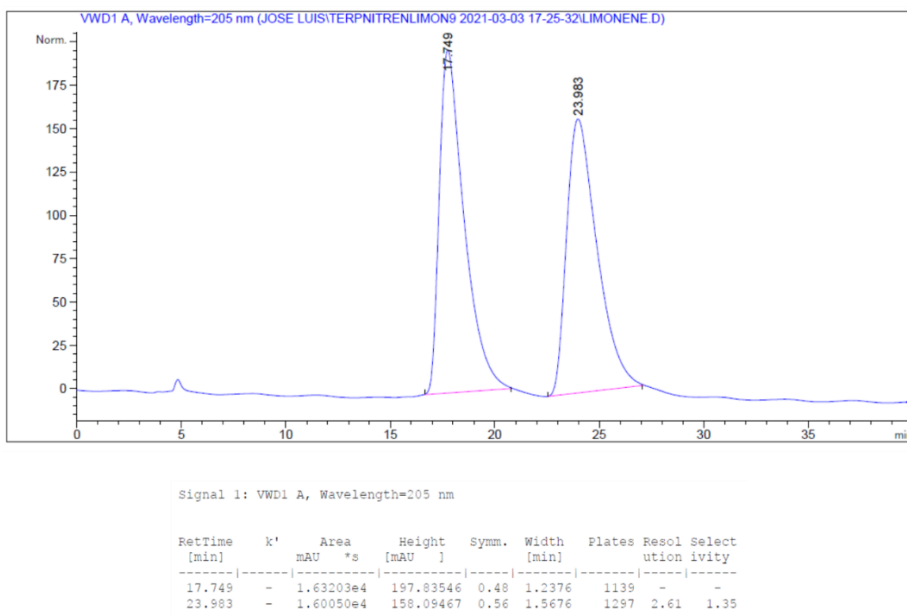
Figure 179. Chromatographic separation and values of limonene (205 nm).

195

Chromatographic Separation of Enantiomers Using TAMOF-1 as Chiral Stationary Phase

Signal 1: DAD1 B, Sig=205,16 Ref=360,100

RetTime [min]	k'	Area [mAU*s]	Height [mAU]	Symm.	Width [min]	Plates	Resolution	Selectivity
31.040	5.47	3312.37476	14.83394	0.60	3.6000	412	-	-
38.464	7.01	3793.39355	12.03454	0.72	4.9867	329	1.02	1.28
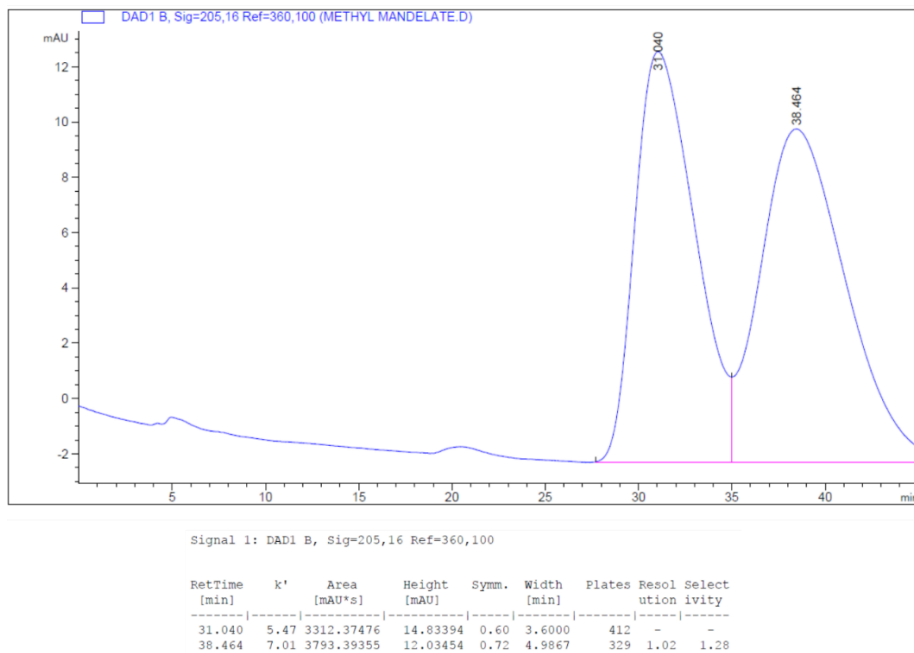
Figure 180. Chromatographic separation and values of methyl mandelate (205 nm).

Signal 1: DAD1 C, Sig=230,8 Ref=360,100

RetTime [min]	k'	Area [mAU*s]	Height [mAU]	Symm.	Width [min]	Plates	Resolution	Selectivity
1.760	7.3e-2	2237.89795	98.19496	0.16	0.4111	101	-	-
2.501	0.53	4112.11768	52.71293	0.18	1.0045	34	0.61	7.17
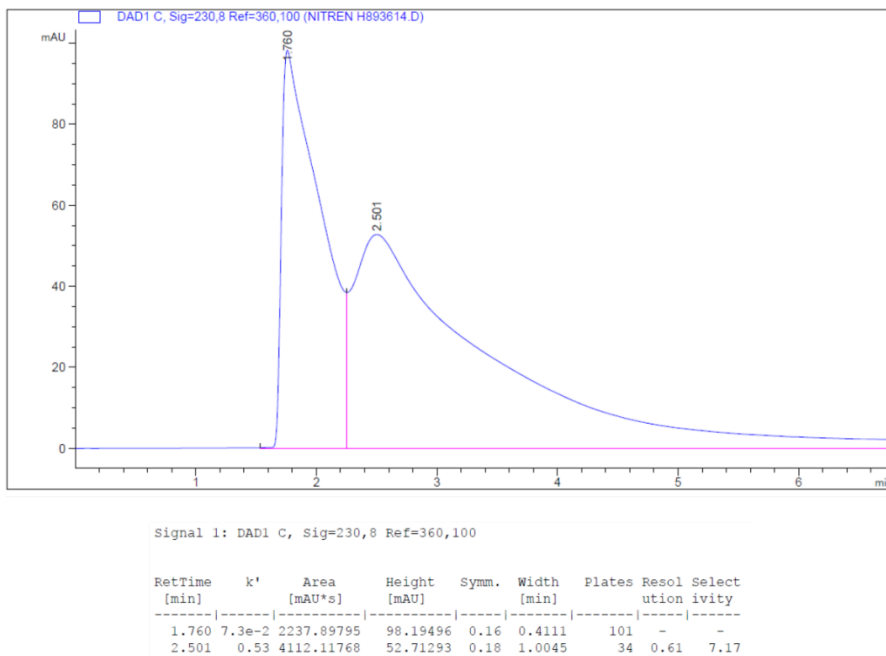
Figure 181. Chromatographic separation and values of nitrendipine (230 nm).

196

Signal 1: DAD1 C, Sig=210,8 Ref=360,100

RetTime [min]	k'	Area [mAU*s]	Height [mAU]	Symm.	Width [min]	Plates	Resolution	Selectivity
16.745	3.08	2002.79004	21.53926	0.77	1.5200	672	-	-
19.397	3.73	1642.37280	19.29841	1.65	1.4400	1006	1.05	1.21
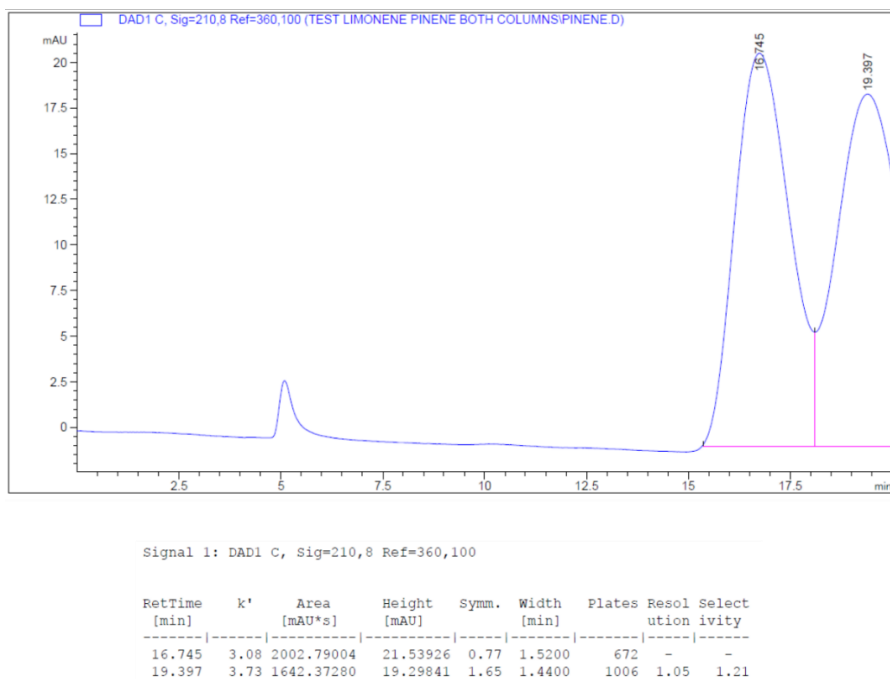
Figure 182. Chromatographic separation and values of α-pinene (210 nm).

Signal 1: DAD1 A, Sig=205,4 Ref=360,100

RetTime [min]	k'	Area [mAU*s]	Height [mAU]	Symm.	Width [min]	Plates	Resolution	Selectivity
9.378	1.29	2880.15356	63.09251	1.72	0.7764	809	-	-
10.206	1.49	6585.89648	77.95178	0.48	1.4269	283	0.44	1.16
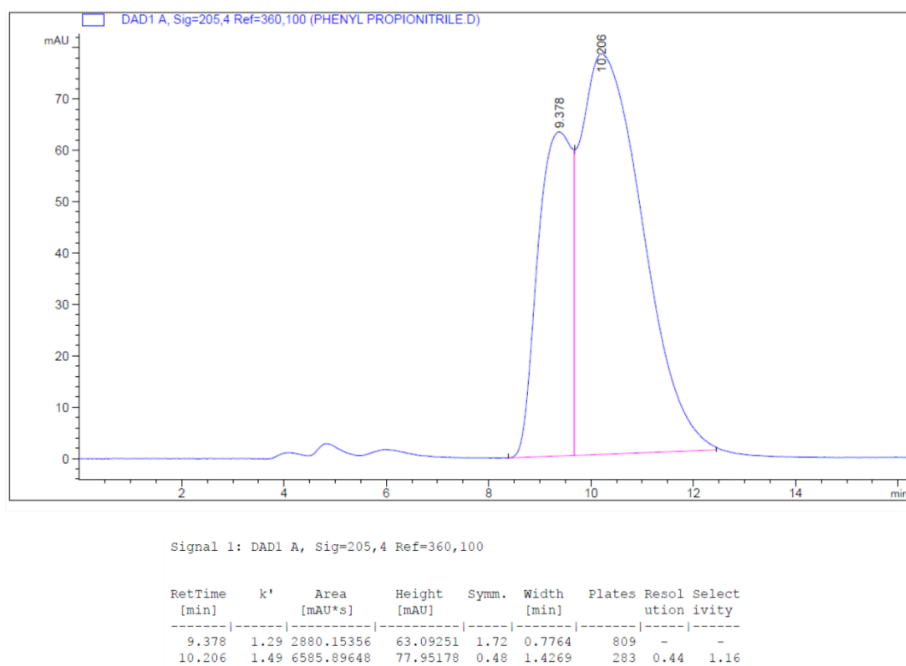
Figure 183. Chromatographic separation and values of 2-phenylpropionitrile (210 nm).

Chapter III

197

Chromatographic Separation of Enantiomers Using TAMOF-1 as Chiral Stationary Phase


```
Signal 1: VWD1 A, Wavelength=205 nm

RetTime   k'      Area       Height    Symm.  Width   Plates Resol Select
 [min]           mAU  *s    [mAU  ]           [min]          ution ivity
-------|------|----------|----------|-----|-------|-------|-----|------
11.299    -    2.32643e4  271.57153  0.94  1.5759   285    -     -
12.916    -    2.51118e4  228.75511  0.48  1.6453   341   0.59  1.14
```
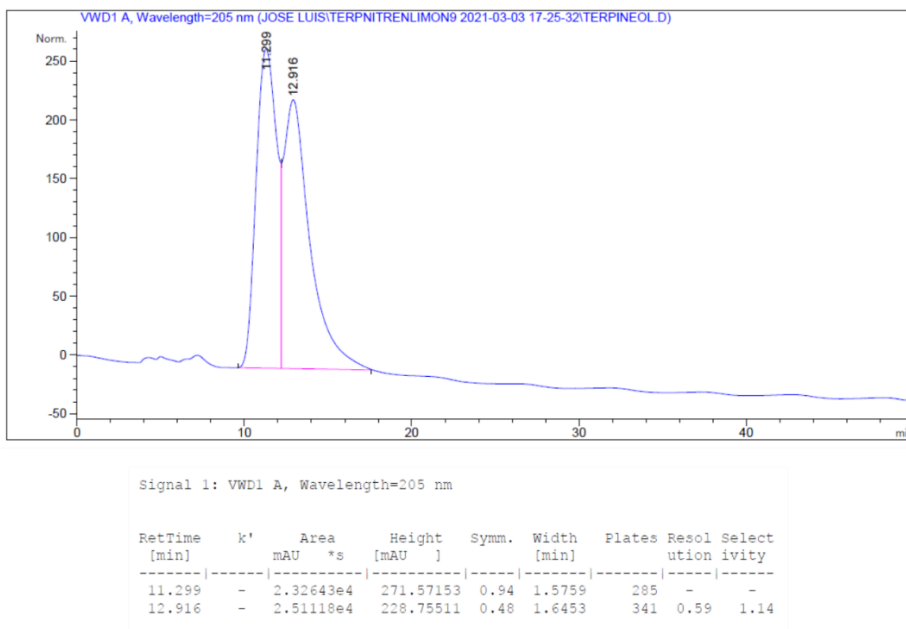
Figure 184. Chromatographic separation and values of α-terpineol (205 nm).


```
Signal 1: DAD1 A, Sig=254,4 Ref=360,100

RetTime   k'     Area      Height    Symm.  Width   Plates Resol Select
 [min]          [mAU*s]    [mAU]            [min]          ution ivity
-------|------|----------|----------|-----|-------|-------|-----|------
 5.264   0.28 1268.96802  40.12624   0.58  0.4833   656    -     -
13.618   2.32 1304.07959  12.99172   0.77  1.6000   401   4.71  8.17
```
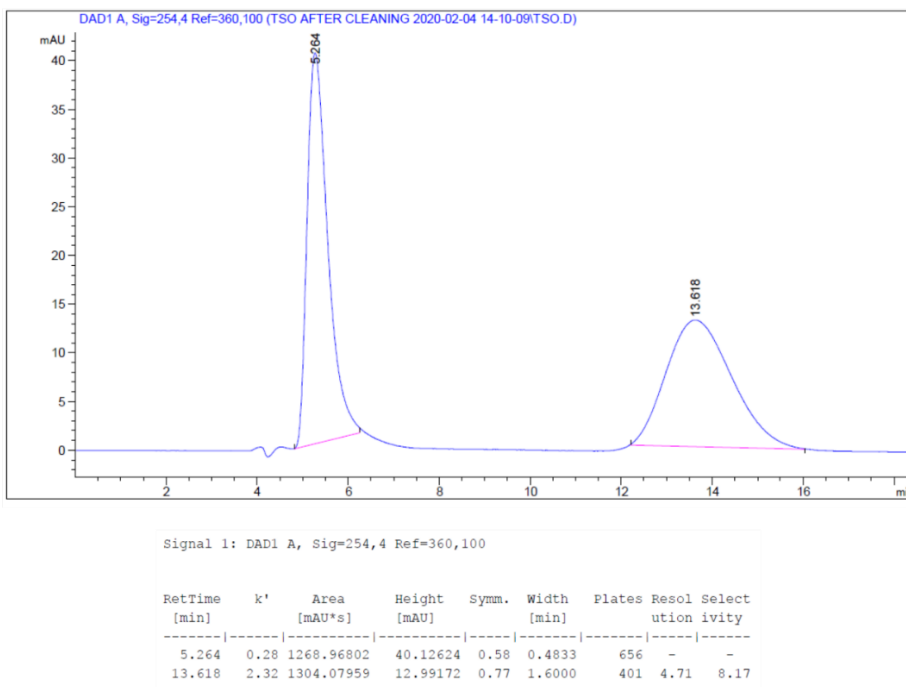
Figure 185. Chromatographic separation and values of TSO (254 nm).

198

3.5.11. Mass spectra analysis
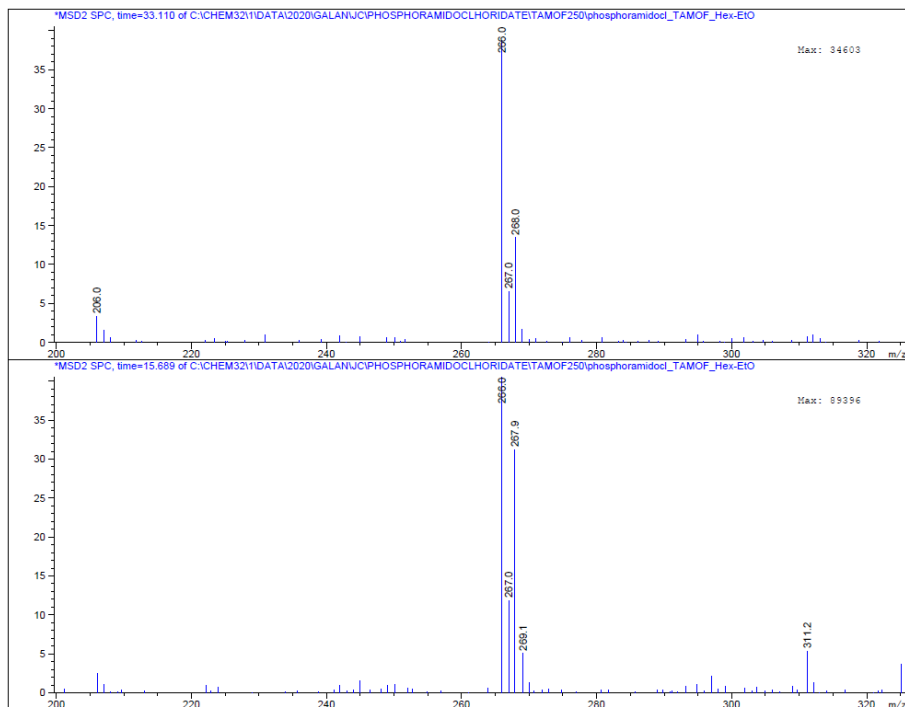
Figure 186. Mass spectra of PNPPCl peaks at t_R = 33.64 min (top) and t_R = 15.92 min (bottom). [M–H]⁻ calcd. for $C_{12}H_{11}ClNO_2P$, 266.02; found 266.0.
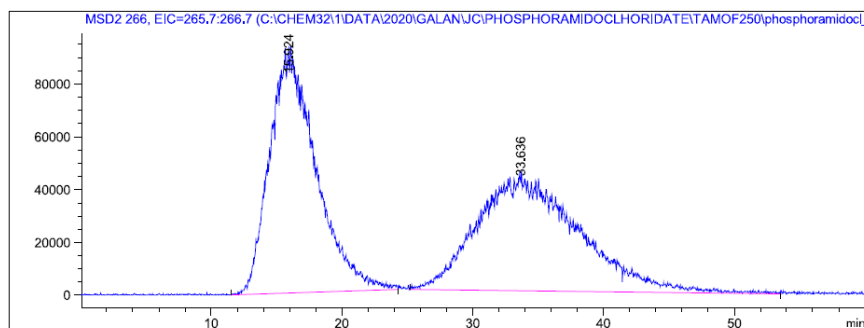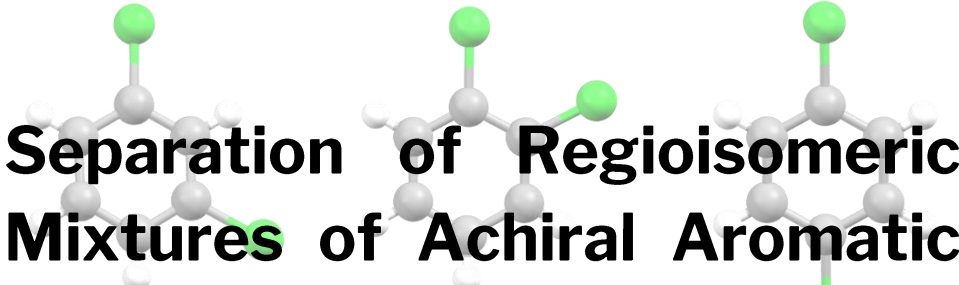

```
Signal 1: MSD2 266, EIC=265.7:266.7

Peak RetTime Type  Width     Area        Height      Area
 #   [min]        [min]                              %
----|-------|----|-------|----------|----------|--------|
  1  15.924 BB    3.9809  2.28144e7  9.00787e4  49.3537
  2  33.636 BBA   6.7503  2.34119e7  4.20617e4  50.6463
```

Figure 187. Integration of the mass spectra of PNPPCl.

Chapter III

Chromatographic Separation of Enantiomers Using TAMOF-1 as Chiral Stationary Phase

CHAPTER IV

Separation of Regioisomeric Mixtures of Achiral Aromatic Compounds Using TAMOF-1 as Stationary Phase

UNIVERSITAT ROVIRA I VIRGILI
INSIGHTS IN HOMOCHIRAL METAL-ORGANIC FRAMEWORKS: FROM THEIR SYNTHESIS TO ENANTIOSELECTIVE
APPLICATIONS
Juanjo Cabezas Giménez

4.1. ABSTRACT

After proving the potential of TAMOF-1 as a CSP, the separation of structurally diverse families of achiral positional isomers of aromatic compounds using TAMOF-1 as stationary phase was achieved in this chapter, either partially or completely.

The separation of the by-products in the industrial production of styrene (benzene, toluene and ethylbenzene) as well as the mixture of cresol regioisomers are separated excellently. The latter has retention times superior to 60 min, an issue that could be overtaken by slightly increasing the polarity of the mobile phase. TAMOF-1 has been demonstrated to be a good CSP and a good stationary phase for the separation of achiral positional isomers of aromatic compounds.

4.2. INTRODUCTION

The development of new purification platforms is a scientific challenge to overcome the current expensive and energy-demanding processes, such as fractional distillation. For instance, the purification of a mixture of xylenes is arduous due to the similar physicochemical properties of the *m-* and *p*-xylene isomers, whose boiling points differ only by 1 °C.[198]

MOFs have already been used in the separation of the components of mixtures of positional isomers in liquid and gas phases. Among these mixtures, the most representative examples are mixtures of hexanes,[199] xylenes,[200] BTEX[201] and dihalobenzenes,[202] which are key chemicals produced in tons every year in industry. However, most of these MOFs are limited for their relatively low chemical and thermal stabilities. Furthermore, they are selective towards the separation of the components of a specific mixture, lacking versatility for the purification of other mixtures, which would be desirable on a hypothetical industrial scale.

Chapter IV

---

[198] See section **4.3.3. Xylenes**.
[199] Henrique, A.; Maity, T.; Zhao, H.; Brântuas, P. F.; Rodrigues, A. E.; Nouar, F.; Ghoufi, A.; Maurin, G.; Silva, J. A. C.; Serre, C. *J. Mater. Chem. A* **2020**, *8*, 17780-17789.
[200] Gonzalez, M. I.; Kapelewski, M. T.; Bloch, E. D.; Milner, P. J.; Reed, D. A.; Hudson, M. R.; Mason, J. A.; Barin, G.; Brown, C. M.; Long, J. R. *J. Am. Chem. Soc.* **2018**, *140*, 3412-3422.
[201] See reference **186c**.
[202] Alaerts, L.; Maes, M.; van der Veen, M. A.; Jacobs, P. A.; De Vos, D. E. *Phys. Chem. Chem. Phys.* **2009**, *11*, 2903-2911.

Separation of Regioisomeric Mixtures of Achiral Aromatic Compounds Using TAMOF-1

As described in Chapter 3, TAMOF-1 has been proven to be an excellent CSP for separating several racemic mixtures in up to milligram scale. In this chapter, we report the role of TAMOF-1 as a stationary phase for the separation of achiral positional isomers of aromatic compounds in liquid chromatography, such as xylenes, cresols and dihalobenzenes, among others. The performance of these separations and the previously reported chiral separations disclose the benefits of TAMOF-1 as a stationary phase in chromatographic systems.

4.3. RESULTS AND DISCUSSION

4.3.1. Dihalobenzenes

Dihalobenzenes are disubstituted benzene rings that contain two halogen atoms either in *ortho* (*o*-), *meta* (*m*-) or *para* (*p*-) disposition. These molecules can be classified by the halogen that the ring contains (*e.g.,* fluorine, chlorine, bromine or iodine). Although there are several dihalobenzenes with different halogen atoms (*e.g.,* bromochlorobenzene), in this section we focused on the separation of dihalobenzenes with only one halogen species. Specifically, we tested the separation of dichlorobenzene, dibromobenzene and diiodobenzene (**Figure 188**).
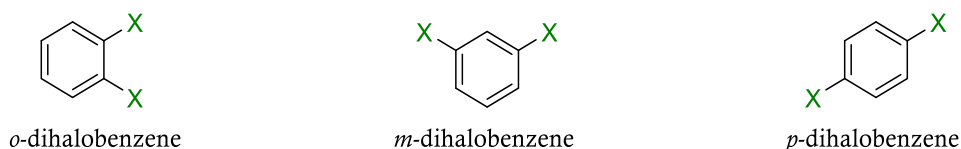
Figure 188. Dihalobenzene regioisomers. X = chloro (Cl), bromo (Br) or iodo (I).

4.3.1.1. Dichlorobenzenes

Each isomer of dichlorobenzene has its use in industry. *o*-Dichlorobenzene (b.p. 180.48 °C)[203] is used as a precursor for the synthesis of agrochemicals, and it is also used for cleaning and degreasing. *m*-dichlorobenzene (b.p. 173.0 °C)[203] is the least abundant of the three isomers and is mainly used as a solvent or chemical intermediate. Finally, *p*-dichlorobenzene (b.p. 174.12 °C)[203] is

---

[203] Ginzburg, B. M.; Tuichiev, S. *Russ. J. Appl. Chem.* **2009**, *82*, 1178-1187.

204

widely used as a repellent against insects and animals, and it has been appointed as toxic and carcinogenic for humans[204] although no human study has been carried out. *o*-dichlorobenzene purification is easier by distillation, whereas the *m*- and *p*- isomers only differ 0.9 ºC in b.p., difficulting their purification by distillation. Hence, we tested the separation of these three dihalobenzenes with TAMOF-1 (**Table 19**).

Table 19. Chromatographic parameters of the separation of dichlorobenzenes.

Analyte	Mobile phase	t_R (min)	$w_{1/2}$ (min)	Chromatogram
1,2-dichlorobenzene		31.5	2.6	
1,3-dichlorobenzene	*n*-Hex/CHCl₃ 97:3 0.15 mL min⁻¹	14.2	1.7	Figure 189
1,4-dichlorobenzene		17.8	1.4	
1,2-dichlorobenzene		33.3	2.6	
1,3-dichlorobenzene	*n*-Hex/CHCl₃ 97:3[a] 0.15 mL min⁻¹	18.6	1.7	Figure 190
1,4-dichlorobenzene		22.2	1.4	
1,2-dichlorobenzene		12.2	1.8	
1,3-dichlorobenzene	*n*-Hex/CHCl₃ 97:3 0.4 mL min⁻¹	6.8	1.1	Figure 191
1,4-dichlorobenzene		8.1	1.3	
1,2-dichlorobenzene		12.5	1.9	
1,3-dichlorobenzene	*n*-Hex/CHCl₃ 97:3[a] 0.4 mL min⁻¹	7.0	1.1	Figure 192
1,4-dichlorobenzene		8.2	1.3	
1,2-dichlorobenzene		4.3	0.7	
1,3-dichlorobenzene	*n*-Hex/CHCl₃ 97:3 1 mL min⁻¹	2.7	0.6	Figure 193
1,4-dichlorobenzene		3.1	0.6	
1,2-dichlorobenzene		5.1	1.0	
1,3-dichlorobenzene	*n*-Hex/CHCl₃ 97:3[a] 1 mL min⁻¹	2.9	0.5	Figure 194
1,4-dichlorobenzene		3.1	0.6	

[a] *o*-, *m*- and *p*-dichlorobenzene were mixed in solution prior to HPLC analysis. Ratio *o*-, *m*- and *p*-dichlorobenzene 1:1:1, concentration: 1 mg mL⁻¹.

Chapter IV

[204] Chin, J. Y.; Godwin, C.; Jia, C.; Robins, T.; Lewis, T.; Parker, E.; Max, P.; Batterman, S. *Indoor Air* **2013**, *23*, 40-49.

The separation of the positional isomers was tested separately and as a mixture. In all separations, the isomer that is better separated is the *o*-dichlorobenzene. Regarding the separation of the *m*- and *p*-dichlorobenzene isomers, the best conditions were found to be *n*-Hex/CHCl$_3$ 97:3 at a flow rate of 0.3 mL min^{-1} (**Figure 189**), *n*-Hex/CHCl$_3$ 97:3 at a flow rate of 0.15 mL min^{-1} (**Figure 190**) and *n*-Hex/CHCl$_3$ 97:3 at a flow rate of 0.4 mL min^{-1} (**Figure 191**).
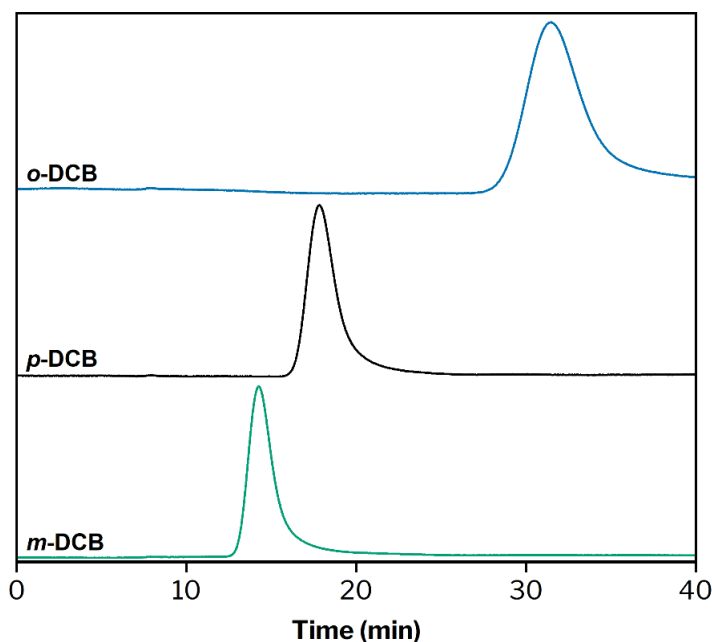
Figure 189. Chromatograms of dichlorobenzene isomers. Conditions: *n*-Hex/CHCl$_3$ 97:3, 0.15 mL min^{-1}.

206
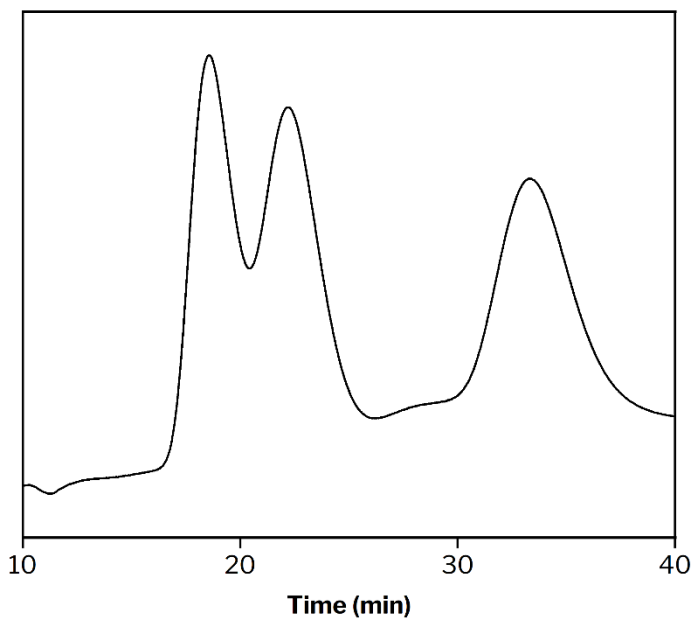
Figure 190. Chromatogram of a mixture of dichlorobenzenes. Conditions: *n*-Hex/CHCl₃ 97:3, 0.15 mL min⁻¹. From left to right: *m*-, *p*- and *o*-dichlorobenzene.
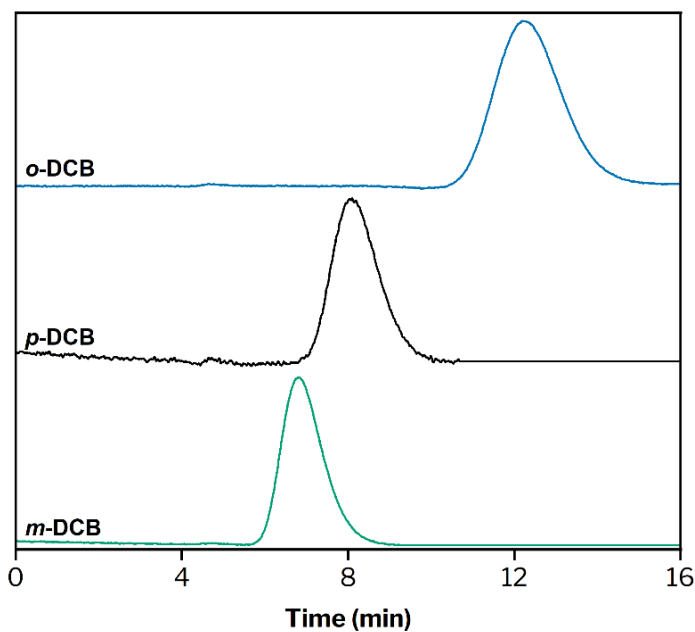
Figure 191. Chromatograms of dichlorobenzene isomers. Conditions: *n*-Hex/CHCl₃ 97:3, 0.4 mL min⁻¹.

Chapter IV

207

Separation of Regioisomeric Mixtures of Achiral Aromatic Compounds Using TAMOF-1
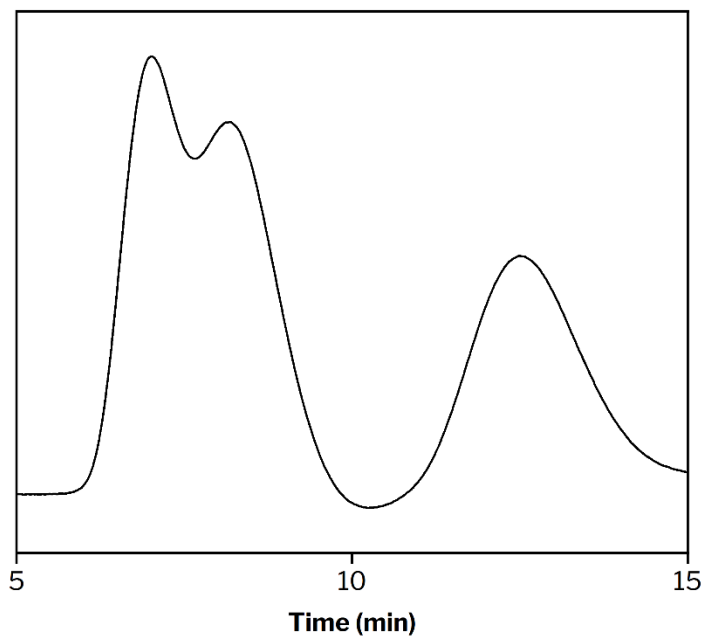
Figure 192. Chromatogram of a mixture of dichlorobenzene isomers. Conditions: *n*-Hex/CHCl₃ 97:3, 0.4 mL min⁻¹. From left to right: *m*-, *p*- and *o*-dichlorobenzene.
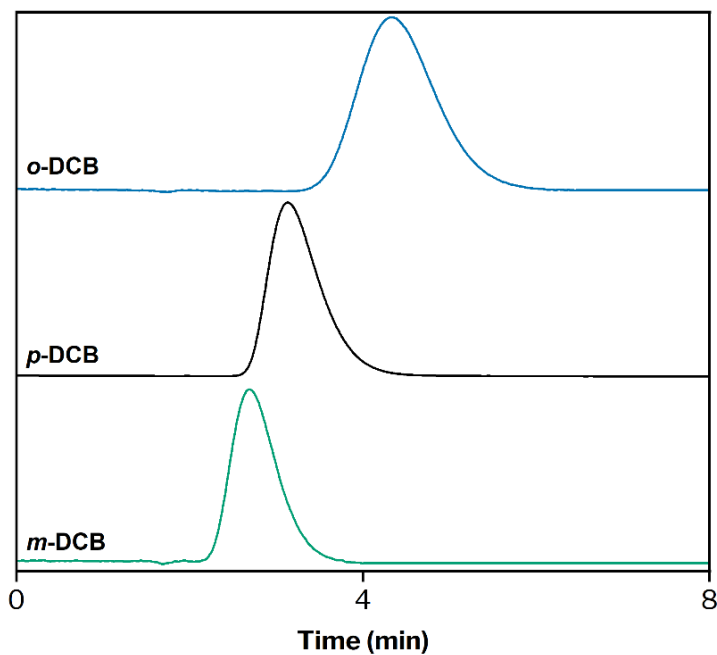
Figure 193. Chromatograms of dichlorobenzene isomers. Conditions: *n*-Hex/CHCl₃ 97:3, 1 mL min⁻¹.

208
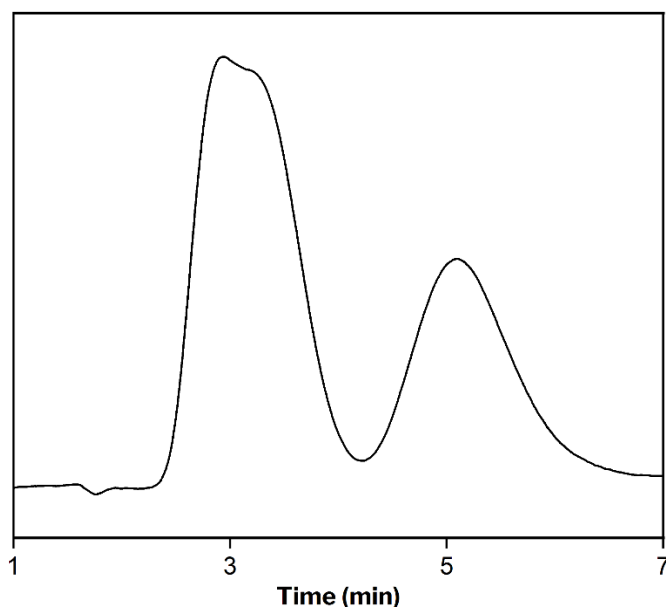
Figure 194. Chromatogram of a mixture of dichlorobenzene isomers. Conditions: *n*-Hex/CHCl$_3$ 97:3, 1 mL min^{-1}. From left to right: *m*-, *p*- and *o*-dichlorobenzene.

We can conclude that the best conditions for separating a mixture of the *m*- and *p*-dichlorobenzene isomers are the ones described in **Figure 190**.

4.3.1.2. Dibromobenzenes

Dibromobenzene isomers have a similar limitation to dichlorobenzene isomers in regards to physical properties – the *m*- and *p*- isomers have close boiling points that limit their separation by distillation, and these are 218.0-219.0 °C and 218.0 °C respectively.[205] *o*-dibromobenzene has a boiling point of 225 °C,[205] making the distillative separation feasible.

Dibromobenzenes, like dichlorobenzenes, are mainly used as chemical intermediates due to their facile use in cross-coupling and substitution reactions. *o*-dibromobenzene utility in industry is to act as a precursor for many 1,2-disubstituted derivatives of benzene, such as 1,2-dicyanobenzene.[206] *m*-dibromobenzene can be used in the synthesis of [n]metacyclophanes.[207]

---

[205] Sigma-Aldrich, C. In *Aldrich Chemistry: Handbook of Fine Chemicals*; Sigma-Aldrich: Milwaukee, WI, 2012-2014; p 880.

[206] Schareina, T.; Zapf, A.; Mägerlein, W.; Müller, N.; Beller, M. *Chem. Eur. J.* **2007**, *13*, 6249-6254.

[207] Smith, B. B.; Hill, D. E.; Cropp, T. A.; Walsh, R. D.; Cartrette, D.; Hipps, S.; Shachter, A. M.; Pennington, W. T.; Kwochka, W. R. *J. Org. Chem.* **2002**, *67*, 5333-5337.

209

Finally, *p*-dibromobenzene has more applications outside being a building block – it is useful as a heavy liquid solvent and motor oil additive. It can be used as well as a precursor to the dye 6,6-dibromoindigo.[208]

The separation of the three isomers was tried with TAMOF-1 emulating some of the conditions used for dichlorobenzenes (**Table 20**). In this case, we began by exploring the positional isomers separately to decide later if the separation of the mixture would be necessary.

Table 20. Chromatographic parameters of the separation of dibromobenzenes.

Analyte	Mobile phase	t_R(min)	$w_{1/2}$(min)	Chromatogram
1,2-dibromobenzene		11.6	3.1	
1,3-dibromobenzene	*n*-Hex/IPA 97:3 0.3 mL min^{-1}	11.1	3.1	Figure 195
1,4-dibromobenzene		13.4	3.9	
1,2-dibromobenzene		28.5	3.9	
1,3-dibromobenzene	*n*-Hex/CHCl$_3$ 98:2 0.3 mL min^{-1}	20.5	3.9	Figure 196
1,4-dibromobenzene		26.4	3.8	

---

[208] Wolk, J. L.; Frimer, A. A. *Molecules* **2010**, *15*, 5561-5580.
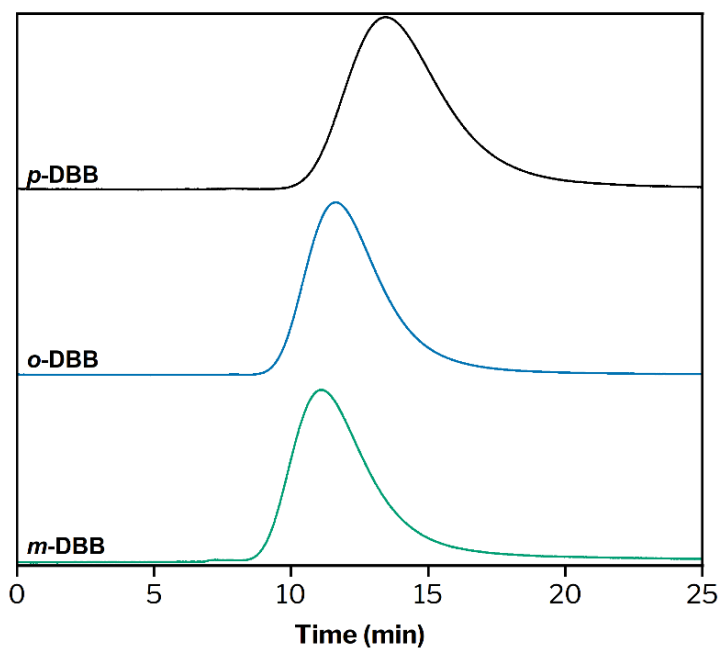
Figure 195. Chromatograms of dibromobenzene isomers. Conditions: n-Hex/IPA 97:3, 0.3 mL min^{-1}.
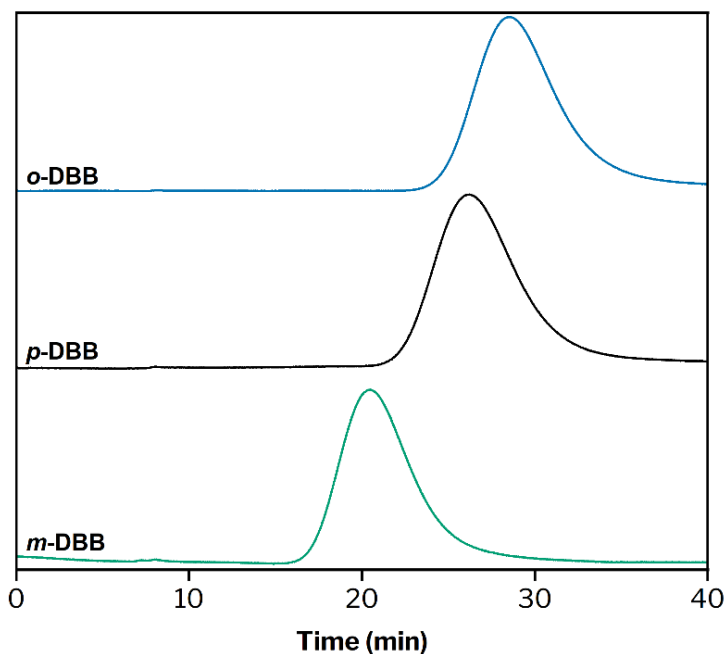
Figure 196. Chromatograms of dibromobenzene isomers. Conditions: n-Hex/CHCl$_3$ 98:2, 0.3 mL min^{-1}.

Chapter IV

211

Separation using *n*-Hex/IPA 97:3 did not provide convincing results to explore these conditions further. Secondly, separation using *n*-Hex/CHCl₃ 98:2 and a flow rate of 0.3 mL min⁻¹ (**Figure 196**) successfully separated the *m*- and *p*-dibromobenzene isomers, setting a precedent for the scale-up of this separation.

4.3.1.3. Diiodobenzenes

Diiodobenzene is widely used in Suzuki reactions. Like dichlorobenzenes and dibromobenzenes, diiodobenzene main application is as building block for cross-coupling reactions. The three isomers have similar boiling points, 287.0 °C for the *o*- isomer and 285.0 °C for the *m*- and *p*-diiodobenzene isomers,[209] that put us in the same situation than the former two dihalobenzenes – the *m*- and *p*- isomers have very similar boiling points, thus making difficult the separation by distillation.

Regarding other applications, *o*-diiodobenzene photolysis has been studied for the obtention of benzyne.[210] *m*-diiodobenzene is a precursor for the thiophene–benzene–thiophene triad[211] and is used for the synthesis of epitaxially aligned polyphenylene lines on Cu(110).[212] *p*-diiodobenzene can be used in the total synthesis of martinellic acid, a bradykinin receptor antagonist.[213]

Following the previous procedures for other dihalobenzenes, we emulated the same separation conditions for the diiodobenzene regioisomers (**Table 21**).

Table 21. Chromatographic parameters of the separation of diiodobenzenes.

Analyte	Mobile phase	t_R (min)	$w_{1/2}$ (min)	Chromatogram
1,2-diiodobenzene		16.3	7.3	
1,3-diiodobenzene	*n*-Hex/IPA 97:3 0.3 mL min⁻¹	26.9	10.7	Figure 197
1,4-diiodobenzene		28.4	8.4	

[209] Haynes, W. M.; Lide, D. R.; Bruno, T. J. In *Crc Handbook of Chemistry and Physics*; 97th ed.; CRC Press: Boca Raton, Florida, 2016-2017; pp 3-194.
[210] Kampmeier, J. A.; Hoffmeister, E. *J. Am. Chem. Soc.* **1962**, *84*, 3787-3788.
[211] Cornacchio, A. L. P.; Price, J. T.; Jennings, M. C.; McDonald, R.; Staroverov, V. N.; Jones, N. D. *J. Org. Chem.* **2009**, *74*, 530-544.
[212] Lipton-Duffin, J. A.; Ivasenko, O.; Perepichka, D. F.; Rosei, F. *Small* **2009**, *5*, 592-597.
[213] Ma, D.; Xia, C.; Jiang, J.; Zhang, J. *Org. Lett.* **2001**, *3*, 2189-2191.
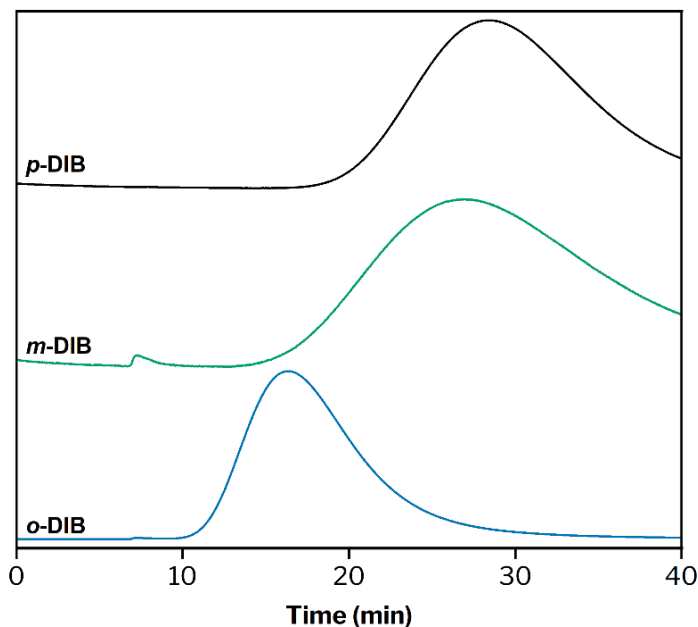
Figure 197. Overlayed HPLC chromatograms of diiodobenzene isomers. Conditions: *n*-Hex/IPA 97:3, 0.3 mL min^{-1}.

As shown in **Figure 197**, only the *o-* isomer is slightly separated from the other two compounds. Moreover, the peak widths have increased dramatically compared to the choro and bromo analogues. This fact could be associated with the greater atomic volume of the iodine atoms.

4.3.2. Benzene, toluene, ethylbenzene and styrene

Styrene (**Figure 198**) is a hydrocarbon with high importance in industry. It is produced in tons every year to fabricate polystyrene (PS),[214] a thermolabile polymer widely used for rubber, plastics, pipes and, isolating materials,

benzene   toluene   ethylbenzene   styrene
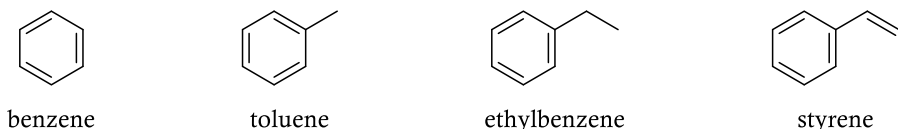
Figure 198. Chemical structures of benzene, toluene, ethylbenzene and styrene.

[214] Maul, J.; Frushour, B. G.; Kontoff, J. R.; Eichenauer, H.; Ott, K.-H.; Schade, C., Polystyrene and Styrene Copolymers. In *Ullmann's Encyclopedia of Industrial Chemistry*, Wiley-VCH: Weinheim, 2007; pp 475-522.

213

UNIVERSITAT ROVIRA I VIRGILI
INSIGHTS IN HOMOCHIRAL METAL-ORGANIC FRAMEWORKS: FROM THEIR SYNTHESIS TO ENANTIOSELECTIVE
APPLICATIONS
Juanjo Cabezas Gimenez

Separation of Regioisomeric Mixtures of Achiral Aromatic Compounds Using TAMOF-1

The industrial synthesis of styrene uses ethylbenzene as a precursor.[215] The ethylbenzene is dehydrogenated to styrene using superheated steam (up to 600 °C) over a catalyst, typically Fe_2O_3, supported on alumina. This process yields a complex mixture of styrene (b.p. 145.15 °C),[215] ethylbenzene (b.p. 136.3 °C),[216] benzene (b.p. 80 °C)[216] and toluene (b.p. 110.8 °C).[216] This mixture needs then to be separated by distillation, although the difference in b.p. of ethylbenzene and styrene is only 9 °C, a difficult distillation process to which is added the possibility of styrene to polymerise to polystyrene, which requires the continuous addition of the corresponding inhibitor (*e.g.,* di-*n*-butyl phthalate).[217]

To avoid these expensive and complex processes, we proposed TAMOF-1 as a stationary phase to separate these four molecules in solution. The selected mobile phases for this process were *n*-Hex, *n*-Hex/IPA 97:3, *n*-Hex/CHCl$_3$ 98:2 and 97:3 at different flow rates (**Table 22**).

[215] James, D. H.; Castor, W. M., Styrene. In *Ullmann's Encyclopedia of Industrial Chemistry*, Wiley-VCH: Weinheim, 2011; pp 529-543.
[216] Shao, X.; Wang, G.; Sun, Y. a.; Zhang, R.; Xie, K.; Liu, H. *J. Chromatogr. Sci.* **2006**, *44*, 141-147.
[217] Motyakin, M. V.; Wasserman, A. M.; Stott, P. E.; Zaikov, G. E. *J. Appl. Polym. Sci.* **2004**, *91*, 1599-1603.

Table 22. Chromatographic parameters of the separation of benzene, toluene, ethylbenzene and styrene.

Analyte	Mobile phase	t_R (min)	$w_{1/2}$ (min)	Chromatogram
benzene		53.5	5.3	
toluene	n-Hex	28.6	2.3	Figure 199
ethylbenzene	0.15 mL min^{-1}	24.7	2.0	
styrene		36.3	3.8	
benzene		38.3	2.8	
toluene	n-Hex/CHCl$_3$ 98:2	26.5	2.5	Figure 200
ethylbenzene	0.15 mL min^{-1}	23.1	2.3	
styrene		32.7	3.2	
benzene		30.0	2.5	
toluene	n-Hex/CHCl$_3$ 97:3[a]	21.0	2.2	Figure 201
ethylbenzene	0.15 mL min^{-1}	17.2	1.8	
styrene		24.5	2.2	
benzene		15.2	1.7	
toluene	n-Hex/CHCl$_3$ 97:3[a]	10.7	1.3	Figure 202
ethylbenzene	0.3 mL min^{-1}	8.8	1.1	
styrene		12.3	1.3	
benzene		3.9	0.6	
toluene	n-Hex/CHCl$_3$ 97:3	3.1	0.5	Figure 203
ethylbenzene	1 mL min^{-1}	2.6	0.5	
styrene		3.6	0.7	

[a] Benzene, toluene, ethylbenzene and styrene were mixed in solution prior to HPLC analysis. Ratio 1:1:1:1, concentration: 1 mg mL^{-1}.

The best separations, in which there is no baseline resolution but the peaks are differentiated, are the ones that use n-Hex/CHCl$_3$ 98:2 and 97:3, both at 0.15 mL min^{-1} (**Figure 200** and **Figure 201**).
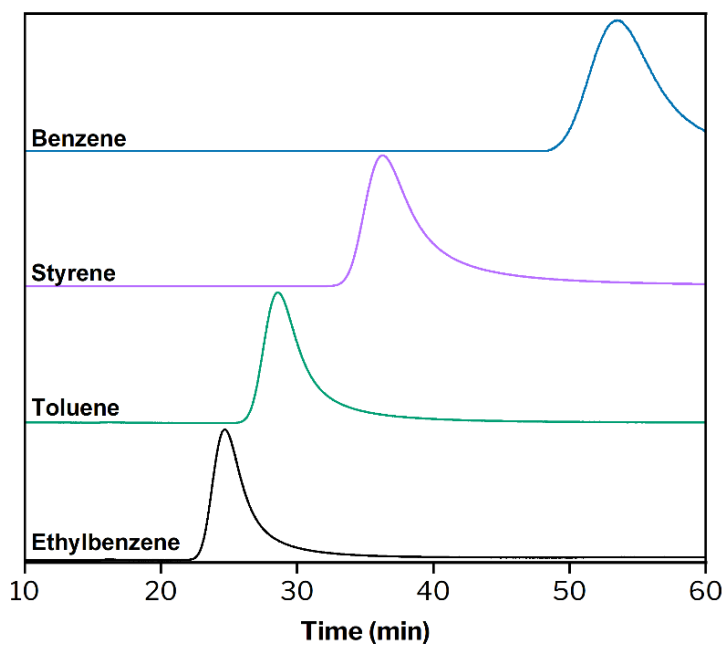
Chapter IV

215

Separation of Regioisomeric Mixtures of Achiral Aromatic Compounds Using TAMOF-1

Figure 199. Overlayed chromatograms of benzene, toluene, ethylbenzene and styrene. Conditions: *n*-Hex 0.15 mL min^{-1}, 1 mg mL^{-1}. From left to right: benzene, ethylbenzene, toluene and styrene.
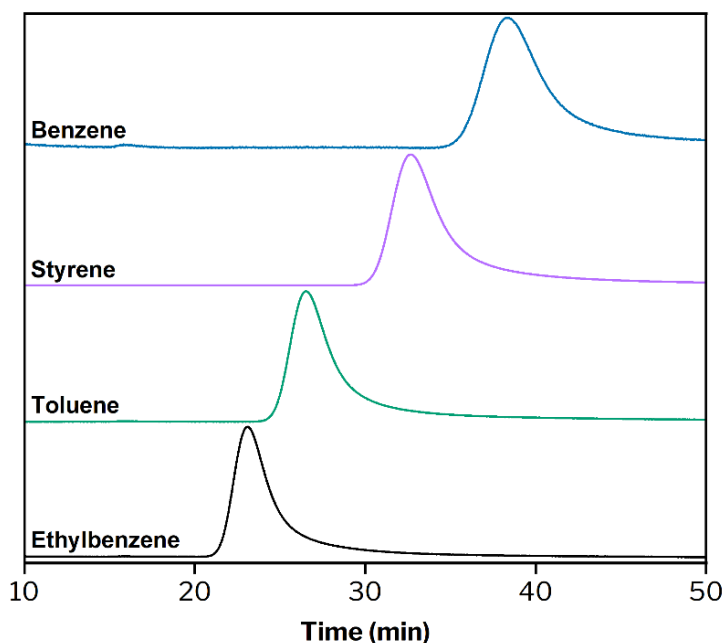
Figure 200. Chromatograms of benzene, toluene, ethylbenzene and styrene. Conditions: *n*-Hex/CHCl$_3$ 98:2, 0.15 mL min^{-1}.
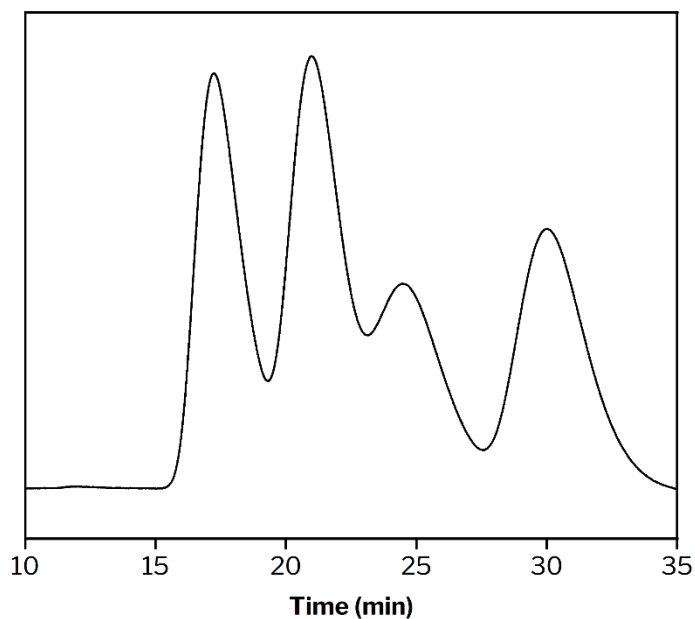
Figure 201. Chromatogram of a mixture of benzene, toluene, ethylbenzene and styrene. Conditions: n-Hex/CHCl$_3$ 97:3, 0.15 mL min^{-1}. From left to right: ethylbenzene, toluene, styrene and benzene.
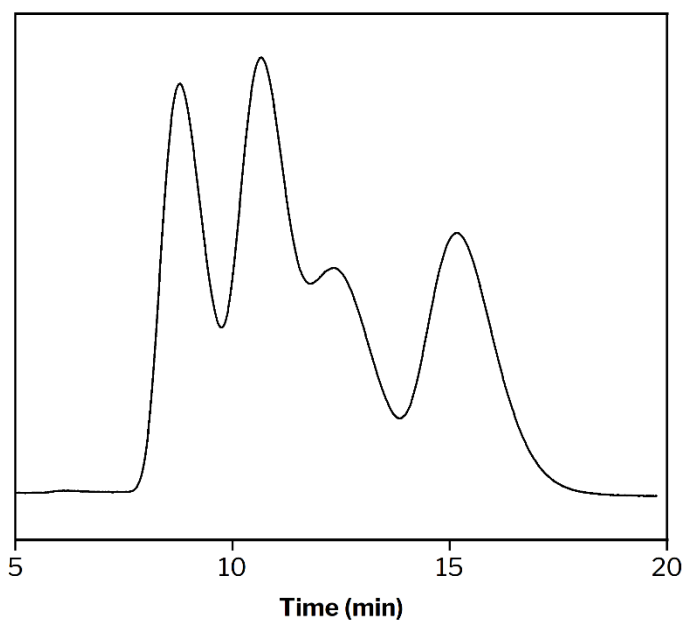
Figure 202. Chromatogram of a mixture of benzene, toluene, ethylbenzene and styrene. Conditions: n-Hex/CHCl$_3$ 97:3, 0.3 mL min^{-1}, 1 mg mL^{-1}. From left to right: ethylbenzene, toluene, styrene and benzene.

Chapter IV

Separation of Regioisomeric Mixtures of Achiral Aromatic Compounds Using TAMOF-1
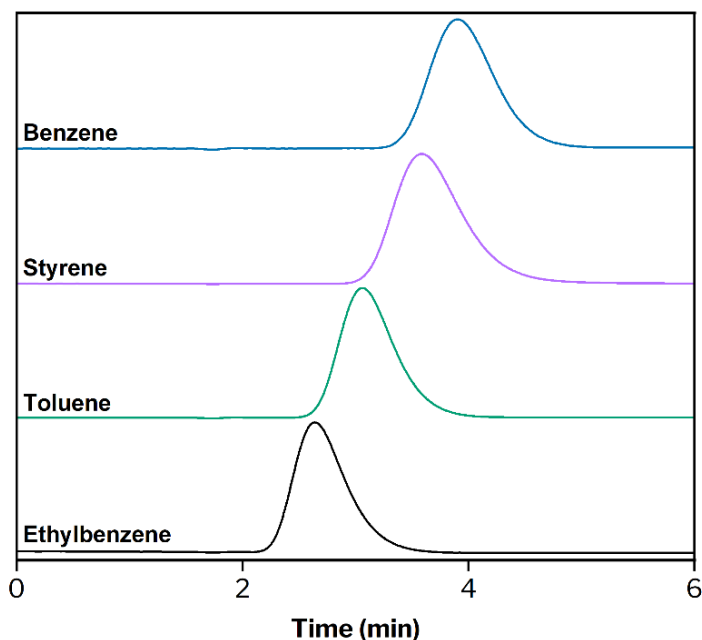
Figure 203. Chromatograms of benzene, toluene, ethylbenzene and styrene. Conditions: *n*-Hex/CHCl$_3$ 98:2, 1 mL min^{-1}.

We observed that styrene overlapped with the rest of the analytes in most cases. If styrene could be separated from the other analytes by distillation, the mixture of benzene, toluene and ethylbenzene could be separated by HPLC. Thereby, we tested the separation of these three analytes (**Table 23**).

Table 23. Chromatographic parameters of the separation of a mixture of benzene, toluene and ethylbenzene.

Analyte	Mobile phase	t_R (min)	$w_{1/2}$ (min)	Chromatogram
benzene	*n*-Hex/CHCl$_3$ 97:3 0.15 mL min^{-1}	30.3	2.2	Figure 204
toluene		21.5	2.2	
ethylbenzene		17.8	1.9	
benzene	*n*-Hex/CHCl$_3$ 97:3 0.3 mL min^{-1}	15.2	1.5	Figure 205
toluene		10.8	1.3	
ethylbenzene		9.0	1.1	

Despite the overlap between ethylbenzene and toluene, both separations are excellent and allowed us to isolate benzene (**Figure 204** and **Figure 205**).

218
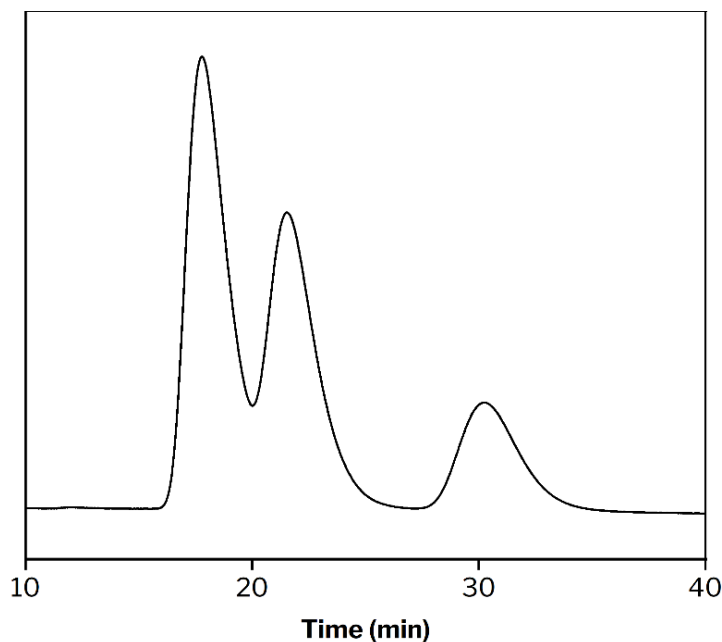
Figure 204. Chromatogram of a mixture of benzene, toluene and ethylbenzene. Conditions: *n*-Hex/CHCl$_3$ 97:3, 0.15 mL min^{-1}. From left to right: ethylbenzene, toluene and benzene.
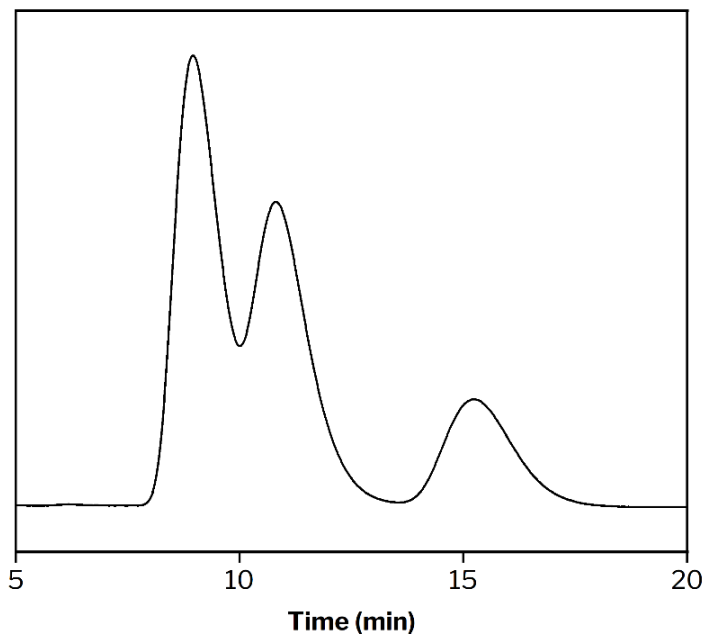
Figure 205. Chromatogram of a mixture of benzene, toluene and ethylbenzene. Conditions: *n*-Hex/CHCl$_3$ 97:3, 0.3 mL min^{-1}. From left to right: ethylbenzene, toluene and benzene.

Chapter IV

219

UNIVERSITAT ROVIRA I VIRGILI
INSIGHTS IN HOMOCHIRAL METAL–ORGANIC FRAMEWORKS: FROM THEIR SYNTHESIS TO ENANTIOSELECTIVE
APPLICATIONS
Juanjo Cabezas Gimenez

Separation of Regioisomeric Mixtures of Achiral Aromatic Compounds Using TAMOF-1

These results indicate that TAMOF-1 could be an interesting stationary phase for the purification of impurities in the industrial synthesis of styrene.

4.3.3. Xylenes

Xylenes, or dimethylbenzenes (**Figure 206**), are a mixture of *o*-xylene, *m*-xylene and *p*-xylene. These can be found naturally in petroleum (~1 wt%), or they can be produced by catalytic reforming[218] as part of the BTX or BTEX aromatics.[219]

o-xylene   *m*-xylene   *p*-xylene
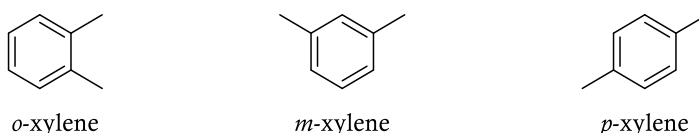
Figure 206. Chemical structures of *o*-, *m*- and *p*-xylene.

As a mixture, commercial xylene, which contains 40–65% *m*-xylene and up to 20% each of *o*-, *p*-xylene and ethylbenzene, is mainly used as a solvent, but its positional isomers possess different applications. *o*-xylene is widely used in the production of phthalic anhydride,[220] *m*-xylene is used for the preparation of isophthalic acid by catalytic oxidation,[221] and *p*-xylene is used in the production of terephthalic acid for polyesters (*e.g.*, PET).[222]

Resembling other disubstituted benzenes, xylene isomers have similar boiling points: 144 °C (*ortho*),[223] 139 °C (*meta*)[224] and 138 °C (*para*).[222] Their melting points could provide an alternative way for their separation (-25 °C for *o*-xylene, -48 °C for *m*-xylene and 13 °C for *p*-xylene), but due to the formation of a eutectic mixture,[225] crystallisation is not an easier way to separate them. Separation with TAMOF-1 could help overcome these challenges. Thus, we analysed the separation of xylenes (**Table 24**).

[218] Speight, J. G. In *The Refinery of the Future (Second Edition)*; Speight, J. G., Ed.; Gulf Professional Publishing: 2020; pp 43-84.
[219] (a) Chareonpanich, M.; Zhang, Z.-G.; Nishijima, A.; Tomita, A. *Fuel* **1995**, *74*, 1636-1640. (b) Kim, Y.; Yun, G.-N.; Lee, Y.-K. *Catal. Commun.* **2014**, *45*, 133-138.
[220] Bond, G. C. *J. Catal.* **1989**, *116*, 531-539.
[221] (a) Lv, H.-f.; Wu, S.-q.; Liu, N.; Long, X.-l.; Yuan, W.-k. *Chem. Eng. J.* **2011**, *172*, 1045-1053. (b) Long, X.; Wang, Z.; Wu, S.; Wu, S.; Lv, H.; Yuan, W. *J. Ind. Eng. Chem.* **2014**, *20*, 100-107.
[222] Partenheimer, W. *J. Mol. Catal. A* **2003**, *206*, 105-119.
[223] Gibbons, L. C.; Thompson, J. F.; Reynolds, T. W.; Wright, J. I.; Chanan, H. H.; Lamberti, J. M.; Hipsher, H. F.; Karabinos, J. V. *J. Am. Chem. Soc.* **1946**, *68*, 1130-1131.
[224] Pines, H.; Arrigo, J. T. *J. Am. Chem. Soc.* **1958**, *80*, 4369-4378.
[225] Shiau, L.-D.; Wen, C.-C.; Lin, B.-S. *AlChE J.* **2008**, *54*, 337-342.

Table 24. Chromatographic parameters of the separation of a o-, m- and p-xylene.

Analyte	Mobile phase	t_R (min)	$w_{1/2}$ (min)	Chromatogram
o-xylene		19.9	2.1	
m-xylene	n-Hex 0.3 mL min^{-1}	10.9	1.8	Figure 207
p-xylene		13.6	2.6	
o-xylene		19.9	3.2	
m-xylene	n-Hex^a 0.3 mL min^{-1}	11.1	1.2	Figure 208
p-xylene		12.7	2.4	

^{a} o-xylene, m-xylene and p-xylene were mixed in solution prior to HPLC analysis. Ratio 1:1:1, concentration: 1 mg mL^{-1}.

In these separations, as the results were good enough using only n-Hex, we discarded more polar additives like IPA and CHCl$_3$. The o-isomer is separated successfully from the m- and p- isomers, with a very differentiated retention time. The retention times of the three xylene isomers are differentiated in separate injections (**Figure 207**). Although the resolution of the three peaks in an equimolar mixture decreases (**Figure 208**), further exploration will be required to improve these results.
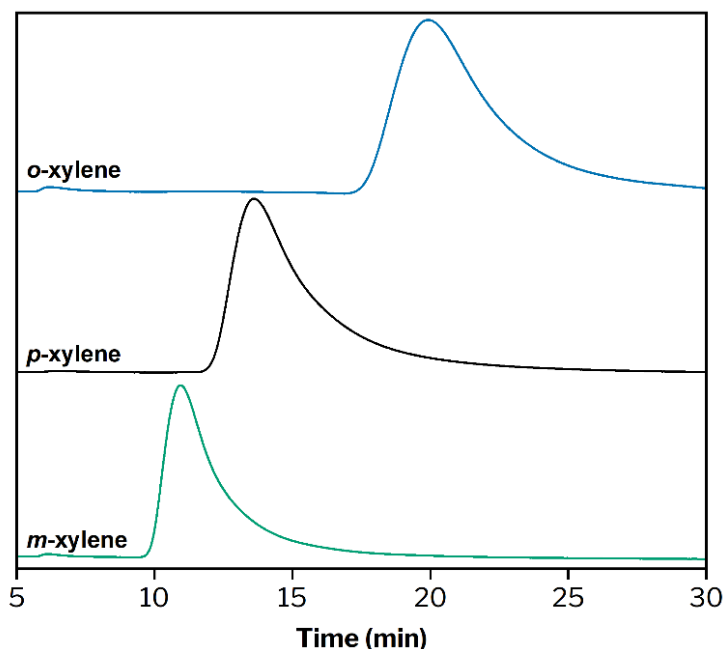
Figure 207. Chromatograms of o-, m- and p-xylene. Conditions: n-Hex, 0.3 mL min^{-1}.

Separation of Regioisomeric Mixtures of Achiral Aromatic Compounds Using TAMOF-1
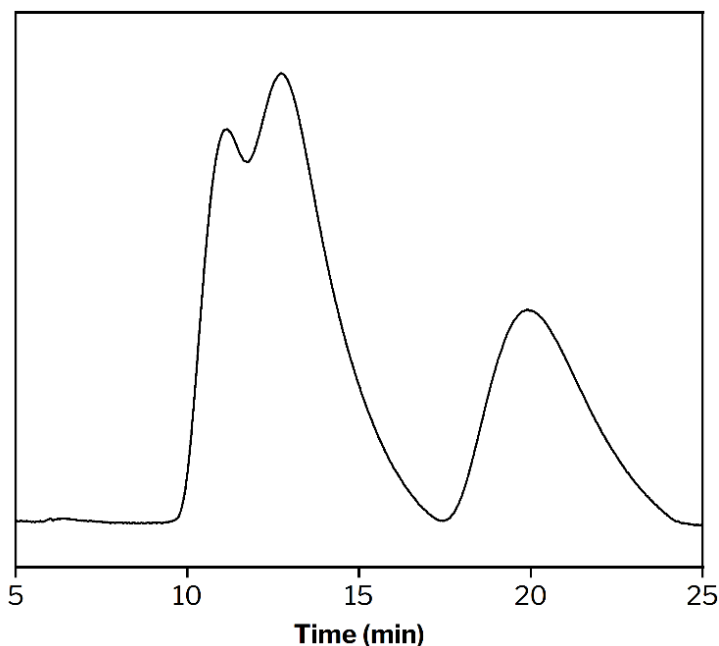
Figure 208. Chromatogram of a mixture of *o*-, *m*- and *p*-xylene. Conditions: *n*-Hex, 0.3 mL min⁻¹, 1 mg mL⁻¹. From left to right: *m*-, *p*- and *o*-xylene.

4.3.4. Cresols

The last family of achiral positional isomers analysed with TAMOF-1 as stationary phase was cresols. Cresols, methylphenols or hydroxytoluenes (**Figure 209**) are a group of aromatic compounds that can be found in nature or can be produced in industry.

o-cresol   *m*-cresol   *p*-cresol
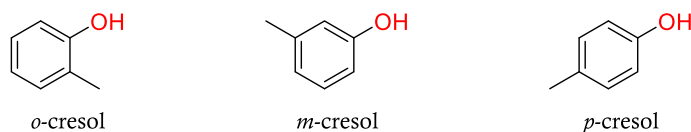
Figure 209. Chemical structures of *o*-, *m*- and *p*-cresol.

The natural source of cresols is coal tar, from where it proceeds up to half of the world's supply.[226] Industrial production involves processes such as hydrolysis of chlorotoluenes or methylation of phenol, among others.

---

[226] Meng, H.; Ge, C.-T.; Ren, N.-N.; Ma, W.-Y.; Lu, Y.-Z.; Li, C.-X. *Ind. Eng. Chem. Res.* **2014**, *53*, 355-362.

The mixture of the three cresol isomers is called tricresol, and its uses go from disinfectant to the manufacture of synthetic resins. *o*-cresol is mainly a chemical precursor in the synthesis of herbicides or pharmaceutical intermediates (*e.g., o*-cresotinic acid).[227] *m*-Cresol is also a valuable precursor for synthetic vitamin E and thymol.[228] However, it also has use as a solvent for polymers or as a preservative. Then, *p*-cresol main application is its role in the production of antioxidants (*e.g.,* BHT).[229]

The boiling point of the *o*-isomer differs from the *m*- and *p*-, like the previously explored families. The latter two possess an almost identical boiling point (202.0 ºC and 201.9 ºC, respectively). Therefore, the separation of these analytes was also explored (**Table 25**).

Table 25. Chromatographic parameters of the separation of a *o*-, *m*- and *p*-cresol.

Analyte	Mobile phase	t_R (min)	$w_{1/2}$ (min)	Chromatogram
o-cresol		66.5	7.6	
m-cresol	*n*-Hex/IPA 95:5[a] 0.6 mL min^{-1}	35.4	5.1	Figure 210
p-cresol		46.2	7.9	
o-cresol		32.0	2.1	
m-cresol	*n*-Hex/IPA 9:1 0.6 mL min^{-1}	17.4	1.8	Figure 211
p-cresol		21.7	2.6	
o-cresol		31.3	4.8	
m-cresol	*n*-Hex/IPA 9:1[a] 0.6 mL min^{-1}	17.0	3.0	Figure 212
p-cresol		23.3	4.5	

[a] *o*-xylene, *m*-xylene and *p*-xylene were mixed in solution prior to HPLC analysis. Ratio 1:1:1, concentration: 1 mg mL^{-1}.

In all three cases, the separation of the *o*- isomer is excellent, as previously seen for other families. In this specific case, the separation of *m*-cresol and *p*-cresol is excellent, explicitly using *n*-Hex/IPA 95:5 at a flow rate of 0.6 mL min^{-1} (**Figure 210**).

[227] Luo, J.; Preciado, S.; Xie, P.; Larrosa, I. *Chem. Eur. J.* **2016**, *22*, 6798-6802.
[228] (a) Ali, A. A.; Gaikar, V. G. *Ind. Eng. Chem. Res.* **2011**, *50*, 6543-6555. (b) Wang, Z.; Mao, S.; Li, H.; Wang, Y. *Act. Phys. -Chim. Sin.* **2018**, *34*, 598-617.
[229] Selvaraj, M.; Kawi, S. *Microporous Mesoporous Mater.* **2007**, *98*, 143-149.

Chapter IV

Separation of Regioisomeric Mixtures of Achiral Aromatic Compounds Using TAMOF-1
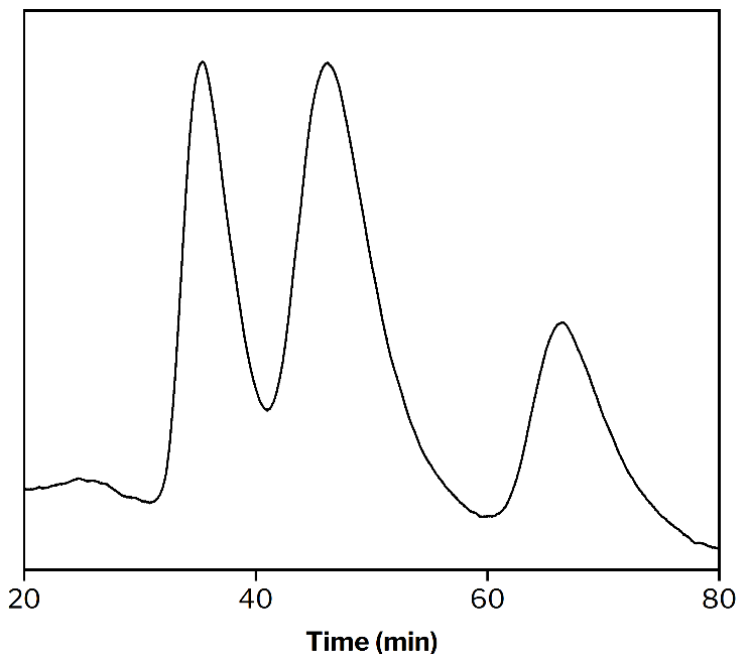
Figure 210. HPLC chromatogram of a mixture of *o*-, *m*- and *p*-cresol. Conditions: *n*-Hex/IPA 95:5, 0.6 mL min⁻¹, 1 mg mL⁻¹. From left to right: *m*-, *p*- and *o*-cresol.

Figure 211. Overlayed chromatograms of *o*-, *m*- and *p*-cresol. Conditions: *n*-Hex/IPA 9:1, 0.6 mL min⁻¹, 1 mg mL⁻¹. From left to right: *m*-, *p*- and *o*-cresol.

224
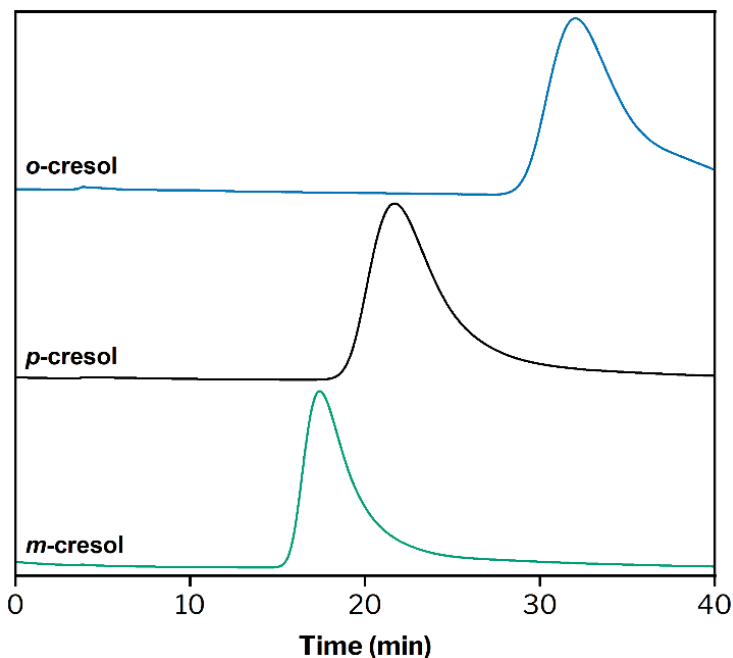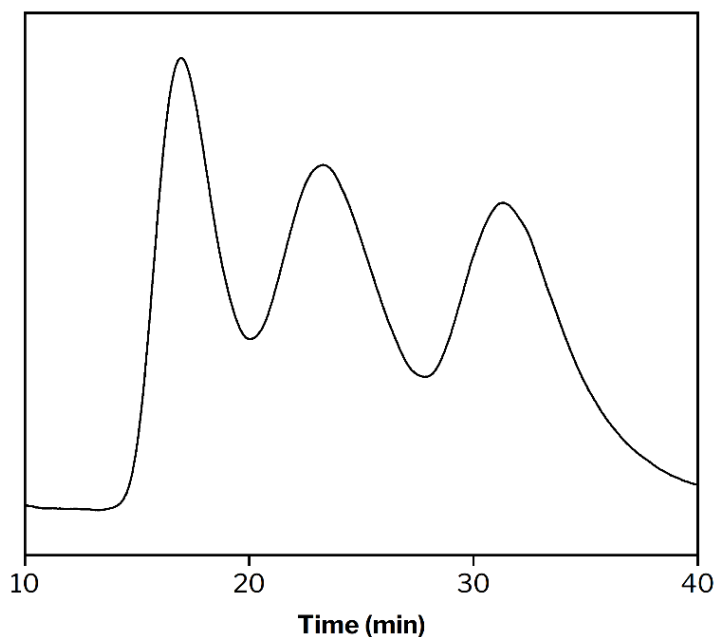
Figure 212. HPLC chromatogram of a mixture of *o*-, *m*- and *p*-cresol. Conditions: *n*-Hex/IPA 9:1, 0.6 mL min^{-1}, 1 mg mL^{-1}. From left to right: *m*-, *p*- and *o*-cresol.

The conditions used in this screening required higher polarities and flow rates due to a higher polarity of cresol isomers compared to its nonpolar analogues, xylenes and alkyl/vinyl benzenes.

Chapter IV

225

4.4. CONCLUSIONS

The chromatographic separation of structurally diverse achiral positional isomers of aromatic compounds has been studied employing TAMOF-1 as the chromatographic phase. In all cases, the mixtures of compounds have been either totally or partially separated using TAMOF-1 as a stationary phase. The peak widths in the dihalobenzenes family retrogress with the atomic volume – diiodobenzene isomers show peak widths superior to five minutes.

The separation of the by-products in the industrial synthesis of styrene (benzene, toluene and ethylbenzene) are successfully separated with low polarity mobile phases.

The mixture of cresol regioisomers is excellently resolved using low polarity solvents. Due to the polarity of cresols, retention times are high (up to 60 min), which could be reduced by slightly increasing the polarity of the mobile phase.

This work proves that TAMOF-1 is not only an excellent chiral stationary phase but also a promising stationary phase for separating structurally diverse achiral positional isomers of aromatic compounds. Among all the examples reported in this chapter, the purification of unreacted starting material and by-products of the industrial synthesis of styrene stands out on its excellent performance.

4.5. EXPERIMENTAL SECTION

4.5.1. Materials and general

All reagents were of commercial grade and used without further purification: *o*-dichlorobenzene (99%, Sigma-Aldrich), *m*-dichlorobenzene (98%, Sigma-Aldrich), *p*-dichlorobenzene (≥99%, Sigma-Aldrich), *o*-dibromobenzene (98%, Sigma-Aldrich), *m*-dibromobenzene (97%, Sigma-Aldrich), *p*-dibromobenzene (98%, Sigma-Aldrich), *o*-diiodobenzene (98%, Sigma-Aldrich), *m*-diiodobenzene (98%, Sigma-Aldrich), *p*-diiodobenzene (99%, Sigma-Aldrich), styrene (≥99%, Sigma-Aldrich), ethylbenzene (99%, Sigma-Aldrich), toluene (≥99.9%, Sigma-Aldrich), benzene (99.8%, Sigma-Aldrich), *o*-xylene (97%, Sigma-Aldrich), *m*-xylene (≥99%, Sigma-Aldrich), *p*-xylene (≥99%, Sigma-Aldrich), *o*-cresol (≥99%, Sigma-Aldrich), *m*-cresol (99%, Sigma-Aldrich), *p*-cresol (99%, Sigma-Aldrich). All solvents were of commercial grade and used without further purification: HPLC-grade MeOH, EtOH, IPA, *n*-Hex, ACN and TBME (VWR, Chem-Lab and Sigma Aldrich), *N*,*N*-dimethylformamide (peptide grade, ≥99.9%, Iris Biotech GMBH) and diethyl ether (≥99%, VWR). The analytes and their mixtures were analysed by HPLC chromatography with an Agilent 1200 series system equipped with a diode array detector. The information about the preparation of the packed columns can be found in Chapter 3, page **178**.
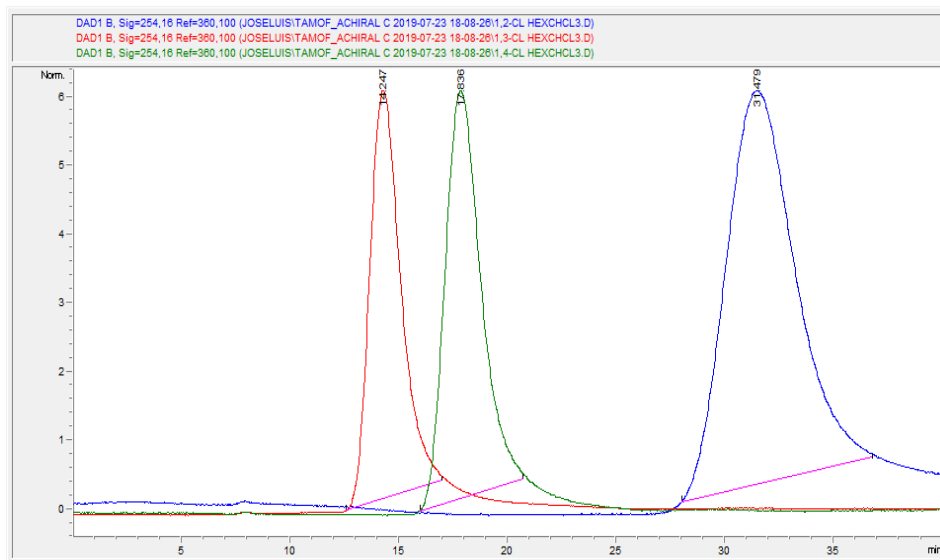
Separation of Regioisomeric Mixtures of Achiral Aromatic Compounds Using TAMOF-1

4.5.2. Chromatograms

Figure 213. Overlayed HPLC chromatograms of dichlorobenzene isomers. Conditions: *n*-Hex/CHCl$_3$ 97:3, 0.15 mL min^{-1}, 1 mg mL^{-1}. From left to right: *m-*, *p-* and *o*-dichlorobenzene.
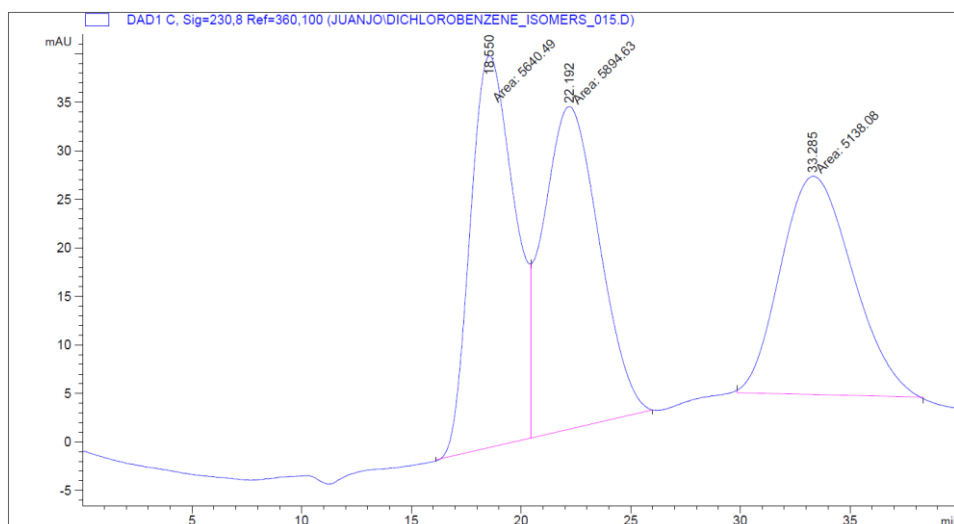
Figure 214. HPLC chromatogram of the mixture of dichlorobenzene isomers. Conditions: *n*-Hex/CHCl$_3$ 97:3, 0.15 mL min^{-1}, 1 mg mL^{-1}. From left to right: *m-*, *p-* and *o*-dichlorobenzene.

228
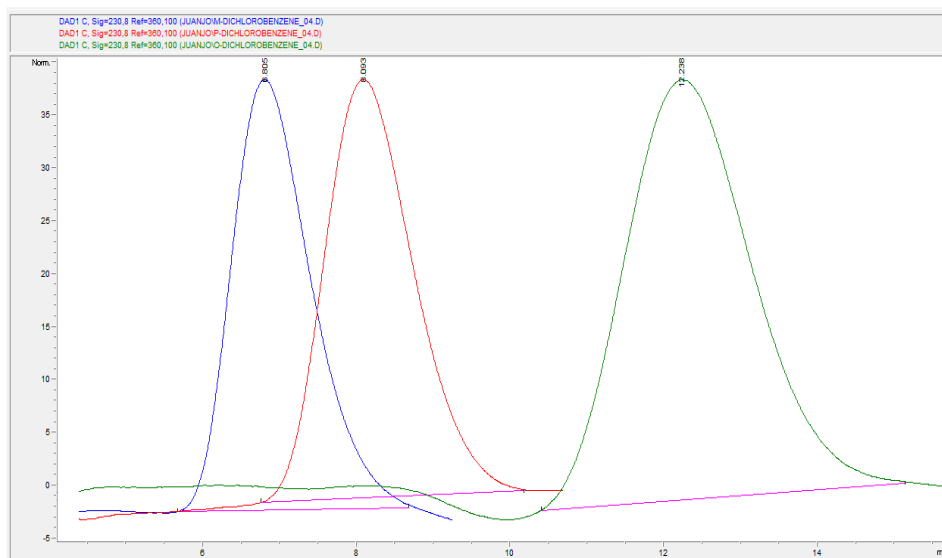
Figure 215. Overlayed HPLC chromatograms of dichlorobenzene isomers. Conditions: n-Hex/CHCl$_3$ 97:3, 0.4 mL min^{-1}, 1 mg mL^{-1}. From left to right: m-, p- and o-dichlorobenzene.
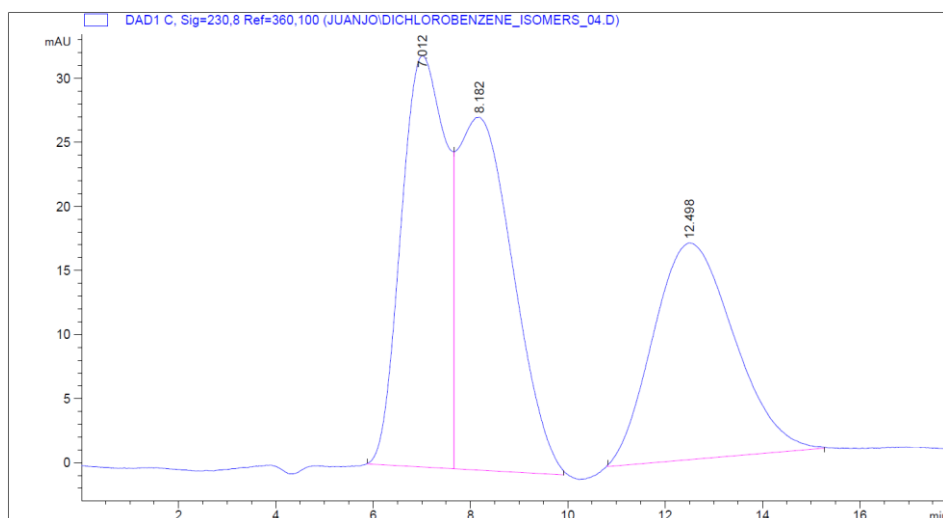
Figure 216. HPLC chromatogram of a mixture of dichlorobenzene isomers. Conditions: n-Hex/CHCl$_3$ 97:3, 0.4 mL min^{-1}, 1 mg mL^{-1}. From left to right: m-, p- and o-dichlorobenzene.

Separation of Regioisomeric Mixtures of Achiral Aromatic Compounds Using TAMOF-1
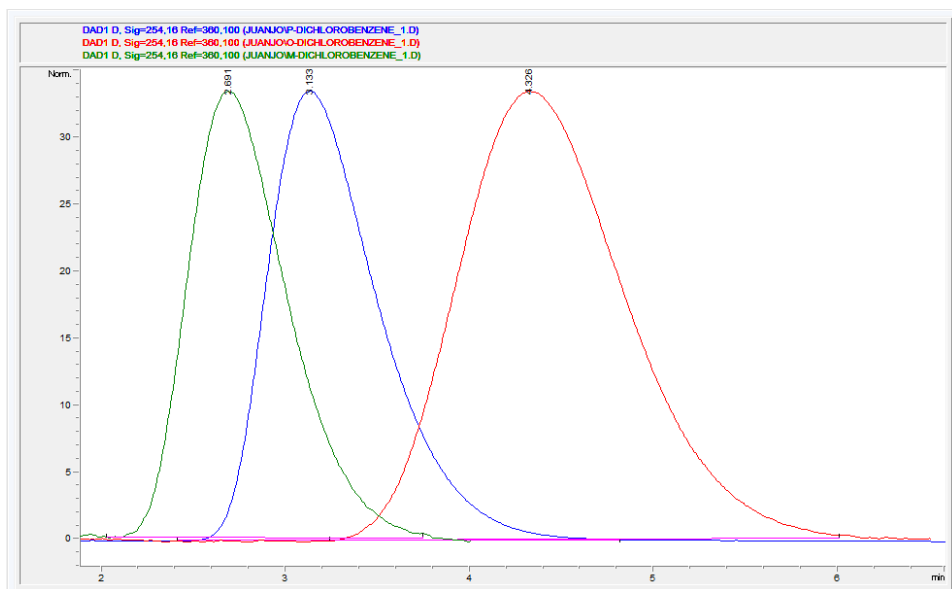
Figure 217. Overlayed HPLC chromatograms of dichlorobenzene isomers. Conditions: *n*-Hex/CHCl$_3$ 97:3, 1 mL min^{-1}, 1 mg mL^{-1}. From left to right: *m*-, *p*- and *o*-dichlorobenzene.
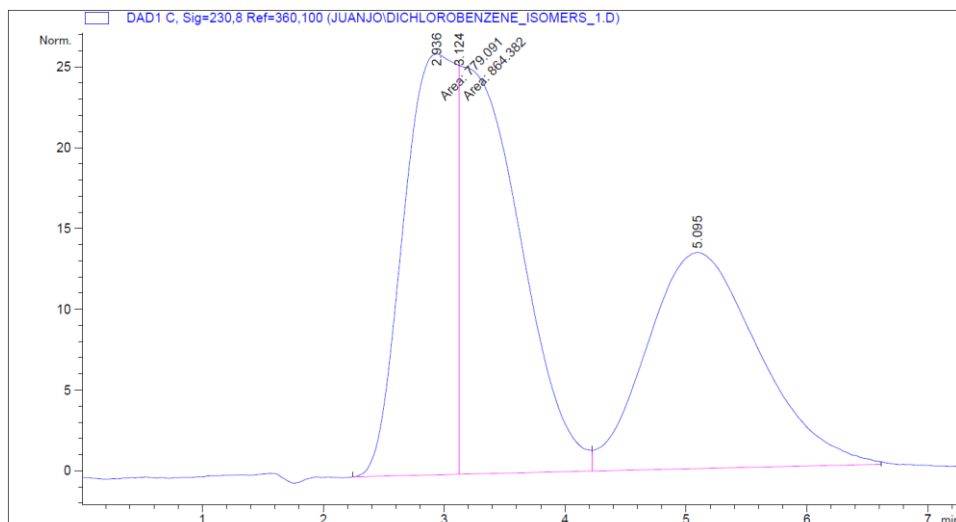
Figure 218. HPLC chromatogram of a mixture of dichlorobenzene isomers. Conditions: *n*-Hex/CHCl$_3$ 97:3, 1 mL min^{-1}, 1 mg mL^{-1}. From left to right: *m*-, *p*- and *o*-dichlorobenzene.

230
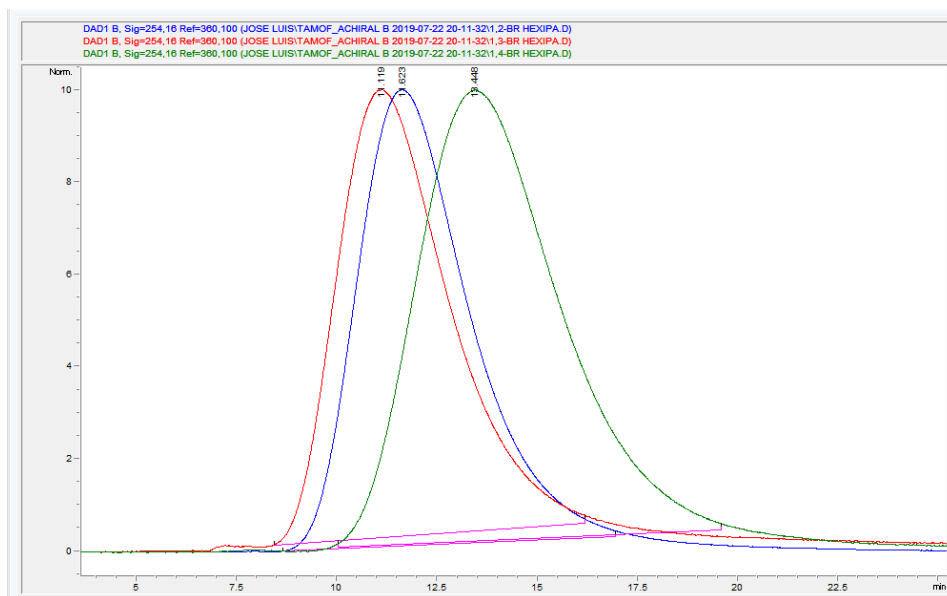
Figure 219. Overlayed HPLC chromatograms of dibromobenzene isomers. Conditions: *n*-Hex/IPA 97:3, 0.3 mL min^{-1}, 1 mg mL^{-1}. From left to right: *m*-, *p*- and *o*-dibromobenzene.
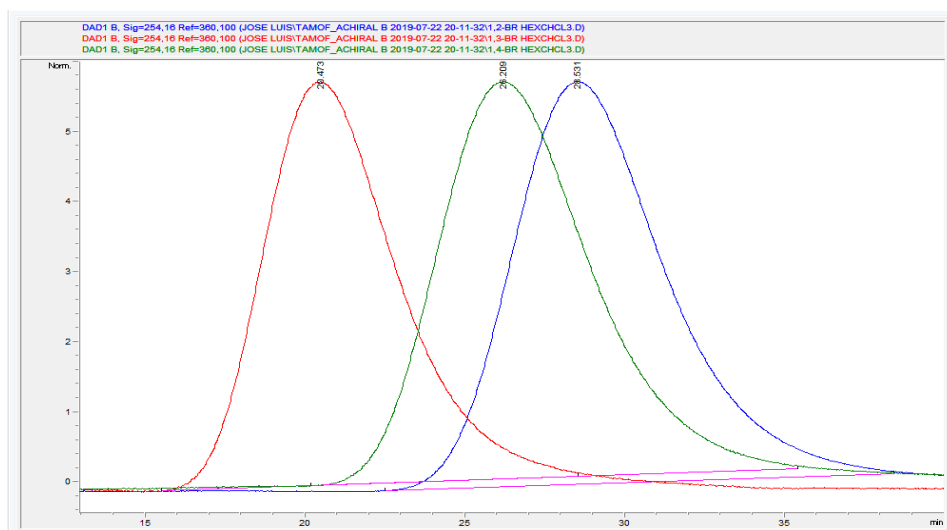
Figure 220. Overlayed HPLC chromatograms of dibromobenzene isomers. Conditions: *n*-Hex/CHCl$_3$ 98:2, 0.3 mL min^{-1}, 1 mg mL^{-1}. From left to right: *m*-, *p*- and *o*-dibromobenzene.
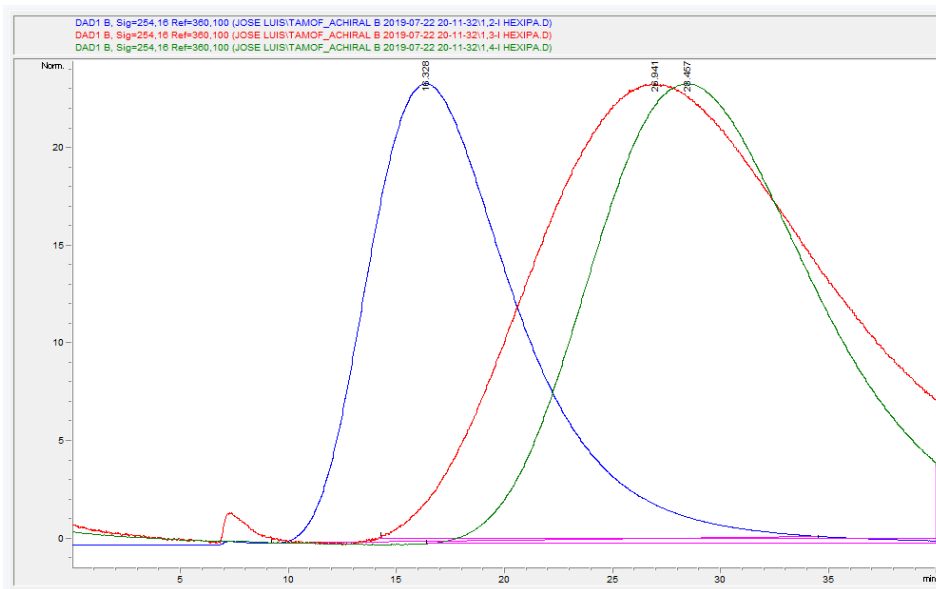
Chapter IV

231

Separation of Regioisomeric Mixtures of Achiral Aromatic Compounds Using TAMOF-1

Figure 221. Overlayed HPLC chromatograms of diiodobenzene isomers. Conditions: *n*-Hex/IPA 97:3, 0.3 mL min^{-1}, 1 mg mL^{-1}. From left to right: *o*-, *m*- and *p*-diiodobenzene.
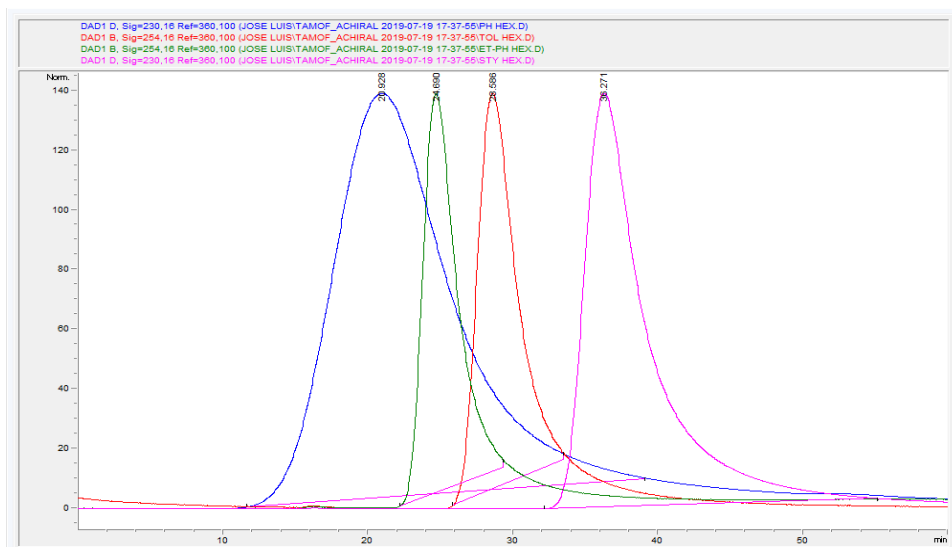
Figure 222. Overlayed chromatograms of benzene, toluene, ethylbenzene and styrene. Conditions: *n*-Hex 0.15 mL min^{-1}, 1 mg mL^{-1}. From left to right: benzene, ethylbenzene, toluene and styrene.

232
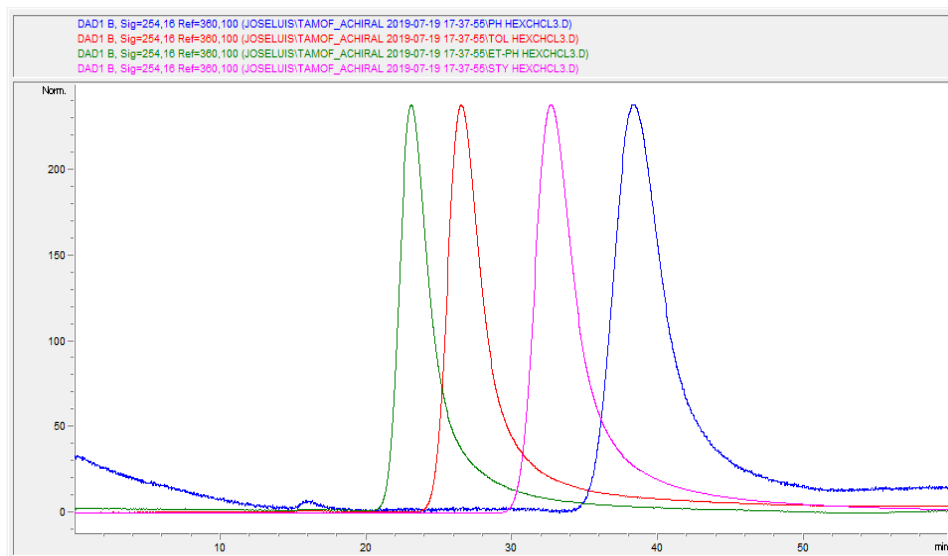
Figure 223. Overlayed chromatograms of benzene, toluene, ethylbenzene and styrene. Conditions: n-Hex/CHCl$_3$ 98:2, 0.15 mL min^{-1}, 1 mg mL^{-1}. From left to right: ethylbenzene, toluene, styrene and benzene.
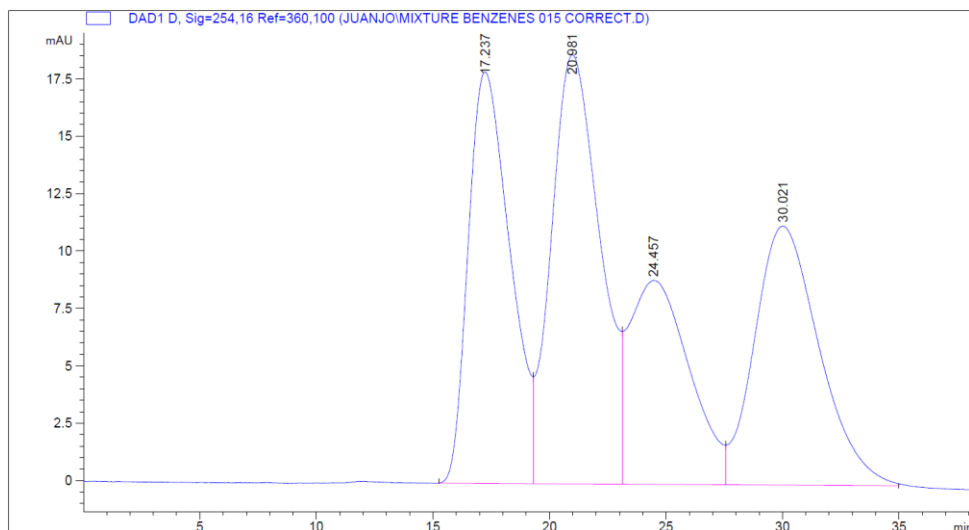
Figure 224. HPLC chromatogram of a mixture of benzene, toluene, ethylbenzene and styrene. Conditions: n-Hex/CHCl$_3$ 97:3, 0.15 mL min^{-1}, 1 mg mL^{-1}. From left to right: ethylbenzene, toluene, styrene and benzene.

Chapter IV

233

Separation of Regioisomeric Mixtures of Achiral Aromatic Compounds Using TAMOF-1
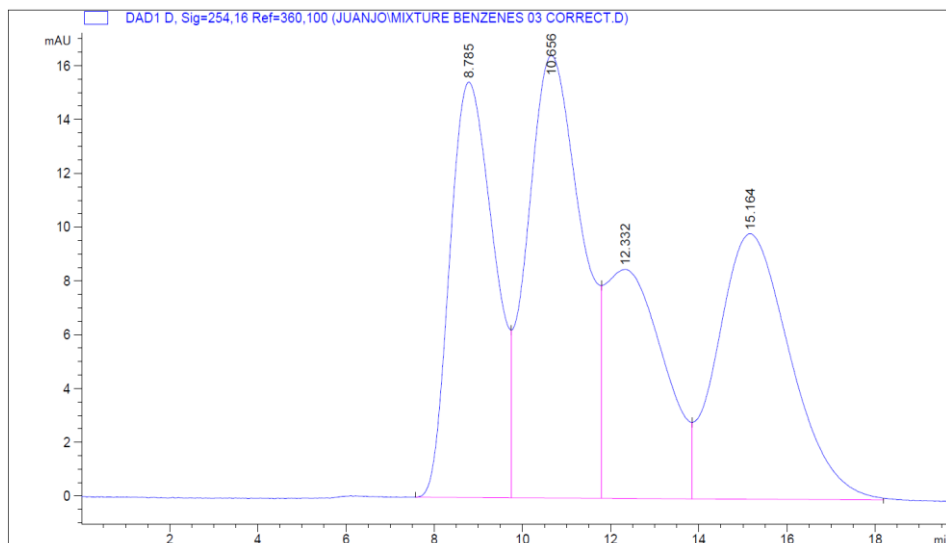
Figure 225. HPLC chromatogram of a mixture of benzene, toluene, ethylbenzene and styrene. Conditions: n-Hex/CHCl$_3$ 97:3, 0.3 mL min^{-1}, 1 mg mL^{-1}. From left to right: ethylbenzene, toluene, styrene and benzene.
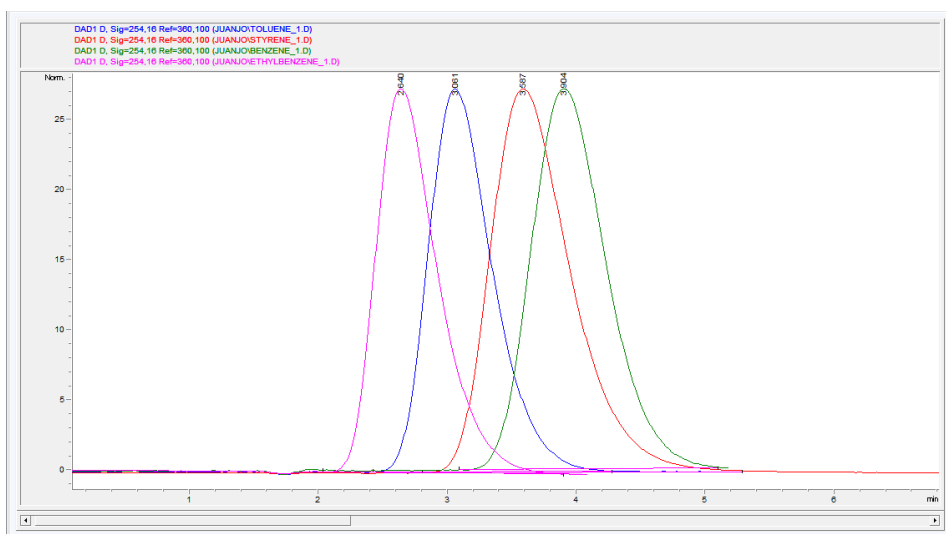
Figure 226. Overlayed chromatograms of benzene, toluene, ethylbenzene and styrene. Conditions: n-Hex/CHCl$_3$ 98:2, 1 mL min^{-1}, 1 mg mL^{-1}. From left to right: ethylbenzene, toluene, styrene and benzene.

234
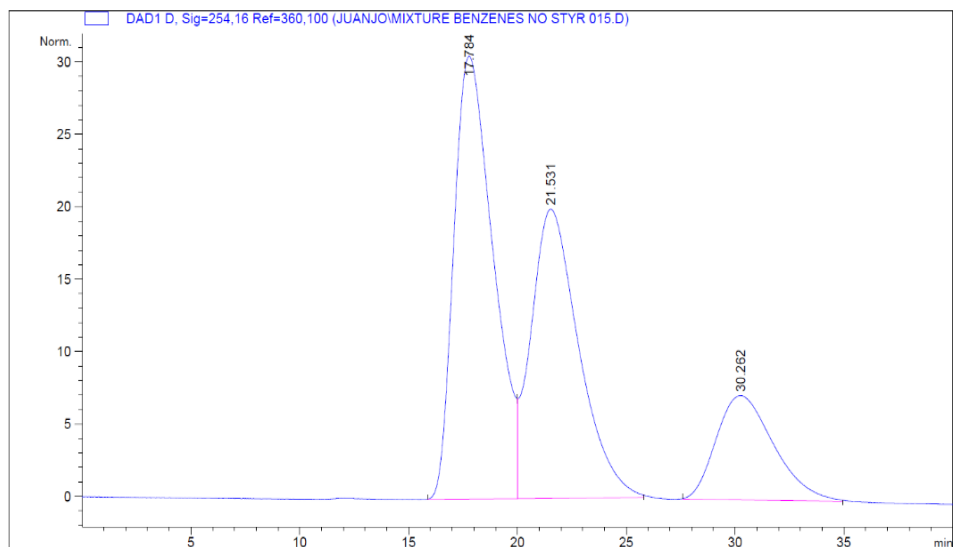
Figure 227. HPLC chromatogram of a mixture of benzene, toluene and ethylbenzene. Conditions: n-Hex/CHCl$_3$ 97:3, 0.15 mL min^{-1}, 1 mg mL^{-1}. From left to right: ethylbenzene, toluene and benzene.

Chapter IV
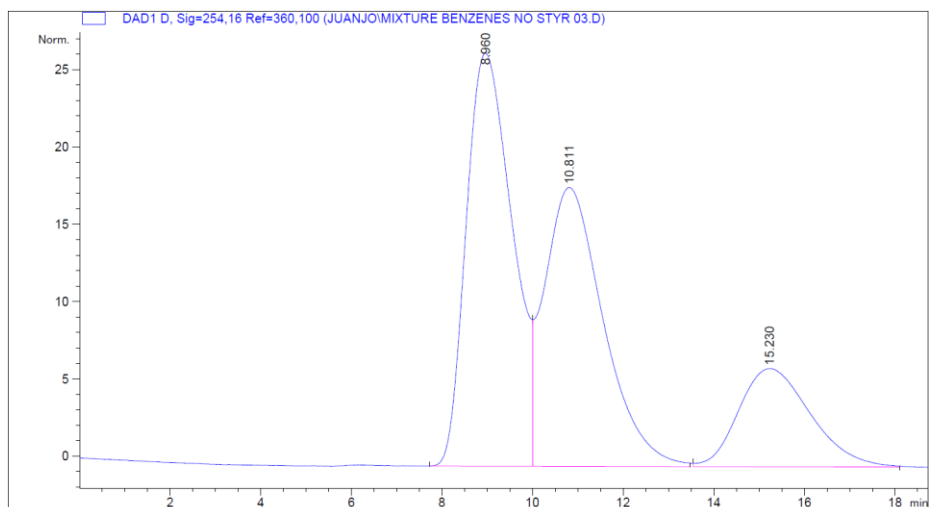
Figure 228. HPLC chromatogram of a mixture of benzene, toluene and ethylbenzene. Conditions: n-Hex/CHCl$_3$ 97:3, 0.3 mL min^{-1}, 1 mg mL^{-1}. From left to right: ethylbenzene, toluene and benzene.

235

Separation of Regioisomeric Mixtures of Achiral Aromatic Compounds Using TAMOF-1
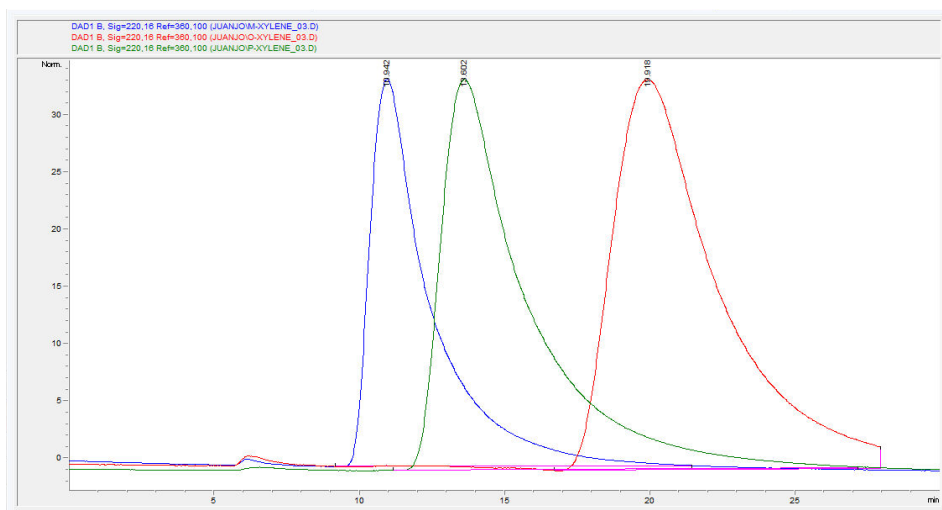
Figure 229. Overlayed chromatograms of *o*-, *m*- and *p*-xylene. Conditions: *n*-Hex, 0.3 mL min⁻¹, 1 mg mL⁻¹. From left to right: *m*-, *p*- and *o*-xylene.
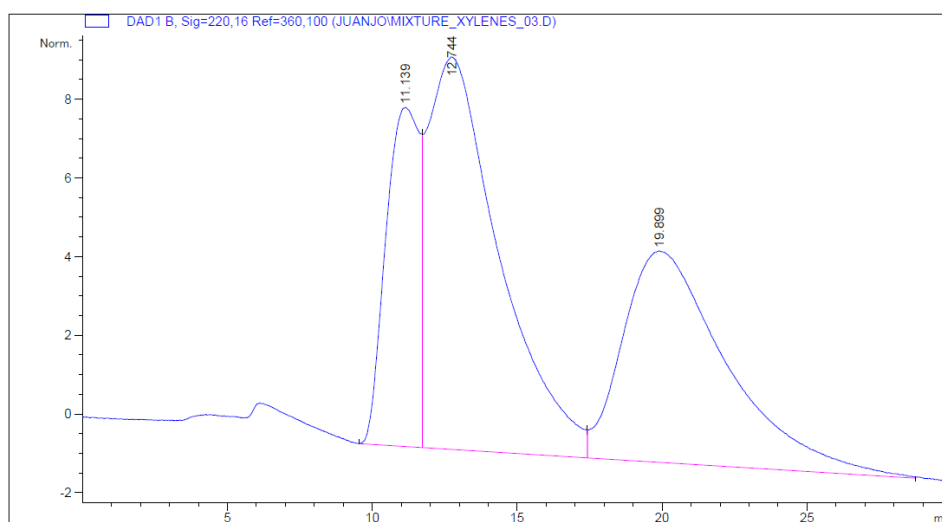
Figure 230. HPLC chromatogram of a mixture of *o*-, *m*- and *p*-xylene. Conditions: *n*-Hex, 0.3 mL min⁻¹, 1 mg mL⁻¹. From left to right: *m*-, *p*- and *o*-xylene.

236
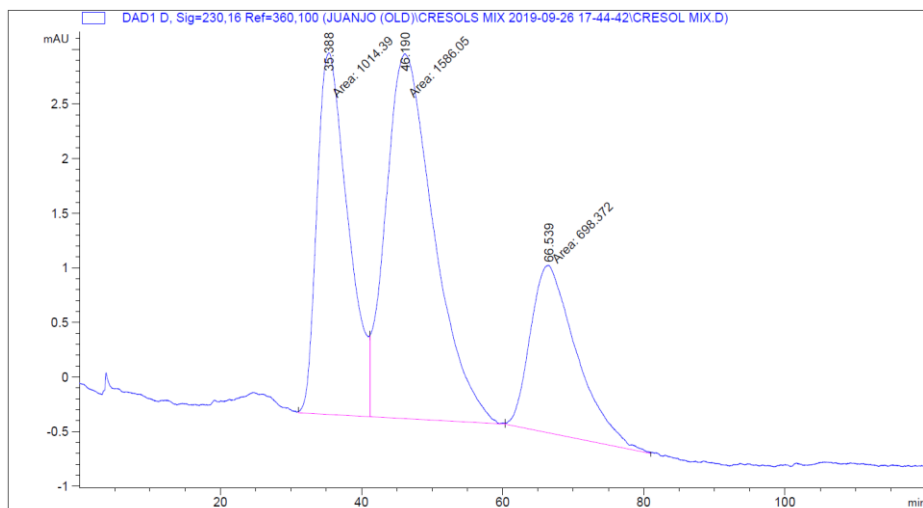
Figure 231. HPLC chromatogram of a mixture of *o*-, *m*- and *p*-cresol. Conditions: *n*-Hex/IPA 95:5, 0.6 mL min⁻¹, 1 mg mL⁻¹. From left to right: *m*-, *p*- and *o*-cresol.

Figure 232. Overlayed chromatograms of *o*-, *m*- and *p*-cresol. Conditions: *n*-Hex/IPA 9:1, 0.6 mL min⁻¹, 1 mg mL⁻¹. From left to right: *m*-, *p*- and *o*-cresol.

237

Separation of Regioisomeric Mixtures of Achiral Aromatic Compounds Using TAMOF-1
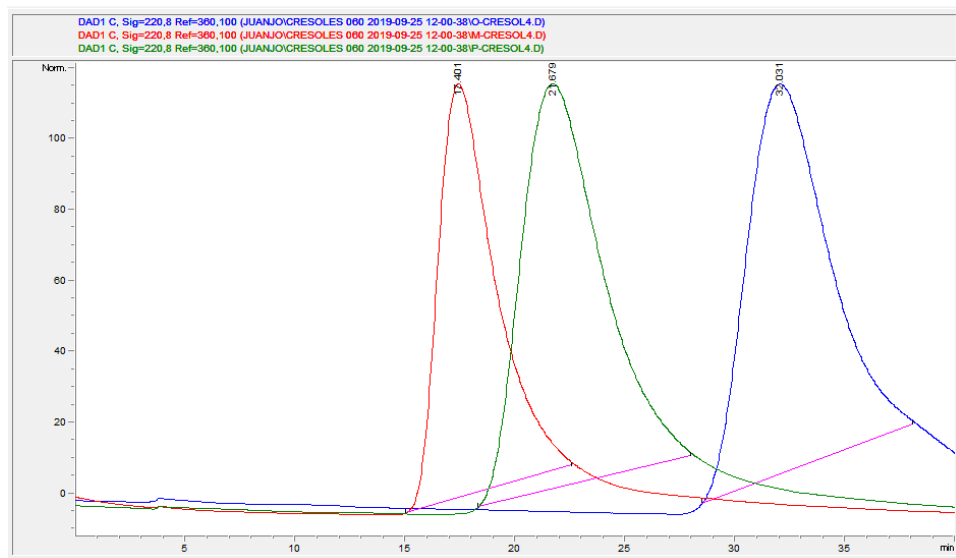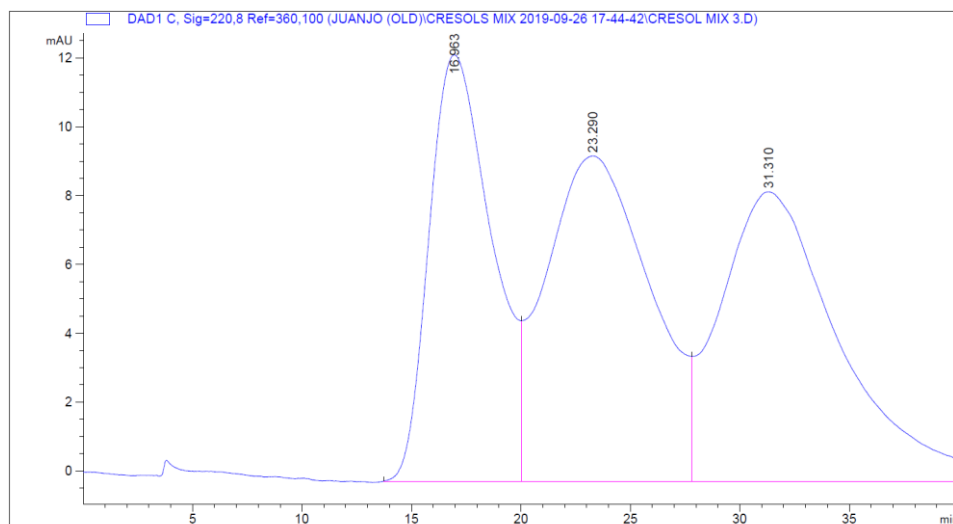
Figure 233. HPLC chromatogram of a mixture of *o*-, *m*- and *p*-cresol. Conditions: *n*-Hex/IPA 9:1, 0.6 mL min⁻¹, 1 mg mL⁻¹. From left to right: *m*-, *p*- and *o*-cresol.

CHAPTER V

Attempts to Expand the TAMOF-1 Family: Synthesis of Structurally Related Ligands

UNIVERSITAT ROVIRA I VIRGILI
INSIGHTS IN HOMOCHIRAL METAL-ORGANIC FRAMEWORKS: FROM THEIR SYNTHESIS TO ENANTIOSELECTIVE
APPLICATIONS
Juanjo Cabezas Giménez

5.1. ABSTRACT

In the search for new CMOFs, we selected an array of structurally related ligands to *S*-HTA with longer distances between the coordinating moieties. Several amino acid derivatives, *i.e.* L-Carnosine, L-Lysine, Homohistidine, 4-amino-L-Phenylalanine and (*S*)-2-amino-3-(1*H*-benzo[*d*]imidazol-2-yl)propanoic acid were successfully transformed into their 4*H*-1,2,4-triazole analogues.

These compounds were fully characterised and further used in coordination attempts with different metal salts in the quest for the obtention of TAMOF-1's analogues, ideally with wider channels and with improved BET surface areas and pore sizes to expand the scope of applications of these materials to underdeveloped enantiomeric separations and enantioselective transformations.

5.2. INTRODUCTION

One of the unique characteristics that make MOFs highly desired materials is pore tunability.[230] This feature allows the design of the size of the pores and the functional groups for interaction with the desired analytes/substrates in terms of size and selective binding. One of the most representative examples of this phenomenon was described in the UiO-X family, where longer ligands drastically increased the pore size (**Figure 234**).[15]
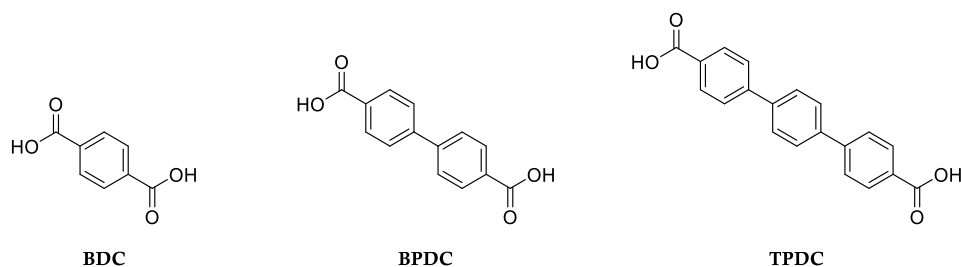
Figure 234. Ligands used in the synthesis of UiO-66 (left), UiO-67 (centre) and UiO-68 (right).

Chapter V

---

[230] (a) Feng, L.; Wang, K.-Y.; Lv, X.-L.; Yan, T.-H.; Zhou, H.-C. *Natl. Sci. Rev.* **2020**, *7*, 1743-1758. (b) Ji, Z.; Wang, H.; Canossa, S.; Wuttke, S.; Yaghi, O. M. *Adv. Funct. Mater.* **2020**, *30*, 2000238.

Attempts to Expand the TAMOF-1 Family: Synthesis of Structurally Related Ligands

The pore tunability methods encompass the design of ligands by modifying their length or adding functional groups oriented towards inside the pore. For instance, the addition of a $-NH_2$ group in the benzylic ring of BDC or the replacement of the phenyl rings with pyridyl groups in BPDC confer the pores with new chemical properties (**Figure 235**).[231]
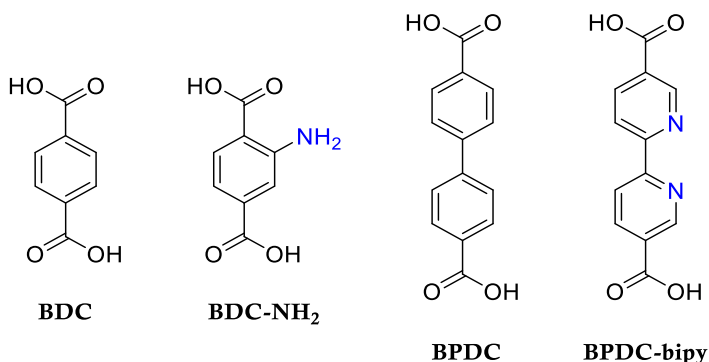
Figure 235. Modification of the UiO-66 and UiO-67 ligands.

The ligand modification can be performed by PSM to avoid inconveniences in the synthetic outcome of the desired MOF. For instance, Maspoch and co-workers reported in 2018 a mixed-ligand MOF where one of the ligands was sensible to ozonolysis, transforming a microporous MOF into a mesoporous one (**Figure 236**).[232]
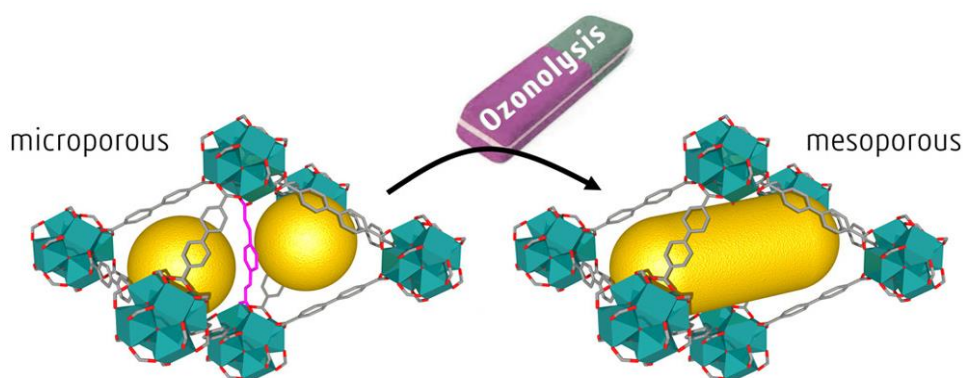
Figure 236. Transformation of a microporous MOF into mesoporous by PSM. Adapted with permission of *J. Am. Chem. Soc.* **2018**, *140*, 15022-15030. Copyright 2018 American Chemical Society.

[231] DeCoste, J. B.; Peterson, G. W.; Jasuja, H.; Glover, T. G.; Huang, Y.-g.; Walton, K. S. *J. Mater. Chem. A* **2013**, *1*, 5642-5650.
[232] Guillerm, V.; Xu, H.; Albalad, J.; Imaz, I.; Maspoch, D. *J. Am. Chem. Soc.* **2018**, *140*, 15022-15030.

242

Another example would be the one reported by Zhou and co-workers in 2017, where they incorporated labile ligand to the MOF PCN-160[233] in different ratios by post-synthetic ligand exchange. The incorporated ligand was known to be easily cleaved by the addition of acetic acid Thus, by using different AcOH concentrations with the different MOFs, they obtained a wide array of hierarchically porous MOFs (**Figure 237**).[234]
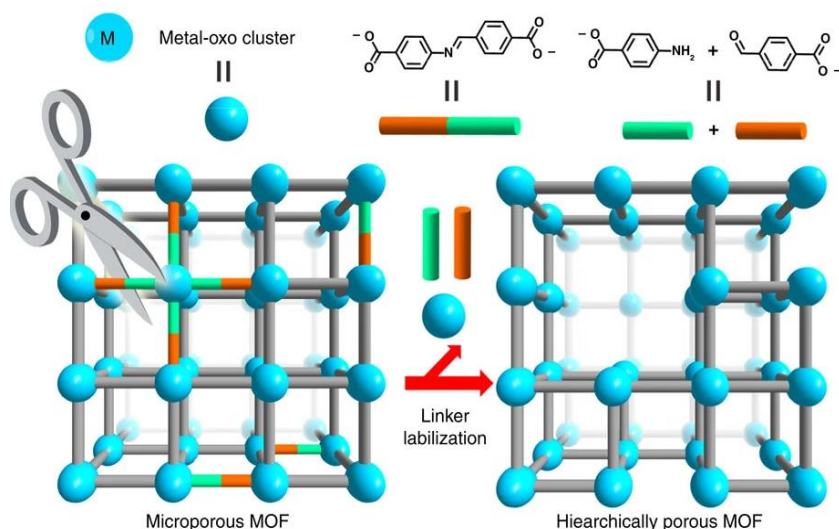
Figure 237. Development of hierarchical porosity by post-synthetic ligand labilisation. Image reproduced from *Nat. Commun.* **2017**, *8*, 15356. Licensed under CC BY 4.0.

Inspired by these examples, we wanted to create further generations of analogues of TAMOF-1 by ligand modification. Due to the robustness of *S*-HTA to be modified by PSM, we aimed at exploring the synthetic transformation of several amino acids into their triazole derivatives and studying their further coordination with Cu^{2+}. In this chapter, to increase the pore size we envisioned the use of ligands similar to *S*-HTA with greater separations between the functional groups involved in the coordination to the metal centre. 4*H*-1,2,4-Triazole motifs derived from different amino acids were synthesised, with different distances and geometries between the coordinating moieties. Once the ligands were properly characterised, we performed an extensive screening of synthetic conditions for the obtention of the corresponding MOFs.

Chapter V

[233] Yang, Q.; Guillerm, V.; Ragon, F.; Wiersum, A. D.; Llewellyn, P. L.; Zhong, C.; Devic, T.; Serre, C.; Maurin, G. *Chem. Commun.* **2012**, *48*, 9831-9833.
[234] Yuan, S.; Zou, L.; Qin, J.-S.; Li, J.; Huang, L.; Feng, L.; Wang, X.; Bosch, M.; Alsalme, A.; Cagin, T.; Zhou, H.-C. *Nat. Commun.* **2017**, *8*, 15356.

UNIVERSITAT ROVIRA I VIRGILI
INSIGHTS IN HOMOCHIRAL METAL-ORGANIC FRAMEWORKS: FROM THEIR SYNTHESIS TO ENANTIOSELECTIVE
APPLICATIONS
Juanjo Cabezas Giménez

Attempts to Expand the TAMOF-1 Family: Synthesis of Structurally Related Ligands

5.3. RESULTS AND DISCUSSION

5.3.1. Synthesis of the ligands

5.3.1.1. Trz-Carnosine-OH (2)

L-Carnosine (**1**), or β-alanyl-L-histidine, is a dipeptide formed by β-alanine and L-Histidine. It is synthesised naturally by the body in the liver, and it is highly concentrated in muscle and brain tissue.[235] The elongation of the ligand through the addition of the β-alanyl moiety by formation of a peptide bond increases the distance between the imidazolyl and the triazolyl groups, thus being a promising ligand for a CMOF with increased pore size.

To find the optimal conditions for the synthesis of (3-(4*H*-1,2,4-triazol-4-yl)propanoyl)-L-histidine **2** (or Trz-Carnosine, **Scheme 21**), we started by emulating the same conditions than those used for the synthesis of *S*-HTA, described in Chapter 1 (these were azine A, EtOH, 80 °C for 72 h). Sadly, these conditions did not yield any conversion.

We decided to modify several components of the reaction, such as the solvent, the temperature, reaction time or pH of the azine to find the optimal conditions for the obtention of **2** (**Table 26**).
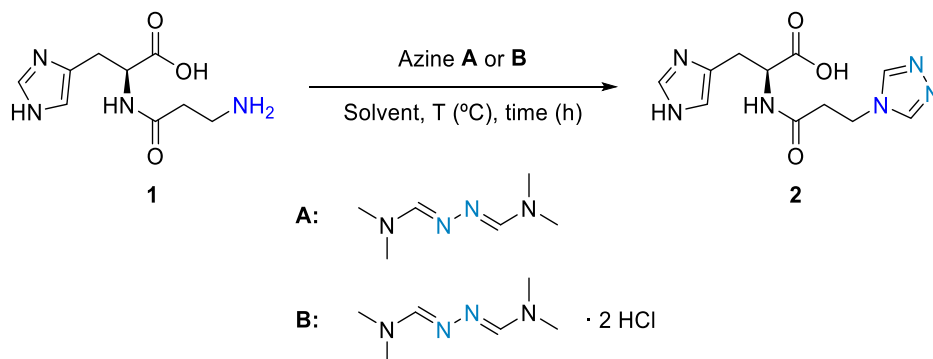
Scheme 21. Schematic synthesis of **2**.

[235] Boldyrev, A. A.; Aldini, G.; Derave, W. *Physiol. Rev.* **2013**, *93*, 1803-1845.

244

Table 26. Screening of the reaction conditions for the synthesis of **2**.

Entry	Solvent	pH	T (ºC)	Time (h)	Azine	Conv. (%)[a]	Yield (%)
1	EtOH	–	80	24	A[c]	–	–
2	H_2O	–	100	24	A[c]	38	–
3	H_2O	6	92	24	A[c]	>95	75
4	H_2O	6	92	72	A[c]	>95	43
5	H_2O	6	92	24	B[d]	>95	57

[a] Calculated by ^{1}H-NMR without internal standard. [b] The adjustment of the pH = 6 was done for the whole reaction mixture. [c] Adjustment of the azine **A** (pH$_0$ ~ 9) to pH = 6 was done with HCl 2M. [d] Adjustment of the azine **B** (pH$_0$ ~ 1) to pH = 6 was done with Na_2CO_3.

Changing the solvent to H_2O (Entries 2–5) allowed us to observe conversion; therefore, we discarded any alcohol as the reaction solvent. By taking the reaction mixture to reflux (Entry 2), a lower conversion was observed than performing the reaction at 92 ºC (Entries 3–5). Comparing reaction times, 24 h of reaction afforded a 75 % yield, but increasing the reaction time to 72 h only yielded a 43 %. Last, we tested the same conditions but with azine B (Entry 5), and the reaction worked smoothly but with a lower yield than with azine A (57 % and 20 %, respectively).

Among many synthetic trials, we manage to isolate monocrystals of compounds **2** (**Figure 238**). The crystal structure allowed us to determine the relative position of the two coordinating moieties in the solid state.
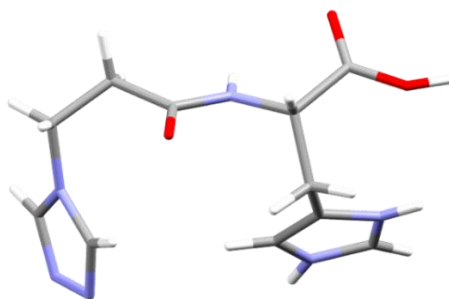
Figure 238. Crystal structure of **2**.

This ligand possesses more DoF than *S*-HTA, *i.e.* flexible alkyl chains that allow free rotation of C_{sp3}–C_{sp3} bonds, thus making it more challenging to create robust bonds between the metallic centre and the nitrogenated moieties. Furthermore, the peptide bond could also coordinate with the metallic salt, preventing the formation of a robust coordination compound.

Chapter V

245

5.3.1.2. Trz-Carnosine-OMe (3)

Prior to the coordination reaction, we envisaged that it would be beneficial to protect the carboxylate as a methyl ester to avoid coordination of the carboxylate group with the Cu^{2+} centre. Then, deprotection of the carboxylate by PSM could yield a structure without counteranions in the channels. This could achieve coordination by the imidazole and triazole moieties, like in TAMOF-1.

We protected **2** as the methyl ester **3** following a literature procedure,[236] where the carboxylate is converted to an acyl halide with thionyl chloride, and then transformed into an ester by reaction with an alcohol (**Scheme 22**).
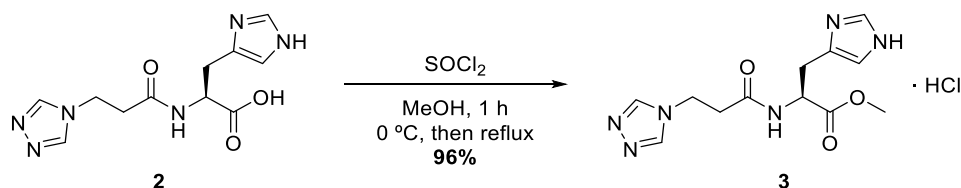
Scheme 22. Synthesis of **3**.

5.3.1.3. Trz-Lysine-OH (5)

L-Lysine **4** is a proteinogenic amino acid with a basic side chain (-$(CH_2)_4NH_2$). This amino acid has two amino groups separated by an alkyl chain, and these amino groups could be transformed into the 4*H*-1,2,4-triazole derivatives to obtain (*S*)-2,6-di(4*H*-1,2,4-triazol-4-yl)hexanoic acid **5**. The distance between the triazole moieties could yield a highly porous material. Thus, we explored the synthesis of **5**.

The synthesis of **5** proceeded smoothly using DMF and PTSA at reflux for 48 h (**Scheme 23**). Furthermore, the only by-product of the reaction was dimethylamine, easily removable by changing the pH of the crude mixture. To accomplish the maximum purity (>95%), purification by flash column chromatography using C_{18}-functionalised silica and H_2O as mobile phase allowed us to isolate **5** in an analytically pure form.

---

[236] Astete, C. E.; Songe Meador, D.; Spivak, D.; Sabliov, C. *Synth. Commun.* **2013**, *43*, 1299-1313.
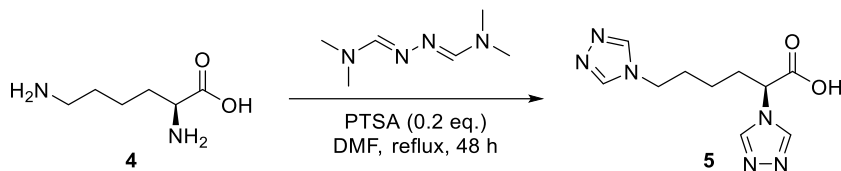
Scheme 23. Schematic synthesis of **5**.

We found in the characterisation process that **5** epimerised at some point of the process. The epimerisation could have been caused by the formation of an imine intermediate catalysed by acid and further hydrolysis (**Scheme 24**). This process has been previously described in the literature, where the use of acetic acid and catalytic amounts of salicylaldehyde at 100 °C yielded D/L-lysine.[237]
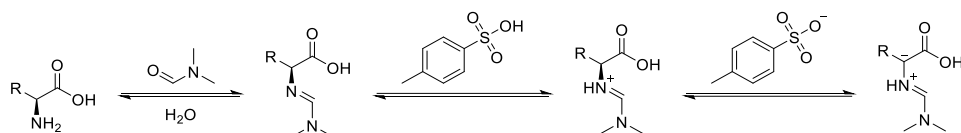
Scheme 24. Proposed route for the epimerisation of **4** in acidic media by Shigeki Yamada and co-workers.

To avoid epimerisation of **5**, we reproduced the synthetic conditions of **2** and, although more by-products were found in the crude (*e.g.* mono triazole products), we were able to isolate **5** with good purity (**Scheme 25**).
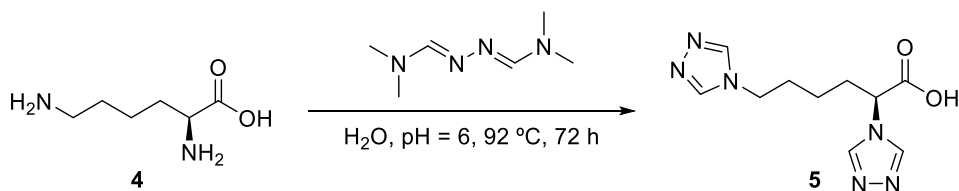
Scheme 25. Schematic synthesis of enantiopure **5**.

Chapter V

---

[237] Yamada, S.; Hongo, C.; Yoshioka, R.; Chibata, I. *J. Org. Chem.* **1983**, *48*, 843-846.

Attempts to Expand the TAMOF-1 Family: Synthesis of Structurally Related Ligands

5.3.1.4. Trz-Homohistidine-OH (13)

In search of new ligands for a second generation of TAMOF-1, we came up with the idea of expanding the alkyl chain of L-histidine. Expanding the alkyl chain of L-histidine by one methylene unit results in **homohistidine**.

Homohistidine (**12**) can be synthesised following a 6-step synthesis, with urocanic acid **6** as starting material (**Scheme 26**).[238]
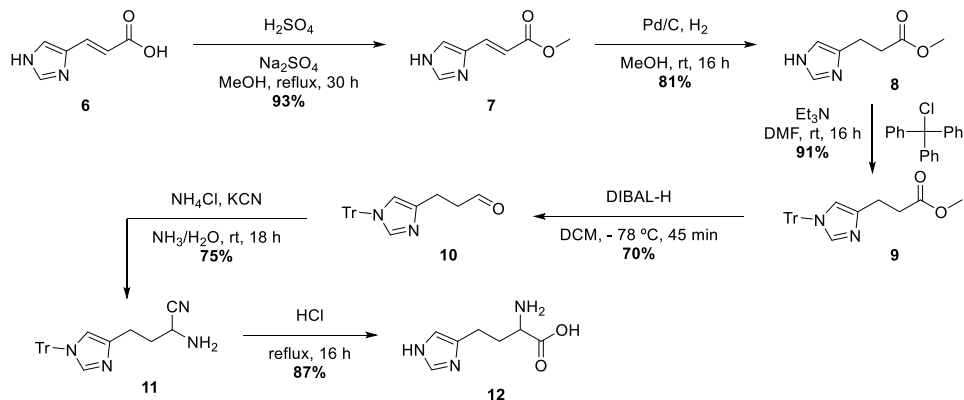
Scheme 26. Synthetic route for the obtention of homohistidine **12**.

The synthetic route comprises several synthetic transformations, *i.e.* esterification, hydrogenation of double bonds, imidazole protection with trityl chloride, reduction of an ester group to an aldehyde and, from this point, **12** is synthesised by the Strecker process for the synthesis of α-amino acids.[239] Finally, **12** is converted into Trz-homohistidine **13** by transamination of DMFA (**Scheme 27**).
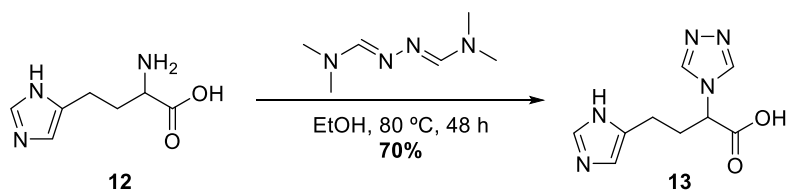
Scheme 27. Synthetic scheme for the obtention of **13**.

[238] Pirrung, M. C.; Pei, T. *J. Org. Chem.* **2000**, *65*, 2229-2230.
[239] Strecker, A. *Justus Liebigs Ann. Chem.* **1850**, *75*, 27-45.

Curiously, despite following a synthetic route for the obtention of racemic **13**, when crystals were found in the RBF and were analysed by single-crystal X-ray diffraction, we found that the compound crystallises as a conglomerate (a 1:1 mixture of enantiopure (*R*)- or (*S*)-**13** crystals (**Figure 239**)).
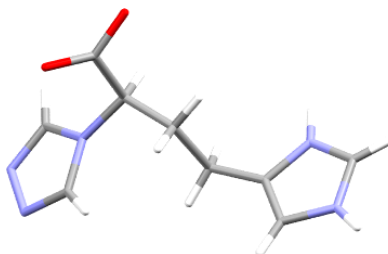
Figure 239. Crystal structure of **13**.

This is a common phenomenon in the crystallisation process of organic molecules, called conglomerate crystallisation, and approximately 10% of the racemates known to date belong to this group.[240] The space group of the crystal is *P*2$_1$, therefore chiral.[241]

5.3.1.5. Trz-4-amino-L-Phenylalanine-OH (16)

Until this point, the ligands explored for the 2nd generation of TAMOF-1 contained longer alkyl chains than L-Histidine, conferring the ligands higher flexibility or solubility, which could be at the origin of the complex formation of extended networks from the solution. For this reason, we looked into a ligand with two 4*H*-1,2,4-triazole moieties separated by a rigid spacer between them – like a phenyl ring.

L-phenylalanine is an amino acid containing a phenyl ring in the side chain. If this amino acid contained an amino functional group in the *para* position of the phenyl ring, we could transform it into a 4*H*-1,2,4-triazole group altogether with the α-amino group, and a ligand with two coordinating moieties with a longer distance between them would be formed. We explored the transformation of the amino groups into triazoles to obtain (*S*)-3-(4-(4*H*-1,2,4-triazol-4-yl)phenyl)-2-(4*H*-1,2,4-triazol-4-yl)propanoic acid **16**.

[240] Lorenz, H.; Perlberg, A.; Sapoundjiev, D.; Elsner, M. P.; Seidel-Morgenstern, A. *Chem. Eng. Process.* **2006**, *45*, 863-873.
[241] Pidcock, E. *Chem. Commun.* **2005**, 3457-3459.

Chapter V

Attempts to Expand the TAMOF-1 Family: Synthesis of Structurally Related Ligands

The design of the synthetic route comprised the transamination of DMFA with both amino groups separately, for one of them is alkylic and the other, arylic – they would require different reaction conditions. For this reason, we decided to selectively protect the aryl amino group with Fmoc-Cl[242] first to transform the α-amino group following a literature procedure,[243] then finally deprotect it and transform the aryl amino group into the desired triazole derivative (**Scheme 28**).
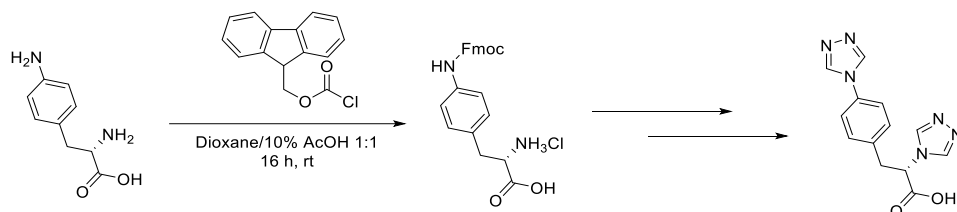
Scheme 28. Planned synthetic route for the synthesis of **16**.

The reaction conditions for the formation of the first 4*H*-1,2,4-triazole required an acid in catalytic amounts at reflux in toluene. We observed that the Fmoc protecting group was removed in the process, but we also observed that the protected amino group was successfully transformed into the desired 4*H*-1,2,4-triazole altogether with the α-amino group in good yields (**Scheme 29**).
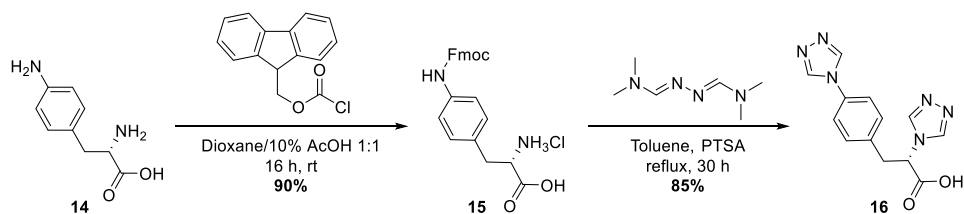
Scheme 29. Synthetic route for the obtention of **16**.

[242] Perron, V.; Abbott, S.; Moreau, N.; Lee, D.; Penney, C.; Zacharie, B. *Synthesis* **2009**, *2009*, 283-289.
[243] Tahli, A.; Elshaarawy, R. F. M.; Köc, Ü.; Kautz, A. C.; Janiak, C. *Polyhedron* **2016**, *117*, 579-584.

5.3.1.6. (*S*)-3-(1*H*-benzo[*d*]imidazol-2-yl)-2-(4*H*-1,2,4-triazol-4-yl)propanoic acid (19)

The last ligand designed possesses a close structure to *S*-HTA, but instead of an imidazolyl moiety, it contains a benzo[*d*]imidazole ring system (**Figure 240**). The hydrophobicity of the additional benzene ring could limit the solvent uptake inside the pores, facilitating the activation process.
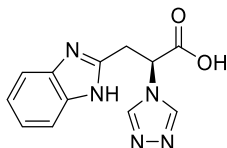
Figure 240. Structure of **19**.

This ligand, (*S*)-3-(1*H*-benzo[*d*]imidazol-2-yl)-2-(4*H*-1,2,4-triazol-4-yl) propanoic acid **19**, is affordable in two steps, starting with the condensation of *o*-phenylenediamine dihydrochloride and L-aspartic acid **17** to yield the benzimidazole moiety **18** (**Scheme 30**).[244] Then, the α-amino group is transformed to the corresponding triazole by transamination of DMFA following a similar procedure to the one described for the previous examples. The overall yield is low (25 %), but **19** is obtained pure.
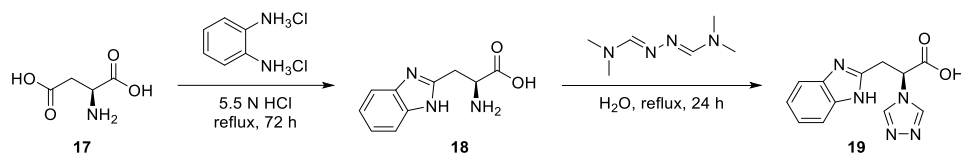
Scheme 30. Synthetic route for the obtention of **19**.

5.3.2. Coordination compounds

After successfully synthesising and properly characterising the ligands described in the previous section, we tried synthesising coordination compounds – ideally porous MOFs – using several transition and lanthanide metallic salts. The synthetic procedures and characterisation of the resulting coordination experiments are described in the sections that follow.

---

[244] Do Quyen-Quyen, T.; Guo, C.; Humphries Paul, S.; Marakovits Joseph, T.; Dong, L.; Hou, X.; Johnson Mary, C. WO 2006/040646 A1, 2006.

Attempts to Expand the TAMOF-1 Family: Synthesis of Structurally Related Ligands

5.3.2.1. Cu-2

The exploration of the coordination of **2** with Cu^{2+} began by replicating the experimental conditions for the synthesis of TAMOF-1 (**Scheme 31**).
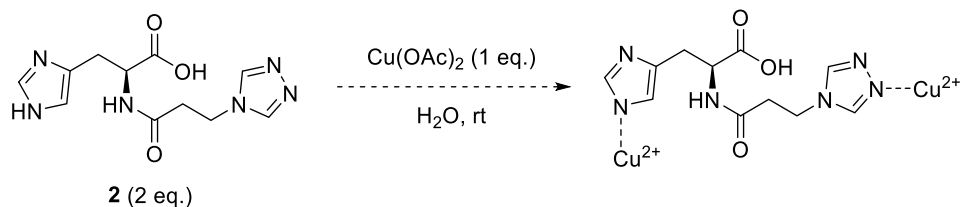
Scheme 31. Schematic synthesis of the coordination compound **Cu-2**.

In order to discard any pH incompatibilities, we experimentally measured the pK_a of **2** (**Figure 241**). Titration of an acidified solution of **2** with NaOH 0.1 N allowed the determination of its pK_a values (pK_{a1} = 5.0 and pK_{a2} = 9.19).
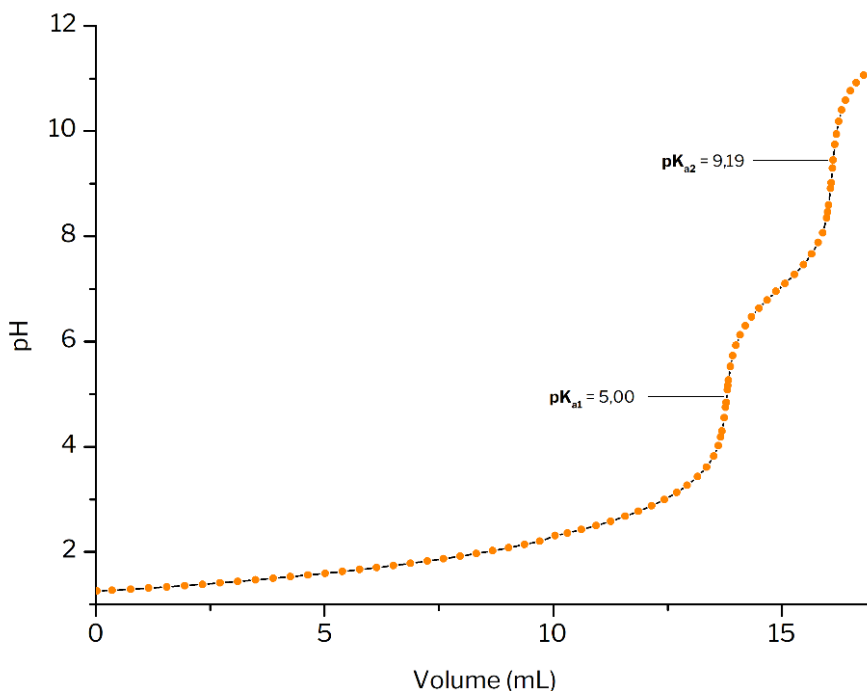
Figure 241. Determination of the pK_a values of **2** by titration with 0.1 N NaOH.

Analogously to *S*-HTA (page **52**), the pK_a values were assigned to the carboxylate (pK_{a1} = 5.0) and the imidazole ring (pK_{a2} = 9.19). Sadly, no precipitate was obtained by reproducing the synthetic conditions of TAMOF-1. Therefore, we decided to expand the screening conditions by using different Cu^{2+} salts, solvents and temperatures.

The use of Cu^{2+} salts under the same reaction conditions for the synthesis of TAMOF-1 was unsuccessful. At this point, we started a collaboration with Dr. Carlos Martí-Gastaldo in the Institute of Molecular Science (ICMol). After exploring other conditions, we obtained a blue polycrystalline powder by replacing the reaction solvent for MeOH in layering conditions (**Figure 242**).
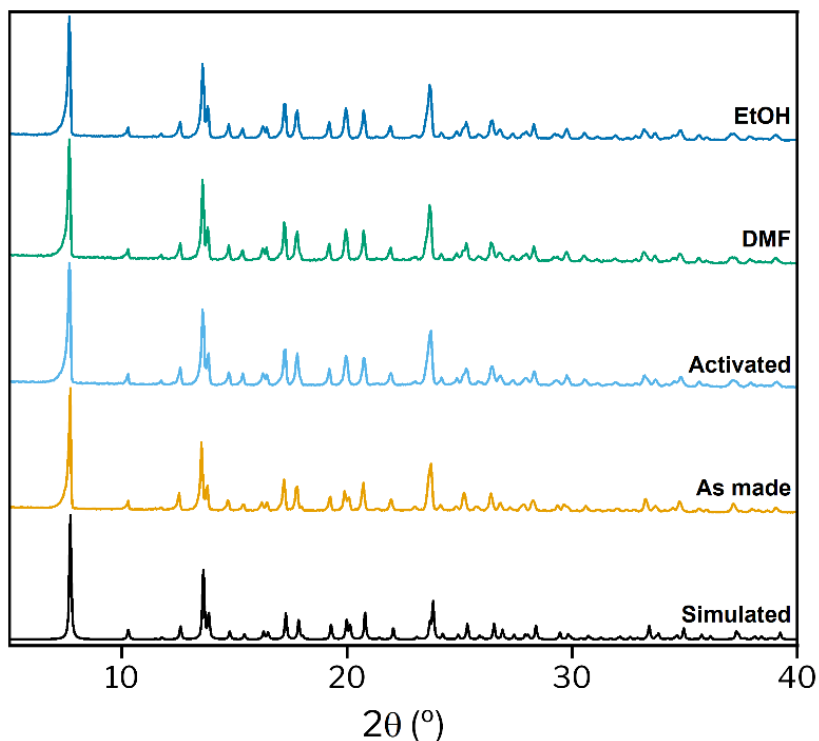
Figure 242. PXRD of the polycrystalline powder **Cu-2**. From top to bottom: as made, activated 4 h at 80 °C, soaked in DMF and soaked in EtOH.

We observed that the structure is quite robust as no significant structural changes were observed after activation *in vacuo* or after soaking the material in DMF or EtOH. TGA analysis (**Figure 243**) showed that the solid is stable up to 200 °C, and N_2 adsorption isotherm showed that **Cu-2** was, unfortunately, non-porous.

Chapter V

253

Attempts to Expand the TAMOF-1 Family: Synthesis of Structurally Related Ligands
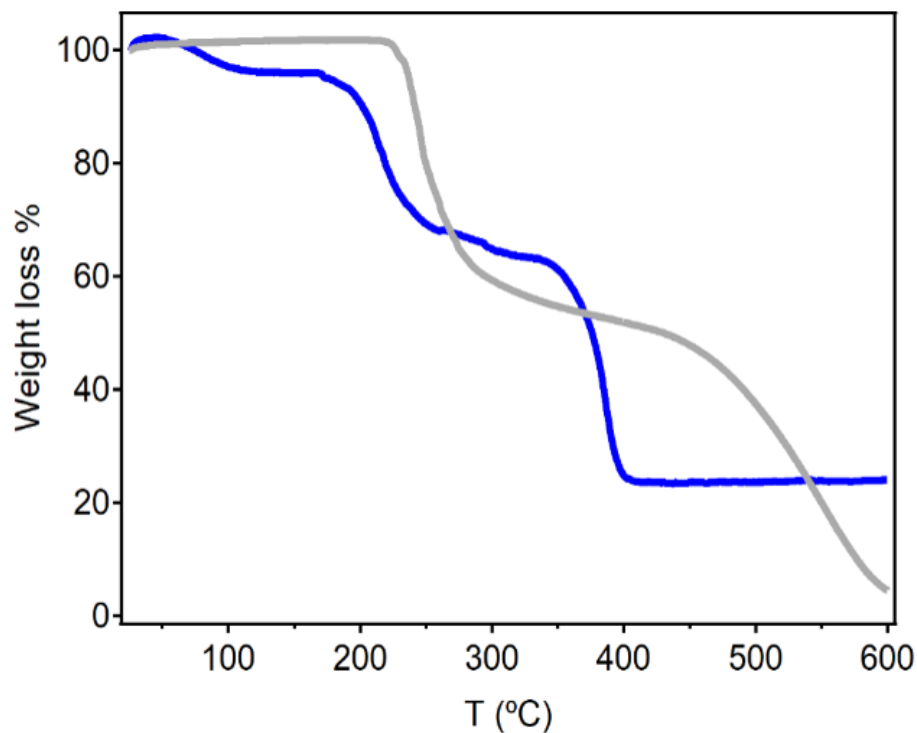
Figure 243. TGA of the coordination compound **Cu-2** (blue) and **2** (grey).

Single crystals of **Cu-2** were obtained by slow diffusion in a layering tube. Single-crystal X-ray structure of **Cu-2** showed that the Cu^{2+} centres are coordinated to two triazoles, one imidazole, one carboxylate group, one water molecule and a bridging water molecule (**Figure 244**).
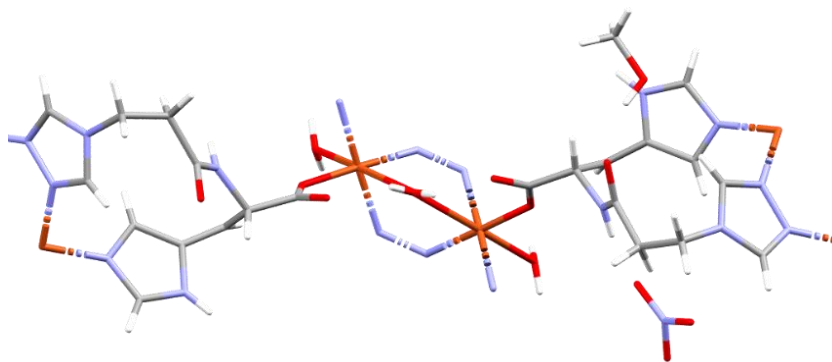
Figure 244. Crystal structure of **Cu-2**.

254

The coordination of the carboxylate moiety with the Cu^{2+} makes the structure require a counteranion, specifically NO_3^- groups. The fact that the structure contains counteranions negatively affects the porosity of the material, as seen in BET analysis and the crystal structure (**Figure 245**).
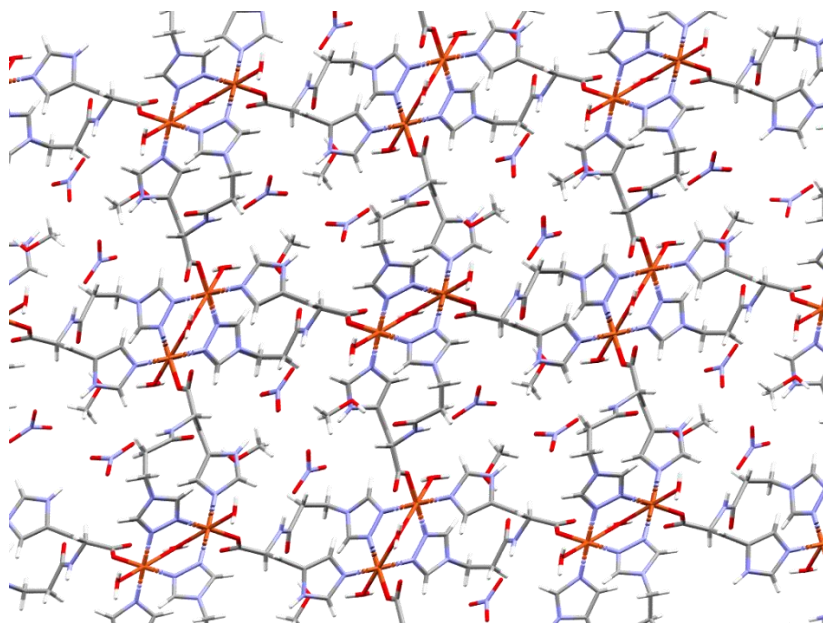
Figure 245. Layered structure of **Cu-2**.

We repeated the experimental conditions for the obtention of **Cu-2** with ligand **3**, and no precipitate was observed after days. A plausible explanation for the unsuccessful trial to reproduce the synthesis of TAMOF-1 with **2** and **3** is that the coordination conditions change radically by increasing the number of DoF.

5.3.2.2. Zn-5

With ligand **5** in hand, we found that mixing the ligand with $ZnCl_2$ in water under solvothermal conditions (100 ºC) yielded a white crystalline solid, which was named **Zn-5**.

Single-crystal X-ray diffraction of **Zn-5** was collected at 298 K (**Figure 246**). The solid crystallised in the chiral monoclinic space group $P2_1$. The asymmetric unit contains two molecules of **5** and two Zn^{2+} ions, compensated by two Cl^- ions and two carboxylates (–COO$^-$). Zn^{2+} showed a tetrahedral

Chapter V

environment, which is connected to two triazoles of two different **5** molecules, one carboxylate of a third **5** molecule, and a chlorido ligand.
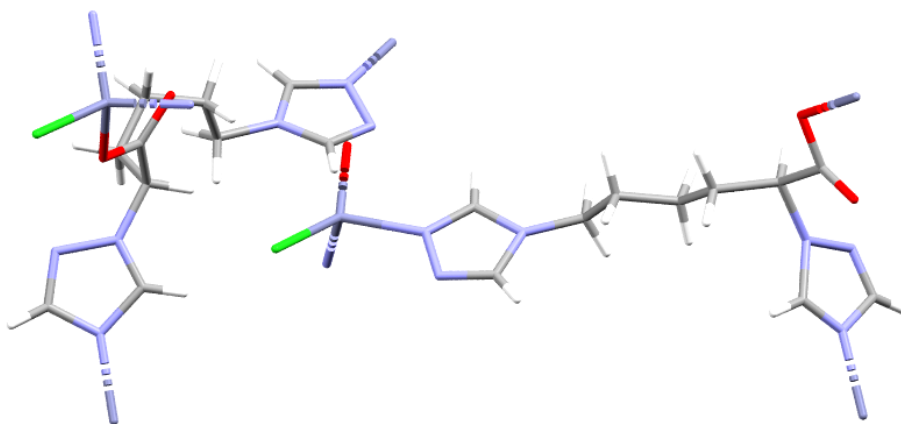
Figure 246. Crystal structure of **Zn-5**.

Zn-5 is a 2D MOF – each Zn is connected to two triazole moieties that form a 1D chain, and the carboxylates link the 1D chains forming a 2D layer (**Figure 247**). The fourth position that should connect the 2D layers is occupied by the chloride counteranion, thus prohibiting the formation of a 3D network and drastically reducing the porosity of **Zn-5**.
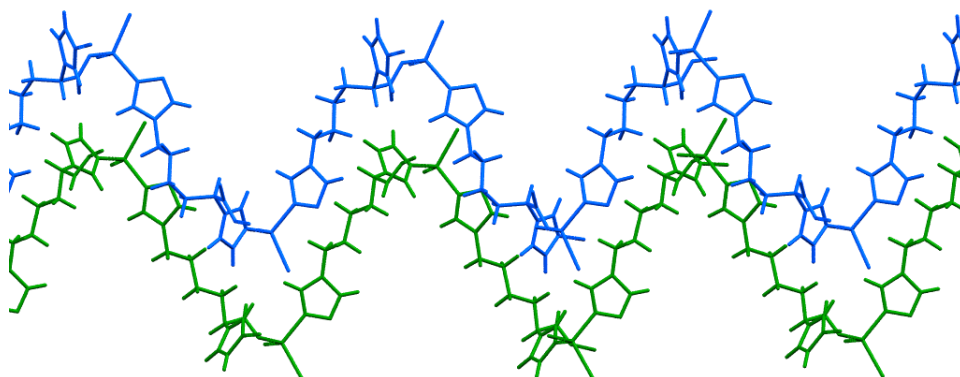
Figure 247. Layered structure of **Zn-5**. Green and blue colours denote the different 2D layers.

Thermogravimetric analysis (TGA) showed that **Zn-5** has excellent thermal stability, being stable up to 340 ºC (**Figure 248**). The BET surface area

of **Zn-5** is low, precisely 95 $m^2 g^{-1}$, which is consistent with that for every Zn^{2+} centre, there is a chloride anion bonded, reducing the pore volume drastically due to the two-dimensional structure.
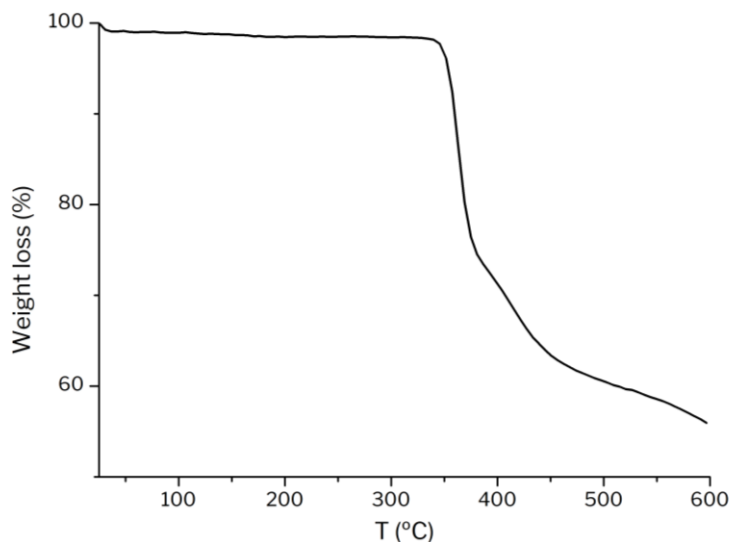
Figure 248. TGA of the coordination compound **Zn-5**.

5.3.2.3. Cu-5

Following the steps taken in the previous section, coordination of Cu^{2+} with ligand **5** was achieved with the same conditions but using $Cu(BF_4)_2$ as a metal salt, yielding green crystals. Single-crystal X-ray diffraction of **Cu-5** was also examined at 298 K (**Figure 249**). The solid crystallised in the tetragonal space group $P4_2/m$. It is a complex structure in which the asymmetric unit is formed by one ligand **5**, three Cu^+ metallic centres, one Cu^{2+}, two BF_4^- counteranions, a bridging H_2O molecule and two chloride anions (Cl^-)

This structure comprises cages constructed of four ligand **5** units and eight Cu^+ centres. The Cu^+ ions appear as a result of the reduction of Cu^{2+} in the reaction, probably due to oxidation of the organic ligand. Each carboxylate binds with a Cu^{2+} centre, which is square planar (as in dehydrated TAMOF-1) and holds together four cages. Analysis by TGA showed that this coordination compound is thermally stable up to 200 °C (**Figure 250**).

A similar analysis to that made for **Zn-5** revealed that **Cu-5** was not a porous structure, which was further confirmed by N_2 adsorption/desorption isotherms with a BET surface area of 9 $m^2 g^{-1}$.

Chapter V

257

Attempts to Expand the TAMOF-1 Family: Synthesis of Structurally Related Ligands
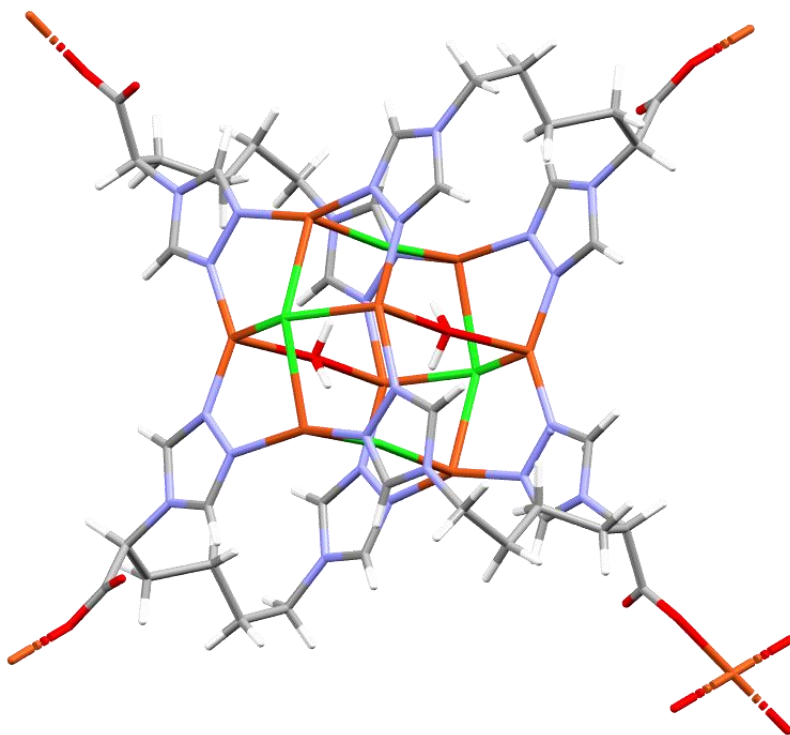
Figure 249. Structure of **Cu-5**. Solvent and BF_4^- ions are omitted for clarity.
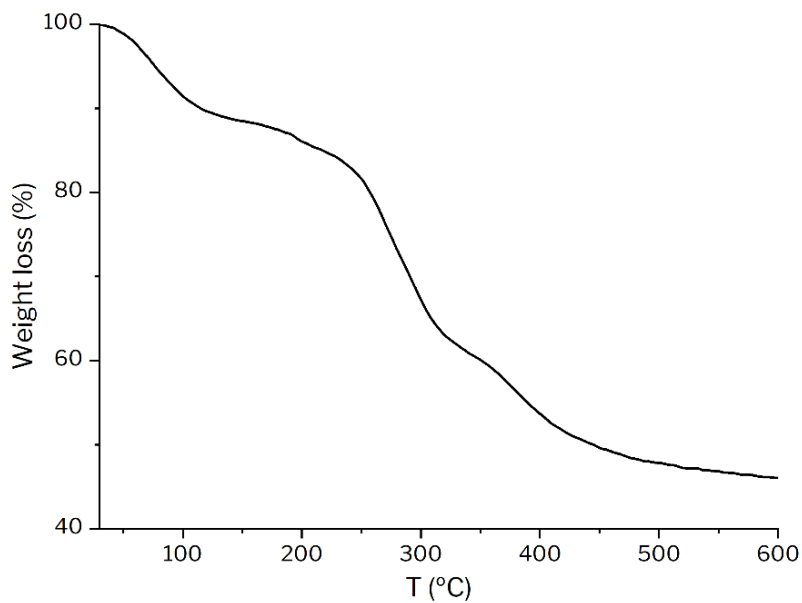
Figure 250. TGA of the coordination compound **Cu-5**.

258

5.4. CONCLUSIONS

Six new ligands containing 4*H*-1,2,4-triazole moieties, five of them enantiopure, have been successfully synthesised and characterised. The scaling up of ligand **2** allowed us to obtain up to 20 g of product.

Minor changes in the structure of the ligand have translated into major changes in the porosity. Contrary to *S*-HTA, coordination complexes of ligands **2** and **5** with Cu and Zn precursors have led to non-porous coordination networks.

These new ligands have undergone complexation tests with different metal salts to obtain new metal-organic frameworks. All attempts made yielded non-porous MOFs with interesting and complex structures. Due to time restraints, the main effort was put in synthesising, purifying, and characterising the organic ligands rather than in the coordination chemistry. Furthermore, difficulties in scaling up most of the ligands severely limited the number of experiments that could be performed.

Chapter V

259

Attempts to Expand the TAMOF-1 Family: Synthesis of Structurally Related Ligands

5.5. EXPERIMENTAL SECTION

5.5.1. Materials and general

All syntheses were carried out on chemicals purchased from commercial sources unless otherwise indicated. Air and moisture sensitive manipulations or reactions were run under inert atmosphere using anhydrous solvents and Schlenk techniques. All solvents were purchased commercially anhydrous or dried using a Solvent Purification System (SPS). NMR spectra were recorded on a Bruker Advance 300, 400 or 500 MHz Ultrashield spectrometers. ^{1}H and ^{13}C-NMR chemical shifts are quoted in ppm relative to residual solvent peaks. Data for ^{1}H-NMR are given as follows: chemical shift, multiplicity (s = singlet, d = doublet, t = triplet, m = multiplet, dd = doublet of doublets, tt = triplet of triplets), coupling constants and intensities. High-resolution mass spectra (HRMS) were recorded by using ESI as ionisation method in positive mode. IR spectra were recorded using Attenuated Total Reflection (ATR) spectroscopy. Specific optical rotation ($[\alpha]_\lambda^T$) was recorded using a Jasco P1030 Polarimeter with a wavelength of 589 nm (sodium, D line) at 25 ºC in the corresponding solvent, in a 10 cm cell, unless otherwise indicated. Powder X-ray diffraction analysis was performed using a Bruker Apex II Duo Single-crystal Diffractometer. N_2 adsorption/desorption isotherms were recorded at 77 K using an AUTOSORB-6 apparatus. TGA was performed in a thermogravimetric balance Mettler Toledo TGA/SDTA851. DMFA and *S*-HTA synthesis are described in Chapter 1, page **48**.

5.5.2. Synthesis of Trz-Carnosine-OH (2)

DMFA (1.26 g, 8.84 mmol) was dissolved in H_2O (7 mL, 0.62 M), then the pH was adjusted to pH = 6 with 2 M HCl. **1** (1 g, 4.42 mmol) was added to the solution, and the reaction mixture was heated to 92 ºC and stirred overnight. The reaction mixture was left to cool at rt, filtered and the solvent was removed *in vacuo*. The solvent was concentrated *in vacuo*, the residue dispersed in MeOH and filtered to yield **2** as a white solid (928 mg, 75%). **^{1}H NMR** (400 MHz, D_2O) δ 8.53 (dd, J =1.5 Hz, 1H, H$_1$), 8.41 (s, 2H, H$_2$), 7.01 (s, 1H, H$_3$), 4.50 – 4.38 (m, 2H, H$_4$), 4.38 – 4.29 (m, 1H, H$_5$), 3.20 (dd, J = 15.6, 4.0, 1H, H$_6$), 2.97 (dd, J = 15.6, 9.3 Hz, 1H, H$_7$), 2.89 – 2.74 (m, 2H, H$_8$) ppm. **^{13}C NMR** (101 MHz, D_2O): δ 176.2 (C, C$_a$), 171.4 (C, C$_b$), 143.9 (CH, C$_c$), 133.1 (CH, C$_d$), 129.6 (C, C$_e$), 116.3 (CH, C$_f$), 53.8 (CH, C$_g$), 41.3 (CH$_2$, C$_h$), 36.0 (CH$_2$, C$_i$), 27.2 (CH$_2$, C$_j$) ppm. **HRMS-ESI-TOF** (*m/z*): [M+H]$^+$

calcd for $C_{11}H_{15}N_6O_3$, 279.1200; found, 279.1199. **[α]$_D^{25}$**= -4.36 (c = 1.4, H_2O). **IR** (neat, cm^{-1}) $\bar{v}$ 3305, 3110, 2853, 1631, 1539, 1435, 1375, 1293, 1173, 1077, 983, 817, 621. **mp** 216.3 – 216.5 °C (decomposition).

5.5.3. Synthesis of Trz-Carnosine-OMe (3)

2 (2 g, 7.19 mmol) was suspended in MeOH (80 mL, 0.09 M) and the suspension was cooled to 0 °C. Then, $SOCl_2$ (1 mL, 13.8 mmol) was added dropwise to the suspension, and it was stirred until no solid was observed (10 min). Then, the reaction mixture was stirred at reflux for 1 h. The reaction mixture was left to cool at rt, then the solvent was removed *in vacuo* to yield quantitatively **3** as a white solid. *The solid was kept in the glovebox due to its highly hygroscopic nature.* **¹H NMR** (500 MHz, D_2O) δ 9.08 (s, 2H), 8.63 (s, 1H), 7.26 (s, 1H), 4.58 (t, *J* = 6.2 Hz, 2H), 3.76 (s, 3H), 3.34 (dd, *J* = 15.6, 5.4 Hz, 2H), 3.16 (dd, *J* = 15.6, 9.0 Hz, 1H), 3.05 – 2.85 (m, 2H). **¹³C NMR** (126 MHz, D_2O) δ 172.29, 171.89, 144.01, 133.85, 128.87, 117.39, 53.60, 52.08, 43.24, 35.13, 26.28. **HRMS-ESI-TOF** (*m/z*): [M+H]$^+$ calcd for $C_{12}H_{17}N_6O_3$, 293.1300; found, 293.1356. **[α]$_D^{25}$**= -2.82 (c = 1.0, MeOH). **IR** (neat, cm^{-1}) $\bar{v}$ 3233, 3122, 3014, 2837, 1730, 1656, 1652, 1543, 1437, 1399, 1214, 1176, 1038, 942, 831, 624.

5.5.4. Synthesis of Trz-Lysine-OH (5)

DMFA (17.6 mmol, 2.5 g) was dissolved in H_2O (0.6 M), and the pH of the solution was adjusted to pH = 6 with 2 M HCl. Then, **4** (4.4 mmol, 0.64 g) was added to the solution, and the reaction mixture was stirred at 92 °C for 48 h. The solvent was concentrated *in vacuo*, and the crude was redissolved in a solution of KOH (2 eq.) in EtOH (10 mL). Et_2O (20 mL) was added to the solution, and after a few minutes, an oil precipitated. The crude oil was redissolved in EtOH, and the pH was adjusted to pH = 4 with HCl 2M. The KCl precipitate was filtered, and the solution was concentrated *in vacuo* to give **5** as a yellow oil (685 mg, 62%). **¹H NMR** (300 MHz, D_2O) δ 8.72 (d, *J* = 7.1 Hz, 4H), 4.92 (dd, *J* = 9.7, 5.3 Hz, 1H), 4.17 (t, *J* = 7.1 Hz, 2H), 2.32 – 2.17 (m, 1H), 2.17 – 2.02 (m, 1H), 1.99 – 1.79 (m, 2H), 1.39 – 1.11 (m, 2H). **¹³C NMR** (126 MHz, D_2O) δ 174.88, 143.92, 61.67, 49.24, 45.99, 31.94, 29.11, 22.50. **HRMS-ESI-TOF** (*m/z*): [M–H]$^-$ calcd for $C_{10}H_{13}N_6O_2$, 249.1200; found, 249.1105. **[α]$_D^{25}$**= +18.5 (c = 0.6, H_2O). **IR** (neat, cm^{-1}) $\bar{v}$ 3382, 3111, 2954, 2870, 2785, 1720, 1618, 1529, 1464, 1376, 1188, 1077, 1022, 995, 874, 635.

Chapter V

Attempts to Expand the TAMOF-1 Family: Synthesis of Structurally Related Ligands

5.5.5. Synthesis of Trz-homohistidine-OH (13)

5.5.5.1. Methyl urocanate (7)

6 (10 g, 72.4 mmol) and anhydrous Na_2SO_4 (1.41 g, 9.85 mmol) were added to anhydrous MeOH (105 mL, 0.68 M). Concentrated H_2SO_4 (5.7 mL, 101 mmol) was added to the reaction mixture, and it was stirred at reflux overnight. The solid was filtered, and the solvent was concentrated *in vacuo*. The resulting solid was dissolved in a small amount of water (10 mL) and further neutralised with $NaHCO_3$ (sat) until no CO_2 evolved. The aqueous fraction was then extracted with EtOAc, dried over Na_2SO_4 and concentrated *in vacuo* to give **7** as a white solid (10.2 g, 92.6%). **^{1}H NMR** (400 MHz, $CDCl_3$) δ 7.72 – 7.68 (m, 1H), 7.61 (d, J = 15.7 Hz, 1H), 7.29 – 7.27 (m, 1H), 6.49 (d, J = 15.7 Hz, 1H), 3.78 (s, 3H). **^{13}C NMR** (101 MHz, $CDCl_3$) δ 167.89, 136.72, 134.96, 115.93, 51.61.

5.5.5.2. Methyl 3-(1*H*-imidazol-4-yl)propanoate (8)

7 (5 g, 32.9 mmol) was dissolved in MeOH (40 mL, 0.775 M) and 10% Pd/C (0.5 g) was added to the solution. Then, the reaction mixture was stirred under H_2 atmosphere (1 atm) at rt overnight. The solid was then filtered and the solvent concentrated *in vacuo* to yield **8** as a white solid (4.11 g, 81%). **^{1}H NMR** (400 MHz, MeOD) δ 7.58 (s, 1H), 6.81 (s, 1H), 3.65 (s, 3H), 2.88 (t, J = 7.5 Hz, 2H), 2.65 (t, J = 7.5 Hz, 2H). **^{13}C NMR** (101 MHz, MeOD) δ 175.02, 137.42, 135.95, 117.18, 52.09, 34.73, 23.23.

5.5.5.3. Methyl 3-(1-trityl-1*H*-imidazol-4-yl)propanoate (9)

To a solution of **8** (4.11 g, 26.7 mmol) and Et_3N (7.5 mL, 53.3 mL) in dry DMF (26.7 mL, 1 M), trityl chloride (8.18 g, 29.3 mmol) in dry DMF (22 mL, 1.32 M) was added, and the reaction mixture was stirred overnight. *The reaction mixture turned cloudy after addition and generated heat*. Then, the reaction mixture was poured into ice (250 g), and the resulting solid was filtered, washed with water (20 mL) and a small volume of Et_2O to yield **9** as a light-yellow solid (9.6 g, 91%). **^{1}H NMR** (300 MHz, CDCl3) δ 7.34 – 7.26 (m, 11H), 7.13 – 7.08 (m, 5H), 6.54 (s, 1H), 3.61 (s, 3H), 2.86 (t, J = 7.7 Hz, 2H), 2.65 (t, J = 7.7 Hz, 2H). **^{13}C NMR** (75 MHz, $CDCl_3$) δ 173.66, 142.53, 139.98, 138.45, 129.85, 128.08, 127.86, 118.16, 75.24, 51.57, 33.97, 23.93.

5.5.5.4. Methyl 3-(1-trityl-1*H*-imidazol-4-yl)propanal (10)

To a solution of **9** (3.44 g, 8.68 mmol) in DCM (45 mL, 0.2 M) at –78 ºC under N_2 atmosphere, DIBAL-H (1 M in toluene, 17.5 mL) was added dropwise, and the reaction mixture was stirred for 45 min. Then, 5 mL of MeOH and 35 mL of water were added to the reaction mixture to quench the DIBAL-H excess, and the mixture was allowed to warm to rt. Then, the mixture was filtered through Celite®, the organic layer separated, dried over Na_2SO_4 and concentrated *in vacuo* to yield **10** as a yellowish solid (2.67 g, 72%). Although the primary alcohol was present (~20%), the product was used without further purification. **¹H NMR** (300 MHz, CDCl₃) δ 9.80 (t, *J* = 1.5 Hz, 1H), 7.37 – 7.28 (m, 10H), 7.15 – 7.09 (m, 6H), 6.60 – 6.53 (m, 1H), 2.92 – 2.83 (m, 2H), 2.83 – 2.75 (m, 2H). **¹³C NMR** (75 MHz, CDCl₃) δ 202.34, 142.50, 139.65, 138.59, 129.87, 128.15, 118.29, 43.31, 21.23.

5.5.5.5. Methyl 3-(1-trityl-1*H*-imidazol-4-yl)-2-aminobutyronitrile (11)

To a solution of **10** (2.5 g, 6.82 mmol) in MeOH (25 mL, 0.27 M) was added NH₄Cl (1.32 g, 24.6 mmol) in NH₄OH (20 mL, 1.23 mL), and the reaction mixture was stirred for 40 min. Then, KCN (808 mg, 12.3 mmol) was added to the reaction mixture and stirred at rt overnight. The solvent was then concentrated *in vacuo*, and the remaining solid was redissolved in EtOAc (25 mL) and H_2O (25 mL). The layers were separated, the organic layer dried over Na_2SO_4 and concentrated *in vacuo* to yield **11** as a white solid (2.15 g, 75%). The impure product (~30 % impurity) was used without further purification. **¹fH NMR** (500 MHz, CDCl₃) δ 7.36 – 7.30 (m, 10H), 7.16 – 7.09 (m, 6H), 6.60 (s, 1H), 3.71 (t, *J* = 7.1 Hz, 1H), 2.81 – 2.72 (m, 2H), 2.12 – 2.03 (m, 2H). **¹³C NMR** (126 MHz, CDCl₃) δ 142.52, 138.79, 137.97, 129.85, 128.20, 118.55, 118.19, 42.82, 35.11, 24.30.

5.5.5.6. Homohistidine (12)

To 10 mL of concentrated HCl (0.15 M) **11** (589 mg, 1.5 mmol) was added and the reaction mixture was refluxed overnight. The solution was extracted with Et_2O (10 x 2 mL), and the aqueous layer was concentrated *in vacuo* to give **12** (220 mg, 87%). **¹H NMR** (400 MHz, D₂O) δ 7.81 (d, *J* = 1.2 Hz, 1H), 7.00 (d, *J* = 1.2 Hz, 1H), 3.76 (dd, *J* = 6.9, 5.6 Hz, 1H), 2.82 – 2.67 (m, 2H), 2.28 – 2.05 (m, 2H). **¹³C NMR** (101 MHz, D₂O) δ 174.59, 135.69, 135.50, 115.89, 54.29, 30.27, 21.94.

Chapter V

263

Attempts to Expand the TAMOF-1 Family: Synthesis of Structurally Related Ligands

5.5.5.7. Trz-homohistidine-OH (13)

PTSA (370 mg, 1.3 mmol) and **12** (220 mg, 1.3 mmol) were dissolved in EtOH (10 mL, 0.13 M) and the reaction mixture was refluxed at 80 ºC for 48 h. Then, the solution was filtered to remove the unreacted **12** and the solvent was concentrated *in vacuo* to obtain **13** as a dark brown oil (2.15 g, 75%). **¹H NMR** (300 MHz, D$_2$O) δ 8.53 (s, 2H), 8.38 (d, J = 1.4 Hz, 1H), 7.10 (s, 1H), 4.87 (dd, J = 10.3, 4.5 Hz, 1H), 2.78 – 2.70 (m, 2H), 2.68 – 2.53 (m, 1H), 2.49 – 2.32 (m, 1H). **¹³C NMR** (101 MHz, D$_2$O) δ 174.80, 143.62, 133.54, 132.33, 115.80, 60.69, 31.12, 21.27. **HRMS-ESI-TOF** (*m/z*): [M − H]⁻ calcd for C$_9$H$_{11}$N$_5$O$_2$, 220.0900; found, 220.0837. **IR** (neat, cm⁻¹) $\bar{v}$ 3391, 3110, 3099, 2779, 2451, 1622, 1528, 1466, 1410, 1357, 1182, 1080, 1019, 982, 925, 877, 843, 764, 731, 670, 639, 493, 435.

5.5.6. Synthesis of (*S*)-3-(4-(4*H*-1,2,4-triazol-4-yl)phenyl)-2-(4*H*-1,2,4-triazol-4-yl)propanoic acid (17)

5.5.6.1. (*S*)-3-(4-((((9*H*-fluoren-9-yl)methoxy)carbonyl)amino)phenyl)-2-aminopropanoic acid (15)

To a solution of **14** (414 mg, 2.3 mmol) in an aqueous solution of 10% AcOH (20 mL, 0.115 M), FmocCl (622 mg, 2.4 mmol) in 1,4-dioxane (20 mL, 0.12 M) was added and the resulting emulsion was stirred at rt overnight. Then, Et2O (2 x 30 mL) was added to the reaction mixture to extract the non-polar impurities. The aqueous layer was acidified with 2M HCl to pH=1, and the precipitate was collected by filtration, washed with Et2O (15 mL) and dried *in vacuo* to yield **15·HCl** as a white solid (903 mg, 90%). **¹H NMR** (400 MHz, DMSO) δ 7.91 (d, J = 7.5 Hz, 2H), 7.74 (d, J = 7.5 Hz, 2H), 7.42 (td, J = 7.5, 1.2 Hz, 2H), 7.40 – 7.37 (m, 2H), 7.34 (td, J = 7.5, 1.2 Hz, 2H), 7.16 (d, J = 8.3 Hz, 2H)f, 4.47 (d, J = 6.6 Hz, 2H), 4.30 (t, J = 6.6 Hz, 1H), 3.70 (dd, J = 7.4, 5.2 Hz, 1H), 3.07 (dd, J = 14.3, 5.2 Hz, 1H), 2.91 (dd, J = 14.3, 7.4 Hz, 1H). **¹³C NMR** (101 MHz, DMSO) δ 170.03, 153.43, 143.77, 140.81, 137.77, 130.24, 129.75, 127.70, 127.13, 125.13, 120.20, 118.40, 65.49, 54.56, 46.65, 35.77.

264

5.5.6.2. (S)-3-(4-(4H-1,2,4-triazol-4-yl)phenyl)-2-(4H-1,2,4-triazol-4-yl)propanoic acid (16)

15 (200 mg, 0.46 mmol), DMFA (214 mg, 1.5 mmol) and PTSA (10.4 mg, 0.055 mmol) were dissolved in toluene (4.6 mL, 0.1 M) and the reaction mixture was stirred at reflux for 30 h. Then, toluene was decanted, and the remaining dark residue was redissolved in hot EtOH (5 mL). To this solution an alcoholic solution (5 mL) of KOH (25 mg, 0.46 mmol) was added, and the solution was stirred for 10 min at 80 ºC. The resulting solution was left to cool and Et_2O (10 mL) was added, yielding a yellow precipitate. The precipitate was filtered, redissolved in a hot solution of MeOH/EtOH (10 mL. 1:1) and acidified to pH=4 with HCl in EtOH. Finally, KCl was removed by filtration and the solvent was concentrated *in vacuo* to yield **16** as a light-yellow solid (110 mg, 85%). **^{1}H NMR** (300 MHz, DMSO) δ 9.06 (s, 2H), 8.43 (s, 2H), 7.55 (d, $J = 8.5$ Hz, 2H), 7.30 (d, $J = 8.5$ Hz, 2H), 5.21 (dd, $J = 11.0, 4.6$ Hz, 1H), 3.52 (dd, $J = 14.4, 4.6$ Hz, 1H), 3.36 (dd, $J = 14.4, 11.0$ Hz, 1H). **^{13}C NMR** (101 MHz, DMSO) δ 170.26, 142.90, 141.24, 137.34, 132.43, 130.27, 120.94, 60.05, 37.43. **HRMS-ESI-TOF** (*m/z*): $[M-H]^-$ calcd for $C_{13}H_{12}N_6O_2$, 283.1000; found, 283.0960. $[\alpha]_D^{25} = $ -20.4 (c = 0.35, H_2O). **IR** (neat, cm^{-1}) $\bar{\upsilon}$ 3371, 3114, 2930, 1674, 1622, 1528, 1372, 1229, 1186, 1091, 1000.

5.5.7. Synthesis of (S)-3-(1H-benzo[d]imidazol-2-yl)-2-(4H-1,2,4-triazol-4-yl)propanoic acid (19)

5.5.7.1. (S)-2-amino-3-(1H-benzo[d]imidazol-2-yl) propanoic acid (18)

To a 5.5 N HCl solution (50 mL, 1 M) of **17** dihydrochloride (9.05 g, 50 mmol), L-aspartic acid (10 g, 75 mmol) was added and the reaction mixture was refluxed for 72 h. The reaction mixture was then cooled to rt, filtered and the filtrate was adjusted to pH = 1 with Na_2CO_3. The precipitate was collected by filtration and recrystallised in 67% EtOH in water (10 mL, v/v) to yield **18** as a light-green solid (3.5 g, 34%). **^{1}H NMR** (400 MHz, D_2O) δ 7.79 (dt, $J = 6.2, 3.4$ Hz, 2H), 7.60 (dt, $J = 6.2, 3.4$ Hz, 2H), 4.30 (d, $J = 7.8$ Hz, 1H), 3.78 – 3.73 (m, 2H). **^{13}C NMR** (101 MHz, D_2O) δ 171.32, 148.34, 130.78, 126.31, 113.83, 52.07, 27.95.

Chapter V

Attempts to Expand the TAMOF-1 Family: Synthesis of Structurally Related Ligands

5.5.7.2. (S)-3-(1H-benzo[d]imidazol-2-yl)-2-(4H-1,2,4-triazol-4-yl)propanoic acid (19)

PTSA (139 mg, 0.975 mmol) and **18** (100 mg, 0.487 mmol) were dissolved in H_2O (5 mL, 0.13 M) and the reaction mixture was stirred at reflux for 24 h. Then, the solvent was concentrated *in vacuo* and the resulting crude was redissolved in EtOH. The precipitate was removed, and the filtrate was concentrated *in vacuo*. The crude was then dispersed in acetone, the solvent decanted, and the remaining gel was dried *in vacuo* to yield **19** as a brown gel (88 mg, 70 %). **^{1}H NMR** (300 MHz, D_2O) δ 8.43 (s, 2H), 7.55 (dt, J = 6.7, 3.4 Hz, 2H), 7.31 (dt, J = 6.7, 3.4 Hz, 2H), 5.41 (dd, J = 10.5, 5.0 Hz, 1H), 3.87 (dd, J = 15.4, 5.0 Hz, 1H), 3.62 (dd, J = 15.4, 10.5 Hz, 1H). **^{13}C NMR** (101 MHz, D_2O) δ 172.99, 150.58, 143.55, 123.22, 114.53, 59.79, 32.46. **HRMS-ESI-TOF** (*m/z*): $[M - H]^-$ calcd for $C_{12}H_{10}N_5O_2$, 256.0900; found, 256.0843. **$[α]_D^{25}$**= -7.92 (c = 0.11, H_2O). **IR** (neat, cm^{-1}) $\bar{\upsilon}$ 3358, 3059, 2786, 2471, 1582, 1467, 1372, 1345, 1273, 1222, 1192, 1023, 751.

5.5.8. Synthesis of Cu-2

$Cu(NO_3)_2 \cdot 3H_2O$ (12.1 mg, 0.05 mmol) was dissolved in 0.5 mL of MeOH and the resulting solution was slowly added to a solution of **2** (13.2 mg, 0.05 mmol) in 1 mL of MeOH and 0.2 ml H_2O. The solution was kept still for 2 days. The blue polycrystalline powder was washed with MeOH (3 x 5 mL) and dried in air. Single crystals of **Cu-2** were obtained by slow diffusion of the Cu^{2+} salt and **2** solutions in a layering tube.

5.5.9. Synthesis of Zn-5

$ZnCl_2$ (32.7 mg, 0.24 mmol) and **5** (20 mg, 0.08 mmol) were added to a Teflon vessel, then H_2O (2 mL) was slowly added without dissolving the reagents. The Teflon vessel was introduced into an autoclave reactor, and the reaction mixture was left at 120 ºC for 48 h. The resulting white crystals of **Zn-5** were filtered and dried in air.

5.5.10. Synthesis of Cu-5

Cu(BF$_4$)$_2$·H$_2$O (56.9 mg, 0.24 mmol) and **5** (20 mg, 0.08 mmol) were added to a Teflon vessel, then H$_2$O (2 mL) was slowly added without dissolving the reagents. The Teflon vessel was introduced into an autoclave reactor, and the reaction mixture was left at 120 ºC for 48 h. The resulting green crystals of **Cu-5** were filtered and dried in air.

5.5.11. NMR spectra
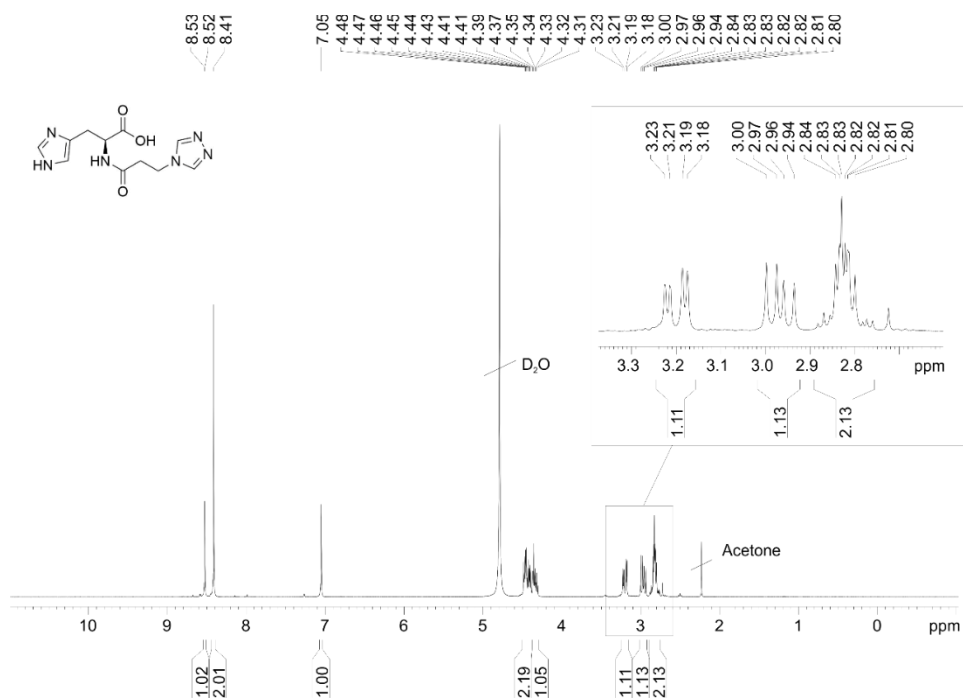
Figure 251. ^{1}H-NMR spectra of **2**.

Chapter V

Attempts to Expand the TAMOF-1 Family: Synthesis of Structurally Related Ligands
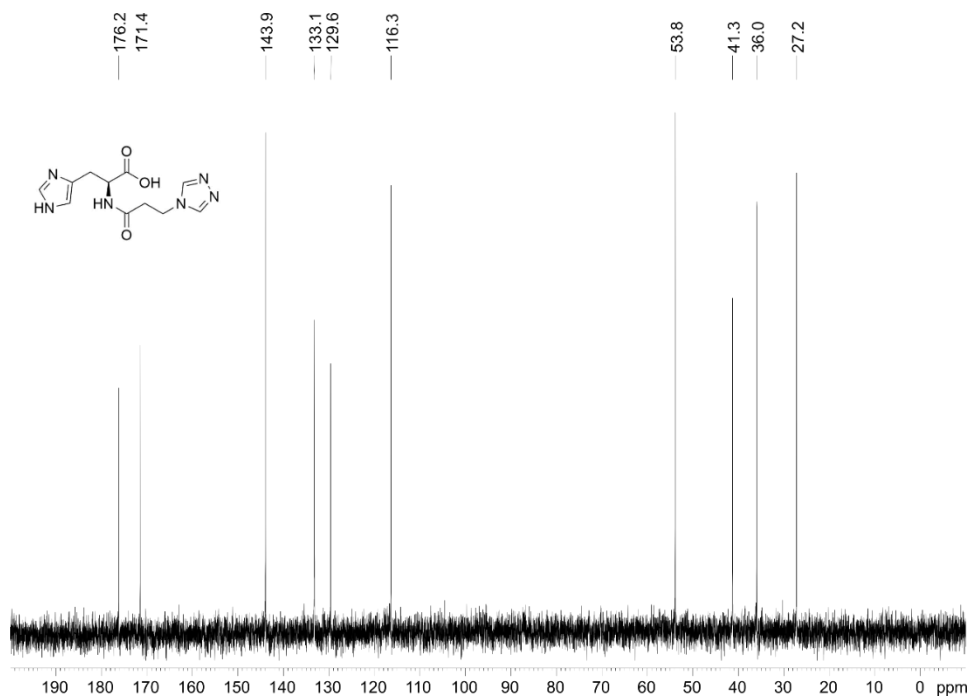
Figure 252. ^{13}C-NMR spectra of **2**.
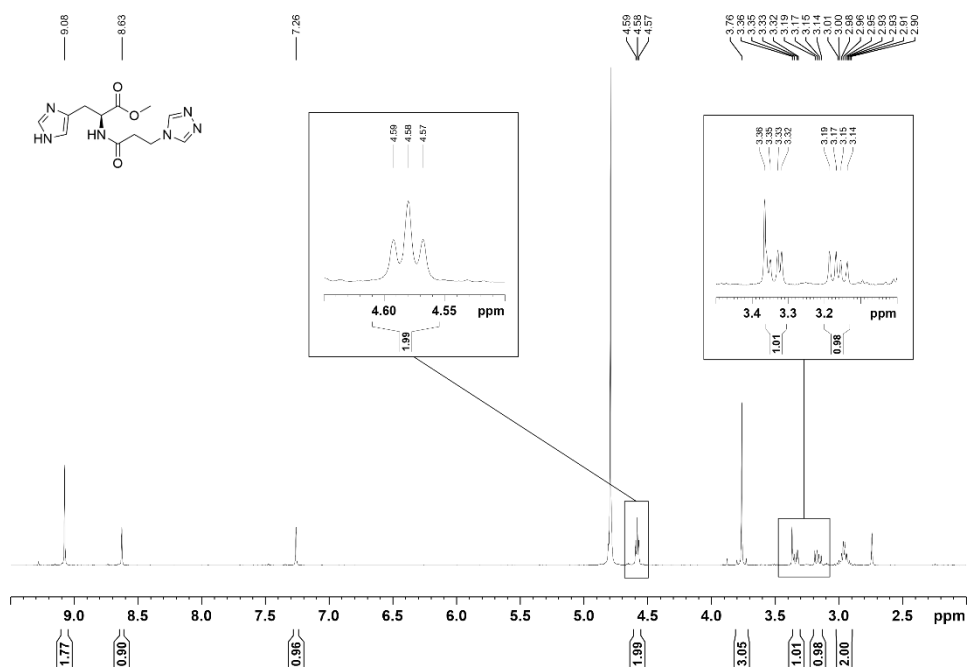
Figure 253. ^{1}H-NMR spectra of **3**.

268
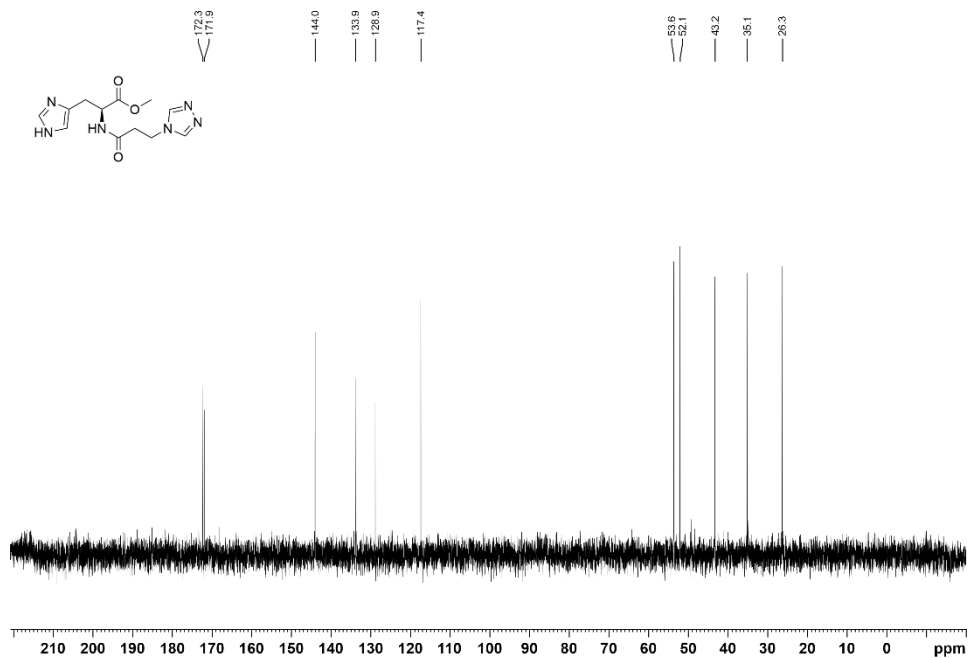
Figure 254. ^{13}C-NMR spectra of **3**.
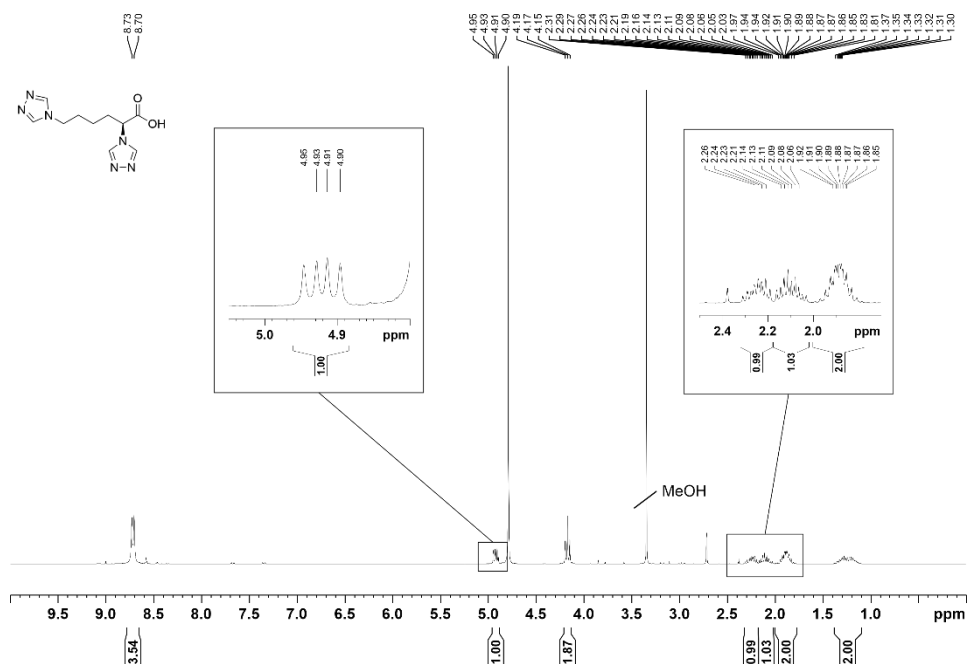
Figure 255. ^{1}H-NMR spectra of **5**.

269

Attempts to Expand the TAMOF-1 Family: Synthesis of Structurally Related Ligands
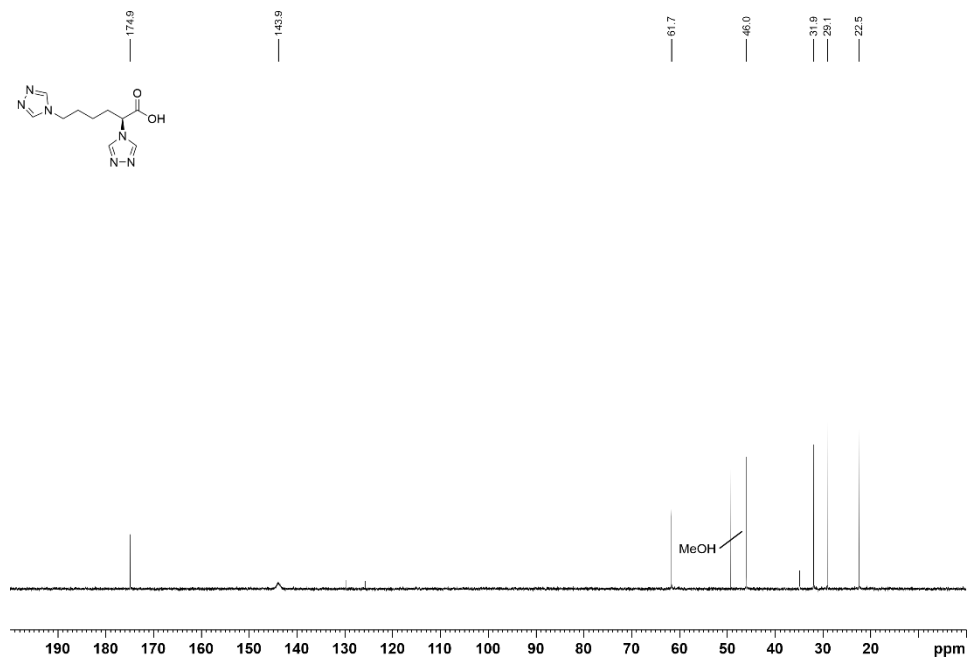
Figure 256. ^{13}C-NMR spectra of **5**.
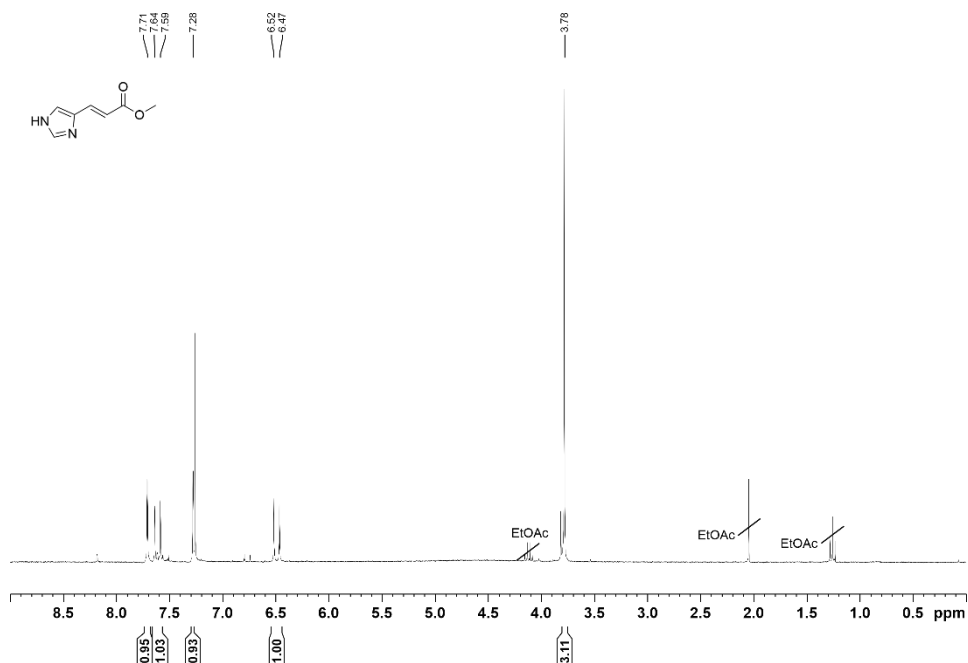
Figure 257. ^{1}H-NMR spectra of **7**.

270
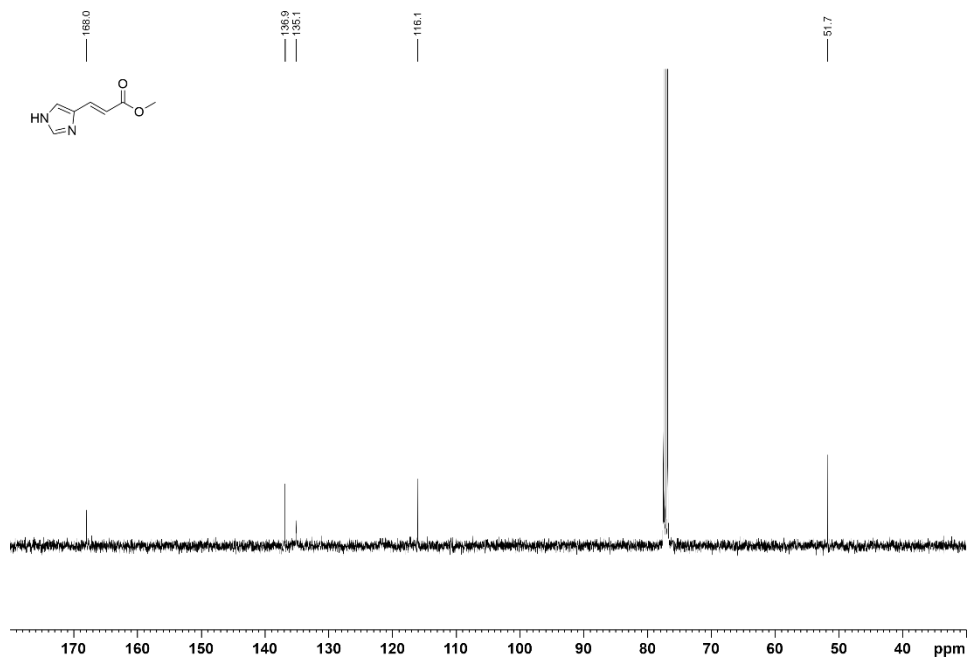
Figure 258. ^{13}C-NMR spectra of **7**.
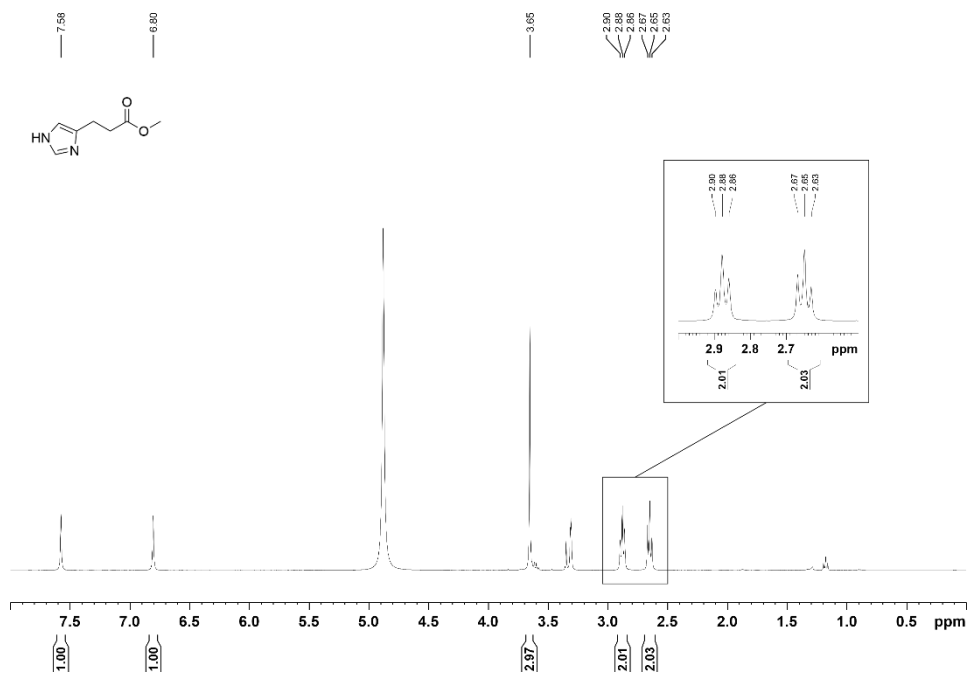
Figure 259. ^{1}H-NMR spectra of **8**.

271

Attempts to Expand the TAMOF-1 Family: Synthesis of Structurally Related Ligands

Figure 260. ^{13}C-NMR spectra of **8**.

Figure 261. ^{1}H-NMR spectra of **9**.
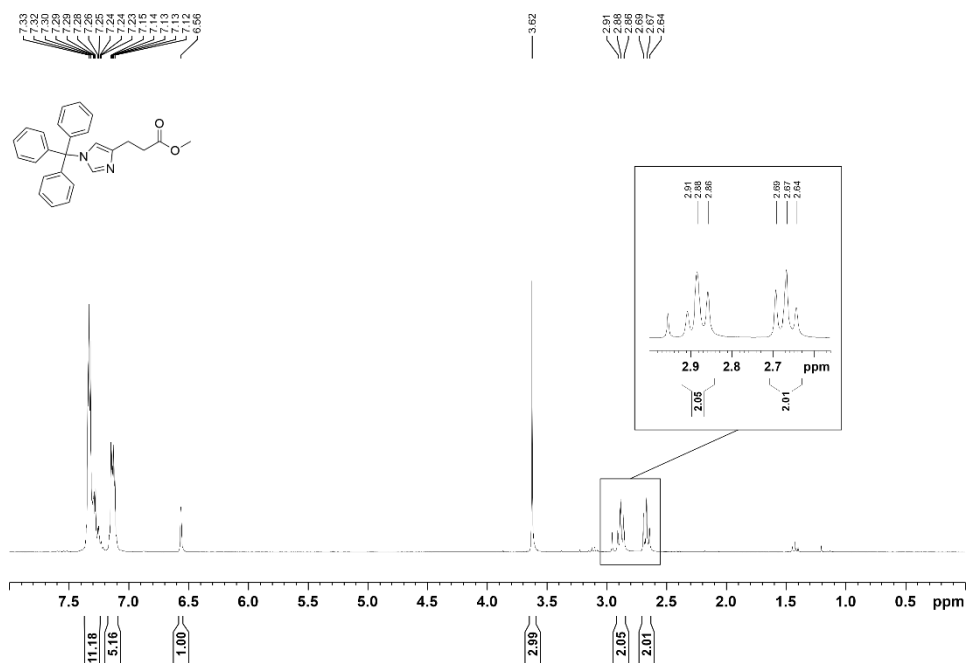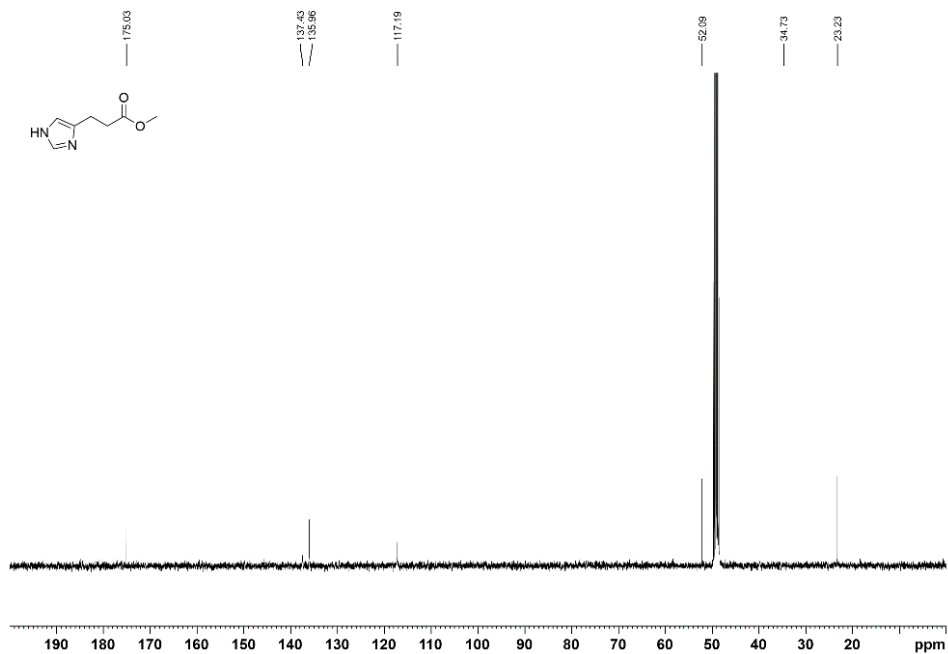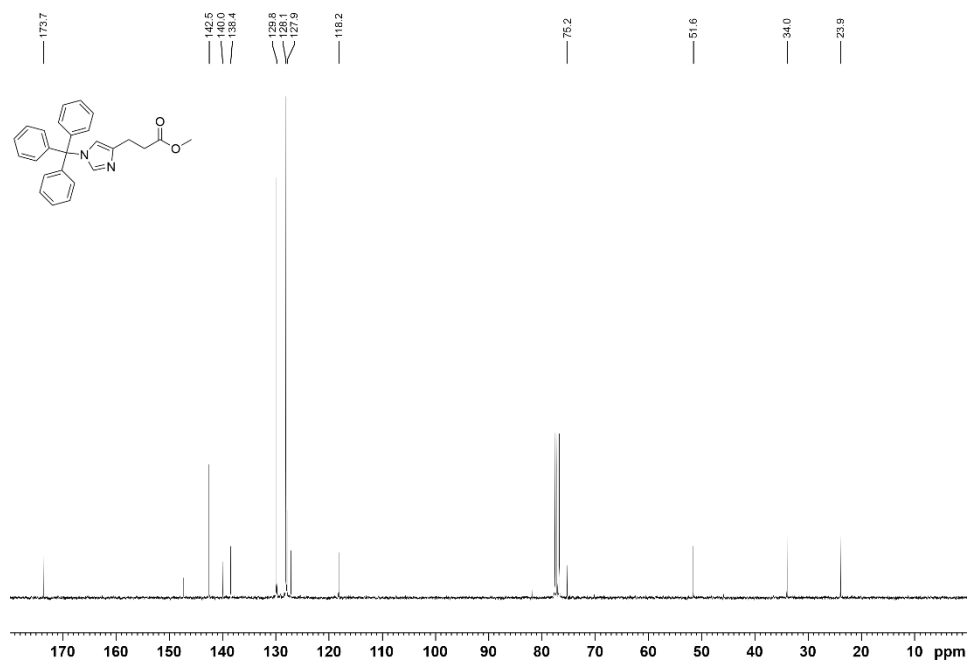
Figure 262. ^{13}C-NMR spectra of **9**.
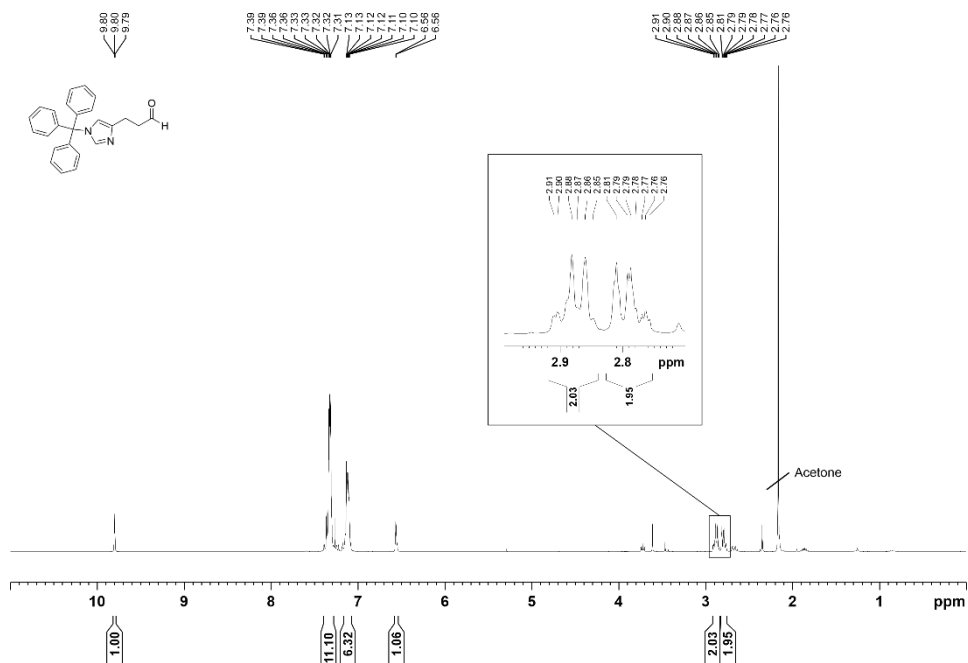
Figure 263. ^{1}H-NMR spectra of **10**.

273

Attempts to Expand the TAMOF-1 Family: Synthesis of Structurally Related Ligands
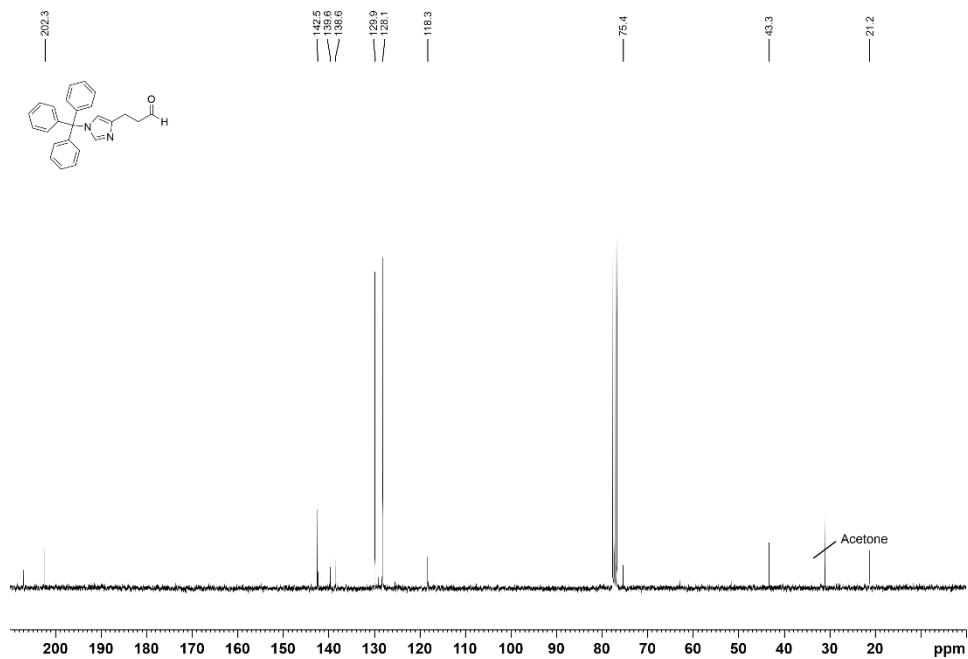
Figure 264. ¹³C-NMR spectra of **10**.
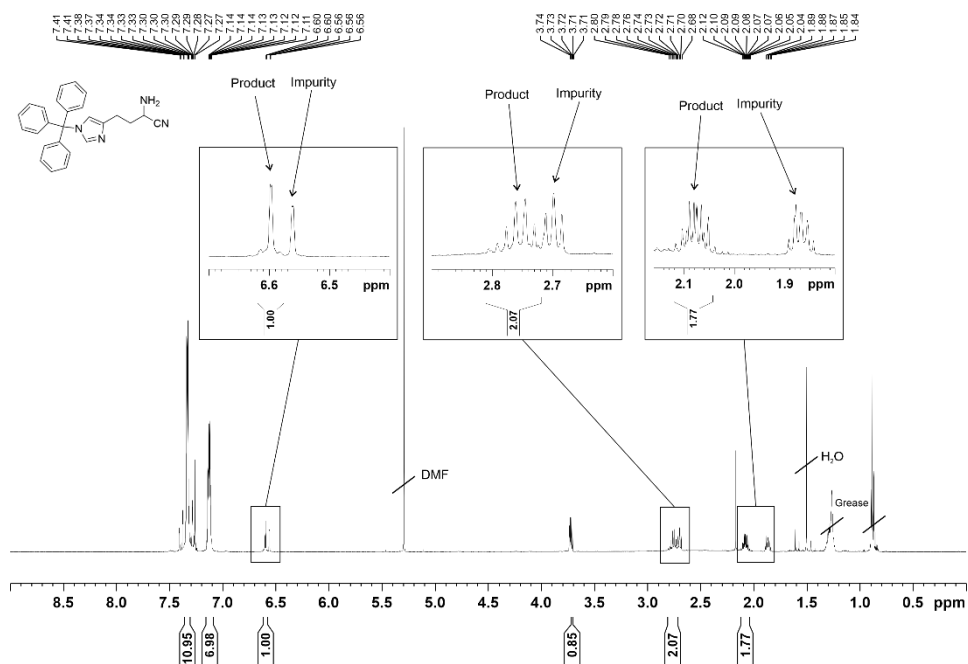
Figure 265. ¹H-NMR spectra of **11**.
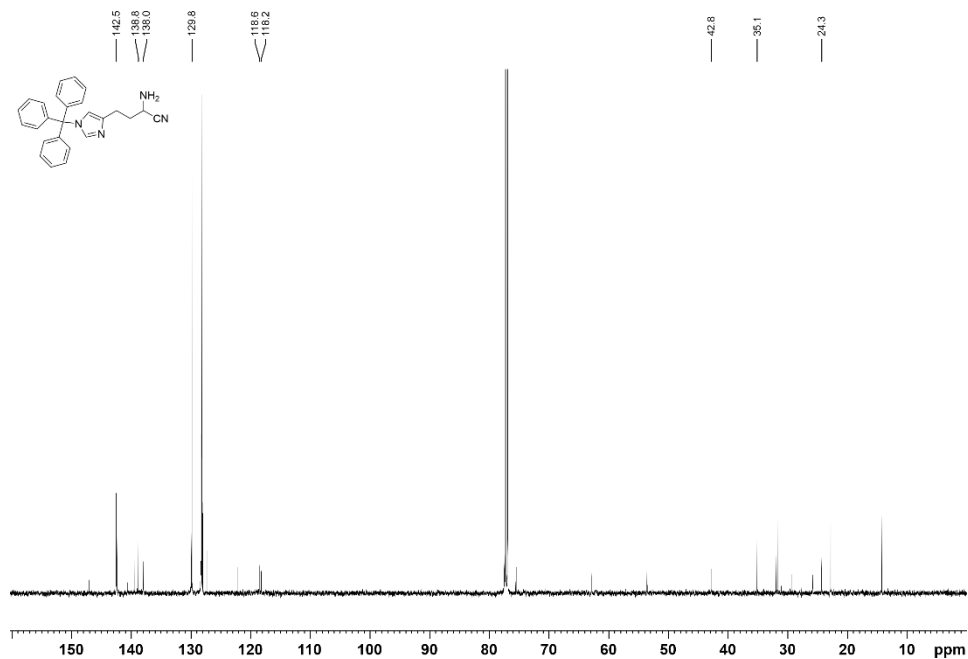
Figure 266. ^{13}C-NMR spectra of **11**.
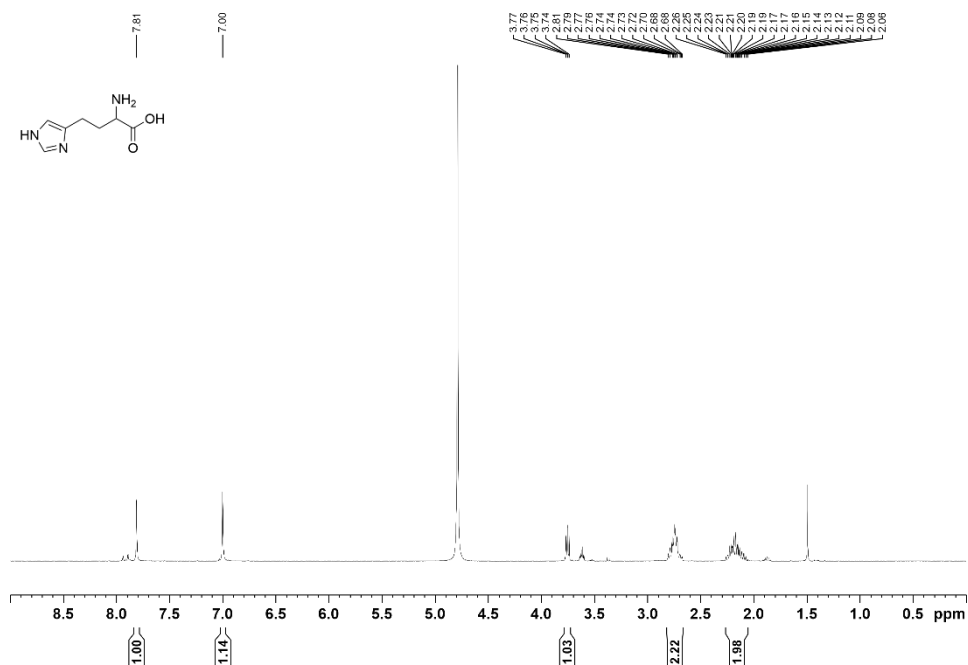
Figure 267. ^{1}H-NMR spectra of **12**.

Chapter V

275

Attempts to Expand the TAMOF-1 Family: Synthesis of Structurally Related Ligands
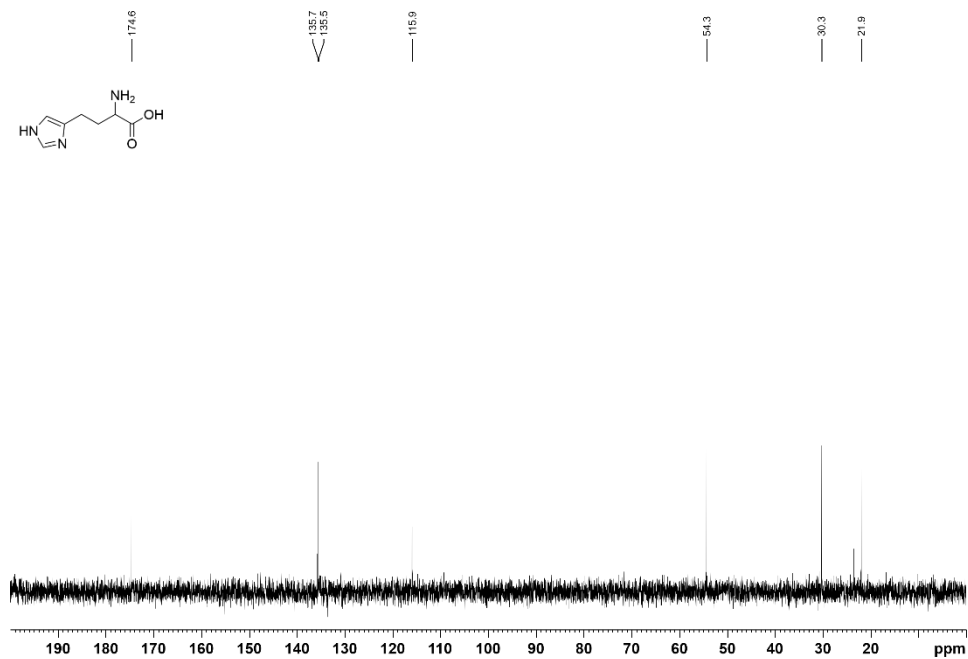
Figure 268. ^{13}C-NMR spectra of **12**.
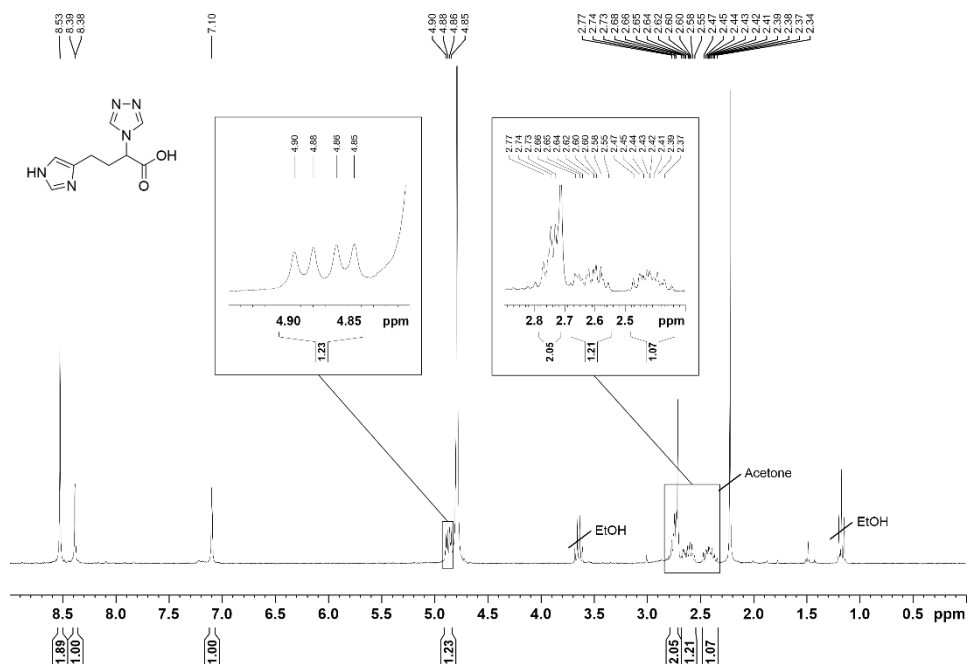
Figure 269. ^{1}H-NMR spectra of **13**.

276
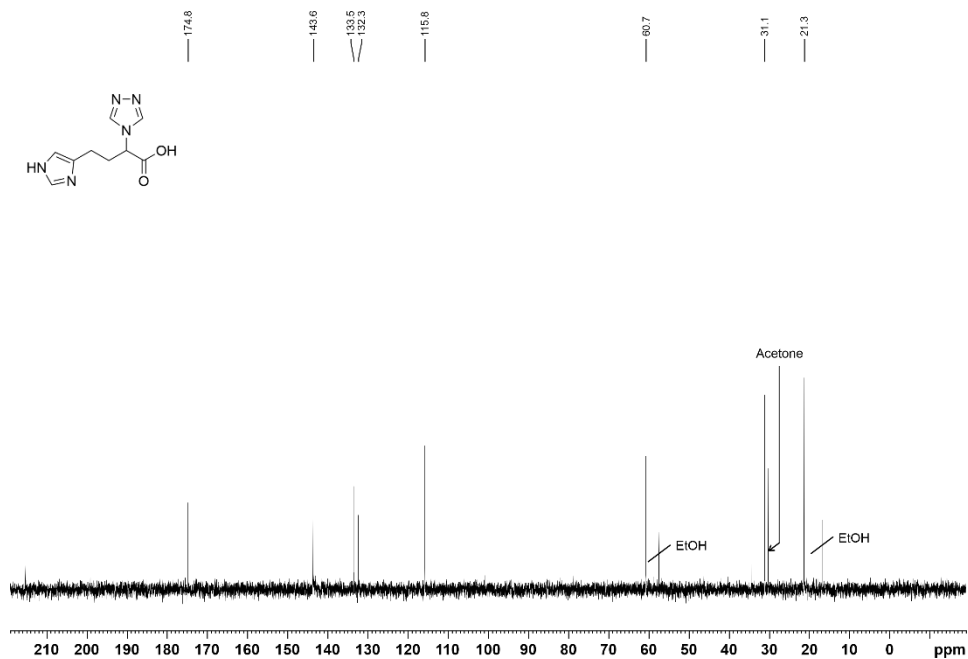
Figure 270. ^{13}C-NMR spectra of **13**.
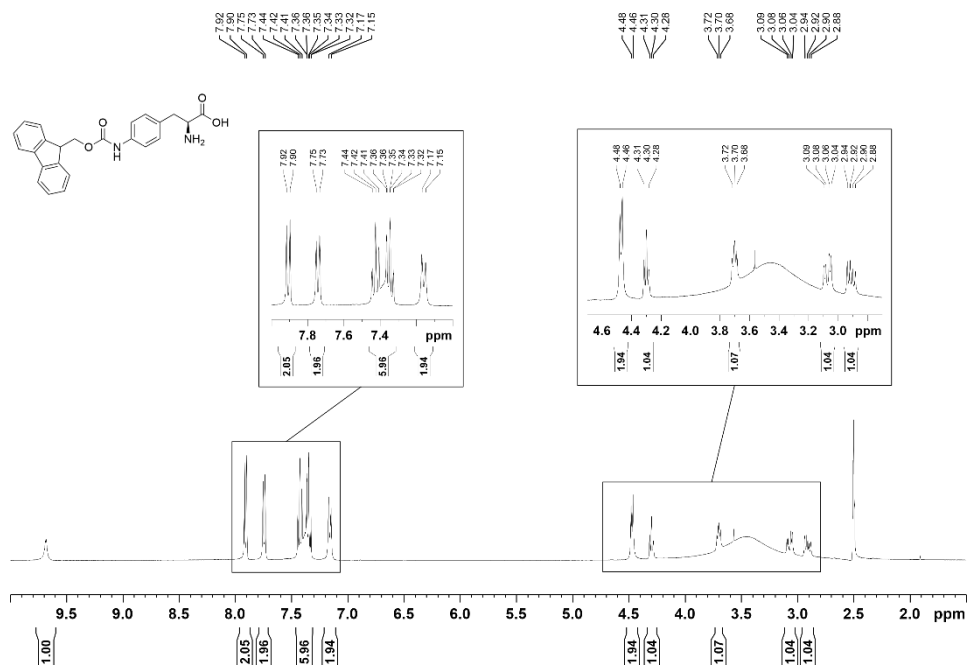
Figure 271. ^{1}H-NMR spectra of **15**.

Chapter V

277

Attempts to Expand the TAMOF-1 Family: Synthesis of Structurally Related Ligands
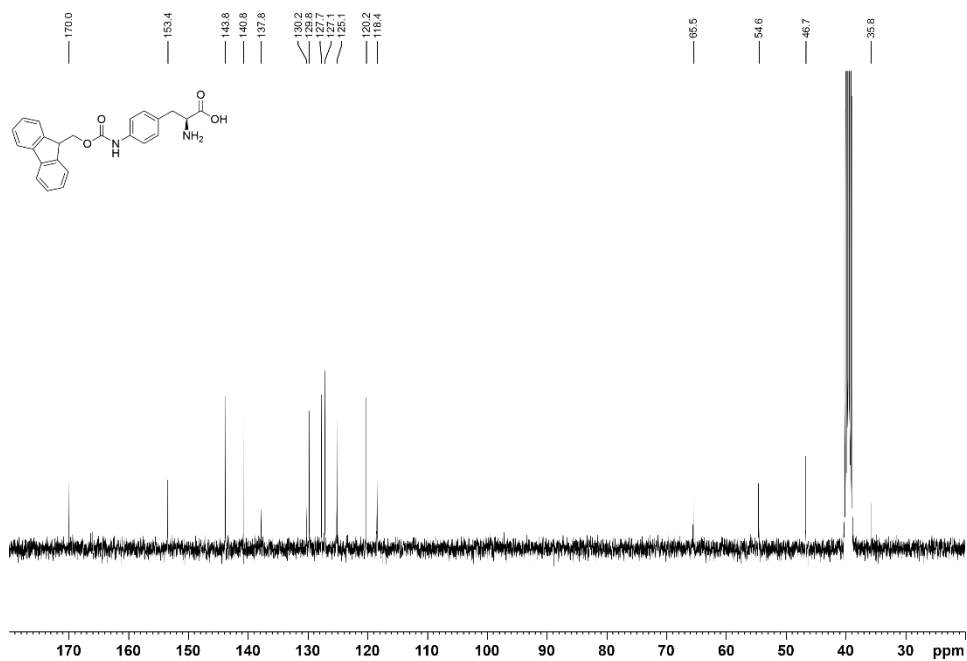
Figure 272. ^{13}C-NMR spectra of **15**.
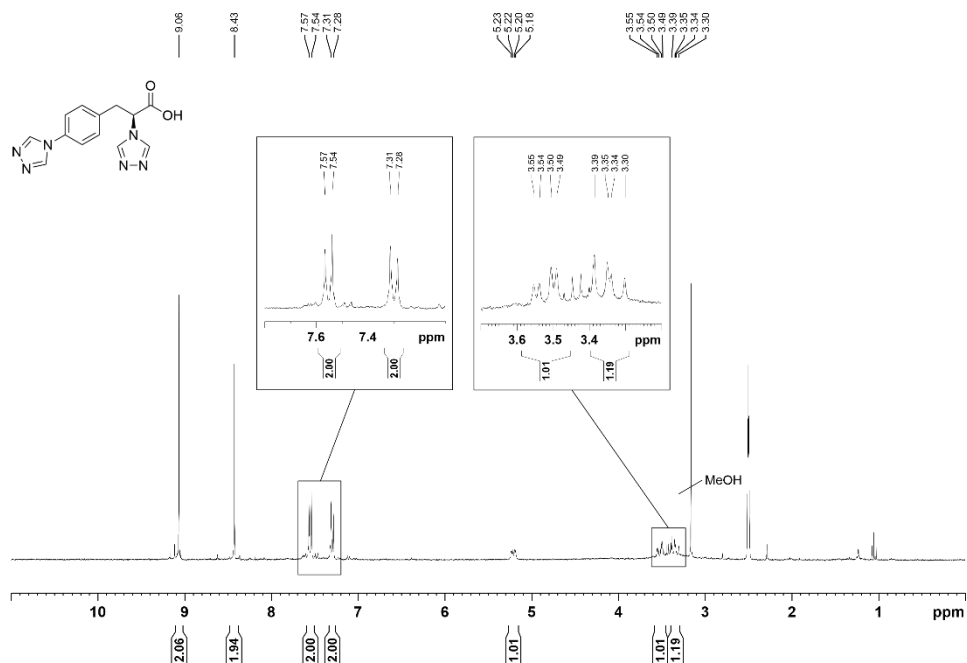
Figure 273. ^{1}H-NMR spectra of **16**.
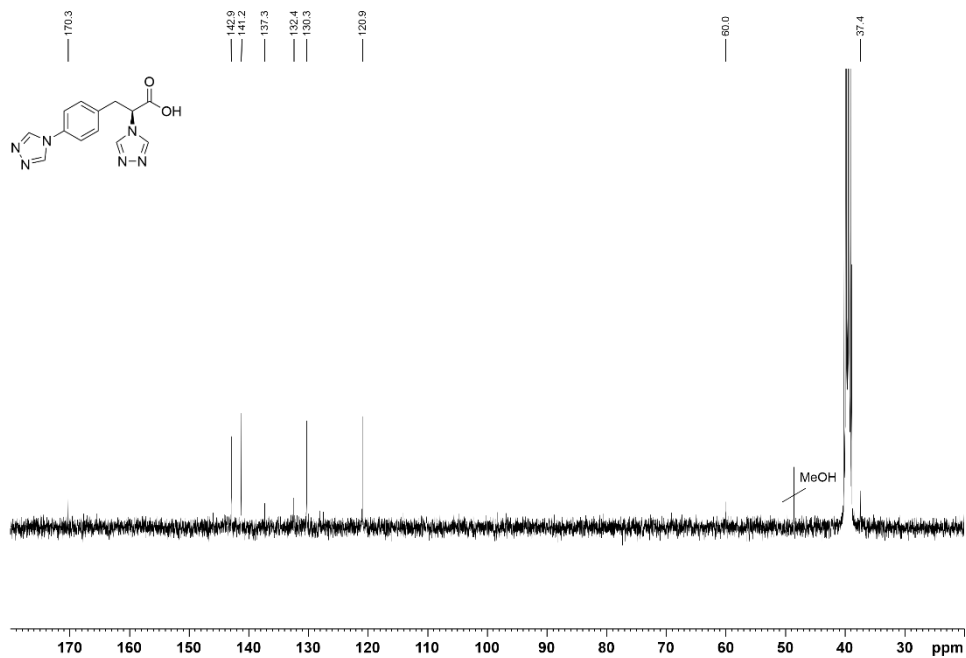
Figure 274. ^{13}C-NMR spectra of **16**.
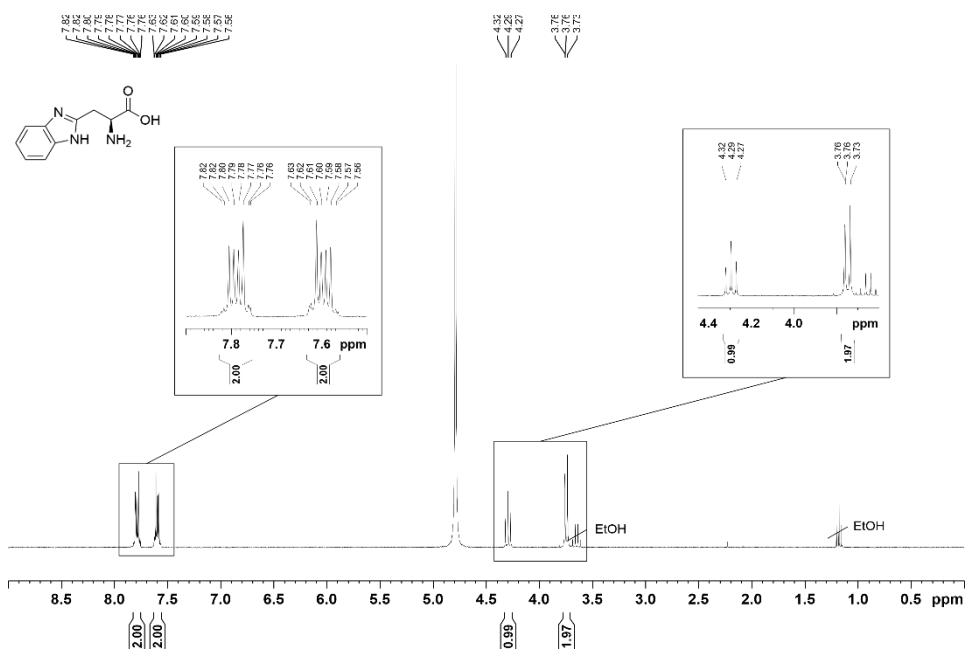
Figure 275. ^{1}H-NMR spectra of **18**.

Chapter V

279
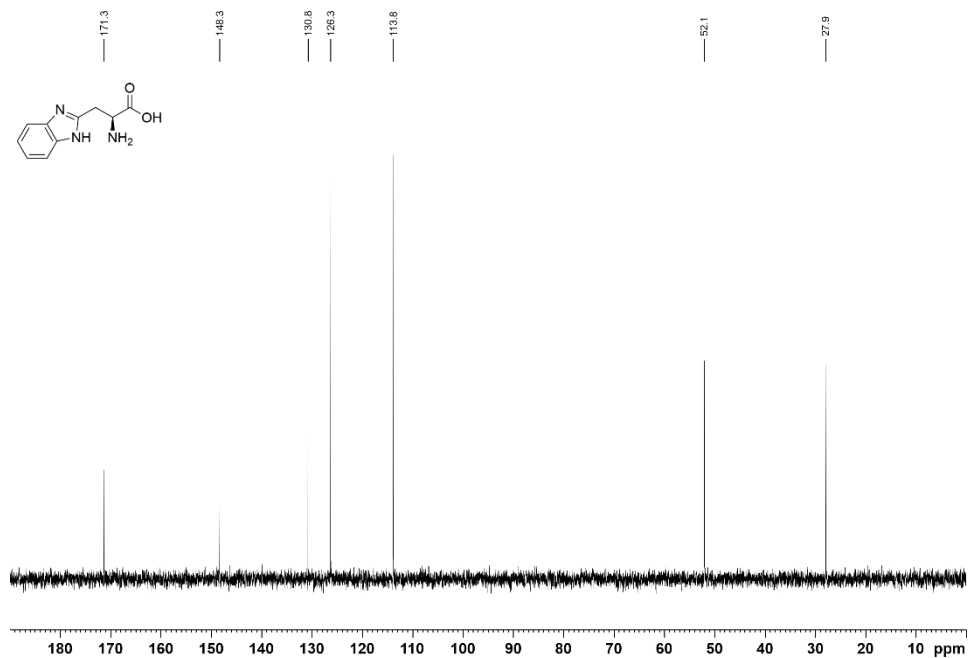
Figure 276. ^{13}C-NMR spectra of **18**.
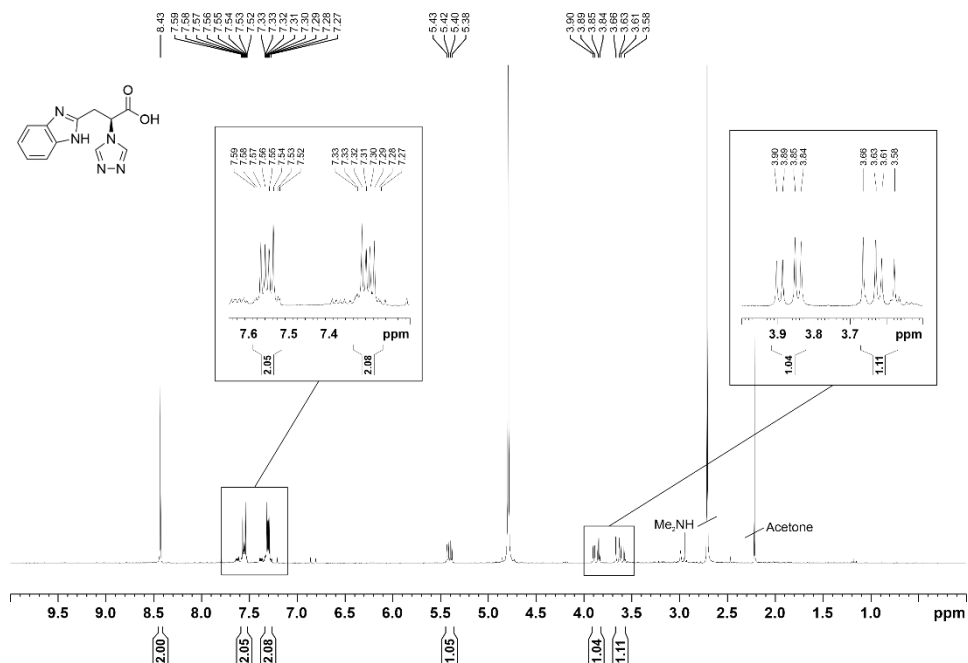
Figure 277. ^{1}H-NMR spectra of **19**.
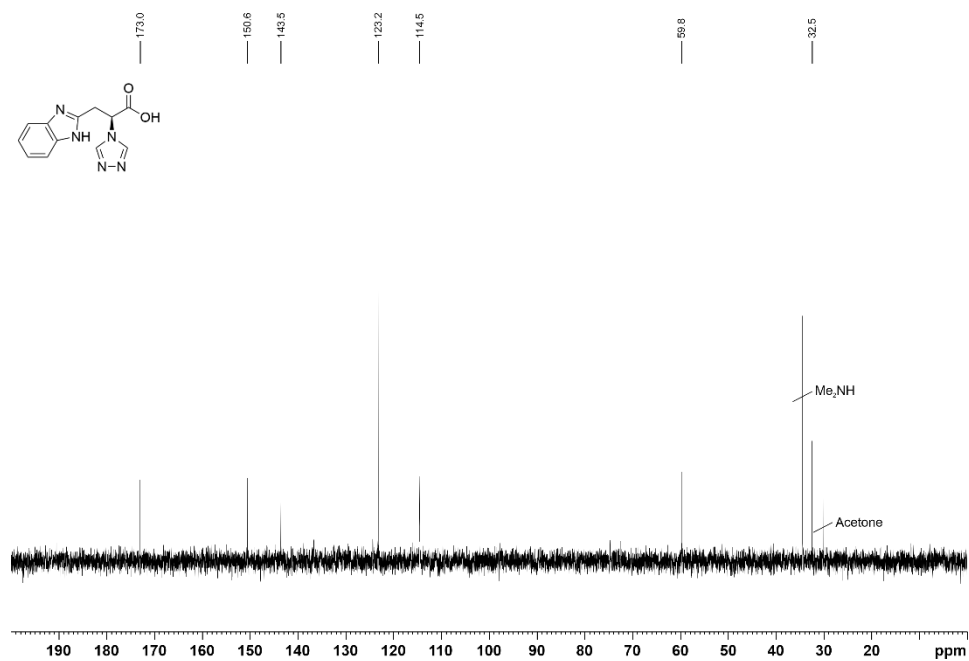
Figure 278. ^{13}C-NMR spectra of **19**.

Attempts to Expand the TAMOF-1 Family: Synthesis of Structurally Related Ligands

CONCLUSIONS

1. In conclusion, the synthesis and crystallisation of TAMOF-1 have been reproduced. The synthesis optimisation was explored to control the particle size, and it was found that there is a correlation between the particle size and the BET surface area (*i.e.* the faster the addition and the faster the stirring rate, the smaller the particle size and the greater the BET surface area). The study of the pH in the synthesis of TAMOF-1 allowed us to conclude that the ligand must be in zwitterionic form for TAMOF-1 precipitation to occur, which is favoured by the acetate ion by acting as a buffer by capturing the released proton of *S*-HTA. The obtention of crystals up to mm scale allowed us to determine the interaction of CO_2 molecules with the trinuclear Cu^{2+} pores, which is a CO_2 molecule per trinuclear pore. TAMOF-1 has been modified by incorporating Pt and Rh NPs in the structure, and preliminary catalytic trials with Pt@TAMOF-1 showed that was inactive in the hydrogenation of a functionalised alkene. Finally, a preliminary monolithic structure of TAMOF-1 was obtained by decreasing the reaction temperature to 0 ºC. The glassy surface and the increased mesoporosity indicates that the TAMOF-1 particle size was substantially decreased, which was confirmed by ESEM.

2. Investigation of the catalytic behaviour of TAMOF-1 resulted in the elucidation of a double matched kinetic resolution of styrene oxide with aniline. The first kinetic resolution process consumes the (*S*)- enantiomer of styrene oxide faster, increasing the e.e. of the (*R*)- counterpart and resulting in a preferential formation of the (*R*)-branched aminoalcohol. The second kinetic resolution process occurs in the linear aminoalcohol, where the preferential consumption of the (*S*)- enantiomer amplifies the e.e. of the unreacted (*R*)- isomer. The result of the consecutive kinetic resolutions is the enhancement of the stereoselectivity towards the formation of the (*R*)-linear isomer. This phenomenon is also known as subtractive Horeau amplification. Computational studies are in complete agreement with the experimental observations. The structural stability and recyclability of TAMOF-1 after several catalytic cycles remains unaltered, proving the robustness of the MOF.

3. Packing of TAMOF-1 inside a preparative column allowed us to quantitatively separate *rac*-ibuprofen and *rac*-thalidomide enantiomers. Computational studies corroborated the elution order and the interaction of the enantiomers inside the pores of TAMOF-1. The fabrication of TAMOF-1 HPLC analytical columns permitted the automation of chiral

Conclusions

283

separations, which facilitated the screening of racemic mixtures with a wide array of solvents, both polar and non-polar. Furthermore, the flow rate for optimal separations was determined through the Van Deemter equation, being 0.4 mL min^{-1}, which was the flow rate used for most separations. So far, 13 examples of separations of structurally diverse analytes have been achieved using those columns, among which are terpenes and terpenoids, calcium channel blockers and a *P*-stereogenic phosphorus compound. TAMOF-1 columns have a lifespan of over two years, and more than 180 consecutive injections of TSO demonstrated the reproducibility of the separations using these columns. Separations of *rac*-limonene and *rac*-carvone were scaled up to milligram scale using a semi-preparative TAMOF-1 column.

4. TAMOF-1 analytical HPLC columns have been used in the study of the chromatographic separation of achiral positional isomers of aromatic compounds, separating either totally or partially all the mixtures of compounds tested. Among all the examples tested, it is worth to highlight the separation of cresol regioisomers and the purification of unreacted starting material and by-products of the industrial synthesis of styrene. Although the retention times in the cresol family are high due to the polarity of the molecules (>60 min), they could be reduced by increasing the polarity of the mobile phase.

5. The transamination reaction of DMFA with primary amines in AA-based molecules has been performed with six different ligands, obtaining products with yields ranging from low to excellent. Furthermore, in the specific case of **2**, this reaction can be scaled up to gram scale (up to 20 g). These new ligands have been used in the synthesis of new CMOFs, although all attempts afforded non-porous materials. The main effort has been put in the synthesis of structurally diverse ligands rather than synthesising new TAMOF-1 analogues, as difficulties in the scaling up of most ligands severely limited the number of experiments that could be performed in a hypothetical screening.

ANNEX I

Crystallographic Data

UNIVERSITAT ROVIRA I VIRGILI
INSIGHTS IN HOMOCHIRAL METAL-ORGANIC FRAMEWORKS: FROM THEIR SYNTHESIS TO ENANTIOSELECTIVE
APPLICATIONS
Juanjo Cabezas Giménez

Annex I

Crystallographic data of TAMOF-1

Table 27. Crystallographic data and refinement parameters for TAMOF-1 collected at 100 K, 298 K, in desolvated state at 403 K, and again at 100 K after rehydration.[103]

	100(2) K	298(2) K	403(2) K	Rehydrated
Empirical formula	$C_{16}H_{31.33}CuN_{10}O_{11.67}$	$C_{16}H_{25.67}CuN_{10}O_{8.83}$	$C_{16}H_{16}CuN_{10}O_4$	$C_{16}H_{31}CuN_{10}O_{11.5}$
Formula weight	614.05	563.00	475.93	611.04
T/K	100(2)	298(2)	404(2)	100(2)
Wavelength/Å	0.71073	0.71073	0.71073	0.71073
Crystal system	Cubic	Cubic	Cubic	Cubic
Space group	$P4_332$	$P4_332$	$P4_332$	$P4_332$
a/Å	20.120(4)	20.172(2)	20.262(2)	20.1133(7)
b/Å	20.120(4)	20.172(2)	20.262(2)	20.1133(7)
c/Å	20.120(4)	20.172(2)	20.262(2)	20.1133(7)
$\alpha/°$	90	90	90	90
$\beta/°$	90	90	90	90
$\gamma/°$	90	90	90	90
Volume/Å^3	8145(4)	8208(2)	8319(3)	8136.7(8)
Z	12	12	12	12
ρ_{calc}/g cm^{-3}	1.502	1.367	1.140	1.496
μ/mm^{-1}	0.878	0.857	0.822	0.878
$F(000)$	3836	3496	2916	3816
Crystal size/mm^3	0.05 × 0.05 × 0.03	0.05 × 0.05 × 0.03	0.05 × 0.05 × 0.03	0.05 × 0.05 × 0.03
θ range /°	1.753 to 35.178	1.749 to 32.062	1.741 to 27.108	1.754 to 33.716
Index ranges	$-12 \leq h \leq 27$	$-11 \leq h \leq 26$	$-6 \leq h \leq 21$	$-31 \leq h \leq 7$
	$-6 \leq k \leq 32$	$-7 \leq k \leq 26$	$-14 \leq k \leq 20$	$-21 \leq k \leq 26$
	$-27 \leq l \leq 8$	$-6 \leq l \leq 30$	$-5 \leq l \leq 25$	$-31 \leq l \leq 17$
Reflections	18098	14121	11230	53327
Independent reflections	5693	4677	3063	5445
R_{int}	0.0310	0.0578	0.0358	0.0400
Completeness/%	98.9	97.5	99.3	99.9
Abs. correction	None	Multi-scan	Multi-scan	Multi-scan
Data/restraints/parameters	5693/78/263	4677/51/222	3063/0/141	5445/78/263
GOF on F^2	1.043	0.986	1.071	1.085
Final R^a indexes [I>=2σ (I)]	$R_1 = 0.0341$ wR$_2$ = 0.0884	$R_1 = 0.0439$ wR$_2$ = 0.1012	$R_1 = 0.0331$ wR$_2$ = 0.0807	$R_1 = 0.0290$ wR$_2$ = 0.0796
Final R^a indexes [all data]	$R_1 = 0.0406$ wR$_2$ = 0.0914	$R_1 = 0.0625$ wR$_2$ = 0.1083	$R_1 = 0.0442$ wR$_2$ = 0.0850	$R_1 = 0.0333$ wR$_2$ = 0.0819
Flack parameter	−0.014(4)	0.004(9)	−0.016(9)	−0.008(3)
Largest diff. peak/hole/ e Å^{-3}	0.458/−0.353	0.431/−0.278	0.182/−162	0.509/−0.271

UNIVERSITAT ROVIRA I VIRGILI
INSIGHTS IN HOMOCHIRAL METAL-ORGANIC FRAMEWORKS: FROM THEIR SYNTHESIS TO ENANTIOSELECTIVE
APPLICATIONS
Juanjo Cabezas Giménez

Crystallographic Data

Table 28. Bond lengths (Å) of TAMOF-1 at 100 K.

Cu1	N4	1.976	C7	H7	0.951
Cu1	O1W	2.457	O1W	H1WA	0.84(3)
Cu1	N2	2.029	O1W	H1WB	0.86(2)
Cu1	O1W	2.457	O1	C8	1.228(4)
Cu1	N2	2.029	O2	C8	1.262(4)
Cu1	N4	1.976	N1	C1	1.469(4)
O1	C8	1.228(4)	N1	C2	1.351(4)
O2	C8	1.262(4)	N1	C3	1.355(4)
N1	C1	1.469(4)	N2	N3	1.388(3)
N1	C2	1.351(4)	N2	C2	1.309(4)
N1	C3	1.355(4)	N3	C3	1.306(4)
N2	N3	1.388(3)	N4	C6	1.375(4)
N2	C2	1.309(4)	N4	C7	1.320(4)
N2	Cu1	2.029	N4	Cu1	1.976
N3	C3	1.306(4)	N5	H5	0.880
N4	C6	1.375(4)	N5	C5	1.376(4)
N4	C7	1.320(4)	N5	C7	1.346(4)
N5	H5	0.880	C1	H1	1.000
N5	C5	1.376(4)	C1	C4	1.530(4)
N5	C7	1.346(4)	C1	C8	1.547(4)
C1	H1	1.000	C2	H2	0.950
C1	C4	1.530(4)	C3	H3	0.950
C1	C8	1.547(4)	C4	H4A	0.990
C2	H2	0.950	C4	H4B	0.991
C3	H3	0.950	C4	C5	1.489(4)
C4	H4A	0.990	C5	C6	1.356(4)
C4	H4B	0.991	C6	H6	0.950
C4	C5	1.489(4)	C7	H7	0.951
C5	C6	1.356(4)	O1W	H1WA	0.84(3)
C6	H6	0.950	O1W	H1WB	0.86(2)

Annex I

Table 29. Bond angles (º) of TAMOF-1 at 100 K.

N4	Cu1	O1W	90.74	N2	C2	H2	125.2
N4	Cu1	N2	174.3	N1	C3	N3	111.6(2)
N4	Cu1	O1W	98.79	N1	C3	H3	124.1
N4	Cu1	N2	87.6	N3	C3	H3	124.3
N4	Cu1	N4	89.3	C1	C4	H4A	109.2
O1W	Cu1	N2	85.07	C1	C4	H4B	109.2
O1W	Cu1	O1W	166.62	C1	C4	C5	112.0(2)
O1W	Cu1	N2	85.98	H4A	C4	H4B	107.9
O1W	Cu1	N4	98.79	H4A	C4	C5	109.3
N2	Cu1	O1W	85.98	H4B	C4	C5	109.2
N2	Cu1	N2	95.9	N5	C5	C4	122.5(2)
N2	Cu1	N4	87.6	N5	C5	C6	105.7(2)
O1W	Cu1	N2	85.07	C4	C5	C6	131.7(3)
O1W	Cu1	N4	90.74	N4	C6	C5	109.6(3)
N2	Cu1	N4	174.3	N4	C6	H6	125.1
C1	N1	C2	128.7(2)	C5	C6	H6	125.2
C1	N1	C3	126.4(2)	N4	C7	N5	110.6(3)
C2	N1	C3	105.0(2)	N4	C7	H7	124.7
N3	N2	C2	108.3(2)	N5	C7	H7	124.7
N3	N2	Cu1	120.9	O1	C8	O2	126.4(3)
C2	N2	Cu1	130.0	O1	C8	C1	119.0(3)
N2	N3	C3	105.4(2)	O2	C8	C1	114.5(3)
Cu1	N4	C6	124.9	Cu1	O1W	H1WA	127
Cu1	N4	C7	128.7	Cu1	O1W	H1WB	126
C6	N4	C7	106.2(2)	H1WA	O1W	H1WB	105(3)
H5	N5	C5	126.1	C1	N1	C2	128.7(2)
H5	N5	C7	126.1	C1	N1	C3	126.4(2)
C5	N5	C7	107.8(2)	C2	N1	C3	105.0(2)
N1	C1	H1	106.9	Cu1	N2	N3	120.9
N1	C1	C4	111.2(2)	Cu1	N2	C2	130.0
N1	C1	C8	110.7(2)	N3	N2	C2	108.3(2)
H1	C1	C4	107.0	N2	N3	C3	105.4(2)
H1	C1	C8	106.9	C6	N4	C7	106.2(2)
C4	C1	C8	113.8(2)	C6	N4	Cu1	124.9
N1	C2	N2	109.7(2)	C7	N4	Cu1	128.7
N1	C2	H2	125.1	H5	N5	C5	126.1

H5	N5	C7	126.1	H4A	C4	C5	109.3
C5	N5	C7	107.8(2)	H4B	C4	C5	109.2
N1	C1	H1	106.9	N5	C5	C4	122.5(2)
N1	C1	C4	111.2(2)	N5	C5	C6	105.7(2)
N1	C1	C8	110.7(2)	C4	C5	C6	131.7(3)
H1	C1	C4	107.0	N4	C6	C5	109.6(3)
H1	C1	C8	106.9	N4	C6	H6	125.1
C4	C1	C8	113.8(2)	C5	C6	H6	125.2
N1	C2	N2	109.7(2)	N4	C7	N5	110.6(3)
N1	C2	H2	125.1	N4	C7	H7	124.7
N2	C2	H2	125.2	N5	C7	H7	124.7
N1	C3	N3	111.6(2)	O1	C8	O2	126.4(3)
N1	C3	H3	124.1	O1	C8	C1	119.0(3)
N3	C3	H3	124.3	O2	C8	C1	114.5(3)
C1	C4	H4A	109.2	Cu1	O1W	H1WA	127
C1	C4	H4B	109.2	Cu1	O1W	H1WB	126
C1	C4	C5	112.0(2)	H1WA	O1W	H1WB	105(3)
H4A	C4	H4B	107.9				

Table 30. Bond lengths (Å) of TAMOF-1 at 298 K.

Cu1	N4	1.982		N4	C6	1.369(4)
Cu1	O1W	2.494		N4	C7	1.321(4)
Cu1	N2	2.032		N5	H5	0.880
Cu1	O1W	2.494		N5	C5	1.360(4)
Cu1	N2	2.032		N5	C7	1.336(5)
Cu1	N4	1.982		C1	H1	1.001
O1	C8	1.225(4)		C1	C4	1.530(5)
O2	C8	1.266(4)		C1	C8	1.547(4)
N1	C1	1.470(4)		C2	H2	0.950
N1	C2	1.352(4)		C3	H3	0.950
N1	C3	1.348(4)		C4	H4A	0.990
N2	N3	1.390(3)		C4	H4B	0.990
N2	C2	1.312(4)		C4	C5	1.491(5)
N2	Cu1	2.032		C5	C6	1.360(5)
N3	C3	1.306(4)		C6	H6	0.949

UNIVERSITAT ROVIRA I VIRGILI
INSIGHTS IN HOMOCHIRAL METAL-ORGANIC FRAMEWORKS: FROM THEIR SYNTHESIS TO ENANTIOSELECTIVE
APPLICATIONS
Juanjo Cabezas Giménez

Annex I.

C7	H7	0.949	N5	C5	1.360(4)
O1W	H1WA	0.85(2)	N5	C7	1.336(5)
O1W	H1WB	0.85(3)	C1	H1	1.001
O1	C8	1.225(4)	C1	C4	1.530(5)
O2	C8	1.266(4)	C1	C8	1.547(4)
N1	C1	1.470(4)	C2	H2	0.950
N1	C2	1.352(4)	C3	H3	0.950
N1	C3	1.348(4)	C4	H4A	0.990
N2	N3	1.390(3)	C4	H4B	0.990
N2	C2	1.312(4)	C4	C5	1.491(5)
N3	C3	1.306(4)	C5	C6	1.360(5)
N4	C6	1.369(4)	C6	H6	0.949
N4	C7	1.321(4)	C7	H7	0.949
N4	Cu1	1.982	O1W	H1WA	0.85(2)
N5	H5	0.880	O1W	H1WB	0.85(3)

Table 31. Bond angles (°) of TAMOF-1 at 100 K.

N4	Cu1	O1W	99.4	N3	N2	Cu1	120.7
N4	Cu1	N2	174.1	C2	N2	Cu1	130.6
N4	Cu1	O1W	90.6	N2	N3	C3	105.4(2)
N4	Cu1	N2	88.0	Cu1	N4	C6	125.1
N4	Cu1	N4	89.1	Cu1	N4	C7	128.9
O1W	Cu1	N2	85.7	C6	N4	C7	105.9(3)
O1W	Cu1	O1W	166.0	H5	N5	C5	125.9
O1W	Cu1	N2	84.8	H5	N5	C7	125.9
O1W	Cu1	N4	90.6	C5	N5	C7	108.3(3)
N2	Cu1	O1W	84.8	N1	C1	H1	106.8
N2	Cu1	N2	95.3	N1	C1	C4	111.1(2)
N2	Cu1	N4	88.0	N1	C1	C8	110.7(2)
O1W	Cu1	N2	85.7	H1	C1	C4	106.8
O1W	Cu1	N4	99.4	H1	C1	C8	106.8
N2	Cu1	N4	174.1	C4	C1	C8	114.1(3)
C1	N1	C2	128.8(2)	N1	C2	N2	109.6(3)
C1	N1	C3	126.1(2)	N1	C2	H2	125.2
C2	N1	C3	105.1(2)	N2	C2	H2	125.2
N3	N2	C2	108.0(2)	N1	C3	N3	111.8(3)

UNIVERSITAT ROVIRA I VIRGILI
INSIGHTS IN HOMOCHIRAL METAL-ORGANIC FRAMEWORKS: FROM THEIR SYNTHESIS TO ENANTIOSELECTIVE
APPLICATIONS
Juanjo Cabezas Giménez

Crystallographic Data

N1	C3	H3	124.0	C5	N5	C7	108.3(3)
N3	C3	H3	124.2	N1	C1	H1	106.8
C1	C4	H4A	109.2	N1	C1	C4	111.1(2)
C1	C4	H4B	109.2	N1	C1	C8	110.7(2)
C1	C4	C5	112.2(3)	H1	C1	C4	106.8
H4A	C4	H4B	107.9	H1	C1	C8	106.8
H4A	C4	C5	109.1	C4	C1	C8	114.1(3)
H4B	C4	C5	109.1	N1	C2	N2	109.6(3)
N5	C5	C4	122.9(3)	N1	C2	H2	125.2
N5	C5	C6	105.7(3)	N2	C2	H2	125.2
C4	C5	C6	131.2(3)	N1	C3	N3	111.8(3)
N4	C6	C5	109.5(3)	N1	C3	H3	124.0
N4	C6	H6	125.2	N3	C3	H3	124.2
C5	C6	H6	125.2	C1	C4	H4A	109.2
N4	C7	N5	110.7(3)	C1	C4	H4B	109.2
N4	C7	H7	124.7	C1	C4	C5	112.2(3)
N5	C7	H7	124.7	H4A	C4	H4B	107.9
O1	C8	O2	125.9(3)	H4A	C4	C5	109.1
O1	C8	C1	119.3(3)	H4B	C4	C5	109.1
O2	C8	C1	114.8(3)	N5	C5	C4	122.9(3)
Cu1	O1W	H1WA	145	N5	C5	C6	105.7(3)
Cu1	O1W	H1WB	106	C4	C5	C6	131.2(3)
H1WA	O1W	H1WB	105(3)	N4	C6	C5	109.5(3)
C1	N1	C2	128.8(2)	N4	C6	H6	125.2
C1	N1	C3	126.1(2)	C5	C6	H6	125.2
C2	N1	C3	105.1(2)	N4	C7	N5	110.7(3)
Cu1	N2	N3	120.7	N4	C7	H7	124.7
Cu1	N2	C2	130.6	N5	C7	H7	124.7
N3	N2	C2	108.0(2)	O1	C8	O2	125.9(3)
N2	N3	C3	105.4(2)	O1	C8	C1	119.3(3)
C6	N4	C7	105.9(3)	O2	C8	C1	114.8(3)
C6	N4	Cu1	125.1	Cu1	O1W	H1WA	145
C7	N4	Cu1	128.9	Cu1	O1W	H1WB	106
H5	N5	C5	125.9	H1WA	O1W	H1WB	105(3)
H5	N5	C7	125.9				

Table 32. Bond lengths (Å) of TAMOF-1 at 403 K.

Cu01	N4	1.968	C6	H6	0.950
Cu01	N2	1.997	C7	H7	0.950
Cu01	N2	1.997	O1	C8	1.225(4)
Cu01	N4	1.968	O2	C8	1.247(4)
O1	C8	1.225(4)	N1	C1	1.473(4)
O2	C8	1.247(4)	N1	C2	1.348(4)
N1	C1	1.473(4)	N1	C3	1.353(4)
N1	C2	1.348(4)	N2	N3	1.382(4)
N1	C3	1.353(4)	N2	C2	1.307(4)
N2	N3	1.382(4)	N3	C3	1.302(4)
N2	C2	1.307(4)	N4	C6	1.366(4)
N2	Cu01	1.997	N4	C7	1.317(4)
N3	C3	1.302(4)	N4	Cu01	1.968
N4	C6	1.366(4)	N5	H5	0.880
N4	C7	1.317(4)	N5	C5	1.363(4)
N5	H5	0.880	N5	C7	1.331(5)
N5	C5	1.363(4)	C1	H1	1.001
N5	C7	1.331(5)	C1	C4	1.522(4)
C1	H1	1.001	C1	C8	1.554(4)
C1	C4	1.522(4)	C2	H2	0.949
C1	C8	1.554(4)	C3	H3	0.950
C2	H2	0.949	C4	H4A	0.991
C3	H3	0.950	C4	H4B	0.991
C4	H4A	0.991	C4	C5	1.493(5)
C4	H4B	0.991	C5	C6	1.360(5)
C4	C5	1.493(5)	C6	H6	0.950
C5	C6	1.360(5)	C7	H7	0.950

Table 33. Bond angles (°) of TAMOF-1 at 403 K.

N4	Cu01	N2	173.3	C1	N1	C2	129.7(2)
N4	Cu01	N2	88.9	C1	N1	C3	125.5(2)
N4	Cu01	N4	89.4	C2	N1	C3	104.8(2)
N2	Cu01	N2	93.5	N3	N2	C2	108.1(2)
N2	Cu01	N4	88.9	N3	N2	Cu01	118.9
N2	Cu01	N4	173.3	C2	N2	Cu01	132.7

293

UNIVERSITAT ROVIRA I VIRGILI
INSIGHTS IN HOMOCHIRAL METAL-ORGANIC FRAMEWORKS: FROM THEIR SYNTHESIS TO ENANTIOSELECTIVE
APPLICATIONS
Juanjo Cabezas Giménez

Crystallographic Data

N2	N3	C3	105.7(2)	C1	N1	C2	129.7(2)
Cu01	N4	C6	125.7	C1	N1	C3	125.5(2)
Cu01	N4	C7	127.5	C2	N1	C3	104.8(2)
C6	N4	C7	105.9(3)	Cu01	N2	N3	118.9
H5	N5	C5	126.1	Cu01	N2	C2	132.7
H5	N5	C7	126.0	N3	N2	C2	108.1(2)
C5	N5	C7	107.9(3)	N2	N3	C3	105.7(2)
N1	C1	H1	106.8	C6	N4	C7	105.9(3)
N1	C1	C4	111.1(2)	C6	N4	Cu01	125.7
N1	C1	C8	110.7(2)	C7	N4	Cu01	127.5
H1	C1	C4	106.8	H5	N5	C5	126.1
H1	C1	C8	106.8	H5	N5	C7	126.0
C4	C1	C8	114.2(3)	C5	N5	C7	107.9(3)
N1	C2	N2	109.9(3)	N1	C1	H1	106.8
N1	C2	H2	125.1	N1	C1	C4	111.1(2)
N2	C2	H2	125.1	N1	C1	C8	110.7(2)
N1	C3	N3	111.5(3)	H1	C1	C4	106.8
N1	C3	H3	124.3	H1	C1	C8	106.8
N3	C3	H3	124.2	C4	C1	C8	114.2(3)
C1	C4	H4A	109.2	N1	C2	N2	109.9(3)
C1	C4	H4B	109.3	N1	C2	H2	125.1
C1	C4	C5	111.9(3)	N2	C2	H2	125.1
H4A	C4	H4B	107.9	N1	C3	N3	111.5(3)
H4A	C4	C5	109.3	N1	C3	H3	124.3
H4B	C4	C5	109.2	N3	C3	H3	124.2
N5	C5	C4	123.1(3)	C1	C4	H4A	109.2
N5	C5	C6	105.8(3)	C1	C4	H4B	109.3
C4	C5	C6	130.9(3)	C1	C4	C5	111.9(3)
N4	C6	C5	109.3(3)	H4A	C4	H4B	107.9
N4	C6	H6	125.3	H4A	C4	C5	109.3
C5	C6	H6	125.3	H4B	C4	C5	109.2
N4	C7	N5	111.0(3)	N5	C5	C4	123.1(3)
N4	C7	H7	124.5	N5	C5	C6	105.8(3)
N5	C7	H7	124.4	C4	C5	C6	130.9(3)
O1	C8	O2	127.3(3)	N4	C6	C5	109.3(3)
O1	C8	C1	118.3(3)	N4	C6	H6	125.3
O2	C8	C1	114.4(3)	C5	C6	H6	125.3

UNIVERSITAT ROVIRA I VIRGILI
INSIGHTS IN HOMOCHIRAL METAL-ORGANIC FRAMEWORKS: FROM THEIR SYNTHESIS TO ENANTIOSELECTIVE
APPLICATIONS
Juanjo Cabezas Giménez

Annex I

N4	C7	N5	111.0(3)		O1	C8	O2	127.3(3)
N4	C7	H7	124.5		O1	C8	C1	118.3(3)
N5	C7	H7	124.4		O2	C8	C1	114.4(3)

Table 34. Bond lengths (Å) of TAMOF-1 at 100 K (rehydrated).

Cu1	N4	1.968		C6	H6	0.950
Cu1	N2	1.997		C7	H7	0.950
Cu1	N2	1.997		O1	C8	1.225(4)
Cu1	N4	1.968		O2	C8	1.247(4)
O1	C8	1.225(4)		N1	C1	1.473(4)
O2	C8	1.247(4)		N1	C2	1.348(4)
N1	C1	1.473(4)		N1	C3	1.353(4)
N1	C2	1.348(4)		N2	N3	1.382(4)
N1	C3	1.353(4)		N2	C2	1.307(4)
N2	N3	1.382(4)		N3	C3	1.302(4)
N2	C2	1.307(4)		N4	C6	1.366(4)
N2	Cu1	1.997		N4	C7	1.317(4)
N3	C3	1.302(4)		N4	Cu1	1.968
N4	C6	1.366(4)		N5	H5	0.880
N4	C7	1.317(4)		N5	C5	1.363(4)
N5	H5	0.880		N5	C7	1.331(5)
N5	C5	1.363(4)		C1	H1	1.001
N5	C7	1.331(5)		C1	C4	1.522(4)
C1	H1	1.001		C1	C8	1.554(4)
C1	C4	1.522(4)		C2	H2	0.949
C1	C8	1.554(4)		C3	H3	0.950
C2	H2	0.949		C4	H4A	0.991
C3	H3	0.950		C4	H4B	0.991
C4	H4A	0.991		C4	C5	1.493(5)
C4	H4B	0.991		C5	C6	1.360(5)
C4	C5	1.493(5)		C6	H6	0.950
C5	C6	1.360(5)		C7	H7	0.950

UNIVERSITAT ROVIRA I VIRGILI
INSIGHTS IN HOMOCHIRAL METAL-ORGANIC FRAMEWORKS: FROM THEIR SYNTHESIS TO ENANTIOSELECTIVE
APPLICATIONS
Juanjo Cabezas Giménez

Crystallographic Data

Table 35. Bond angles (º) of TAMOF-1 at 100 K (rehydrated).

N4	Cu1	N2	173.3	H4B	C4	C5	109.2
N4	Cu1	N2	88.9	N5	C5	C4	123.1(3)
N4	Cu1	N4	89.4	N5	C5	C6	105.8(3)
N2	Cu1	N2	93.5	C4	C5	C6	130.9(3)
N2	Cu1	N4	88.9	N4	C6	C5	109.3(3)
N2	Cu1	N4	173.3	N4	C6	H6	125.3
C1	N1	C2	129.7(2)	C5	C6	H6	125.3
C1	N1	C3	125.5(2)	N4	C7	N5	111.0(3)
C2	N1	C3	104.8(2)	N4	C7	H7	124.5
N3	N2	C2	108.1(2)	N5	C7	H7	124.4
N3	N2	Cu1	118.9	O1	C8	O2	127.3(3)
C2	N2	Cu1	132.7	O1	C8	C1	118.3(3)
N2	N3	C3	105.7(2)	O2	C8	C1	114.4(3)
Cu1	N4	C6	125.7	C1	N1	C2	129.7(2)
Cu1	N4	C7	127.5	C1	N1	C3	125.5(2)
C6	N4	C7	105.9(3)	C2	N1	C3	104.8(2)
H5	N5	C5	126.1	Cu1	N2	N3	118.9
H5	N5	C7	126.0	Cu1	N2	C2	132.7
C5	N5	C7	107.9(3)	N3	N2	C2	108.1(2)
N1	C1	H1	106.8	N2	N3	C3	105.7(2)
N1	C1	C4	111.1(2)	C6	N4	C7	105.9(3)
N1	C1	C8	110.7(2)	C6	N4	Cu1	125.7
H1	C1	C4	106.8	C7	N4	Cu1	127.5
H1	C1	C8	106.8	H5	N5	C5	126.1
C4	C1	C8	114.2(3)	H5	N5	C7	126.0
N1	C2	N2	109.9(3)	C5	N5	C7	107.9(3)
N1	C2	H2	125.1	N1	C1	H1	106.8
N2	C2	H2	125.1	N1	C1	C4	111.1(2)
N1	C3	N3	111.5(3)	N1	C1	C8	110.7(2)
N1	C3	H3	124.3	H1	C1	C4	106.8
N3	C3	H3	124.2	H1	C1	C8	106.8
C1	C4	H4A	109.2	C4	C1	C8	114.2(3)
C1	C4	H4B	109.3	N1	C2	N2	109.9(3)
C1	C4	C5	111.9(3)	N1	C2	H2	125.1
H4A	C4	H4B	107.9	N2	C2	H2	125.1
H4A	C4	C5	109.3	N1	C3	N3	111.5(3)

UNIVERSITAT ROVIRA I VIRGILI
INSIGHTS IN HOMOCHIRAL METAL-ORGANIC FRAMEWORKS: FROM THEIR SYNTHESIS TO ENANTIOSELECTIVE
APPLICATIONS
Juanjo Cabezas Giménez

Annex I

N1	C3	H3	124.3	C4	C5	C6	130.9(3)
N3	C3	H3	124.2	N4	C6	C5	109.3(3)
C1	C4	H4A	109.2	N4	C6	H6	125.3
C1	C4	H4B	109.3	C5	C6	H6	125.3
C1	C4	C5	111.9(3)	N4	C7	N5	111.0(3)
H4A	C4	H4B	107.9	N4	C7	H7	124.5
H4A	C4	C5	109.3	N5	C7	H7	124.4
H4B	C4	C5	109.2	O1	C8	O2	127.3(3)
N5	C5	C4	123.1(3)	O1	C8	C1	118.3(3)
N5	C5	C6	105.8(3)	O2	C8	C1	114.4(3)

UNIVERSITAT ROVIRA I VIRGILI
INSIGHTS IN HOMOCHIRAL METAL-ORGANIC FRAMEWORKS: FROM THEIR SYNTHESIS TO ENANTIOSELECTIVE
APPLICATIONS
Juanjo Cabezas Giménez

Crystallographic Data

Crystallographic data of TAMOF-1 neutron diffraction

Table 36. Crystallographic data and refinement parameters for the crystal structure of TAMOF-1 immersed in CO_2 at 100 K.

Empirical formula	$C_{17.96}H_{16}N_{10}O_{7.92}Cu$
Formula weight	562.17
T/K	100(2)
Wavelength/Å	1.45566
Crystal system	Cubic
Space group	$P4_332$
a/Å	20.1760(14)
b/Å	20.1760(14)
c/Å	20.1760(14)
$\alpha/°$	90
$\beta/°$	90
$\gamma/°$	90
Volume/Å^3	8213.1(17)
Z	12
ρ_{calc}/g cm^{-3}	1.364
μ/mm^{-1}	0.117
$F(000)$	2482
Crystal size/mm^3	1.000 x 0.600 x 0.400 mm^3
θ range for data collection/°	9.254 to 121.33
Index ranges	$-20 \leq h \leq 10, -1 \leq k \leq 23, -9 \leq l \leq 23$
Reflections collected	2431
Independent reflections	2431[R_{int} = 0.0736, R_{sigma} = 0.0496]]
Completeness/%	98.5%
Absorption correction	Multi-scan
Max. and min. transmission	?
Refinement method	?
Data/restraints/parameters	2431/141/348
Goodness-of-fit on F^2	1.782
Final R indices [I>=2σ (I)]	R_1 = 0.0866, wR_2 = 0.2175
R indices (all data)	R_1 = 0.0935, wR_2 = 0.2210
Flack parameter	?
Largest diff. peak and hole	0.91 and –0.90 e.Å^{-3}

Table 37. Bond lengths (Å) of TAMOF-1 immersed in CO_2 at 100 K.

C1	N1	1.452(7)	N4	C7	1.346(9)
C1	C4	1.516(9)	N4	C6	1.381(8)
C1	C8	1.561(9)	C5	C6	1.367(9)
N1	C2	1.366(7)	C5	N5	1.370(8)
N1	C3	1.367(7)	N5	C7	1.348(8)
O1	C8	1.235(10)	O1C	C1C	1.179(12)
Cu1	N4	1.959(7)	C1C	O2C	1.170(12)
Cu1	N4	1.959(7)	O1D	C1D	1.165(12)
Cu1	N2	2.014(7)	C1D	O2D	1.165(13)
Cu1	N2	2.014(7)	O1F	C1F	1.163(12)
C2	N2	1.306(7)	C1F	O2F	1.163(12)
N2	N3	1.388(6)	O1E	C1E	1.164(13)
O2	C8	1.258(10)	C1E	O2E	1.166(13)
C3	N3	1.311(7)	O1L	C1L	1.164(12)
C4	C5	1.501(9)	C1L	O2L	1.162(12)

Table 38. Bond angles (º) of TAMOF-1 immersed in CO_2 at 100 K.

N1	C1	C4	111.1(5)	C3	N3	N2	106.1(4)
N1	C1	C8	110.1(5)	C5	C4	C1	111.7(5)
C4	C1	C8	114.3(5)	C7	N4	C6	106.7(5)
C2	N1	C3	105.0(4)	C7	N4	Cu1	127.4(4)
C2	N1	C1	129.5(5)	C6	N4	Cu1	125.4(4)
C3	N1	C1	125.5(5)	C6	C5	N5	107.1(6)
N4	Cu1	N4[1]	89.3(4)	C6	C5	C4	130.7(6)
N4	Cu1	N2[2]	88.73(17)	N5	C5	C4	121.9(6)
N4[1]	Cu1	N2[2]	173.7(2)	C7	N5	C5	108.0(5)
N4	Cu1	N2[3]	173.7(2)	C5	C6	N4	108.3(6)
N4[1]	Cu1	N2[3]	88.73(17)	N4	C7	N5	109.8(6)
N2[2]	Cu1	N2[3]	93.9(4)	O1	C8	O2	127.6(7)
N2	C2	N1	109.5(5)	O1	C8	C1	118.7(6)
C2	N2	N3	108.7(4)	O2	C8	C1	113.8(6)
C2	N2	Cu1[4]	132.0(4)	O2C	C1C	O1C	163(3)
N3	N2	Cu1[4]	119.0(3)	O2D	C1D	O1D	172(8)
N3	C3	N1	110.8(5)	O2F	C1F	O1F	175(10)

Crystallographic data of Pt@TAMOF-1

Table 39. Crystallographic data and refinement parameters for the crystal structure of Pt@TAMOF-1 collected at 100 K.

Empirical formula	$C_{11.29}H_{22.82}Cu_{0.71}N_{7.06}O_{8.59}$
Formula weight	439.80
T/K	100(2) K
Wavelength/Å	0.71073
Crystal system	Cubic
Space group	$P4_332$
a/Å	20.24600(10)Å
b/Å	20.24600(10)Å
c/Å	20.24600(10)Å
$\alpha/°$	90°
$\beta/°$	90°
$\gamma/°$	90°
Volume/Å^3	8298.85(12) Å^3
Z	17
ρ_{calc}/g cm^{-3}	1.496 g cm^{-3}
μ/mm^{-1}	0.864 mm^{-1}
F(000)	3896
Crystal size/mm^3	0.400 x 0.200 x 0.020 mm^3
θ range for data collection/°	2.846 to 32.049°
Index ranges	$-25 \leq h \leq 26, -29 \leq k \leq 29, -15 \leq l \leq 30$
Reflections collected	29269
Independent reflections	4631[R_{int} = 0.0481]
Completeness/%	96.8%
Absorption correction	Multi-scan
Max. and min. transmission	1.00 and 0.92
Refinement method	Full-matrix least-squares on F^2
Data/restraints/parameters	4631/23/276
Goodness-of-fit on F^2	1.212
Final R indices [I>=2σ (I)]	R1 = 0.0378, wR2 = 0.0924
R indices (all data)	R1 = 0.0403, wR2 = 0.0931
Flack parameter	x =0.022(4)
Largest diff. peak and hole	0.379 and -0.337 e.Å^{-3}

Table 40. Bond lengths (Å) of Pt@TAMOF-1.

Cu1	N4#	1.984(2)	C3	C4	1.547(4)
Cu1	N4#	1.984(2)	C3	H3	1.0000
Cu1	N2#	2.036(2)	N4	C8	1.322(4)
Cu1	N2	2.036(2)	N4	C7	1.373(4)
O1	C4	1.243(4)	N5	C8	1.348(4)
N1	C2	1.356(3)	N5	C6	1.383(4)
N1	C1	1.363(3)	N5	H5	0.8800
N1	C3	1.467(4)	C5	C6	1.492(4)
C1	N3	1.312(4)	C5	H5A	0.9900
C1	H1	0.9500	C5	H5AB	0.9900
N2	C2	1.316(4)	C6	C7	1.370(4)
N2	N3	1.390(3)	C7	H7	0.9500
O2	C4	1.270(4)	C8	H8	0.9500
C2	H2	0.9500	O1W	H1WA	0.7299
C3	C5	1.537(4)	O1W	H1WB	0.7621

Table 41. Bond angles (º) of Pt@TAMOF-1 at 100 K.

N4#	Cu1	N4#	89.57(14)	C1	N3	N2	105.5(2)
N4#	Cu1	N2#	174.31(10)	N1	C3	C5	111.2(2)
N4#	Cu1	N2#	87.37(9)	N1	C3	C4	110.8(2)
N4#	Cu1	N2	87.37(9)	C5	C3	C4	113.7(2)
N4#	Cu1	N2	174.31(10)	N1	C3	H3	106.9
N2#	Cu1	N2	96.07(13)	C5	C3	H3	106.9
C2	N1	C1	104.6(2)	C4	C3	H3	106.9
C2	N1	C3	129.0(2)	C8	N4	C7	106.4(2)
C1	N1	C3	126.4(2)	C8	N4	Cu1#	128.5(2)
N3	C1	N1	111.7(2)	C7	N4	Cu1#	124.9(2)
N3	C1	H1	124.1	O1	C4	O2	126.0(3)
N1	C1	H1	124.1	O1	C4	C3	119.0(3)
C2	N2	N3	108.2(2)	O2	C4	C3	115.0(3)
C2	N2	Cu1	129.75(19)	C8	N5	C6	108.0(2)
N3	N2	Cu1	121.31(17)	C8	N5	H5	126.0
N2	C2	N1	110.0(2)	C6	N5	H5	126.0
N2	C2	H2	125.0	C6	C5	C3	111.8(2)
N1	C2	H2	125.0	C6	C5	H5A	109.2

C3	C5	H5A	109.2	C6	C7	N4	109.8(3)
C6	C5	H5AB	109.2	C6	C7	H7	125.1
C3	C5	H5AB	109.2	N4	C7	H7	125.1
H5A	C5	H5AB	107.9	N4	C8	N5	110.7(3)
C7	C6	N5	105.1(3)	N4	C8	H8	124.7
C7	C6	C5	131.9(3)	N5	C8	H8	124.7
N5	C6	C5	122.9(3)	H1WA	O1W	H1WB	108.6

UNIVERSITAT ROVIRA I VIRGILI
INSIGHTS IN HOMOCHIRAL METAL-ORGANIC FRAMEWORKS: FROM THEIR SYNTHESIS TO ENANTIOSELECTIVE
APPLICATIONS
Juanjo Cabezas Giménez

Annex I

Crystallographic data of 2

Table 42. Crystallographic data and refinement parameters for the crystal structure of **2** collected at 100 K.

Empirical formula	$C_{11}H_{14}N_6O_3$
Formula weight	278.78
Wavelength/Å	0.71073
Crystal system	Monoclinic
Space group	$P2_1$
a/Å	4.8299(5)Å
b/Å	13.4847(13)Å
c/Å	9.7074(9)Å
α/°	90°
β/°	92.218(3)°
γ/°	90°
Volume/Å^3	631.77(11) Å^3
Z	2
ρ_{calc}/g cm^{-3}	1.463 g cm^{-3}
μ/mm^{-1}	0.111 mm^{-1}
$F(000)$	292
Crystal size/mm^3	0.200 x 0.100 x 0.050 mm^3
θ range for data collection/°	2.100 to 26.455°
Index ranges	$-5 \leq h \leq 6, -10 \leq k \leq 16, -10 \leq l \leq 12$
Reflections collected	3693
Independent reflections	2054[R_{int} = 0.0395]
Completeness/%	99.0%
Absorption correction	Multi-scan
Max. and min. transmission	0.74 and 0.46
Refinement method	Full-matrix least-squares on F^2
Data/restraints/parameters	2045/3/196
Goodness-of-fit on F^2	1.046
Final R indices [I>=2σ (I)]	R1 = 0.0393, wR2 = 0.1028
R indices (all data)	R1 = 0.0407, wR2 = 0.1040
Flack parameter	x =-1.9(10)
Largest diff. peak and hole	0.190 and -0.241 e.Å^{-3}

UNIVERSITAT ROVIRA I VIRGILI
INSIGHTS IN HOMOCHIRAL METAL-ORGANIC FRAMEWORKS: FROM THEIR SYNTHESIS TO ENANTIOSELECTIVE
APPLICATIONS
Juanjo Cabezas Giménez

Crystallographic Data

Table 43. Bond lengths (Å) of **2** at 100 K.

O1	C1	1.267(4)	N6	C10	1.309(4)
N1	C6	1.340(4)	C1	C2	1.539(4)
N1	C4	1.378(4)	C2	C3	1.543(4)
O2	C1	1.239(3)	C3	C4	1.497(4)
N2	C6	1.321(4)	C7	C8	1.516(4)
N2	C5	1.376(4)	C8	C9	1.519(4)
O3	C7	1.238(4)	O1	C1	1.267(4)
N3	C7	1.340(4)	N1	C6	1.340(4)
N3	C2	1.458(4)	N1	C4	1.378(4)
N4	C11	1.366(4)	O2	C1	1.239(3)
N4	C10	1.367(5)	N2	C6	1.321(4)
N4	C9	1.462(4)	N2	C5	1.376(4)
N5	C11	1.303(5)	O3	C7	1.238(4)
N5	N6	1.392(4)	N3	C7	1.340(4)
C5	C4	1.368(5)			

Table 44. Bond angles (°) of **2** at 100 K.

C6	N1	C4	109.0(3)	N3	C2	C3	112.7(3)
C6	N2	C5	107.8(3)	C1	C2	C3	114.2(2)
C7	N3	C2	121.4(3)	C4	C3	C2	114.3(2)
C11	N4	C10	103.5(3)	C5	C4	N1	105.5(3)
C11	N4	C9	128.6(3)	C5	C4	C3	132.1(3)
C10	N4	C9	127.9(2)	N1	C4	C3	122.4(3)
C11	N5	N6	106.7(3)	O3	C7	N3	122.7(3)
C4	C5	N2	108.4(3)	O3	C7	C8	121.4(3)
C10	N6	N5	106.8(3)	N3	C7	C8	115.8(3)
N2	C6	N1	109.3(3)	C7	C8	C9	112.4(2)
O2	C1	O1	126.5(3)	N4	C9	C8	112.2(2)
O2	C1	C2	118.8(2)	N6	C10	N4	111.3(3)
O1	C1	C2	114.6(2)	N5	C11	N4	111.7(3)
N3	C2	C1	109.4(2)				

Crystallographic data of 13

Table 45. Crystallographic data and refinement parameters for the crystal structure of **13** collected at 293 K.

Empirical formula	$C_9H_{11}N_5O_2$
Formula weight	221.23
T/K	293(2) K
Wavelength/Å	0.71073
Crystal system	Monoclinic
Space group	$P2_1$
a/Å	9.9742(12) Å
b/Å	5.0008(4) Å
c/Å	11.0838(12) Å
α/°	90°
β/°	115.304(14)°
γ/°	90°
Volume/Å^3	499.80(10) Å^3
Z	2
ρ_{calc}/g cm^{-3}	1.470
μ/mm^{-1}	0.109
F(000)	232
Crystal size/mm^3	?
θ range for data collection/°	2.304 to 29.434°
Index ranges	$-13 \leq h \leq 13, -6 \leq k \leq 6, -14 \leq l \leq 14$
Reflections collected	3129
Independent reflections	3129
Completeness/%	88.1
Absorption correction	Multi-scan
Max. and min. transmission	1.00 and 0.852
Refinement method	Full-matrix least-squares on F^2
Data/restraints/parameters	3129 / 1 / 146
Goodness-of-fit on F^2	1.097
Final R indices [I>=2σ (I)]	$R_1 = 0.0326$, w$R_2 = 0.0891$
R indices (all data)	$R_1 = 0.0341$, w$R_2 = 0.0958$
Flack parameter	x = 0.8(9)
Largest diff. peak and hole	0.306 and -0.242 e· Å^{-3}

UNIVERSITAT ROVIRA I VIRGILI
INSIGHTS IN HOMOCHIRAL METAL-ORGANIC FRAMEWORKS: FROM THEIR SYNTHESIS TO ENANTIOSELECTIVE
APPLICATIONS
Juanjo Cabezas Giménez

Crystallographic Data

Table 46. Bond lengths (Å) of **13** at 100 K.

O1	C1	1.237(3)	N4	C7	1.387(3)
N1	C3	1.347(3)	N4	H4A	0.86
N1	C4	1.366(3)	C5	C6	1.550(3)
N1	C2	1.474(3)	C5	H5A	0.97
C1	O2	1.265(3)	C5	H5AB	0.97
C1	C2	1.555(3)	N5	C9	1.333(3)
N2	C3	1.315(3)	N5	C8	1.384(3)
N2	N3	1.389(3)	N5	H5	0.86
C2	C5	1.526(3)	C8	C7	1.363(3)
C2	H2	0.98	C8	H8	0.93
C3	H3	0.93	C7	C6	1.493(3)
N3	C4	1.315(3)	C6	H6A	0.97
C4	H4	0.93	C6	H6AB	0.97
N4	C9	1.332(3)	C9	H9	0.93

Table 47. Bond angles (°) of **13** at 100 K.

C3	N1	C4	104.59(18)	C2	C5	H5A	108.7
C3	N1	C2	124.78(18)	C6	C5	H5A	108.7
C4	N1	C2	130.19(19)	C2	C5	H5AB	108.7
O1	C1	O2	127.2(2)	C6	C5	H5AB	108.7
O1	C1	C2	119.84(19)	H5A	C5	H5AB	107.6
O2	C1	C2	112.99(18)	C9	N5	C8	109.15(19)
C3	N2	N3	107.85(18)	C9	N5	H5	125.4
N1	C2	C5	112.45(17)	C8	N5	H5	125.4
N1	C2	C1	110.46(17)	C7	C8	N5	106.61(19)
C5	C2	C1	108.48(18)	C7	C8	H8	126.7
N1	C2	H2	108.5	N5	C8	H8	126.7
C5	C2	H2	108.5	C8	C7	N4	106.90(18)
C1	C2	H2	108.5	C8	C7	C6	133.02(19)
N2	C3	N1	110.5(2)	N4	C7	C6	119.80(19)
N2	C3	H3	124.7	C7	C6	C5	108.87(17)
N1	C3	H3	124.7	C7	C6	H6A	109.9
C4	N3	N2	105.63(18)	C5	C6	H6A	109.9
N3	C4	N1	111.4(2)	C7	C6	H6AB	109.9
N3	C4	H4	124.3	C5	C6	H6AB	109.9
N1	C4	H4	124.3	H6A	C6	H6AB	108.3
C9	N4	C7	108.86(18)	N4	C9	N5	108.48(18)
C9	N4	H4A	125.6	N4	C9	H9	125.8
C7	N4	H4A	125.6	N5	C9	H9	125.8
C2	C5	C6	114.20(19)				

Crystallographic data of Cu-2

Table 48. Crystallographic data and refinement parameters for the crystal structure of **Cu-2** collected at 100 K.

Empirical formula	$C_{12.10}H_{19.20}CuN_7O_{8.5}$
Formula weight	462.28
T/K	100(2) K
Wavelength/Å	0.71073
Crystal system	Orthorhombic
Space group	$P2_12_12$
a/Å	15.3496(16)Å
b/Å	17.1992(13)Å
c/Å	7.0146(10)Å
$\alpha/°$	90°
$\beta/°$	90°
$\gamma/°$	90°
Volume/Å^3	1851.9(4) Å^3
Z	4
ρ_{calc}/g cm^{-3}	1.658 g cm^{-3}
μ/mm^{-1}	1.241 mm^{-1}
$F(000)$	951
Crystal size/mm^3	0.120 x 0.080 x 0.050 mm^3
θ range for data collection/°	2.368 to 35.624°
Index ranges	$-24 \leq h \leq 25, -21 \leq k \leq 22, -9 \leq l \leq 10$
Reflections collected	12.642
Independent reflections	5700[R_{int} = 0.0321]
Completeness/%	72.0%
Absorption correction	Multi-scan
Max. and min. transmission	1.00 and 0.80
Refinement method	Full-matrix least-squares on F^2
Data/restraints/parameters	5700/714/462
Goodness-of-fit on F^2	1.076
Final R indices [I>=2σ (I)]	R_1 = 0.0471, wR_2 = 0.1108
R indices (all data)	R_1 = 0.0674, wR_2 = 0.1187
Flack parameter	x =-0.004(7)
Largest diff. peak and hole	0.703 and -0.692 e.Å^{-3}

UNIVERSITAT ROVIRA I VIRGILI
INSIGHTS IN HOMOCHIRAL METAL-ORGANIC FRAMEWORKS: FROM THEIR SYNTHESIS TO ENANTIOSELECTIVE
APPLICATIONS
Juanjo Cabezas Giménez

Crystallographic Data

Table 49. Bond lengths (Å) of **Cu-2** at 100 K.

Cu1	O1	1.835(3)		N6	C11	1.207(6)
Cu1	N5'#	1.90(2)		C5	H5	0.9500
Cu1	N5#	1.958(10)		C6	H6	0.9500
Cu1	N2#	1.998(7)		C7	C8	1.620(10)
Cu1	N6#	2.036(9)		C8	C9	1.519(9)
Cu1	N2'#	2.060(18)		C8	H8A	0.9900
Cu1	N6'#	2.15(2)		C8	H8B	0.9900
O1	C1	1.217(8)		C9	H9A	0.9900
O1	C1'	1.340(16)		C9	H9B	0.9900
O1W	H1W	0.8585		C10	H10	0.9500
O1W	H2W	0.8535		C11	H11	0.9500
C3M	O3M	1.44(3)		N1'	C6'	1.310(11)
C3M	H3M1	0.9800		N1'	C4'	1.392(12)
C3M	H3M2	0.9800		N1'	H1'	0.8800
C3M	H3M3	0.9800		C1'	O2'	1.291(12)
O3M	H3M	0.8400		C1'	C2'	1.459(11)
O2W	H21W	0.7474		N2'	C5'	1.265(11)
O2W	H21W#	0.7473		N2'	C6'	1.492(12)
N1	C6	1.303(7)		C2'	C3'	1.494(12)
N1	C4	1.392(8)		C2'	N3'	1.570(13)
N1	H1	0.8800		C2'	H2'	1.0000
C1	O2	1.281(8)		O3'	C7'	1.253(12)
C1	C2	1.463(7)		N3'	C7'	1.349(12)
N2	C5	1.261(7)		N3'	H3A'	0.8800
N2	C6	1.487(8)		C3'	C4'	1.383(11)
C2	C3	1.490(8)		C3'	H3'	0.9500
C2	N3	1.573(9)		N4'	C10'	1.315(11)
C2	H2	1.0000		N4'	C9'	1.402(10)
O3	C7	1.251(8)		N4'	C11'	1.465(11)
N3	C7	1.346(8)		C4'	C5'	1.473(12)
N3	H3A	0.8800		N5'	C10'	1.309(12)
C3	C4	1.378(7)		N5'	N6'	1.478(12)
C3	H3	0.9500		N6'	C11'	1.209(11)
N4	C10	1.315(7)		C5'	H5'	0.9500
N4	C9	1.403(6)		C6'	H6'	0.9500
N4	C11	1.463(8)		C7'	C8'	1.617(14)
C4	C5	1.472(8)		C8'	C9'	1.520(13)
N5	C10	1.309(8)		C8'	H8'A	0.9900
N5	N6	1.477(7)		C8'	H8'B	0.9900

UNIVERSITAT ROVIRA I VIRGILI
INSIGHTS IN HOMOCHIRAL METAL-ORGANIC FRAMEWORKS: FROM THEIR SYNTHESIS TO ENANTIOSELECTIVE
APPLICATIONS
Juanjo Cabezas Giménez

Annex I

C9'	H9'A	0.9900	C1M	H1M1	0.9800
C9'	H9'B	0.9900	C1M	H1M2	0.9800
C10'	H10'	0.9500	C1M	H1M3	0.9800
C11'	H11'	0.9500	O1M	H1M	0.830(7)
O1A	N1A	1.357(10)	C4M	O4M	1.33(3)
O1A	N1A'	1.38(2)	C4M	H4M1	0.9800
N1A	O2A	1.201(9)	C4M	H4M2	0.9800
N1A	O3A	1.233(10)	C4M	H4M3	0.9800
N1A'	O2A'	1.218(12)	O4M	H4M	0.8400
N1A'	O3A'	1.236(13)	O3W	H3W1	0.9075
C1M	O1M	1.489(9)	O3W	H3W2	0.8333

Table 50. Bond angles (º) of **Cu-2** at 100 K.

O1	Cu1	N5'#	171.4(11)	C3M	O3M	H3M	109.5
O1	Cu1	N5#	176.7(5)	H21W	O2W	H21W#	103.9
O1	Cu1	N2#	84.0(4)	C6	N1	C4	98.1(5)
N5#	Cu1	N2#	98.5(4)	C6	N1	H1	130.9
O1	Cu1	N6#	97.3(7)	C4	N1	H1	130.9
N5#	Cu1	N6#	80.2(8)	O1	C1	O2	130.9(6)
N2#	Cu1	N6#	178.1(5)	O1	C1	C2	112.0(5)
O1	Cu1	N2'#	84.8(9)	O2	C1	C2	117.0(6)
N5#	Cu1	N2'#	97.5(12)	C5	N2	C6	105.4(5)
N2#	Cu1	N2'#	6.6(13)	C5	N2	Cu1#	121.0(7)
N6#	Cu1	N2'#	174.3(14)	C6	N2	Cu1#	130.7(7)
O1	Cu1	N6'#	98.6(17)	C1	C2	C3	107.7(5)
N5'#	Cu1	N6'#	78(2)	C1	C2	N3	114.1(5)
N5#	Cu1	N6'#	79.0(18)	C3	C2	N3	104.6(5)
N2#	Cu1	N6'#	175.1(12)	C1	C2	H2	110.1
N6#	Cu1	N6'#	3.1(17)	C3	C2	H2	110.1
N2'#	Cu1	N6'#	176(2)	N3	C2	H2	110.1
C1	O1	Cu1	124.9(4)	C7	N3	C2	124.8(6)
C1'	O1	Cu1	118.6(6)	C7	N3	H3A	117.6
H1W	O1W	H2W	107.5	C2	N3	H3A	117.6
O3M	C3M	H3M1	109.5	C4	C3	C2	107.9(6)
O3M	C3M	H3M2	109.5	C4	C3	H3	126.0
H3M1	C3M	H3M2	109.5	C2	C3	H3	126.0
O3M	C3M	H3M3	109.5	C10	N4	C9	116.3(7)
H3M1	C3M	H3M3	109.5	C10	N4	C11	113.6(5)
H3M2	C3M	H3M3	109.5	C9	N4	C11	130.1(7)

Crystallographic Data

C3	C4	N1	111.6(6)	O2'	C1'	C2'	121.2(13)
C3	C4	C5	133.7(6)	O1	C1'	C2'	105.8(11)
N1	C4	C5	114.7(5)	C5'	N2'	C6'	106.0(10)
C10	N5	N6	115.6(6)	C1'	C2'	C3'	107.7(11)
C10	N5	Cu1#	119.3(7)	C1'	C2'	N3'	117.3(13)
N6	N5	Cu1#	125.0(7)	C3'	C2'	N3'	104.1(11)
C11	N6	N5	103.4(5)	C1'	C2'	H2'	109.2
C11	N6	Cu1#	127.4(8)	C3'	C2'	H2'	109.2
N5	N6	Cu1#	129.0(7)	N3'	C2'	H2'	109.2
N2	C5	C4	104.9(5)	C7'	N3'	C2'	126.3(13)
N2	C5	H5	127.5	C7'	N3'	H3A'	116.9
C4	C5	H5	127.5	C2'	N3'	H3A'	116.9
N1	C6	N2	116.8(6)	C4'	C3'	C2'	108.1(13)
N1	C6	H6	121.6	C4'	C3'	H3'	126.0
N2	C6	H6	121.6	C2'	C3'	H3'	126.0
O3	C7	N3	118.5(8)	C10'	N4'	C9'	116.8(13)
O3	C7	C8	124.4(6)	C10'	N4'	C11'	112.7(10)
N3	C7	C8	117.1(6)	C9'	N4'	C11'	129.6(14)
C9	C8	C7	122.6(6)	C3'	C4'	N1'	111.3(13)
C9	C8	H8A	106.7	C3'	C4'	C5'	134.9(14)
C7	C8	H8A	106.7	N1'	C4'	C5'	112.1(9)
C9	C8	H8B	106.7	C10'	N5'	N6'	114.5(14)
C7	C8	H8B	106.7	C11'	N6'	N5'	103.0(11)
H8A	C8	H8B	106.6	N2'	C5'	C4'	106.1(10)
N4	C9	C8	108.3(7)	N2'	C5'	H5'	126.9
N4	C9	H9A	110.0	C4'	C5'	H5'	126.9
C8	C9	H9A	110.0	N1'	C6'	N2'	114.2(10)
N4	C9	H9B	110.0	N1'	C6'	H6'	122.9
C8	C9	H9B	110.0	N2'	C6'	H6'	122.9
H9A	C9	H9B	108.4	O3'	C7'	N3'	119.2(15)
N5	C10	N4	99.2(6)	O3'	C7'	C8'	123.8(14)
N5	C10	H10	130.4	N3'	C7'	C8'	117.0(12)
N4	C10	H10	130.4	C9'	C8'	C7'	124.5(14)
N6	C11	N4	107.8(5)	C9'	C8'	H8'A	106.2
N6	C11	H11	126.1	C7'	C8'	H8'A	106.2
N4	C11	H11	126.1	C9'	C8'	H8'B	106.2
C6'	N1'	C4'	101.2(9)	C7'	C8'	H8'B	106.2
C6'	N1'	H1'	129.4	H8'A	C8'	H8'B	106.4
C4'	N1'	H1'	129.4	N4'	C9'	C8'	108.1(14)
O2'	C1'	O1	132.6(12)	N4'	C9'	H9'A	110.1

C8'	C9'	H9'A	110.1	O1M	C1M	H1M1	109.5
N4'	C9'	H9'B	110.1	O1M	C1M	H1M2	109.5
C8'	C9'	H9'B	110.1	H1M1	C1M	H1M2	109.5
H9'A	C9'	H9'B	108.4	O1M	C1M	H1M3	109.5
N5'	C10'	N4'	98.4(11)	H1M1	C1M	H1M3	109.5
N5'	C10'	H10'	130.8	H1M2	C1M	H1M3	109.5
N4'	C10'	H10'	130.8	C1M	O1M	H1M	107(6)
N6'	C11'	N4'	107.5(11)	O4M	C4M	H4M1	109.5
N6'	C11'	H11'	126.2	O4M	C4M	H4M2	109.5
N4'	C11'	H11'	126.2	H4M1	C4M	H4M2	109.5
O2A	N1A	O3A	108.4(9)	O4M	C4M	H4M3	109.5
O2A	N1A	O1A	123.7(10)	H4M1	C4M	H4M3	109.5
O3A	N1A	O1A	127.9(9)	H4M2	C4M	H4M3	109.5
O2A'	N1A'	O3A'	114.5(17)	C4M	O4M	H4M	109.5
O2A'	N1A'	O1A	123.2(16)	H3W1	O3W	H3W2	106.8
O3A'	N1A'	O1A	122.2(16)				

UNIVERSITAT ROVIRA I VIRGILI
INSIGHTS IN HOMOCHIRAL METAL-ORGANIC FRAMEWORKS: FROM THEIR SYNTHESIS TO ENANTIOSELECTIVE
APPLICATIONS
Juanjo Cabezas Giménez

Crystallographic Data

Crystallographic data of Zn-5

Table 51. Crystallographic data and refinement parameters for the crystal structure of **Zn-5** collected at 100 K.

Empirical formula	$C_{11}H_{14}ClN_5O_2Zn$
Formula weight	349.09
T/K	100(2)K
Wavelength/Å	0.71073 Å
Crystal system	Monoclinic
Space group	$P2_1$
a/Å	7.8493(3)Å
b/Å	15.7291(6)Å
c/Å	11.1380(4)Å
α/°	90°
β/°	92.045(3)°
γ/°	90°
Volume/Å^3	1374.25(8) Å^3
Z	4
ρ_{calc}/g cm^{-3}	1.687 g cm^{-3}
μ/mm^{-1}	1.990 mm^{-1}
F(000)	712
Crystal size/mm^3	0.250 x 0.100 x 0.100 mm^3
θ range for data collection/°	2.590 to 31.987°.
Index ranges	$-11 \leq h \leq 11, -20 \leq k \leq 23, -16 \leq l \leq 13$
Reflections collected	22468
Independent reflections	8337[R(int) = 0.0332]
Completeness/%	94.3%
Absorption correction	Multi-scan
Max. and min. transmission	1.00 and 0.67
Refinement method	Full-matrix least-squares on F^2
Data/restraints/parameters	8337/ 337/ 496
Goodness-of-fit on F^2	1.049
Final R indices [I>=2σ (I)]	R$_1$ = 0.0674, wR$_2$ = 0.1902
R indices (all data)	R$_1$ = 0.1240, wR$_2$ = 0.2201
Flack parameter	x =0.007(12)
Largest diff. peak and hole	0.529 and -0.448 e.Å^{-3}

Table 52. Bond lengths (Å) of **Zn-5** at 100 K.

Zn1	O1#	1.980(6)	N7	C22	1.320(12)
Zn1	N4	2.027(9)	N7	C20	1.391(15)
Zn1	N1#	2.076(8)	N7	C19	1.430(11)
Zn1	Cl1	2.244(5)	N7	C19'	1.499(13)
Zn1'	N1#	1.502(11)	C7	H7	0.9500
Zn1'	N4	2.170(12)	C8	H8	0.9500
Zn1'	Cl1'	2.191(12)	C9	H9	0.9500
Zn1'	C11#	2.507(12)	C10	C11	1.321(15)
Zn1'	C9#	2.533(11)	C10	H10	0.9500
N1	C9	1.313(11)	C11	H11	0.9500
N1	C11	1.362(12)	Zn2	O3'#	1.901(13)
O1	C1	1.286(13)	Zn2	N10	1.979(9)
C1	O2	1.224(11)	Zn2	N10'	2.116(10)
C1	C2	1.575(14)	Zn2	O3#	2.135(11)
N2	C9	1.332(11)	Zn2	Cl2	2.246(3)
N2	C10	1.362(12)	N8	C13	1.329(14)
N2	C2	1.455(12)	N8	C14	1.418(19)
C2	C3	1.563(17)	N8	C15	1.462(16)
C2	H2	1.0000	N9	N10	1.351(14)
N3	C8	1.346(14)	N9	C14	1.365(18)
N3	C7	1.347(13)	N10	C13	1.317(15)
N3	C6	1.516(15)	C13	H13	0.9500
C3	C4	1.459(15)	C14	H14	0.9500
C3	H3A	0.9900	C15	C16	1.501(17)
C3	H3B	0.9900	C15	H15A	0.9900
N4	C8	1.368(14)	C15	H15B	0.9900
N4	N5	1.382(12)	C16	C17	1.577(16)
C4	C5	1.547(18)	C16	H16A	0.9900
C4	H4A	0.9900	C16	H16B	0.9900
C4	H4B	0.9900	C17	C18	1.517(18)
N5	C7	1.388(14)	C17	H17A	0.9900
C5	C6	1.573(19)	C17	H17B	0.9900
C5	H5A	0.9900	C18	C19	1.533(6)
C5	H5B	0.9900	C18	C12	1.925(19)
N6	C22	1.346(14)	C18	H18A	0.9900
N6	C21	1.371(12)	C18	H18B	0.9900
N6	Zn2#	2.036(9)	N8'	C13'	1.330(15)
C6	H6A	0.9900	N8'	C14'	1.420(19)
C6	H6B	0.9900	N8'	C15'	1.461(17)

313

Crystallographic Data

N9'	N10'	1.356(15)		C18'	H18C	0.9900
N9'	C14'	1.364(18)		C18'	H18D	0.9900
N10'	C13'	1.323(16)		C19	C12	1.503(7)
C13'	H13'	0.9500		C19	H19	1.0000
C14'	H14'	0.9500		C19'	C12'	1.528(7)
C15'	C16'	1.503(17)		C19'	H19'	1.0000
C15'	H15C	0.9900		C20	C21	1.206(16)
C15'	H15D	0.9900		C20	H20	0.9500
C16'	C17'	1.576(16)		C21	H21	0.9500
C16'	H16C	0.9900		C22	H22	0.9500
C16'	H16D	0.9900		O3	C12	1.302(13)
C17'	C18'	1.516(19)		O4	C12	1.256(14)
C17'	H17C	0.9900		O3'	C12'	1.312(14)
C17'	H17D	0.9900		O4'	C12'	1.270(14)
C18'	C19'	1.585(13)				

Table 53. Bond angles (°) of **Zn-5** at 100 K.

O1#	Zn1	N4	110.3(3)	C9	N2	C10	104.5(8)
O1#	Zn1	N1#	116.9(3)	C9	N2	C2	128.0(8)
N4	Zn1	N1#	101.4(3)	C10	N2	C2	127.5(8)
O1#	Zn1	Cl1	106.1(2)	N2	C2	C3	107.9(9)
N4	Zn1	Cl1	115.0(3)	N2	C2	C1	114.9(8)
N1#	Zn1	Cl1	107.5(3)	C3	C2	C1	109.8(8)
N1#	Zn1'	N4	118.5(6)	N2	C2	H2	108.0
N1#	Zn1'	Cl1'	112.3(7)	C3	C2	H2	108.0
N4	Zn1'	Cl1'	113.8(7)	C1	C2	H2	108.0
N1#	Zn1'	C11#	27.4(4)	C8	N3	C7	106.9(9)
N4	Zn1'	C11#	142.9(5)	C8	N3	C6	126.3(10)
N1#	Zn1'	C9#	24.1(4)	C7	N3	C6	126.6(10)
N4	Zn1'	C9#	94.5(4)	C4	C3	C2	122.3(13)
C11#	Zn1'	C9#	50.7(3)	C4	C3	H3A	106.7
C9	N1	C11	107.7(8)	C2	C3	H3A	106.7
C9	N1	Zn1'#	128.1(8)	C4	C3	H3B	106.7
C11	N1	Zn1'#	122.2(8)	C2	C3	H3B	106.7
C9	N1	Zn1#	127.8(7)	H3A	C3	H3B	106.6
C11	N1	Zn1#	124.4(6)	C8	N4	N5	108.7(9)
C1	O1	Zn1#	111.9(6)	C8	N4	Zn1	128.5(7)
O2	C1	O1	125.6(11)	N5	N4	Zn1	122.6(8)
O2	C1	C2	119.9(10)	C8	N4	Zn1'	128.5(8)
O1	C1	C2	114.6(8)	N5	N4	Zn1'	117.3(7)

C3	C4	C5	115.5(13)	C10	C11	N1	106.2(8)
C3	C4	H4A	108.4	C10	C11	Zn1'#	135.5(7)
C5	C4	H4A	108.4	N1	C11	Zn1'#	30.5(5)
C3	C4	H4B	108.4	C10	C11	H11	126.9
C5	C4	H4B	108.4	N1	C11	H11	126.9
H4A	C4	H4B	107.5	Zn1'#	C11	H11	97.1
N4	N5	C7	104.3(9)	N10	Zn2	N6#	106.5(8)
C4	C5	C6	114.7(11)	O3'#	Zn2	N10'	101.9(6)
C4	C5	H5A	108.6	N6#	Zn2	N10'	101.3(8)
C6	C5	H5A	108.6	N10	Zn2	O3#	106.8(7)
C4	C5	H5B	108.6	N6#	Zn2	O3#	117.3(4)
C6	C5	H5B	108.6	O3'#	Zn2	Cl2	130.0(4)
H5A	C5	H5B	107.6	N10	Zn2	Cl2	111.7(5)
C22	N6	C21	105.9(8)	N6#	Zn2	Cl2	107.1(2)
C22	N6	Zn2#	130.9(7)	N10'	Zn2	Cl2	120.8(6)
C21	N6	Zn2#	123.2(7)	O3#	Zn2	Cl2	107.5(3)
N3	C6	C5	112.6(8)	C13	N8	C14	102.7(12)
N3	C6	H6A	109.1	C13	N8	C15	129.5(14)
C5	C6	H6A	109.1	C14	N8	C15	127.8(12)
N3	C6	H6B	109.1	N10	N9	C14	104.5(11)
C5	C6	H6B	109.1	C13	N10	N9	109.9(9)
H6A	C6	H6B	107.8	C13	N10	Zn2	130.7(9)
C22	N7	C20	105.0(9)	N9	N10	Zn2	119.4(10)
C22	N7	C19	136.0(11)	N10	C13	N8	112.4(12)
C20	N7	C19	117.5(10)	N10	C13	H13	123.8
C22	N7	C19'	116.5(14)	N8	C13	H13	123.8
C20	N7	C19'	137.7(14)	N9	C14	N8	110.2(11)
N3	C7	N5	110.9(9)	N9	C14	H14	124.9
N3	C7	H7	124.5	N8	C14	H14	124.9
N5	C7	H7	124.5	N8	C15	C16	113.6(11)
N3	C8	N4	109.2(9)	N8	C15	H15A	108.9
N3	C8	H8	125.4	C16	C15	H15A	108.9
N4	C8	H8	125.4	N8	C15	H15B	108.9
N1	C9	N2	111.0(8)	C16	C15	H15B	108.9
N1	C9	Zn1'#	27.8(5)	H15A	C15	H15B	107.7
N2	C9	Zn1'#	137.2(7)	C15	C16	C17	111.9(10)
N1	C9	H9	124.5	C15	C16	H16A	109.2
N2	C9	H9	124.5	C17	C16	H16A	109.2
Zn1'#	C9	H9	97.6	C15	C16	H16B	109.2
C11	C10	N2	110.5(9)	C17	C16	H16B	109.2
C11	C10	H10	124.7	H16A	C16	H16B	107.9
N2	C10	H10	124.7	C18	C17	C16	112.3(10)

C18	C17	H17A	109.1	C16'	C17'	H17C	109.0
C16	C17	H17A	109.1	C18'	C17'	H17D	109.0
C18	C17	H17B	109.1	C16'	C17'	H17D	109.0
C16	C17	H17B	109.1	H17C	C17'	H17D	107.8
H17A	C17	H17B	107.9	C17'	C18'	C19'	138(2)
C17	C18	C19	108.1(11)	C17'	C18'	H18C	102.7
C17	C18	C12	153.8(12)	C19'	C18'	H18C	102.7
C19	C18	C12	49.9(5)	C17'	C18'	H18D	102.7
C17	C18	H18A	110.1	C19'	C18'	H18D	102.7
C19	C18	H18A	110.1	H18C	C18'	H18D	105.0
C12	C18	H18A	92.9	N7	C19	C12	129.1(13)
C17	C18	H18B	110.1	N7	C19	C18	106.9(12)
C19	C18	H18B	110.1	C12	C19	C18	78.7(9)
C12	C18	H18B	72.4	N7	C19	H19	112.0
H18A	C18	H18B	108.4	C12	C19	H19	112.0
C13'	N8'	C14'	101.8(12)	C18	C19	H19	112.0
C13'	N8'	C15'	130.3(15)	N7	C19'	C12'	97.6(11)
C14'	N8'	C15'	127.8(12)	N7	C19'	C18'	111.3(15)
N10'	N9'	C14'	105.6(12)	C12'	C19'	C18'	138(2)
C13'	N10'	N9'	108.1(10)	N7	C19'	H19'	101.8
C13'	N10'	Zn2	132.0(10)	C12'	C19'	H19'	101.8
N9'	N10'	Zn2	120.0(11)	C18'	C19'	H19'	101.8
N10'	C13'	N8'	113.9(13)	C21	C20	N7	110.9(10)
N10'	C13'	H13'	123.0	C21	C20	H20	124.5
N8'	C13'	H13'	123.0	N7	C20	H20	124.5
N9'	C14'	N8'	110.4(11)	C20	C21	N6	109.5(10)
N9'	C14'	H14'	124.8	C20	C21	H21	125.2
N8'	C14'	H14'	124.8	N6	C21	H21	125.2
N8'	C15'	C16'	115.3(13)	N7	C22	N6	108.4(9)
N8'	C15'	H15C	108.4	N7	C22	H22	125.8
C16'	C15'	H15C	108.4	N6	C22	H22	125.8
N8'	C15'	H15D	108.4	C12	O3	Zn2#	108.5(7)
C16'	C15'	H15D	108.4	O4	C12	O3	122.1(11)
H15C	C15'	H15D	107.5	O4	C12	C19	138.0(13)
C15'	C16'	C17'	111.8(11)	O3	C12	C19	97.7(11)
C15'	C16'	H16C	109.3	O4	C12	C18	94.3(11)
C17'	C16'	H16C	109.3	O3	C12	C18	142.3(11)
C15'	C16'	H16D	109.3	C19	C12	C18	51.4(5)
C17'	C16'	H16D	109.3	O4'	C12'	O3'	117.8(12)
H16C	C16'	H16D	107.9	O4'	C12'	C19'	125.2(16)
C18'	C17'	C16'	113.1(12)	O3'	C12'	C19'	115.1(13)
C18'	C17'	H17C	109.0				

UNIVERSITAT ROVIRA I VIRGILI
INSIGHTS IN HOMOCHIRAL METAL-ORGANIC FRAMEWORKS: FROM THEIR SYNTHESIS TO ENANTIOSELECTIVE
APPLICATIONS
Juanjo Cabezas Giménez

Annex I

Crystallographic data of Cu-5

Table 54. Crystallographic data and refinement parameters for the crystal structure of **Cu-5** collected at 100 K.

Empirical formula	$C_{20}H_{30.21}BCl1_{.54}Cu_{4.50}N_{12}O_{6.96}$
Formula weight	977.46
T/K	100(2)K
Wavelength/Å	0.71073 Å
Crystal system	Tetragonal
Space group	$P4_2/m$
a/Å	16.1598(8)Å
b/Å	16.1598(8)Å
c/Å	14.8505(8)Å
$\alpha/°$	90°
$\beta/°$	90°
$\gamma/°$	90°
Volume/Å^3	3878.0(4) Å^3
Z	4
ρ_{calc}/g cm^{-3}	1.674 g cm^{-3}
μ/mm^{-1}	2.607 mm^{-1}
F(000)	1950
Crystal size/mm^3	0.100 x 0.100 x 0.050 mm^3
θ range for data collection/°	1.260 to 29.590°.
Index ranges	$-18 \leq h \leq 22, -17 \leq k \leq 22, -20 \leq l \leq 19$
Reflections collected	42499
Independent reflections	5632[R(int) = 0.0373]
Completeness/%	99.6%
Absorption correction	Multi-scan
Max. and min. transmission	0.74 and 0.63
Refinement method	Full-matrix least-squares on F^2
Data/restraints/parameters	5632/633/506
Goodness-of-fit on F^2	1.105
Final R indices [I>=2σ (I)]	$R_1 = 0.0731$, $wR_2 = 0.2094$
R indices (all data)	$R_1 = 0.0872$, $wR_2 = 0.2189$
Largest diff. peak and hole	1.403 and -0.676 e.Å^{-3}

UNIVERSITAT ROVIRA I VIRGILI
INSIGHTS IN HOMOCHIRAL METAL-ORGANIC FRAMEWORKS: FROM THEIR SYNTHESIS TO ENANTIOSELECTIVE
APPLICATIONS
Juanjo Cabezas Giménez

Crystallographic Data

Table 55. Bond lengths (Å) of **Cu-5** at 100 K.

Cu1	N1	1.84(3)	C3	C5	1.511(6)
Cu1	N1#	1.84(3)	C4	O2	1.231(8)
Cu1	Cl1	2.418(14)	C4	O1	1.237(8)
Cu1'	N1'#	1.907(7)	C5	C6	1.536(6)
Cu1'	N1'	1.907(7)	C6	C7	1.527(6)
Cu1'	Cl1	2.469(3)	C7	C8	1.527(6)
Cu2	N6#	1.90(3)	C8	N4	1.467(8)
Cu2	N2'	1.907(7)	N4	C9	1.332(9)
Cu2	N6'#	1.926(8)	N4	C10	1.341(9)
Cu2	N2	2.01(3)	N5	C9	1.307(8)
Cu2	Cl1B	2.4982(9)	N5	N6	1.375(8)
Cu2	Cl1	2.5495(8)	N6	C10	1.317(8)
Cu3	O2#	1.89(2)	N1'	C1'	1.320(7)
Cu3	O2	1.89(2)	N1'	N2'	1.378(8)
Cu3	O2#	1.89(2)	N2'	C2'	1.306(8)
Cu3	O2#	1.89(2)	C1'	N3'	1.317(9)
Cu3	O2'#	1.947(6)	C2'	N3'	1.331(9)
Cu3	O2'#	1.947(6)	N3'	C3'	1.472(7)
Cu3	O2'#	1.947(6)	C3'	C5'	1.507(6)
Cu3	O2'	1.947(6)	C3'	C4'	1.513(9)
Cu4	N5'#	1.906(7)	C4'	O2'	1.229(7)
Cu4	N5'	1.906(7)	C4'	O1'	1.236(8)
Cu4	N5#	1.98(3)	C5'	C6'	1.537(6)
Cu4	N5	1.98(3)	C6'	C7'	1.525(6)
Cu4	Cl1#	2.4778(17)	C7'	C8'	1.524(6)
N1	C1	1.320(8)	C8'	N4'	1.467(7)
N1	N2	1.378(9)	N4'	C9'	1.331(8)
N2	C2	1.305(9)	N4'	C10'	1.340(8)
C1	N3	1.318(9)	N5'	C9'	1.307(7)
C2	N3	1.334(10)	N5'	N6'	1.375(7)
N3	C3	1.472(8)	N6'	C10'	1.317(7)
C3	C4	1.511(10)			

Annex I

Table 56. Bond angles (º) of **Cu-5** at 100 K.

N1	Cu1	N1#	142(4)	N5	Cu4	Cl1#	103.2(11)
N1	Cu1	Cl1	104.6(17)	Cu1	Cl1	Cu4#	151.4(2)
N1#	Cu1	Cl1	104.6(17)	Cu1	Cl1	Cu2#	84.88(7)
N1'#	Cu1'	N1'	156.1(7)	Cu4#	Cl1	Cu2#	87.10(4)
N1'#	Cu1'	Cl1	101.9(4)	Cu1	Cl1	Cu2	84.88(7)
N1'	Cu1'	Cl1	101.9(4)	Cu1'	Cl1	Cu2	86.95(4)
N6#	Cu2	N6'#	9.9(10)	Cu4#	Cl1	Cu2	87.10(4)
N6#	Cu2	N2	157.0(18)	Cu2#	Cl1	Cu2	146.99(7)
N6#	Cu2	Cl1B	90.6(9)	Cu2#	Cl1B	Cu2	172.2(3)
N2	Cu2	Cl1B	97.3(17)	C1	N1	N2	107.5(7)
N6#	Cu2	Cl1	102.2(11)	C1	N1	Cu1	130(3)
N2'	Cu2	Cl1	101.2(3)	N2	N1	Cu1	122(3)
N6'#	Cu2	Cl1	98.9(3)	C2	N2	N1	105.3(6)
N2	Cu2	Cl1	97.1(13)	C2	N2	Cu2	133(2)
Cl1B	Cu2	Cl1	102.60(13)	N1	N2	Cu2	120(3)
O2#	Cu3	O2	180.0	N3	C1	N1	109.6(7)
O2#	Cu3	O2#	113(2)	N2	C2	N3	111.4(7)
O2	Cu3	O2#	67(2)	C1	N3	C2	106.1(7)
O2#	Cu3	O2#	67(2)	C1	N3	C3	121.4(9)
O2	Cu3	O2#	113(2)	C2	N3	C3	130.5(9)
O2#	Cu3	O2#	180.0(13)	N3	C3	C4	111.6(8)
O2#	Cu3	O2'#	13.7(10)	N3	C3	C5	111.1(7)
O2	Cu3	O2'#	166.3(10)	C4	C3	C5	114.1(8)
O2#	Cu3	O2'#	101.0(9)	O2	C4	O1	125.4(9)
O2#	Cu3	O2'#	79.0(9)	O2	C4	C3	114.5(8)
O2#	Cu3	O2'#	101.0(9)	O1	C4	C3	119.8(9)
O2	Cu3	O2'#	79.0(9)	C4	O2	Cu3	124(2)
O2#	Cu3	O2'#	13.7(10)	C3	C5	C6	114.2(8)
O2#	Cu3	O2'#	166.3(10)	C7	C6	C5	109.1(8)
O2#	Cu3	O2'#	79.0(9)	C8	C7	C6	114.2(8)
O2	Cu3	O2'#	101.0(9)	N4	C8	C7	111.1(7)
O2#	Cu3	O2'#	166.3(10)	C9	N4	C10	105.3(6)
O2#	Cu3	O2'#	13.7(10)	C9	N4	C8	126.2(8)
O2'#	Cu3	O2'	180.0(3)	C10	N4	C8	127.9(8)
O2'#	Cu3	O2'	89.8(4)	C9	N5	N6	107.0(6)
O2'#	Cu3	O2'	90.2(4)	C9	N5	Cu4	132.5(19)
N5'#	Cu4	N5'	155.9(6)	N6	N5	Cu4	120.5(18)
N5#	Cu4	N5	153(2)	C10	N6	N5	106.2(6)
N5#	Cu4	Cl1#	103.2(11)	C10	N6	Cu2#	129.2(18)

Crystallographic Data

N5	N6	Cu2#	124.6(17)	O2'	C4'	O1'	125.9(6)
N5	C9	N4	110.7(7)	O2'	C4'	C3'	114.1(6)
N6	C10	N4	110.5(7)	O1'	C4'	C3'	119.9(6)
C1'	N1'	N2'	107.5(5)	C4'	O2'	Cu3	115.8(5)
C1'	N1'	Cu1'	128.0(7)	C3'	C5'	C6'	113.6(5)
N2'	N1'	Cu1'	124.4(7)	C7'	C6'	C5'	109.4(5)
C2'	N2'	N1'	105.4(5)	C8'	C7'	C6'	113.8(6)
C2'	N2'	Cu2	132.9(6)	N4'	C8'	C7'	111.0(5)
N1'	N2'	Cu2	121.5(6)	C9'	N4'	C10'	105.4(5)
N3'	C1'	N1'	109.6(6)	C9'	N4'	C8'	126.5(6)
N2'	C2'	N3'	111.3(6)	C10'	N4'	C8'	128.1(6)
C1'	N3'	C2'	106.3(5)	C9'	N5'	N6'	107.0(5)
C1'	N3'	C3'	121.6(6)	C9'	N5'	Cu4	129.6(6)
C2'	N3'	C3'	132.0(6)	N6'	N5'	Cu4	123.1(5)
N3'	C3'	C5'	110.6(5)	C10'	N6'	N5'	106.2(5)
N3'	C3'	C4'	111.3(5)	N5'	C9'	N4'	110.8(5)
C5'	C3'	C4'	113.6(6)	N6'	C10'	N4'	110.5(6)

ANNEX II

Molecule Index

UNIVERSITAT ROVIRA I VIRGILI
INSIGHTS IN HOMOCHIRAL METAL-ORGANIC FRAMEWORKS: FROM THEIR SYNTHESIS TO ENANTIOSELECTIVE
APPLICATIONS
Juanjo Cabezas Giménez

Introduction

L₁

L₂

L₃

L₄

L₅ (R = Me, H)

L₆ (R = Me, H)

L₇ (R = Me, H)

L₈ (R = Me, H)

UNIVERSITAT ROVIRA I VIRGILI
INSIGHTS IN HOMOCHIRAL METAL-ORGANIC FRAMEWORKS: FROM THEIR SYNTHESIS TO ENANTIOSELECTIVE
APPLICATIONS
Juanjo Cabezas Giménez

Molecule Index
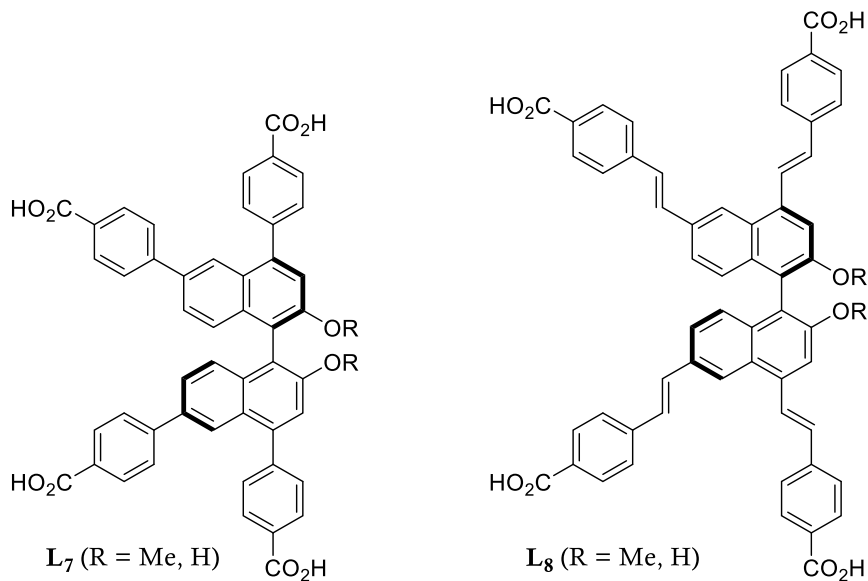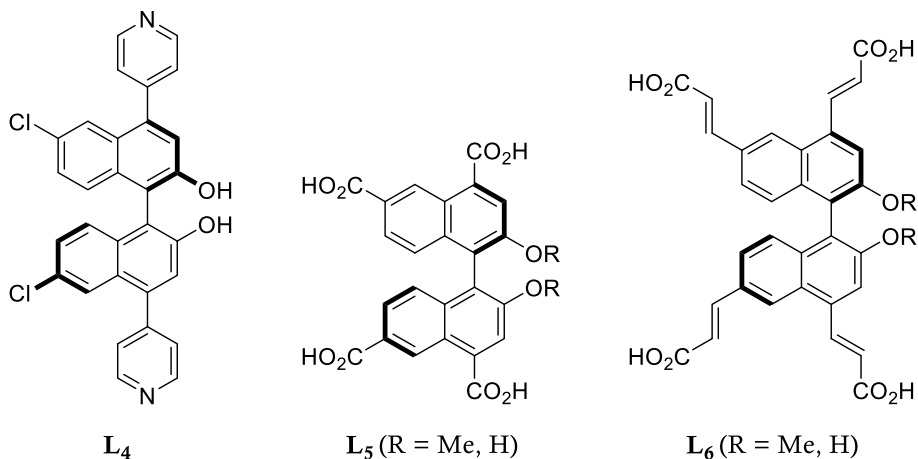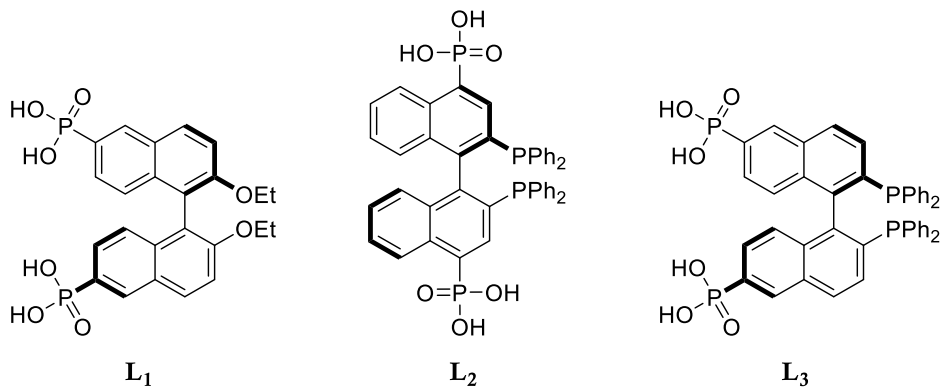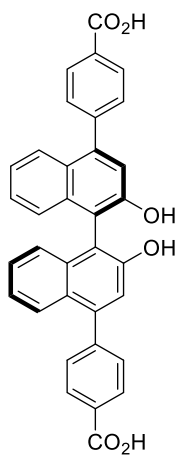
L$_9$
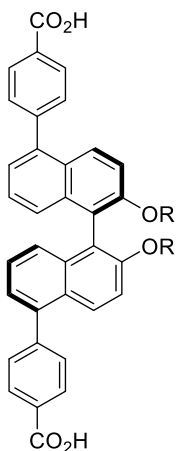
L$_{10a}$: R = H
L$_{10b}$: R = Me
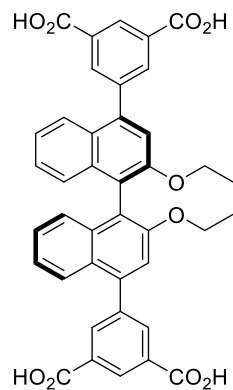
L$_{11}$
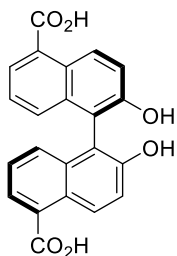
L$_{12}$
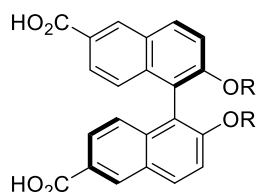
L$_{13a}$: R = H
L$_{13b}$: R = Me
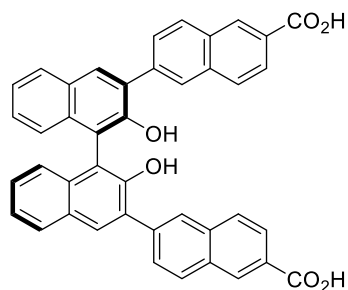
L$_{14}$
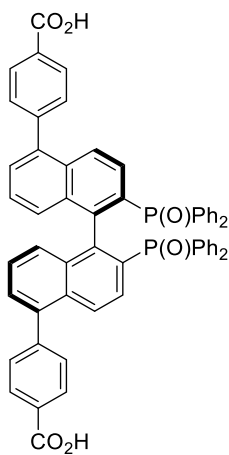
L$_{15}$
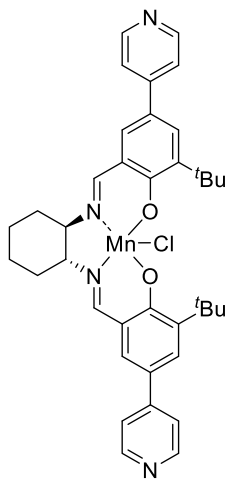
L$_{16}$
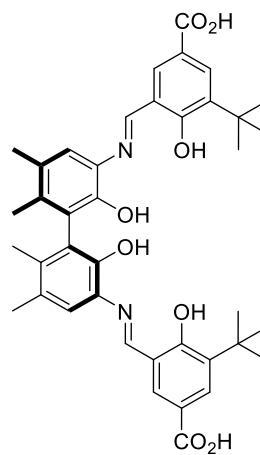
L$_{17}$
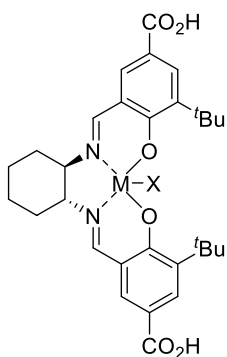
L₁₈
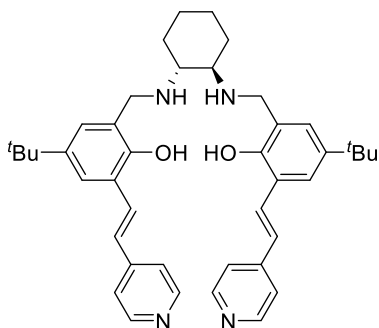
L₁₉
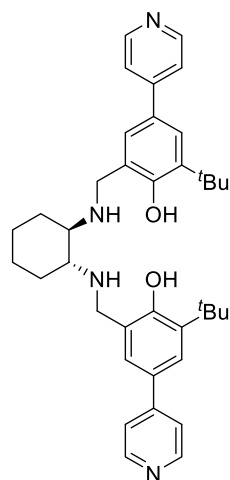
L₂₀
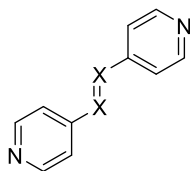
L₂₁ (X = N)
L₂₂ (X = C)
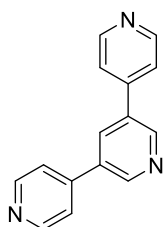
L₂₃
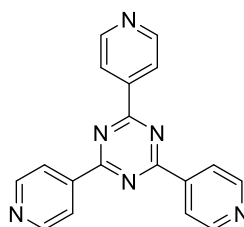
L₂₄
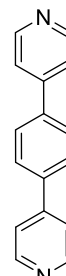
L₂₅
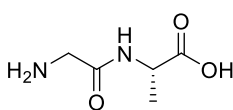
L₂₆
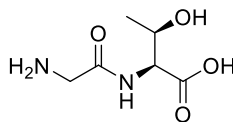
L₂₇
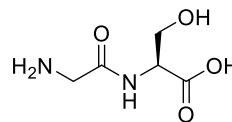
L₂₈
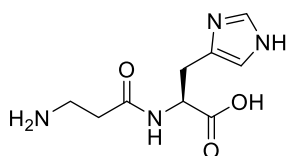
L₂₉
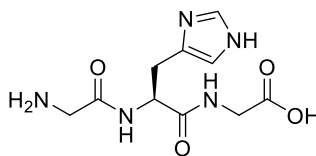
L₃₀
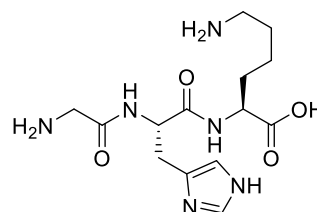
L₃₁
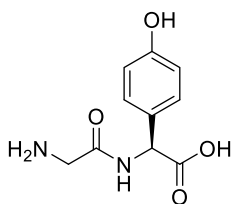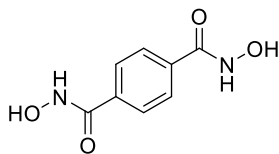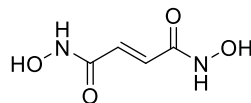
L₃₂   **L₃₃**   **L₃₄**
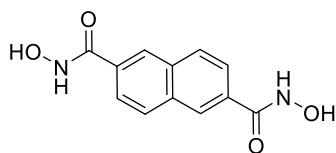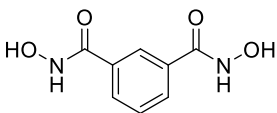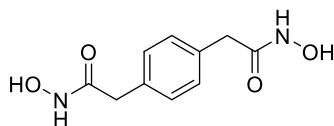
L₃₅   **L₃₆**   **L₃₇**
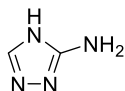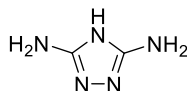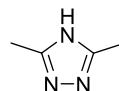
L₃₈   **L₃₉**   **L₄₀**   **L₄₁**
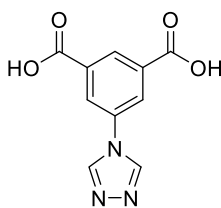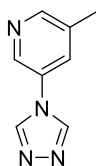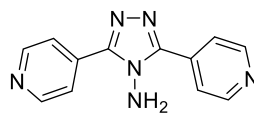
L₄₂   **L₄₃**   **L₄₄.₁**
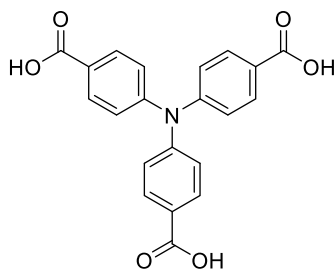
L₄₄.₂   **L₄₅**   **L₄₆ₐ**: R = H
L₄₆ᵦ: R = Me

L₄₇   **L₄₈**   **L₄₉**   **L₅₀**

Annex II
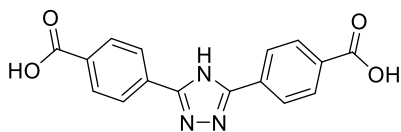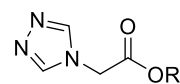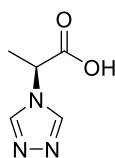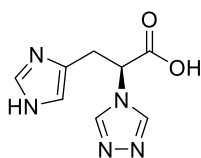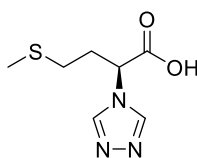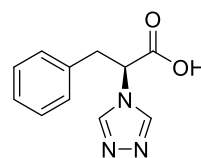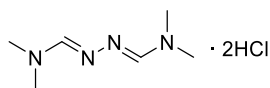
Chapter I

DMFA·2HCl
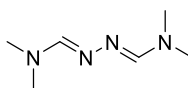
DMFA
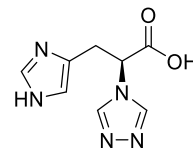
S-HTA
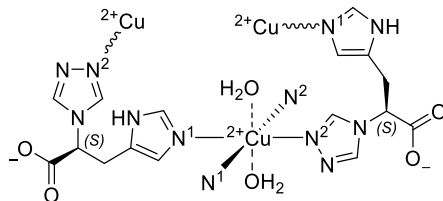
TAMOF-1
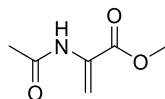
1
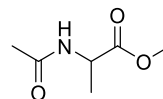
2

Chapter II
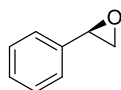
(*R*)-**1**
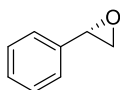
(*S*)-**1**
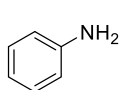
2
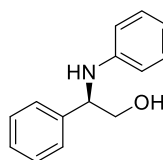
(*R*)-**B1**
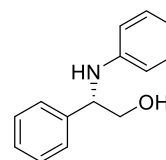
(*S*)-**B1**
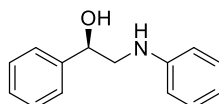
(*R*)-**L1**
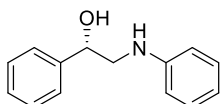
(*S*)-**L1**
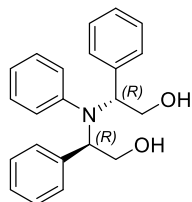
BB1
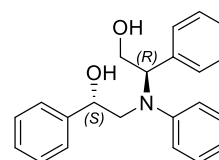
LB1

LL1

ent-**BB1**

ent-**LB1**

BB2

LB2   **LL2**   *ent*-**LL1**   *ent*-**LB2**

3   (*R*)-**4b**   (*S*)-**4l**   **5**   **6**

Chapter III

ibuprofen   **thalidomide**   *trans*-**stilbene oxide**   **furoin**

1-phenylethanol   **flavanone**   **benzoin**   **anisoin**

methyl mandelate   **2-phenylpropionitrile**   **limonene**   **carvone**

camphene   **β-citronellol**   **α-pinene**   **α-terpineol**
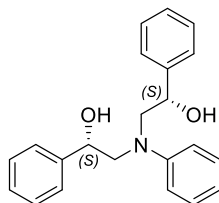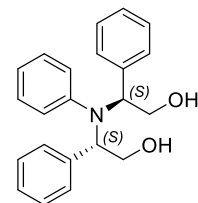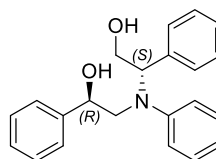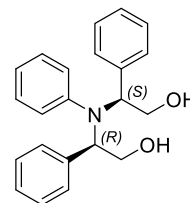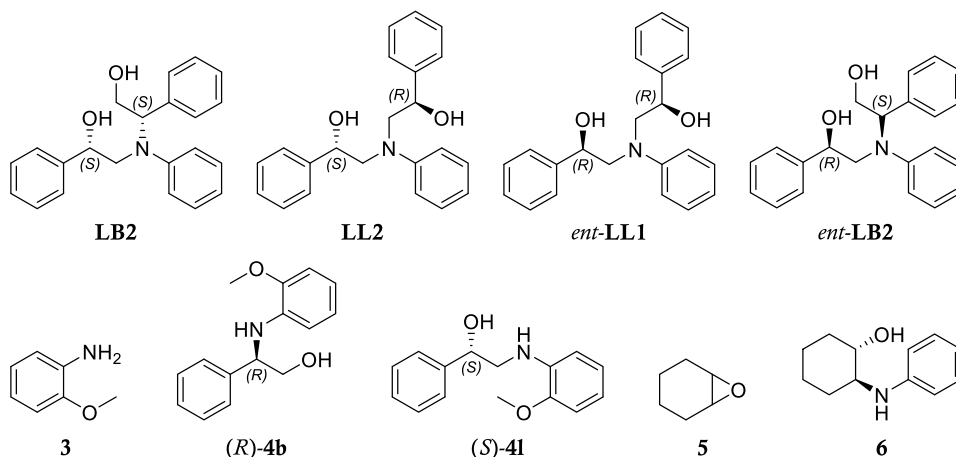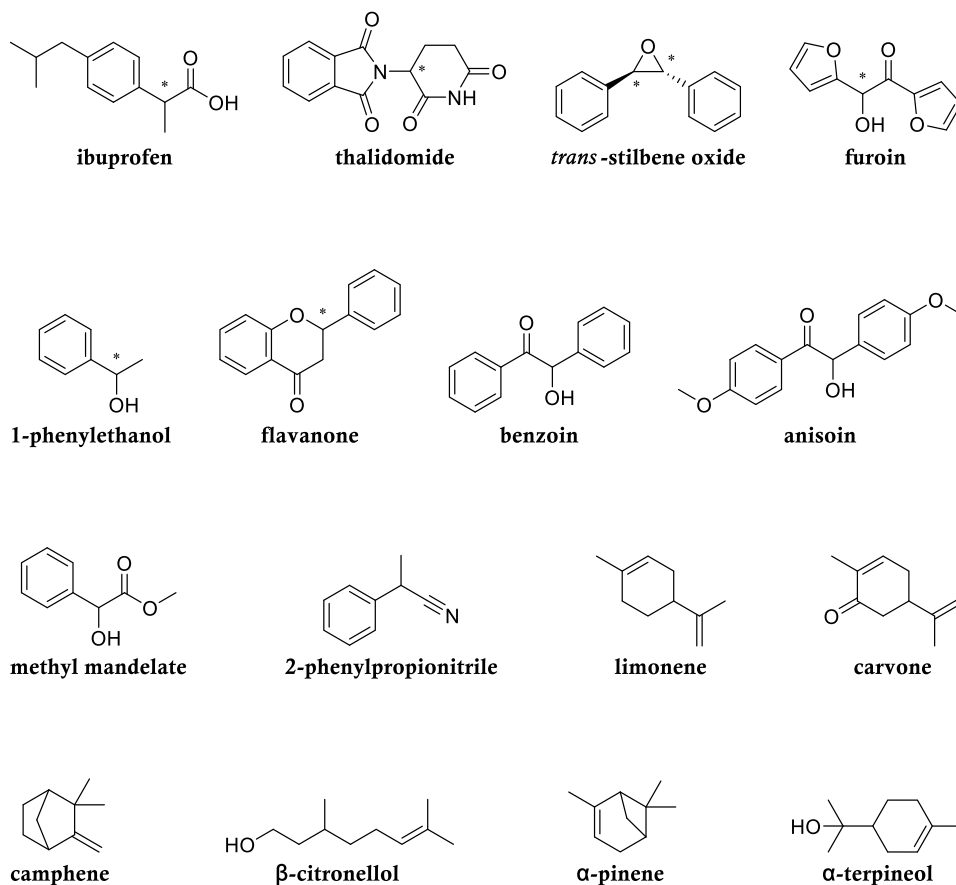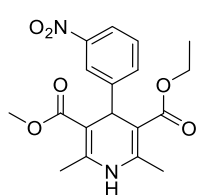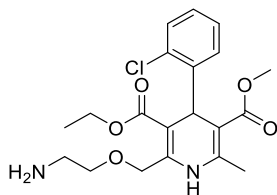
nitrendipine   amlodipine   phenyl *N*-phenylphosphoramidochloridate
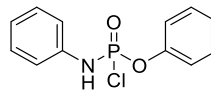
Chapter IV
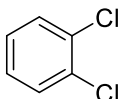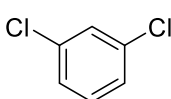
1,2-dichlorobenzene   1,3-dichlorobenzene   1,4-dichlorobenzene
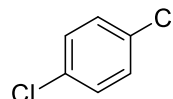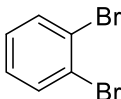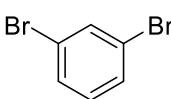
1,2-dibromobenzene   1,3-dibromobenzene   1,4-dibromobenzene
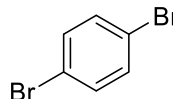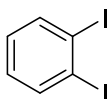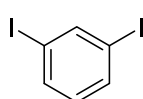
1,2-diiodobenzene   1,3-diiodobenzene   1,4-diiodobenzene
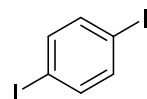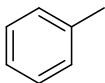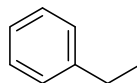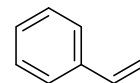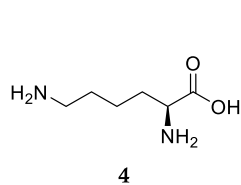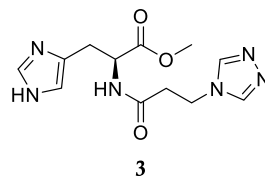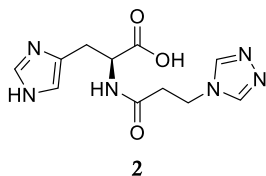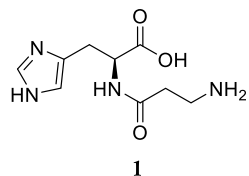

benzene   toluene   ethylbenzene   styrene
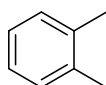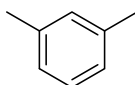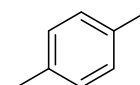
o-xylene   *m*-xylene   *p*-xylene

o-cresol   *m*-cresol   *p*-cresol

UNIVERSITAT ROVIRA I VIRGILI
INSIGHTS IN HOMOCHIRAL METAL-ORGANIC FRAMEWORKS: FROM THEIR SYNTHESIS TO ENANTIOSELECTIVE
APPLICATIONS
Juanjo Cabezas Giménez

Molecule Index

Chapter V

1

2

3

4

5

6

7

8

9

10

11

12

13

14

15

16

17

18

19

UNIVERSITAT ROVIRA I VIRGILI
INSIGHTS IN HOMOCHIRAL METAL-ORGANIC FRAMEWORKS: FROM THEIR SYNTHESIS TO ENANTIOSELECTIVE
APPLICATIONS
Juanjo Cabezas Giménez

UNIVERSITAT ROVIRA I VIRGILI
INSIGHTS IN HOMOCHIRAL METAL-ORGANIC FRAMEWORKS: FROM THEIR SYNTHESIS TO ENANTIOSELECTIVE
APPLICATIONS
Juanjo Cabezas Giménez

UNIVERSITAT ROVIRA I VIRGILI
INSIGHTS IN HOMOCHIRAL METAL-ORGANIC FRAMEWORKS: FROM THEIR SYNTHESIS TO ENANTIOSELECTIVE
APPLICATIONS
Juanjo Cabezas Giménez

UNIVERSITAT
ROVIRA i VIRGILI

ICIQ

Institut
Català
d'Investigació
Química